Full Explanatory Supplement

6 March 2013

Main Page

Very important information for new users: READ ME FIRST.

Very important information for all users: News.

If you are reading the printed version of this ES wiki, the online version can be found at the URL:

http://www.sciops.esa.int/wikiSI/planckpla/index.php?title=Main_Page&instance=Planck_PLA_ES [1].

For help with editing the Explanatory Supplement consult the User's Guide [2] for a detailed User Guide of the MediaWiki software or the Explanatory Supplement Help page for the guidelines on editing the ES.

A set of *books* (a collection of pages that can easily be printed together as a pdf file) can be found here. We also have a page explaining how to create your own book.

PDF Book: A book with the full contents can be found here and a pdf version updated weekly can be found here:.

Explanatory supplement

By Planck Collaboration

The Explanatory Supplement is a reference text to the public data delivered from the operations of the European Space Agency's Planck satellite during its mission.

1. The Planck mission (Dupac)
2. The satellite
    1. The service module
        1. Thermal design(Mendes)
    2. HFI design, qualification, and performance (Lamarre/Pajot)
        1. Overview
        2. Cryogenics
        3. Cold optics
        4. Detection chain
        5. Time response
        6. Operations
        7. Performance summary
        8. Annexes
    3. LFI design, qualification, and performance(Gregorio)
    4. The telescope
    5. Others
        1. The standard radiation environment monitor (Mendes)
        2. The fiber optic gyro unit
3. Ground Segment and Operations
    1. Ground segment overview (Dupac)
    2. Contingencies
    3. Operational history
    4. Survey scanning and performance (Dupac)
    5. Thermal environment
    6. Radiation environment (Mendes)

7. Pointing performance (Dupac)

4. Data processing
    1. Data flow overview
    2. On-board processing
    3. MOC data transfer and storage
    4. HFI Data Processing (Bouchet)
        1. Pre-processing (Vibert)
        2. TOI processing (Desert)
        3. Detectors pointing and beams (Crill/Jones/Jaffe)
        4. Map-making (Perdereau)
        5. Spectral response (Spencer)
        6. Internal overall validation (Ganga)
        7. Power spectra (Hivon)
        8. Summary of HFI data characteristics (Bouchet)
    5. LFI data processing: Introduction (Zacchei)
        1. TOI processing (Mennella)

        1. Detector Pointing (Maris/Galeotta)
        2. Beams (Sandri/Villa/Rocha)
        3. Map-making (Keihanen)
        4. LFI systematic effects uncertainties (Mennella)
        5. LFI internal overall validation (Maino)
        6. LFI specific L3 activities: masks, MCQA, etc
        7. Summary of LFI data characteristics & the RIMO content
    2. HFI/LFI joint data processing
        1. Compact Source catalogues (Ashdown/Nuevo/Caniego)
        2. CMB map cleaning from foreground emissions (Ashdown/Baccigalupi)
        3. CMB Power spectra and Planck likelihood code CLIK(Bouchet/Natoli)
        4. Simulations (TBC, bouchet)
    3. Scientific analyses products (bouchet)
    4. PSO processing (To be removed)
2. Planck Legacy Archive(Dupac)
3. Mission products
    1. Timelines: (Not in 1st Release)

    1. Frequency Maps: Types of maps • List of products • FITS file structure
    2. The RIMOs: Map-level data • Band transmissions • Beam Window Functions
    3. Effective Beams (Rocha??)
    4. Catalogues: ERCSC • Compact Sources • SZ Clusters
    5. Frequency maps angular power spectra (Zacheoi/Bouchet)
    6. Astrophysical component maps: CMB • Foregrounds • Dust opacity • CO emission
    7. Planck CMB spectrum and Likelihood Code (Bouchet/Natoli)
    8. Cosmological Parameters
    9. Specially processed maps: Lensing map
    10. Additional angular power spectra (SZ, CIB...)
    11. The Planck Sky Model (Not in 1st Release)
    12. Scientific data used to generate Planck products

13. Simulation data
14. Survey history data (Dupac) SHoudl this be here or in the next chapter??
15. Satellite history data (Not in 1st release)

2. Payload design, performance and calibration data
    1. Instrument performance
    2. Telescope
    3. Thermal and cooler system
    4. Fiber optic gyro (Not in 1st Release)
    5. Space radiation environment monitor
3. Software utilities
    1. Unpack and display (Not in 1st release)
    2. Unit conversion and Color correction (DPC)
    3. Print and plot (Not in 1st release)
    4. Analysis (Not in 1st release)
    5. Format conversion (Not in 1st release)
4. Appendix
5. Glossary
6. List of acronyms
7. References

References

[1] http://www.sciops.esa.int/wikiSI/planckpla/index.php?title=Main_Page&instance=Planck_PLA_ES
[2] http://meta.wikimedia.org/wiki/Help:Contents

The Planck Mission

The Planck mission

Introduction

Planck is a space telescope of the European Space Agency designed to answer key cosmological questions. Its main goal is to determine the geometry and content of the Universe, and which theories describing the birth and evolution of the Universe are correct. To achieve this ambitious objective, it observed the Cosmic Microwave Background radiation (CMB), emitted about 14 billion years ago, just over 300,000 years after the Big Bang. Today the CMB permeates the Universe and is observed to have an average temperature of 2.7 K. Small deviations from this average value (the so-called anisotropies), observable at angular scales larger than ~5 arcminutes, encode a wealth of information on the properties of the Universe in its infancy. The objective of Planck is to measure these properties with an unprecedented accuracy and level of detail.

The Planck collaboration institutes.

As with all ESA scientific missions, Planck was developed in a partnership with the European scientific community. Two consortia of scientific institutes, each led by a Principal Investigator, developed and delivered to ESA two instruments designed specifically for Planck. Each of these instruments targets a specific number of wavelength bands within the range in which the CMB is observable. Together, the two instruments are capable of collecting data of a quality adequate to measure the CMB signal and distinguish it from other confusing sources. A large telescope collects the light from the sky and deliver it to the instruments for measurement and analysis. The reflectors of the Planck telescope were developed and delivered to ESA by a Danish consortium of institutes. ESA retains overall management of the project, develops and procures the spacecraft, integrates the instruments into the spacecraft, and launches and operates it. Planck was launched on May 14th 2009 on an Ariane 5 rocket together with the Herschel Space Observatory. After launch, they were both placed into orbits around the L2 Lagrange of the Sun-Earth system, located about 1.5 million km from the Earth. From that far vantage point, Planck sweeped the sky regularly in large swaths, and covered it fully about six times. Each of the two instrument consortia operated their respective instrument and processed all the data into usable scientific products. At the end of the mission the consortia delivered the final products to ESA, which archives them and distributes them to the community.

Early operations and transfer to orbit

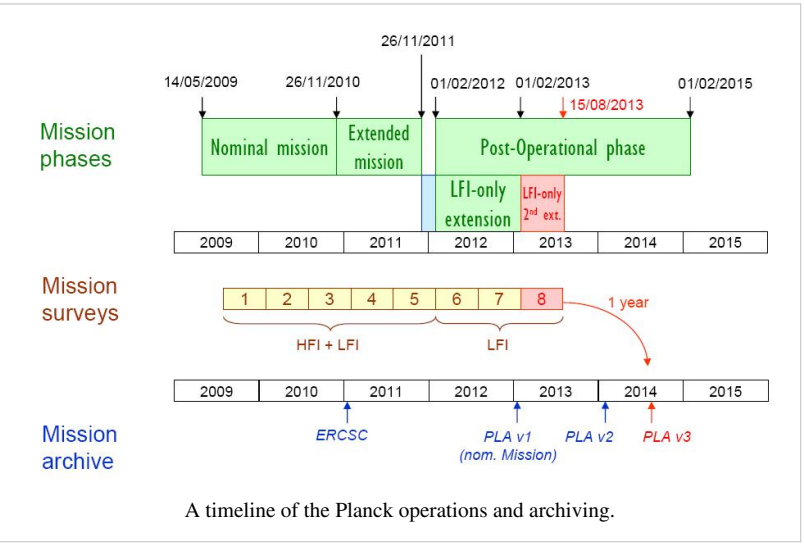

A timeline of the Planck operations and archiving.

Planck was launched from the Centre Spatial Guyanais in Kourou (French Guyana) on 14 May 2009 at its nominal lift-off time of 13:12 UT, on an Ariane 5 ECA rocket of Arianespace2. ESA's Herschel observatory was launched on the same rocket. At 13:37:55 UT, Herschel was released from the rocket at an altitude of 1200 km; Planck followed suit at 13:40:25UT. The separation attitudes of both satellites were within 0.1 deg. of prediction. The Ariane rocket placed Planck with excellent accuracy (semimajor axis within 1.6 % of prediction), on a trajectory towards the second Lagrangian point of the Earth-Sun system (L2) . The orbit describes a Lissajous trajectory around L2 with a ~6 month period that avoids crossing the Earth penumbra for at least 4 years.

After release from the rocket, three large manoeuvres were carried out to place Planck in its intended final orbit. Once in its final orbit, very small manoeuvres are required at approximately monthly intervals (1 ms−1 per year) to keep Planck from drifting away from its intended path around L2. The attitude manoeuvres required to followthe scanning strategy require about 2.6 ms−1 per year. Overall, the excellent performance of launch and orbit manoeuvres will lead to a large amount (~160 kg, or ~40% of initial tank loading) of fuel remaining on board at end of mission operations.

The Herschel and Planck spacecrafts in the launch vehicle configuration.

Planck started cooling down radiatively shortly after launch. Heaters were activated to hold the focal plane at 250 K, which was reached around 5 h after launch. The valve opening the exhaust piping of the dilution cooler was activated at 03:30 UT, and the 4He-JT cooler compressors were turned on at low stroke at 05:20 UT. After these essential operations were completed, on the second day after launch, the focal plane temperature was allowed to descend to 170 K for out-gassing and decontamination of the telescope and focal plane.

Commissioning and initial science operations

Commissioning

The Herschel and Planck launch by an Ariane 5 ECA rocket.

The first period of operations focussed on commissioning activities, i.e., functional check-out procedures of all sub-systems and instruments of the Planck spacecraft in preparation for running science operations related to calibration and performance verification of the payload. Planning for commissioning operations was driven by the telescope decontamination period of 2 weeks and the subsequent cryogenic cool-down of the payload and instruments. The overall duration of the cool-down was approximately 2 months, including the decontamination period. The commissioning activities were executed very smoothly and all sub-systems were found to be in good health. The commissioning activities were formally completed at the time when the HFI bolometer stage reached its target temperature of 100 mK, on 3 July 2009 at 01:00 UT. At this time all the critical resource budgets (power, fuel, lifetime, etc.) were found to contain very significant margins with respect to the original specification.

Calibration and performance verification

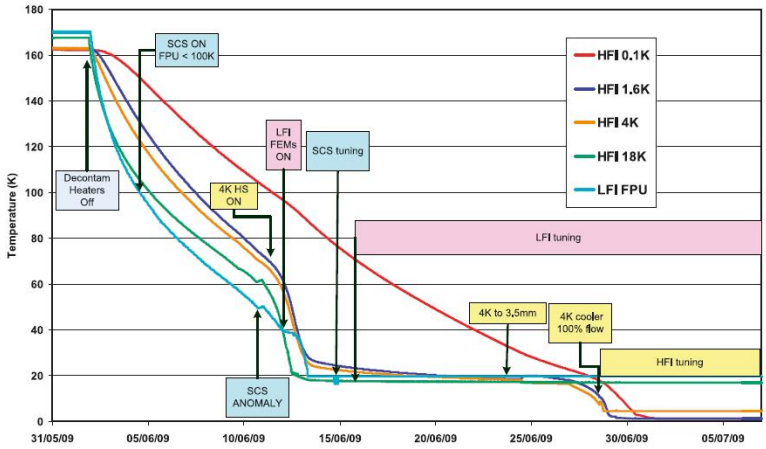

Schematics of the cool-down sequence, from Planck Coll. 2011, A&A 536, A1.

Calibration and performance verification (CPV) activities started during the cool-down period and continued until the end of August 2009. On completion of all the planned activities, it was concluded that the two instruments were fully tuned and ready for routine operations. No further parameter tuning was expected to be needed, except for the sorption cooler, which requires a weekly change in operational parameters. The scientific performance parameters of both instruments was in most respects as had been measured on the ground before launch. The only significant exception was that, due to the high level of Galactic cosmic rays, the bolometers of HFI were detecting a higher number of glitches than expected, causing a modest (~10%) level of systematic effects on their noise properties. The satellite did not introduce any major systematic effects into the science data. In particular, the telemetry transponder did not result in radio-frequency interference, which implies that the data acquired during visibility periods is useable for science.

First-Light Survey

The First Light Survey (FLS) was the last major activity planned before the start of routine surveying of the sky. It was conceived as a two-week period during which Planck would be fully tuned up and operated as if it was in its routine phase. This stable period could have resulted in the identification of further tuning activities required to optimise the performance of Planck in the long-duration surveys to come. The FLS was conducted between 13 and 27 August, and in fact led to the conclusion that the Planck payload was operating stably and optimally, and required no further tuning of its instruments. Therefore the period of the FLS was accepted as a valid part of the first Planck

survey.

Routine operations phase

The routine operations phase of Planck is characterised by continuous and stable scanning of the sky and data acquisition by LFI and HFI. It started with the FLS on 13 August of 2009, at 14:15 UT.

The Planck satellite generates (and stores on-board) data continuously at the following typical rates: 21 kilobit s^{-1} (kbps) of house-keeping (HK) data from all on-board sources, 44 kbps of LFI science data and 72 kbps of HFI science data. The data are brought to ground in a daily pass of approximately 3 h duration. Besides the data downloads, the passes also acquire realtime HK and a 20 min period of real-time science (used to monitor instrument performance during the pass). Planck utilises the two ESA deep-space ground stations in New Norcia (Australia) and Cebreros (Spain), usually the former. Scheduling of the daily telecommunication period is quite stable, with small perturbations due to the need to coordinate the use of the antenna with other ESA satellites (in particular Herschel). At the ground station the telemetry is received by redundant chains of front-end/back-end equipment. The data flows to the mission operations control centre (MOC) located at ESOC in Darmstadt (Germany), where it is processed by redundant mission control software (MCS) installations and made available to the science ground segment. To reduce bandwidth requirements between the station and ESOC only one set of science telemetry is usually transferred. Software is run post-pass to check the completeness of the data. This software check is also used to build a catalogue of data completeness, which is used by the science ground segment to control its own data transfer process. Where gaps are detected, attempts to fill them are made as an offline activity (normally next working day), the first step being to attempt to reflow the relevant data from station. Early in the mission these gaps were more frequent, with some hundreds of packets affected per week (impact on data return of order 50 ppm) due principally to a combination of software problems with the data ingestion and distribution in the MCS, and imperfect behaviour of the software gap check. Software updates implemented during the mission have improved the situation such that gaps are much rarer, with a total impact on data return well below 1 ppm. Redump of data from the spacecraft is attempted when there have been losses in the space link. This has only been necessary on three occasions. In each case the spacecraft redump has successfully recovered all the data.

All the data downloaded from the satellite, and processed products such as filtered attitude information, are made available each day for retrieval from the MOC by the LFI and HFI Data Processing Centres (DPCs).

The scanning strategy is the following: the spin axis follows a cycloidal path on the sky by step-wise displacements of 2 arcmin approximately every 50 min. The dwell time (i.e., the duration of stable data acquisition at each pointing) has varied sinusoidally by a factor of ~2. Planck's scanning strategy results in significantly inhomogeneous depth of integration time across the sky; the areas near the ecliptic poles are observed with greater depth than all others.

The scanning strategy for the second year of Routine Operations (i.e., Surveys 3 and 4) is exactly the same as for the first year, except that all pointings are shifted by 1 arcmin along the cross-scanning direction, in order to provide finer sky sampling for the highest frequency detectors when combining two years of observations.

Orbit maintenance manoeuvres were carried out at approximately monthly intervals6. Although the manoeuvres only required a few minutes, preparations, post-manoeuvre massproperty calibration, and re-entry into scientific slewing mode increased the overhead to several hours. The manoeuvres were carried out without disturbing the path of the spin axis from its nominal scanning law. The dwell times of pointings before and after the execution of the manoeuvre were reduced to allow all pre-planned pointings to be carried out.

While the Planck detectors are scanning the sky, they also naturally observe celestial calibrators. The main objects used for this purpose are the Crab Nebula, and the bright planets Mars, Jupiter and Saturn.

Payload performance

The main achievements in terms of payload performance are the following:

- the angular resolution measured on planets is within a few per cent of that predicted on the ground
- the instantaneous sensitivity of the Planck LFI and HFI channels is estimated to be approximately 10% larger than that measured on the ground and extrapolated to launch conditions
- the photometric calibration uncertainty quoted is conservatively based on the current knowledge of systematic effects and data processing pipelines. There is no reason to believe that the mission goals (1% in CMB channels and 3% at the highest frequencies) will not be reached for all Planck channels in due time.

References

A complete overview of the Planck mission and its science programme can be found in the so-called Blue Book : http://www.sciops.esa.int/SA/PLANCK/docs/Bluebook-ESA-SCI%282005%291_V2.pdf

More details on the Planck mission performance can be found in Planck coll. 2011, A&A 536, A1.

A complete list of Planck publications can be found here [1].

References

[1] http://www.sciops.esa.int/index.php?project=PLANCK&page=Planck_Published_Papers

The Satellite

The satellite

The Planck satellite was designed, built and tested around two major modules:

- **The payload module** containing an off-axis telescope with a projected diameter of 1.5m, focussing radiation from the sky onto a focal plane shared by detectors of the LFI and HFI, operating at 20K and 0.1K respectively; a telescope baffle that simultaneously provides stray-light shielding and radiative cooling; and three conical "V-groove" baffles that provide thermal and radiative insulation between the warm service module and the cold telescope and instruments.
- **The service module** containing all the warm electronics servicing instruments and satellite; and the solar panel providing electrical power. It also contains the cryocoolers, the main on-board computer, the telecommand receivers and telemetry transmitters, and the attitude control system with its sensors and actuators. The most relevant technical characteristics of the Planck spacecraft are detailed in the Table bellow.

Table. Planck satellite characteristics.

Diameter	4.2 m	Defined by the solar array
Height	4.2 m	
Total mass at launch	1912 kg	Fuel mass = 385 kg at launch; He mass = 7.7 kg
Electrical power demand (avg)	1300 W	Instrument part: 685 W (Begining of Life), 780 W (End of Life)
Minimum operational lifetime	18 months	Planck operated for 32 months with both instruments; the LFI continues surveying the sky
Spin rate	1 rpm	± 0.6 arcmin/sec (changes due to manoeuvers); stability during inertial pointing $\sim 6.5 \times 10^{-5}$rpm/h
Max angle of spin axis to Sun	10 deg	To maintain the payload in the shade; default angle is 7.5 deg
Max angle of spin axis to Earth	15 deg	To allow communication to Earth
Angle between spin axis and telescope boresight	85 deg	Max extent of FOV~ 8 deg
On-board data storage capacity	32 Gbit	Two redundant units (only one is operational at any time)
Data transmission rate to ground (max)	1.5 Mbps	Within 15 deg of Earth, using a 35 m ground antenna
Daily contact period	3 h	The effective real-time science data acquisition bandwidth is 130 kbps

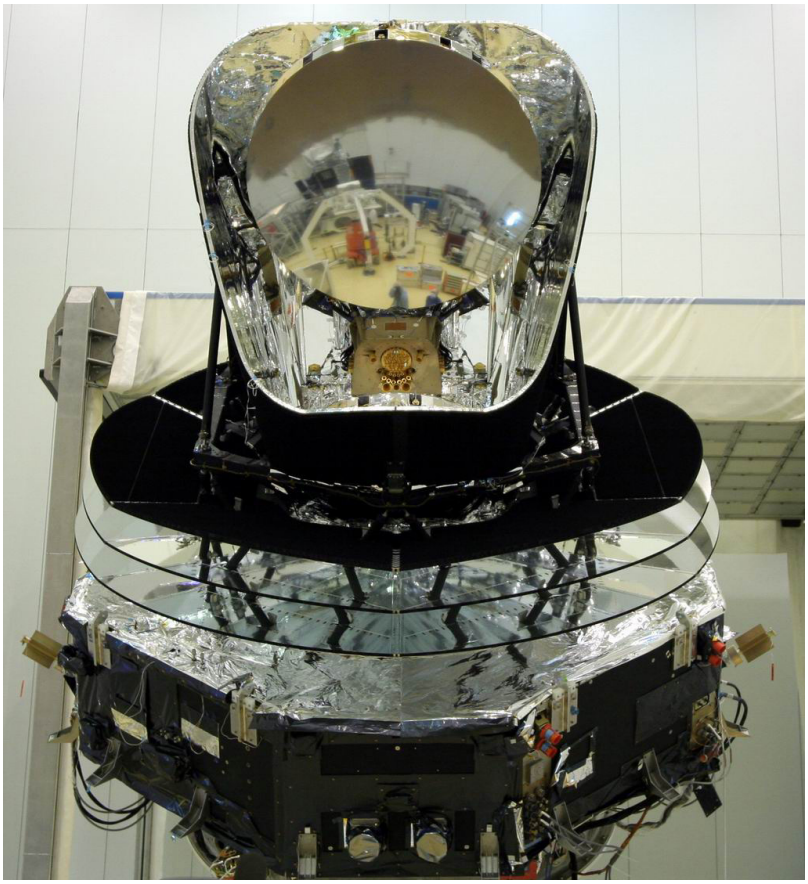

The fully assembled Planck satellite a few days before integration into the Ariane 5 rocket. Herschel is visible by reflection on the primary reflector.

For more information, see #planck2011-1-1.

Contents of this chapter

<biblio force=false>

1. References

</biblio>

The service module

The service module provides the various equipment and instruments housed in it with suitable mechanical and thermal environments during launch and orbit. It is formed by an octagonal box, built around a conical tube, which supports the following subsystems intervening in flight operations:

- Command and data management.
- Attitude control and measurement.
- Power control.
- Reaction control.
- Telemetry, tracking and command.
- Thermal control.

The service module contains all the warm satellite and payload electronic units, with the only exception of the box containing JFETs for impedance-matching to the HFI bolometers, which is mounted on the primary reflector support panel, to allow the operation of the JFETs at an optimal temperature of ~130 K. The service module holds:

- Main computer
- Attitude control computer
- Data processing units
- Star trackers
- LFI electronics
- Dilution control unit
- HFI readout electronics
- 4K compressors
- Helium tanks: 36000 litres of ^{4}He, and 12000 litres of ^{3}He gas are stored in four high-pressure tanks.
- Sorption cooler radiator
- Sorption cooler electronics
- Sorption compressors (2 redundant units)
- Hydrazine tanks
- Medium-gain antenna
- Telemetry subsystem.

For more information, see #tauber2010a.

Contents of this chapter

<biblio force=false>

1. References

</biblio>

Thermal design

(Note: Adapted from Tauber et al. 2010, A&A 520, A1 and Ade et al. 2011, A&A 536)

Introduction

The performance of the Planck instruments in space is enabled by their low operating temperatures, 20 K for LFI and 0.1 K for HFI, achieved through a combination of passive radiative cooling and three active mechanical coolers. The scientific requirement for very broad frequency coverage led to two detector technologies with widely different temperature and cooling needs. Active coolers could satisfy these needs; a helium cryostat, as used by previous cryogenic space missions (IRAS, COBE, ISO, Spitzer, AKARI), could not. Radiative cooling is provided by three V-groove radiators and a large telescope baffle. The active coolers are a hydrogen sorption cooler (<20 K), a ^{4}He Joule-Thomson cooler (4.7 K), and a ^{3}He- ^{4}He dilution cooler (1.4 K and 0.1 K). The flight system was at ambient temperature at launch and cooled in space to operating conditions. The HFI bolometer plate reached 93 mK on 3 July 2009, 50 days after launch. The solar panel always faces the Sun, shadowing the rest of Planck, and operates at a mean temperature of 384 K. At the other end of the spacecraft, the telescope baffle operates at 42.3 K and the telescope primary mirror operates at 35.9 K. The temperatures of key parts of the instruments are stabilized by both active and passive methods. Temperature fluctuations are driven by changes in the distance from the Sun, sorption cooler cycling and fluctuations in gas-liquid flow, and fluctuations in cosmic ray flux on the dilution and bolometer plates. These fluctuations do not compromise the science data.

The contrast between the high power dissipation in the warm service module ($\sim$1000 W at 300 K) and that at the coldest spot in the satellite ($\sim$100 nW at 0.1 K) are testimony to the extraordinary efficiency of the complex thermal system which has to achieve such disparate ends simultaneously while preserving a very high level of stability at the cold end.

Passive cooling

The telescope baffle and V-groove shields (see Figs.) are key parts of the passive thermal system. The baffle (which also acts as a stray-light shield) is a high-efficiency radiator consisting of $\sim$14 m ^{2}of open aluminium honeycomb coated with black cryogenic paint; the effective emissivity of this combination is very high (>0.9). The **V-grooves** are a set of three conical shields with an angle of 5 $^\circ$between adjacent shields; the surfaces (approx 10 m ^{2}on each side) are specular (aluminum coating with an emissivity of $\sim$0.045) except for the outer ($\sim$4.5 m ^{2}) area of the topmost V-groove which has the same high-emissivity coating as the baffle. This geometry provides highly efficient radiative coupling to cold space, and a high degree of thermal and radiative isolation between the warm spacecraft bus and the cold telescope, baffle, and instruments. The cooling provided by the passive system leads to a temperature of 40-45 K for the telescope and baffle. Table 3 lists temperature ranges predicted in flight for various parts of the satellite, based on a thermo-mechanical model which has been correlated to test results; the uncertainty in the prediction for elements in the cold payload is of order (+0.5 K, -2 K).

A more detailed account of the passive cooling stage design can be found here

Active cooling

The active refrigeration chain further reduces the detector temperatures to 20 K (LFI front-end low noise amplifiers) and 0.1 K (HFI bolometers) respectively. It is based on three distinct units working in series (see Fig. 7):

The hydrogen sorption cooler

The hydrogen sorption cooler was designed and built expressly for Planck at NASA's Jet Propulsion Laboratory (USA) (Bhandari et al. 2004; Pearson et al. 2006); it directly cools the LFI low-noise amplifiers to their operating temperature while providing pre-cooling for the HFI cooler chain. The sorption cooler consists of two cold redundant units, each including a six-element sorption compressor and a Joule-Thomson (JT) expansion valve. Each element of the compressor is filled with hydride material (La Ni4.78 Sn0.22) which alternately absorbs and releases hydrogen gas under control of a heat source. The cooler produces liquid hydrogen in two liquid-vapor heat-exchangers (LVHXs) whose temperatures are stabilized by hydrogen absorption into three compressor elements. LVHX1 provides pre-cooling for the HFI 4K cooler, while LVHX2 cools the LFI focal plane unit (FPU). The vapor pressure of the liquid hydrogen in the LVHXs is determined primarily by the absorption isotherms of the hydride material used in the compressor elements. Thus, the heat rejection temperature of the compressor elements determines the instrument temperatures. On the spacecraft the compressor rejects heat to a radiator to space with flight allowable temperatures between 262 and 282 K; the radiator is a single unit which couples the active and redundant sorption coolers via a network of heat pipes. The operating efficiency of the Planck sorption cooler depends on passive cooling by radiation to space, which is accomplished by heat exchange of the gas piping to the three V-groove radiators. The final V-groove is required to be between 45 and 60 K to provide the required cooling power for the two instruments. At the expected operating temperature of $\sim$47 K, with a working pressure of 3.2 MPa, the two sorption coolers produce the 990 mW of required cooling power for the two instruments, with a margin of $\sim$100 mW. The temperature in flight at the heat exchangers will be 17.5 K (LVHX1) and 19 K (LVHX2). LVHX2 is actively stabilised by a closed loop heat control; typical temperature fluctuation spectra are shown in Fig. 8.

The details of the design, calibration and operation of the sorption cooler can be found here

The 4K cooler

The 4 K cooler is based on the closed circuit JT expansion of helium, driven by two mechanical compressors, one for the high pressure side and one for the low pressure side. A description of this system is given in Bradshaw et al. (1997). Similar compressors have already been used for active cooling at 70 K in space. The Planck 4 K cooler was initially developed under an ESA programme to provide 4 K cooling with reduced vibration for the FIRST (now Herschel) satellite. For this reason the two compressors are mounted in a back-to-back configuration, which cancels most of the momentum transfer to the spacecraft. Furthermore, force transducers placed between the two compressors provide an error signal which is used by the drive electronics servo system to control the motion profile of the pistons up to the 7th harmonic of the base compressor frequency ($\sim$40 Hz). The damping of vibration achieved by this system is more than two orders of magnitude at the base frequency and factors of a few at higher harmonics; the residual vibration levels will have a minor heating effect on the 100 mK stage, and negligible impact on the pointing. Pre-cooling of the helium is provided by the sorption cooler described above. The cold end of the cooler consists of a liquid helium reservoir located just behind the JT orifice. This cold tip is attached to the bottom of the 4 K box of the HFI FPU (see Fig. 7). It provides cooling for this screen and also pre-cooling for the gas in the dilution cooler pipe described later in this section. The margin between heat lift and heat load depends sensitively on the pre-cooling temperature provided by the sorption cooler at the LVHX1 interface. The temperature of LVHX1 is thus the most critical interface of the HFI cryogenic chain; system-level tests have shown that it is likely to be <media>\sim</media> 17.5 K, about 2 K below the maximum requirement[*]. At this pre-cooling temperature the heat load is 10.6 mW and the heat lift is 16.1 mW for a compressor stroke amplitude of 3.5 mm (the maximum is 4.4 mm). The heat load of the 4 K cooler onto the sorption cooler is only 30 mW, a very small amount with respect to

the heat lift of the sorption cooler (990 mW); thus there is little back reaction of the 4 K onto the sorption cooler.

Here you will find a more detailed overview of the 4K cooler.

The dilution cooler

The dilution cooler consists of two cooling stages in series, using 36 000 litres of Helium 4 and 12 000 litres of Helium 3 gas stored on-board in 4 high-pressure tanks. The first stage is based on JT expansion, and produces cooling for the 1.6 K screen of the FPU and for pre-cooling of the second stage cooler. The latter is based on a dilution cooler principle working at zero-G, which was invented and tested by A. Benoît (Benoît et al. 1997), and developed into a space-qualified system by the Institut d'Astrophysique Spatiale (Orsay) and DTA Air Liquide (Grenoble), see Triqueneaux et al. (2006). The gas from the tanks (at 300 bars at the start of the mission) is brought down to 19 bars through a pressure regulator and the flow through the dilution is regulated by a set of discrete restrictions which can be switched by telecommand. The gas is vented to space after the dilution process[*], and the cooler therefore has a lifetime limited by the gas supply. The dilution of the two helium isotopes provides the cooling of the bolometers to a temperature around 100 mK which is required to deliver a very high sensitivity for the channels near the peak of the CMB spectrum (noise equivalent power around $10^{-17}\ \mathrm{W}/\sqrt{\mathrm{Hz}}$), limited mostly by the background photon noise.

The details of design, calibration and operation of the dilution cooler can be found here

Qualification and performance

TBW FIGURES STILL TO BE ADDED

HFI design, qualification, and performance

Contents of this chapter

Overview

THIS SECTION IS CURRENTLY IN A VERY PRELIMINARY FORM. It is intended to provide an overview of the instrument and of its different sub-systems. Two papers that include and detail this information are available: LAMARRE, Jean-Michel, PUGET, Jean-Loup et 93 co-auteurs, " Planck pre-launch status: The HFI instrument, from specification to actual performance", Astronomy and Astrophysics, Volume 520, id.A9 (20 pages, A&A Homepage), 09/2010. and Planck-HFI Core Team and 165 co-authors. " Planck early results. IV. First assessment of the High Frequency Instrument in-flight performance", Astronomy & Astrophysics, Volume 536, id.A4 (A&A Homepage) 12/2011." Additional detailed information potentially useful for the use of the HFI data will be included into this section or annexed to it.

(Lamarre/Pajot)

The HFI instrument is designed around 52 bolometers. Twenty of the bolometers (spider-web bolometers or SWBs) are sensitive to total power, and the remaining 32 units are arranged in pairs of orthogonally-oriented polarisation-sensitive bolometers (PSBs). All bolometers are operated at a temperature of ~0.1 K by mean of a space qualified dilution cooler coupled with a high precision temperature control system. A 4He-JT provides an active cooling for 4 K stages using vibration controlled mechanical compressors to prevent excessive warming of the 100 mK stage and minimize microphonic effects in the bolometers. Bolometers and sensitive thermometers are read using AC-bias scheme through JFET amplifiers operated at ~130 K that provide high sensitivity and low frequency stability. The HFI covers six bands centred at 100, 143, 217, 353, 545 and 857 GHz, thanks to a thermo-optical design consisting of three corrugated horns and a set of compact reflective filters and lenses at cryogenic temperatures.

The whole satellite is organized to provide thermal transitions between its warm part exposed to the sun and earth radiation, and the focal plane instruments that include the cold receivers (Sections XXX1 and XXX2). The various parts of the HFI are distributed among three different stages of the satellite in order to provide each sub-system an optimal operating temperature. The "warm" parts, including nearly all the electronics and the sources of fluids of the 4K and 0.1K coolers, are attached and thermally linked to the service module of the satellite. The first stage of the preamplifiers is attached to the back of the passively cooled telescope structure. The focal plane unit is attached to the 20K stage cooled by the sorption cooler. This is detailed in (XXX2).

The telescope and horns selects the geometrical origin of photons. They provide a high transmission efficiency to photons inside the main beam, while photons coming from the intermediate and far-side lobes have very low probability of being detected. This essential characteristics is known by a complex process mixing ground measurements of components (horns, reflectors), modelling the shape of the far side lobes, and measuring in-flight bright sources, especially planets.

The filters and bolometers define the spectral responses and absolute optical efficiency, that will be known mostly

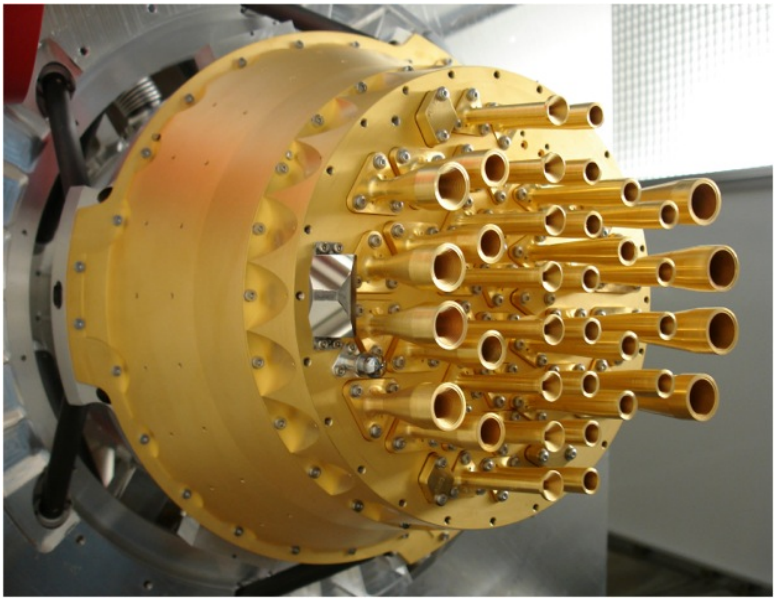

FIGURE 2.4.1.1.a The HFI focal plane optics and 4K thermo-mechanical stage

from ground based measurements performed at component, sub-system and system levels reported in this document. The relations between spectral response and geometrical response will also be addressed.

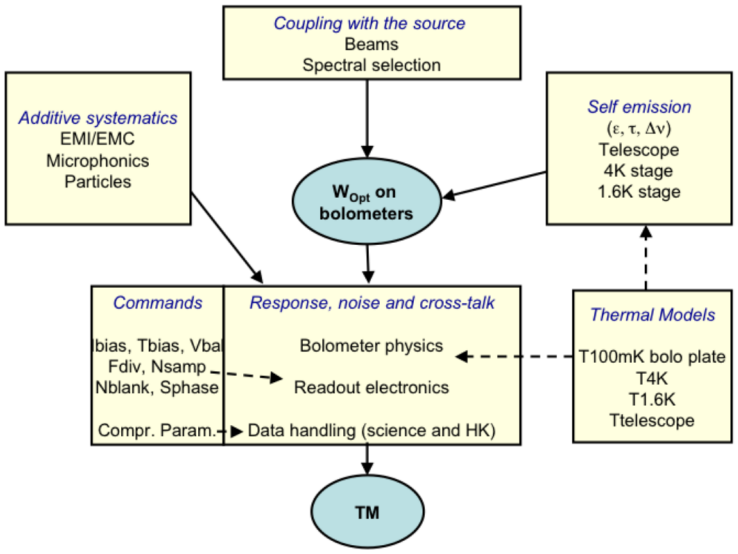

FIGURE 2.4.1.1.C_HFI signal formation

Photons absorbed by a bolometer include the thermal radiation emitted by the various optical devices: telescope, horns and filters. They are transformed in heat that propagates to the bolometer thermometer and influence its temperature which is itself measured by the readout electronics. Temperatures of all these items must stable enough not to contaminate the scientific signal delivered by the bolometers. How this stability is reached is described in section 2.4.1_cryogeny.

The bolometer temperature depends also on the temperature of the bolometer plate, on the intensity of the biasing current and on any spurious inputs, such as cosmic rays and mechanical vibrations. Such systematics are included in the list of section 2.4.1._systematics.

Since the bolometer thermometer is part of an active circuitry that also heats it, the response of this system is complex and has to be considered as a whole. In addition, due to the modulation of the bias current and to the sampling of the data, a complex time response is expected, which modifies the beam shape resulting from the scanning of point sources. Section 2.4.1._time response is dedicated to the description of the time response.

Figure 2.4.1.1_HFI signal formation: Logic of the formation of the signal in HFI. This is an idealized description of the physics that takes place in the instrument. The optical power that is absorbed by the bolometers comes from the observed sky and from the instrument itself. The bolometers and readout electronics, acting as a single and complex chain, transform this optical power in data that is compressed and transmitted for science data reduction.

HFI cryogenics

(F .Pajot)

Dilution cooler

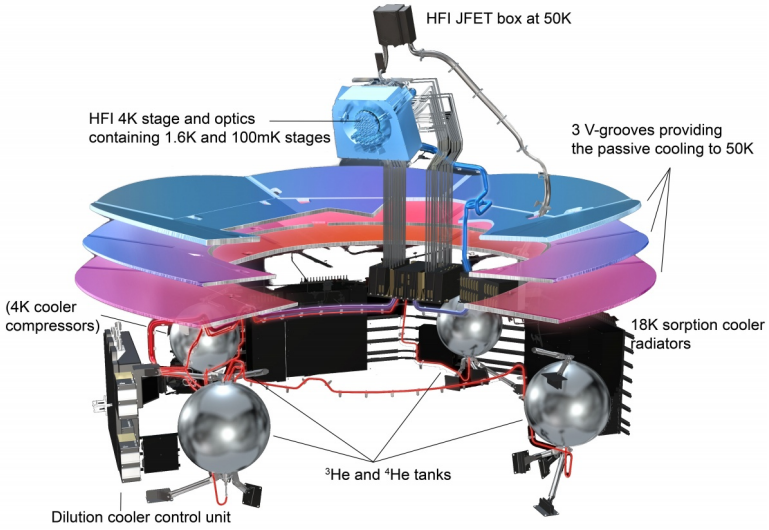

Thermal architecture of Planck/HFI

The HFI dilution cooler cools the bolometers down to 0.1K through the dilution of ^{3}He into ^{4}He and the intermediate optical plate to 1.4K through Joule-Thomson expansion of the ^{3}He and ^{4}He mixture. Two stages of PID regulation are included on the 0.1K stage. The first one (PID1) is at the dilution cold end itself and provides stability on long timescales. When no thermal perturbation is applied to the bolometer plate, the PID1 alone provides the required stability. A passive thermal filter is mounted between the dilution cold end and the bolometer optical plate. It gives a thermal time constant of several hours between these stages. A second regulation system (PID2) is on the bolometer plate, with a similar time constant. The dilution cooler is described in detail in section 2.3.3 of early paper II [1].

The dilution was operated with flows set to the minimum available values, providing a total lifetime of 30.5 months exceeding the nominal lifetime of 16 months by 14.5 months. The dilution stage was stabilized by the PID1 at a temperature close to 101mK using 20 to 30nW of power. The bolometer plate was stabilized by the PID2 at 102.8mK with about 5nW. The cooling power values were in very good agreement with those obtained during the ground tests and calibration.

However, the cosmic particles interactions with the 0.1K stages induced both temperature fluctuations of the 0.1K plates and glitches on the thermometers measurements.

At very low frequency, below 1mHz, the temperature fluctuations are very well correlated with the high energy particles hit rate, as measured by the on-board Standard Radiation Environment Monitor (SREM). At frequencies in the 10mHz to 1Hz range, single events inducing a global or partial temperature change of the bolometer plate are observed. Decorrelation of the bolometers signal from the thermal fluctuations is described in the TOI processing section.

The 1.4K stage is very stable and given the very low coupling coefficients between the 1.4K optical components and the detectors no effect can be measured on the signal. Detailed thermal analysis of the in-flight stability of the dilution cooler can be found in section 5.4 of early paper II [2].

4K J-T cooler

The HFI 4K Joule-Thomson (J-T) cooler produces a temperature of 4K for the HFI 4K stage and optics and the precooling of the dilution gases. Full description of the 4K cooler can be found in in section 2.3.2 of early paper II [1].

The two mechanical compressors produce micro-vibrations and also induce electromagnetic interference affecting the science signals of bolometers. The risks associated with these effects were taken into account early in the design of the HFI by phase-locking the sample frequency of the data to a harmonic of the compressors frequency. The removal of these interferences is addressed in the 4K cooler lines variability section.

Operation of the 4K J-T cooler was flawless during the whole mission, but for an unexpected shutdown during the CPV on August 6th 2009, caused by an SEU on the precharge regulator. It never occured again, and the 4K J-T cooler was then operated without interruption during all the survey phase of the mission. It is still in operation as it also provides the cooling of the optical reference loads of the LFI.

The 4K J-T cooler compressors amplitude was set to 3450 micrometers during the CPV, and was maintained to this value during all the mission. Its cooling power is very stable and gives enough margin to cancel out the fluctuations and drifts induced by the sorption cooler fluctuations and adjustments. The PID stabilizing the temperature of the HFI optics is regulated at 4.81K using a power around 1.8mW.

Details on the in-flight performance of the 4K J-T cooler can be found in in section 5.3 of early paper II [3].

References

[1] http://www.rssd.esa.int/llink/livelink/fetch/-60063/3036676/3065909/3110897/3135828/3135852/PE_paper2.pdf#page=7
[2] http://www.rssd.esa.int/llink/livelink/fetch/-60063/3036676/3065909/3110897/3135828/3135852/PE_paper2.pdf#page=23
[3] http://www.rssd.esa.int/llink/livelink/fetch/-60063/3036676/3065909/3110897/3135828/3135852/PE_paper2.pdf#page=21

HFI cold optics

(Lamarre)

Horns,lenses and filters

links to Peter's paper

Feed horns beams (sub-system level)

In order to meet with straylight, beam shapes and filtering requirements, a design using feedhorn coupled detectors has been chosen, with a triple horn configuration (see Figure 3.1.1). A detailed description of the HFI optical design and beam performances is given in Maffei et al.(2009) and Ade et al.(2009).

Single-moded horns patterns

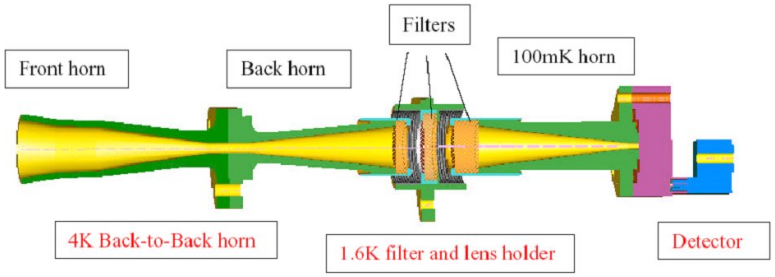

Optics of the HFI Focal plane unit. The back-to-back horn (front and back horns) is coupling the incoming radiation from the telescope to a detector horn which is then coupling the radiation to the bolometer. The filters determining the spectral bands are located in between the two horn assemblies. A lens is refocussing the radiation from the back horn to the detector

The spectral and geometrical properties of the horns have been characterized individually. The measured beam pattern of a typical front horn is compared with the prediction from the design (figure 3.1.2). The fit is excellent down to very low levels, which validates the logics that prevailed for characterizing the horns: modelling and optimizing the horns before implementation. Validating the model with a complete measurement of the beam intensity patterns.

For the single-moded horns, a method has been developed to use the measured intensities, together with the phase information from modeling to derive “worst-case” horn beam patterns that can be used in GRASP simulations of the telescope beams (phase information is mandatory). Worst-case beam patterns have been computed for all single-moded HFI horn types. A .pdf file (IAS-FN-WCB-001-03022009) detailing the algorithm can be found on the optics ftp site at ctwg1.planck.fr, in the following directory: /File_Exchange_Box_GOPT/Files_from_FN/Worst_case_beams”

As an example, in Figure 3.1.3, we show the difference in encircled powers at constant isolevel intervals for the HFI 143_1a channel main beam using both the model and worst-case horns.

Ideal Multi-moded horns simulations

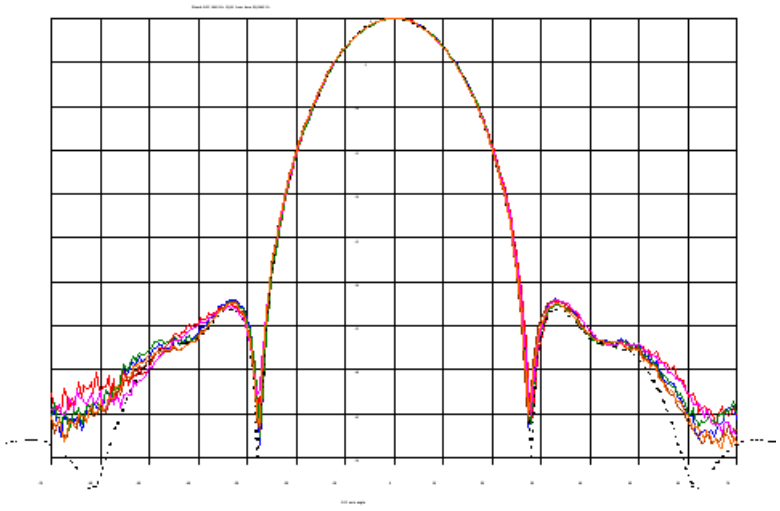

Typical measurement/theory comparison for the back-to-back horn co-pol beam pattern at 100GHz. Dots : model. Color : measurements (Off axis angle in degrees). Noise is limiting accuracy under -35 dB

In the high frequency 545GHz and 857GHz Planck pixels both the back-to-back (BTB) horn and the detector horn have overmoded waveguide filters. The waveguide-horn structures are modelled using the scattering matrix approach used for the single-moded-CMB-channel horns, with the inclusion of modes of azimuthal orders, n = 0, 1, 2, 3 and 4. We assume reciprocity, and that the cavity plus cavity horn and filter behaves like a black-body: since the waveguide filter in the detector horn is wider than that of the BTB, it is reasonable to assume that any mode that can propagate through the BTB filter also propagates through the detector horn filter from the cavity.

Thus, as far as the beam patterns are concerned the BTB is effectively coupled to a black body cavity also and all modes are excited at the back end of the BTB horn. Thus, all waveguide modes are equally excited in power but are also independent of each other so there is no phase relationship between them. Many of these modes may contribute independently (i.e. incoherently) to the beam on the sky. All coherent aperture fields have to be independently propagated through the PLANCK telescope.

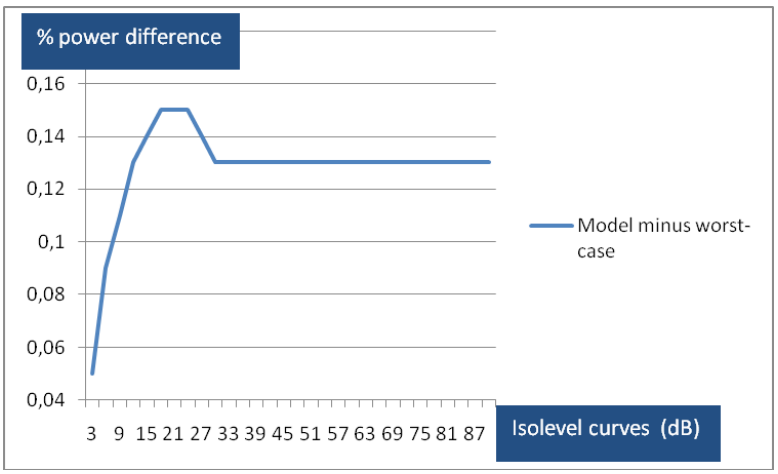

Difference in power encircled within 3dB curves from peak value. Main beam encloses at least 99.5 % (model) and 99.4% (worst-case) of power

From the S21 transmission scattering matrix for the whole BTB we recover the group of true independent hybrid fields that are transmitted by the waveguide filter and horn at the aperture of the BTB. These hybrid fields propagate independently through the telescope and onto the sky at a single frequency. The beam pattern for the band is obtained by adding the filter transmission weighted coherent fields in quadrature across the band (Microwave Horns and Feeds A. David Olver, Institution of Electrical Engineers) ("Shaped Corrugated horns for Cosmic Microwave Background Anisotropy Measurements" B. Maffei, P.A.R. Ade, C.E. Tucker, E. Wakui, R.J. Wylde, J.A. Murphy, R.M. Colgan, Int Jour Infrared & Millimeter waves, 21, (12) 2023-2033, December 2000).

Far field patterns of horns and comparison with test data:

The far-field patterns of the horns (which illuminate the Planck mirrors) have been simulated and are shown in figure 3.1.4a for a few spot frequencies across the 857 GHz band. Note that the edge taper is approx -30dB at 25 degrees as required at the centre of the band. Superimposed is the broadband measurement made at Cardiff (see below) which clearly looks narrower than the majority of the spot frequency measurements and requires explanation. The measured far field beam patterns across the band are narrower than the predicted far field beams right across the band. The simulated beams are too wide suggesting missing higher order modes, either due to attenuation between the cavity and the BTB, or to the experimental setup. Away from the band centre the theoretical beams also appear to be too wide, indicating missing modes (see figure 3.1.4b).

Grouping contributions according to azimuthal order and overlaying the measurement data to investigate missing field distributions, modes of order 2 and higher appear to be absent. The beam containing modes of azimuthal orders n = 0 and 1 appears to fit the measured beams reasonably. Adding modes with azimuthal order n = 2 gives a simulated beam that is too wide, suggesting that these modes are absent from the measured BTB front aperture field.

Spectral response

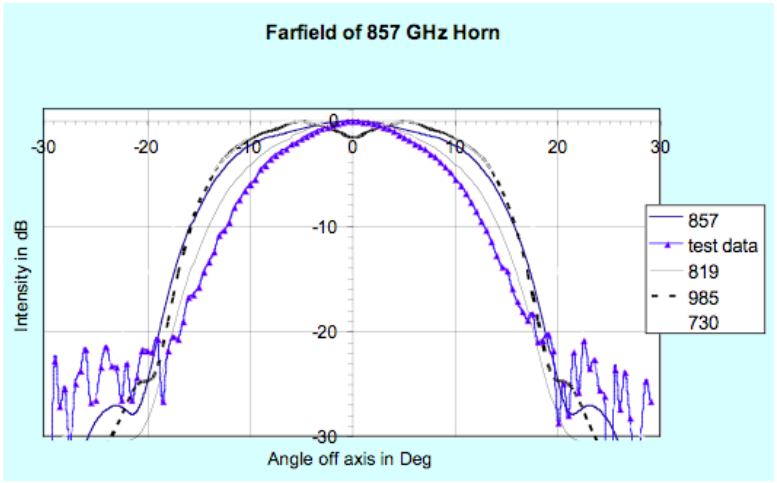

no legend provided

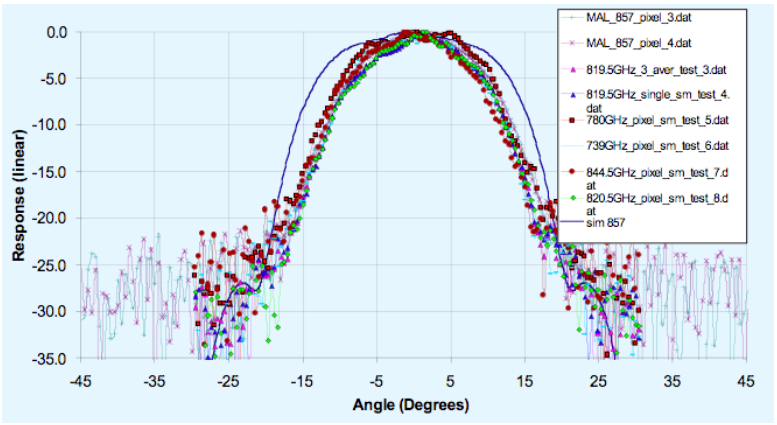

Model / Measurement comparison for the Far field pattern of the 857GHz_Horn ; left (a) : model at spot frequencies, superimposed with the broadband test data; right (b): measurements made at Cardiff for broadband and spot frequencies with the BTB horn both outside and inside the test dewar window (the inside case being more representative of the true Planck pixel)

(Spencer) This section is comprised of excerpts from the *HFI - Spectral Calibration report of the IAS measurements, v3.02,* an internal report describing detailed pre-flight ground based measurements of the HFI focal plane. The experimental setup, data collection, and related data processing are described. The official version of the HFI detector spectral transmission profiles is available within the HFI instrument model and the RIMO files in the Planck Legacy archive [ref.] . This data is comprised of broadband Fourier transform spectrometer (FTS) measurements conducted with the HFI focal plane assembly in a ground-based test cryostat, and includes a waveguide model for the low frequency spectral region, and component-level filter spectra for the remaining out of band spectral regions. Specific attention is given to in-band and near-band spectral regions surrounding CO rotational transitions in order to support the CO extraction component separation effort [ref.] . The spectral transmission profiles are evaluated with parameters such as cut-on, cut-off, centre frequency, effective frequency (including spectral index), and band-width, all provided in this analysis. Further evaluation yields band-average spectra ([ref.]) and unit conversion / colour correction coefficients ([ref.]) and software routines to generate additional unit conversion and colour correction coefficients ([ref.]).

The main goal of the spectral transmission tests of the HFI instrument is to measure the spectral response of all HFI detectors to a known source of EM radiation individually. This was determined by measuring the interferometric output of all detection channels for radiation propagated through a continuously scanned polarising Fourier transform spectrometer (FTS). The required accuracy to which the spectral transmission is to be recovered is 1 %. It is important to note that the absolute spectral calibration cannot be achieved solely from the analysis of the FTS data because of uncertainties in the coupling efficiency of the FTS source through the FTS, input optics, and integrating sphere. The relative FTS measurements must be combined with the optical efficiency tests which used internal black-body sources (EFF Test – see §EFF). A reference bolometer located in an intermediate integrating sphere (accepting 2πsr of incident radiation) within the FTS test setup was used to ratio the HFI detector spectra against to determine the throughput-normalized relative transmission spectra for each HFI detector. Data were collected over a

series of pre-flight test campaigns, and processed/analyzed using standard Fourier data processing techniques.

Additional Experiments

There were two significant additional tests that are used in the derivation of the HFI detector spectral transmission profiles beyond the scope of the IAS HFI FTS measurements. Additional filter measurements were recorded in the Astronomical Instrumentation Group (AIG) test facility at Cardiff during filter stack production. These measurements are used to extend the IAS FTS spectral measurements beyond the HFI spectral passband. The EFF tests are used to obtain optical efficiency parameters for each detector. These parameters, when combined with the respective normalized spectral transmission profiles, provide an estimate of the absolute spectral transmission. The EFF tests are discussed in greater detail by A. Catalano ([ref.]). The filter measurements are described in §Filter Measurements below and the optical efficiency experiments are described in §Optical Efficiency below.

Filter Measurements

Prior to the IAS measurements with the integrated HFI detectors and filter stacks, FTS measurements of the individual filters comprising the filter stacks for each band were conducted at Cardiff. As will be discussed in §[sec:OOB], the independent measure of the filter stack transmission is used for a portion of the HFI detector spectral transmission for regions of the spectrum where it is deemed to be of better quality than the IAS FTS measurements (i.e. for frequencies outside of the band edge filter cut-off(s)). The filter stacks for each of the frequency bands are comprised of 5 filters. There is an additional low frequency cut-on filter for the 545 and 857 GHz bands as the waveguide cut-on is too low for these multi-moded channels. Figures [fig:Filt100] – [fig:Filt857] show the individual filter transmission measurements as well as the combined filter stack product.

Combined (bottom) and individual (top) filter transmission measurements for the 5 filters within the HFI band filter stacks (6 for 545 and 857 GHz).

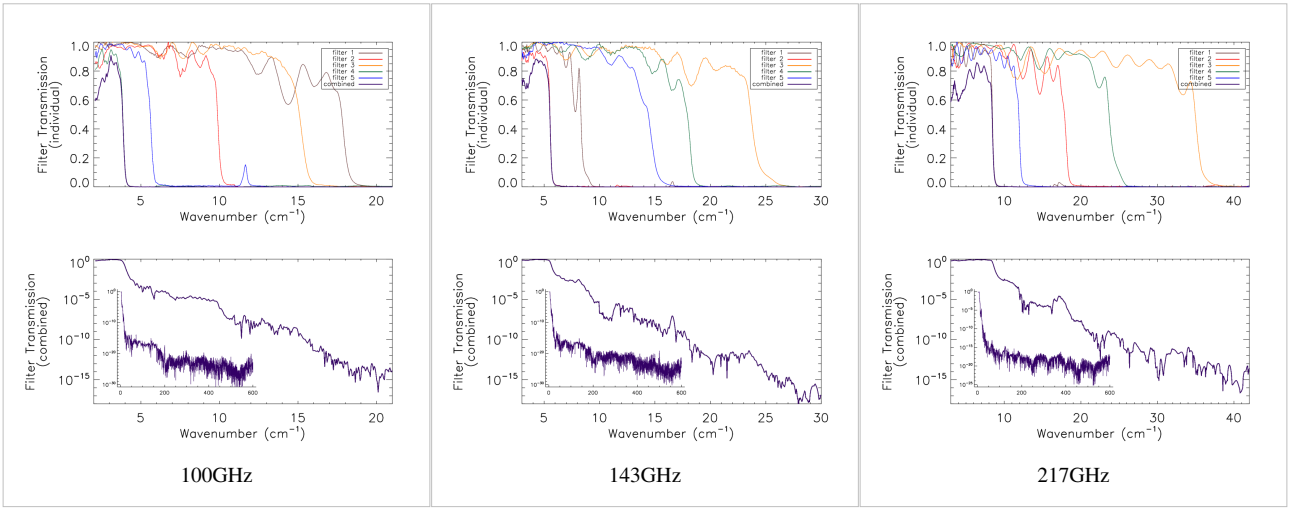

100GHz 143GHz 217GHz

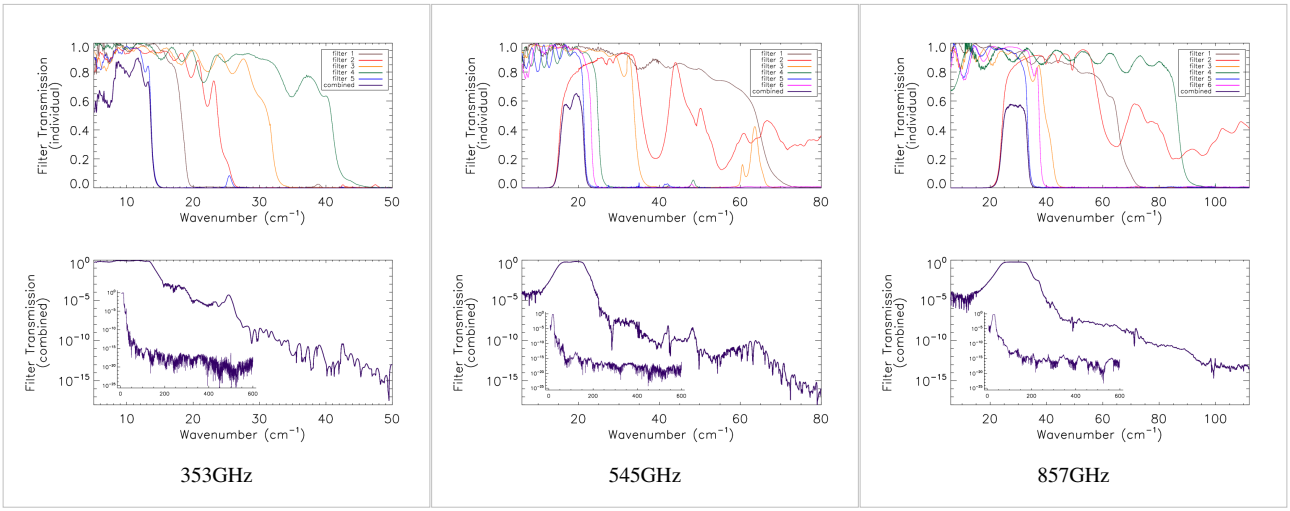

353GHz 545GHz 857GHz

The uncertainty on the combined filter transmission measurement is determined as follows. Let $f_i(\sigma)$ represent the individual filter transmission. The standard deviation of all values of $f_i(\sigma)$ below a threshold of 0.001 is used as an approximate uncertainty for each individual filter measurement, i.e. ς_i. The individual uncertainty estimates are combined to provide an estimate of the combined filter transmission spectral uncertainty through standard error propagation. For the combined filter transmission represented as $F(\sigma)$, the associated uncertainty estimate is given as

As described below, the composite filter spectra illustrated above form part of the official HFI detector spectral response, specifically for a portion of the out-of-band spectral region. The band-average spectra, containing this data as a constituent, is provided in the RIMO files (see here). The RIMO files will also include the detector level spectra for future Planck data releases.

Optical Efficiency

The optical efficiency tests, hereafter the EFF tests, were conducted to allow an estimate of the overall optical efficiency of the HFI detectors. These tests involved exposing the HFI detectors to a known blackbody source and observing the response, and comparing this to a theoretical model in combination with the detector spectral response data. The optical efficiency parameter derived for each detector is meant as a multiplicative factor to be combined with the normalized transmission spectra. This product is an estimate of the absolute spectral transmission of a given HFI detector. The detector optical efficiency parameters are included within the header of the detector spectra in the RIMO files (here).

Further details regarding the derivation of the optical efficiencies are provided here.

Data Processing and Fourier Transformation

Having identified the data sections that are of interest, here follows the data processing sequence used to obtain the resulting spectra. The processing steps taken are as follows:

1. Selection and extraction of time sampled data sets
2. Conversion of time sampled data to arrays of OPD sampled interferogram data sets
3. Fourier transformation and averaging of interferogram data sets
4. Discrimination of poor quality spectra by standard deviation comparison (see §[sec:FTavg])
5. Division of detector spectra by reference bolometer spectra to obtain normalized spectral transmission profiles
6. Combination of relative transmission spectra with filter measurements and waveguide models
7. Determination of optical efficiency through evaluation of normalized spectral transmission in the context of the EFF experiments

8. Addition of over-sampled data into spectrum for the CO transition regions (see §[sec:CO])
9. Identification of common frequency sampling per channel and interpolation of spectra onto the common sampling

Further details regarding the interferogram processing are provided here.

Reference Bolometer Spectra

The reference bolometer spectra are obtained in a fashion similar to that used for the HFI detectors. Wherever possible, the same data processing is applied to the reference bolometer data as was applied to the HFI detector data, including optical filtering, scan speed, scan length, source intensity, apodization, phase correction, etc. This Table (see here) contains the reference bolometer data set properties corresponding to those listed for the HFI detectors in this Table. Figures [fig:BrefL] - [fig:Bref857] (see here) illustrate the resultant spectra and S/N from the reference bolometer data sets. Figure [fig:SNall] (see here) compares the approximate S/N of the average spectrum for each detector against the reference bolometer average spectrum S/N over the same spectral region.

Further details are found here.

Out-of-Band Spectral Transmission Content

The HFI detector spectral transmission profiles have been extended beyond the optical pass-band of the detectors. This is done by using a combination of a waveguide model and external filter measurements for the out-of-band regions of the detector spectral response. An uncertainty estimate for these additional spectral regions is also provided, however, it should be noted that the spectral uncertainty for the waveguide and filter spectra are determined indirectly (as described above/below). There is a transition from IAS FTS data to filter data for every band edge which is defined by an optical filter. For the 100, 143, 217, and 353 GHz bands this is the high frequency cut-off band edge. For the 545 and 857 GHz bands a separate filter is used to define each of the high and low frequency band edges. For the spectral regions outside of the HFI detector optical bands, first the IAS FTS data is used to qualitatively verify that there are no spectral leaks or features, and then the external filter measurements are grafted into the ratioed spectra where they better represent the relative spectral transmission.

The normalized ratioed spectrum and filter are both scaled by the optical efficiency (see §[sec:EFF]). For the 100 - 353 bands, the filter spectrum is also scaled by $\lambda^2$to account for single-moded throughput normalization. This frequency scaling results in a more accurate in- and near-band match between the two sets of spectra, at the cost of less accuracy at much higher frequencies where any transmission will not be single-moded. As ransmission at higher frequencies is significantly reduced, this trade-off is acceptable. The 545 and 857 GHz bands have their filter spectra without the additional frequency scaling as this is not correct for multi-moded propagation. Both lower and upper frequency thresholds, ν_l, and ν_u, are defined for each band, below and above which the IAS-FTS spectra and/or the Cardiff composite filter spectra must be used, respectively. This is done to avoid introducing any detector nonlinearity residuals into the final spectral transmission data products. The region between these two points is defined as the transition region; within this region the amplitudes and slopes of the IAS and filter spectra are used to determine the spectral cross-oveer/transition point. Additional checks are performed to ensure that non-physical data processing artefacts are not introduced into the spectral transition region. Additionally, a similar technique is used, with decreasing frequency instead of increasing, for the 545 and 857 GHz bands with a filter-induced frequency cut-on. Figure [fig:OOBex] illustrates an example of both the FTS and filter spectra used in extending the transmission profiles beyond the HFI optical bands. Similar plots for every detector are shown in §[sec:stitch].

Waveguide Model

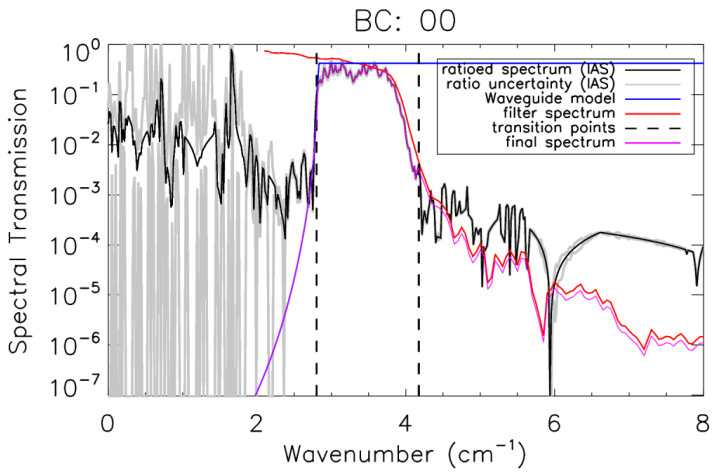

Demonstration of the combination of the waveguide model spectrum (left), the HFI measured spectrum (centre), and the combined filter spectra (right) for a given HFI detector.

A waveguide model is used to provide the data for the lowest frequency portion of the HFI detector spectral transmission. For the 100, 143, 217, and 353 GHz bands the waveguide model is transitioned (with increasing frequency) to the FTS ratioed spectra directly. There is an intermediate transition to the filter data, and then the ratioed spectra for the 545 and 857 GHz bands. For each detector, the waveguide transmission, $W(\sigma)$, is given by the following relation

where $\sigma$is the frequency in cm -1, r_w is the waveguide radius in cm, $l_w$is the waveguide length in cm, and $c_{nm}$is a waveguide specific constant; 1.841 for the TE 11/TM 11(HE 11) hybrid mode in this case . Table [tab:WG] lists the waveguide radii and lengths resultant from the waveguide model fit to the ratioed spectra. As all of the feedhorns for a given band are meant to be identical (i.e. within mechanical manufacturing tolerances) the uncertainty of the waveguide transmission is estimated statistically using all of the waveguide models for each band. I.e. for $n$bands, the uncertainty at each spectral data point is determined by the standard deviation of $n$transmission values at that frequency. As a result of each detector in a given band having a unique cut-on frequency, this method begins to over-estimate the uncertainty for frequencies approaching the cut-on; for regions very near the waveguide cut-on, the uncertainty is extrapolated from the ratioed spectrum as a more accurate representation.

A table of the waveguide fit parameters for each HFI detector is provided here.

CO interpolation

The IAS FTS/Saturne data taken with the HFI detectors is limited to a spectral resolution of ~ 0.017 cm^{-1} (~ 0.5 GHz)by the mechanical travel of the FTS translation stage. This corresponds to an unapodized FTS ILS FWHM of ~ 0.020 cm^{-1} (~ 0.61 GHz). The previous iteration of the spectral transmission (IMO ver. 2_28), in addition to a triangular apodization kernel, has a factor of 3 sub-sampled spectral resolution to improve the signal-to-noise ratio (S/N) of the output spectra. In light of the CO contribution to the 100 GHz spectra, the spectral transmission has been reprocessed at the original full spectral resolution with a different apodization function which provides better noise reduction and less spectral resolution degradation, as discussed above.

In order to provide an improved estimate of the spectral transmission near the CO features, an interpolation of the spectra by a factor of $\sim$10 has been performed. This over-sampling was accomplished by zero-padding the FTS interferograms prior to Fourier transformation , and subsequently incorporated into the Nyquist-sampled spectral data near the CO transitions (see the CO table). Although the data are presented at higher resolution, the resolution of independent data points is not improved, i.e. the ILS line-width remains the same. A flag column has been added to the spectral transmission profile data files to indicate whether a given data point originates from the actual data, or is a result of the ILS-based interpolation. The region of the over-sampled, interpolated, data has been extended to also include other CO isotopes; the COJ1-0 – J9-8 transitions should be oversampled for CO, ^{13}CO, C ^{17}O, and C ^{18}O.

The original data points within the over-sampled region have been preserved (i.e. every tenth data point – the data point that is not an interpolated one – is flagged with a zero rather than a one), as is indicated by the data flag, so a flag filter on the data will restore the independent data points easily. Figure [fig:COflag] illustrates the regions where the over-sampling has been incorporated into the spectral transmission profiles. An example of the over-sampled spectra is shown in Figure [fig:COzoom100] for the 100 GHz detectors. Examples for the other detector bands are shown in §here.

Details of the HFI CO data products are available here.

Regions of HFI spectral transmission profiles near CO transitions.

Band (GHz)	CO transition (J_{Upper}- J_{Lower})	ν_o(GHz)	over-sampled region (GHz)
100	1 – 0	115.2712018	109.67 – 115.39
143	1 – 0	115.2712018	109.67 – 115.39
143	2 – 1	230.5380000	219.34 – 230.77
217	2 – 1	230.5380000	219.34 – 230.77
353	3 – 2	345.7959899	329.00 – 346.15
545	4 – 3	461.0407682	438.64 – 461.51
545	5 – 4	576.2679305	548.28 – 576.85
857	6 – 5	691.4730763	657.89 – 692.17
857	7 – 6	806.6518060	767.48 – 807.46
857	8 – 7	921.7997000	877.04 – 922.73
857	9 – 8	1036.9123930	986.57 – 1037.95

Spectral Response Conclusions and Conformity With Requirements

The two defining requirements indicated in the HFI calibration plan are the acquisition of the spectral transmission of the single pixels with a prescribed accuracy and spectral resolution. The desired accuracy is 3% for the low frequency channels (CMB – 100, 143, and 217 GHz) and 1% for the high frequency channels (353, 545, 857 GHz). The spectral resolution requirement is for a resolution superior to 0.1 cm $^{-1}$.

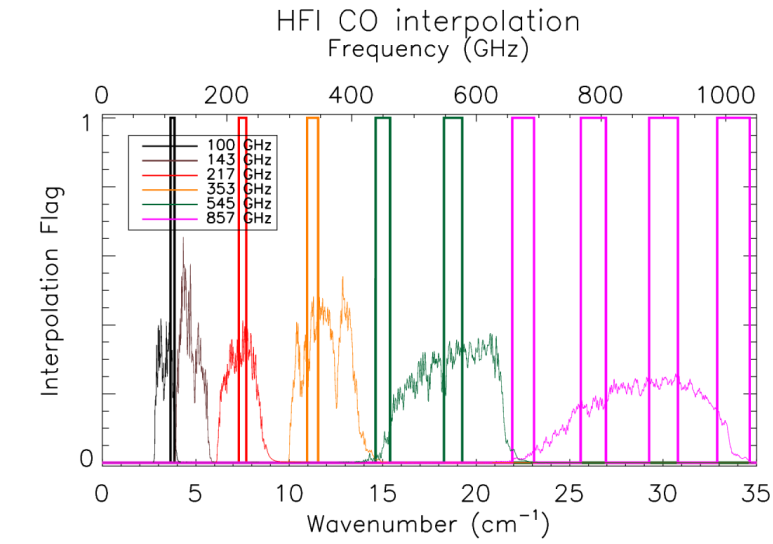

The CO regions over which the spectral transmission was interpolated using the FTS instrument line shape.

The spectral resolution requirement has been exceeded by more than a factor of five. It is also possible to degrade the spectral resolution to the 0.1 cm $^{-1}$requirement to gain an improvement in the S/N.

No quantitative number is present on the document regarding the blocking of high frequency (near IR, visible, UV) radiation outside the range of the instrument. Checks in order to quantify the rejection have been performed at subsystem level and estimates of the out-of-band transmission profiles have been incorporated into the data products. The high level of out-of-band signal attenuation is verified by in-flight observations as demonstrated in the Spectral Response paper ([ref.]).

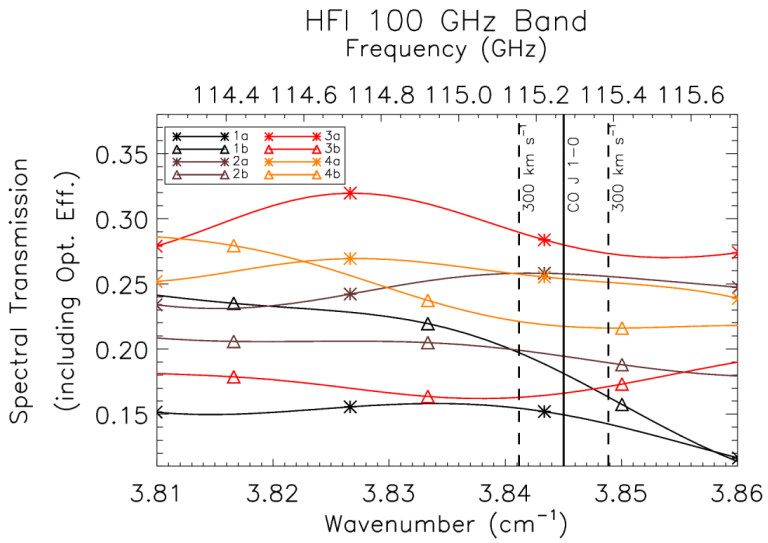

An example of the spectral transmission within 100 GHz detectors about the COJ1-0 rotational transition.

Considering statistical fluctuations in the determination of the spectra, these goals have been achieved. There are, however, caveats regarding the nature of error bars when dealing with frequency space. The nature of uncertainties in spectra determination is less obvious than when dealing with timestream data. Systematic effects produced from instrumental setup, but also by data reduction can in some cases exceed the actual statistical oscillation in the determination of the final spectra. This is the case for the high-frequency data for instance where the statistical fluctuation of the different determinations of the spectra in some case are better than 1 part in 10^3.

A second caveat regards the method of data analysis of the calibration test data, for which the ratio with the reference bolometer data (of which the relative error is a function of frequency) introduces an error that increase with wavelength. With the spectral resolution of the data provided being much higher than the stated 0.1 cm $^{-1}$, the transmission accuracy requirement is not met for the 100 GHz detectors. It is possible to degrade the spectral resolution to the 0.1cm $^{-1}$level to allow the accuracy to achieve the required level, but the higher spectral resolution data has been provided to better assist with the CO contamination removal from the 100 GHz signal.

Figures containing the full spectral response of each HFI detector, and band-average spectra, are provided in the Appendix [ref.]. Details of the generation of band-average spectra, unit conversion coefficients, and colour correction coefficients are provided in the Data Processing sections of the Explanatory Supplement. IDL scripts have been provided alongside the PLA to allow users to generate unit conversion and colour correction coefficients; these are described in the PLA section [ref.].

Further details regarding the use of the spectral response of the HFI detectors are found [FIXME] (include links to other ExSup sections).

HFI detection chain

Bolometers

The heart of the HFI - the detectors - are bolometers, solid-state devices in which the incoming radiation dissipates its energy as heat that increases the temperature of a thermometer. The instrument Flight Model total number of bolometers is 52, split into 6 channels at central frequencies of 100, 143, 217, 353, 545, and 857GHz. Two extra bolometers not optically coupled to the telescope are added to the focal plane to monitor thermal noise (Dark Bolometers).

Thirty two of these bolometers are polarization sensitive allowing a map of the CMB polarisation to be built.

Bolometers consist of (i) an absorber that transforms the in-coming radiation into heat; (ii) a thermometer that is thermally linked to the absorber and measures the temperature changes; and (iii) a weak thermal link to a thermal sink, to which the bolometer is attached.

The detectors are semi-conducting NTD thermistor bolometers. There are two kinds of detector modules:

- SWB, spider web bolometers, are mounted on an absorbing spider-web of metallised silicon nitride
- PSB, polarization sensitive bolometers, are mounted or on a parallel absorbing grid of metallised silicon nitride.

In the spider-web bolometers, or SWBs (Bock et al. 1995; Mauskopf et al. 1997), the absorbers consist of metallic grids deposited on a Si3 N4 substrate in the shape of a spider web. The mesh design and the impedance of the metallic layer are adjusted to match vacuum impedance and maximize the absorption of millimeter waves, while minimizing the cross section to particles. The absorber is designed to offer equal impedance to any linearly polarised radiation. Nevertheless, the thermometer and its electrical leads define a privileged orientation (Fig. SWB) that makes the SWBs slightly sensitive to polarisation, as detailed in (Rosset et al. 2010). The thermometers are made of neutron transmuted doped (NTD) germanium (Haller et al. 1996), chosen to have an impedance of about 10 MΩ at their operating temperature.

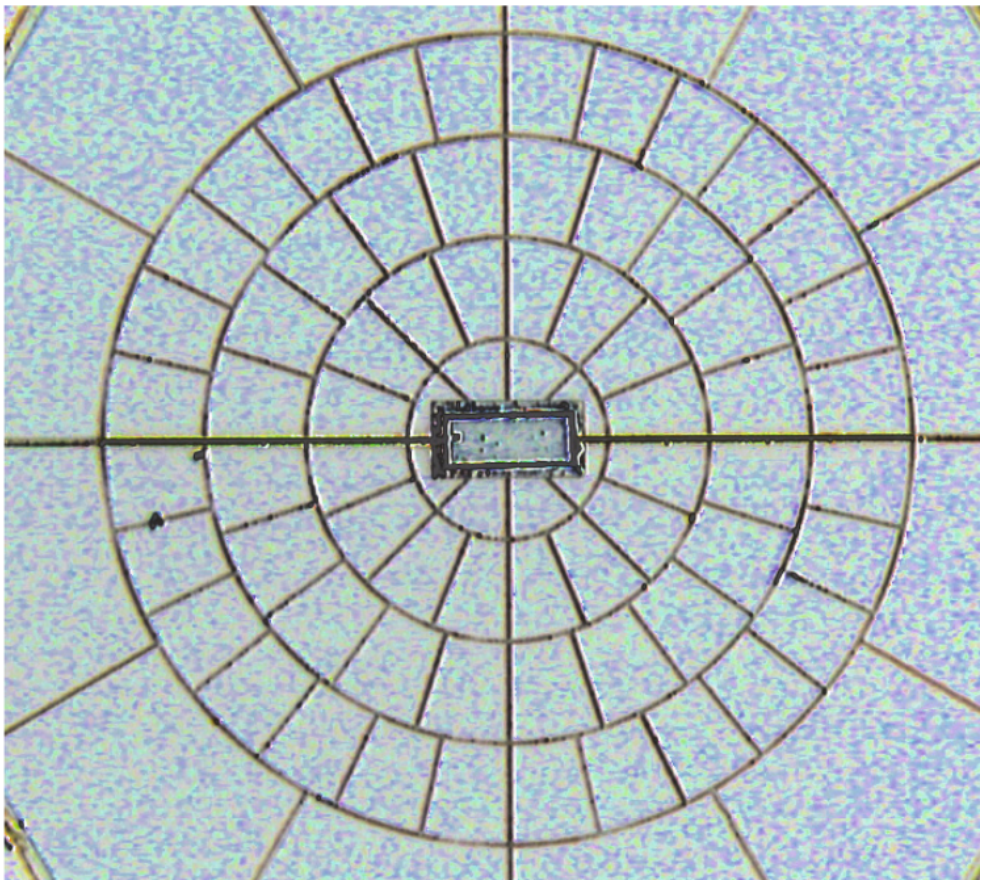

Picture of a spider web bolometer. This a 143 GHz module, The temperature sensor is at the center of the absorbing grid

The absorber of PSBs is a rectangular grid (Fig. PSB) with metallization in one direction (Jones et al. 2003). Electrical fields parallel to this direction develop currents and then deposit some power in the grid, while perpendicular electrical fields propagate through the grid without significant interaction. A second PSB perpendicular to the first one absorbs the other polarisation. Such a PSB pair measures two polarisations of radiation collected by the same horns and filtered by the same devices, which minimises the systematic effects: differences between polarised beams collected by a given horn are typically less than −30 dB of the peak. The differences in the spectral responses of a PSB pair also proved to be a few percent in the worst case. Each pair of PSBs sharing the same horn is able to measure the intensity Stokes parameter and the Q parameter associated with its local frame. An associated pair of PSBs rotated by 45◦ scans exactly the same line (if the geometrical alignment is perfect), providing the U Stokes parameter.

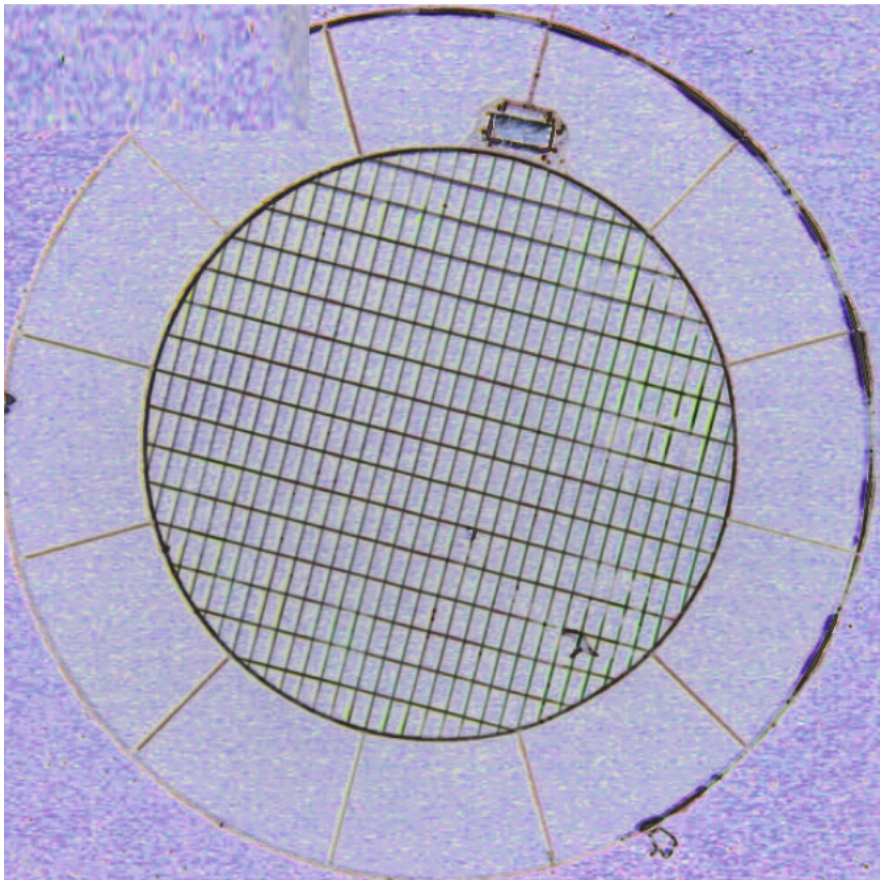

Picture of a polarization sensitive bolometer. This a 217 GHz module, The temperature sensor is at the an edge of the absorbing grid

The detectors operate at a temperature close to 100 mK, while the filters are distributed on the 100mK, 1.6 K, and 4 K stages in such a way that the heat load on the coldest stages is minimized to limit the heat load on the detectors and to decrease the heat lift requirement and thus enhance the mission lifetime. The self-emission of the 4K stage is minimised to limit the photon noise contribution on the detectors from the instrument. The HFI Focal Plane Unit accommodates sub-millimiter absorbing material in order to decrease the scattering inside it.

Table 1. The HFI receivers.

Band	ν_{center} [GHz]	Bandwidth [%]	Number of bolometers
100P	100	33	8
143P	143	32	8
143	143	30	4
217P	217	29	8
217	217	33	4
353P	353	29	8
353	353	28	4
545	545	31	4
857	857	30	4

Notes. The "P" identifies the polarisation sensitive bolometers.

to be change into a real table

Focal plane layout

The layout of the detectors in the focal plane is defined to cope with the scanning strategy. The HFI horns are positioned at the centre of the focal plane, where the optical quality is good enough for the high frequencies. The curvature of rows compensates for the distortion of images by the telescope. A pair of identical SWB will scan the same circle on the sky to provide additional redundancy. Similar horns feeding PSBs are also aligned so that two pairs of PSBs rotated by 45 ◦ with respect to each other scan the same line. This will provide the Q and U Stokes parameters with minimal correction for the pointing (Rosset et al. 2010). Residual systematics will come from the differences between the beam shapes of the two horns. In all cases except for the 100 GHz horns, a measurement is also done by a pair of similar channels shifted by 1.25 arcminutes in the cross-scan direction, to ensure adequate sampling. In the figures focal plane layout is reported.

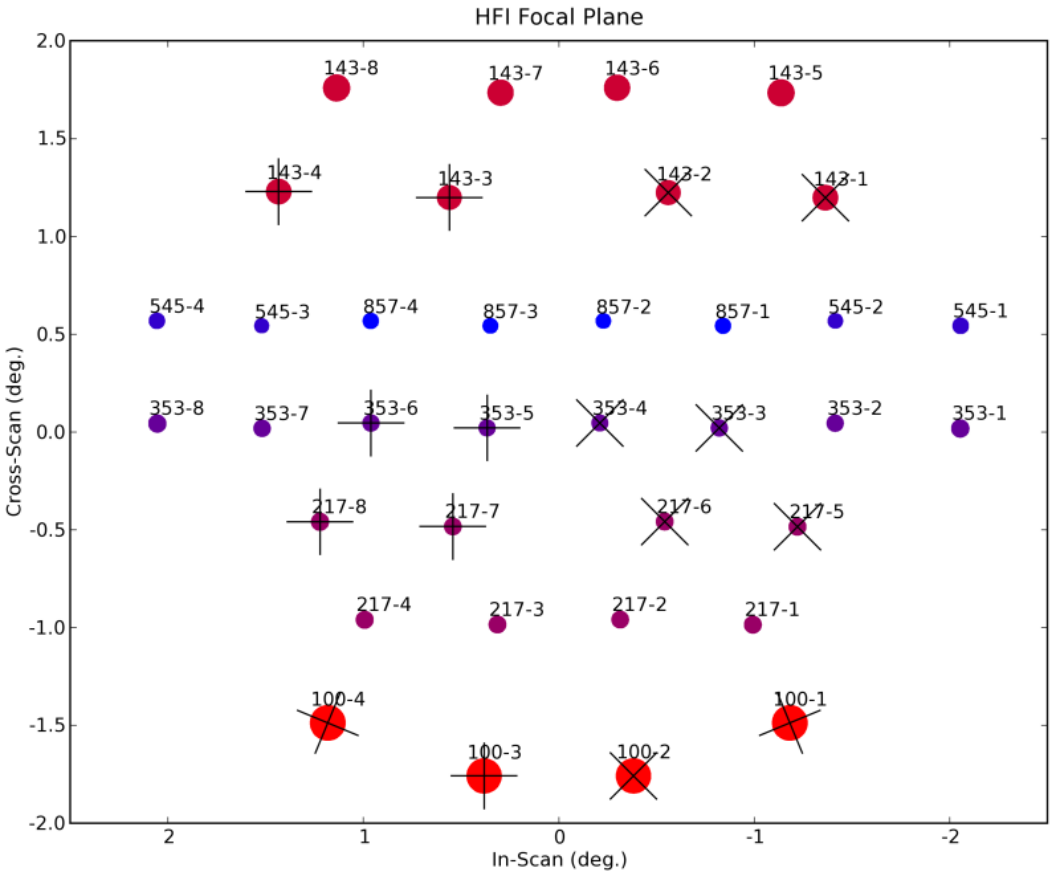

Focal plane layout as seen from outside the celestial sphere. Each spot represents an horn in the focal plane. Coordinates are in pointing direction with respect to the telescope boresight. PSBs detectors are indicated with a cross oriented as the two polarimeters axes. Scan direction is from left to right.

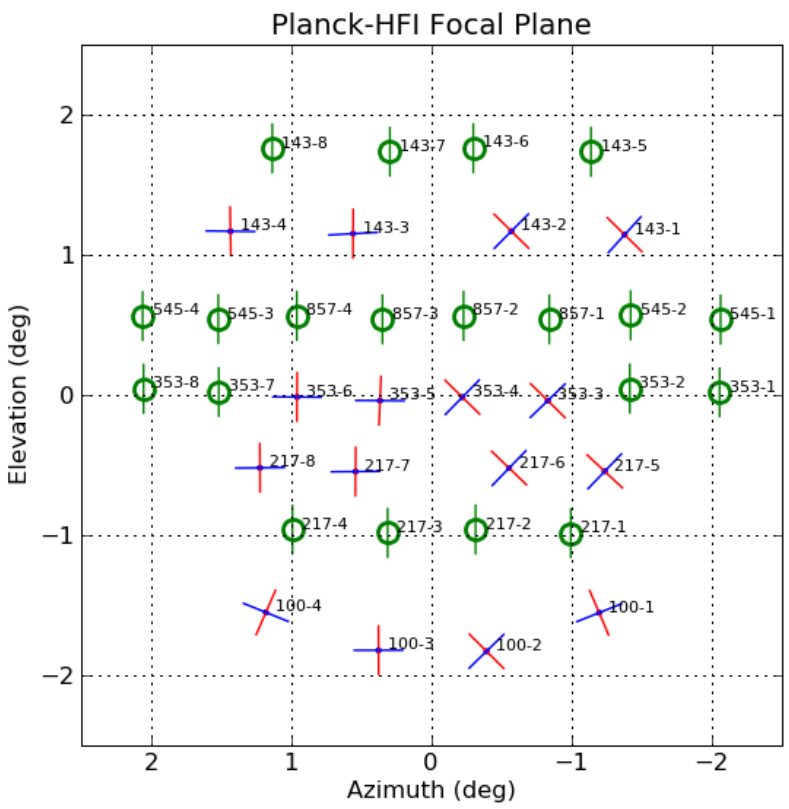

Focal plane layout as seen from outside the celestial sphere. In this case PSBs orientations are reported. Red rod is for a elements of PSBs, blue rod is for b elements.

Readout

The AC bias readout electronics of the HFI instrument (Gaertner et al. 1997) includes a number of original features proposed by several laboratories (CRTBT in Grenoble, CESR in Toulouse and IAS in Orsay), which were validated on the Diabolo experiment and on the balloon-borne Archeops experiment. It was developed for space by the CESR in Toulouse.

The particular features of the HFI AC bias readout are mainly

- i)that the cold load resistors were replaced by capacitors because they have no Johnson noise;
- ii)that the detectors are biased by applying a triangular voltage to the load capacitors

which produces a square current [Ibias] in the capacitors, and a square voltage [T bias] that compensates for the stray capacitance of the wiring (producing a nearly square bias current into the bolometer;

- iii)that a square offset com-pensation signal is subtracted to the bolometric signal to minimise the amplitude of the signal that has to be amplified and digitized;
- iv)that the electronic scheme is symmetrical and uses a differential amplification scheme to optimize the immunity to electromagnetic interferences;
- v)and finally that every parameter of the REU can be set by commands, which

is made possible by using digital-to-analog and analog-to-digital converters extensively.

The readout electronics consist of 72 channels designed to perform low noise measurements of the impedance of 52 bolometers, two blind bolometers, 16 accurate low temperature thermometers, all in the 10 MΩ range, one resistor of 10 MΩ and one capacitor of 100 pF. The semiconductor bolometers and thermometers of Planck-HFI operate at

cryogenic temperature around 100 mK on the focal plane, with impedance of about 10 MΩ when biased at the optimal current. The readout electronics on the contrary have to operate at “room” temperature (300 K). The distance between the two extremities of the readout chain is about 10 m and could represent a point of extreme susceptibility to electromagnetic interference. The readout electronic chain was split into three boxes. These are the JFET box, located on the 50 K stage of the satellite at 2.2 m from the focal plane, the pre-amplifier unit (PAU), located 1.8m further at 300 K, and the REU, located on the opposite side of the satellite, 5 m away. Each of the three boxes (JFET, PAU and REU) consists of 12 belts of six channels. The first nine belts are dedicated to the bolometers, and the three last ones to the accurate thermometers, the resistor and the capacitor (see figure Organization of the HFI readout).

Nbelt / Nchannel	0	1	2	3	4	5
0	100-1a	100-1b	143-1a	143-1b	217-1	353-1
1	143-5	217-5a	217-5b	353-2	545-1	Dark 1
2	100-2a	100-2b	217-2	353-3a	353-3b	857-1
3	143-2a	143-2b	353-4a	353-4b	545-2	857-2
4	100-3a	100-3b	143-6	217-6a	217-6b	353-7
5	143-3a	143-3b	217-3	353-5a	353-5b	545-3
6	143-7	217-7a	217-7b	353-6a	353-6b	857-3
7	143-8	217-8a	217-8b	545-4	857-4	Dark 2
8	100-4a	100-4b	143-4a	143-4b	217-4	353-8
9	Ther_0.1K 1	Ther_PID2 N	Ther_PID1 N	Ther_PID1.6 N	Ther_1.6K 1	Ther_PID4 N
10	**Resistor**	Capa 2	Ther_0.1K 2	Ther_PID1.6 R	Ther_4KH 1	Ther_4KL 1
11	Ther_PID2 R	Ther_PID1 R	Ther_1.6K 2	Ther_PID4 R	Ther_4KH 2	Ther_4KL 2

Organization of the HFI readout. Each row represents a belt. Each belt has 6 channels. (to be change into a real table ?)

Principles of the readout electronics

See figure [Principles of readout electronics]. The bolometer is biased by a square wave AC current obtained by the differentiation of a triangular voltage through a load capacitance, in a completely differential architecture. The presence of the stray capacitance due to losses of charge in the wiring requires a correction of the shape of the square bias current by a transient voltage. Thus the bias voltage generation is controlled by the two parameters I-bias and T-bias that express the amplitude of the triangular and transient voltage. The compensation voltage added to the bolometric signal to optimize the dynamic of the chain is controlled by the V-bal parameter.

Parameters of the Readout Unit can be set to optimize the detectors performance.

The modulation frequency of the AC bias system, fmod of the square bias current can be tuned from 70 Hz to 112 Hz by the telecommand parameters: Nsample, which defines the number of samples per half period of modulated signal, fdiv which determines the sampling frequency of the ADC.

The optimal frequencies are around 90 Hz.

Each channel has its own settings for the following parameters: I-bias, amplitude of the triangular bias voltage;

T-bias, amplitude of the transient bias voltage;

V-bal, amplitude of the square compensation voltage;

G-amp, value of the programmable gain of the REU [1/3, 1, 3, 7.6];

N-blank, number of blanked samples at the beginning of halfperiod not taken into account during integration of the signal;

S-phase, phase shift when computing the integrated signal.

All these parameters influence the effective response of the detection chains, and were optimized during the calibration campaigns and confirmed during the calibration and performance verification (CPV) phase following the launch of Planck. The scientific signal is provided by the integral of the signal on each half-period, between limits fixed by the S-phase and N-blank parameters.

The interaction of modulated readout electronics with semiconductor bolometers is rather different from that of a classical DC bias readout (Jones 1953). The differences were seen during the calibration of the HFI, although the readout electronics was designed to mimic the operation of a DC biased bolometric system as far as possible. With the AC readout the maximum of responsivity is lower and is obtained for higher bias current in the bolometer with respect to the DC model. This is caused by the stray capacitance in the wiring which has negligible effects for a DC bias and a major effect for an AC bias. In our case, a stray capacitance of 150 pF induces increases of NEP ranging from 4% (857 GHz bolometers) to 10% (100 GHz bolometers) and also affects the HFI time response. Details of the effect of the HFI AC bias system into the time response of the detectors are discussed in the Time Response [1] Section.

JFETs

Given the high impedance of the bolometers and the length of the connecting cables, it it is essential that the impedance of the signal is lowered as close as possible to the detectors. In our system this is accomplished by means of JFET source followers, located in boxes connected to the 50 K stage. The JFET box has been designed, developed and tested in the Observational Cosmology group in the Physics Department of the University of Rome "La Sapienza" (Brienza D. et al 2006). There are two JFETs per channel, since the readout is fully differential, and they provide a current amplification of the signal while keeping the voltage amplification very close to unity.

Inside the box, the JFETs are mounted on a thermally insulated plate with an active temperature control to keep them at the optimal temperature of 110 K. With a dissipated power lower than 240 mW, mainly produced by the JFETs and the source resistors, we obtained a noise power spectral density of less than 3 nV Hz1/2 for the frequency range of interest. This increases the total noise ofall bolometer channels by less than 5%.

Time response

The HFI bolometers and readout electronics have a finite response time to changes in incident optical power modeled as a Fourier domain transfer function (called the LFER4 model). LFER4 has two factors. The first one represents the thermal response of the bolometers, driven by their heat capacity, the thermal link to the bolometer plate at 100 mK, and by the thermo-electrical feed-back (ref. Catalano et al.) resulting from the heat deposited in the bolometer by the readout electronics. This factor is empirically obtained from the observation of sources. The second factor is simply the time response of the part of the readout electronics that amplifies and digitizes the signal, without any interaction with the bolometers. It is obtained by modelling the electronics with only a very few free parameters.

The time response of the HFI bolometers and readout electronics is modeled as a Fourier domain transfer function (called the LFER4 model) consisting of the product of an bolometer thermal response $F(\omega)$and an electronics response $H'(\omega)$.

Due to Planck's nearly constant scan rate, the time response is degenerate with the optical beam. However, because of the long time scale effects present in the time response, the time response is deconvolved from the data in the processing of the HFI data (see TOI processing). $F(\omega)$is tuned to optimize the "compactness" of the beams reconstructed with the deconvolved signal from planets.

Details about the time response model are to be found in this annex.

Data compression

The output of the readout electronics unit (REU) consists of one value for each of the 72 science channels (bolometers and thermometers) for each modulation half-period. This number, S_{REU}, is the sum of the 40 16-bit ADC signal values measured within the given half-period. The data processor unit (DPU) performs a lossy quantization of S_{REU}.

Details about data compression scheme, performance of the data compression during the mission, setting the quantization step in flight, impact of the data compression on science are to be found in this annex.

References

[1] http://www.sciops.esa.int/wikiSI/planckpla/index.php?title=HFI_design,_qualification,_and_performance&instance=Planck_PLA_ES#Time_response

HFI time response model

LFER4 model

If we write the input signal (power) on a bolometer as the bolometer physical impedance can be written as: where ω is the angular frequency of the signal and $F(\omega)$is the complex intrinsic bolometer transfer function. For HFI the bolometer transfer function is modelled as the sum of 4 single pole low pass filters: The modulation of the signal is done with a square wave, written here as a composition of sine waves of decreasing amplitude: where we have used the Euler relation $\sin x = (e^{ix} - e^{-ix})/2i$and $\omega_r$is the angular frequency of the square wave. The modulation frequency is $f_{mod} = \omega_r/2\pi$and was set to $f_{mod} = 90.18759$Hz in flight. This signal is then filtered by the complex electronic transfer function $H(\omega)$. Setting: $\omega_k^+ = \omega + (2k+1)\omega_r\, \omega_k^- = \omega - (2k+1)\omega_r$we have: This signal is then sampled at high frequency ($2f_{mod}NS$). $NS$is one of the parameters of the HFI electronics and corresponds to the number of high frequency samples in each modulation semi-period. In order to obtain an output signal sampled every π/ω_rseconds, we must integrate on a semiperiod, as done in the HFI readout. To also include a time shift Δt, the integral is calculated between $n\pi/\omega_r + \Delta t$and $(n+1)\pi/\omega_r + \Delta t$(with $T = 2\pi/\omega_r$ period of the modulation). The time shift $\Delta t$is encoded in the HFI electronics by the parameter S_{phase}, with the relation $\Delta t = S_{phase}/NS/f_{mod}$.

After integration, the n-sample of a bolometer can be written as where

The output signal in equation eqn:output can be demodulated (thus removing the $(-1)^n$) and compared to the input signal in equation bol_in. The overall transfer function is composed of the bolometer transfer function and the effective electronics transfer function, $H'(\omega)$: $TF(\omega) = F(\omega)H'(\omega)$

The shape of $H(\omega)$is obtained combining low and high-pass filters with Sallen Key topologies (with their respective time constants) and accounting also for the stray capacitance low pass filter given by the bolometer impedance combined with the stray capacitance of the cables. The sequence of filters that define the electronic band-pass function $H(\omega) = h_0 * h_1 * h_2 * h_3 * h_4 * h_5$are listed in table table:readout_electronics_filters.

Parameters of LFER4 model

The LFER4 model has are a total of 10 parameters(A_1, A_2, A_3, A_4, τ_1, τ_2, τ_3, τ_4, S_{phase}, τ_{stray}) 9 of which are independent, for each bolometer. The free parameters of the LFER4 model are determined using in-flight data in the following ways:

- $S_{phase}$is fixed at the value of the REU setting.
- $\tau_{stray}$is measured during the QEC test during CPV.
- A_1, τ_1, A_2, $\tau_2$are fit forcing the compactness of the scanning beam.
- A_3, τ_3, A_4 $\tau_4$are fit by forcing agreement of survey 2 and survey 1 maps.
- The overall normalization of the LFER4 model is forced to be 1.0 at the signal frequency of the dipole.

The details of determining the model parameters are given in (reference P03c paper) and the best-fit parameters listed here in table table:LFER4pars.

HFI electronics filter sequence

HFI electronics filter sequence. We define $s = i \omega$

Filter	Parameters	Function
0. Stray capacitance low pass filter	$\tau_{stray} = R_{bolo}C_{stray}$	$h_0 = \frac{1}{1.0 + \tau_{stray} * s}$
1. Low pass filter	$R_1 = 1_{\mathrm{k}}\,\Omega$ $C_1 = 100_{\mathrm{nF}}$	$h_1 = \frac{2.0 + R_1 * C_1 * s}{2.0 * (1.0 + R_1 * C_1 * s)}$
2. Sallen Key high pass filter	$R_2 = 51_{\mathrm{k}}\,\Omega$ $C_2 = 1\mu$	$h_2 = \frac{(R_2 * C_2 * s)^2}{(1.0 + R_2 * C_2 * s)^{2}3}$
3. Sign reverse with gain		$h_3 = -5.1$
4. Single pole low pass filter with gain	$R_4 = 10_{\mathrm{k}}\,\Omega$ $C_4 = 10_{\mathrm{nF}}$	$h_4 = \frac{1.5}{1.0 + R_4 * C_4 * s}$
5. Single pole high pass filter coupled to a Sallen Key low pass filter	$R_9 = 18.7_{\mathrm{k}}\,\Omega$ $R_{12} = 37.4_{\mathrm{k}}\,\Omega$ $C = 10.0_{\mathrm{nF}}$ $R_{78} = 510_{\mathrm{k}}\,\Omega$ $C_{18} = 1.0\mu_{\mathrm{F}}$ $K_3 = R_9^2 * R_{78} * R_{12}^2 * C^2 * C_{18}$ $K_2 = R_9 * R_{12}^2 * R_{78} * C^2 + R_9^2 * R_{12}^2 * C^2 + R_9 * R_{12}^2 * R_{78} * C_{18} * C$ $K_1 = R_9 * R_{12}^2 * C + R_{12} * R_{78} * R_9 * C_{18}$	$h_5 = \frac{2.0 * R_{12} * R_9 * R_{78} * C_{18} * s}{s^3 * K_3 + s^2 * K_2 + s * K_1 + R_{12} * R_9}$

Parameters for LFER4 model.

Bolometer	A_1	τ_1(s)	A_2	τ_2(s)	A_3	τ_3(s)	A_4	τ_4(s)	τ_{stray}(s)	S_{phase}(s)
100-1a	0.392	0.01	0.534	0.0209	0.0656	0.0513	0.00833	0.572	0.00159	0.00139
100-1b	0.484	0.0103	0.463	0.0192	0.0451	0.0714	0.00808	0.594	0.00149	0.00139
100-2a	0.474	0.00684	0.421	0.0136	0.0942	0.0376	0.0106	0.346	0.00132	0.00125
100-2b	0.126	0.00584	0.717	0.0151	0.142	0.0351	0.0145	0.293	0.00138	0.00125
100-3a	0.744	0.00539	0.223	0.0147	0.0262	0.0586	0.00636	0.907	0.00142	0.00125
100-3b	0.608	0.00548	0.352	0.0155	0.0321	0.0636	0.00821	0.504	0.00166	0.00125
100-4a	0.411	0.0082	0.514	0.0178	0.0581	0.0579	0.0168	0.37	0.00125	0.00125
100-4b	0.687	0.0113	0.282	0.0243	0.0218	0.062	0.00875	0.431	0.00138	0.00139
143-1a	0.817	0.00447	0.144	0.0121	0.0293	0.0387	0.0101	0.472	0.00142	0.00125
143-1b	0.49	0.00472	0.333	0.0156	0.134	0.0481	0.0435	0.27	0.00149	0.00125
143-2a	0.909	0.0047	0.0763	0.017	0.00634	0.1	0.00871	0.363	0.00148	0.00125
143-2b	0.912	0.00524	0.0509	0.0167	0.0244	0.0265	0.0123	0.295	0.00146	0.00125
143-3a	0.681	0.00419	0.273	0.00956	0.0345	0.0348	0.0115	0.317	0.00145	0.00125
143-3b	0.82	0.00448	0.131	0.0132	0.0354	0.0351	0.0133	0.283	0.00161	0.000832
143-4a	0.914	0.00569	0.072	0.0189	0.00602	0.0482	0.00756	0.225	0.00159	0.00125
143-4b	0.428	0.00606	0.508	0.00606	0.0554	0.0227	0.00882	0.084	0.00182	0.00125
143-5	0.491	0.00664	0.397	0.00664	0.0962	0.0264	0.0156	0.336	0.00202	0.00139
143-6	0.518	0.00551	0.409	0.00551	0.0614	0.0266	0.0116	0.314	0.00153	0.00111
143-7	0.414	0.00543	0.562	0.00543	0.0185	0.0449	0.00545	0.314	0.00186	0.00139
217-5a	0.905	0.00669	0.0797	0.0216	0.00585	0.0658	0.00986	0.342	0.00157	0.00111
217-5b	0.925	0.00576	0.061	0.018	0.00513	0.0656	0.0094	0.287	0.00187	0.00125
217-6a	0.844	0.00645	0.0675	0.0197	0.0737	0.0316	0.0147	0.297	0.00154	0.00125
217-6b	0.284	0.00623	0.666	0.00623	0.0384	0.024	0.0117	0.15	0.00146	0.00111
217-7a	0.343	0.00548	0.574	0.00548	0.0717	0.023	0.0107	0.32	0.00152	0.00139
217-7b	0.846	0.00507	0.127	0.0144	0.0131	0.0479	0.0133	0.311	0.00151	0.00139
217-8a	0.496	0.00722	0.439	0.00722	0.0521	0.0325	0.0128	0.382	0.00179	0.00111
217-8b	0.512	0.00703	0.41	0.00703	0.0639	0.0272	0.0139	0.232	0.00173	0.00125
217-1	0.0136	0.00346	0.956	0.00346	0.0271	0.0233	0.00359	1.98	0.00159	0.00111
217-2	0.978	0.00352	0.014	0.0261	0.00614	0.042	0.00194	0.686	0.0016	0.00125
217-3	0.932	0.00355	0.0336	0.00355	0.0292	0.0324	0.00491	0.279	0.00174	0.00125
217-4	0.658	0.00135	0.32	0.00555	0.0174	0.0268	0.00424	0.473	0.00171	0.00111
353-3a	0.554	0.00704	0.36	0.00704	0.0699	0.0305	0.0163	0.344	0.0017	0.00125
353-3b	0.219	0.00268	0.671	0.00695	0.0977	0.0238	0.0119	0.289	0.00157	0.00111
353-4a	0.768	0.00473	0.198	0.00993	0.0283	0.0505	0.00628	0.536	0.00181	0.00125
353-4b	0.684	0.00454	0.224	0.0108	0.0774	0.08	0.0149	0.267	0.00166	0.00111
353-5a	0.767	0.00596	0.159	0.0124	0.0628	0.0303	0.0109	0.357	0.00156	0.00111
353-5b	0.832	0.00619	0.126	0.0111	0.0324	0.035	0.0096	0.397	0.00166	0.00111

353-6a	0.0487	0.00176	0.855	0.006	0.0856	0.0216	0.0105	0.222	0.00199	0.00125
353-6b	0.829	0.00561	0.127	0.00561	0.0373	0.0252	0.00696	0.36	0.00228	0.00111
353-1	0.41	0.000743	0.502	0.00422	0.0811	0.0177	0.0063	0.329	0.00132	0.00097
353-2	0.747	0.00309	0.225	0.00726	0.0252	0.0447	0.00267	0.513	0.00154	0.00097
353-7	0.448	0.0009	0.537	0.0041	0.0122	0.0273	0.00346	0.433	0.00178	0.00125
353-8	0.718	0.00223	0.261	0.00608	0.0165	0.038	0.00408	0.268	0.00177	0.00111
545-1	0.991	0.00293	0.00743	0.026	0.00139	2.6	0	0	0.00216	0.00111
545-2	0.985	0.00277	0.0128	0.024	0.00246	2.8	0	0	0.00187	0.00097
545-4	0.972	0.003	0.0277	0.025	0.000777	2.5	0	0	0.00222	0.00111
857-1	0.974	0.00338	0.0229	0.025	0.00349	2.2	0	0	0.00176	0.00111
857-2	0.84	0.00148	0.158	0.00656	0.00249	3.2	0	0	0.0022	0.00125
857-3	0.36	4.22e-05	0.627	0.0024	0.0111	0.017	0.002	1.9	0.00152	0.00126
857-4	0.278	0.0004	0.719	0.00392	0.00162	0.09	0.00152	0.8	0.00149	0.000558

HFI operations

All satellite operations including the HFI instrument ones are under ESA MOC responsibilty for obvious safety reasons.The HFI instrument operations are nevertheless delegated to the HFI Instrument Operations Team (IOT) built from the HFI consortium and under the HFI Principal Investigator responsibility. Instrument management, operations and parameter monitoring are thus prepared and controlled by the IOT and serviced by MOC either in near real time during the DTCP or uploaded in the satellite mission timeline for defered execution. The HFI instrument health and science data quality has been monitored daily by the IOT from launch till the end of the HFI extension mission phase. Apart from ground based tests, different operations phases did occur:

- 14/05/2009-18/05/2009 **Launch Early Operational Phase**
- 18/05/2009-09/07/2009 **Commissioning Phase**. The operations during this phase were under ESA's Planck Project responsibilty. The main HFI activities have been functional tests of the instrument and its cooldown till 100 mK. Given the performance, the helium flow has been set to the minimal one giving an End Of Life estimation second half of January 2012.
- 10/07/2009-12/08/2009 **Calibration and Performance Verification Phase**. The operations during this phase were under ESA's Planck Science Office responsibilty. The main HFI operations have been performance tests and activities to mesure the effects of several systematics. The only instrument failure happened the 6th of August were the electronic part of the 4K cooler has been switched off probably due to a major cosmic particle. It has to be noted that no tuning of the HFI parameters have been executed in flight till the end of the full HFI mission, excepted in December 2009 for an adjustment of the on-board numerical compression parameters.
- 12/08/2009-28/11/2010 **HFI Nominal mission**
- 28/11/2010-13/01/2012 **HFI Extended mission**
- 13/01/2012-(to be continued) **LFI "only" extension phase**

The detailled operation timeline for HFI is given in this annex.

HFI perfsummary

HFI inst annexes

This page lists all annexes about the HFI instrument section.

- Cold optics:
  - HFI Spectral Response Optical Efficiency measurements
  - HFI Spectral Response Reference Bolometer Measurements
  - HFI Spectral Response Data Processing and Fourier Transformation
  - HFI Detector Feedhorn Waveguide Model Parameters
  - HFI Spectral Response over the CO rotational transition regions
- Detection chain:
  - HFI time response model
  - HFI data compression
- Operations:
  - HFI operations timeline

HFIspecEFF

The EFF tests involved exposing the HFI detectors to a known blackbody source and observing the response. Sufficient details for the HFI detector spectral transmission profiles are provided here while full details of the EFF experiments and results are provided in a separate technical report . A blackbody source internal to the Saturne cryostat was set to a variety of temperatures ($\sim 1 - 6$ K) and the bolometer detector response was recorded. A bolometer model was applied to the recorded response in order to obtain the radiative optical power absorbed by the detector, in units of W, i.e. $P_{\rm abs}(T_i)$ where T_i represents the blackbody source temperature. Using the measured source temperature, the theoretical radiative optical power incident on the detector is also calculated using the Planck function. The ratio of the received power and the theoretical power provides the optical efficiency term. To remove any offsets in the measurement, a ratio of differences between unique temperature settings is used. The measured absorbed optical power difference is given by

where T_j and T_i represent two unique source temperature settings. The theoretical incident power is determined using the HFI detector spectral transmission profiles. Let $\tau(\nu)$ represent the normalized detector transmission spectrum (i.e. it has been ratioed and had the waveguide model and filter data appropriately grafted). The spectral transmission is scaled for λ^2 throughput and then re-normalized as follows

where $\mathrm{Norm}\,(f(x))$ is the division of $f(x)$ by its maximum value, and c is the speed of light. The normalized spectral transmission is then used with the Planck function at the temperature setting to determine the theoretical power, $P_{\rm th}(T_i)$, as follows

where h is the Planck constant, k is the Boltzmann constant, the integration limits are given by ν_1 and ν_2, and n_m is the expected mode content of the frequency band. Table [tab:modes] lists the n_m values used for each band . In this case the integration is performed over the range $\nu \in [67\ \mathrm{GHz}, 1142\ \mathrm{GHz}]$. The difference between the theoretical power loading is given by

which allows the optical efficiency term to be determined as follows

Thus, if $\epsilon\tau'(\nu)$ were used in Equation [eq:EFFPth] in place of $\tau'(\nu)$, the resultant optical efficiency would be unity, indicating that the transmission losses have already been taken into account.
The uncertainty estimate of the optical efficiency is statistically based on the results from the multiple temperature settings used in the EFF test sequences.

Mode Content for the HFI detector bands.

Band (GHz)	100	143	217	353	545	857
n_m	1	1	1	1	3.4	8.3

HFIspecBREF

Properties of Ref. Bolometer Spectra

Band (GHz)	# Ifgm.	# Spec.	MPD (cm)	ILS $\mathrm{FWHM}_{(\mathrm{cm}^{-1})}$	avg. S/N
100	164	164	29.644698	0.020357772	11.478057
143	164	164	29.644698	0.020357772	37.361317
217	164	164	29.644698	0.020357772	126.14280
353	24	24	29.652306	0.020352549	136.06159
545	24	24	29.652306	0.020352549	314.58093
857	24	24	29.652306	0.020352549	388.23050

Reference bolometer spectra and S/N.

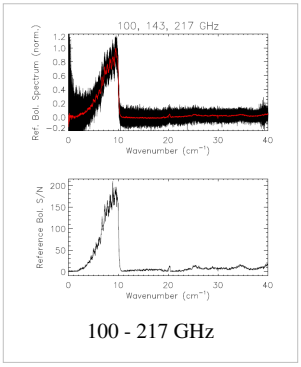

100 - 217 GHz

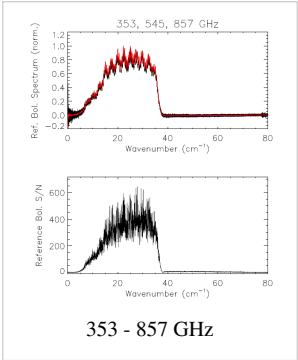

353 - 857 GHz

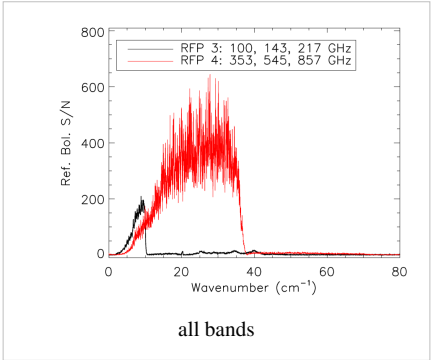

all bands

Reference bolometer spectra (top) and S/N (bottom) for each of the HFI bands (vertical bars represent band edges).

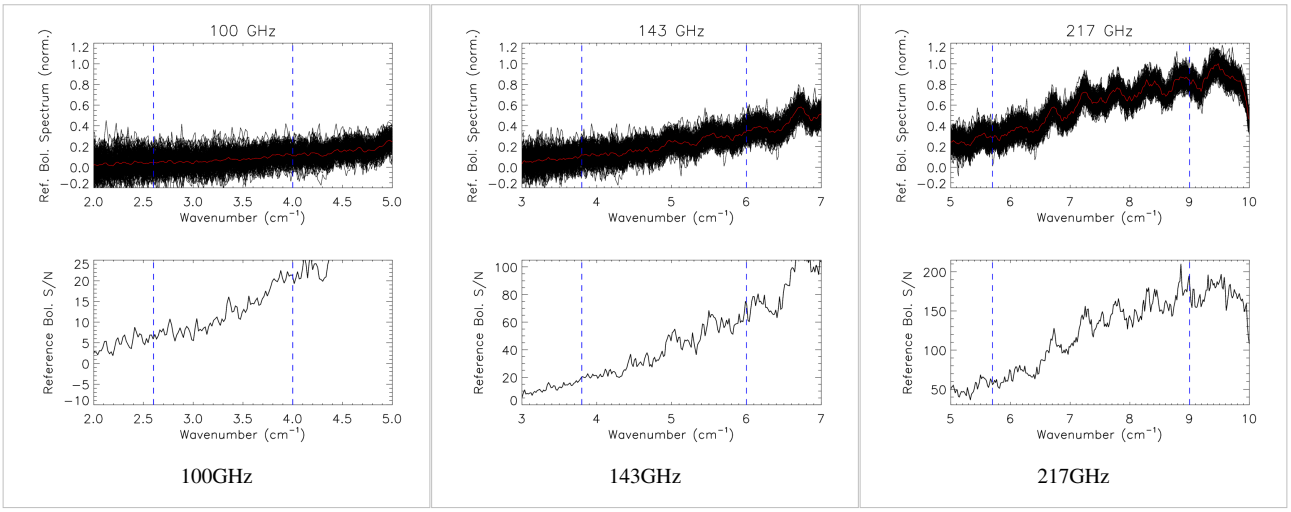

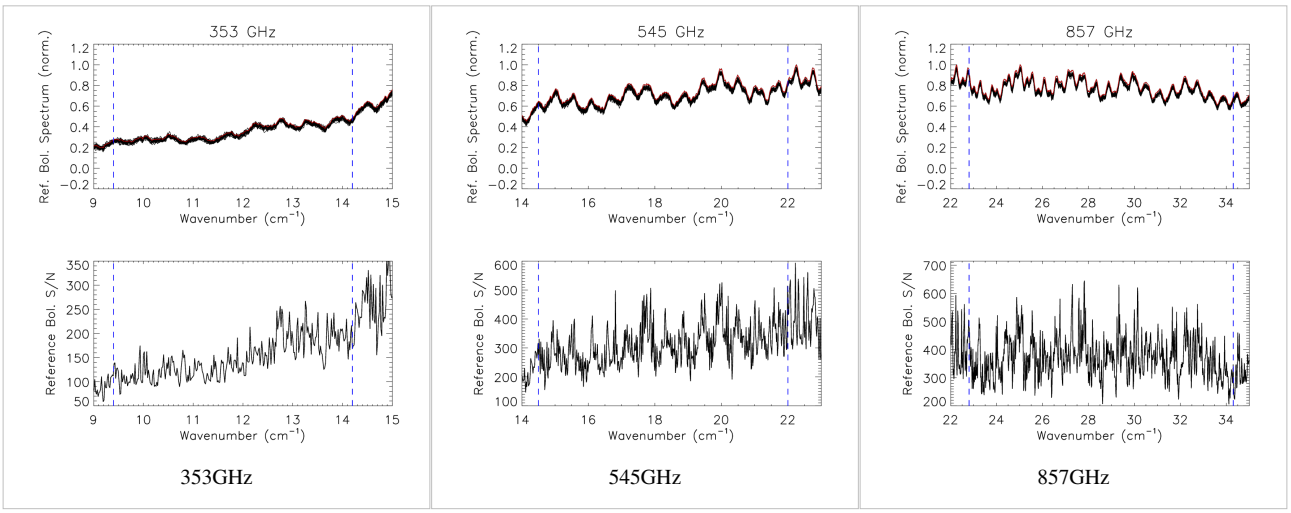

FIXME: This figure needs updated.

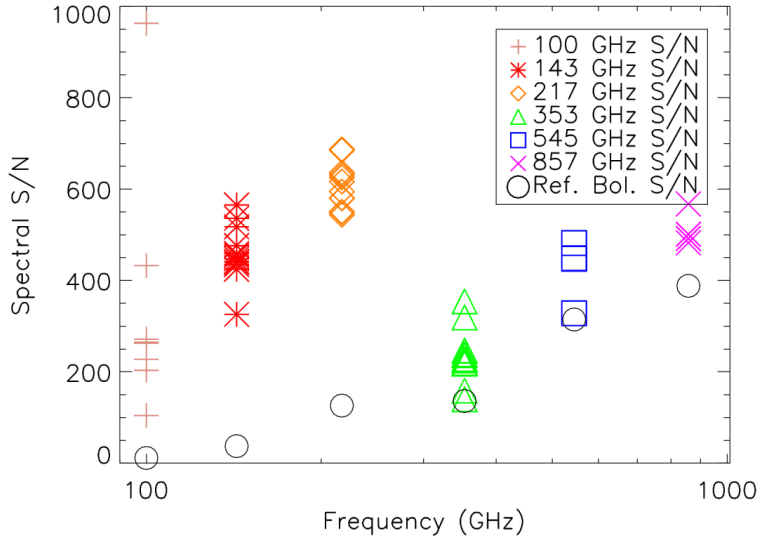

Approximate S/N ratio for the individual HFI detector spectra and the reference bolometer spectra.

HFIspecFT

HFI Spectral Response Pre-Flight Spectral Characterization Data Processing and Fourier Transformation

The bolometer signal is stored within the initial database in several formats: raw ADU, signal voltage, resistance, current, temperature, total power, electrical power, and radiant power, all of which may be exported as a function of sample time. A bolometer model was applied to the raw data to produce interferograms in units of absorbed optical power. This both reduced the in-band effects of detector nonlinearities, and allowed another comparison of optical efficiency to complement the EFF tests. The location of Zero Optical Path Difference (ZPD) is estimated for each interferogram, and the interferogram boundaries are determined as the mid-points between subsequent interferograms, less a small number of buffer points ($\sim$10) to ensure that the extracted interferograms include regions associated with the FTS stage travel having constant velocity while excluding the acceleration regions. Visual verification of the extracted interferograms is performed prior to subsequent processing and averaging to ensure that each ZPD was identified correctly, and to remove any low-quality interferograms. The overlap of the extracted interferograms is also verified visually. Once interferograms have been extracted from each data set, the overall spectral resolution is evaluated and an evenly sampled Optical Path Difference (OPD) grid onto which each interferogram in the combined data is then interpolated is generated. This ensures that each individual interferogram is sampled at ZPD and that each spectrum has identical frequency sampling and can thus be averaged together. An example of a combined interferogram data set is illustrated in Figure [fig:CombinedIFGMex] where the central portions of the recorded interferograms are shown. A similar plot for each HFI detector is included in the Appendices (see §[sec:allIFGMs]). The MPD value for each detector, and corresponding spectral resolution, is shown in Fig. [fig:MPD].

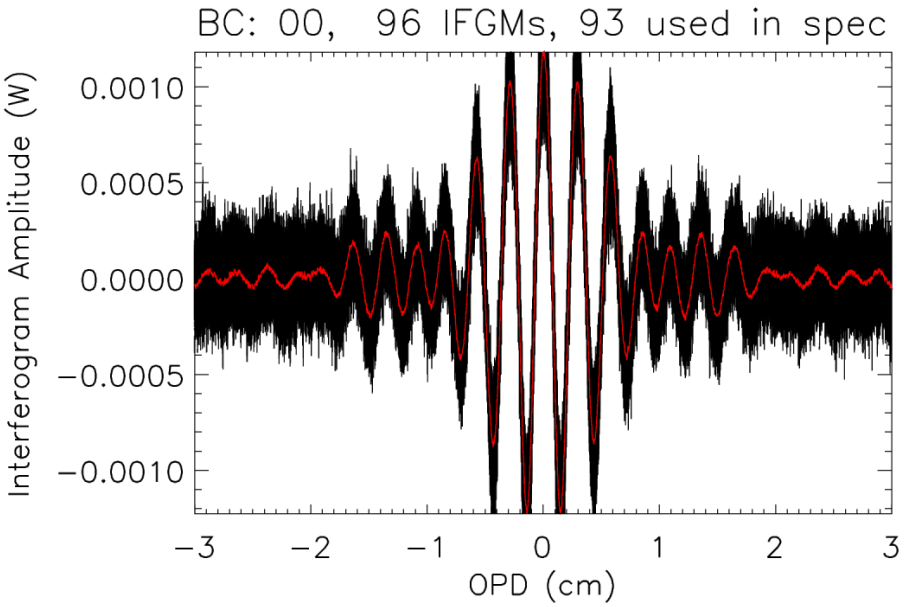

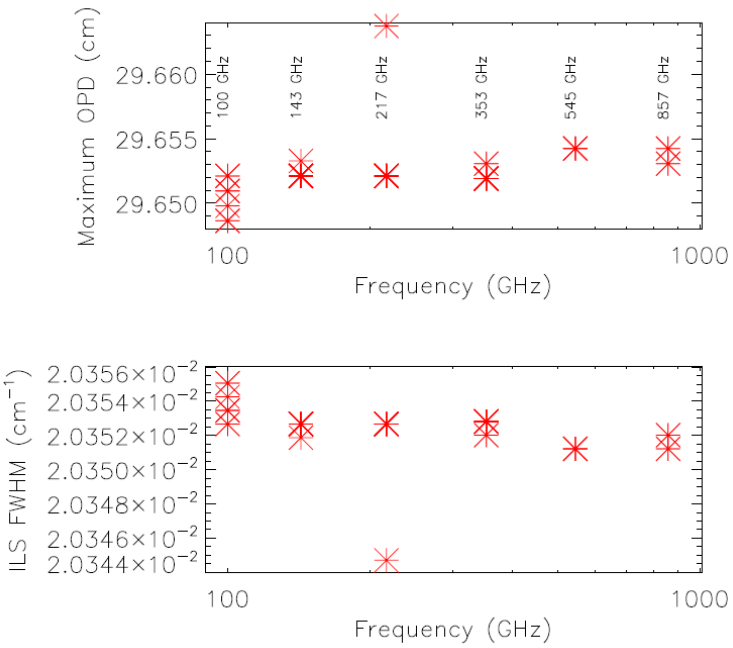

In preparation for Fourier transformation, a low-order polynomial baseline removal is performed on the individual interferograms. Consequently, no information can be recovered from the spectrum below $\sim 0.1\ \mathrm{cm}^{-1}$, but this is of no concern as this region of the spectrum is replaced by a waveguide fit in the final data product (see §[sec:WG]). An average interferogram is determined and used to identify glitches for removal from the interferogram data. Following glitch removal, individual interferograms undergo standard Fourier data processing. The modified Norton-Beer 1.5 apodization function ([ref.]) has been selected to be used for the final spectral transmission profile data set as it represents a good compromise between the desired ILS sidelobe reduction and improved S/N with marginal reduction in spectral resolution. Data averaging is then performed in the spectral domain. The uncertainty for every spectral data point is determined statistically through the standard deviation at a given frequency. A check for poor quality spectra is performed by comparing the overall standard deviation including and excluding any given spectrum. An example of the individual spectra and uncertainty for bc00 is shown in Fig. [fig:CombinedSpecEx], along with the corresponding S/N of the reference bolometer spectrum; similar plots for all of the detectors are shown in §[sec:allSpecs]. An estimate of the spectral S/N for each detector is obtained using the average spectrum and its statistical uncertainty, averaged across the in-band region of the spectrum. The averaged spectra are then normalized and divided by a (normalized) reference bolometer spectrum (see §[sec:setup] & §[sec:Bref]) to obtain the HFI detector relative spectral response.

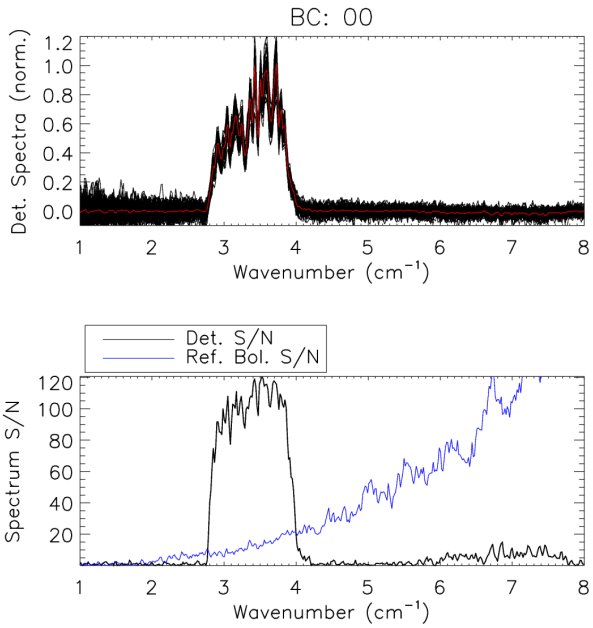

Properties of HFI Detector Spectra

Band (GHz)	bc	# Ifgm.	# Spec.	MPD (cm)	ILS FWHM$_{(cm^{-1})}$	avg. S/N
100	00	96	93	29.648639	0.020355066	104.70555
100	01	96	95	29.648639	0.020355066	203.34226
100	20	96	96	29.649801	0.020354268	271.38262
100	21	95	94	29.650962	0.020353471	264.65385
100	40	96	94	29.652124	0.020352674	432.40921
100	41	96	96	29.652124	0.020352674	962.98064
100	80	95	95	29.650962	0.020353471	262.71036
100	81	96	96	29.650962	0.020353471	227.35782
143	02	96	95	29.652124	0.020352674	434.93136
143	03	96	96	29.652124	0.020352674	458.86741
143	10	95	95	29.652124	0.020352674	565.21311
143	30	92	92	29.653286	0.020351876	424.53824
143	31	92	92	29.652124	0.020352674	447.50343
143	42	92	92	29.652124	0.020352674	536.23423
143	50	96	96	29.652124	0.020352674	441.68983
143	51	96	96	29.652124	0.020352674	476.22684
143	60	96	96	29.652124	0.020352674	517.43269
143	70	95	94	29.652124	0.020352674	326.06542
143	82	96	96	29.652124	0.020352674	454.23293
143	83	96	96	29.652124	0.020352674	439.50612
217	04	96	96	29.652124	0.020352674	625.92713
217	11	96	96	29.652124	0.020352674	580.32904

217	12	67	67	29.663741	0.020344703	549.24264
217	22	96	96	29.652124	0.020352674	550.65242
217	43	95	95	29.652124	0.020352674	616.57750
217	44	96	96	29.652124	0.020352674	543.78288
217	52	95	94	29.652124	0.020352674	684.91039
217	61	92	92	29.652124	0.020352674	594.70296
217	62	95	95	29.652124	0.020352674	579.69385
217	71	96	96	29.652124	0.020352674	631.30065
217	72	96	96	29.652124	0.020352674	687.10844
217	84	92	92	29.652124	0.020352674	636.36790
353	05	55	55	29.651916	0.020352816	354.15815
353	13	57	57	29.651916	0.020352816	319.09858
353	23	55	55	29.651916	0.020352816	218.05772
353	24	64	64	29.651916	0.020352816	236.44464
353	32	56	56	29.651916	0.020352816	238.40018
353	33	55	55	29.651916	0.020352816	219.60443
353	45	64	64	29.653078	0.020352019	246.97889
353	53	57	57	29.651916	0.020352816	225.27621
353	54	57	57	29.651916	0.020352816	228.47058
353	63	57	56	29.651916	0.020352816	140.16991
353	64	55	55	29.651916	0.020352816	158.85037
353	85	57	57	29.653078	0.020352019	246.18460
545	14	63	63	29.654240	0.020351221	448.67624
545	34	64	64	29.654240	0.020351221	481.87111
545	55	57	57	29.654240	0.020351221	328.07835
545	73	57	57	29.654240	0.020351221	447.49901
857	25	64	64	29.653078	0.020352019	501.25106
857	35	64	64	29.654240	0.020351221	567.55125
857	65	42	42	29.653078	0.020352019	482.41906
857	74	64	64	29.654240	0.020351221	491.89133

HFIspecWG

HFI Detector Feedhorn Waveguide Cut-On Model Parameters

This section proviedes a table of the waveguide parameters used in modelling the low frequency cut-on for the various HFI detectors.

Waveguide model parameters for the HFI detectors.

Band (GHz)	bc	Det.	r^{W}(mm)	r^{W}(mm)
100	00	1a	1.039705	12.1000
100	01	1b	1.038040	12.5813
100	20	2a	1.038375	14.3000
100	21	2b	1.041035	12.3750
100	40	3a	1.042370	12.9250
100	41	3b	1.042370	12.5125
100	80	4a	1.033050	13.2000
100	81	4b	1.033050	12.6500
143	02	1a	0.740345	9.4500
143	03	1b	0.737550	9.5625
143	10	5	0.736155	9.4500
143	30	2a	0.740345	9.4500
143	31	2b	0.739880	9.2250
143	42	6	0.741275	9.4500
143	50	3a	0.741275	9.4500
143	51	3b	0.741275	9.4500
143	60	7	0.729635	9.7875
143	70	8	0.739415	9.4500
143	82	4a	0.739415	9.4500
143	83	4b	0.738480	9.4500
217	04	1	0.4740750	7.8000
217	11	5a	0.4814250	7.8000
217	12	5b	0.4817310	8.0000
217	22	2	0.4749935	7.8000
217	43	6a	0.4832625	8.0000
217	44	6b	0.4832625	8.0000
217	52	3	0.4753000	8.0000
217	61	7a	0.4820375	8.0000
217	62	7b	0.4820375	8.0000
217	71	8a	0.4838750	8.0000
217	72	8b	0.4838750	8.1000

217	84	4	0.4740750	7.6000
353	05	1	0.2921850	6.47500
353	13	2	0.2914300	7.00000
353	23	3a	0.2891650	7.70000
353	24	3b	0.2893535	7.52500
353	32	4a	0.2869000	7.35000
353	33	4b	0.2870890	7.39375
353	45	7	0.2876550	6.12500
353	53	5a	0.2936950	7.35000
353	54	5b	0.2936950	7.61250
353	63	6a	0.2929400	6.73750
353	64	6b	0.2925625	6.62500
353	85	8	0.2889765	6.73750
545	14	1	0.3861000	3.600
545	34	2	0.3865875	3.525
545	55	3	0.3800065	3.525
545	73	4	0.3787875	3.525
857	25	1	0.2985	2.4
857	35	2	0.2985	2.4
857	65	3	0.2985	2.4
857	74	4	0.2985	2.4

HFIspecCOtable

HFI CO response

This is a temporary placeholder until the DPC CO section is updated. Below is a table of the spectral transmission over the CO rotational transition/emission regions.

Spectral transmission for CO transitions for HFI detectors.

Band	BC	Det.	CO transition ($J_{\mathrm{upper}} - J_{\mathrm{lower}}$)	Transmission
100	00	1a	1 – 0	0.1495 ±0.0054
100	01	1b	1 – 0	0.1812 ±0.0052
100	20	2a	1 – 0	0.2577 ±0.0119
100	21	2b	1 – 0	0.1944 ±0.0086
100	40	3a	1 – 0	0.2798 ±0.0133
100	41	3b	1 – 0	0.1660 ±0.0093
100	80	4a	1 – 0	0.2538 ±0.0114
100	81	4b	1 – 0	2173 ±0.0105
217	04	1	2 – 1	0.3781 ±0.0026
217	11	5a	2 – 1	0.4530 ±0.0029
217	12	5b	2 – 1	0.4174 ±0.0030
217	22	2	2 – 1	0.3773 ±0.0026
217	43	6a	2 – 1	0.3149 ±0.0023
217	44	6b	2 – 1	0.3609 ±0.0030
217	52	3	2 – 1	0.3924 ±0.0025
217	61	7a	2 – 1	0.3428 ±0.0022
217	62	7b	2 – 1	0.2770 ±0.0017
217	71	8a	2 – 1	0.4623 ±0.0031
217	72	8b	2 – 1	0.4340 ±0.0031
217	84	4	2 – 1	0.3506 ±0.0025
353	05	1	3 – 2	0.4487 ±0.0036
353	13	2	3 – 2	0.5461 ±0.0044
353	23	3a	3 – 2	0.3443 ±0.0030
353	24	3b	3 – 2	0.4706 ±0.0037
353	32	4a	3 – 2	0.3099 ±0.0024
353	33	4b	3 – 2	0.2801 ±0.0027
353	45	7	3 – 2	0.2923 ±0.0022
353	53	5a	3 – 2	0.3150 ±0.0024
353	54	5b	3 – 2	0.3181 ±0.0023
353	63	6a	3 – 2	0.2059 ±0.0014
353	64	6b	3 – 2	0.2113 ±0.0017

353	85	8	3 – 2	0.3509 ±0.0028
545	14	1	4 – 3	0.0747 ±0.0003
545	34	2	4 – 3	0.0731 ±0.0003
545	55	3	4 – 3	0.0521 ±0.0002
545	73	4	4 – 3	0.0473 ±0.0002
545	14	1	5 – 4	0.3306 ±0.0012
545	34	2	5 – 4	0.3183 ±0.0011
545	55	3	5 – 4	0.2428 ±0.0009
545	73	4	5 – 4	0.2597 ±0.0009
857	25	1	6 – 5	0.0280 ±0.0001
857	35	2	6 – 5	0.0241 ±0.0001
857	65	3	6 – 5	0.0292 ±0.0001
857	74	4	6 – 5	0.0159 ±0.0001
857	25	1	7 – 6	0.1636 ±0.0005
857	35	2	7 – 6	0.1427 ±0.0004
857	65	3	7 – 6	2176 ±0.0007
857	74	4	7 – 6	0.1168 ±0.0003
857	25	1	8 – 7	0.2554 ±0.0009
857	35	2	8 – 7	0.2218 ±0.0007
857	65	3	8 – 7	0.2744 ±0.0009
857	74	4	8 – 7	0.1119 ±0.0004
857	25	1	9 – 8	0.0053 ±0.0000
857	35	2	9 – 8	0.0060 ±0.0000
857	65	3	9 – 8	0.0085 ±0.0000
857	74	4	9 – 8	0.0001 ±0.0000

HFI data compression

Data compression

Data compression scheme

The output of the readout electronics unit (REU) consists of one value for each of the 72 science channels (bolometers and thermometers) for each modulation half-period. This number, S_{REU}, is the sum of the 40 16-bit ADC signal values measured within the given half-period. The data processor unit (DPU) performs a lossy quantization of S_{REU}.

We define a compression slice of 254 S_{REU}values, corresponding to about 1.4 s of observation for each detector and to a strip on the sky about 8 degrees long. The mean $\langle S_{REU} \rangle$of the data within each compression slice is computed, and data are demodulated using this mean:

$S_{demod,i} = (S_{REU,i} - \langle S_{REU} \rangle) * (-1)^i$

where $1 < i < 254$is the running index within the compression slice.

The mean $\langle S_{demod} \rangle$of the demodulated data $S_{demod,i}$is computed and subtracted, and the resulting slice data is quantized according to a step size Q that is fixed per detector:

$S_{DPU,i} = \mathrm{round}\left[(S_{demod,i} - \langle S_{demod} \rangle)/Q\right]$

This is the lossy part of the algorithm: the required compression factor, obtained through the tuning of the quantization step Q, adds a noise of variance $\simeq 2\%$to the data. This will be discussed below.

The two means $\langle S_{REU} \rangle$and $\langle S_{demod} \rangle$are computed as 32-bit words and sent through the telemetry, together with the $S_{DPU,i}$values. Variable-length encoding of the $S_{DPU,i}$values is performed on board, and the inverse decoding is applied on ground.

Performance of the data compression during the mission

Optimal use of the bandpass available for the downlink was obtained initially by using a value of Q = σ/2.5 for all bolometer signals. After the 12th of December 2009, and only for the 857 GHz detectors, the value was reset to Q = σ/2.0 to avoid data loss due to exceeding the limit of the downlink rate. With these settings the load during the mission never exceeded the allowed band-pass width as is seen on the next figure.

Setting the quantization step in flight

The only parameter that enters the PLANCK-HFI compression algorithm is the size of the quantization step, in units of σ, the white noise standard deviation for each channel. It has been adjusted during the mission by studying the mean frequency of the central quantization bin [-Q/2,Q/2], $p_0$within each compression slice (254 samples). For a pure Gaussian noise, this frequency is related to the step size (in units of σ) by $\hat{Q} = 2\sqrt{2}\mathrm{Erf}^{-1}(p_0) \simeq 2.5p_0$ where the approximation is valid up to $p_0 < 0.4$. In PLANCK however the channel signal is not a pure Gaussian, since glitches and the periodic crossing of the Galactic plane add some strong outliers to the distribution. By using the frequency of these outliers, p_{out}, above 5σ, simulations show that the following formula gives a valid estimate:

$\hat{Q}_{\mathrm{cor}} = 2.5\frac{p_0}{1 - p_{\mathrm{out}}}$

The following figure shows an example of the $\hat{Q}$and $\hat{Q}_{\mathrm{cor}}$timelines that were used to monitor and adjust the quantization setting.

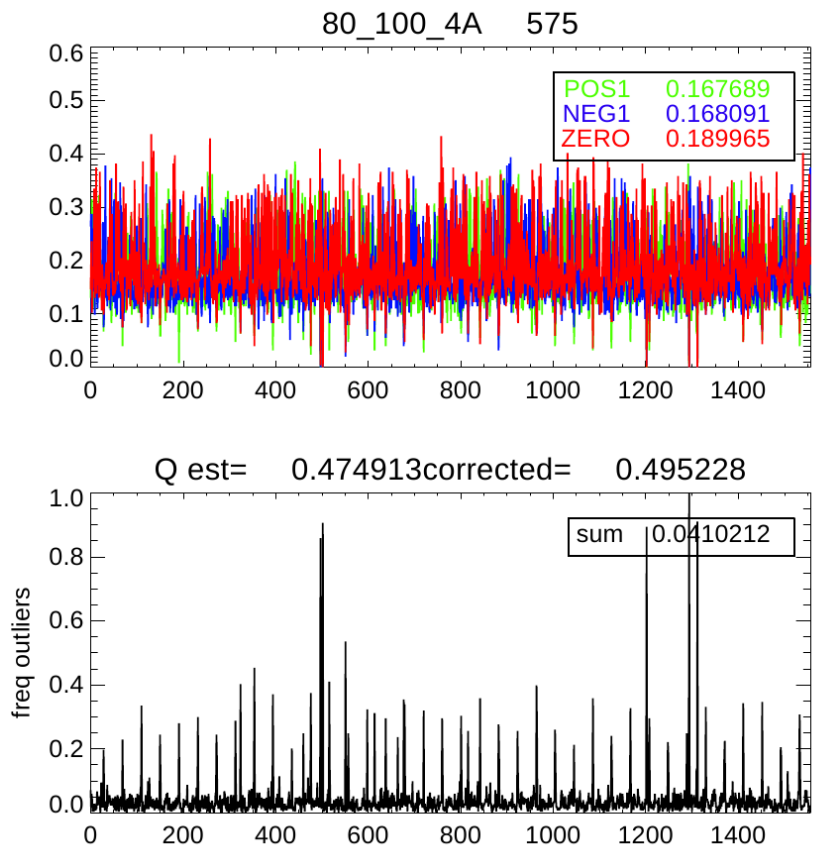

Example of the "bin0" frequency timeline (1 point per compression slice) p_0 (labeled "ZERO") for one of the channels. The -1 ("NEG1") and +1 ("POS1") bin frequencies are also shown. The lower plot shows the frequency timeline of outliers, where the glitches and periodic crossing of the Galaxy are visible. The estimated raw step size \hat Q=0.47 and corrected value \hat Q_\text{cor}=0.49 are automatically computed and the step size can be adjusted according to these control plots.

Impact of the data compression on science

The effect of a pure quantization process of step Q(in units of σ) on the statistical moments of a signal is well known (#widrow) When the step is typically below the noise level (which is largely the PLANCK case) one can apply the Quantization Theorem which states that the process is equivalent to the addition of a uniform random noise in the $[-Q/2, Q/2]$range. The net effect of quantization is therefore to add quadratically to the signal a $Q^2/12$ variance. For $Q \simeq 0.5$this corresponds to a 2%noise level increase. The spectral effect of the non-linear quantization process is theoretically much more complicated and depends on the signal and noise details. As a rule of thumb, a pure quantization adds some auto-correlation function that is suppressed by a $\exp[-4\pi^2(\frac{\sigma}{Q})^2]$factor #banta. Note however that PLANCK does not perform a pure quantization process. A baseline which depends on the data (mean of each compression slice value), is subtracted. Furthermore, for the science data, circles on the sky are coadded. Coaddition is again performed when projecting the rings onto the sky (map-making). To study the full effect of the PLANCK-HFI data compression algorithm on our main science products, we have simulated a realistic data timeline corresponding to the observation of a pure CMB sky. The compressed/decompressed signal was then back-projected onto the sky using the PLANCK scanning strategy. The two maps were analyzed using the \texttt{anafast} Healpix procedure and both reconstructed $C_\ell$were compared. The result is shown for a quantization step $Q = 0.5$.

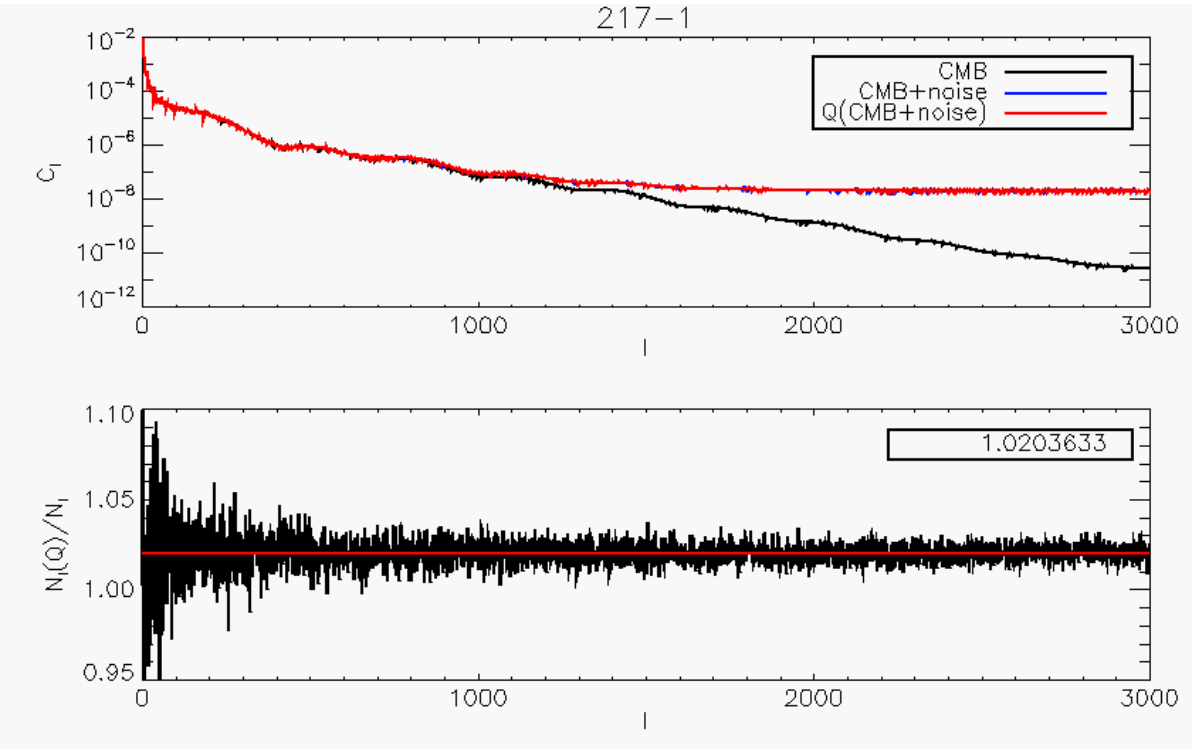

Effect of the PLANCK compression algorithm on the reconstructed power spectrum (C_ℓ) after data projection and map-making, according to the simulation. The upper plot shows the input reconstructed CMB power spectrum (black), the CMB+noise spectrum for this channel (blue, barely visible) and the reconstructed C_ℓ) when including the data compression in the chain (red). The lower plot shows these last two ratios and confirms the white nature of the final added noise at a level that can still be computed by the Quantization Theorem ($2\%$for $Q = 0.5$used here).

It is remarkable that the full procedure of baseline-subtraction+quantization+ring-making+map-making still leads to the 2%increase of the variance that is predicted by the simple timeline quantization (for $Q/\sigma = 2$). Furthermore we check that the noise added by the compression algorithm is white.

It is not expected that the compression brings any non-gaussianity, since the pure quantization process does not add any skewness and less than 0.001 kurtosis, and coaddition of circles and then rings erases any non-gaussian contribution according to the Central Limit Theorem.

<biblio force=false>

1. References

</biblio>

HFI operations timeline

The following list gives some known events and activities that have affected or might have affected the HFI data. The time information is the start time of the event in On Board Time. The label contains few keywords:

- **dtcp** : (for Daily Tele-Communication Period) refers to extended pass
- **HFI** : refers to HFI instrument operations (when during the Commissioning of the Calibration and Performance Verification phases, labels are usually followed bu the activity label)
- **period**: refers to the different phases of the mission
- **test** : refers to End Of Life tests executed on the HFI
- **therm** : refers to satellite events that might have a thermal impact on the HFI
- **sat** : refers to operations on the satellite SerVice Module that might have an impact on the HFI data
- **slew** : refers to thruster activity
- **solar flare** : refers to all solar events as detected by a thermal fluctuation on the HFI bolometer plate

14/05/2009 13:12:00 EPC Vulcain Engine ignition 14/05/2009 16:58:36 HFI: LCLs nominal switch on 14/05/2009 17:30:59 HFI: go from startup to standby 14/05/2009 17:36:08 HFI: choose DPU FDIR mode Desynchro 14/05/2009 17:39:39 HFI: open dilution cooler valves 14/05/2009 18:48:52 HFI: setup REU Ns (40 Hz) and Fdiv (124) parameters 14/05/2009 18:52:33 HFI: set 4K cooler internal frequency at 40Hz 14/05/2009 19:05:45 HFI: activate the 6 nominal cernox thermometers 14/05/2009 19:08:51 HFI: synchronise the 4K cooler clock (External) 14/05/2009 19:23:47 HFI: set the 4K cooler amplitude demand at 2000 microns 14/05/2009 19:28:42 HFI: power on the nominal 4K getter heater 14/05/2009 19:35:31 HFI: start the 4K cooler compressors 15/05/2009 12:00:00 therm: stop the Focal Plane Unit 250K heating 15/05/2009 19:17:06 slew: OCM LEOP (MAN-01a) 16/05/2009 12:06:55 HFI: switch on all REU analog belts 16/05/2009 12:17:23 HFI: REU FPGA reset 16/05/2009 12:26:40 HFI: start the 4K cooler compressors 16/05/2009 12:31:16 HFI: set the JFET PID heaters at 110K 16/05/2009 12:49:26 HFI: set the channel compression parameters 16/05/2009 12:54:37 HFI: raw signal cycle on channels 16/05/2009 14:20:15 HFI: science data production starts 16/05/2009 14:48:30 HFI: channel setup [all channels] 16/05/2009 15:41:23 HFI: VI measurement [bolos, thermos, resistor] 16/05/2009 16:00:00 HFI: test end of slew 16/05/2009 17:51:43 HFI: set Cernox thermistor [4K-1.6K switch, 4K, 1.6K at 100K-200K] 17/05/2009 12:28:32 HFI: set Cernox thermistor [0.1K nominal at 100K-200K] 18/05/2009 00:00:00 period: end of LEOP / start of Commissioning phase 01/06/2009 21:36:00 therm: end of reflectors anticontamination 02/06/2009 16:40:20 HFI: set the JFET PID heaters at 130K 02/06/2009 17:00:06 HFI: REU hardware test 02/06/2009 17:20:06 HFI: start the 4K cooler compressors 02/06/2009 17:39:56 HFI: save REU configuration in EEPROM 03/06/2009 17:24:00 therm: SCS active cooldown starts 05/06/2009 17:28:18 slew: OCM-z (MAN-02a) 06/06/2009 18:19:21 HFI: set Cernox thermistor [4K-1.6K switch, 4K, 1.6K at 40K-100K] 09/06/2009 16:29:33 HFI: activate the 18K-4K heat switch nominal (repeated every day till 24/06) 09/06/2009 22:28:02 HFI: Single Event Upset 11/06/2009 21:15:00 HFI: set Cernox thermistor [0.1K nominal at 40K-100K] 12/06/2009 03:00:00 HFI: QEC1 at 100K 12/06/2009 05:08:20 HFI: QEC1 at 100K [end] 12/06/2009 15:26:07 HFI: set Cernox thermistor [4K-1.6K switch, 4K, 1.6K at 19K-40K] 12/06/2009 15:32:10 HFI: PID setup [4K-1.6K switch PID activated at max power] 12/06/2009 15:33:31 HFI: PID setup [4K PID nominal at max power] 15/06/2009 03:00:00 HFI: LFER_A_test 15/06/2009 04:54:52 HFI: LFER_A_test [end] 17/06/2009 16:46:58 slew: OCM-z touch-up (MAN-02b) 18/06/2009 18:29:57 HFI: LFER_A 19/06/2009 13:12:53 HFI: LFER_A [end] 22/06/2009 10:11:08 HFI: set Cernox thermistor [0.1K nominal at 19K-40K] 23/06/2009 11:00:34 HFI: set Cernox thermistor [4K-1.6K switch, 4K, 1.6K at 9K-19K] 24/06/2009 10:40:15 HFI: PID setup [4K-1.6K switch PID desactivated] 24/06/2009 10:40:35 HFI: PID setup [4K PID nominal] 24/06/2009 10:44:36 HFI: activate the 18K-4K heat switch nominal for LFI test [1st attempt] 24/06/2009 10:49:01 HFI: set the 4K cooler amplitude demand at 3500 microns 24/06/2009 10:52:48 HFI: set the dilution cooler flow to FNOM2 24/06/2009 11:18:58 HFI: activate the 18K-4K heat switch nominal for LFI test [5th and last attempt] 26/06/2009 23:00:00 HFI: desactivate the 18K-4K heat switch nominal 27/06/2009 13:34:34 HFI: set Cernox thermistor [0.1K, 1.6K, 4K and

4K-1.6K switch at <9K] 28/06/2009 12:22:14 HFI: channel setup [R & C] 28/06/2009 12:53:22 HFI: 4K cooler amplitude tuning 1/2 29/06/2009 09:38:15 HFI: 4K cooler amplitude tuning 2/2 29/06/2009 11:58:41 HFI: channel setup [all 1.6K thermometers] 29/06/2009 12:08:27 HFI: VI measurement [1.6K thermometers] 29/06/2009 12:21:10 HFI: set the channel compression parameters [4K thermometers] 29/06/2009 12:29:51 HFI: channel setup [all 4K thermometers] 29/06/2009 12:38:30 HFI: VI measurement [4K thermometers] 29/06/2009 13:28:40 HFI: channel setup [4K PID nominal thermometer] 29/06/2009 13:31:24 HFI: PID setup [4K PID nominal] 29/06/2009 13:41:00 HFI: channel setup [4K PID nominal thermometer] 29/06/2009 14:56:15 HFI: channel setup [1.6K PID nominal thermometer] 29/06/2009 14:58:58 HFI: PID setup [1.6K PID nominal] 29/06/2009 15:07:42 HFI: set Cernox thermistor [0.1K nominal at 3.5K-9K] 29/06/2009 15:45:02 HFI: PID setup [4K PID nominal] (8 times hourly) 29/06/2009 21:59:57 HFI: LFER-B 30/06/2009 04:16:13 HFI: LFER-B [end] 30/06/2009 09:35:52 HFI: set Cernox thermistor [0.1K nominal at 2.2K-3.5K] 30/06/2009 10:41:53 HFI: channel setup [1.6K PID nominal thermometer] 30/06/2009 10:43:58 HFI: PID setup [1.6K PID nominal] 30/06/2009 10:57:31 HFI: channel setup [0.1K thermometers] 30/06/2009 12:35:07 HFI: set Cernox thermistor [0.1K nominal at 1.4K-2.2K] 30/06/2009 13:42:12 HFI: PID setup [1.6K PID nominal] 30/06/2009 14:20:51 HFI: VI measurement [] 30/06/2009 18:09:59 HFI: set Cernox thermistor [0.1K nominal at <1.4 K] 30/06/2009 18:20:51 HFI: VI measurement [] 30/06/2009 19:10:01 HFI: QEC2 at 1K 30/06/2009 21:18:31 HFI: QEC2 at 1K [end] 01/07/2009 00:20:51 HFI: VI measurement 01/07/2009 04:20:51 HFI: VI measurement 01/07/2009 12:10:01 HFI: QEC3 at 300mK 01/07/2009 14:18:21 HFI: QEC3 at 300mK [end] 01/07/2009 14:18:31 HFI: channel setup [bolometers at 200mk] 01/07/2009 15:20:51 HFI: VI measurement [] 01/07/2009 19:20:51 HFI: VI measurement [] 01/07/2009 23:20:51 HFI: VI measurement [] 02/07/2009 04:20:51 HFI: VI measurement [] 02/07/2009 08:20:51 HFI: VI measurement [] 02/07/2009 09:24:41 HFI: channel setup [0.1K thermometers] 02/07/2009 10:35:26 HFI: channel setup [1.6K PID nominal thermometer] 02/07/2009 10:36:58 HFI: PID setup [1.6K PID nominal] 02/07/2009 11:15:46 slew: OCM Insertion (MAN-03a) 02/07/2009 12:34:36 HFI: set the dilution cooler flow to FNOM1 02/07/2009 13:58:16 HFI: set the channel compression parameters 03/07/2009 09:37:20 HFI: VI measurement [100mK bolometers] 03/07/2009 10:10:01 HFI: channel setup [bolometers at 100mk] 03/07/2009 10:17:56 HFI: set the dilution cooler flow to FMIN2 03/07/2009 12:50:00 HFI: PID setup [bolo PID activated] 03/07/2009 13:09:45 HFI: channel setup [thermo PID1R] 03/07/2009 13:10:58 HFI: PID setup [dilu PID activated] 03/07/2009 13:26:04 HFI: channel setup [1.6K PID nominal thermometer to 1.39 K] 03/07/2009 13:52:29 HFI: channel setup [1.6K PID nominal thermometer to 1.41 K] 03/07/2009 14:03:43 HFI: set the channel compression parameters 03/07/2009 16:15:01 HFI: QEC4 at 100mK 03/07/2009 18:23:21 HFI: QEC4 at 100mK [end] 03/07/2009 19:05:51 HFI: VI measurement [] 03/07/2009 20:05:26 HFI: PID setup [1.6K PID nominal] 03/07/2009 22:00:02 HFI: pre-RAW72 03/07/2009 23:13:08 HFI: pre-RAW72 [end] 04/07/2009 02:00:00 therm: aphelion 04/07/2009 09:43:13 HFI: channel setup [1.6K PID nominal thermometer to 1.39 K] 04/07/2009 09:45:27 HFI: PID setup [1.6K PID nominal] 04/07/2009 20:26:32 HFI: channel setup [1.6K PID nominal thermometer] 04/07/2009 22:30:01 HFI: CPVA_01 05/07/2009 01:55:49 HFI: CPVA_01 [end] 05/07/2009 10:47:08 HFI: channel setup [1.6K PID nominal thermometer to 1.35 K] 05/07/2009 11:28:57 HFI: channel setup [1.6K PID nominal thermometer to 1.34 K] 05/07/2009 13:25:03 HFI: IBTU_01 06/07/2009 09:47:49 HFI: IBTU_01 [end] 06/07/2009 09:58:51 HFI: channel setup [1.6K PID nominal thermometer to 1.33 K] 06/07/2009 12:38:33 HFI: channel setup [1.6K PID nominal thermometer to 1.35 K] 06/07/2009 13:15:21 HFI: channel setup [100mK PID redundant to 98.5 mK] 07/07/2009 11:30:14 HFI: VI measurement [resistor, bolometers] 07/07/2009 13:24:37 HFI: set the channel compression parameters 07/07/2009 14:20:03 HFI: IBTU_02 08/07/2009 10:42:49 HFI: IBTU_02 [end] 08/07/2009 11:04:39 HFI: channel setup [1.6K PID nominal thermometer to 1.39 K] 08/07/2009 11:16:02 HFI: PID setup [1.6K PID redundant at 200 microW] 08/07/2009 11:24:40 HFI: channel setup [100mK PID redundant to 100.0 mK] 08/07/2009 23:00:01 HFI: LFER-B 09/07/2009 17:39:59 HFI: LFER-B [end] 09/07/2009 19:30:01 HFI: IBTU_03 10/07/2009 00:00:00 Start of CPV phase 10/07/2009 15:08:03 HFI: IBTU_03 [end] 10/07/2009 16:00:01 HFI: PHTU_01 11/07/2009 00:01:47 HFI: PHTU_01 [end] 11/07/2009 10:24:00 HFI: channel setup [4K PID nominal thermometer at 4.73 K] 11/07/2009 10:26:00 HFI: PID setup [desactivation of 4K PID redundant] 11/07/2009 10:50:16 HFI: 4KFT (bis) 11/07/2009 12:49:50 HFI: 4KFT (bis) [end] 11/07/2009

12:59:35 HFI: channel setup [1.6K PID nominal thermometer to 1.37 K] 11/07/2009 13:05:25 HFI: PID setup [1.6K PID redundant desactivated] 11/07/2009 14:10:01 HFI: XTLK_01 12/07/2009 00:34:38 HFI: Single Event Upset 12/07/2009 00:42:05 HFI: XTLK_01 [end] 12/07/2009 01:00:02 HFI: RAW72_02 12/07/2009 07:00:10 HFI: RAW72_02 [end] 12/07/2009 11:53:22 HFI: DPU soft reboot 12/07/2009 12:18:13 HFI: back to nominal 12/07/2009 13:02:33 HFI: channel setup [capacitor] 12/07/2009 13:22:13 HFI: set the channel compression parameters 12/07/2009 13:31:21 HFI: 01TO_01 13/07/2009 01:30:01 HFI: 01TO_01 [end] 13/07/2009 11:12:32 HFI: channel setup [4K PID nominal thermometer at 4.80 K] 13/07/2009 13:03:50 HFI: channel setup [4K PID nominal thermometer at 4.66 K] 13/07/2009 13:26:23 HFI: channel setup [4K PID nominal thermometer at 4.64 K] 14/07/2009 09:50:15 HFI: PID setup [1.6K PID redundant to 200 microW] 14/07/2009 13:12:01 HFI: PID setup [1.6K PID redundant to 260 microW] 14/07/2009 13:14:22 HFI: channel setup [1.6K PID nominal thermometer to 1.38 K] 15/07/2009 09:16:02 slew: OCM Insertion touch-up (MAN-03b) 15/07/2009 09:46:54 HFI: channel setup [4K PID nominal thermometer at 4.66 K] 16/07/2009 09:21:29 HFI: PID setup [4K PID redundant to 0.8 mW] 16/07/2009 09:23:30 HFI: channel setup [4K PID nominal thermometer at 4.68 K] 17/07/2009 09:26:56 HFI: PID setup [4K PID redundant to 1.2 mW] 17/07/2009 09:30:08 HFI: channel setup [4K PID nominal thermometer at 4.70 K] 17/07/2009 11:12:09 HFI: channel setup [1.6K PID nominal thermometer to 1.39 K] 17/07/2009 11:23:02 HFI: channel setup [thermometers] 17/07/2009 14:00:01 HFI: LFER_02 18/07/2009 08:40:59 HFI: LFER_02 [end] 18/07/2009 09:51:16 HFI: channel setup [1.6K PID nominal thermometer to 1.40 K] 18/07/2009 19:10:19 therm: elephant 19/07/2009 11:09:09 HFI: channel setup [100mK PID redundant to 100.5 mK] 20/07/2009 10:59:16 HFI: PID setup [1.6K PID redundant desactivated] 20/07/2009 12:53:40 HFI: channel setup [1.6K PID nominal thermometer to 1.37 K] 21/07/2009 10:05:59 HFI: channel setup [4K PID nominal thermometer at 4.72 K] 21/07/2009 13:02:01 HFI: channel setup [bolo PID at 102.3 mK] 21/07/2009 13:11:48 HFI: PID setup [bolo PID] 22/07/2009 10:21:20 HFI: channel setup [1.6K PID nominal thermometer to 1.38 K] 22/07/2009 10:26:49 HFI: PID setup [bolo PID] 23/07/2009 09:23:42 HFI: decrease the 4K cooler amplitude demand to 3450 microns 23/07/2009 09:47:32 HFI: PID setup [4K PID redundant at max power] 23/07/2009 09:54:04 HFI: channel setup [4K PID nominal thermometer at 4.77 K] 23/07/2009 10:53:39 HFI: channel setup [4K PID nominal thermometer at 4.80 K] 24/07/2009 10:44:08 HFI: PID setup [bolo PID] 24/07/2009 22:30:00 HFI: 4KTO 25/07/2009 08:30:00 HFI: 4KTO [end] 27/07/2009 01:56:42 HFI: Single Event Upset 27/07/2009 09:21:28 HFI: PID setup [4K PID redundant to 0,84 mW] 27/07/2009 09:27:54 HFI: 4K memory HCT dump 27/07/2009 09:56:06 HFI: channel setup [bolo PID at 103.0 mK] 27/07/2009 13:01:32 HFI: set the channel compression parameters (increase of the HFI telemetry rate) 28/07/2009 09:31:34 HFI: channel setup [nominal bolo PID] 28/07/2009 09:38:16 HFI: channel setup [100mK PID redundant to 101.0 mK] 28/07/2009 12:30:34 HFI: channel setup [nominal bolo PID] 28/07/2009 12:46:13 HFI: channel setup [nominal bolo PID] 31/07/2009 16:00:00 HFI: SUNI_1_1 01/08/2009 00:00:00 HFI: SUNI_1_2 01/08/2009 10:55:00 HFI: SPIN day 1 : RPM@1.05 02/08/2009 12:20:00 HFI: SPIN day 2 : RPM@0.95 03/08/2009 11:53:37 HFI: SPIN day 3 : RPM@1.00 03/08/2009 11:53:37 HFI: SPIN day 4 : RPM@1.00 05/08/2009 09:36:01 slew: 1.7' slews test 06/08/2009 10:00:00 HFI: SUNI_2_1 06/08/2009 17:31:31 HFI: 4K Charge Regulator Unit anomalous shutdown 06/08/2009 18:00:00 HFI: SUNI_2_2 07/08/2009 12:20:01 HFI: set Cernox thermistor [4K-1.6K switch, 4K, 1.6K] 07/08/2009 13:40:43 HFI: 4K CDE software reset 07/08/2009 13:45:43 HFI: activate the 4K VCS 07/08/2009 13:46:23 HFI: select the harmonic forces 07/08/2009 13:47:56 HFI: set the 4K cooler amplitude demand at 2000 microns 07/08/2009 13:49:28 HFI: start the 4K cooler compressors 07/08/2009 13:53:23 HFI: set the 4K cooler amplitude demand at 2500 microns 07/08/2009 13:55:16 HFI: set the 4K cooler amplitude demand at 3000 microns 07/08/2009 13:58:50 HFI: 4K getter on 07/08/2009 17:54:56 HFI: stop the 4K cooler compressors 07/08/2009 17:57:22 HFI: desactivate the 4K VCS 07/08/2009 17:58:17 HFI: set the 4K cooler amplitude demand at 3500 microns 07/08/2009 17:59:41 HFI: start the 4K cooler compressors 07/08/2009 18:41:27 HFI: PID setup [4K PID redundant] 08/08/2009 10:05:25 HFI: stop the 4K cooler compressors 08/08/2009 10:07:41 HFI: activate the 4K VCS 08/08/2009 10:08:09 HFI: select the harmonic forces 08/08/2009 10:08:52 HFI: set the 4K cooler amplitude demand at 3450 microns 08/08/2009 10:10:26 HFI: start the 4K cooler compressors 08/08/2009 10:48:56 HFI: set Cernox thermistor [4K-1.6K switch, 4K, 1.6K] 08/08/2009 11:48:33 HFI: PID setup [dilu PID

activated] 08/08/2009 11:55:25 HFI: PID setup [4K PID redundant to 0,84 mW] 08/08/2009 14:05:36 period: first light survey 09/08/2009 03:58:53 star tracker switchover #1 11/08/2009 09:44:16 HFI: channel setup [100mK thermometers] 12/08/2009 10:24:46 HFI: channel setup [100mK PID redundant] 12/08/2009 10:29:52 HFI: PID setup [dilu PID] 12/08/2009 14:13:45 period: DPC survey#1 (ring#240) 14/08/2009 12:30:10 slew: orbit maintenance manoeuvre #1 18/08/2009 11:43:42 long ring #440 for CDMU patch day 1 18/08/2009 12:39:09 sat: CDMU patch (day 1) 18/08/2009 12:39:20 sat: CDMU patch (end of day 1) 19/08/2009 11:49:40 long ring #474 for CDMU patch day 2 19/08/2009 12:45:31 sat: CDMU patch (day 2) 19/08/2009 12:45:34 sat: CDMU patch (end of day 2) 20/08/2009 11:53:46 long ring #509 for CDMU patch day 3 20/08/2009 12:45:32 sat: CDMU patch (day 3) 20/08/2009 12:45:36 sat: CDMU patch (end of day 3) 21/08/2009 11:56:03 long ring #544 for CDMU patch 21/08/2009 14:18:48 HFI: clock resynchronisation 22/08/2009 09:36:51 dtcp: transition to 3 h DTCP duration 31/08/2009 12:09:14 long ring #897 to allow the execution of the ACMS warm reset 31/08/2009 13:40:00 thrusters catbed heaters are switched off by error 31/08/2009 13:40:01 sat: FOG telemetry is disabled by error 31/08/2009 13:41:05 long ring #898 to allow the execution of the ACMS warm reset 04/09/2009 15:01:00 thurster under/over performed 11/09/2009 21:00:41 slew: orbit maintenance manoeuvre #2 16/09/2009 20:31:41 thrusters catbed heaters are switched back on 18/09/2009 19:06:15 planet: HFI Crab scan#1 20/09/2009 19:36:00 dtcp: extra pass CEB 20/10/2009 23:44:24 therm: HFI elephant LONG deltaT>10uK 22/10/2009 19:34:56 planet: HFI Mars scan#1 24/10/2009 11:01:39 therm: HFI elephant LONG deltaT>10uK 25/10/2009 15:30:49 planet: HFI Jupiter scan#1 28/10/2009 23:06:00 thurster under/over performed 01/11/2009 00:41:04 planet: HFI Neptune scan# 1 20/11/2009 18:52:25 long ring #3589 (29 hours) : no slew due to MTL uplink problem 21/11/2009 23:39:54 slew : resumption of SL after the MTL problem 22/11/2009 19:48:41 slew to SGR position 23/11/2009 08:47:54 slew to catchup 23/11/2009 19:48:10 SGR (end): back to nominal scanning law 25/11/2009 05:56:00 HFI: 1.6K stage event 26/11/2009 14:32:00 thurster under/over performed 04/12/2009 17:49:29 slew: orbit maintenance manoeuvre #3 05/12/2009 09:43:53 planet: HFI Uranus scan# 1 16/12/2009 20:42:11 sat: FOG telemetry is enabled back 21/12/2009 19:59:54 HFI: set the channel compression parameters 22/12/2009 11:46:18 dtcp: extra pass 03/01/2010 00:00:00 therm: perihelia 04/01/2010 00:25:49 planet: HFI Saturn scan#1 11/01/2010 19:16:32 star tracker switchover #2 15/01/2010 21:57:45 slew: orbit maintenance manoeuvre #4 25/01/2010 21:16:41 sat: transponder always on 08/02/2010 20:51:32 period: DPC survey#2 (ring#5721) 26/02/2010 12:43:37 star tracker switchover #3 26/02/2010 23:02:49 slew: orbit maintenance manoeuvre #5 06/03/2010 05:04:43 planet: HFI Crab scan#2 01/04/2010 06:41:00 thurster under/over performed 02/04/2010 13:48:21 therm: major elephant 05/04/2010 10:00:00 solar flare: geomagnetic storm 10/04/2010 10:36:35 planet: HFI Mars scan#2 26/04/2010 17:55:37 slew: orbit maintenance manoeuvre #6 29/04/2010 17:34:58 therm: SCS TSA setpoint increase 06/05/2010 17:02:08 therm: SCS TSA setpoint increase 13/05/2010 16:30:13 therm: SCS TSA setpoint increase 17/05/2010 17:51:09 planet: HFI Neptune scan# 2 12/06/2010 01:00:00 solar flare 12/06/2010 01:57:16 planet: HFI Saturn scan#2 24/06/2010 18:31:09 therm: SCS TSA setpoint increase 30/06/2010 19:00:53 planet: HFI Uranus scan#2 03/07/2010 20:01:43 planet: HFI Jupiter scan#2 06/07/2010 11:00:00 therm: aphelion 14/07/2010 20:45:50 dtcp: extra pass 15/07/2010 18:13:43 therm: SCS TSA setpoint increase 18/07/2010 04:28:00 thurster under/over performed 21/07/2010 21:08:44 therm: moon transit 22/07/2010 00:42:59 therm: moon transit (end) 24/07/2010 16:36:11 therm: HFI elephant LONG deltaT>10uK 29/07/2010 17:45:52 therm: SCS TSA setpoint increase 03/08/2010 19:00:00 solar flare: possible geomagnetic storm 11/08/2010 10:14:37 long ring #11149 for SCS switchover 11/08/2010 11:00:00 therm: SCS switchover 11/08/2010 11:00:30 HFI: PID setup [1.6K PID nominal and 4K PIDs desactivated] 11/08/2010 17:17:50 HFI: deselect all 4K harmonics for VCS 11/08/2010 18:50:15 HFI: select all 4K harmonics for VCS 11/08/2010 18:52:44 HFI: PID setup [1.6K PID nominal and 4K PIDs reactivated] 11/08/2010 21:34:10 dtcp: extra pass CEB 12/08/2010 00:06:59 HFI: PID setup [4K PID redundant set to 1.14 mW] 12/08/2010 19:27:28 period: DPC survey#3 (ring#11195) 13/08/2010 23:59:21 slew to interleaved pointings for survey#3 14/08/2010 11:00:00 solar flare 16/08/2010 18:00:09 slew: orbit maintenance manoeuvre #7 18/08/2010 08:35:00 solar flare 25/08/2010 17:51:58 HFI: 4K memory HCT dump 18/09/2010 18:28:04 planet: HFI Crab scan#3 04/10/2010 04:25:00 HFI:

1.6K stage event 04/10/2010 04:57:05 therm: HFI elephant SHORT deltaT>10uK 06/10/2010 19:00:46 dtcp: extra pass CEB 11/10/2010 13:26:47 long ring #13333: manoeuvre failed 03/11/2010 08:11:34 planet: HFI Neptune scan#3 04/11/2010 13:20:14 therm: change of the DPU2 thermal control 04/11/2010 19:19:00 dtcp: extra pass NNO 11/11/2010 12:45:00 therm: SCS TSA setpoint increase 21/11/2010 03:02:51 therm: HFI elephant LONG deltaT>10uK 24/11/2010 11:23:01 long ring #14627 for star tracker tests 24/11/2010 12:29:29 star tracker switchover for intercalibration test (STR1->STR2) 24/11/2010 20:23:53 slew back 25/11/2010 17:02:45 long ring #14653 for star tracker tests 25/11/2010 17:59:37 star tracker switchover STR2->STR1 26/11/2010 01:55:21 slew back to nominal scanning strategy 27/11/2010 20:20:00 solar flare 02/12/2010 13:21:13 slew: orbit maintenance manoeuvre #8 06/12/2010 20:38:00 planet: HFI Jupiter scan#3 10/12/2010 14:55:44 planet: HFI Uranus scan#3 15/12/2010 08:19:00 thurster under/over performed 15/12/2010 10:30:00 thurster under/over performed 22/12/2010 16:33:14 HFI: Single Event Upset 23/12/2010 15:44:53 therm: SCS TSA setpoint increase 03/01/2011 19:00:00 therm: perihelia 18/01/2011 05:25:24 planet: HFI Saturn scan#3 24/01/2011 13:20:09 therm: SCS warm radiator warming 24/01/2011 17:28:00 dtcp: extra pass CEB 28/01/2011 02:00:00 solar flare 31/01/2011 14:06:49 slew: orbit maintenance manoeuvre #9 01/02/2011 13:31:33 therm: SCS TSA setpoint increase 08/02/2011 20:55:48 period: DPC survey#4 (ring#16692) 10/02/2011 02:48:02 HFI: 1.6K stage event 15/02/2011 06:00:00 solar flare: X ray solar flare 18/02/2011 00:00:00 solar flare: X ray solar flare 24/02/2011 14:05:28 therm: SCS TSA setpoint increase 28/02/2011 23:20:41 slew: acceleration for Crab scan 06/03/2011 04:12:44 planet: HFI Crab scan#4 07/03/2011 21:00:00 solar flare: coronal mass ejection 10/03/2011 19:44:00 dtcp: extra pass CEB 15/03/2011 17:42:31 therm: SCS desorption power gap jump 15/03/2011 20:35:00 dtcp: extra pass 18/03/2011 15:15:00 dtcp: long pass (5h30mn) 21/03/2011 03:30:00 solar flare: radiation event 21/03/2011 21:10:17 slew: orbit maintenance manoeuvre #10 31/03/2011 21:02:52 therm: SCS TSA setpoint increase 07/04/2011 20:38:16 therm: SCS TSA setpoint increase 14/04/2011 21:03:33 therm: SCS TSA setpoint increase 21/04/2011 20:33:20 therm: SCS TSA setpoint increase 10/05/2011 16:48:13 therm: SCS TSA setpoint increase 20/05/2011 14:18:21 planet: HFI Neptune scan#4 04/06/2011 22:00:00 solar flare: geomagnetic storm 07/06/2011 07:00:00 solar flare: solar proton enhancement 23/06/2011 04:55:03 thurster under/over performed 29/06/2011 17:03:39 planet: HFI Saturn scan#4 04/07/2011 15:00:00 therm: aphelion 05/07/2011 22:00:17 planet: HFI Uranus scan#4 25/07/2011 17:38:00 slew: orbit maintenance manoeuvre #11 27/07/2011 16:51:00 on board mass properties update 29/07/2011 17:13:00 slew to survey#5 29/07/2011 17:43:32 period: DPC survey#5 (ring#21721) 02/08/2011 07:00:00 solar flare: M1 class 03/08/2011 21:09:40 planet: HFI Jupiter scan#4 04/08/2011 04:30:00 solar flare 04/08/2011 15:55:38 therm: SCS TSA setpoint increase 08/08/2011 16:53:00 SGR: scanning law is interrupted 08/08/2011 17:32:00 slew back 08/08/2011 18:00:00 solar flare: X7 class 08/08/2011 18:44:00 planet: HFI Jupiter scan#4 (bis) 09/08/2011 01:54:00 slew to the catchup position 09/08/2011 08:00:00 solar flare 09/08/2011 17:23:00 SGR (end): back to nominal scanning law 06/09/2011 02:20:00 solar flare: M5.3 06/09/2011 23:00:00 solar flare: X2.1 13/09/2011 09:34:22 planet: HFI Crab scan#5 17/09/2011 08:00:00 solar flare: magnetic storm 20/09/2011 09:43:00 slew setting-up the second crab scan 20/09/2011 10:41:38 planet: HFI Crab scan#5 (bis) 21/09/2011 16:43:41 planet: HFI Crab scan#6 21/09/2011 18:33:00 dtcp: extra pass 22/09/2011 12:00:00 solar flare: complexe event 24/09/2011 00:42:34 slew back to survey 5 scanning strategy 26/09/2011 12:29:45 slew : station keeping manoeuvre half failed 04/10/2011 12:35:07 slew: orbit maintenance manoeuvre #12 bis 11/10/2011 12:35:13 HFI: temperature steps on bolometer PID 12/10/2011 10:30:00 HFI: EOL-Fast VI at 100mK 22/10/2011 14:00:00 solar flare: small event 27/10/2011 12:38:38 therm: SCS TSA setpoint increase 04/11/2011 00:00:00 solar flare: X2 class 07/11/2011 09:00:00 HFI : pre-EOL-LFER-1 07/11/2011 11:06:54 HFI : pre-EOL-LFER-1 [end] 08/11/2011 10:42:00 HFI: EOL-IBTU 08/11/2011 16:10:03 HFI: EOL-IBTU [end] 14/11/2011 09:00:00 HFI: 2nd pre-EOL-LFER-1 14/11/2011 11:08:42 HFI: 2nd pre-EOL-LFER-1 [end] 14/11/2011 23:58:33 slew: beginning of dwell duration compression phase 18/11/2011 00:00:00 HFI: EOL-LFER-1 20/11/2011 14:33:42 HFI: EOL-LFER-1 [end] 26/11/2011 07:00:00 solar flare: Radiation storm and Coronal Mass Ejection 28/11/2011 17:10:00 dtcp: extra pass 07/12/2011 17:00:00 spinup test at 1.4RPM 08/12/2011 10:00:00 planet: HFI Mars scan @ 1.4 RPM 09/12/2011 16:43:00 star tracker unhealthy 16/12/2011 18:35:00 slew: back to

scanning law 17/12/2011 18:00:00 planet: HFI Mars scan#3 23/12/2011 15:10:06 HFI: He3 flow rate 0 -> 1 25/12/2011 14:45:16 HFI: HFI: PID setup [1.6K PID redundant add 153.4 uW] 25/12/2011 20:00:00 solar flare: C-class 27/12/2011 11:42:10 HFI: temperature steps on the bolometer plate II 27/12/2011 13:48:45 HFI: temperature steps on the bolometer plate II [end] 29/12/2011 14:24:29 HFI: He3 flow rate 1 -> 2 02/01/2012 13:58:00 HFI: He3 flow rate 2 -> 3 03/01/2012 14:20:19 HFI: temperature steps on bolo plate III (1st part) 04/01/2012 13:52:00 HFI: He3 flow rate 3 -> 4 04/01/2012 16:00:00 HFI: temperature steps on bolo plate III (2nd part) 06/01/2012 00:00:00 HFI: temperature steps on bolo plate III (2nd part) [end] 07/01/2012 14:10:52 HFI: He3 flow rate 4 -> 5 08/01/2012 07:20:00 slew to Jupiter deep annuli scan 09/01/2012 14:23:36 HFI: He3 flow rate 5 -> 6 10/01/2012 04:20:00 planet: HFI Jupiter scan 11/01/2012 14:48:04 HFI: He3 flow rate 6 -> 7 13/01/2012 15:04:33 HFI: HFI: PID setup [1.6K PID and dilu PID desactivated] 14/01/2012 16:00:00 period: end of HFI nominal operations 16/01/2012 15:00:00 HFI channel setup [100mK thermometers] 16/01/2012 15:00:12 HFI: bolo plate at 110mK 16/01/2012 15:45:09 HFI: bolo plate at 300mK 17/01/2012 14:13:54 HFI: set Cernox thermistor [0.1K nominal at 1.4K] 18/01/2012 15:20:10 HFI: set the channel compression parameters 18/01/2012 16:15:11 HFI: EOL-Fast VI at 300 mK 19/01/2012 14:30:52 HFI: channel setup [bolometers] 20/01/2012 19:58:08 HFI: EOL-RAW54 at 300mK 21/01/2012 13:29:58 HFI: EOL-RAW54 at 300mK [end] 22/01/2012 00:18:00 therm: loss of satellite thermal control 22/01/2012 15:00:00 CDMU PM-A reset 22/01/2012 22:59:58 HFI: DPU soft reboot 23/01/2012 05:00:00 solar flare: major one 25/01/2012 14:45:00 HFI: set the channel compression parameters 27/01/2012 19:00:00 solar flare 30/01/2012 21:53:00 period: slew to survey#6 07/02/2012 00:00:00 slew: large orbit correction manœuvre 10/02/2012 16:30:00 HFI: EOL-Fast VI at 600 mK 14/02/2012 14:20:00 therm: CDMU PM-A switch over 20/02/2012 10:00:00 HFI: set the channel compression parameters (EOL#0) 20/02/2012 14:57:00 slew: touchup manœuvre 21/02/2012 15:00:00 HFI: set the channel compression parameters (EOL#1) 21/02/2012 15:16:00 HFI: set the channel compression parameters (EOL#2) 22/02/2012 16:50:00 HFI: set the channel compression parameters (EOL#3) 23/02/2012 15:20:00 HFI: set the channel compression parameters (EOL#4)

LFI design, qualification, and performance

Overview

The Planck-LFI instrument is an array of 11 radiometric receivers in the Ka, Q and V bands, with centre frequencies close to 30, 44 and 70 GHz. The exact centre frequencies for each receiver are reported in #planck2011-1-4 [Planck early results. The heart of the LFI instrument is a compact, multi-frequency array of differential receivers with ultra-low-noise amplifiers based on cryogenic indium phosphide (InP) high-electron-mobility transistors (HEMTs). To minimise power dissipation in the focal plane unit, which is cooled to 20 K, the radiometers are split into two subassemblies connected by a set of waveguides, as shown in figure 1, left panel. [[File:lfi_instrument.jpg|thumb|center|600px|Figure 1. Left Panel: the LFI instrument with main thermal stages, focal plane, waveguides and sorption cooler piping highlighted. Right Panel: Labelling of feed horns on the LFI focal plane. [1]]

The LFI horns are situated in a ring around the HFI, see figure 1 – right panel. Each horn collects radiation from the telescope and feeds it to one or more detectors. The radiometer design is driven by the need to suppress 1/f-type noise induced by gain and noise temperature fluctuations in the amplifiers, which would be unacceptably high for a simple total power system. A differential pseudo-correlation scheme is adopted, in which signals from the sky and from a black-body reference load are combined by a hybrid coupler, amplified in two independent amplifier chains, and separated out by a second hybrid (figure 2). The sky and the reference load power can then be measured and differenced. Since the reference signal has been subject to the same gain variations in the two amplifier chains as the sky signal, the true sky power can be recovered. Insensitivity to fluctuations in the back-end amplifiers and detectors is realized by switching phase shifters at ~8 kHz synchronously in each amplifier chain. The rejection of 1/f noise as

well as the immunity to other systematic effects is optimised if the two input signals are nearly equal. For this reason the reference loads are cooled to ~4 K by mounting them on the 4-K structure of the HFI. In addition, the effect of the residual offset (< 2 K in nominal conditions) is reduced by introducing a gain modulation factor in the on-board processing to balance the output signal (#Seiffert2002). The differencing receiver greatly improves the stability of the measured signal.

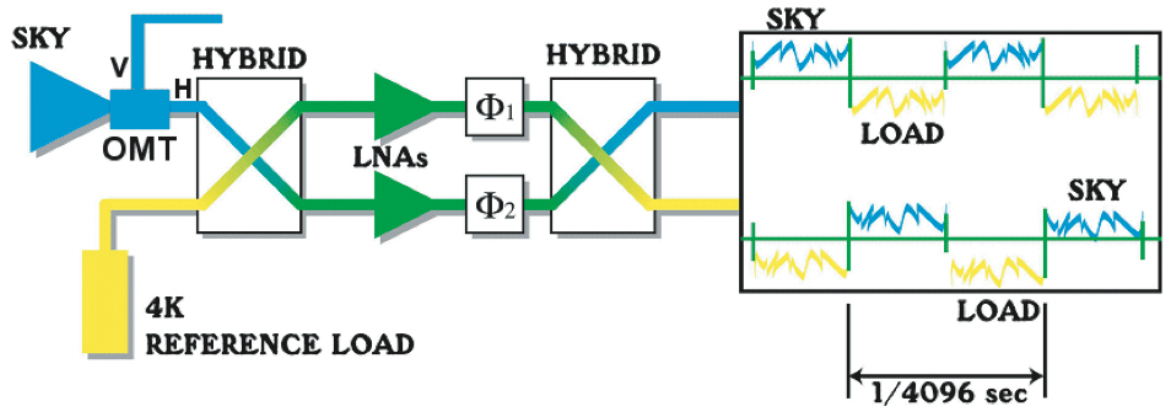

Figure 2. Schematic of the LFI front-end radiometer. The front-end unit is located at the focus of the Planck telescope, and comprises: dual profiled corrugated feed horns; low-loss (~0.2 dB), wide-band (> 20%) ortho-mode transducers; and radiometer front-end modules with hybrids, cryogenic low noise amplifiers, and phase switches.

First assessment of the Low Frequency Instrument in-flight performance]]; for simplicity, here we will refer to the three channels using their nominal centre frequency. A detailed description of the LFI instrument is given in #bersanelli2010 [Planck pre-launch status: Design and description of the Low Frequency Instrument [2]], and references therein.

The LFI description

The LFI instrument (see figure 1 above) consists of a 20 K focal plane unit hosting the corrugated feed horns, the orthomode transducers (OMTs) and the receiver front-end modules (FEMs). Forty four composite waveguides #darcangelo2009a are interfaced with three conical thermal shields and connect the front-end modules to the warm (~300 K) back-end unit (BEU) containing a further radio frequency amplification stage, detector diodes and all the electronics for data acquisition and bias supply.

Best LFI noise performance is obtained with receivers based on InP High Electron Mobility Transistor (HEMT) low noise amplifiers (LNAs) for minimal power dissipation and best performance. To further minimise power consumption in the focal plane, the radiometers are split into two sub-assemblies connected by waveguides, one located at the telescope focal area, the other on the 300 K portion of the Planck satellite. These design features allow the entire front-end LNAs dissipation to be <0.55 W, which enables the active cooling of the focal assembly. This is achieved with a vibration-less hydrogen sorption cooler, which also provides 18 K pre-cooling to the HFI helium J-T cooler. Two sorption cooler units are included in the flight hardware.

As shown schematically in Figure 3 below, the LFI consists of the following subsystems:

- Radiometer Array Assembly (RAA)
- Sorption Cooler Subsystem (SCS)
- Radiometer Electronics Box Assembly (REBA)

The RAA includes the Front End Unit (FEU) and the Back End Unit (BEU), connected via waveguides. The FEU is located at the focus of the telescope, as one component of the joint LFI/HFI focal assembly (see sections below). The BEU is mounted on the top of the Planck service module (SVM). The REBA (Radiometer Electronics Box

Assembly) and the warm parts of the Sorption Cooler System (SCS) are located on one of the lateral panels of the SVM. The FEU and the Sorption Cooler Compressor (SCC) are connected by concentric stainless steel tubes. The smaller tube carries hydrogen at ~60 atmospheres from the cooler compressors to the FEU, while the larger tube returns the hydrogen at ~0.3 atmospheres. These units are described in following sections and in the LFI Appendix, the SCS is described in details in the Sorption Cooler section. All LFI units are linked together by the LFI harness, which also connects to the spacecraft interface.

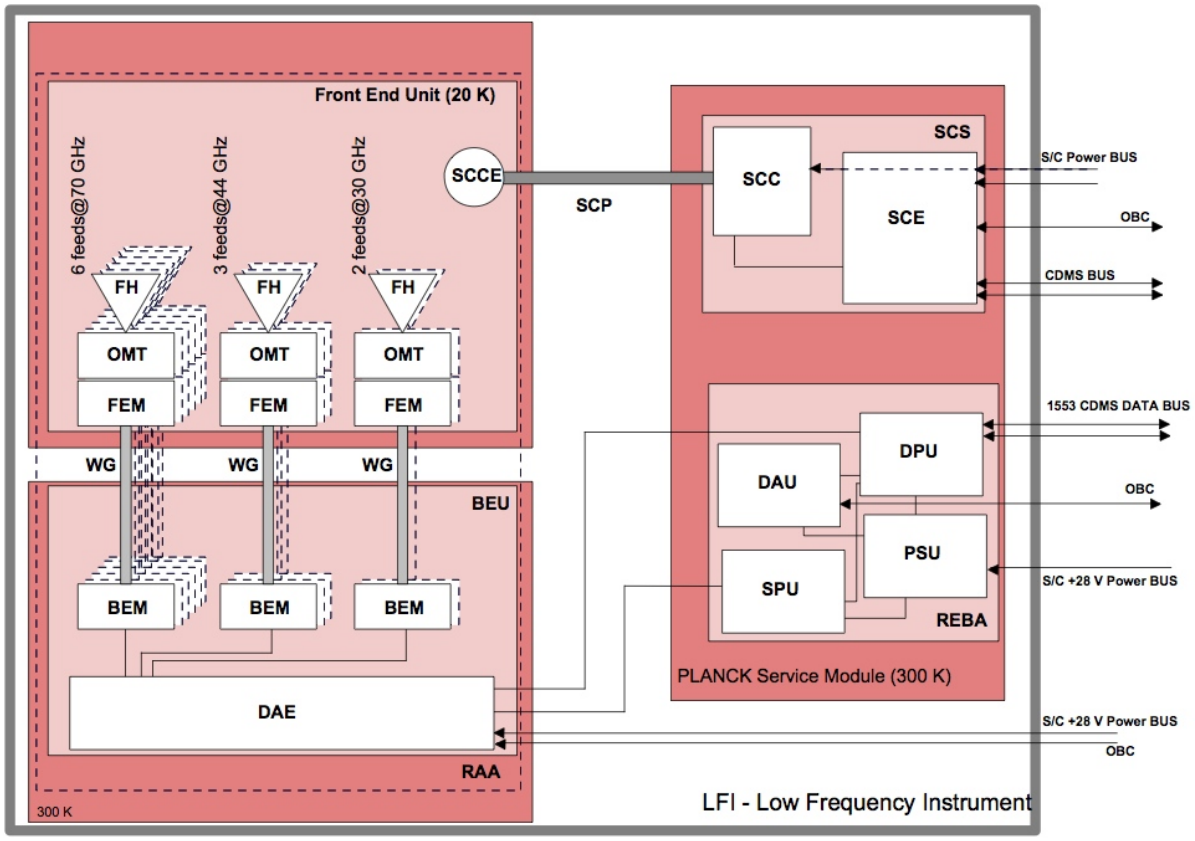

Figure 3. Block Diagram of LFI

Radiometer Array Assembly (RAA)

The Radiometer Array Assembly (RAA) consists of two main units (the front end unit, FPU and the Back End Unit, BEU), connected by a set of waveguides. The Focal Plane Unit (FPU) is the heart of the LFI instrument and it contains the feed array and associated orthomode transducers (OMTs) and FEMs, all cooled to 20 K by the sorption cooler. The FPU comprises a set of 11 modules, which are mounted on a mechanical support which meets the thermo-mechanical requirements of the instrument and adds thermal inertia. The BEU comprises the radiometer Back End Modules (BEM) and the Data Acquisition Electronics (DAE), which are connected by an internal harness. The HFI Unit is located inside the LFI FPU and supported by the LFI structure. The LFI structure gives the mechanical and thermal interface to the HFI unit with the proper stiffness and thermal de-coupling. The LFI structure also guarantees the proper alignment of the HFI detector with the telescope focal plane.

The time scale of the stability of the receiver is driven by the 1 rpm rotation speed of the spacecraft, which requires a very low 1/f-noise or gain variation of the low noise amplifiers and other components. The LFI uses a pseudo-correlation receiver concept (Figure 4 below). This radiometer concept is chosen to maximise the stability of the instrument by reducing the effect of non-white noise generated in the radiometer itself. In this scheme, the difference between the inputs to each of the chains (the signal from the telescope and that from a reference black body respectively) is continuously being observed. To remove the effect of instability in the back-end amplifiers and

detector diodes, it is necessary to switch the signal detected at the diodes at high rate. The signals from the sky and from a reference load are combined by a hybrid coupler, amplified in two independent amplifier chains, and separated out by another hybrid. The sky and the reference load power can then be measured and differenced. Since the reference signal has been subject to the same gain variations in the two amplifier chains as the sky signal, the true sky power can be recovered. The differencing receiver greatly improves the stability if the two input signals are almost equal, at a cost of a factor of $\sqrt{2}$in sensitivity compared to a perfectly stable total-power radiometer with the same noise temperature and bandwidth. This radiometer concept is capable of greatly reducing the knee frequency. We define as Radiometer Chain Assembly (RCA, see Figure 4) each functional unit from the feed horn to the BEM. The RAA therefore includes a set of 11 RCAs and the Data Acquisition Electronics (see also Figure 3 above), all mounted on a suitable mechanical structure. Although there are differences in the details of the radiometer chains at different frequencies, their overall configuration is similar, and a general description of its design is provided in this section. Planck LFI has 11 Radiometer Chain Assembly (RCA). Each RCA is constituted by feed horn and FEM in the FEU (at 20 K), BEM (at 300 K) in the BEU and four waveguides that connect each FEM-BEM couple. The frequency distribution of the RCA is the following:

- 2 RCAs at 30 GHz;
- 3 RCAs at 44 GHz;
- 6 RCAs at 70 GHz.

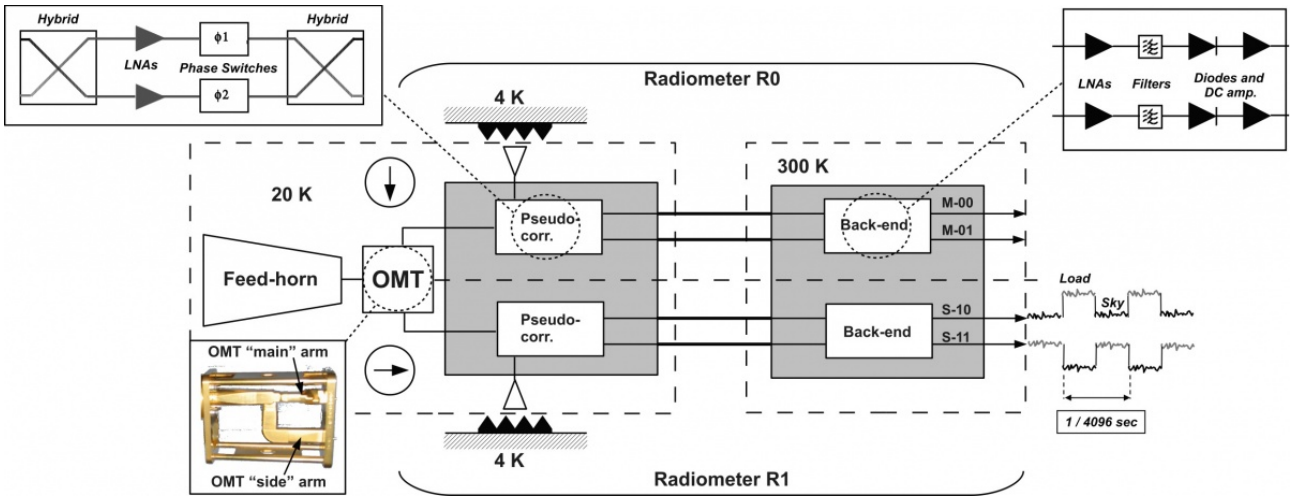

Figure 4. A complete RCA from feed-horn to analog voltage output. The insets show the OMT, the details of the 20 K pseudo-correlator and of the back-end radio-frequency amplification, low-pass filtering, detection and DC amplification.

Radiometer Chain Assembly (RCA)

Every RCA consists of two radiometers, each feeding two diode detectors (see Figure 4 above), for a total of 44 detectors. The 11 RCAs are labelled by a numbers from 18 to 28 as outlined in Figure 1, right panel.

Figure 4 provides a more detailed description of each radiometric receiver. In each RCA, the two perpendicular linear polarisation components split by the OMT propagate through two independent pseudo-correlation differential radiometers, labelled as *M* or *S* depending on the arm of the OMT they are connected to (*Main* or *Side*, see lower-left inset of Figure 4).

In each radiometer the sky signal coming from the OMT output is continuously compared with a stable 4 K blackbody reference load mounted on the external shield of the HFI 4 K box #valenziano2009. After being summed by a first hybrid coupler, the two signals are amplified by ~30 dB, see upper-left inset of Figure 4. The amplifiers were selected for best operation at low drain voltages and for gain and phase match between paired radiometer legs, which is crucial for good balance. Each amplifier is labelled with codes *1*, *2* so that the four outputs of the LNAs can be named with the sequence: *M1*, *M2* (radiometer *M*) and *S1*, *S2* (radiometer *S*). Tight mass and power constraints

called for a simple design of the Data Acquisition Electronics (DAE) box so that power bias lines were divided into five common-grounded power groups with no bias voltage readouts; only the total drain current flowing through the front-end amplifiers is measured and is available to the house-keeping telemetry (this design has important implications for front-end bias tuning, which depends critically on the satellite electrical and thermal configuration and was repeated at all integration stages, during on-ground and in-flight satellite tests). A phase shift alternating between $0^{\circ}$and 180°at the frequency of 4096 Hz is applied in one of the two amplification chains and then a second hybrid coupler separates back the sky and reference load components that are further amplified and detected in the warm BEU, with a voltage output ranging from -2.5 V to +2.5 V.

Each radiometer has two output diodes which are labelled with binary codes *00*, *01* (radiometer *M*) and *10*, *11* (radiometer *S*), so that the four outputs of each radiometric chain can be named with the sequence: *M-00*, *M-01*, *S-10*, *S-11*.

After detection, an analog circuit in the DAE box removes a programmable offset in order to obtain a nearly null DC output voltage and a programmable gain is applied to increase the signal dynamics and optimally exploit the ADC input range. After the ADC, data are digitally down-sampled, re-quantised and compressed in the REBA according to a scheme described in #herreros2009, maris2009, before preparing telemetry packets. On ground, telemetry packets are converted to sky and reference load time ordered data after calibrating the ADU samples into volt considering the applied offset and gain factors.

To first order, the mean differential power output for each of the four receiver diodes can be written as follows #seiffert2002, mennella2003, bersanelli2010 [Planck pre-launch status: Design and description of the Low Frequency Instrument [3]]:

where $G_{\rm tot}$is the total gain, $k$is the Boltzmann constant, $\beta$the receiver bandwidth and $a$is the diode constant. $T_{\rm sky}$ and $T_{\rm ref}$are the average sky and reference load antenna temperatures at the inputs of the first hybrid and $T_{\rm noise}$is the receiver noise temperature.
The gain modulation factor #mennella2003, planck2011-1-6 [Planck early results. The Low Frequency Instrument data processing [1]], r, is defined by:

and is used to balance (in software) the temperature offset between the sky and reference load signals and minimise the residual 1/ $f$noise in the differential datastream. This parameter is calculated from the average uncalibrated total power data using the relationship:

where $< V_{\rm sky} >$and $< V_{\rm ref} >$are the average sky and reference voltages calculated in a defined time range. The white noise spectral density at the output of each diode is essentially independent from the reference-load absolute temperature and is given by:
If the front-end components are not perfectly balanced, then the separation of the sky and reference load signals after the second hybrid is not perfect and the outputs are mixed. First-order deviations in white noise sensitivity from the ideal behaviour are caused mainly by noise temperature and phase-switch amplitude mismatches. Following the notation used in #seiffert2002, we define ϵ_{Tn}, the imbalance in front end noise temperature, and $\epsilon_{A1}$and ϵ_{A2}, the imbalance in signal attenuation in the two states of the phase switch. Equation above for the two diodes of a slightly imbalanced radiometer then becomes

which is identical for the two diodes apart from the sign of the term , representing the phase switch amplitude imbalance. This indicates that the isolation loss caused by this imbalance generates an anti-correlation between the white noise levels of the single-diode data streams. For this reason, the LFI scientific data streams are obtained by averaging the voltage outputs from the two diodes in each radiometer:

where $w_1$and $w_2$are inverse-variance weights calculated from the data as discussed in #planck2011-1-6. This way, the diode-diode anti-correlation is cancelled, and the radiometer white noise becomes

In Equations above, , while $\alpha$is a term given by:

See Diode Combination section for the details of the diode combination procedure.

In Figure 5 below we show a close-up of the two front end modules of an RCA with the four phase switches which are labelled with the four letters *A* and *B* (main arm), *C* and *D* (side arm). Each phase switch is characterised by two states: state 0 (no phase shift applied to the incoming wave) and state 1 (180° phase shift applied) and can either stay fixed in a state or switch at 4 kHz between the two states.

Phase switches are clocked and biased by the DAE and their configuration can be programmed via telecommand. In order to simplify the instrument electronics, phase switches are configured and operated in pairs: *A/C* and *B/D*. This means that if phase switches *A* and *C* are switching at 4 kHz then *B* and *D* are fixed both in the same state (either 0 or 1). This simplification, required during the design phase to comply with mass and power budgets, comes at the price of loosing some setup redundancy.

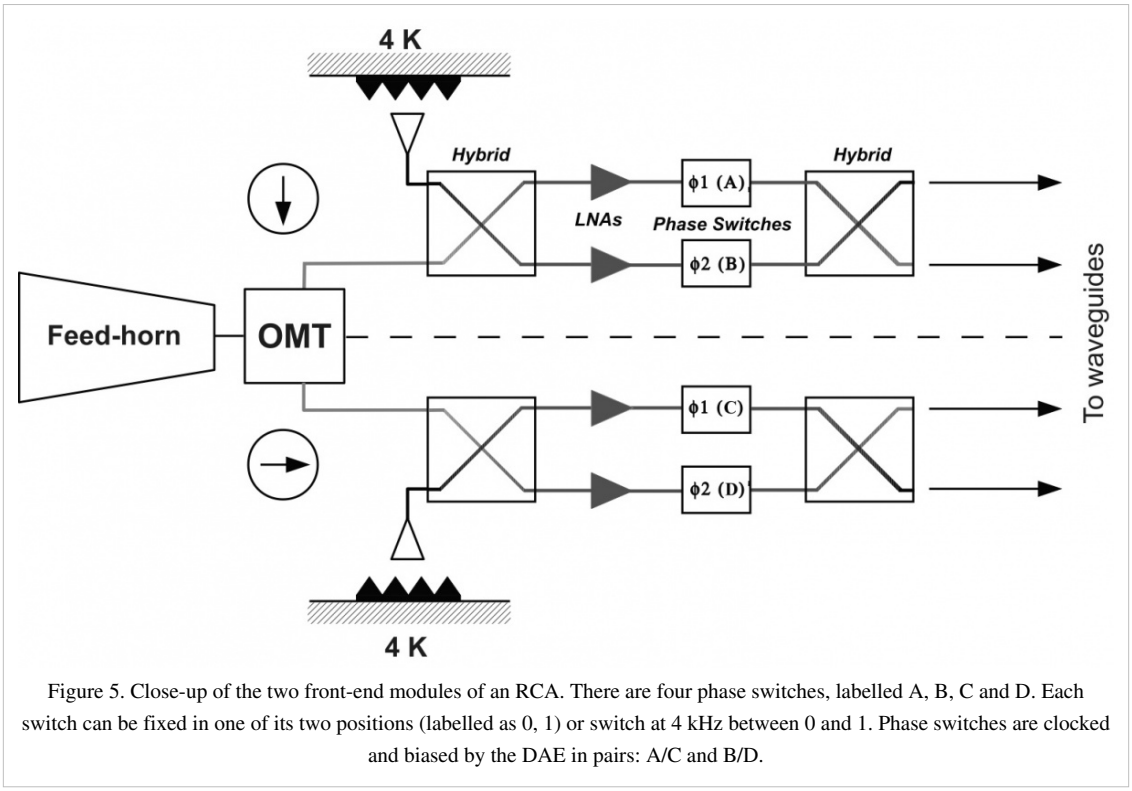

Figure 5. Close-up of the two front-end modules of an RCA. There are four phase switches, labelled A, B, C and D. Each switch can be fixed in one of its two positions (labelled as 0, 1) or switch at 4 kHz between 0 and 1. Phase switches are clocked and biased by the DAE in pairs: A/C and B/D.

Feed Horns (FH)

Dual profiled corrugated horns have been selected at all LFI frequencies as the best design in terms of shape of the main lobe, level of the side lobes, control of the phase centre, and compactness. Details of the design, flight model and tests of Planck-LFI feed horns can be found in #villa2009 and in the corresponding Appendix section.

OrthoMode Transducers (OMT)

The Ortho–Mode Transducer (OMTs) separates the radiation collected by the feed horn in two orthogonal polarisation components. It consists of a circular to square waveguide transition (directly connected to the FH), a square waveguide section and two separate rectangular waveguide (the through and side arms, which separate and pick up the orthogonal polarisation, connected with the FEU). On the side arms is always present a 90 degrees bend, while a twist is also necessary on the main (30 and 44 GHz) and side (70 GHz) arm, in order to math the FEU polarisation.

The details of the flight models and measurements of the Planck LFI ortho-mode transducers can be found in #darcangelo2009b and in the corresponding Appendix section.

Front End Modules (FEM)

Front End Modules are located in the FPU, just in cascade of the Feed Horn and the Ortho Mode Transducers. 70 GHz FEMs are mounted onto the inner wall of the mainframe (the wall facing HFI instrument) from the HFI side. 44 and 30 GHz FEMs are inserted into the mainframe from the WG side and fixed to the bottom plate. Screws to bottom plate are inserted from WG side. The LFI FEMs are the first active stage of amplification of the radiometer chain. Each FEM contains four amplification paths. Each path is composed by several cascaded LNAs followed by a phase switch. Two passive hybrids, at the input and output of the FEM, are used to mix couples of signals of the same radiometer (see Figure 5). This makes the instabilities of each chain to be applied to both the sky and load signals.

The passive hybrid coupler (magic-tee) combines the signals from the sky and cold load with a fixed phase offset of either 90 deg or 180 deg between them. It has a 20% bandwidth, low loss, and amplitude balance needed at the output to ensure adequate signal isolation.

The details of the design, development and verification of the 70 GHz front-end modules for the Planck Low Frequency Instrument can be found in #varis2009 and in the corresponding Appendix section.

Waveguides

The LFI Front End Unit (FEU) is connected to the Back End Unit (BEU) by 44 rectangular waveguides approximately 1.5-2.0 meter long. Each waveguide exhibits low voltage standing wave ratio, low thermal conductivity, low insertion loss, and low mass. In addition, the waveguide path shall permit the LFI/HFI integration and the electrical bonding between FPU and BEU. Because of the Focal Plane Unit arrangement, the waveguides are in general twisted and bended in different planes and with different angles, depending on the particular waveguide. From the thermal point of view the waveguides have to connect 2 systems (BEM and FEM) that are at very different temperatures. At BEM level the waveguides are at a temperature of 300K while at FEM level the temperature is 20K. The waveguides have to reduce the thermal flow from 300K to 20K. In Figure 1 (left panel) a conceptual sketch of the LFI configuration is shown.

Details of the Planck-LFI flight model of the composite waveguides can be found in #darcangelo2009a and in the corresponding Appendix section.

Back End Modules (BEM)

The BEMs are composed by four identical channels each made of Low Noise Amplifiers (LNA), RF Band Pass Filter, RF to DC diode detector and DC amplifiers. The FEM output signals are connected by waveguide from the Focal Plane Unit (FPU) assembly to the Back End Modules (BEM's) housed adjacent to the Data Acquisition Electronics (DAE) assembly. To maintain compatibility with the FEM's, each BEM accommodates four receiver channels from the four waveguide outputs of each FEM. The BEM internal signal routes are not cross coupled and can be regarded as four identical parallel circuits. Each BEM is constructed as two mirror halves. The two amplifier/detector assemblies each contain two amplifier/detector circuits. Each is supplied from one of a pair of printed circuit boards which also house two DC output amplifiers.

The details of the design, development and verification of the 30 and 44 GHz back-end modules for the Planck Low Frequency Instrument can be found in #artal2009. The details of the design, development and verification of the 70 GHz back-end modules for the Planck Low Frequency Instrument can be found in #varis2009. Details are reported also in the corresponding Appendix section.

4K Load

The purpose of the 4 K reference load is to provide the radiometer with a stable reference signal. Reducing the input offset (the radiometric temperature difference between the sky and the reference load) reduces the minimum achievable radiometer 1/f noise knee frequency for a given amplifier fluctuation spectrum. A reference load temperature that matches the sky temperature (approximately 2.7 K) would be ideal.

Details of the design, characteristics and performance of the LFI 4K reference load units are given in #valenziano2009 and in the corresponding section of the LFI Appendix.

LFI Naming Convention

The naming of all the LFI elements is described in the previous sections but here is summarized again for clarity.

The 11 RCAs are labelled by a numbers from 18 to 28 as outlined in Figure 1, right panel. In each RCA, the two perpendicular linear polarisation components are labelled as *M* or *S* according to the arm of the OMT they are connected to (*Main* or *Side*, see lower-left inset of Figure 4).

Each front-end amplifier (see upper-left inset of Figure 4) is labelled with codes *1*, *2* so that the four outputs of the FEM LNAs can be named with the sequence: *M1*, *M2* (radiometer *M*) and *S1*, *S2* (radiometer *S*).

Each radiometer has two output diodes (see upper-right inset of Figure 4) which are labelled with binary codes *00*, *01* (radiometer *M*) and *10*, *11* (radiometer *S*), so that the four outputs of each radiometric chain can be named with the sequence: *M-00*, *M-01*, *S-10*, *S-11*.

REBA

The Radiometer Electronics Box Assembly (REBA) is the electronic box in charge of processing the digitized scientific data and to manage the overall instrument. It is also in charge of the communication with the spacecraft. There are two REBA boxes, one nominal and one redundant. The redundancy concept is cold, which means that both boxes are never ON at the same time; the operation of each unit shall be managed by the spacecraft switching-on the corresponding unit. The REBA ASW (Application SoftWare) is the same in each REBA box.

A detailed description of the Planck LFI REBA can be found in #herreros2009 and in the corresponding section of the LFI Appendix.

Instrument On-board Software

The REBA software is the on board software of LFI. It is installed in the two computing subunits of REBA: the DPU (Digital Processing Unit), responsible of the control and monitoring of the instrument and the interface with the spacecraft and; the SPU (Signal Processing Unit), responsible of the data reduction and compression.

Details can be found in the corresponding section of the LFI Appendix.

Reduction and Compression of Science Data

To asses stability against 1/f noise, the Low Frequency Instrument (LFI) on-board the Planck mission will acquire data at a rate much higher than the data rate allowed by the science telemetry bandwidth of 35.5 kbps. The data are processed by an on-board pipeline, followed on-ground by a decoding and reconstruction step, to reduce the volume of data to a level compatible with the bandwidth while minimizing the loss of information. The on-board processing of the scientific data used by Planck/LFI to fit the allowed data-rate is an intrinsically lossy process which distorts the signal in a manner which depends on a set of five free parameters (N_{aver}, r_1, r_2, q, O) for each of the 44 LFI detectors. A brief description of the characteristics of this algorithm and the level of distortion introduced by the on-board processing as a function of these parameters can be found in the corresponding section of the LFI Appendix, a full description of the Planck LFI on-board data handling system and the tuning and optimization method of the on-board processing chain in #maris2009.

The strategy adopted to fit into the bandwidth relies on three on-board processing steps: downsampling, pre-processing the data to ensure loss-less compression, and loss-less compression itself. To demonstrate these steps, a model of the input signal shall be used. It has to be noted that while the compression is loss-less, the pre-processing is not, due to the need to rescale the data and convert them in integers, (a process named data re-quantization). However, the whole strategy is designed to asses a strict control of the way in which lossy operations are done, of the amount of information loss in order to asses optimal compression rate with minimal information loss.

Instrument Operations

LFI Operational Modes

The operations of the LFI are designed to be automatic and require little if any intervention from the ground. A small amount of commands is required for operating the instrument and eventually for diagnostic and reconfiguration purposes. Each sky survey is conducted by the LFI with the instrument in the Normal Operations Mode mode. No deployable elements, or mechanically moving parts are included in the instrument. The scanning of the sky is achieved by progressive repointing of the satellite spin axis, with the Sun direction always within a cone 10 degrees from the spin axis. Within the Normal Science Mode the instrument can be configured in order to fit with different science or diagnostic needs without changing the power consumption and thus the temperature in the FPU. Changes in power consumption in the FPU are minimised and should occur only in the case that failures in the radiometers that could create interference problems require an RCA to be switched off. Power adjustments on the first stage of the HEMT amplifiers which are contemplated, require extremely small power level variations.

A brief summary of the LFI Operational Modes and the transitions between them is given in the corresponding section of the LFI Appendix.

In-flight Operations

TBW

Anomalies

TBW

LFI Ground Tests

During its development, the LFI flight model was calibrated and tested at various integration levels from sub-systems #davis2009 to individual integrated receivers #villa2010 [[Planck pre-launch status: Calibration of the Low Frequency Instrument flight model radiometers [4]] and the whole receiver array #mennella2010 [Planck pre-launch status: Low Frequency Instrument calibration and expected scientific performance [5]]. In every campaign we performed tests according to the following classification:

- *Functionality tests*, performed to verify the instrument functionality.
- *Tuning tests*, to tune radiometer parameters (biases, DC electronics gain and offset, digital quantisation and compression) for optimal performance in flight-like thermal conditions.
- *Basic calibration and noise performance tests*, to characterise instrument performance (photometric calibration, isolation, linearity, noise and stability) in tuned conditions.
- *Susceptibility tests*, to characterise instrument susceptibility to thermal and electrical variations.

Where possible, the same tests were repeated in several test campaigns, in order to ensure enough redundancy and confidence in the instrument behaviour repeatability. A matrix showing the instrument parameters measured in the various test campaigns is provided in Table 1 of #mennella2010 [Planck pre-launch status: Low Frequency Instrument calibration and expected scientific performance [5]].

The ground test campaign was developed in three main phases: cryogenic tests on the individual RCAs, cryogenic tests on the integrated receiver array (the so-called radiometer array assembly, RAA) and system-level tests after the integration of the LFI and HFI instruments onto the satellite. The first two phases were carried out at the Thales Alenia Space - Italia laboratories located in Vimodrone (Milano, Italy) (note that receiver tests on 70 GHz RCAs were carried out in Finlad, at Yilinen laboratories), system level tests (SLT) were conducted in a dedicated cryofacility at the Centre Spatiale de Liege (CSL) located in Liege (Belgium).

In Table 1 below we list the temperature of the main cold thermal stages during ground tests compared to in-flight nominal values. These values show that system-level tests were conducted in conditions that were as much as possible flight-representative, while results obtained during RCA and RAA tests needed to be extrapolated to flight conditions to allow comparison. Details about the RCA test campaign are discussed in #villa2010 [Planck pre-launch status: Calibration of the Low Frequency Instrument flight model radiometers [4]] while the RAA tests and the extrapolation methods are presented in #mennella2010 [Planck pre-launch status: Low Frequency Instrument calibration and expected scientific performance [5]].

Table 1. Temperatures of the main cold stages during the various ground test campaigns compared to in-flight nominal values

Temperature	Nominal	RCA tests	RAA tests	System-level
Sky	~ 3 K	≳ 8 K	≳ 18.5 K	~ 4 K
Ref. load	~ 4.5 K	≳ 8 K	≳ 18.5 K	~ 4.5 K
Front-end unit	~ 20 K	~ 20 K	~ 26 K	~ 20 K

During the various test campaigns the instrument was switched off and moved several times in a time period of about three years. A series of functional tests were always repeated at each location and also in flight, in order to verify the instrument functionality and the response repeatability. No failures or major problems have been identified due to transport and integration procedures.

The expected Planck LFI scientific performance, resulting mainly from cryogenic system level tests, are described in #mennella2010 [Planck pre-launch status: Low Frequency Instrument calibration and expected scientific performance [5]].

LFI In-flight Calibration

The LFI Commissioning and Calibration and Performance Verification (CPV) phases started on June, 4^{th}2009 and lasted until August, $12^{\mathrm{th}}$when Planck started scanning the sky in nominal mode. At the onset of CPV, the active cooling started when the radiating surfaces on the payload module reached their working temperatures (~50 K on the 3^{rd}V-groove, and ~40 K on the reflectors) by passive cooling. This was achieved during the transfer phase. Nominal temperatures were achieved on July, 3^{rd}2009, when the dilution cooler temperature reached 0.1 K #planck2011-1-3, meinhold2009 [Planck early results. The thermal performance of Planck [6]]. The cooldown of the HFI 4K stage (see Figure 6 below), was key during CPV for the LFI as it provided a variable input signal that was exploited during bias tuning.

The LFI Commissioning and CPV was carried out in four phases:

- LFI switch on and basic functionality verification (Commissioning),
- Tuning of front-end biases and back-end electronics (CPV),
- Preliminary calibration tests (CPV),
- Thermal tests (CPV).

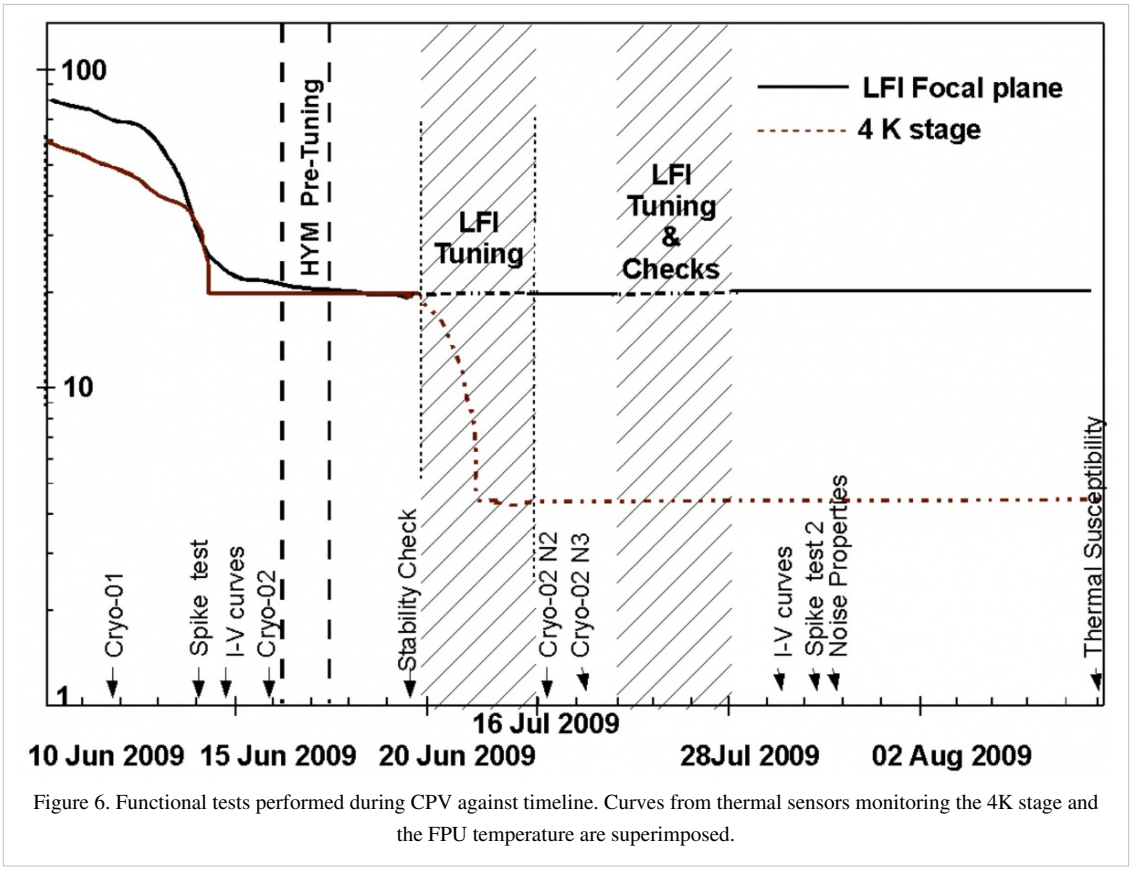

Figure 6. Functional tests performed during CPV against timeline. Curves from thermal sensors monitoring the 4K stage and the FPU temperature are superimposed.

Details of the LFI Commissioning and CPV test campaign are given in #gregorio2013.

LFI Performance

Instrument Scientific Performance

Optical Parameters

The most accurate measurements of the LFI main beams have been made with Jupiter, the most powerful unresolved (to Planck) celestial source in the LFI frequency range. Since the LFI feed horns point to different positions on the sky, they detect the signal at different times. To map the beam, each sample in the selected timelines was projected in the (u, v)-plane perpendicular to the nominal line-of-sight (LOS) of the telescope (and at 85 ◦ to the satellite spin axis). The $u$and $v$coordinates are defined in terms of the usual spherical coordinates :

To increase the signal-to-noise ratio, data were binned in an angular region of 2′ for the 70 GHz channels and 4′ for the 30 and 44 GHz channels. We recovered all beams down to −20 dB from the peak. An elliptical Gaussian was fit to each beam for both M and S radiometers. Differences between the M and S beams caused by optics and receiver non-idealities are inevitable at some level, but they appear to be well within the statistical uncertainties, and for the purposes of point-source extraction, the beams may be considered identical. For the details of the typical FWHM and ellipticity averaged over each frequency channel, refer to #planck2011-1-4 [Planck early results. First assessment of the Low Frequency Instrument in-flight performance [1]]). Exhaustive details on all LFI beam parameters are presented in the LFI data processing section - Beams.

Photometric Calibration

Photometric calibration, i.e., conversion from voltage to antenna temperature, is performed for each radiometer after total power data have been cleaned of 1 Hz frequency spikes (see the LFI data processing section - Spikes Removal section and #planck2011-1-6 [Planck early results. The Low Frequency Instrument data processing [1]]), and differenced. Here we report a brief overview of the photometric calibration, for the details see the LFI data processing section - Photometric Calibration.

Our calibrator is the well-known dipole signal induced by Earth and spacecraft motions with respect to the CMB rest frame. The largest calibration uncertainty comes from the presence of the Galaxy and of the CMB anisotropies in the measured signal. We therefore use an iterative calibration procedure in which the dipole is fitted and subtracted, producing a sky map that is then removed from the original data to enhance the dipole signal for the next iteration. Typically, convergence is obtained after a few tens of iterations.

In our current calibration model we use as calibration signal the sum of the solar dipole $\Delta T_{Sun}$and the orbital dipole ΔT_{orb}, which is the contribution from Planck's orbital velocity around the Sun,

where $\theta_{axis}$is the angle between the spacecraft axis and the overall dipole axis (solar + orbital). In this equation, the absolute calibration uncertainty is dominated by the uncertainty in T_{Sun}= 3.355 mK ± 0.008 mK hinshaw2009, which is known to about 0.2%. The modulation of the orbital dipole by the Earth motion around the Sun is known with an uncertainty almost three orders of magnitude smaller; however, at least one complete Planck orbit is needed for its measurement. The accuracy of our current calibration can be estimated by taking into account two components: 1) the statistical uncertainty in the regions of weak dipole; and 2) the systematic uncertainty caused by neglecting gain fluctuations that occur on periods shorter than the smoothing window. In our calibration procedure the gain is estimated for every pointing period: if we call $G_i$the gain estimate from the i_{th}pointing period we have that the associated uncertainty is

where $N$is the overall number of pointing and $< G >$is the average of the Ngains. We then approximate the effect of the smoothing filter as an average over Mconsecutive pointings, so that the overall uncertainty can be estimated as:

Noise Properties

The noise characteristics of the LFI datastreams are closely reproduced by a simple (white + $1/f$) noise model,

where $P(f)$is the power spectrum and . In this model, noise properties are characterised by three parameters, the white noise limit σ, the knee frequency f_{knee}, and the exponent of the $1/f$component α, also referred to as slope.
Here we give noise performance estimates based on one year of operations, details of the analysis are given in LFI data processing section - Noise Estimation and in #planck2011-1-6, planck2011-1-4 [Planck early results. The Low Frequency Instrument data processing [1], Planck early results. First assessment of the Low Frequency Instrument in-flight performance [1]].
Noise properties have been calculated following two different and complementary approaches: 1) fitting equation above to time-ordered data for each radiometer; and 2) building normalised noise maps by differencing data from the first half of the pointing period with data from the second half of the pointing period to remove the sky signal ("jackknife" data sets).

Typical uncertainties are ~0.5% for the white noise, between 5 and 10% for the slope, and between 10 and 20% for the knee frequency.

White Noise Sensitivity

Details of the white noise sensitivity can be found in #planck2011-1-4 [Planck early results. First assessment of the Low Frequency Instrument in-flight performance [1]].

Table 2 summarizes the sensitivity numbers calculated during the first year of operations using methods and procedures described in detail in #planck2011-1-6 [Planck early results. The Low Frequency Instrument data processing [1]], compared with scientific requirements. The measured sensitivity is in very good agreement with pre-launch expectations. While the white noise moderately exceeds the design specification, this performance is fully in line with the LFI science objectives.

Table 2. White noise sensitivity of the LFI frequency channels compared with requirements

Channel	Measurement [$\mu K\, CMB_S\, ^{1/2}$]	Requirement [$\mu K\, CMB_S\, ^{1/2}$]
70 GHz	152.5	119
44 GHz	173.1	119
30 GHz	146.8	119

Instrument Technical Performance

Spectral Response

The in-band receiver response has been thoroughly modelled and measured for all the LFI detectors during ground tests. The complete set of bandpass curves has been published in #zonca2009 where all the details of the LFI radiometer's spectral response are given. From each curve we have derived the effective centre frequency according to:

where is the receiver bandwidth and $g(\nu)$is the bandpass response. Details about colour corrections, $C(\alpha)$, needed to derive the brightness temperature of a source with a power-law spectral index α, are provided in #planck2011-1-6.

Some details are also given in the corresponding section of the LFI Appendix.

Bandpass Estimation

As detailed in #zonca2009, our most accurate method to measure the LFI bandpasses is based on measurements of individual components integrated into the LFI Advanced RF Model (LARFM) to yield a synthesised radiometer bandpass. The LARFM is a software tool based on the open-source Quasi Universal Circuit Simulator (QUCS). The measured frequency responses of the various subsystems (feed-OMT, FEM, BEM) are considered as lumped S-parameter components. Measurements of single components are obtained with standard methods and provide highly reliable results, with precision of order 0.1-0.2 dB over the entire band. Waveguides are simulated with an analytical model, in order to reproduce the effect of their temperature gradient and the effect of standing waves caused by impedance mismatch at the interfaces between the FEM and BEM. This is because the 1.8-meter long waveguides were not measured at unit level in cryogenic conditions. The model provides accurate agreement with the measured waveguide response in the conditions of the test measurements (300 K). The composite bandpasses are estimated to have a precision of about 1.5 to 2 dB.

Some details are also given in the corresponding section of the LFI Appendix.

Stability

Thanks to its differential scheme, the LFI is insensitive to many effects caused by 1/f noise, thermal fluctuations, or electrical instabilities. As detailed in #planck2011-1-4 [Planck early results. First assessment of the Low Frequency Instrument in-flight performance [1]], one effect detected during the first survey was the daily temperature fluctuation in the back-end unit induced by the downlink transponder, which was powered on each day for downlinks during the first 258 days of the mission. As expected, the effect is highly correlated between the sky and reference load signals. In the difference, the variation is reduced by a factor , where $r$is the gain modulation factor defined above (see eq. \ref{eq:erre1}).

A particular class of signal fluctuations occasionally observed during operations is due to electrical instabilities that appear as abrupt increases in the measured drain current of the front-end amplifiers, with a relaxation time variable from few seconds to some hundreds of seconds. Typically, these events cause a simultaneous change in the sky and reference load signals. Because they are essentially common-mode, their residual on the differenced data is negligible, and the data are suitable for science production. In a few cases the residual fluctuation in the differential output was large enough (a few millikelvin in calibrated antenna temperature units) to be flagged, and the data were not used. The total amount of discarded data for all LFI channels until Operational Day 389 was about 2000 s per detector, or 0.008%.

A further peculiar effect appeared in the 44 GHz detectors, where single isolated samples, either on the sky or the reference voltage output, were far from the rest. Over a reference period of four months, 15 occurrences of single-sample spikes (out of 24 total anomaly events) were discarded, an insignificant loss of data.

Thermal Susceptibility

As mentioned in section LFI In-flight Calibration above and detailed in #gregorio2013, during the CPV campaign, susceptibility tests were performed in order to characterise the LFI instrument susceptibility to thermal and electrical variations.

The effect of temperature fluctuations on the LFI radiometers is originated in the Planck cold end interface of the hydrogen sorption cooler to the instrument focal plane. The temperature is actively controlled through a dedicated stage, the Thermal Stabilization Assembly (TSA), providing a first reduction of the effect. The thermal mass of the focal plane strongly contribute to reduce residual fluctuations. The physical temperature fluctuations propagated at the front end modules cause a correlated fluctuation in the radiometer signal degrading the quality of scientific data. The accurate characterization of this effect is crucial for possibly removing it from raw data by exploiting the housekeeping information of thermal sensors.

The propagation of the temperature oscillations through the focal plane and the instrument response to thermal changes were characterized through two main tests:

- the thermal dynamic response aimed at measuring the dynamic thermal behaviour of the LFI Focal Plane;
- the radiometers thermal susceptibility.

Some details are also given in the corresponding section of the LFI Appendix.

Instrument Budgets

LFI power, mass and telemetry budget are given in the corresponding section of the LFI Appendix.

LFI Systematics Effects

The LFI design was driven by the need to suppress systematic effects well below instrument white noise. The differential receiver scheme, with reference loads cooled to 4 K, greatly minimises the effect of 1/f noise and common-mode fluctuations, such as thermal perturbations in the 20K LFI focal plane. The use of a gain modulation factor (see Eq. \ref{eq:erre1} in RCA section above) largely compensates for spurious contributions from input

offsets. Furthermore, diode averaging (Eq. \ref{eq:v1} in RCA section above) allows us to cancel second-order correlations such as those originating from phase switch imbalances.

We have developed an error budget for systematic effects (#planck2011-1-4, bersanelli2010 [Planck early results. First assessment of the Low Frequency Instrument in-flight performance [1]],Planck pre-launch status: Design and description of the Low Frequency Instrument [2]]) as a reference for both instrument design and data analysis. Our goal is to ensure that each systematic effect is rejected to the specified level, either by design or by robust removal in software. At this stage, the following effects are relevant:

- 1/f noise;
- 1 Hz frequency spikes;
- receivers non-linearities;
- thermal fluctuations in the back-end modules driven by temperature oscillations from the transponder during the first survey;
- thermal fluctuations in the 20 K focal plane;
- thermal fluctuations of the 4 K reference loads.

For each of these effects we used flight data and information from ground tests to build timelines, maps, and angular power spectra that represent our best knowledge of their impact on the scientific analysis. The details of the systematic effect analysis is given in section LFI data processing section - Systematic Effects uncertainties.

Acronyms

BEM Back End Module

BEU Back End Unit

CCE Central Check-out Equipment

CDMS Command and Data Management Subsystem

CDMU Central Data Management Unit

CoG Centre of Gravity

CPV Calibration and Performance Verification

CSL Centre Spatiale de Liege

DAE Data Acquisition Electronics

DC Direct Current

DPC Data Processing Centre

DPU Digital Processing Unit

EMC Electro-Magnetic Compatibility

EMI Electro-Magnetic Interference

FEM Front End Module

FEU Front End Unit

FH Feed Horn

FOV Field Of View

FPU Focal Plane Unit

HK House Keeping

ILT Instrument Level Test

IST Integrated System Test

JFET Junction Field Effect Transistor

LEOP Launch and Early Orbit Phase

MLI Multilayer Insulation

MoI Moment of Inertia

MOS Margin Of Safety

OMT Ortho Module Transducer

PCS Power Control Subsystem

PSF Point Spread Function

RAA Radiometer Array Assembly

RAM Random Access Memory

RCA Radiometer Chain Assembly

REBA Radiometer Electronics Box Assembly

S/C Spacecraft

SCC Sorption Cooler Compressor assembly

SCCE Sorption Cooler Cold End

SCE Sorption Cooler Electronics

SCOS Spacecraft Control and Operations System

SCP Sorption Cooler Piping

SCS Sorption Cooler Subsystem

SLT System Level Test

SPU Signal Processing Unit

SS Stainless Steel

SVM Service Module

TCS Thermal Control System

TM Telemetry

TSA Thermal Stabilization Assembly

TTC Telemetry, Tracking and Command

VSWR Voltage Standing Wave Ratio

WG Waveguide

Glossary

Feed Horns xxx

REBA Radiometer Electronics Box Assembly

References

<biblio force=false>

1. References

</biblio>

References

[1] http://www.rssd.esa.int/llink/livelink/fetch/-60063/3036676/3065909/3110897/3135828/3135852/PE_paper3.pdf#page=1
[2] http://www.rssd.esa.int/llink/livelink/fetch/-60063/3036676/3065909/3110897/3135828/3135930/PL_paper4.pdf#page=1
[3] http://www.rssd.esa.int/llink/livelink/fetch/-60063/3036676/3065909/3110897/3135828/3135852/PE_paper4.pdf#page=1
[4] http://www.rssd.esa.int/llink/livelink/fetch/-60063/3036676/3065909/3110897/3135828/3135930/PL_paper6.pdf#page=1
[5] http://www.rssd.esa.int/llink/livelink/fetch/-60063/3036676/3065909/3110897/3135828/3135930/PL_paper5.pdf#page=1
[6] http://www.rssd.esa.int/llink/livelink/fetch/-60063/3036676/3065909/3110897/3135828/3135852/PE_paper2.pdf#page=1

LFIAppendix

Appendix: LFI Instrument

Here we report a more detailed definition of each component of the LFI instrument, briefly described in the main LFI instrument page.

Radiometer Array Assembly (RAA) Components

Feed Horns (FH)

Dual profiled corrugated horns have been selected at all LFI frequencies as the best design in terms of shape of the main lobe, level of the side lobes, control of the phase centre, and compactness. Dual profiled LFI horns are composed by a Sine Squared profiled section, and an exponential profile near the aperture plane. In order to optimise the optical matching of the feeds phase centres to the telescope focal surface, while preventing obscuration between horns, LFI has 6 different feed horn designs. For each frequency, the number of feeds and the number of different designs are reported in Table 1 below.

Table 1. Number of LFI feed horns and number of different feed horn designs

Frequency (GHz)	Number of Horns	Number of designs
30	2	1
44	3	2
70	6	3

LFI feed horn design specifications are reported in the table 2 below.

Table 2. LFI feed horn design specifications. The edge taper is the taper used to optimize the optical response; the return loss and the cross polarization are the maximum design values over the whole bandwidth; The phase center location is defined as the distance between the horn flange and the focal surface of the telescope.

	D401	D405	D861	D428	D862	D863
FH ID	27;28	24	25;26	18;23	20;21	19;22
ν_0 [GHz]	30	44	44	70	70	70
$\Delta\nu$ [GHz]	6	8.8	8.8	14	14	14
Edge Taper [dB@22°]	30	30	30	17	17	17
Return Loss [dB]	−30	−30	−30	−30	−30	−30
Cross Polarization [dB]	−30	−30	−30	−30	−30	−30
Phase Center Location [mm]	119.60	122.23	83.83	59.18	66.13	63.63
Total Length [mm]	156.12	150.44	133.04	61.54	68.49	66.00

The design process led to a corrugation profile composed by a mixture of a sine-squared section, starting from the throat, and an exponential section near the aperture plane. The length of this last has a direct impact on the location of the phase center. The analytical expression of the corrugation profile, $R(z)$, is the following

in the sine section, and

in the exponential region. Here, $R_{th}$is the throat radius, $R_s$is the sine squared region end radius (or exponential region initial radius), $R_{ap}$is the aperture radius, $L_s$is the sine squared region length and $L_e$is the exponential region length. The parameter modulates the first region profile between linear and pure sine squared type. The parameters $L_e/(L_e + L_s)$, $A$and $R_s$can be used to control, as far as possible, the position and frequency stability of the phase center and the compactness of the structure. The feed horn parameters are reported in table 3 below.

Table 3. LFI feed horn parameters.

	D401	D405	D861	D428	D862	D863
R_{th}	0.49	0.49	0.49	0.5156	0.5156	0.5156
N_s	26	35	32	34	40	39
R_s	1.80	2.00	1.94	1.65	1.65	1.67
A	0.80	0.75	0.67	1.0	1.0	1.0
N_e	15	27	20	12	10	10
R_{ap}	2.60	2.65	3.00	2.15	2.12	2.15
β	2	2	3/2	2	2	2

The qualification campaign, mainly focused on RF return loss and pattern (amplitude and phase) measurements, was successfully concluded. The agreement between the pattern measurements and the expected performances (simulated using nominal corrugation profile) is excellent both in amplitude and in phase. Moreover reflection measurements show a good impedance match for all the horns, the return loss being better than -30 dB over the whole 20% of

operational bandwidth.

Details of the design, flight model and tests of Planck-LFI feed horns can be found in #villa2009.

OrthoMode Transducers (OMT)

The Ortho–Mode Transducer (OMTs) separates the radiation collected by the feed horn in two orthogonal polarisation components. It consists of a circular to square waveguide transition (directly connected to the FH), a square waveguide section and two separate rectangular waveguide (the through and side arms, which separate and pick up the orthogonal polarisation, connected with the FEU). On the side arms is always present a 90 degrees bend, while a twist is also necessary on the main (30 and 44 GHz) and side (70GHz) arm, in order to math the FEU polarisation.

The required and measured performances for the LFI OMTs at all frequencies are reported in the following tables 4 and 5:

Table 4. Performance Characteristics of the LFI OMTs based on measurements. The values are the worst values over the entire 20% of bandwidth.

OMT ID	Bandwidth [GHz]	X–Pol [dB] (Main)	X–Pol [dB] (Side)	Return–Loss [dB] (Main)	Return–Loss [dB] (Side)
18	14	<29	<30	-15.0	-20.0
19	14	<26	<28	-15.0	-20.0
20	14	<32	<35	-15.0	-20.0
21	14	<32	<37	-15.0	-18.0
22	14	<26	<28	-15.0	-18.0
23	14	<26	<28	-15.0	-20.0
24	8.8	<38	<40	-13.0	-18.0
25	8.8	<31	<32	-13.0	-18.0
26	8.8	<27	<25	-13.0	-17.0
27	6	<38	<44	-16.0	-23.0
28	6	<36	<38	-16.0	-22.0

Table 5. Mean value of the IL over LFI bandwidth estimated at 20K and measured at room temperature.

	IL @ T room		IL @ 20 K	
	main [dB]	side [dB]	main [dB]	side [dB]
30 GHz				
RCA 27	0.11	0.12	0.10	0.10
RCA 28	0.12	0.14	0.11	0.10
44 GHz				
RCA 24	0.12	0.19	0.10	0.17
RCA 25	0.16	0.16	0.15	0.14
RCA 26	0.14	0.14	0.13	0.12
70 GHz				
RCA 18	0.17	0.14	0.16	0.07
RCA 19	0.18	0.20	0.16	0.10
RCA 20	0.18	0.24	0.16	0.16
RCA 21	0.16	0.14	0.15	0.06
RCA 22	0.12	0.18	0.09	0.09
RCA 23	0.20	0.22	0.18	0.11

The details of the flight models and measurements of the Planck LFI ortho-mode transducers can be found in #darcangelo2009b.

Front End Modules (FEM)

Front End Modules are located in the FPU, just in cascade of the Feed Horn and the Ortho Mode Transducers. 70 GHz FEMs are mounted onto the inner wall of the mainframe (the wall facing HFI instrument) from the HFI side. 44 and 30 GHz FEMs are inserted into the mainframe from the WG side and fixed to the bottom plate. Screws to bottom plate are inserted from WG side. The LFI FEMs are the first active stage of amplification of the radiometer chain. Each FEM contains four amplification paths. Each path is composed by several cascaded LNAs followed by a phase switch. Two passive hybrids, at the input and output of the FEM, are used to mix couples of signals of the same radiometer (see Figure 4 in LFI instrument section). This makes the instabilities of each chain to be applied to both the sky and load signals.

The passive hybrid coupler (magic-tee) combines the signals from the sky and cold load with a fixed phase offset of either 90 deg or 180 deg between them. It has a 20% bandwidth, low loss, and amplitude balance needed at the output to ensure adequate signal isolation.

The FEM LNAs (InP MMIC) are biased providing 1 drain line per channel (that is 4 per FEM) and 2 gate lines per channel (that is 8 per FEM). The FEM Phase switches are biased providing 2 lines per channel (that is 8 per FEM) each capable of providing a direct bias current or a reverse bias voltage.

The LFI FEM parameters necessary to meet the science objectives at 30 and 44 GHz were given as requirements and goals and are summarised in table 6 below where they are compared with the values actually achieved. The FEM units meet the requirements, within the measurement errors, for most parameters and in particular the noise temperature. The units come close to the more stringent goals in several parameters. Of particular note are the noise temperatures achieved; these along with the wide bandwidths are critical for the high sensitivity required for the Planck mission. Some LNAs within the FEMs met the goals at 30 GHz and 44 GHz within the measurements errors and reached 3 and 5 times the theoretical quantum limit respectively at the band centres. Furthermore, a range of tests showed that LNAs and FEMs achieved the stability levels required to meet the observing strategy of Planck. In particular, the 1/f noise knee frequency ≤29 mHz, close to the goal, met the conditions imposed by the 60 second rotation period of the spacecraft. The linear polarization performance of the FEMs exceeded the requirements of the mission. The isolation between the E- and H- polarizations was measured to be between 51 and 58 dBs for the

various FEMs. The LFI radiometers have very well determined position angle precision, being determined by the accuracy of the waveguide engineering. The 30 and 44 GHz geometry is accurate to ~ 0.1°; the corresponding precision is ~ 1° in the HFI polarimeters. The temperature stability requirement values are also given in the table 6 below.

Table 6. Summary of the FEM goals, requirements and mean achieved performances.

	Centre Frequency (GHz)	Goal	Requirement	Achieved
Gain, excluding phase switch insertion loss	30	33 dB	30 dB (including phase switch)	31.1 dB (mean)
	44	33 dB	30 dB (including phase switch)	32.3 dB
Noise temperature of the FEMs	30	6.1 K	8.6 K	8.9 K (mean across band)
	44	10.4 K	14.1 K	15.6 (mean across band)
Bandwidth	30	6 GHz	6 GHz	5.7 GHz
	44	8.8 GHz	8.8 GHz	7.3 GHz
Isolation	30	<5%	10%	~ 4.0%
	44	<5%	10%	4.1%
1/f knee frequency	30	20 mHz	<50 mHz	~ 28 mHz
	44	20 mHz	<50 mHz	~ 29 mHz
Temperature stability requirements			$10\mu KHz^{-1/2}$ >10 mHz	
			$100\mu KHz^{-1/2}$ <10 mHz	

The details of the design, development and verification of the 30 and 44 GHz front-end modules for the Planck Low Frequency Instrument can be found in #davis2009.

For what regards the 70 GHz channels, for the LNA selection of the FEMs, nine different wafers from various processing runs were evaluated, only the LNAs with the best performance were assembled as the first stage amplifiers in the FEM ACAs. For the phase switch selection, four different wafers were evaluated. When the signal is passed to an output, the gain is 35 dB or higher for almost the entire required range, and on average, the Planck requirement was fulfilled. In all FEMs, the average channel gains ranged from 34.0-40.0 dB (uncertainty ±0.1 dB). When the signal is isolated from an output, the gain is 20 dB lower or more at all frequencies. This difference in gain is used as the measure for isolation. In all the six FEMs, the channel isolation values ranged from 11.3-22.1 dB (uncertainty ±0.1 dB).

Table 7 below summarises the best, the worst and the average values of the key performance parameters. The shown uncertainties are based on worst case estimates.

Table 7. Summary of the 70 GHz Protoflight Model radiometer performance.

Parameter	Requirement	PFM radiometers best values	PFM radiometers average values	PFM radiometers worst values
FEM PERFORMANCE				
FEM gain, dB	≥ 35	40.0±0.1	37.0±0.1	34.0±0.1
FEM isolation, dB	≥ 13	22.1±0.1	18.5±0.1	11.3±0.1
FEM power consumption, mW	≤ 24	21	23	25
BEM PERFORMANCE				
BEM filter pass band, GHz	14	18.50±0.06	19.00±0.06	19.50±0.06
BEM power consumption, mW	≤ 604	575	627	725
RADIOMETER PERFORMANCE				
System noise temperature, K	≤ 29.2	28±5	35±5	39±5
White noise floor, $\times 10^{-5} V/\sqrt{Hz}$		1.5	2.8	4.8
1/f noise spectrum knee frequency, mHz	≤ 50	38	104	248
Effective bandwidth, GHz	≥ 14	16	13	10

The details of the design, development and verification of the 70 GHz front-end modules for the Planck Low Frequency Instrument can be found in #varis2009.

Waveguides

The LFI Front End Unit (FEU) is connected to the Back End Unit (BEU) by 44 rectangular waveguides approximately 1.5-2.0 meter long. Each waveguide exhibits low VSWR (Voltage Standing Wave Ratio), low thermal conductivity, low insertion loss, and low mass. In addition, the waveguide path shall permit the LFI/HFI integration and the electrical bonding between FPU and BEU. Because of the Focal Plane Unit arrangement, the waveguides are in general twisted and bended in different planes and with different angles, depending on the particular waveguide. From the thermal point of view the waveguides have to connect 2 systems (BEM and FEM) that are at very different temperatures. At BEM level the waveguides are at a temperature of 300K while at FEM level the temperature is 20K. The waveguides have to reduce the thermal flow from 300K to 20K. In Figure 1 (left panel) of LFI instrument section, a conceptual sketch of the LFI configuration is shown.

All the required characteristics cannot be realized with single material waveguide configuration; a composite waveguide configuration is needed. The WGs can be considered divided in three sections: 1. 400 mm of Stainless Steel (gold plated) straight waveguide section, attached to the BEU, ending after the 3rd V−groove; 2. 300 mm of non−plated Stainless Steel (SS). The SS-sections are identical for all the channels except for internal dimensions, depending on frequency. These guides are connected to all the V-grooves in order to dissipate the heat produced at BEU level. 3. bended and twisted 400 microns thin electroformed copper waveguide starting at the end of the SS−section and attached to the FEU, whose length varying from around 800 mm to 1300 mm, with 2 to 4 Cu-joints. The copper waveguides section is connected to a mechanical support structure in five points in order to increase the stiffness of the waveguide.

The performance for the LFI waveguides at all frequencies are reported in the following table 8:

Table 8. Number of LFI waveguides and performances. The Insertion Loss (IL), Return Loss (RL) and Electrical Resistance (R) values are the requirements. In between parenthesis the goal is reported also. Note that the RL value includes possible degradation due to presence of flanges.

Frequency	νband [GHz]	Number	IL [dB] @20 K	RL [dB]	Isolation [dB]	R [mΩ] @20 K	R [mΩ] @300 K
30	27-33	8	<2.5 (1.0)	<-25	<-30	11.8	27.3
44	39.6-48.4	12	<3.0 (1.5)	<-25	<-30	14.7	34.1
70	63-77	24	<5.0 (3.5)	<-25	<-30	26.2	60.5

From the thermal point of view the waveguides have to connect 2 systems (BEM and FEM) that are at different temperatures. At BEM level the waveguides are at a temperature of 300K while at FEM level the temperature is 20K. Along the Stainless Steel section the waveguides have to reduce the thermal flow from 300K to 20K. The Stainless Steel waveguide is connected to all the V-grooves in order to dissipate the heat produced at BEU level.

Details of the Planck-LFI flight model of the composite waveguides can be found in #darcangelo2009a.

Back End Modules (BEM)

The BEMs are composed by four identical channels each made of Low Noise Amplifiers (LNA), RF Band Pass Filter, RF to DC diode detector and DC amplifiers. The FEM output signals are connected by waveguide from the Focal Plane Unit (FPU) assembly to the Back End Modules (BEM's) housed adjacent to the Data Acquisition Electronics (DAE) assembly. To maintain compatibility with the FEM's, each BEM accommodates four receiver channels from the four waveguide outputs of each FEM. The BEM internal signal routes are not cross coupled and can be regarded as four identical parallel circuits. Each BEM is constructed as two mirror halves. The two amplifier/detector assemblies each contain two amplifier/detector circuits. Each is supplied from one of a pair of printed circuit boards which also house two DC output amplifiers.

In the 30 GHz BEM, each LNA consists of two cascaded MMIC amplifiers. The Band Pass Filter is based on microstrip coupled line structure. Its design is a three order Chebyshev response band pass filter. The detector is composed by a hybrid reactive/passive matching network, and a Schottky diode. A commercial Agilent beam-lead and zero-bias diode was selected. The detector diode is followed by a low noise operational amplifier that provides most of the DC amplification. A second stage is implemented using an operational amplifier to provide a balanced bipolar output.

In the 44 GHz BEM, each LNA consists of self designed MMIC amplifiers manufactured with the process ED02AH from OMMIC which employs a 0.2 μm gate length Pseudomorphic-High Mobility Transistor (P-HEMT) on GaAs. The topology chosen for the band-pass filter is a third order Chebyshef band pass filter made on a PTFE substrate, based on microstrip coupled line structure. The detector is composed by a hybrid reactive/passive matching network and a Schottky diode. A commercial Agilent beam-lead and zero-bias diode was selected. The detector diode is followed by a low noise operational amplifier that provides most of the DC amplification. A second stage is implemented using an operational amplifier to provide a balanced bipolar output.

Table 9 below shows the values of the equivalent noise temperature for each flight model BEM at three different temperatures in the range of possible operating temperature. The large variability of the equivalent noise temperature of 44 GHz BEM units was due to their large dependence on the input matching network result, which was observed to be a very critical parameter, not easy to control during the assembly process of MMIC.

Table 9. Equivalent noise temperature of the BEM Flight models in Kelvin. (One unit of each band is a Flight Spare). Estimated error: ± 20 K.

	Channel *A*			Channel *B*			Channel *C*			Channel *D*		
BEM	T_{low}	T_{nom}	T_{high}	T_{low}	T_{nom}	T_{high}	T_{low}	T_{nom}	T_{high}	T_{low}	T_{nom}	T_{high}
30 GHz FM1	196	317	365	159	294	349	231	349	413	150	292	346
30 GHz FM2	176	288	324	179	299	332	202	316	357	167	307	350
30 GHz FM3	164	286	347	129	272	323	257	342	410	185	301	364
44 GHz FM1	923	856	1006	734	676	745	798	662	744	546	643	881
44 GHz FM2	346	494	397	513	674	587	349	426	386	299	405	509
44 GHz FM3	419	467	525	520	595	755	385	437	591	392	437	484
44 GHz FM4	342	561	939	464	459	609	271	380	609	342	510	598

The raw measurements of the output spectrum are used for the determination of the 1/f knee frequency. The results for the four channels of a 30 GHz BEM unit are given in the table below.

Table 10. 1/f knee frequency (Hz) of 30 GHz BEM unit.

Channel	T_{low}	T_{nom}	T_{high}
A	75	90	103
B	75	100	94
C	74	100	117
D	87	100	100

The details of the design, development and verification of the 30 and 44 GHz back-end modules for the Planck Low Frequency Instrument can be found in #artal2009.

The 70 GHz BEM is constructed of machined aluminium with separate filter, amplifier/detector assemblies and an overall housing for other circuits and components. The BEM filter characteristics hold very accurately for every channel in the six BEMs. The -3 dB pass band, 62-81 GHz, was the same in every filter within 0.5 GHz. The BEM frequency response was measured as a function of input microwave power. Also, the pass bands roll at almost exactly 63 GHz and 77 GHz. The linearity of the channel is very good as well, especially from -57 dBm upwards. The dynamic range was at least 15 dB from -57 dBm to -42 dBm. In three cases, the BEMs fulfilled the power consumption requirement, while the limit was exceeded for the other three. For the total six BEMs, the limit, 3.6 W, was exceeded by approximately 140 mW. Table 7 above summarises the best, the worst and the average values of the key performance parameters. The shown uncertainties are based on worst case estimates.

The details of the design, development and verification of the 70 GHz back-end modules for the Planck Low Frequency Instrument can be found in #varis2009.

4K Load

The purpose of the 4 K reference load is to provide the radiometer with a stable reference signal. Reducing the input offset (the radiometric temperature difference between the sky and the reference load) reduces the minimum achievable radiometer 1/f noise knee frequency for a given amplifier fluctuation spectrum. A reference load temperature that matches the sky temperature (approximately 2.7 K) would be ideal. In the 4KRL design, the reference temperature is provided by the HFI outer radiation shield, at a temperature around 4K. The 4KRL performance are reported in Table 11 below.

Table 11. RF measured performance for the 4KRL: RH (+WaveGuide) Insertion Loss, RH (+WG) RL, RH (+WG) + RT Return Loss. 70 GHz performance have been measured using a representative Reference Horn and waveguide, since RHs are internal to FEMs: this value is reported in the table. RCAs 24-26 are the LFI 44 GHz channels, 27 and 28 the 30 GHz ones. M and S refer to Main and Side OMT arm, respectively.

LFI RCA	Average IL (dB)	Average RL (dB)	
	RH	RH only	RH + RT
18 -M	0.16	-20.99	-20.14
18 - S	-	-	-20.18
19 - M	-	-	-20.54
19 - S	-	-	-20.25
20 - M	-	-	- 20.18
20 - S	-	-	-19.56
21 - M	-	-	-20.58
21 - S	-	-	-20.48
22 - M	-	-	-20.07
22 - S	-	-	-20.29
23 - M	-	-	-19.57
23 - S	-	-	-19.83
24 - M	0.09	-24.13	-24.21
24 - S	0.08	-24.20	-23.42
25 - M	0.08	-22.39	-23.92
25 - S	0.11	-22.27	-24.04
26 - M	0.09	-22.27	-23.85
26 - S	0.08	-21.01	-23.22
27 - M	0.11	-26.59	-24.49 *
27 - S	0.10	-25.15	- 26.45 *
28 - M	0.09	-24.48	-24.49
28 - S	0.10	-25.78	-23.92

The 4K reference load unit is formed by single targets, one for each radiometer (two for each FEM). The horns used to couple to the 4 K reference load targets need to be relatively small because the targets themselves are small. An optimisation process produced a different horn design for each LFI band: their dimensions increase with reducing frequency. Due to the LFI Focal Plane design, where higher frequency radiometers (70 GHz) are placed around the HFI cryostat and the lower frequency radiometers (30 and 44 GHz) in a second row, the target mounting structure is separated in two parts, see Figure 1 below. The upper one is located around the conical part of the HFI outer shield. Reference targets are mounted on a supporting structure, thermally and mechanically connected to the HFI outer shield. Each target faces a reference horn, two for each FEM. This ensemble is fixed to a support structure on the HFI 4K shield. Thermal link between the mounting structure and the HFI is obtained via fixation point only. Thermal washers are interposed to damp temperature fluctuations on targets induced by the HFI outer shield temperature oscillations. The lower part is fixed in the cylindrical part. It is made with the same target geometry of the upper part, and it is fixed on the HFI shield. The reference horns face the loads and are connected to the FEMs through WGs. Reference WGs and RH (Reference Horns) are either included in the FEM (70 GHz) or external to FEM (30 and 44 GHz).

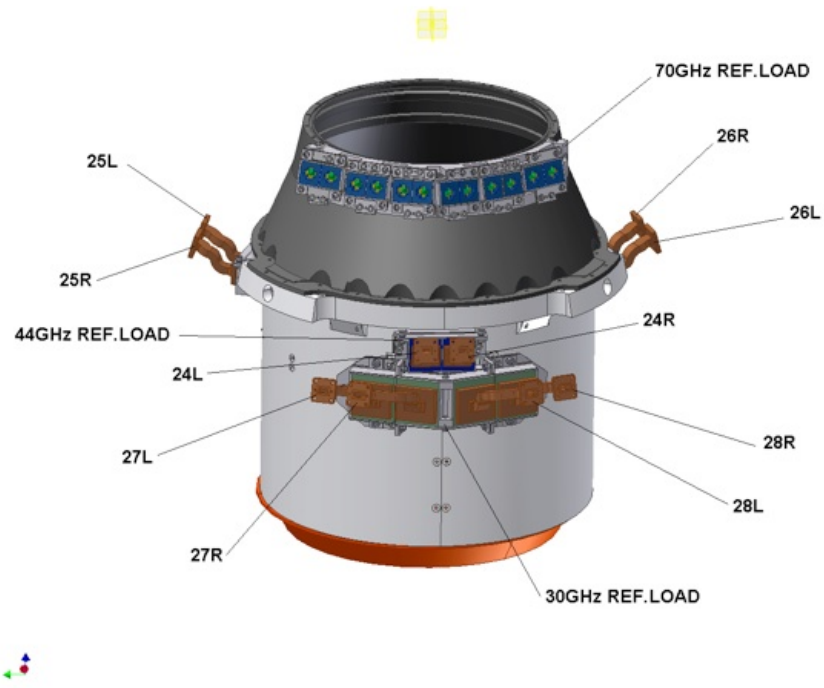

Figure 1. 4K reference load targets mounted on the HFI 4K shield

Targets are formed of a back section, made of ECCOSORB CR117, which shows higher RF absorption but also high reflectivity. To reduce the target global reflectivity, a front section, assembled with an ECCOSORB specific cement to the back one, faces the radiometer Reference Horn. This last is casted from ECCOSORB CR110, whose RF reflectivity is lower than that of CR117. Target design is optimised to further reduce both reflectivity and leakage. Each target is metal backed and it is mounted in a metal enclosure.

Thermal tests were performed in the IASF-Bo 4K cryo facility, equipped with a GM cooler, with an heat lift up to 1.5 W at 4K. The setup simulated the real environment in the payload, where targets are mounted on the HFI 4K shield in front of the quasi-cylindrical LFI main frame at about 20 K. It was also used to test the susceptibility to fluctuations of the LFI.

The thermo-mechanical damping was evaluated from the transient test, inducing sinusoidal temperature fluctuation with periods of 60, 600, 667 (typical Sorption Cooler period) and 1000 seconds at the level of the attachment point of the loads on the support structures. The fluctuation at the level of the targets is then acquired and the transfer function (amplitude and phase) are estimated by the ratio of the amplitudes. The final results are summarized in the table 12.

Table 12. Thermal fluctuation damping measured for the reference loads at different frequencies.

Freq.	D (60s)	D (600s)	D (667s)	D (1000s)
30 GHz	0.080 ± 0.004	0.60 ± 0.03	0.64 ± 0.03	0.78 ± 0.04
44 GHz	0.133 ± 0.007	0.81 ± 0.04	0.85 ± 0.04	0.91 ± 0.05
70 GHz	0.131 ± 0.007	0.72 ± 0.04	0.75 ± 0.04	0.85 ± 0.04

Details of the design and performance of the LFI 4K reference load units are given in #valenziano2009.

REBA

The Radiometer Electronics Box Assembly (REBA) is the electronic box in charge of processing the digitized scientific data and to manage the overall instrument. It is also in charge of the communication with the spacecraft. There are two REBA boxes, one nominal and one redundant. The redundancy concept is cold, which means that both boxes are never ON at the same time; the operation of each unit shall be managed by the spacecraft switching-on the corresponding unit. The REBA ASW (Application SoftWare) is the same in each REBA box.

Each REBA consists of the following subunits:

- The Power Supply Unit (PSU) which feeds the REBA unit. It consists of a DC/DC converter that converts the primary power received from the spacecraft PDU to the secondary regulated voltages required only by the REBA and provides galvanic isolation towards the spacecraft side of the interface. The PSU DC/DC converter also receives the On-Board Clock (OBC) from the CDMS that is used to increment the internal On Board Time register. There is no software interface with the REBA ASW.
- The Data Acquisition Unit (DAU) performs the analogue to digital conversion of the analogue housekeeping data of the REBA itself (temperatures and voltages). The REBA ASW collects from the DAU the HK data.
- The Signal Processing Unit (SPU) is a computing subunit in charge of the reduction and compression of the science data and implements part of the REBA ASW, the SPU ASW (stored in the EEPROM located in the DPU board and transferred to the SPU by the DPU ASW). It receives the science data from the DAE through a IEEE 1355 link implemented in a SMCS chip. A second IEEE 1355 link is used to control by link the remote DAE SMCS chip. The third IEEE 1355 link communicates with the DPU. A “Data Ready” electrical signal is connected between DAE and the SPU, this signal produces an interruption in the SPU when the DAE is ready to transfer data.
- The Digital Processing Unit (DPU) is a computing subunit and implements part of the REBA ASW, the DPU ASW. The DPU is in charge of the control and monitoring of the instrument as well as the communication with the spacecraft (CDMS). It contains another SMCS chip with 3 IEEE 1355 links that communicate with the SPU, and the DAE. A MIL-STD 1553B link is used to communicate with the CDMS. One IEEE 1355 link is used by the DPU ASW to communicate with the DAE to control by link the SMCS chip of DAE, the second one is used to communicate with the DAE to transfer commands and HK and the third one is used by DPU ASW to communicate with the SPU (commands and TM). Two Reset electrical lines are provided by the DPU to reset each of the two SMCS chips of DAE. The DPU ASW is stored in the EEPROM.

A detailed description of the Planck LFI REBA can be found in #herreros2009.

Instrument On-board Software

The REBA software is the on board software of LFI. It is installed in the two computing subunits of REBA: the DPU, responsible of the control and monitoring of the instrument and the interface with the spacecraft and; the SPU, responsible of the data reduction and compression. The REBA software can be classified (see Figure 2) into:

1. the REBA Start-up Software (SUSW), installed in the PROM memories, which is the bootstrap code to switch on both the subunits;

2. the Application Software (ASW), which performs the nominal operations of the REBA;

3. the REBA Low Level Software Drivers (LLSWDRV) which are functions provided to the ASW to access the hardware capabilities.

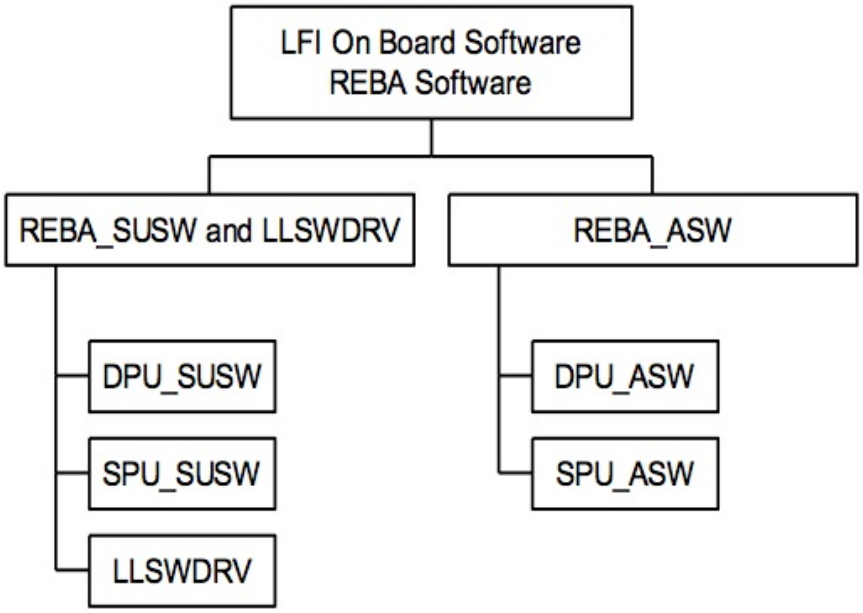

Figure 2. REBA Software, high level product tree

The SPU SUSW and DPU SUSW, located in the PROM memories of SPU and DPU, respectively, are in charge of the booting of the subunits.

The REBA ASW performs the following main functions:

- SPU ASW reduction and compression of the scientific data;
- DPU ASW: control and monitoring of the instrument, interface with the spacecraft to transfer data and receive commands to/from ground, communication with the SPU SUSW during the start-up procedure to load the SPU ASW.

The REBA ASW checks periodically the following parameters:

- Science TM rate produced on board in order to control the filling of the spacecraft mass memory;
- CPU load of the SPU;
- Focal Plane temperature sensors;
- The communication links between REBA and DAE.

In case of deviations from nominal values, the REBA ASW activates autonomy functions that put the instrument in a safe state or recover from non-nominal situations. Autonomy functions allows to:

- Re-enable, in some cases, previously disabled science processing;
- Switch-off the Front End Unit by sending Disable RCA DC/DC commands to the DAE;
- Try to resume the communication between REBA and DAE or ask the CDMS to switch off the RAA.

The DPU ASW reports the activation of any autonomous function by sending to the CDMS an event report. The REBA monitors some LFI HK parameters in order to manage to some extent the safety of the instrument.

Reduction and Compression of Science Data

To asses stability against 1/f noise, the Low Frequency Instrument (LFI) on-board the Planck mission will acquire data at a rate much higher than the data rate allowed by the science telemetry bandwidth of 35.5 kbps. The data are processed by an on-board pipeline, followed on-ground by a decoding and reconstruction step, to reduce the volume of data to a level compatible with the bandwidth while minimizing the loss of information. The on-board processing of the scientific data used by Planck/LFI to fit the allowed data-rate is an intrinsically lossy process which distorts

the signal in a manner which depends on a set of five free parameters (N_{aver}, r_1, r_2, q, O) for each of the 44 LFI detectors. Her briefly describe the characteristics of this algorithm and the level of distortion introduced by the on-board processing as a function of these parameters. A full description of the Planck LFI on-board data handling system and the tuning and optimization method of the on-board processing chain can be found in #maris2009.

The strategy adopted to fit into the bandwidth relies on three on-board processing steps: downsampling, pre-processing the data to ensure loss-less compression, and loss-less compression itself. To demonstrate these steps, a model of the input signal shall be used. It has to be noted that while the compression is loss-less, the pre-processing is not, due to the need to rescale the data and convert them in integers, (a process named data re-quantization). However, the whole strategy is designed to asses a strict control of the way in which lossy operations are done, of the amount of information loss in order to asses optimal compression rate with minimal information loss.

A schematic representation of the sequence in which these steps are applied on-board and whenever possible reversed on-ground is given in figure 3 below.

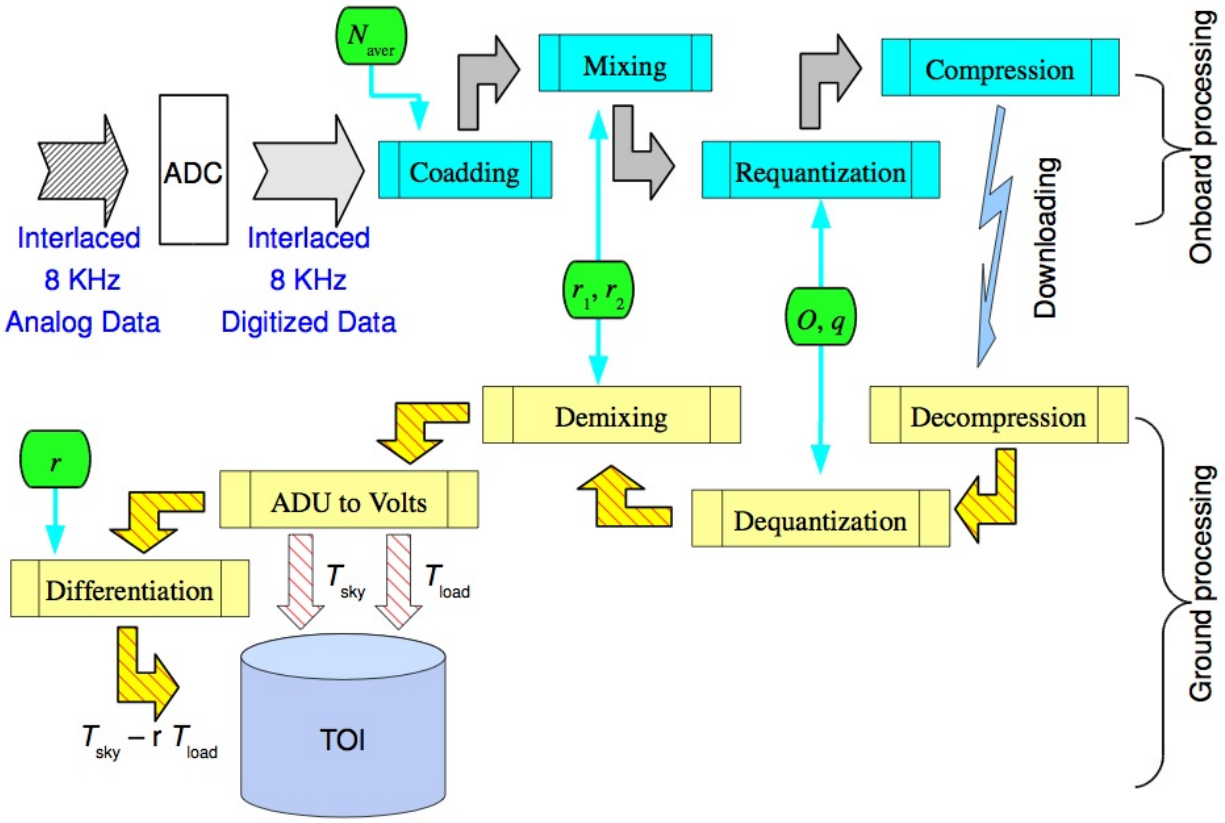

Figure 3. Schematic representation of the scientific onboard and ground processing for the Planck/LFI. Cyan boxes represent REBA operations, yellow boxes ground operations. Green pads specify the parameters needed by each operation. TOI could be produced both in undifferentiated form (T_{sky}, T_{load}stored separately) or in differentiated form.

The figure refers to a single radiometer chain and is ideally splitted into two parts: the upper part depicts the on-board processing with cyan boxes denoting the main steps. The corresponding on-ground processing is depicted in the lower part with the main steps colored in yellow. Green pads represents the processing parameters. The first four of them are referred to as REBA parameters, and they are applied both on-board and on-ground. The parameters are: the number of ADC raw samples to be coadded to form an instrumental sample, N_{aver}, the two mixing parameters r_1, r_2, the offset $O$to be added to data after mixing and prior to re-quantization, and the re-quantization step q. It is important to note that the on-board parameters are set by telecommands and are stamped in each scientific packet. The gain modulation factor, r(see Eq. \ref{eq:erre1} in RCA section above), is a parameter of the ground processing and is computed from the total power data received on ground. The final products in the form of

Time Ordered Data (TOI) either in total power or differentiated are stored in an archive represented by the light-blue cylinder.

All the needed optimization steps are performed by an automated software tool, the Onboard Computing Analysis (OCA), which simulates the on-board processing, explores the space of possible combinations of parameters, and produces a set of statistical indicators, among them: the compression rate $C_r$and the processing noise ϵ_Q. For Planck/LFI it is required that $C_r = 2.4$while, as for other systematics, $\epsilon_Q$would have to be less than 10% of rms of the instrumental white noise. An analytical model is developed that is able to extract most of the relevant information on the processing errors and the compression rate as a function of the signal statistics and the processing parameters to be tuned. This model is of interest for the instrument data analysis to asses the level of signal distortion introduced in the data by the on-board processing.

Once the instrument is completed tuned and stable, a tuning process is applied in order to optimize the REBA parameters. The procedure foresees to acquire chunks of about 15 minutes of *averaged data* to be analyzed by OCA. After setting the (optimized) REBA parameters, another session of 15 minutes of acquisition is applied, this time with the nominal processing.

The values for the optimal REBA parameters are mainly determined by the frequency of the radiometric channel with some dispersion from detector to detector. Table 13 below gives representative median values for r_1, r_2, q from on ground System Level tests (CSL) as well as for the quantities in figure 4 below and the resulting data rate. O is omitted since it is the most variable parameter and it has no significant impact on $\epsilon_q$and C_r. Table 13 below reports also the number of detectors for each frequency channel, the N_{aver}values which are kept constant, the compressed data rate per detector, per frequency channel and for the instrument as a whole. Quantities are reported in the form where δxrepresents the standard deviation taken as a measure of the internal dispersion of $x$within the given subset of detectors, this number must not be interpreted as an error and it must not be propagated.

The performance has been verified against the requirements with the result that the required data rate of 35.5 kbps has been achieved while keeping the processing error at a level of 3.8% of the instrumental white noise and well below the target 10% level.

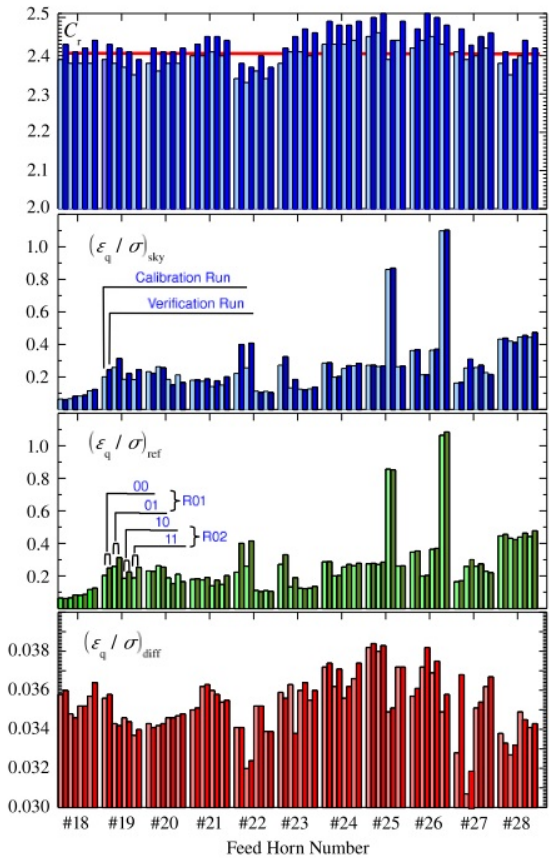

Figure 4. Results for a typical session of REBA parameters tuning during the CSL test campaign. From top to bottom the figure reports for each detector the mean C_r, $\epsilon_{q,sky}/\sigma_{sky}$, $\epsilon_{q,load}/\sigma_{load}$, $\epsilon_{q,diff}/\sigma_{diff}$ where σ_{diff} is the r.m.s. of the differentiated data. The red line in background of the top frame denotes the target $C_r^{Tgt} = 2.4$. Values are represented by bars. Light-bars are the results from the calibration phase, where raw data from the instrument are processed by OCA. Dark-bars are results from the verification phase, where processing is performed on-board. The second frame from Top gives an example for detector 00 of Feed-Horn #19. Feed-horns are numbered according to the internal Planck/LFI convention assigning at Planck/LFI the Feed-Horns numbers from #18 to #28. Detectors belonging to the same Feed-Horn are grouped together as shown in the third frame from top.

Table 13. Representative REBA Parameters, the measured

	Frequency Channel		
	30 GHz	44 GHz	70 GHz
Detectors	8	12	24
N_{aver}	126	88	53
r_1	1.042 ± 0.032	1.042 ± 0.024	1.042 ± 0.012
r_2	0.917 ± 0.065	0.917 ± 0.025	0.958 ± 0.020
q [ADU]	0.297 ± 0.034	0.198 ± 0.044	0.279 ± 0.048
C_r	2.400 ± 0.024	2.440 ± 0.019	2.380 ± 0.023
$(\varepsilon_q/\sigma)_{sky}$	0.420 ± 0.278	0.269 ± 0.184	0.177 ± 0.063
$(\varepsilon_q/\sigma)_{load}$	0.432 ± 0.267	0.271 ± 0.183	0.178 ± 0.063
$(\varepsilon_q/\sigma)_{diff}$	0.0341 ± 0.0016	0.0369 ± 0.0010	0.0351 ± 0.0010
ΔT_q [μK]	1.759 ± 0.148	2.412 ± 0.356	1.905 ± 0.287
Data Rate per Detector [bits/sec]	454.9 ± 4.1	640.8 ± 4.7	1108.2 ± 9.8
Data Rate per Frequency Channel [bits/sec]	3641.8	7689.9	26600.3
Total Data Rate [bits/sec]		37932	

In flight the procedure is to acquire continuously data by using the nominal processing. Short chunks of unprocessed data is daily acquired in turn from each detector. The comparison of unprocessed with processed data allows to monitor of the processing error. In addition the REBA tuning might be repeated daily on the chunk of unprocessed data in order to test whether some REBA parameters on-board the satellite should be changed or not.

Instrument Operations

LFI Operational Modes

The operations of the LFI are designed to be automatic and require little if any intervention from the ground. A small amount of commands is required for operating the instrument and eventually for diagnostic and reconfiguration purposes. Each sky survey is conducted by the LFI with the instrument in the Normal Operations Mode mode. No deployable elements, or mechanically moving parts are included in the instrument. The scanning of the sky is achieved by progressive repointing of the satellite spin axis, with the Sun direction always within a cone 10 degrees from the spin axis. Within the Normal Science Mode the instrument can be configured in order to fit with different science or diagnostic needs without changing the power consumption and thus the temperature in the FPU. Changes in power consumption in the FPU are minimised and should occur only in the case that failures in the radiometers that could create interference problems require an RCA to be switched off. Power adjustments on the first stage of the HEMT amplifiers which are contemplated, require extremely small power level variations.

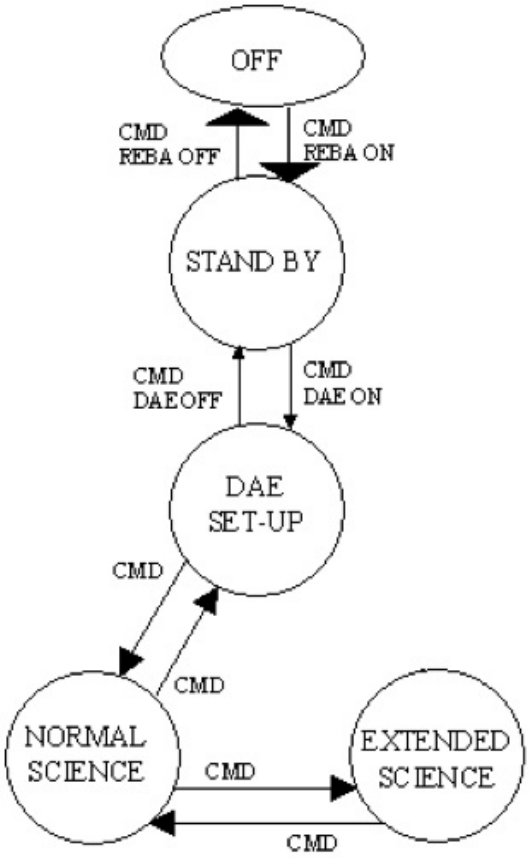

Figure 5. LFI Operating Modes and their nominal transitions

A scheme of the nominal transitions between the LFI Operation Modes are shown in Figure 5, a brief summary is given below.

1. OFF MODE: During this operating mode the instrument is completely off for example during the launch.

2. STAND-BY: During this mode only the REBA can be operated. It is the first interface to the instrument whenever the LFI is switched on. When the instrument is in this mode the RAA must be OFF because no data can be received and no control is possible on the radiometer chains.

3. DAE SET-UP: During this mode the REBA and the DAE are ON, but no radiometer chains are active. Nevertheless science data can be generated and contain only the background noise of the instrument.

4. NORMAL SCIENCE: During this mode the RAA is seen by the REBA as a set of 44 independent instruments. This means that each instrument can be operated, by the same SW, in different modes without affecting the LFI modes. Science data from the DAE are continuously acquired by the REBA that decides, on the basis of the activation table, which packets (either science or diagnostic) have to be produced. The whole set of HK is continuously acquired and sent to ground. This mode is the nominal for the LFI observation operations.

5. EXTENDED SCIENCE: This mode is similar to the previous except that for the total amount of telemetry sent to the ground. In fact this mode shall be used when, in particular cases, (e.g. calibration…) a larger telemetry rate is needed and made available by an agreement with HFI and the CDMS.

During launch, for contingency situations and/or to allow diagnostics of other spacecraft subsystems (e.g. HFI or others) LFI is in the OFF mode. When, upon a command from ground the REBA is powered on, the instrument is in its STAND-BY mode. A step-by-step bootstrap procedure commanded from ground documented by HK is initialized to turn the DAE on. This sets-up the internal communications, and allows the LFI subsystems to collect and deliver a

full set of HK. The instrument is in DAE SET-UP mode. The following step is to upload from ground the DAE settings and processing parameters; then, to switch on the RCA on ground command. At this stage, on ground command, the acquisition of science data can start. A further step is needed to move to NORMAL SCIENCE, namely start processing and compressing the science raw data. When this is accomplished, science packets can be sent to ground.

Instrument Technical Performance

Spectral Response

The in-band receiver response has been thoroughly modelled and measured for all the LFI detectors during ground tests. The complete set of bandpass curves has been published in #zonca2009 where all the details of the LFI radiometer's spectral response are given. From each curve we have derived the effective centre frequency according to:

where is the receiver bandwidth and $g(\nu)$is the bandpass response. Table 14 below gives the centre frequencies of the 22 LFI radiometers. For each radiometer, $g(\nu)$is calculated by weight-averaging the bandpass response of the two individual diodes with the same weights used to average detector timestreams. For simplicity and for historical reasons, we will continue to refer to the three channels as the 30, 44, and 70 GHz channels.

Table 14. LFI centre frequencies.

RCA	Radiometer M ν_0 [GHz]	Radiometer S ν_0 [GHz]
***V* band; "70 GHz"** ...		
LFI18	71.7	70.1
LFI19	67.5	69.6
LFI20	69.2	69.5
LFI21	70.4	69.5
LFI22	71.5	72.8
LFI23	70.8	71.3
Average	70.3	
***Ka* band; "44 GHz"** ..		
LFI24	44.4	44.1
LFI25	44.0	44.1
LFI26	43.9	44.1
Average	44.1	
***K* band; "30 GHz"** ...		
LFI27	28.3	28.5
LFI28	28.8	28.2
Average	28.5	

Colour corrections, $C(\alpha)$, needed to derive the brightness temperature of a source with a power-law spectral index α, are given in the table 15 below. The values are averaged for the 11 RCAs and for the three frequency channels. Details about the definition of colour corrections are provided in #planck2011-1-6.

Table 15. Colour corrections for the 11 LFI RCAs individually and averaged by frequency.

RCA	Spectral Index α −2.00	−1.00	0.00	1.00	2.00	3.00	4.00
LFI18	1.054	1.028	1.011	1.003	1.003	1.010	1.026
LFI19	1.170	1.113	1.066	1.026	0.994	0.969	0.949
LFI20	1.122	1.079	1.044	1.017	0.997	0.983	0.975
LFI21	1.087	1.053	1.028	1.010	1.000	0.996	0.998
LFI22	0.973	0.971	0.976	0.988	1.007	1.033	1.066
LFI23	1.015	1.004	0.999	0.998	1.003	1.012	1.026
70 GHz average	**1.070**	**1.041**	**1.021**	**1.007**	**1.001**	**1.001**	**1.007**
LFI24	1.028	1.015	1.007	1.002	1.000	1.003	1.009
LFI25	1.039	1.024	1.013	1.005	1.000	0.999	1.000
LFI26	1.050	1.032	1.017	1.007	1.000	0.997	0.997
44 GHz average	**1.039**	**1.024**	**1.012**	**1.004**	**1.000**	**0.999**	**1.002**
LFI27	1.078	1.049	1.026	1.010	1.000	0.996	0.998
LFI28	1.079	1.049	1.026	1.009	1.000	0.997	1.002
30 GHz average	**1.079**	**1.049**	**1.026**	**1.010**	**1.000**	**0.997**	**1.000**

Bandpass Estimation

As detailed in #zonca2009, our most accurate method to measure the LFI bandpasses is based on measurements of individual components integrated into the LFI Advanced RF Model (LARFM) to yield a synthesised radiometer bandpass. The LARFM is a software tool based on the open-source Quasi Universal Circuit Simulator (QUCS). The measured frequency responses of the various subsystems (feed-OMT, FEM, BEM) are considered as lumped S-parameter components. Measurements of single components are obtained with standard methods and provide highly reliable results, with precision of order 0.1-0.2 dB over the entire band. Waveguides are simulated with an analytical model, in order to reproduce the effect of their temperature gradient and the effect of standing waves caused by impedance mismatch at the interfaces between the FEM and BEM. This is because the 1.8-meter long waveguides were not measured at unit level in cryogenic conditions. The model provides accurate agreement with the measured waveguide response in the conditions of the test measurements (300 K). The composite bandpasses are estimated to have a precision of about 1.5 to 2 dB.

We also attempted an end-to-end measurement of the RCA spectral response in the cryo-facility as an independent check. Unfortunately, these measurements suffered some subtle systematic effects in the test setup (standing waves at 70 GHz; polarisation mismatch and narrow frequency coverage at 30 and 44 GHz), preventing an accurate cross-check. However, the comparison shows a general agreement within limits of the test reliability and repeatability.

Figures 6 and 7 below show all the LFI bandpasses obtained by the frequency response data of each radiometer unit assembled by the LARFM. The 70 GHz channels show a low bandpass ripple, of about 10 dB, which is within scientific requirements. The spike between 60 and 61 GHz, below the low frequency cut-off, is due to a systematic effect present in all the BEM gain measurements and caused by the test setup. We removed this range from the bandpasses made available at the Data Processing Center in order to avoid possible spurious effects and therefore the frequency coverage is 61-80 GHz. The high frequency cut-off is not well defined in most of the channels. The 30 and 44 GHz bandpasses show a more complex shape, driven by the BEM spectral response, but still within ± 10dB. The low frequency cut-off is always well defined, while the high frequency cut-off is not well defined in RCA 24 and 26. However, comparing with the high frequency cut-off of RCA 25, it is expected that the additional bandwidth is very low. Frequency coverage is 25-50 GHz for the 44 GHz channels and 21.3-40 GHz for the 30 GHz channels.

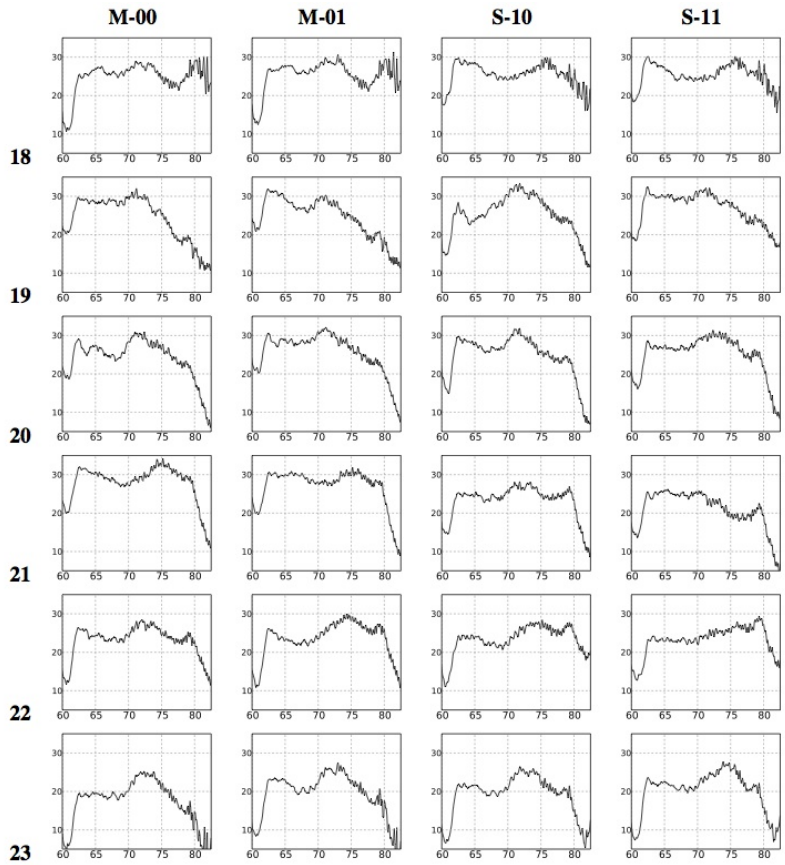

Figure 6. LFI 70 GHz channels' bandpasses. Each row shows the 4 bandpasses of a RCA ordered as M-00, M-01, S-10 and S-11. Units are [dB] $10log(\frac{V_{out}}{V_{in}})$ plotted against frequency [GHz].

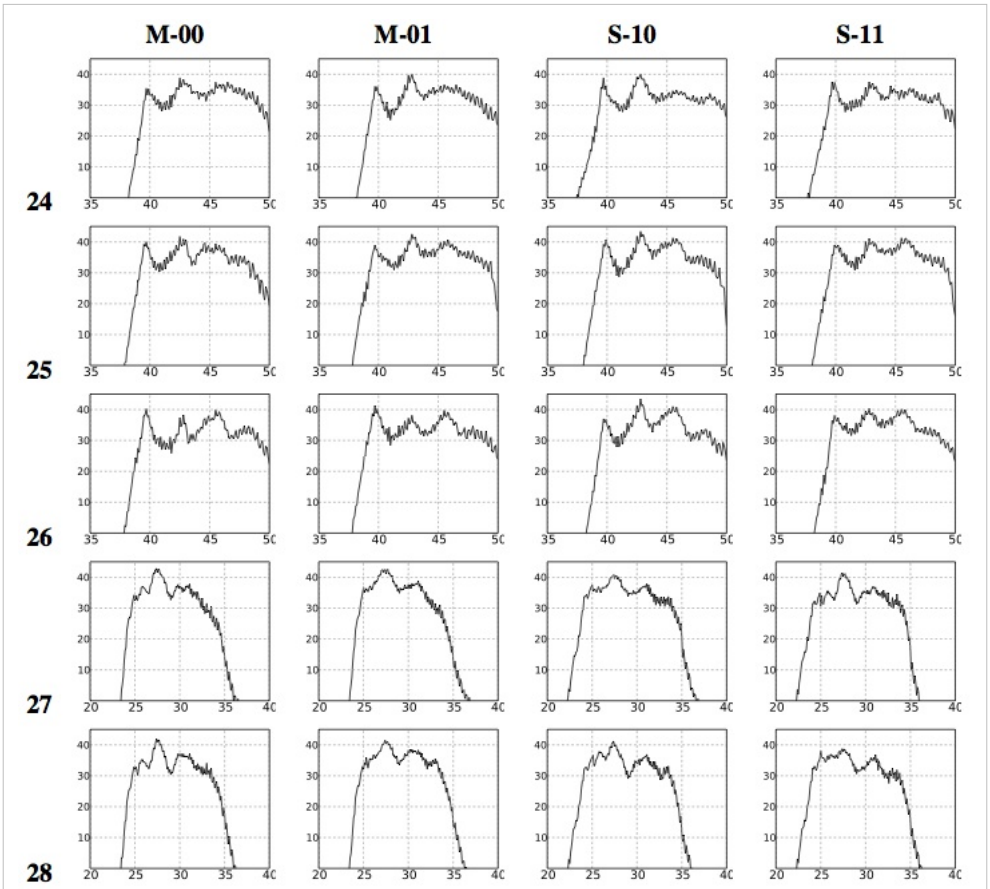

Figure 7. LFI30 and 44 GHz channels' bandpasses. Each row shows the 4 bandpasses of a RCA ordered as M-00, M-01, S-10 and S-11. Units are [dB] $10log(\frac{V_{out}}{V_{in}})$ plotted against frequency [GHz].

Stability

Thanks to its differential scheme, the LFI is insensitive to many effects caused by 1/f noise, thermal fluctuations, or electrical instabilities. As detailed in #planck2011-1-4 [Planck early results. First assessment of the Low Frequency Instrument in-flight performance [1]], one effect detected during the first survey was the daily temperature fluctuation in the back-end unit induced by the downlink transponder, which was powered on each day for downlinks during the first 258 days of the mission. As expected, the effect is highly correlated between the sky and reference load signals. In the difference, the variation is reduced by a factor , where r is the gain modulation factor defined above.

A particular class of signal fluctuations occasionally observed during operations is due to electrical instabilities that appear as abrupt increases in the measured drain current of the front-end amplifiers, with a relaxation time variable from few seconds to some hundreds of seconds. Typically, these events cause a simultaneous change in the sky and reference load signals. Because they are essentially common-mode, their residual on the differenced data is negligible (figure 8), and the data are suitable for science production. In a few cases the residual fluctuation in the differential output was large enough (a few millikelvin in calibrated antenna temperature units) to be flagged, and the data were not used. The total amount of discarded data for all LFI channels until Operational Day 389 was about 2000 s per detector, or 0.008%.

A further peculiar effect appeared in the 44 GHz detectors, where single isolated samples, either on the sky or the reference voltage output, were far from the rest. Over a reference period of four months, 15 occurrences of single-sample spikes (out of 24 total anomaly events) were discarded, an insignificant loss of data.

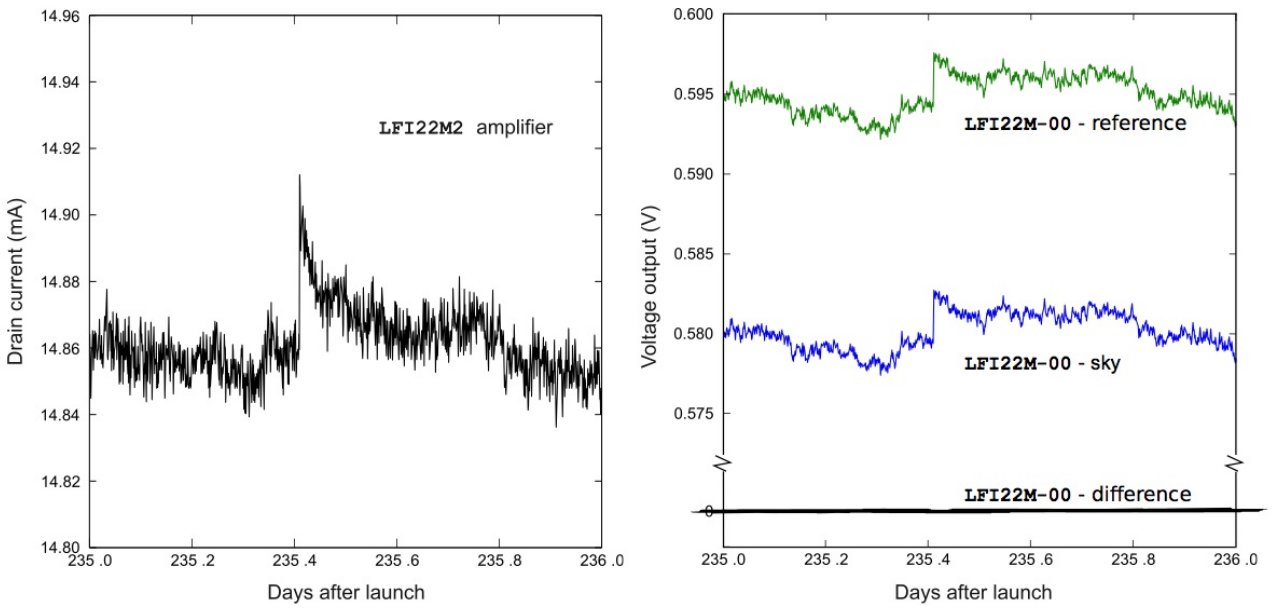

Figure 8. Short spikes in the drain current (left) affect total power signals (right). The jumps are strongly correlated in sky and reference signals, so that in the difference data the effect essentially disappears.

Thermal Susceptibility

As already mentioned in section LFI In-flight Calibration above and detailed in #gregorio2013, during the CPV campaign, susceptibility tests were performed in order to characterise the LFI instrument susceptibility to thermal and electrical variations.

The effect of temperature fluctuations on the LFI radiometers is originated in the Planck cold end interface of the hydrogen sorption cooler to the instrument focal plane. The temperature is actively controlled through a dedicated stage, the Thermal Stabilization Assembly (TSA), providing a first reduction of the effect. The thermal mass of the focal plane strongly contribute to reduce residual fluctuations. The physical temperature fluctuations propagated at the front end modules cause a correlated fluctuation in the radiometer signal degrading the quality of scientific data. The accurate characterization of this effect is crucial for possibly removing it from raw data by exploiting the housekeeping information of thermal sensors.

The propagation of the temperature oscillations through the focal plane and the instrument response to thermal changes were characterized through two main tests:

- the thermal dynamic response aimed at measuring the dynamic thermal behaviour of the LFI Focal Plane;
- the radiometers thermal susceptibility.

Thermal Dynamic Response

In order to amplify the effect and to get a more accurate measurement, the active control from the TSA was switched off. The resulting increased fluctuations, propagating at the cooler frequencies, were used to evaluate transfer functions between the TSA stage and the FPU sensors (see figure 9 below). The analysis produced damping factors of 2–5 at about 1 mHz. The source of fluctuations was characterized by two typical periods of the sorption cooler during the final CPV phase: (i) the single bed cycle time, 940 s, (ii) the complete cooler period, six times larger, 5640 s.

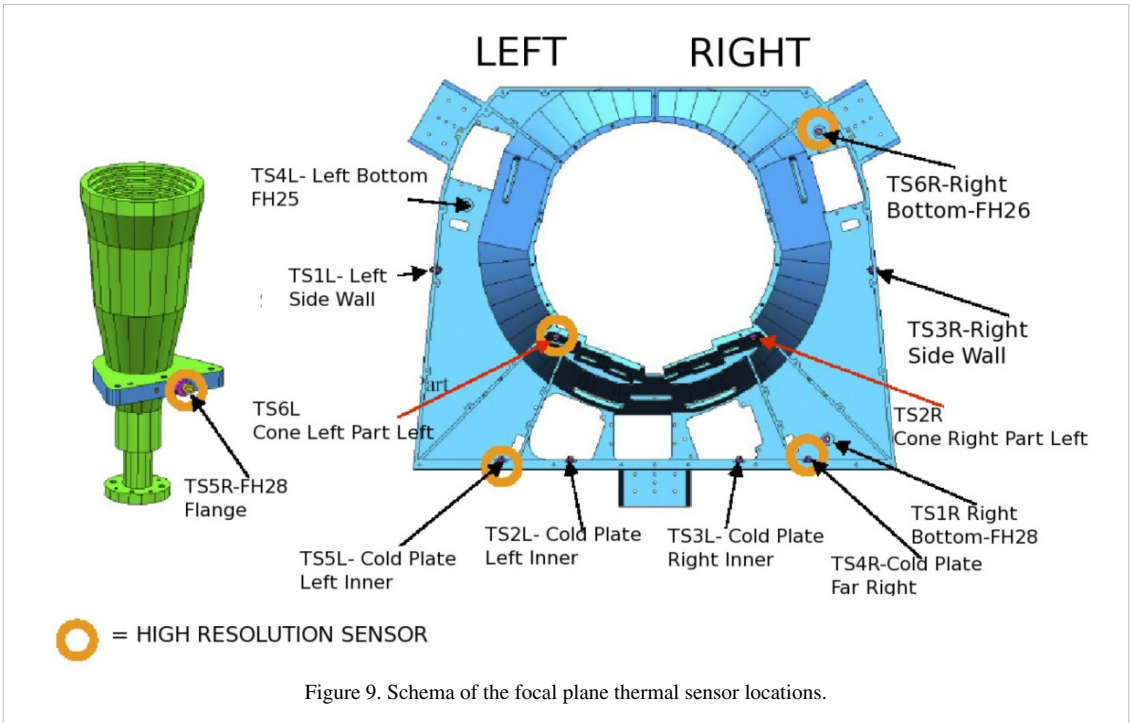

Figure 9. Schema of the focal plane thermal sensor locations.

Results are shown in Table 16. Sorting the sensors by the transfer function amplitudes in descending order (second column of the table), the route of the propagation of temperature fluctuations through the focal plane sensors (shown in figure 9) was reproduced as expected: the largest amplitudes are in the sensor closest to the right bottom corner interface with the working cooler and they decrease in the direction left upwards. The measured values in flight showing a good agreement with what measured during the CSL ground test.

Table 16. Transmission amplitudes and phases of fluctuations at the two main cooler frequencies during the transient test. Typical fit parameters uncertainties are at 1% level.

	Results	1.064 mHz	Results	0.177 mHz
Sensor ID	Ampl. (V)	Phase (rad)	Ampl. (V)	Phase (rad)
TSL1	0.113	1.79	0.520	0.95
TSL2	0.153	1.13	0.560	0.81
TSL3	0.266	0.60	0.600	0.60
TSL4	0.112	1.83	0.522	0.96
TSL5	0.136	1.37	0.554	0.87
TSL6	0.110	1.70	0.483	0.98
TSR1	0.402	0.33	0.660	0.41
TSR2	0.218	0.86	0.583	0.68
TSR3	0.222	0.84	0.589	0.68
TSR4	0.313	0.49	0.616	0.52
TSR5	0.224	0.84	0.586	0.68
TSR6	0.158	1.23	0.545	0.81

Radiometer Thermal Susceptibility

Fluctuations of the focal plane temperature would cause variations of important parameters (mainly the low noise amplifier gains and noise temperatures), impacting the radiometer output signal. The response of the LFI radiometers to thermal fluctuations was estimated by inducing discrete temperature steps on the focal plane through TSA set-point changes. The set-point was changed over four values (Fig. 47, left) and after a stabilization of at least two hours, the measured receivers output was characterized as a function of each temperature variation of about 0.3 K.

The slope of the resulting T_{ant}vs T_{phys}plot is the measured response of the receivers to a change in the temperature. Results, reported in the Table 17, confirmed that physical temperature fluctuations in the main frame are furtherly reduced when convolved with the radiometer thermal susceptibility coefficients: the derived output fluctuations, measured in antenna temperature, were actually reduced by an extra factor of 10 to 200 (according to the channel considered), of the same order of ground test results. This corresponds to reduce the mean peak-to-peak amplitudes of fluctuations measured by high resolution sensors, of the order of 4 mK in steady condition, of at least one order of magnitude in the output timestream.

Table 17. Results of thermal susceptibility test. Units are

Radiometer (sensor)	M - 00	M - 01	S - 10	S - 11
RCA 18 (TS2R)	0.040 ± 0.010	0.030 ±0.010	0.031 ± 0.009	0.027 ± 0.009
RCA 19 (TS2R)	0.040 ± 0.010	0.050 ±0.010	0.030 ± 0.010	0.040 ± 0.010
RCA 20 (TS2R)	0.050 ± 0.010	0.060 ±0.010	0.040 ± 0.010	0.050 ± 0.010
RCA 21 (TS6L)	0.029 ± 0.009	0.039 ±0.009	0.060 ± 0.010	0.070 ± 0.010
RCA 22 (TS6L)	0.080 ± 0.010	0.069 ±0.009	0.100 ± 0.010	0.100 ± 0.010
RCA 23 (TS6L)	0.050 ± 0.010	0.040 ±0.010	0.050 ± 0.010	0.050 ± 0.010
RCA 24 (TS2L)	0.013 ± 0.008	0.013 ±0.009	0.014 ± 0.007	–
RCA 25 (TS4L)	0.012 ± 0.007	0.008 ±0.007	0.001 ± 0.007	0.001 ± 0.007
RCA 26 (TS6R)	-0.020± 0.008	-0.009± 0.009	0.006 ± 0.008	0.010 ± 0.007
RCA 27 (TS2L)	-0.007± 0.005	0.000 ±0.005	-0.007 ± 0.005	0.001 ± 0.005
RCA 28 (TS5R)	0.041 ± 0.006	0.027 ±0.006	0.034 ± 0.005	0.011 ± 0.005

Instrument Budgets

Power Budget

Table 18. LFI sub-system power budget.

Subsystem	Unit	Assembly	Sub-Assembly	Budget [W]
RAA				45.599
	FEU			0.329
		FE structure		N/A
		Feed Horns		N/A
		OMTs		N/A
		FEMs		0.329
			30 GHz	0.056
			44 GHz	0.121

			70 GHz	0.152
	BEU			45.270
		DAE		31.986
		BEMs		13.284
			30 GHz	4.914
			44 GHz	4.633
			70 GHz	3.737
		Waveguides		N/A
		RAA harness		N/A
	4K Load			N/A
REBA				22.700
System Harness				N/A
Total				68.299

Mass Budget

The maximum allocated mass for the Planck Instruments is 445 kg, 89 kg are allocated for the LFI instrument. The distribution of the instrument and cooler mass to the different interfaces in the system is as given in table 19 below.

Table 19. LFI sub-system mass budget.

Subsystem	Unit	Assembly	Sub-Assembly	Budget [kg]
RAA				77.900
	FEU			22.935
		FE structure		17.680
		Feed Horns+OMTs		2.825
			30 GHz	0.680
			44 GHz	0.732
			70 GHz	1.413
		FEMs		2.430
			30 GHz	0.810
			44 GHz	1.110
			70 GHz	0.510
	BEU			25.542
		DAE		23.130
		BEMs		2.412
			30 GHz	0.624
			44 GHz	0.864
			70 GHz	0.924
	Waveguides			23.005
		WG structure		15.940
		WGs		7.065

	RAA harness			5.491
		BEU internal harness		4.489
		DAE-FEU cryo-harness		1.002
	4K Load			0.927
REBA (2 units)				8.480
System Harness				3.495
Total				89.875

Telemetry Budget

All the science data flow coming from the foreseen on-board data processing can be summarised in the following table 20.

Table 20. Data processing and compression results.

	30 GHz	**44 GHz**	**70 GHz**	**Total**
Total samples	65	94	154	
Compression factor	2.4	2.4	2.4	
Compressed samples	27	39	64	
Science data available (word)	490	490	490	
Time per packet (s)	18.035	12.570	7.651	
Corresponding sky arc (°)	108	75	46	
Packet frequency (Hz)	0.444	0.955	3.317	
Net Data Volume (word/s)	217.352	467.778	1536.986	2222.116
Net Data Volume (kbps)	3.478	7.484	24.592	35.554

This result refers to the net science telemetry rate that LFI sends to ground. If we add the overhead due to the packet header (protocol) and the tertiary header we obtain a gross science telemetry rate of 37.150 kbps. This number should be added to the data coming from the calibration channel (uncompressed data used to verify the correct functionalities of the on-board compression algorithm, see Reduction and Compression of Science Data section) sent to ground in parallel. This channel has a worst case gross data production of 5.140 kbps for a total science data of 42.290 kbps.

The gross housekeeping telemetry budget is 2.425 kbps for a total budget of 44.715 kbps. The total data budget allocated to the LFI is 53.5 kbps well above the LFI total telemetry budget.

References

<biblio force=false>

1. References

</biblio>

The telescope

The telescope is an off-axis aplanatic design with two elliptical reflectors and a 1.5 m projected diameter and an overall emissivity $\lesssim 1\%$. The optical system was optimized for a set of representative detectors (eight HFI and eight LFI). The performance of the aplanatic configuration is not quite as good on the optical axis as the so-called Dragone-Mizuguchi Gregorian configuration, which eliminates astigmatism on the optical axis, but is significantly better over the large focal surface required by the many HFI and LFI feeds.

The Planck telescope consists of:

1. **The primary and secondary reflectors** (PR and SR), designed and manufactured by Astrium (Friedrichshafen, Germany);

2. **The support structure**, designed and manufactured by Oerlikon Space (Zurich, Switzerland).

For more information, see Tauber et al. 2010, A&A 520, A2.

For more information, see #tauber2010b.

Contents of this chapter

<biblio force=false>

1. References

</biblio>

The standard radiation environment monitor

(NOTE: Adapted from IEEE TRANSACTIONS ON NUCLEAR SCIENCE, VOL. 50, NO. 6, DECEMBER 2003)

Introduction

The standard radiation environment monitor (SREM) is a particle detector developed for satellite applications. It measures high-energy electrons and protons of the space environment with a $\pm 20^{\circ}$ angular resolution, spectral information and provides the host spacecraft with radiation information. SREM was developed and manufactured by Contraves Space in cooperation with Paul Scherrer Institute under a development contract of the European Space Agency. SREM is the second generation of instruments in a programme, which was established by ESA's European Research and Technology Centre (ESTEC) to:

1. Provide minimum intrusive radiation detectors for space applications;
2. Provide radiation hazard alarm function to instruments on board spacecraft;
3. Assist in investigation activities related to possible radiation related anomalies observed on spacecraft;
4. Assist in in-flight Technology Demonstration Activities.

The design goals are low weight, small dimensions, low power consumption, combined with the ability to provide particle species and spectral information.

In the case of Planck, the use of the SREM was entirely within the scope of bullets 1 and 3 above as due to the nature of operations no real time alarms where possible

The instrument

The SREM consists of three detectors (D1, D2, and D3) in two detector heads configurations. One system is a single silicon diode detector (D3). The main entrance window is covered with 0.7 mm aluminum, which defines the lower energy threshold for electrons to ∼0.5 MeV and for protons to ∼10MeV. The other system uses two silicon diodes (detectors D1/D2) arranged in a telescope configuration. The main entrance of this detector is covered with 2 mm aluminum giving a proton and electron threshold of 20 and 1.5 MeV, respectively.A 1.7-mm-thick aluminum and 0.7−mm-thick tantalum layer separate the two diodes of the telescope configuration.

The telescope detector allows measurement of the high-energy proton fluxes with enhanced energy resolution. In addition, the shielding between the two diodes in the telescope prevents the passage of electrons. However, protons with energies greater than ∼30 MeVgo through. Thus, using the two diodes in coincidence gives pure proton count rates allowing subtraction of the proton contribution from the electron channels. A total of 15 discriminator levels are available to bin the energy of the detected events. Any two of the levels can be used to raise an alarm flag when the count rates exceed a programmable threshold. This alarm signal can then be used to control the operation of the spacecraft and its instruments. The detector electronics is capable of processing a detection rate of 100 kHz with dead-time correction below 20%. The SREM is contained in a single box of 20 ×12 ×10 and weighs 2.6 kg (see Fig. 1). The box contains the detector systems with the analog and digital front-end electronics, a power supply, and a TTC-B-01 telemetry and Telecommand interface protocol. By virtue of a modular buildup, the interface can be adapted to any spacecraft system. The power consumption is approximately 2.5 W. An essential input for the interpretation of the detection rates, in terms of particle fluxes, are the energy dependent

The data

The SREM data are provided in the Planck Legacy Archive in the following form:

- individual FITS files per calendar day

The fiber optic gyro unit

The Fiber-Optic Gyro unit (FOG) is an extra payload on-board Planck which is not used as part of the attitude control system. The FOG functioning is based on the physical phenomenon called *Sagnac effect*::

"*a solid-state optical interferometer enclosing a surface located on a rotating support will detect a phase difference of the optical signal, which is proportional to the angular rate and to the surface enclosed by the optical path*".

The FOG features the following architecture:

- An optical path enclosing a maximal surface: this is realized through the 1 km long fibre optic, winded many time round, in order to make a reasonable sized interferometer (< 120 mm in diameter).
- A source, to deliver the light to the interferometer.
- A multifunction Integrated Optical Circuit, which closes the interferometer, to share the light between the two extremities of the fiber optic coil, to filter undesirable polarization.
- A coupler to extract the optical signal coming back from the ring interferometer, which is the signal carrying the Sagnac inertial information, and to direct it towards an optical detector.
- A detection module to convert this light signal into an electrical signal.
- A closed-loop signal processing to increase the dynamic range and remove the effect of fluctuations of the optical power and of the gain of the detection chain, allowing an easy auto-calibration of the system and excellent scale factor stability and linearity.
- A biasing modulation allowing the measurement of very low rotation rates as well as the sign of those rotations.

Redundancy is offered by providing four skewed gyro channels, allowing the Attitude Control and Measurement Subsystem to use any triplet among the four axes to determine the spacecraft three axes rates. Nominally the four channels are activated, in case of failure or thermal criticalities a subset of channels could be used.

There is no dangerous FOG flight command. The FOG is designed to operate five years ON in orbit, withstanding 1000 ON/OFF cycles, and its performance is guaranteed under rotations of ± 10deg/second, and at the temperature range of 253 K up to 333 K. Power dissipations are in the range of 5.5 up to 6.7 W/channel.

Ground Segment and Operations

Ground segment overview

Geographical distribution of the Planck Ground Segment

The Planck Ground Segment is made of four geographically distributed centres:

The Mission Operations Centre

The mission operations centre (MOC), located at ESA's operations centre in Darmstadt (Germany), is responsible for all aspects of flight control and of the health and safety of the Planck satellite, including both instruments. It plans and executes all necessary satellite activities, including instrument commanding requests by the instrument operations centres.

MOC communicates with the satellite using ESA's 35-m antenna located in New Norcia (Australia), or that in Cebreros (Spain), over a daily 3-h period, during which it uplinks a scheduled activity timeline which is autonomously executed by the satellite, and downlinks the science and housekeeping (HK) data acquired by the satellite during the past 24 h. The downlinked data are transferred from the antenna to the MOC over a period of typically 8 h; at MOC they are put onto a data server from where they are retrieved by the two Data Processing Centres.

The European Space Operations Centre in Darmstadt, Germany, home of the Planck Mission Operations Centre.

The Planck Science Office

The Planck Science Office (PSO)is located at ESA's European Space Astronomy Centre in Villanueva de la Cañada surroundings (Madrid, Spain).

Its main responsibilities include:

- coordinating scientific operations of the Planck instruments
- designing, planning and executing the Planck observation strategy.

It provides to MOC a detailed pointing plan with a periodicity of about one month.

- creating and updating the specifications of the Planck Legacy Archive developed by the Science Archives Team at ESAC
- testing and operating the PLA

The European Space Astronomy Centre in Villanueva de la Cañada, Madrid, Spain, see of the Planck Science Office.

The LFI instrument operations and data-processing centre

The LFI instrument operations and data processing centre, located at the Osservatorio Astronomico di Trieste (Italy), is notably responsible for:

- the optimal operation of the LFI instrument
- the processing of the data acquired by LFI into the final scientific products of the mission.

The HFI instrument operations and data-processing centre

The HFI instrument operations and data processing centres, located respectively at the Institut d'Astrophysique Spatiale in Orsay (France) and at the Institut d'Astrophysique de Paris (France), are similarly responsible for the optimal operation of the HFI instrument, and (with several other institutes in France and the UK) for the processing of the data acquired by HFI into the final scientific products of the mission.

The data flow in the Planck Ground Segment

The Planck Science Office (PSO), located at ESAC, Spain, sends the pointing lists (Pre-Programmed Pointing Lists) to the Mission Operations Centre at ESOC in Darmstadt, Germany. The Flight Dynamics team at ESOC adapts them into Augmented Pre-Programmed Pointing Lists (APPL) taking into account ground station scheduling, Operational Day (OD) boundaries and other issues.

MOC sends pointing and instrument commands to the spacecraft, and receives the house-keeping telemetry and science data through the ground stations (for Planck, mostly the New Norcia and Cebreros ones).

Science data is then transferred to both Data Processing Centres (DPC) which process the data and send quality reports to PSO.

Science products (timelines, maps, etc) are exchanged between DPCs in order to help calibration and other scientific issues.

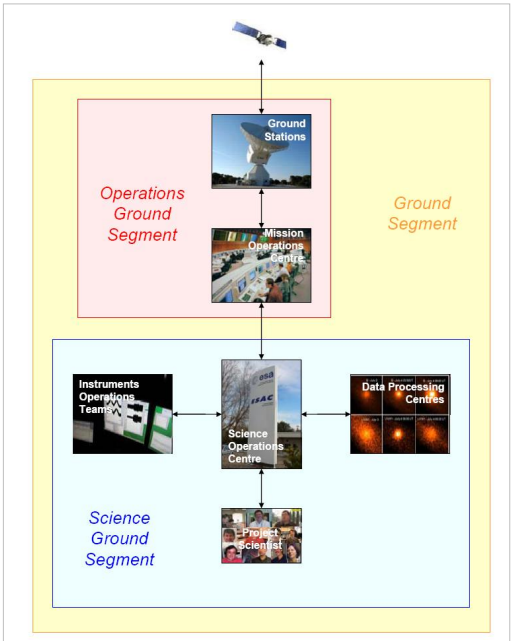

General schematics of European Space Agency Science Ground Segments. This picture exhibits the way ESA Ground Segments are generally organized.

References

Tauber et al. 2010, A&A 520, A1

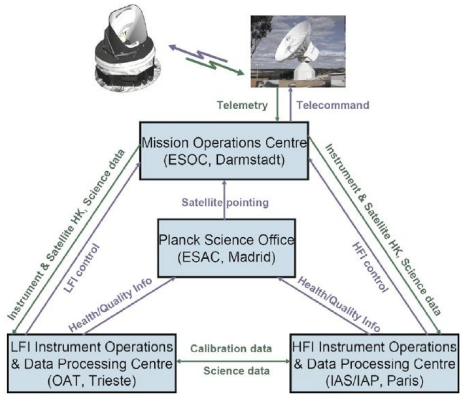

Specific schematics of the Planck Science Ground Segment. This picture exhibits the way the specific Planck Science Ground Segment works.

Contingencies

NOTE: THE LIST IS STILL INCOMPLETE.

The main unplanned events included the following:

- Very minor deviations from the scanning law include occasional (on the average about once every two months) under-performance of the 1-N thrusters used for regular manoeuvres, which implied the corresponding pointings were not at the intended locations. These deviations had typical amplitudes of 30 arcsec, and have no significant impact on the coverage map.
- The thruster heaters were unintentionally turned off between 31 August and 16 September 2009 (the so-called “catbed” event).
- An operator error in the upload of the on-board command timeline led to an interruption of the normal sequence of manoeuvres and therefore to Planck pointing to the same location on the sky for a period of 29 h between 20 and 21 November 2009 (“the day Planck stood still”). Observations of the nominal scanning pattern resumed on 22 November, and on 23 November a recovery operation was applied to survey the previously missed area. During the recovery period the duration of pointing was decreased to allow the nominal law to be caught up with. As a side effect, the RF transmitter was left on for longer than 24 h, which had a significant thermal impact on the warm part of the satellite.
- As planned, the RF transmitter was initially turned on and off every day in synchrony with the daily visibility window, in order to reduce potential interference by the transmitter on the scientific data. The induced daily temperature variation had a measurable effect throughout the satellite. An important effect was on the temperature of the 4He-JT cooler compressors, which caused variations of the levels of the interference lines that they induce on the bolometer data (Planck HFI Core Team 2011a). Therefore the RF transmitter was left permanently on starting from 25 January 2010 (257 days after launch), which made a noticeable improvement on the daily temperature variations.
- During the coverage period, the operational star tracker switched autonomously to the redundant unit on two occasions (11 January 2010 and 26 February 2010); the nominal star tracker was restored a short period later (3.37 and 12.75 h, respectively) by manual power-cycling. Although the science data taken during this period have normal quality, they have not been used because the redundant star tracker's performance is not fully characterised.

For more information, see Planck Collaboration 2011, A&A 536, A1.

Operational history

(Note: Adapted from Planck Collaboration 2011, A&A 536, A1)

Provide a description of the product Planck Operational State History.

The major operational phases and milestones are:

Launch and transfer to orbit: (provide date, and summary overview)

Planck was launched from the Centre Spatial Guyanais in Kourou (French Guyana) on 14 May 2009 at its nominal lift-off time of 13:12 UT, on an Ariane 5 ECA rocket of Arianespace2. ESA's Herschel observatory was launched on the same rocket. At 13:37:55 UT, Herschel was released from the rocket at an altitude of 1200 km; Planck followed suit at 13:40:25UT. The separation attitudes of both satellites were within 0.1 deg of prediction. The Ariane rocket placed Planck with excellent accuracy (semimajor axis within 1.6% of prediction), on a trajectory towards the second Lagrangian point of the Earth-Sun system (L2). After release from the rocket, three large manoeuvres were carried out to place Planck in its intended final orbit. The first (14.35 ms−1), intended to correct for errors in the rocket injection, was executed on 15 May at 20:01:05 UT, with a slight overperformance of 0.9% and an error in direction of 1.3 deg (a touch-up manoeuvre was carried out on 16 May at 07:17:36 UT). The second and major (mid-course) manoeuvre (153.6ms−1) took place between 5 and 7 June, and a touch-up (11.8 ms−1) was executed on 17 June. The third and final manoeuvre (58.8ms−1), to inject Planck into its final orbit, was executed between 2 and 3 July. The total fuel consumption of these manoeuvres, which were carried out using Planck's coarse (20N) thrusters, was 205 kg. Once in its final orbit, very small manoeuvres are required at approximately monthly intervals (1 ms−1 per year) to keep Planck from drifting away from its intended path around L2. The attitude manoeuvres required to follow the scanning strategy require about 2.6 ms−1 per year. Overall, the excellent performance of launch and orbit manoeuvres will lead to a large amount (~160 kg, or ~40% of initial tank loading) of fuel remaining on board at end of mission operations.

Planck started cooling down radiatively shortly after launch. Heaters were activated to hold the focal plane at 250 K, which was reached around 5 h after launch. The valve opening the exhaust piping of the dilution cooler was activated at 03:30 UT, and the 4He-JT cooler compressors were turned on at low stroke at 05:20 UT. After these essential operations were completed, on the second day after launch, the focal plane temperature was allowed to descend to 170 K for out-gassing and decontamination of the telescope and focal plane.

Commissioning: (provide date, and summary overview)

The first period of operations focussed on commissioning activities, i.e., functional check-out procedures of all sub-systems and instruments of the Planck spacecraft in preparation for running science operations related to calibration and performance verification of the payload. Planning for commissioning operations was driven by the telescope decontamination period of 2 weeks and the subsequent cryogenic cool-down of the payload and instruments. The overall duration of the cool-down was approximately 2 months, including the decontamination period. The sequence of commissioning activities covered the following areas:

- on-board commanding and data management;
- attitude measurement and control;
- manoeuvreing ability and orbit control;
- telemetry and telecommand;
- power control;

- thermal control;
- payload basic functionality, including:
- the LFI;
- the HFI;
- the cryogenic chain;
- the Standard Radiation Environment Monitor;
- the Fibre-Optic Gyro unit (FOG), a piggy-back experiment which is not used as part of the attitude control system.

The commissioning activities were executed very smoothly and all sub-systems were found to be in good health. The most significant unexpected issues that had to be addressed during these early operational phases were the following.

- The X-band transponder showed an initialisation anomaly during switch-on which was fixed by a software patch.
- Large reorientations of the spin axis were imperfectly completed and required optimisation of the on-board parameters of the attitude control system.
- The data rate required to transmit all science data to the ground was larger than planned, due to the unexpectedly high level of Galactic cosmic rays, which led to a high glitch rate on the data stream of the HFI bolometers (Planck HFI Core Team 2011a); glitches increase the dynamic range and consequently the data rate. The total data rate was controlled by increasing the compression level of a few less critical thermometers.
- The level of thermal fluctuations in the 20-K stage was higher than originally expected. Optimisation of the sorption cooler operation led to an improvement, though they still remained ~25% higher than expected (Planck Collaboration 2011b).
- The 20-K sorption cooler turned itself off on 10 June 2009, an event which was traced to an incorrectly set safety threshold.
- A small number of sudden pressure changes were observed in the 4He-JT cooler during its first weeks of operation, and were most likely due to impurities present in the cooler gas (Planck Collaboration 2011b). The events disappeared after some weeks, as the impurities became trapped in the cooler system.
- The 4He-JT cooler suffered an anomalous switch to standby mode on 6 August 2009, following a current spike in the charge regulator unit which controls the current levels between the cooler electronics and the satellite power supply (Planck Collaboration 2011b). The cooler was restarted 20 h after the event, and the thermal stability of the 100-mK stage was recovered about 47 h later. The physical cause of this anomaly was not found, but the problem has not recurred.
- Instabilities were observed in the temperature of the 4He-JT stage, which were traced to interactions with lower temperature stages, similar in nature to instabilities observed during ground testing (Planck Collaboration 2011b). They were fixed by exploring and tuning the operating points of the multiple stages of the cryo-system.
- The length of the daily telecommunications period was increased from 180 to 195 min to improve the margin available and ensure completion of all daily activities.

The commissioning activities were formally completed at the time when the HFI bolometer stage reached its target temperature of 100 mK, on 3 July 2009 at 01:00 UT. At this time all the critical resource budgets (power, fuel, lifetime, etc.) were found to contain very significant margins with respect to the original specification

Calibration and Performance Verification: (provide date, and summary overview)

Calibration and performance verification (CPV) activities started during the cool-down period and continued until the end of August 2009. Their objectives were to:

- verify that the instruments were optimally tuned and their performance characterised and verified;
- perform all tests and characterisation activities which could not be performed during the routine phase;
- characterise the spacecraft and telescope characteristics of relevance for science;
- estimate the lifetime of the cryogenic chain.

CPV activities addressed the following areas:

- tuning and characterisation of the behaviour of the cryogenic chain;
- characterisation of the thermal behaviour of the spacecraft

and payload;

- for each of the two instruments: tuning; characterisation and/or verification of performance, calibration (including thermal, RF, noise and stability, optical response); and data compression properties;
- determination of the focal plane footprint on the sky;
- verification of scanning strategy parameters;
- characterisation of systematic effects induced by the spacecraft and the telescope, including:
- dependence on solar aspect angle;
- dependence on spin;
- interference from the RF transmitter;
- straylight rejection;
- pointing performance.

The schedule of CPV activities consumed about two weeks longer than initially planned, mainly due to:

- the anomalous switch to standby mode of the 4He-JT cooler on 6 August (costing 6 days until recovery);
- instabilities in the cryo-chain, which required the exploration of a larger parameter phase space to find an optimal setting point;
- additional measurements of the voltage bias space of the LFI radiometers, which were introduced to optimise its noise performance, and led to the requirement of artificially slowing the natural cool-down of the 4He-JT stage.

A more detailed description of the relevant parts of these tests can be found in Mennella et al. (2011) and Planck HFI Core Team (2011a). On completion of all the planned activities, it was concluded that:

- the two instruments were fully tuned and ready for routine operations. No further parameter tuning was expected to be needed, except for the sorption cooler, which requires a weekly change in operational parameters (Planck Collaboration 2011b);
- the scientific performance parameters of both instruments was in most respects as had been measured on the ground before launch. The only significant exception was that, due to the high level of Galactic cosmic rays, the bolometers of HFI were detecting a higher number of glitches than expected, causing a modest (~10%) level of systematic effects on their noise properties (see details in Planck HFI Core Team 2011a);
- the telescope survived launch and cool-down in orbit without any major distortions or changes in its alignment;
- the lifetime of the cryogenic chain was adequate to carry the mission to its foreseen end of operations in November 2010, with a margin of order one year;
- the pointing performance was better than expected, and no changes to the planned scanning strategy were required;
- the satellite did not introduce any major systematic effects into the science data. In particular, the telemetry transponder did not result in radio-frequency interference, which implies that the data acquired during visibility periods is useable for science.

Nominal Mission: (provide date, and summary overview)

The routine operations phase of Planck is characterised by continuous and stable scanning of the sky and data acquisition by LFI and HFI. It started with the First Light Survey (FLS) on 13 August of 2009, at 14:15 UT.

The FLS was the last major activity planned before the start of routine surveying of the sky. It was conceived as a two-week period during which Planck would be fully tuned up and operated as if it was in its routine phase. This stable period could have resulted in the identification of further tuning activities required to optimise the performance of Planck in the long-duration surveys to come. The FLS was conducted between 13 and 27 August, and in fact led to the conclusion that the Planck payload was operating stably and optimally, and required no further tuning of its instruments. Therefore the period of the FLS was accepted as a valid part of the first Planck survey.

Survey scanning and performance

The observation strategy

The Planck *observation strategy*, or *scanning strategy*, makes use of the characteristics of the Planck spacecraft and orbit in order to achieve the survey goals in terms of sky coverage and scanning directions.

The Planck focal plane scans the sky in the way explained in the figure below.

The 353 GHz row scans the sky in small circles with a 85 deg. bore-sight angle from the spin axis. 545 GHz, 857 GHz, 143 GHz bolometers as well as LFI 25-26 radiometers have a slightly smaller bore-sight angle, while the other part of the Planck focal plane have larger ones (up to ~ 89 deg.). The Planck spacecraft spins at a rate of 1 rpm.

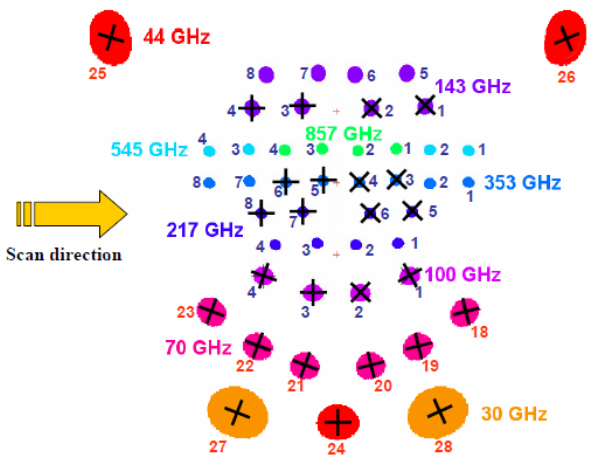

The Planck focal plane with the direction of scanning. Polarization-sensitive detectors are drawn with crosses indicating the polarization direction.

Planck, being at L2, moves along the Ecliptic at ~ one degree per day, and needs to keep the Solar aspect angle below ~ 9 degrees at all times. In practice, during the surveys, the limit considered is 8 deg. Another celestial constraint is that the angle between the Planck spin axis and the anti-Earth direction cannot exceed 15 deg. (relaxed to 17 deg. from Survey 5 onward). These constraints have a very direct influence on the chosen scanning strategy.

The path followed by the Planck spin axis is defined with respect to the Ecliptic plane. It corresponds to a motion in longitude which maintains an anti-Sun pointing (about one degree per day), to which is added a cycloidal motion (precession) of the spin axis around the anti-Sun position (fiducial point). The cycloidal path is defined by the following functions:

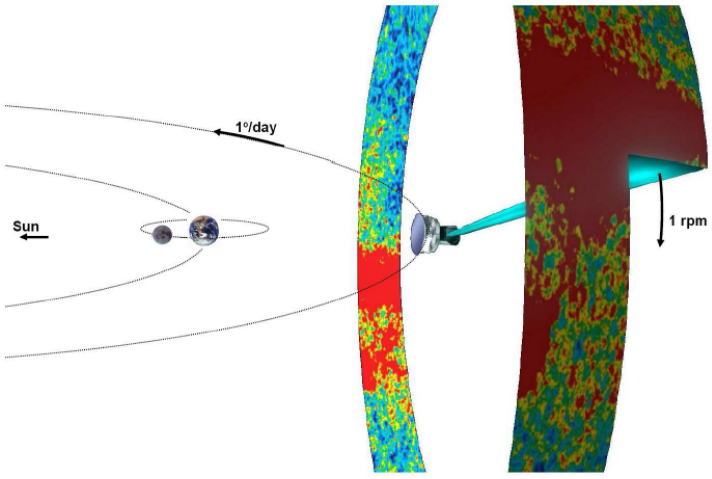

Simplified way to show the Planck scanning strategy, without additional motion of the spin axis

$ \lambda = \theta \sin((-1)^n \omega (t-t_0)+\varphi) $ (eq. 1)

$ \beta = -\theta \cos((-1)^n \omega(t-t_0) + \varphi) $ (eq. 2)

where λ is the angular distance from the fiducial point in Ecliptic longitude, β the angular distance from the fiducial point in Ecliptic latitude, θ the spin axis precession amplitude, ω the pulsation of the precession, φ its phase, n the parameter which controls the motion direction of the precession, t is the time, and t_0 is the first time during the Planck survey at which the fiducial point crosses the 0 Ecliptic longitude line.

The reasons to decide to use such a precession of the spin axis are the following :

- An excursion of the spin axis from the anti-Sun direction is required to fully observe the whole sky (no excursion would leave a large area unobserved around the Ecliptic poles)
- The precession motion allows to keep the Sun aspect angle constant during the whole survey, therefore minimizing the thermal constraint variations on the spacecraft

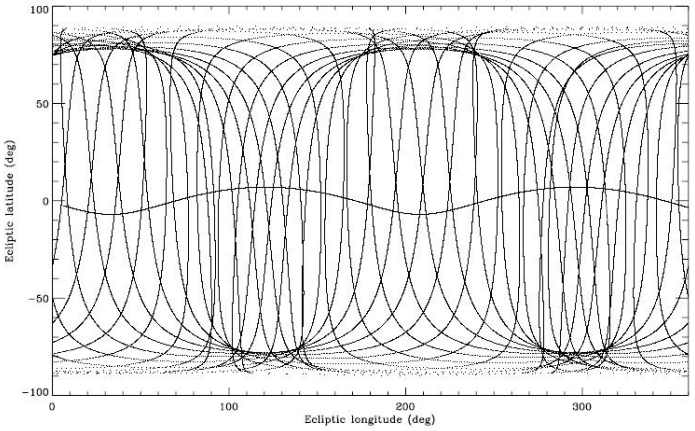

Spin axis path with a 7 degree amplitude cycloidal scanning, from Dupac & Tauber 2005, A&A 430, 363

The following precession parameters have been chosen for the BSS:

- amplitude $\theta = 7.5^o$ (this value is the lowest possible which allows to cover the whole sky with all detectors)
- n = 1 (anti-clockwise motion as seen from the Sun)
- pulsation $\omega = 2\pi$ / (half a year). Faster precession was considered, and has interesting advantages, but is not possible given the constraints if one wants to keep a 7.5 deg. amplitude (which is necessary to cover the whole sky).
- The phase of the precession was decided according to this set of criteria (in order of importance):

a) respecting the operational constraints,

b) allowing the largest possible angle between two scans on the Crab,

c) avoiding null dipole amplitude for the whole mission,

d) optimizing the position of the planets in the beginning of the survey and with respect to the feasibility of their recovery,

e) placing the two “deep fields” where Galactic foregrounds are minimum,

f) allowing a reasonable survey margin (i.e. the time allowed to recover lost pointings if a problem occurs)

The phase is 340 deg. for Surveys 1 to 4, and 250 deg. for Surveys 5 to 8.

The scanning strategy for the second year of Routine Operations (i.e. Surveys 3 and 4) is exactly the same as for the first year, except that all pointings are shifted by 1 arcmin along the cross-scanning direction, in order to provide finer sky sampling for the highest frequency detectors when combining two years of observations.

The change of phase between Survey 4 and Survey 5 occurred because it was found essential especially on the HFI side that scanning direction crossings are increased in the Planck survey. By choosing a phase 90 deg. away from the original one, one optimizes the scanning strategy in this respect.

The details of the justifications for these parameters can be found in PL-WG9-TN-001.

The scanning strategy parameters are input to the PSO Survey Planning and Performance Tool, which is the software which generates the series of pointing records to be sent out to MOC for implementation.

An approximate visualisation of the Planck scanning strategy can be found here [1] and there [2].

Spin axis manoeuvres and exact pointings

The motion of the spin axis is not continuous. Every change in the spin axis position is initiated by a manoeuvre which requires less than 5 minutes time to complete.

The duration between spin-axis manoeuvres is hereafter referred to as “dwelling times"; and the angular distance between manoeuvres along the spin axis path is hereafter referred to as “spacing”.

The dwelling times and spacings are defined as follows:

- The spacings are fixed to 2’ which roughly corresponds to Nyquist criterion for sampling the highest-frequency HFI detectors.
- The dwell times vary from 2360 s to 3904 s.

The exact series of coordinates and dwell times are set by equations 1 and 2 when one has fixed the spacings.

Data gap recoveries

Gaps in the data flow can occur because of various reasons:

- Anomalies may occur at spacecraft or instrument level, but also due to failures in the ground-to-spacecraft link or the ground segment itself. The adverse effects of such anomalies may be the loss of scientific data corresponding to one or several planned pointings, which have either not been acquired and/or stored in memory.
- Failure to acquire proper scientific data may occur to one or both instruments

In case a gap occurs, scientific criteria are applied to decide whether to recover the data through the Small-Gap Recovery procedure.

The Small-Gap Recovery (SGR) procedure can be applied by MOC or PSO:

- **MOC-triggered SGR**: Within its nominal scheduling procedure for an OD, the MOC searches the PPL for PREF corresponding to the OD being processed and any pointings which are subject of a Small Gap Recovery. As the PREF are sorted in chronological order according to their nominal start time, those corresponding to a small gap will naturally be the earliest. After checking attitude constraints, all observable pointings are listed and their dwell times reduced (initially) to the Minimum Dwell Time (MDT) as given in the PPL.

Having included all valid PREF the required slew times are calculated. With the required slew times and minimum dwell times for all pointings, the OD schedule may be under-populated; in this case the dwell times of all scheduled pointings will be increased equally to make use of all available time in the OD. If the resulting schedule is over-populated, even with MDT for all pointings, the recovery cannot be constrained to a single OD. The sequence

of pointings for the ODs involved will be optimized in PREF scheduling and dwell times in order to effect the recovery and revert to the nominal timeline as quickly as possible.

- **PSO-triggered SGR**:

PSO declares a small gap when pointings that have been executed result in data of insufficient quality or inadequate frequency coverage. This assessment is based on data quality and instrument health information provided by the DPCs. The algorithm that is used by the PSO to check the scientific validity of a pointing is implemented within the SPPT software tool. The SPPT ingests on a weekly basis a Weekly Health Report (WHR) for the HFI and LFI containing information on the current working status of each detector and their expected condition over the next four weeks. On a daily basis, a Daily Quality Report (DQR) provided by the DPCs for both instruments, includes a set of parameters that describe the quality of the detection achieved by each individual detector for every pointing executed.

The scheme for declaring a Small-Gap Recovery from PSO is the following:

- If a pointing fails to meet the chosen requirement, it becomes an SGR candidate

- If there are at least 12 consecutive pointings which are declared SGR candidates, and the problem has been identified and solved, then an SGR is triggered Recoveries are only carried out if the recovery slewing out is guaranteed to be in OCM. MOC carries out this analysis and decides whether they perform the SGR accordingly.

- The start and end times of the gap and the list of the pointing numbers (or just the numbers of the first and last pointings to be recovered) are then sent to MOC by E-mail, with the notification to start a Small-Gap Recovery

- MOC implements the Small-Gap Recovery, provided the pointings can still be scheduled with respect to their latest start time, using the same scheme as described in the MOC-triggered SGR section

Throughout the Planck mission, data losses have been very rare. Small-Gap Recovery has been applied only a couple of times.

Special observations

The special observations are:

- normal scanning on Solar System objects for calibration purposes

This concerns the following objects (planets): Mars, Jupiter, Saturn, Uranus and Neptune whose thermal emission in the far-infrared and their point-source-like quality make them essential calibrators for spider-web bolometers and radiometers.

Mars is a particularly interesting calibrator for Planck because of its proper motion. However this proper motion makes it difficult to observe it many times during the mission.

Jupiter is the brightest source for (non-polarized) calibration. Saturn is also used a lot, and Uranus and Neptune are secondary calibrators.

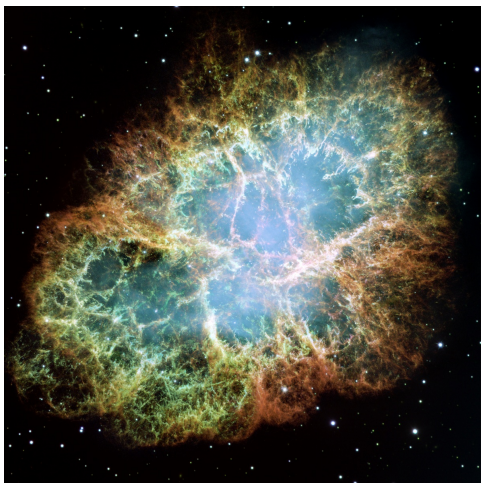

The Crab Nebula (Messier 1, NGC 1952, Taurus A), here seen by the Hubble Space Telescope

- normal scanning on other (non-moving) sources for calibration purposes

This concerns mostly the Crab Nebula for polarizer calibration purposes. This supernova remnant is highly polarized and as such represents the main polarization calibrator for Planck.

- special pointings during the calibration phase, not relative to celestial sources

- "deep rings" : these special observations are performed on each passage of Jupiter and the Crab Nebula, from January 2012 onward.

They consist of very deeply sampled observations (0.5') with the spin axis along the Ecliptic plane, during typically two to three weeks.

These observations benefit from special relaxing of the celestial constraints with Solar Aspect Angles < 9 deg. rather than < 8 deg. during cycloidal surveying.

- "drift scans" : these special observations are performed on Mars, making use of its proper motion

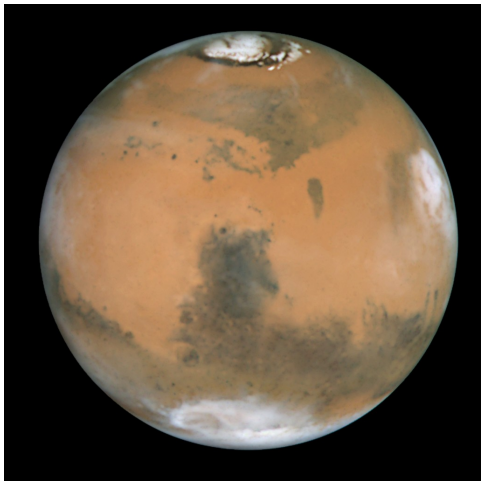

Mars as seen by the Hubble Space Telescope in 1999

Start and end of surveys

The completion of a given “survey” is declared when the logical AND of all frequency-coverage maps is greater than 95 %, OR the sky has been surveyed over a consecutive period of 7.5 months. Note that this definition is that of the Project Scientist and Planck Science Office. Data Processing Centres do not use the same concept of surveys to create "survey" maps.

In practice, since the gaps during the surveys have always been very small, it results in ~ six months per survey.

- **Survey 1**: starts August 13, 2009, ends Feb. 13, 2010
- **Survey 2**: starts Feb. 14, 2010, ends Aug. 13, 2010
- **Survey 3**: starts Aug. 14, 2010, ends Feb. 13, 2011
- **Survey 4**: starts Feb. 14, 2011, ends July 29th, 2011

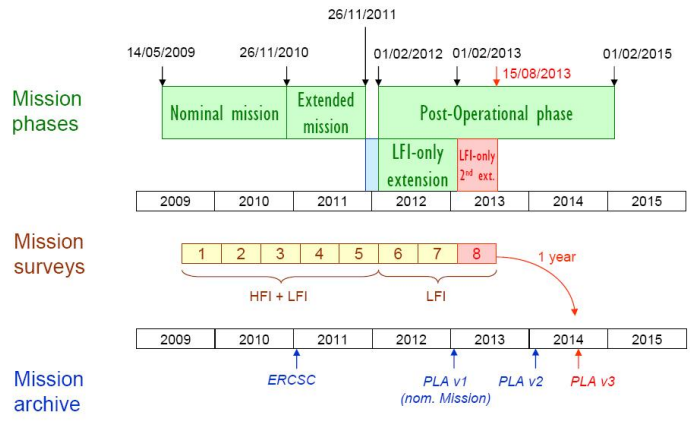

The Planck mission timeline with the distribution of the "sky surveys".

This survey was shortened in ordered to start earlier with the new scanning strategy (see above).

- **Survey 5**: starts July 29th, 2011, ends January 30th, 2012
- **Survey 6** (LFI only): starts January 30th, 2012, ends July 31st, 2012
- **Survey 7** (LFI only): starts July 31st, 2012, ends January 31st, 2013
- **Survey 8** (LFI only): starts February 1st, 2013, ends August 1st, 2013

Completion of full sky coverage during Surveys 1-2

The picture gallery below exhibits the progress of sky coverage during the first months of survey (black color = unobserved areas).

The HFI 353 GHz integration time after N months of survey. Unit is seconds per square degree, normalized to one detector.

Main planet and Crab observations during Surveys 1-7

Solar System objects and the Crab Nebula have been observed many times during the Planck surveys. Here is a complete list of these observations. Note that the *deep rings* and *drift scans* (Mars only) are in **boldface**.

- Crab: Sept. 16-22, 2009
- Mars: Oct. 17-29, 2009
- Jupiter: Oct. 25 – Nov. 1, 2009
- Neptune: Nov. 1-8, 2009
- Uranus: Dec. 6-16, 2009
- Saturn: Jan. 2-8, 2010
- Crab: March 6-12, 2010
- Mars: April 9-18, 2010
- Neptune: May 15-23, 2010
- Saturn: June 13-22, 2010
- Uranus: June 27 – July 5, 2010
- Jupiter: July 1-9, 2010
- Crab: Sept. 15-21, 2010
- Neptune: Nov. 3-11, 2010
- Jupiter: Dec. 9-18, 2010
- Uranus: Dec. 12-21, 2010
- Saturn: Jan. 15-22, 2011
- Crab: March 7-12, 2011
- Neptune: May 18-26, 2011
- Saturn: June 30 - July 9, 2011
- Uranus: July 3-11, 2011
- Jupiter: Aug. 9-15, 2011
- Crab: Sept. 10-18, 2011

This Crab scan was performed with the 250 deg. phase cycloidal strategy.

- Crab: Sept. 20-23, 2011

This Crab scan was performed with the 340 deg. phase cycloidal strategy.

- **Mars**: Dec. 8-16, 2011 ("drift scan": Mars is let move through the Planck focal plane via its proper motion)
- Mars: Dec. 17-26, 2011 (normal scanning)
- **Jupiter**: Jan. 8-30, 2012 (deep ring)

- **Crab**: Feb. 26 - March 16, 2012 (deep ring)
- **Jupiter**: Sept. 1-14, 2012 (deep ring)
- **Crab**: Sept. 14 - Oct. 1, 2012 (deep ring)
- Neptune: Nov. 19-27, 2012
- Uranus: Dec. 24-30, 2012
- Saturn: Jan. 30 - Feb. 5, 2013
- **Jupiter**: Feb. 2013 (deep ring)

Resulting integration time distribution

The integration time after the end of HFI operations (January 2012) is shown in the following picture gallery.

Units are seconds per square degree, normalized to one detector, for all maps. The projection is full-sky Mollweide centered on the Galactic Centre.

Integration time after the end of HFI operations (January 2012). Units are seconds per square degree, normalized to one detector.

References

[1] http://www.youtube.com/watch?v=WwFXuZ0B3B8
[2] http://www.youtube.com/watch?v=7Zu-aiEiDtY

Thermal environment

(Note: Adapted from Planck Collaboration 2011, A&A 536, A1)

The satellite design and its location at L2 provide an extremely stable thermal environment. The main temperature variation on long timescales is driven by the total radiative power absorbed by the solar panels, which varies depending on distance from the Sun and the solar aspect angle (i.e. the angle between the solar direction and the spin axis). On shorter timescales, temperature variations are driven by active thermal regulation cycles. Both seasonal and shorter-timescale variations are observed across the satellite's service module (SVM), but are heavily damped and almost unobservable within the payload module (PLM).

Specific operations and deviations from the scanning strategy have a thermal influence on the satellite and payload. Some significant effects are listed below.

– The thruster heaters were unintentionally turned off between 31 August and 16 September 2009 (the so-called "catbed" event).

– As planned, the RF transmitter was initially turned on and off every day in synchrony with the daily visibility window, in order to reduce potential interference by the transmitter on the scientific data. The induced daily temperature variation had a measurable effect throughout the satellite. An important effect was on the temperature of the 4He-JT cooler compressors, which caused variations of the levels of the interference lines that they induce on the bolometer data (Planck HFI Core Team 2011a). Therefore the RF transmitter was left permanently on starting from 25 January 2010 (257 days after launch), which made a noticeable improvement on the daily temperature variations.

– A significant thermal effect arises from the (approximately) weekly adjustments to the operation of the Sorption Cooler.

The thermal environment of the payload module is – by design – extremely well decoupled from that of the service module. As a consequence, in spite of the significant thermal perturbations originating in the SVM, the thermal variability affecting the detectors is essentially completely due to the operation of the cryogenic cooling chain (described in detail in Planck Collaboration 2011b), which ensures their cold environment.

Radiation environment

(Note: Adapted from Planck Collaboration 2011, A&A 536, A1)

The Standard Radiation Environment Monitor on board Planck (SREM, Buehler et al. 1996) is a particle detector which is being flown on several ESA satellites. The SREM consists of several detectors sensitive to different energy ranges, which can also be used in coincidence mode. In particular, the SREM measures count rates of high energy protons with E>20 MeV, electrons with E>0.5 MeV and Ions with 150 MeV < E < 185 MeV.

Particle fluxes measured by the SREM on board Planck are shown in Fig. 8. The radiation environment of Planck is characterised by the current epoch near the minimum in the solar cycle. As a consequence, the particle flux is dominated by Galactic cosmic rays, rather than by the solar wind. The time evolution of the SREM measurements is well correlated with that of identical units flying simultaneously on other satellites (e.g., Herschel, Rosetta) and with indicators of Galactic cosmic rays, and is anti-correlated with solar flare events and with the solar cycle (Fig. 8). More importantly for Planck, the SREM measurements are very well correlated with the heat deposition on the coldest stages of the HFI, and with glitch rates measured by the detectors of HFI. A more detailed interpretation of these data is provided in Planck HFI Core Team (2011a).

Pointing performance

The pointing performance of Planck can be measured by the difference between the executed pointings as described in the Attitude History Files (using the Star Trackers and the Fiber Optics Gyroscope), and the planned pointings by PSO in the Pre-Programmed Pointing Lists.

The MOC makes available to DPCs and PSO the reconstituted pointing information:

- the positions on the sky of the three axes bound to the ACMS system (ASTR) every second (quaternions or equivalent information).

The accuracy of this information complies with the requirements stated in the SRS document.

- For each circle (i.e. nominally a 60 second observation period), the spin axis position on the sky and spin velocity averaged over this circle plus the spin

phase.

- For each ring (i.e. nominally a ~ 1 hr observation period), the spin axis position on the sky, spin velocity and nutation parameters averaged over this ring.
- Any information the MOC has that might help the DPCs in assessing the quality of the above information.

The attitude history file contains high frequency data for slews, post slew and stable pointing periods at a maximum frequency of one record every 0.25 seconds. It also contains data averaged over a spin period and data averaged over an observation period. For the spin period and observation period, the information used to construct these data records is restricted to stable pointing periods.

The pointing performance of Planck has been very good throughout operations, as the plots in the right panel show.

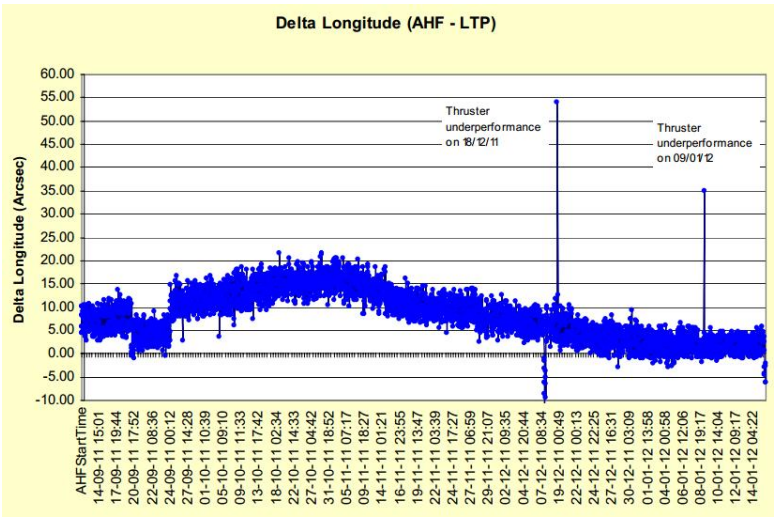

This plot exhibits the pointing errors in Ecliptic longitude for the period Sept. 2011 - Jan. 2012.

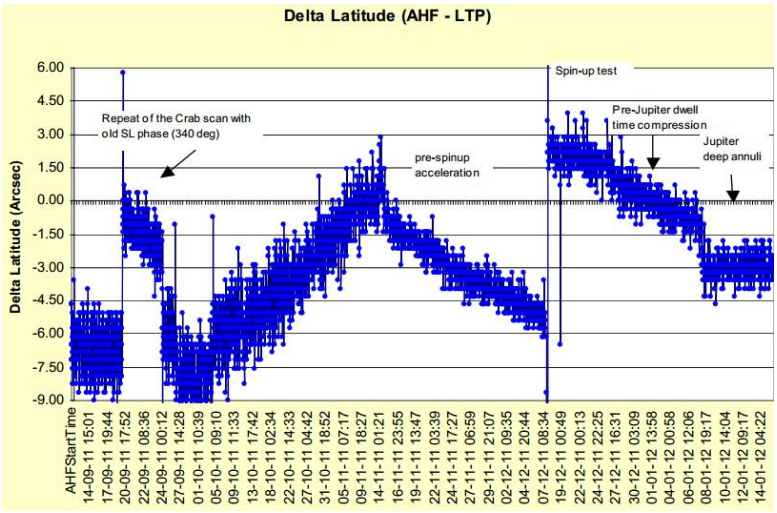

This plot exhibits the pointing errors in Ecliptic latitude for the period Sept. 2011 - Jan. 2012.

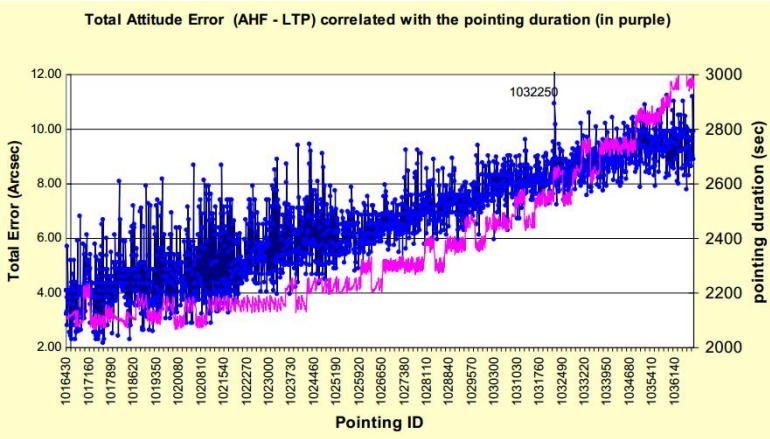

This plot exhibits a correlation between the periodic component of the pointing error and the duration of the pointing. This suggests a Solar drift origin to this component.

Data Processing

Data flow overview

The Planck satellite generates (and stores on-board) data continuously at the following typical rates: 21 kilobit s^{-1} (kbps) of house-keeping (HK) data from all on-board sources, 44 kbps of LFI science data and 72 kbps of HFI science data. The data are brought to ground in a daily pass of approximately 3 h duration. Besides the data downloads, the passes also acquire realtime HK and a 20 min period of real-time science (used to monitor instrument performance during the pass). Planck utilises the two ESA deep-space ground stations in New Norcia (Australia) and Cebreros (Spain), usually the former. Scheduling of the daily telecommunication period is quite stable, with small perturbations due to the need to coordinate the use of the antenna with other ESA satellites (in particular Herschel).

At the ground station the telemetry is received by redundant chains of front-end/back-end equipment. The data flows to the mission operations control centre (MOC) located at ESOC in Darmstadt (Germany), where it is processed by redundant mission control software (MCS) installations and made available to the science ground segment. To reduce bandwidth requirements between the station and ESOC only one set of science telemetry is usually transferred. Software is run post-pass to check the completeness of the data. This software check is also used to build a catalogue of data completeness, which is used by the science ground segment to control its own data transfer process. Where gaps are detected, attempts to fill them are made as an offline activity (normally next working day), the first step being to attempt to reflow the relevant data from station. Early in the mission these gaps were more frequent, with some hundreds of packets affected per week (impact on data return of order 50 ppm) due principally to a combination of software problems with the data ingestion and distribution in the MCS, and imperfect behaviour of the software gap check. Software updates implemented during the mission have improved the situation such that gaps are much rarer, with a total impact on data return well below 1 ppm.

Redump of data from the spacecraft is attempted when there have been losses in the space link. This has only been necessary on three occasions. In each case the spacecraft redump has successfully recovered all the data.

An operational principle of the mission is to avoid impact on the nominal science of a completely missed ground station pass. Commanding continuity is managed by keeping more than 24 h of commanding-timeline queued on-board. The telemetry resides on board the satellite in a ~60 h circular buffer in solidstate memory, and can be recovered subsequently using the margin in each pass, or more rapidly by seeking additional station coverage after an event. The lost-pass scenario has in fact occurred only once (on 21 December 2009), when snow on the dish at Cebreros led to the loss of the entire pass. A rapid recovery was made by using spare time available on the New Norcia station. Smaller impacts on the pass occur more often (e.g., the first ~10 min of a pass may be lost due to a station acquisition problem) and these can normally be recovered simply by restarting a software task or rebooting station equipment. Such delays are normally accommodated within the margin of the pass itself, or during the subsequent pass.

All the data downloaded from the satellite, and processed products such as filtered attitude information, are made available each day for retrieval from the MOC by the LFI and HFI Data Processing Centres (DPCs). Typically, the data arrive at the LFI (resp. HFI) DPC 2 (resp. 4) hours after the start of the daily acquisition window. Automated processing of the incoming telemetry is carried out each day by the LFI (resp. HFI) DPCs and yields a daily data quality report which is made available to the rest of the ground segment typically 22 (resp. 14) hours later. More sophisticated processing of the data in each of the two DPCs is described in Zacchei et al. (2011) and Planck HFI Core Team (2011b).

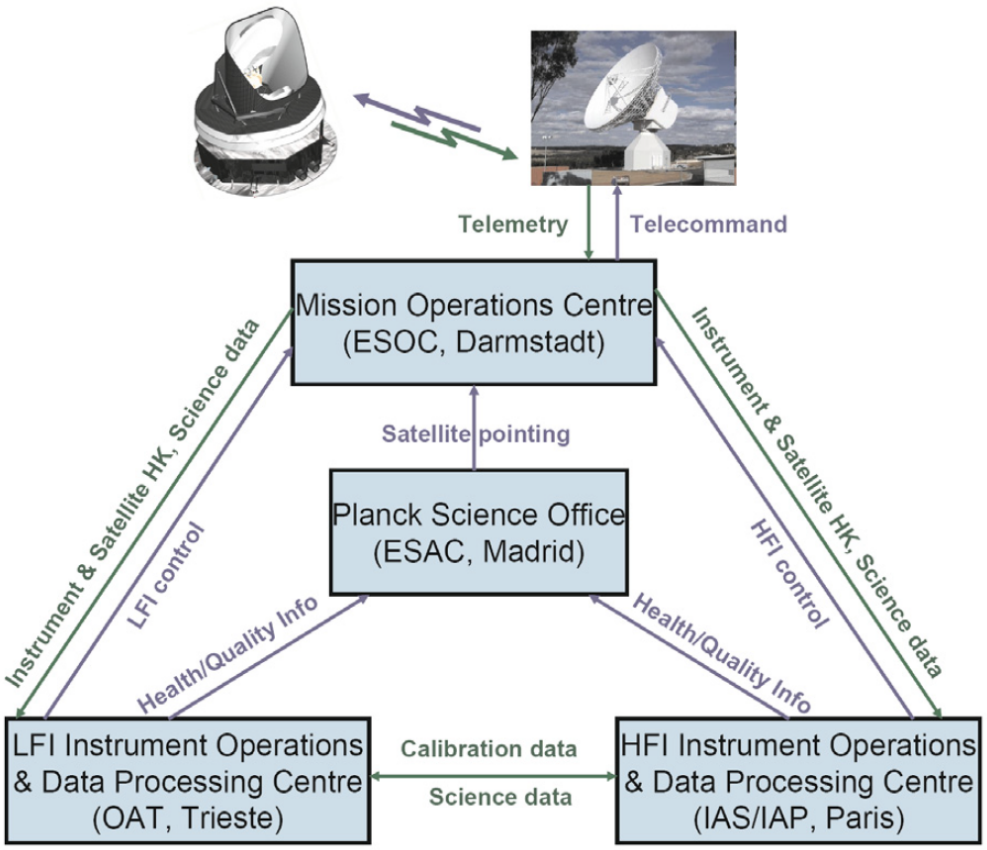

A sketch of the centres involved in the Planck ground segment and the main data exchanges between them.

For more information, see #tauber2010a, #planck2011-1.1.

Contents of this chapter

<biblio force=false>

1. References

</biblio>

On-board processing

MOC data transfer and storage

The Mission Operations Centre (MOC), located at ESA's operations centre in Darmstadt (Germany), is responsible for all aspects of flight control and of the health and safety of the Planck satellite, including both instruments. It plans and executes all necessary satellite activities, including instrument commanding requests by the instrument operations centres. MOC communicates with the satellite using two ESA deep-space ground stations in New Norcia (Australia) and Cebreros (Spain), usually the former, over a daily 3-h period, during which it uplinks a scheduled activity timeline which is autonomously executed by the satellite, and downlinks the science and housekeeping data acquired by the satellite during the past 24 h. The downlinked data are transferred from the ground station to the MOC over a period of typically 8 h; at MOC they are put onto a data server from where they are retrieved by the two Data Processing Centres.

There is no data processing done at MOC. Only transfer and storage of data is performed at this stage. MOC verifies the reception of all telemetry packets, which are transfered from the spacecraft via the ground station, as given by the Source Sequence Count related to each Virtual Channel and Application ID. All data are stored in the Long Term Archive as telemetry packets (duplicated in A and B archives), which present an archive of all data, both science and housekeeping, acquired through the whole mission.

The HFI DPC

Contents of this chapter

Summary of HFI data characteristics

Overview

The first stage of HFI data processing is performed on-board in order to generate the telemetry as described in this page. On the ground, the HFI DPC has been organized into different "Levels": 1, 2, 3, 4 and "S". In brief, during operations, L1 feeds the database resulting in time-ordered information (TOI) objects. L2 is the core of the processing, which turns TOIs into clean calibrated sky maps. L3 transforms these maps at specific frequencies into more scientific products, like catalogues, maps and spectra of astrophysical components. L3 can rely on simulation provided by the LS, while L4 refers to delivering the DPC products to ESA. This processing relies on dedicated software and hardware infrastructures developed pre-launch.

The data processing applied for the *"Early Planck results"* series of publications was described in early paper VI [1]. The and its co-papers provide the reference for the processing done for the 2013 Data release. An Annex of P03 specifies what had been done (and resulting characteristics) for the *"Intermediate Planck results"* series of publications.

Level 1: building the reference database during flight operations

(L1): consists in receiving the telemetry and ancillary data files and ingesting them into the DPC database. This involves decompressing, in some cases changing data formats, computing the time of individual data samples from the time of the compression slices, but otherwise no processing proper. Other steps are:

- data ingestion (science, HK, ancillary, other?)
- construction of ToS in science data group
- pointing interpolation
- construction of other TOI and ROI objects from AHF, ...

This is further described in the Pre-processing section.

Level 2: converting temporal information into clean calibrated maps

(L2): this is where the data are processed from timelines into maps. The main processing steps are

- Timeline (or Time-Ordered Information = TOI) processing, which includes conversion from ADUs to engineering units (Volts), demodulation, deglitching, conversion from engineering to physical units (Watts), removal of known systematic effects (non-linearities, 4K lines, Jumps, ring flagging), removal of the instrumental signature (time transfer function), temporal noise Estimation. Details here.
- Pointing and beam of each detector. See section Pointing&Beams.
- map-making & photomoetric calibration: projecting the TOIs onto all-sky maps, etc. See section Map-making.
- Characterisation/validation through angular power spectra. See section PowerSpectra.
- Overal HFI data validation, through difference tests, comparison to detailed simulations, etc., See section HFI-Validation
- The resulting data characteristics are given in section Summary.

Level 3: Basic analyses of (Level 2) Frequency maps

(L3): This is where the data in the form of frequency maps are converted to catalogues and full sky astrophysical component maps. Much of this is done in common with the LFI DPC, and is further described in the HFI/LFI common sections .

Level 4 : Delivering results

Level 4 is the "Archive Level". No processing done, but rather exporting, reformating, documenting.

Level S : A common HFI/LFI simulation software

Level S is the so-called "Simulation Level" software suite common to both consortia, which, given a sky model (generated by the Planck sky model, `PSM`), detectors pointing and beams, generates the infalling power on each

detector. It can also provide a simplified description of eg. the noise. It is further described in the HFI/LFI common section. HFI specific developments (configuration control & MC bench, specific effects like 4K lines, glitches, ADC non-linearity, etc.) are described in the HFI data validation section.

HFI DPC Infrastructures The HFI Data Processing Centre can be thought of as a centralized backbone providing hardware and software infrastructures to a relatively large number of geographically distributed groups of developers and other R&D groups in the HFI and LFI core teams.
An overview was given in the HFI data processing paper of the *"Planck Early Results"* series. In particular:

- Code and configuration management can be found at early paper VI [2].
- Data management at early paper VI [2].
- Instrument model (IMO) database at early paper VI [3].
- Data flow management at early paper VI [3].
- Hardware at early paper VI [4].

References

[1] http://www.rssd.esa.int/llink/livelink/fetch/-60063/3036676/3065909/3110897/3135828/3135852/PE_paper6.pdf#page=1
[2] http://www.rssd.esa.int/llink/livelink/fetch/-60063/3036676/3065909/3110897/3135828/3135852/PE_paper6.pdf#page=34
[3] http://www.rssd.esa.int/llink/livelink/fetch/-60063/3036676/3065909/3110897/3135828/3135852/PE_paper6.pdf#page=35
[4] http://www.rssd.esa.int/llink/livelink/fetch/-60063/3036676/3065909/3110897/3135828/3135852/PE_paper6.pdf#page=36

Pre-processing

Overview

In terms of data processing, the HFI ground segment handles two types of data, both made available via the MOC:

- telemetry data transmitted from the satellite. These come from the different subsystems of the satellite service module, from the sorption cooler and from the two instruments.
- auxiliary data. These are data produced by MOC. The only 3 products used by the HFI DPC are the pointing data, the orbit data, and the time correlation data.

All data are retrieved by the HFI level 1 software and stored in the HFI database.

Telemetry data

The digitized data from the satellite are assembled on board in packets according to the ESA Packet Telemetry Standard and Packet Telecommand Standard, the CCSDS Packet Telemetry recommendations and the ESA Packet Utilization Standard.The packets are dumped to the ground during the Daily Tranmission Control Period, consolidated by and stored at MOC. Telemetry data contain the housekeeping data and the bolometer (ie science) data.

Housekeeping data

For several reasons (systems monitoring, potential impact of the environment, understanding of the bolometer data), the HFI level 1 software gathers and stores in its database the satellite subsystems housekeeping parameters:

- Command and Data Management System
- Attitude Control & Measurement Subsystem
- Thermal Control System
- Sorption Cooler System
- HFI housekeeping parameters

The structure and the frequency of the packets built by these subsystems and the format of the house keeping parameters are described in the Mission Information Bases [refer to an hypothetical MIB section under MOC responsibility]. The HFI L1 software uses these MIBs to extract the house keeping parameters from the packets. Given the status of each subsystem, the parameters are gathered in the HFI database in groups. The HFI L1 software builds in each group a vector of time (usually named TIMESEC) and a single vector per housekeeping parameter.

Bolometer data

The HFI science data is retrieved and reconstructed as described in section 3.1 of early paper VI [1].

The first stage of HFI data processing is performed on-board in order to generate the telemetry. This is described in this page.

On board, the signal from the 72 HFI channels is sampled at 180.4Hz by the Read-out Electronic Unit. 254 samples per channel are grouped into a compression slice. The Data Processing Unit then builds a set of several telemetry packets containing the compression slice data and adds to the first packet the start time of the compression slice. When receiving this set of telemetry packets, the L1 software extracts the samples and computes the time of each sample based on the compression slice start time (digitized with $2^{-16}s = 15.26$µs quantization steps) and a mean sample time between samples. For the nominal instrument configuration, the sample integration time is measured to be Tsamp = 5.54404 ms

The two plots show the histogram of time differences between two successive samples for the full mission. 6 samples intervals (> 6 ms) correspond to 3 occurences of packets lost on board when the on board sofwtare of the Command and Data Management Unit has been patched (18, 19 and 20th of August 2009). The right plot is a blow up of the left one. It shows the distribution around the mean value of 5,54 ms and the 15 µs quantization step.

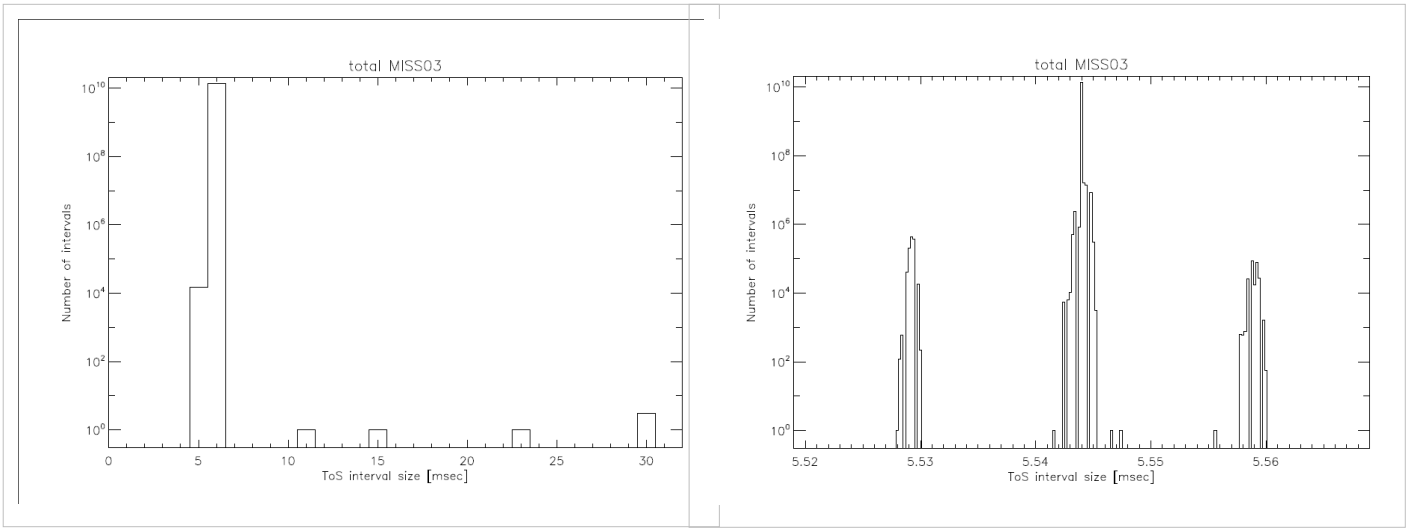

Transfer functions

In order to ease the reading data in the HFI database, so called transfer functions are created. They allow software items to read data on which functions are applied on the fly. A simple example of a transfer function is the conversion of a thermometer data in Analogic to Digital Units (ADU) to Kelvins. Here we show the 2 transfer functions applied on the bolometer samples in the data processing pipelines:

From raw signal to non demodulated signal in Volts (transf1_nodemod)

$$Signal\_ND\_V_{bc} = \frac{\frac{C_{bc}}{N_{sample} - Nblanck_{bc}} - offset_{bc}}{F1_{bc}} \times \frac{Gamp_{ETAL}}{Gamp_{bc}}$$

where:

- bcrefers to a bolometer usually labelled by its electronic belt and channel. Eg. bc=00 refers to the *a* part of the first 100 GHz Polarized Sentivite Bolometer.
- $C_{bc}$is the bolometer sample in Analogic Digital Units (ADU)
- $N_{sample}$is the number of samples in half a modulation period. This parameter is common to all bolometer channels and - although kept fixed during the whole mission - is read from the housekeeping parameter. $N_{sample} = 40$
- $Nblanck_{bc}$is the number of samples suppressed at the beginning oft each half modulation period. Although kept fixed during the whole mission, it is read from the housekeeping parameter. For bc=00, $Nblanck_{00} = 0$
- $F1_{bc}$is a calibration factor. For bc=00, $F1_{00} \simeq 1.8 \times 10^7$.
- $offset_{bc}$is close to 32768
- $Gamp_{ETAL}$is the gain amplifier mesured during the calibration phase. For bc=00, $Gamp_{ETAL} = 1$
- $Gamp_{bc}$is the current gain amplifier. Although kept fixed during the whole mission, it is read from the housekeeping parameter. For bc=00, $Gamp_{00} = 1$

From raw signal to demodulated signal in Volts (transf1)

The same formula as above is used but with the demodulation and a 3-point filter computed as:

$$Signal\_V_{bc}[n] = -\tfrac{1}{4}(-1)^{parity_{n-1}} Signal\_ND\_V_{bc}[n-1] + \tfrac{1}{2}(-1)^{parity_n} Signal\_ND\_V_{bc}[n] - \tfrac{1}{4}(-1)^{parity_{n+1}} Signal\_ND\_V_{bc}[n+1]$$

where:

- $n-1$, and $n+1$refer to the samples before and after the given $n$sample to demodulate
- $parity$is computed by the HFI L1 software

Statistics on the telemetry data

The table gives some statistics about the data handled at the pre-processing level:

-	**Nominal mission**[1]	**Full mission**[1]	**From launch to the end of full mission**[1]
Duration	473days	884days	974days
Number of HFI packets generated onboard (HSK/science)[2]	19 668 436/ 376 294 615	37 762 493/ 704 852 262	41 689 4090/765 043 713
Number of HFI packets lost [3] **(HSK/science)**	2/20	2/20	2/20
ratio of HFI lost packets vs generated on board (HSK/science)	$1 \times 10^{-7}/5 \times 10^{-8}$	$5 \times 10^{-8}/3 \times 10^{-8}$	$5 \times 10^{-8}/3 \times 10^{-8}$
Number of different housekeeping parameters stored in the database (HFI/SCS/sat)	3174/708/12390		
Number of science samples stored in the database	530 632 594 653	991 929 524 565	1 090 125 748 960

Number of missing science samples	2 537 499	6 634 491[4]	7 521 758
Ratio of missing science samples vs samples stored	5×10^{-6}	7×10^{-6}	7×10^{-6}

- [1] : mission periods are defined in this page.
- [2] : science packets refer to the number of telemetry packets containing science data (ie: bolometer data and *fine thermometer* data) when the instrument is in observation mode (Application Program IDentifier = 1412). HSK packets refer to the number of HFI *non essential* housekeeping telemetry packets (Application Program IDentifier = 1410).
- [3] : all lost packets have been lost on board ; no HFI packet has been lost at ground segment level.
- [4] : this amount of lost science samples is distributed as
  - 0.3% are due to Single Event Unit
  - 18.5% have been lost during the 3 CDMU patch days and the consecutive clock resynchronisation
  - 29.1% have been lost because of compression errors
  - 52.1% have been lost due to the EndOfSlew buffer overflow being triggered by solar flare events

Pointing data

The pointing data are built by the MOC Flight Dynamics team. The pointing data are made available to the DPC via AHF files. See AHF description document [2] and AHF files repository [3]. All data contained in the AHF files are ingested in the HFI database. The present section describes the steps to produce the HFI pointing solution.

- During the stable pointing period (ie during the dwell), data sampling rate is given at 8 Hz while it is at 4 Hz during the satellite slews. Those data are thus interpolated to the bolometer sampling rate using a sphericallinear interpolation as described in section 3.4 of of early paper VI [4].
- The pointing solution is then amended from the wobble effect as delivered by MOC Flight Dynamics in the AHF files.
- A final correction is then applied based on the study of main planets and point sources seen by the bolometers.

Note **HFI ring** : a ring corresponds to a duration during each stable pointing period, when the spin axis is pointing towards an essentially fixed direction in the sky and the detectors repeatedly scan the same circle on the sky. More precisely the **HFI ring** start time is defined as the *time of the first thurster firing*. The end time of the HFI ring is the start time of the following ring.

The plot shows the evolution of the ring duration along the whole mission. It mainly reflects the scanning strategy and few *long* rings due to operational constraints or tests.

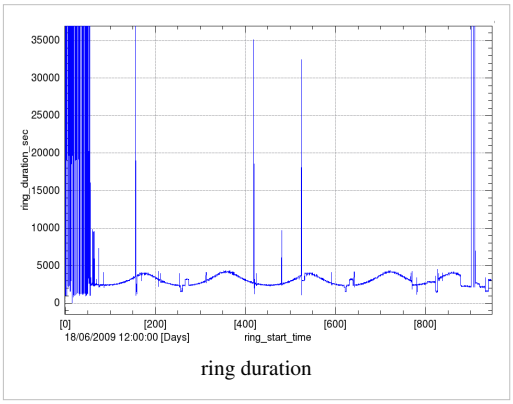

ring duration

Orbit data

Satellite orbit velocity is built by the MOC Flight Dynamics team and made available to the HFI DPC via orbit files. See Orbit description document [5] and orbit files repository [6]. As those orbit files contain both effective and predictive data, they are regularly ingested updated in the HFI database.
*Note: these same data are also ingested in parallel into the NASA JPL Horizons system (*http://ssd.jpl.nasa.gov/*) under ESA's responsibility.*

The satellite orbit data preprocessing is the following.

- The sampling of the MOC provided orbit velocity data is appromximately 1 every 5 mn. These data are interpolated to the time of the middle of the HFI rings.

- The reference frame of the orbit data is translated from the MOC given Earth Mean Equator and Equinox J2000 (EME2000) reference frame to the ecliptic reference frame in cartesian coordinates.
- The earth velocity provided by the NASA JPL Horizons system (http://ssd.jpl.nasa.gov/) is interpolated to the time of the middle of the HFI rings. It is then added to the satellite velocity data.

The use of the satellite orbit velocity is three-fold:

1. computation of the CMB orbital dipole (see calibration section)
2. computation of th positions of solar system objects (see data masking section)
3. computation of the abberation correction.

Time correlation data

The MOC is responsible for providing information about the relationship between the satellite On Board Time (OBT) and Coordinated Universal Time (UTC). This information comes via several measurements of OBT and UTC pairs each day, measured during the satellite ranging. See Time Correlation document [7] and [refer to the PLA TCO folders] Time Correlation files repository.

The plot shows the (OBT, UTC) data couples provided by MOC since Planck launch. The x axis is in number of days since the 17th of May 2009 while the y axis is the difference of OBT and UTC in seconds. The very slow drift is approximately 0.05 seconds per day. The small wiggles are due to the satellite global temperature trends due to its orbit and distance to the sun. *Note: The extra couple on the 1st of June 2010 is not significant and due to a misconfiguration of the ground station parameters.*

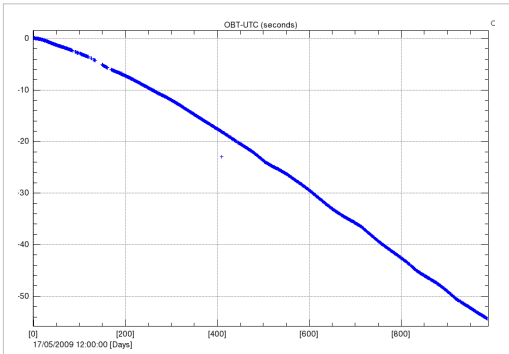

OBT-UTC correlation data

An order 3 polynomial is then fitted to the data. As the whole HFI data management and processing uses OBT, the OBT-UTC information is only used when importing orbit data from Horizons.

References

[1] http://www.rssd.esa.int/llink/livelink/fetch/-60063/3036676/3065909/3110897/3135828/3135852/PE_paper6.pdf#page=5
[2] http://www.rssd.esa.int/llink/livelink/fetch/-60063/3036676/3065909/3110897/3139172/ICD_AHF.pdf#page=1
[3] http://pla.esac.esa.int/pla/aio/metadata-action?PAGE_SIZE=1500&PAGE=1&RESOURCE_CLASS=OPERATIONAL_FILE&SELECTED_FIELDS=OPERATIONAL_FILE&OPERATIONAL_FILE_TYPE.NAME=AHF&RETURN_TYPE=HTML
[4] http://www.rssd.esa.int/llink/livelink/fetch/-60063/3036676/3065909/3110897/3135828/3135852/PE_paper6.pdf#page=6
[5] http://www.rssd.esa.int/llink/livelink/fetch/-60063/3036676/3065909/3110897/3139172/ICD_ODAT.pdf#page=1
[6] http://pla.esac.esa.int/pla/aio/metadata-action?PAGE_SIZE=1500&PAGE=1&RESOURCE_CLASS=OPERATIONAL_FILE&SELECTED_FIELDS=OPERATIONAL_FILE&OPERATIONAL_FILE_TYPE.NAME=ORB&RETURN_TYPE=HTML
[7] http://www.rssd.esa.int/llink/livelink/fetch/-60063/3036676/3065909/3110897/3139172/ICD_TCO.pdf#page=1

TOI processing

This Section is kept short as this Planck release does not contain TOIs. The main information in the HFI processing paper is not duplicated here.

Overview

We describe here the how the TOIs are processed in order to be used for map production. We do not repeat the general features of the pipeline which are given in the HFI Data Processing article #planck2013-p03. Here we give complementary explanations on some details. The TOI of each bolometer is processed independently of the other bolometers, so as to keep the noise properties as uncorrelated as possible. The processing involves modifying the TOI itself for what concerns the conversion to absorbed power and the correction of glitch tails. It also adds a flag TOI that masks the TOI samples that are not to be projected on maps for various reasons.

Acronyms and definitions

- 4K lines: EMI/EMC influence of the 4K cooler mechanical motion on the bolometer readout electronics.
- ADC : analog to digital converter
- IMO : instrument model
- Jump : sudden change of the baseline level inside a ring
- LFER : low frequency excess response
- PBR : phase binned ring
- RIMO : reduced IMO
- Ring : pointing period
- ROI : ring ordered information
- RTS : random telegraphic signal
- SSO : solar system object
- TOI : time ordered information

Input TOI

The input TOI consists in the AC modulated voltage output of the readout of each bolometer. The input has previously been decompressed, and converted from internal digital units to voltage via a constant factor. The TOI has a regular sampling at the acquisition frequency of facq=180.373700+-0.000050 Hz. There are almost no missing data in the TOIs, except for few hundred samples of 545 and 857GHz TOIs which are lost in the on-board compression due to saturation on the Galactic Center crossings.

General Pipeline Structure

The figure on the right shows how the initial TOI is transformed and how flags are produced:

Output TOIs and products

A TOI of clean calibrated samples (ccTOI) and a combined flag TOI (fTOI) are the outputs of the processing. The ccTOI is calibrated so as to represent the instantaneous power absorbed by the detector up to a constant (which will be determined by the map-making destriper). It is worth mentioning how the ccTOI is changed with respect to the input TOI, beyond the harmless constant conversion factor from voltage to absorbed power. The demodulation stage allows to get the demodulated bolometer voltage. The non-linearity correction is a second-order polynomial correction based on the physical but static bolometer model. In order to avoid too much masking after glitches, a

glitch tail is subtracted after an occurrence of a glitch in the TOI. The 4K cooler lines noise is substituted at a series of 9 single temporal frequencies. Finally, the temporal response of the bolometer is deconvolved. This affects mostly the high-temporal frequency part of the TOI, although a small but significant low frequency (the long time response) tail is corrected too. Although flagged samples are not projected, their value influences the valid samples somehow. Hence interpolation procedures introduce some indirect modifications of the TOI. The flag TOI is a combination a dozen flags with an OR logic. Only unflagged data are projected. The exhaustive list of flags is given here: CompressionError, NoData, SSO, UnstablePointing, Glitch, BoloPlateFluctuation, RTS, Jump, PSBab. A complete qualification of the data is obtained at the ring level. If the TOI shows an anomalous behaviour on a given ring, this ring is discarded from projection. A special production of TOIs is also made as an input to the beam analysis with Mars, Jupiter and Saturn.

Examples of clean TOIs

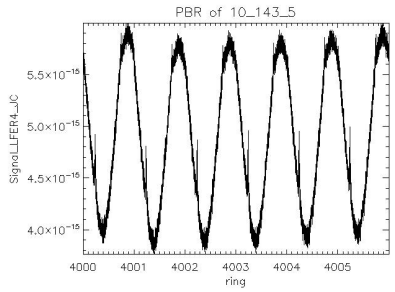

Phase-binned signal (PBR) for 6 consecutive rings from 4000 to 4005

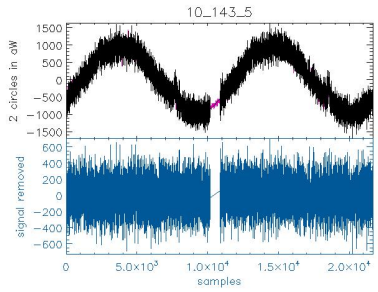

Valid signal (up) and noise (bottom) for 2 consecutive circles of the ring 4000

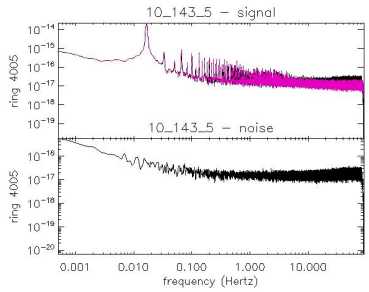

Fourier power spectral density of the first 30 minutes of the ring 4005 with signal before (pink) and after (black) deconvolution (top) and noise (bottom)

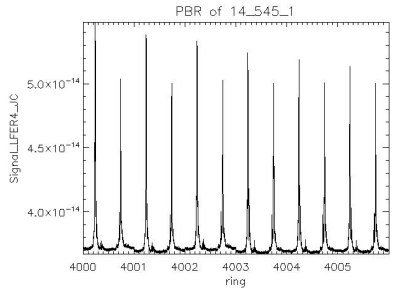

Phase-binned signal (PBR) for 6 consecutive rings from 4000 to 4005

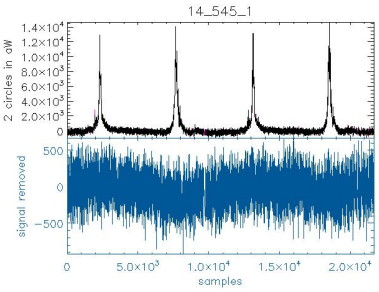

Valid signal (up) and noise (bottom) for 2 consecutive circles of the ring 4000

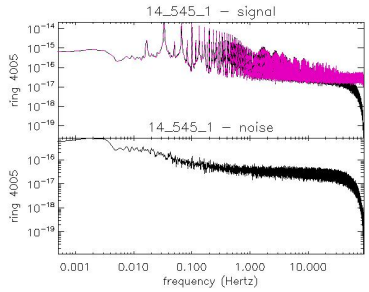

Fourier power spectral density of the first 30 minutes of the ring 4005 with signal before (pink) and after (black) deconvolution (top) and noise (bottom)

Samples of PBR, TOIs, and PSDs of all detectors are shown in this file

Trends in the output processing variables

Here we intend to show the trend of the systematic effects that are dealt with in the TOI processing. The full impact of each of them is analyzed in HFI-Validation.

ADC baseline

The following figure shows the ADC baseline which is used prior to demodulation (a constant offset is removed for clarity). This baseline is obtained by smoothing on an hour block average the undemodulated TOI on unflagged samples.

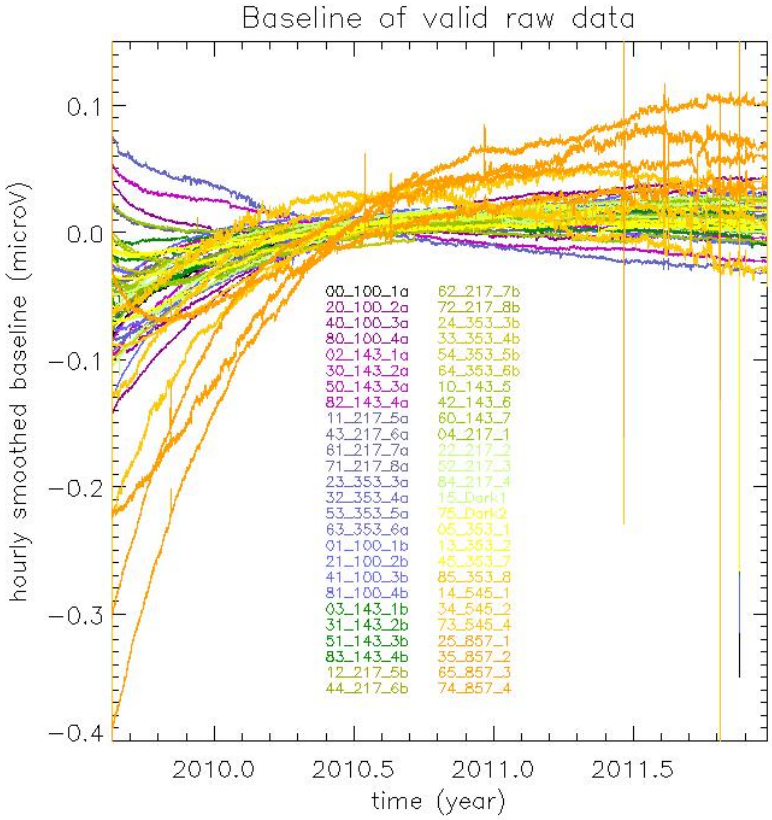

Glitch statistics

The glitch rate per channel is shown in this figure. For details, see copap.

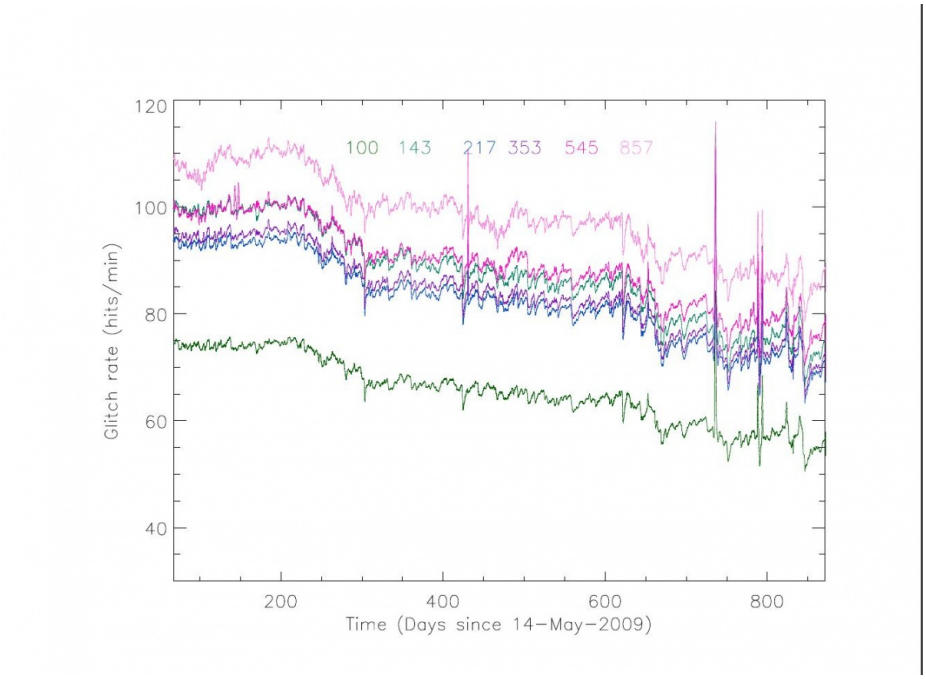

The percentage of flagged data (mostly due to Cosmic Rays) at the ring level is shown in these examples. No smoothing was applied. Only valid rings are shown.

Percentage of flagged data

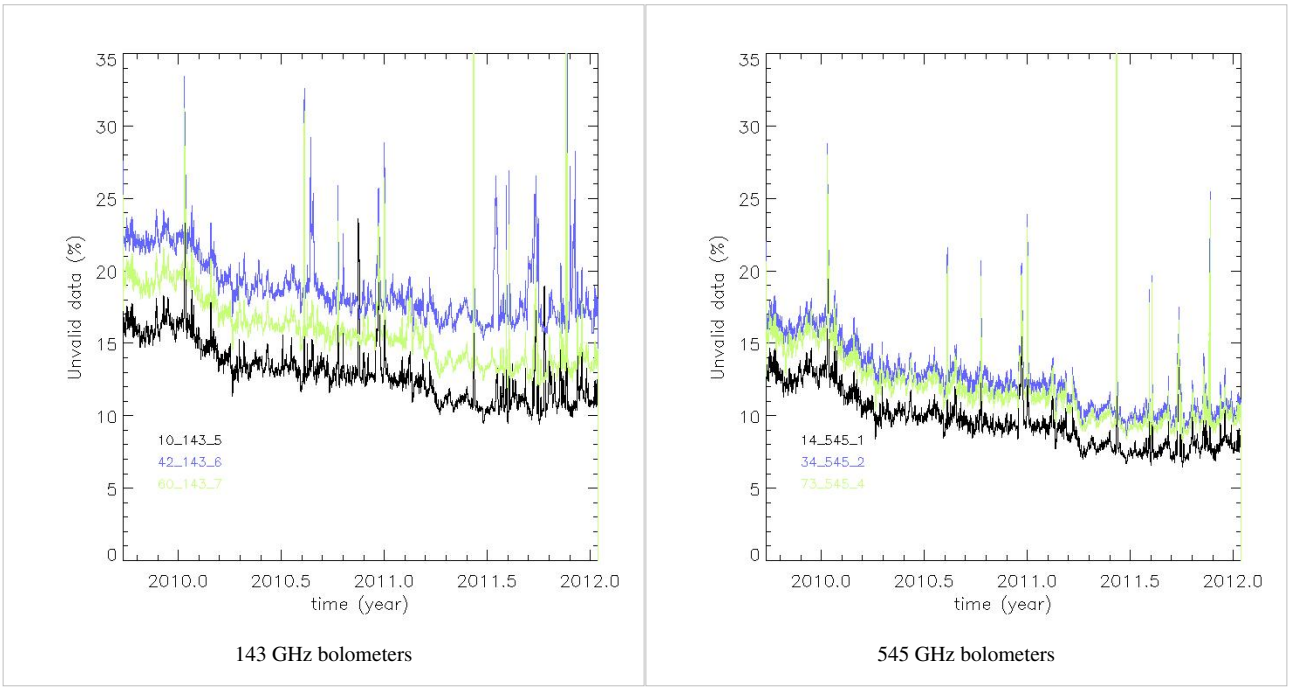

143 GHz bolometers

545 GHz bolometers

The complete set of plots is here

Thermal template for decorrelation

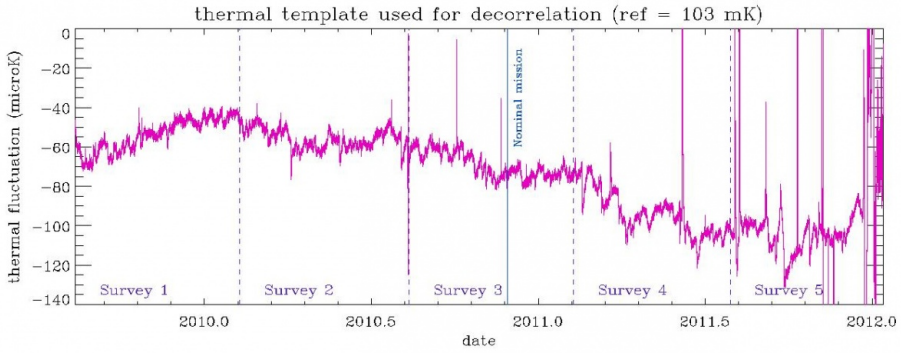

A simple linear decorrelation is performed using the 2 dark bolometers as a proxy of the bolometer plate temperature. Coupling coefficients were measured during the CPV phase.

4K cooler lines variability

The amplitude of the nine 4K cooler lines in aW at 10, 20, 30, 40, 50, 60, 70, 80 and 17 Hz is shown for 2 bolometers in the following figures. The trend is smoothed over 31 ring values after having discarded measurements done at a ring which is discarded for all bolometers.

Amplitude of the nine 4K cooler lines

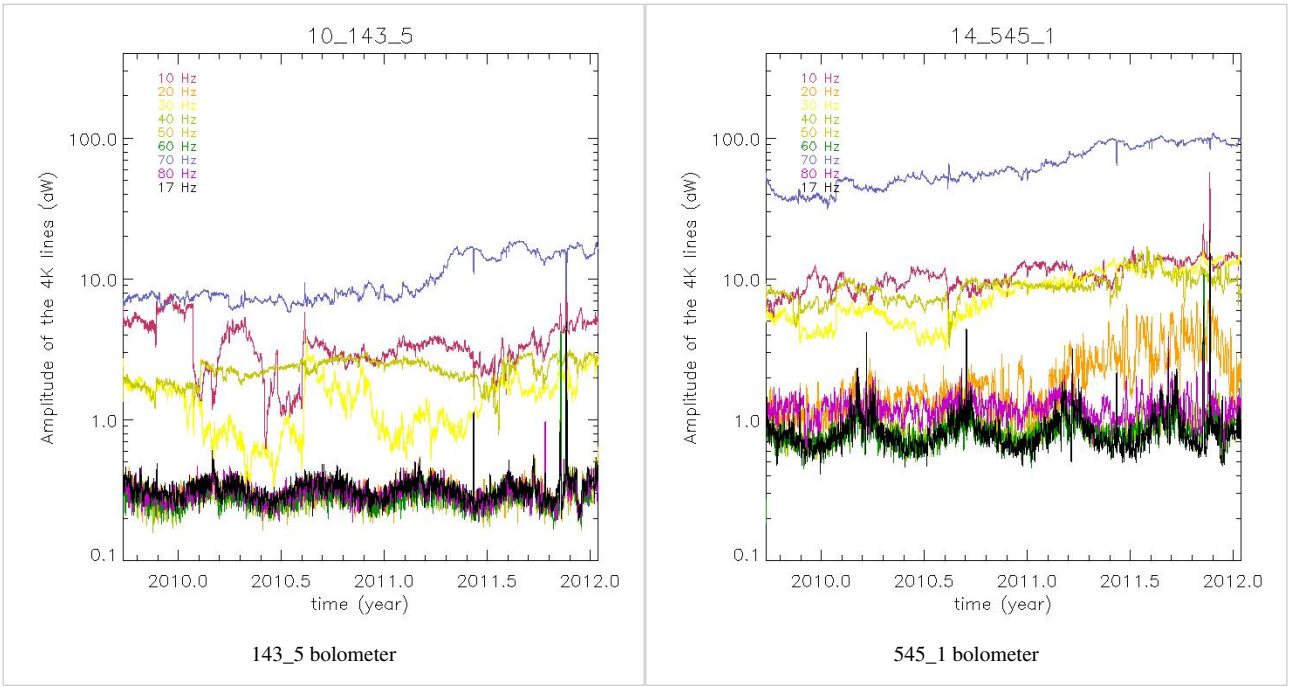

143_5 bolometer

545_1 bolometer

The 4K cooler line coefficients of all bolometers are shown in this file

The 4K cooler lines project onto the maps only for a limited fraction of rings, the so-called resonant rings. This is graphically shown in the following figure. For each ring (stable pointing period), the spin rate is very stable at about 1 rpm. From one ring to another, the spin frequency (shown as diamonds) changes around that value. The sky signal is imprinted at the corresponding spin frequency and its 5400 (60x90) harmonics. If one of the nine 4K cooler lines happens to coincide with one of the spin frequency harmonics (a resonant ring), it will project a sine-wave systematic on the maps. The horizontal coloured bars show the zone of influence of a particular 4K line (labeled on the left side of the plot), when folded around 16.666 mHz. When the spin frequency hits one of these zones, we have a resonant ring. The 4K line coefficient is interpolated for this ring and an estimate of the systematic effect is

subtracted from the TOI. Resonant rings are different for different 4K lines. Note the two-level oscillation pattern of the spin frequency is due to the satellite attitude control system.

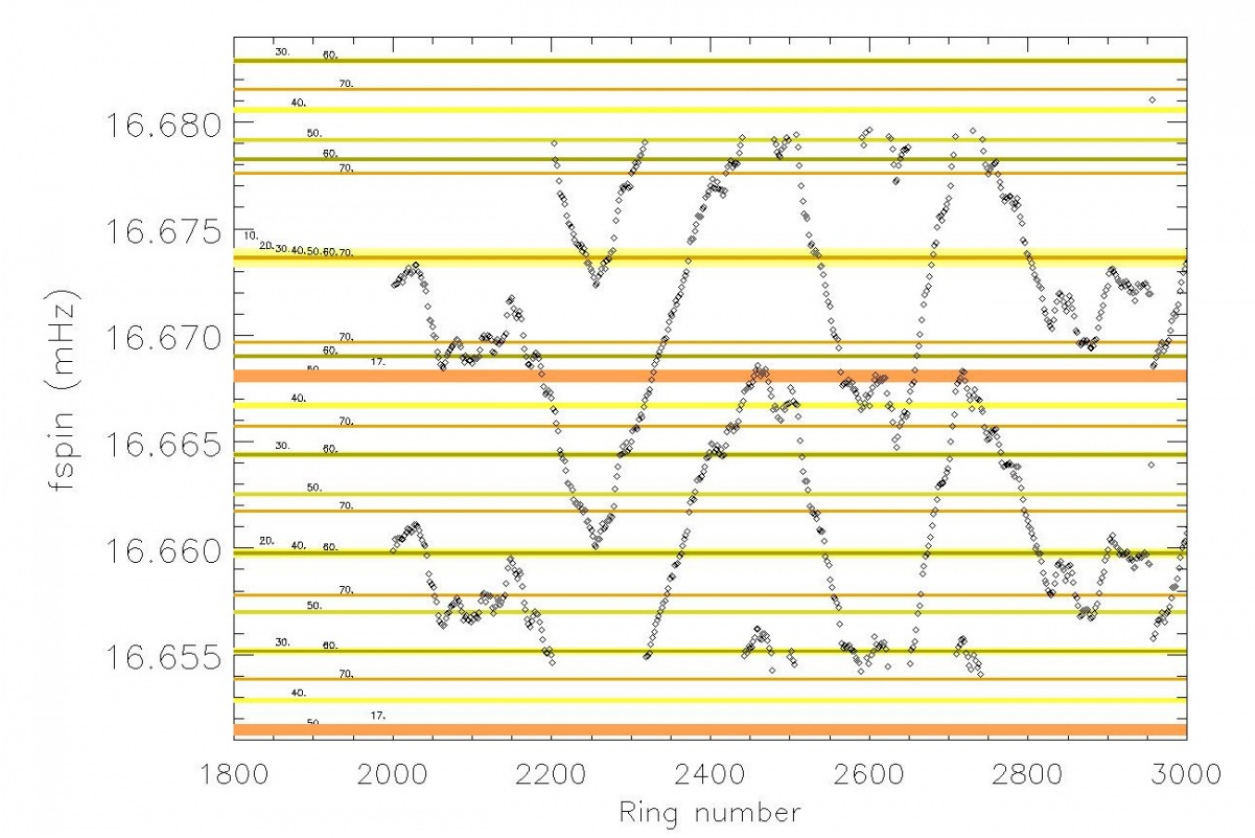

jump correction

A piecewise constant value is removed to the TOI if a jump is detected. See a jump example in this figure:

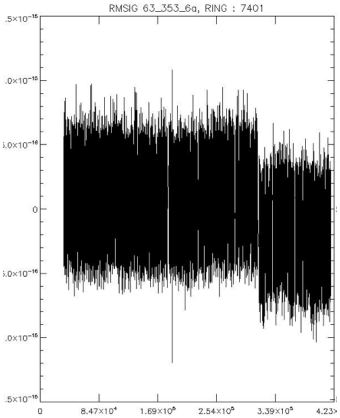

The number of jumps per day (all bolometers included) is shown in this figure:

The jumps are uncorrelated from bolometer to bolometer. The total number of jumps detected in the nominal and full mission is shown here:

Trends in noise and signal

Signal (top) and noise (bottom) smoothed at 1 minute. All values falling in a discarded ring are not plotted.

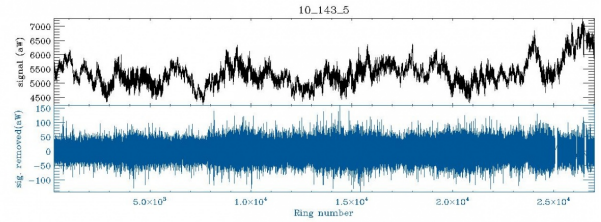

143_5 bolometer

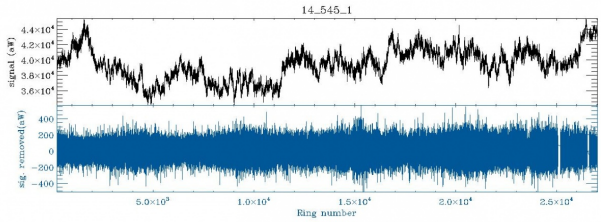

545_1 bolometer

The smooth TOIs of all detectors are shown in this file

Noise stationarity

This is not the final version but gives a good idea of power spectra at the detector level of rmsigTOIs. All PSDs can be seen in this file

The standard deviation per ring corrected by ring duration bias is given here, one per bolometer using only valid rings. No smoothing is applied (except a 31-point smoothing for the 545 and 857 GHz channels) but values for rings discarded for all bolometers (see below) are not used. The standard deviation is computed on samples valid for map-making which are also not affected by the Galaxy or the point-sources using the usual flags. Two examples are given here.

Standard deviation per ring

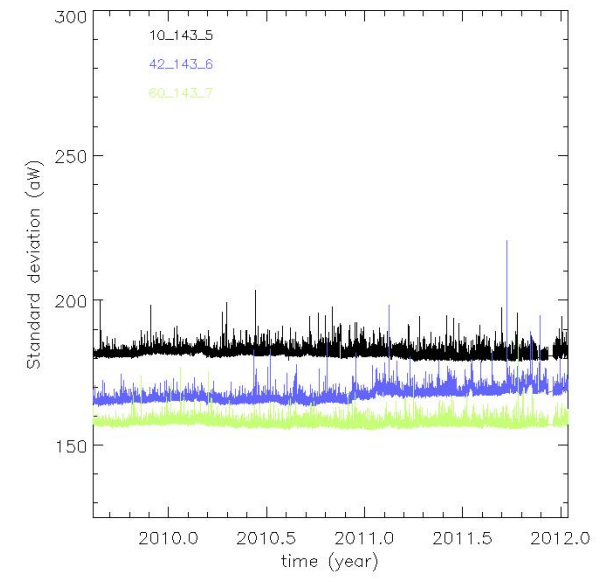

143_5 bolometer

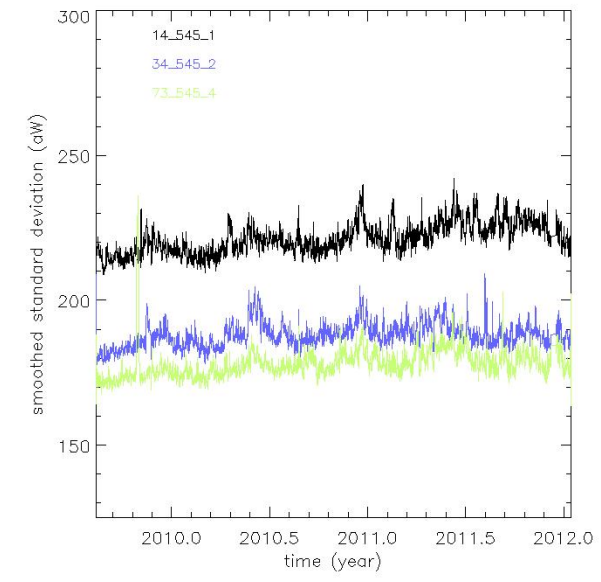

545_1 bolometer

The full series of plots is here: Standard deviation of rmsig TOIs at the ring level

Note the presence for 3 bolometers of a two-level noise system. No correction can be done for that effect. See one example here:

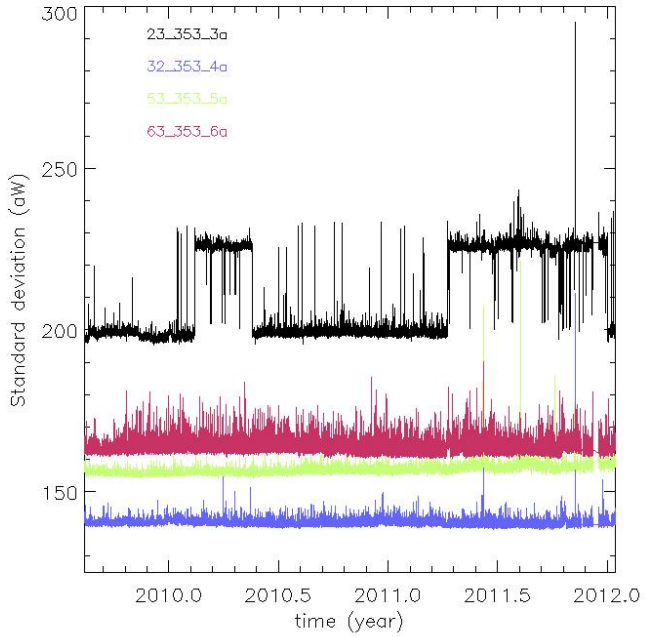

An example of the higher order statistics which are used to unveil rings affected by RTS problems.

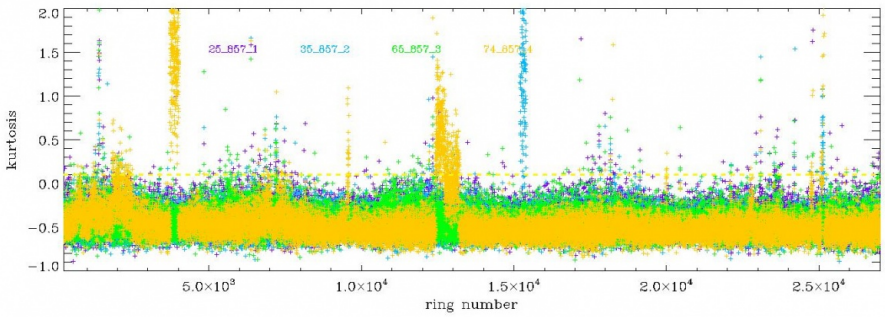

Discarded rings

Some rings are discarded (flagged) from further use (beam making, map making) by using ring statistics (see above and #planck2013-p03). For each statistic, we compare each ring value to the ring values averaged (RVA) over a large selection of rings (between 3000 and 21700). We also define the modified standard deviation (MSD) of a ring quantity as the standard deviation of that quantity over the rings that deviate by less than five nominal standard deviations. This truncation is necessary to be robust against extreme deviant rings.

More specifically, a ring is discarded if it matches one of the following criteria:

- the | mean-median | deviates from the RVA by more than fifteen times the MSD.
- the standard deviation deviates from the RVA by more than -5 times the MSD (all cases corresponding to almost empty rings) or +15 times the MSD.
- the Kolmogorov-Smirnov test deviates from the RVA by more than 15 times the MSD.
- the ring duration is more than 90 min.
- the ring is contaminated by RTS with an amplitude of more than one standard deviation of the noise. It concerns a few hundreds of rings for 3 bolometers (44_217_6b, 71_217_8a, 74_857_4). Notice that two bolometers are completely discarded for maps: 55_545_3 and 70_143_8, which present RTS at all time.

For the three first criteria, a visual inspection of the rmsigTOI at each of the incriminated rings has shown that all these anomalous rings are due to either a drift, a small jump in the TOI trend or a sudden change of noise level, the origin of which is unknown at present.

Once the list of discarded rings per bolometer is produced, a common list of discarded rings can be extracted for all bolometers (by using discarded rings for at least half the bolometers). Such rings correspond to identified phenomena, as can be seen on the following table.

Furthermore, an isolated valid ring stuck between two common discarded rings becomes discarded as well.

Table of **common discarded rings** of the nominal mission (rings 240-14723).

Cause	ring number
manoeuvre	304 1312 3590 3611 3642 3922 4949 6379 8456 11328
Sorption Cooler Switchover	11149 11150 11151 11152
Rings too long	440 474 509 544 897 898 3589 13333 14627 14653
Star tracker switchover	14628 14654
Massive Glitch Event	7665
Solar Flare	11235

The following figure is a summary of the impact of the discarding process **for each bolometer** (the solid black line is the common discarded ring percentage). The outlier bolometers have some RTS problems as mentionned above.

Effective integration time

The following figure summarizes the effective integration time per bolometer. For that purpose the number of unflagged samples in non-discarded pointing periods have been used within the nominal mission. The average value is of about 335 days of effective integration time.

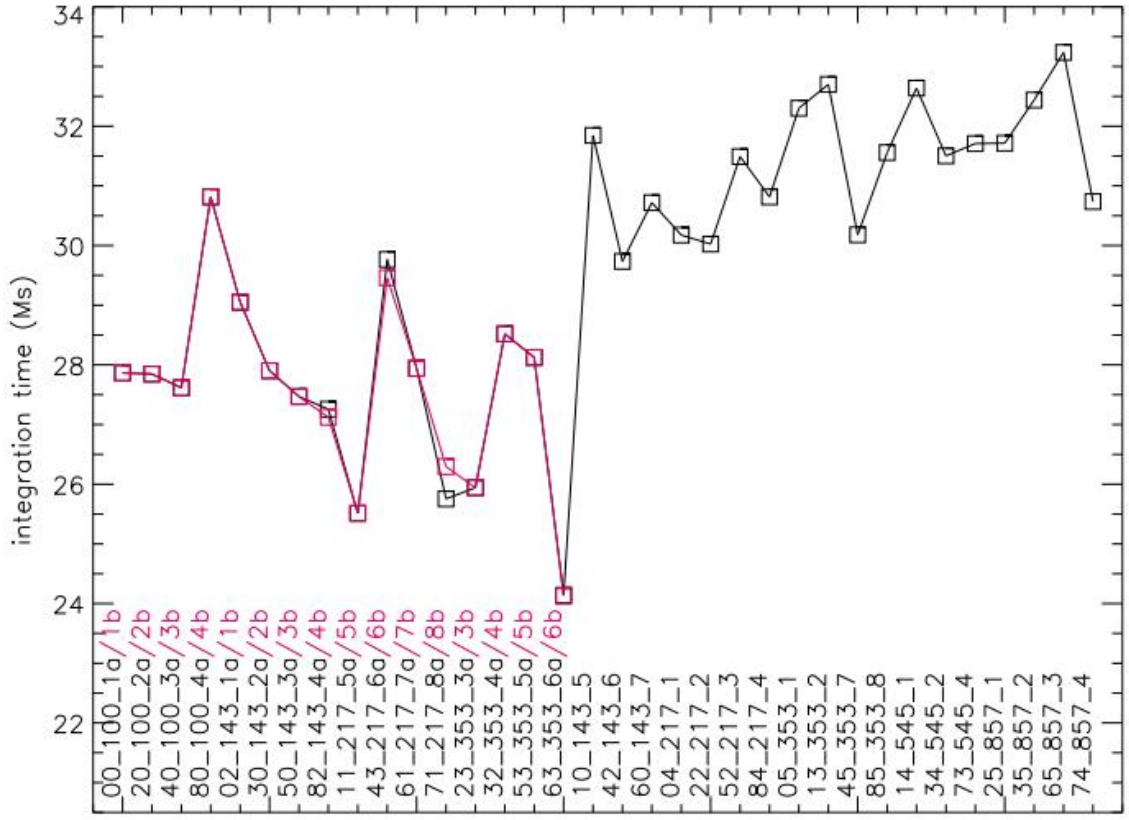

Flag description

Input flags

These flags are used as inputs to the TOI processing

The point-source flag (PSflag)

> An earlier version of HFI point-source catalog is read back into a flag TOIs, at a given frequency. In practice, 5 sigma sources are masked within a radius of 1.3 FWHM (9, 7, 5, 5, 5, 5 arcmin at 100,143,217,353,545,857 GHz) TBC.

the galactic flag (Galflag

> An earlier version of HFI maps is thresholded and apodized. The produced masks are read into flag TOIs. The retained threshold corresponds to a sky coverage of respectively 70, 70, 80, 90, 90, 90% at 100,143,217,353,545,857 GHz.

Solar System Object flag

> For the TOI flag, Mars, Jupiter, Saturn are flagged up to a radius of NbBeam= 2,3,3,4,4,4 times the fiducial SSO_FWHM with SSO_FWHM= 9, 7, 5, 5, 5, 5 arcmin at 100,143,217,353,545,857 GHz.
>
> As an input to planet mask for maps, Mars, Jupiter, Saturn are flagged with a radius computed as a coefficient depending on the planet (Factor_per_source) times NbBeam times SSO_FWHM, with Factor_per_source = 1.1, 2.25, 1.25 for Mars, Jupiter, Saturn respectively and NbBeam = 2.25, 4.25, 4.0, 5.0,.6.0, 8.0 at 100, 143, 217, 353, 545, 857 GHz. This flag is called SSOflag4map.
>
> A small trailing tail is added to the mask to take into account the non-deconvolution of the planet signal which has been replaced by background values. The width of that tail is 10 % of the main flag diameter. The number of samples which are additionnaly flagged are the Factor_per_Source times AddSNafter with (trail) times (Factor_per_source)^3 samples where trail = 10, 30, 20, 20, 30, 40 at 100, 143, 217, 353, 545, 857 GHz.
>
> Uranus and Neptune together with detected asteroids are masked by HFI. They are masked at the TOI level using an exclusion radius of 1.5 SSO_FWHM. At 857 GHz, 24 asteroids have been detected with HFI : 1Ceres, 2Pallas, 3Juno, 4Vesta, 7Iris, 8Flora, 9Metis, 10Hygiea, 11Parthenope, 12Victoria, 13Egeria, 14Irene, 15Eunomia, 16Psyche, 18Melpomene, 19Fortuna, 20Massalia, 29Amphitrite, 41Daphne, 45Eugenia, 52Europa, 88Thisbe, 704Interamnia, 324Bamberga.

Local maps showing the SSO flag. The colors correspond to the surveys involved in the nominal mission (green = Survey I, yellow = Survey II, red = Survey III).

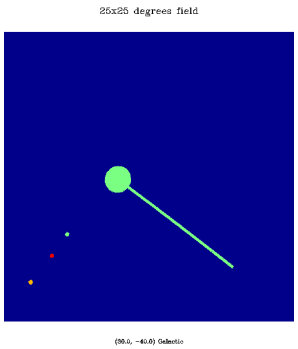

143 SWB row, around Jupiter 1st crossing

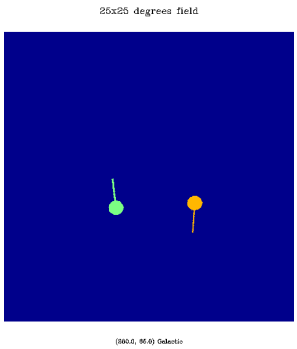

143 SWB row, around Saturn

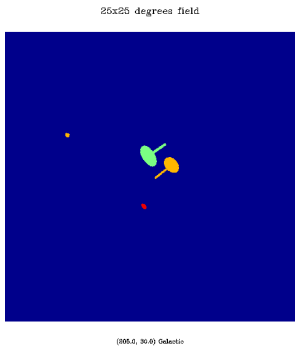

143 SWB row, around Mars

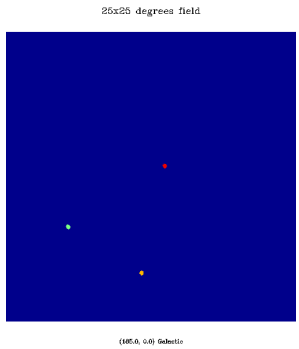

143 SWB row, random field in the ecliptic plane

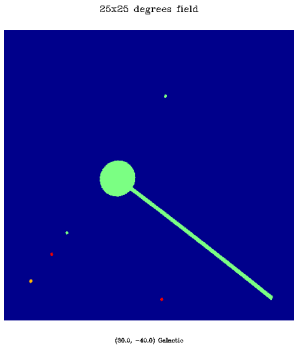

545/857 row, around Jupiter 1st crossing

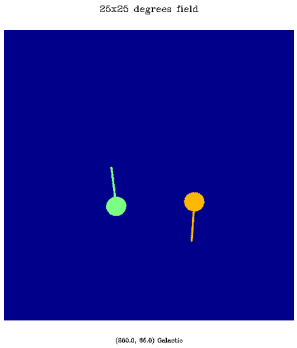

545/857 row, around Saturn

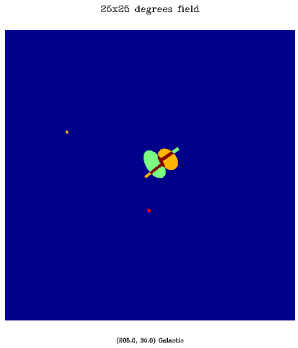

545/857 row, around Mars

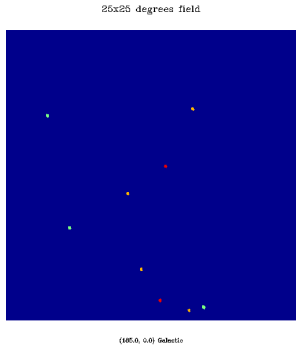

545/857 row, random field in the ecliptic plane

Output flags

A FlagTOIproc is produced by the TOIprocessing. It marks measurements which are not reliable for any of the following reasons:

- gap (no valid input data), enlarged by one sample on each side. It flags less than 0.00044% (resp. 0.00062%) of the nominal (resp. complete) mission. It is equivalent to less than 3 (resp. 8) minutes of data.
- "glitch" on dark bolometers: as the thermal template used for decorrelation is computed from these bolometer data, chunks of one minute-length data are discarded for all bolometers if at least 50\% of the data for at least one dark bolometer are flagged during this time. It is efficient to flag the data around the maximum of thermal events.
- "glitch" on individual bolometers : samples where the signal from a cosmic ray hit dominates the sky signal at more than 3 σ are discarded.
- jump as 100 samples are flagged around the computed position of the jump to take into account the error on this reconstructed position.

So the flag produced for the map making, called Total_flag, is defined by:

- Total_flag = UnstablePointing Flag OR FlagTOIproc OR SSOflag4map OR SSOflag seen

where FlagTOIproc = gap OR flag thermal template OR glitch OR jump and for PSB bolometers, FlagTOIproc_AB = FlagTOIproc_A OR FlagTOIproc_B. Note that the Total_flag is then identical for the A and B bolometers of a PSB pair.

At the destriping stage, a more restricted flag, called Total_flag_PS, is used. It is defined by Total_flag_PS = Total_flag OR PS_flag.

References

<biblio force=false>

1. References

</biblio>

Pointing&Beams

Detector Pointing and Beams (and Errors)

Detector Pointing

Introduction and Summary

The overall geometry of the Planck focal plane is shown here:

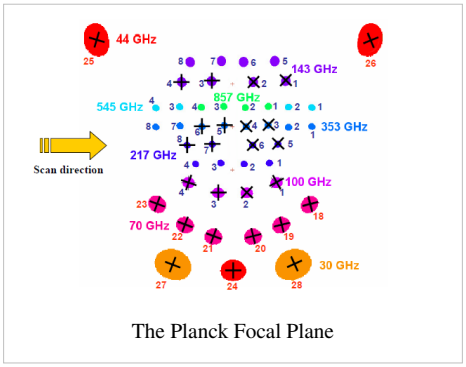

The Planck Focal Plane

In order to take full advantage of the HFI beams, we must know the individual detector positions to a precision of better than several arcseconds, over the course of the entire mission. Spacecraft pointing comes from the on-board star tracker at 4 Hz. This is translated via a series of three-dimensional rotations to a pointing for the centre of the focal plane and resampled to the HFI TOI data rate for convenience. We must then further translate this focal-plane boresight pointing to the individual detector locations. Because neither the rotations from the star tracker to the boresight nor those from the boresight to the individual detectors are known exactly a priori, we must calibrate using flight data. Specifically, measurements of HFI Detector pointing are based largely on observations of individual planets, with information from the much more frequent observation of lower-flux galactic and extragalactic high-frequency sources used to monitor and build a model of overall pointing drift. This long-term drift of the spacecraft attitude is due to changes in the moment of inertia and includes specific events which may induce sudden changes, essentially random as far as our ability to predict the effects thereof. Note that the resulting pointing model cannot easily be directly compared to a physical/optical model: in particular, it includes an unmeasured phase shift in the scan direction from the convolution and deconvolution of the detector transfer function, which is complex in the Fourier domain (Planck Collaboration P03c). Comparison with the initial optical model indicates that the in-scan change due to this phase shift is of the order of 1 arcminute. Note also that aberration is corrected in all observations. The final pointing model is measured to be better than 2 arcsecond rms in the co-scan and cross-scan directions averaged over ten-day periods.

Initial measurements: Mars 1 and other planets

The first observation of Mars, which occured around OD 80, is the baseline against which other objects are compared. Here, we show the relative pointing of Mars 1 to the pre-launch RFFM.

Focal plane drift: map-based measurement of detector positions

Prior to modeling of systematic changes in the Planck pointing, we find secular drifts of order one arcminute over the course of the nominal mission. We monitor this by making point-source catalogs based on single Planck surveys, only counting those objects which are observed over the course of less than seven days (this limits us to observations away from the ecliptic poles where Planck's observing strategy is highly cross-linked). We cross-match these catalog

positions to the known IRAS point-source catalog (Wang and Rowan-Robinson 2008) and average the deviations in ten-day blocks (the individual measurements are shown as lighter points; error bars assume equal weighting for all points, but the results are not sensitive to any imposed S/N cutoff):

A similar analysis performed directly in the timestream gives similar results, below.

A model for Planck Pointing

These analyses allow us to build a model for the pointing drift.

The correction is based on the measurement of pointing offset directly from the timeline, on a small sample of known and bright radio sources and planets. First the beam shape of each detector is measured by stacking individual timeline observation of bright planets. This process is of course amperes by pointing error, but those are reduced by allowing each pass on the planet to be slightly displaced in order to correct for the observed location of the planet. This process yield a very clean estimate of the beam of each detector.

Then those beam are used to determine the offset of observed location of planets (Mars, Saturn & Jupiter) as well as a few (~10) bright radio sources.

This offset are estimated for all detectors for the planet, and only for 100Ghz to 217Ghz one for the radio sources.

From the planet observations, one can recover the alignment of each detector in the focal plane, as well as a first pointing correction at the time of planet observations. This pointing correction is obtained by fitting splines on the planet observation from each detector. We further allow this correction to have a sharp jump between the first and second survey (SCS switchover).

This first pointing correction is further refined using the point sources observations in order to fill the period between planet observations. The radio sources offsets require further treatment than the planet based offsets. First, the brightness of the sources being much smaller than planets, the offset on individual detector observation are very noisy, and we filter out the noise by building median offsets for each point source observation. Second, since the sources can be slightly extended we still observe systematic offset above and below the planet based pointing correction in a regular alternating pattern. This is due to the fact that we are observing those extended objects scanning in alternating directions, and our fit of those extended sources to our beam translate into this systematic alternating pattern. We thus allow for a small, arcsec correction of those offsets : i.e. each object is allowed a single offset displacement of order arc seconds in order to minimize the offset between different observations of the same object at different time.

The resulting list of point source offsets is then merged with the planet offsets. Again a spline based correction is built fitting all of this data, and allowing rupture of continuity at the time of the SCS switchover and other major onboard event (typically between each surveys).

Once we assume the full Planck pointing model and re-measure the position of Mars for this observation, we see sub-arcsecond deviations (as expected); this gives an indication of the purely numerical limitations of the method. Further planet observations show the small remaining uncorrected drift present in the pointing model (note that cross-scan positions are measured with considerably less data than in-scan positions due to the scan strategy): Redoing the single-survey map- and catalog-based computation with the corrected pointing shows that Planck has achieved the arcsecond-scale goal of pointing rms:

Scanning Beams

The scanning beams describe the instrument's instantaneous beam profile. Due to the near constant spin rate of the spacecraft, time domain effects (including residual time response and lowpass filtering) are degenerate with the spatial response due to the optical system. The scanning beam reconstruction recovers both of these effects, aside from residual time domain effects on a longer time scale than can be captured with the extent of the scanning beam model.

In the paper cite P03c we consider two models of the beam in order to better understand systematics in the reconstruction. Here we describe only the BSpline beams which are used to compute the delivered effective beam (see next section).

BSpline Beam construction

We use seasons 1 and 2 of the Mars observation to reconstruct the beam. The data are processed with the bigPlanets TOI processing. We use JPL Horizons ephemerides to determine the pointing of each detector relative to the planet. We subtract the astrophysical background in the time domain using a bicubic interpolation of the Planck maps.

The time ordered data are used to fit a two dimensional BSpline surface using a least square minimization and a smoothing criterion to minimize the effects of high spatial frequency variations. We therefore assume the scanning beam to be smooth. The smoothing criterion as well as the locations of the nodes used to compute the B-Spline basis functions are set using GRASP physical optics simulations as inputs which are the best assumptions on the spatial frequency content of the in-flight beams.

The smoothing criterion is defined as follows:

And the global inversion criterion :

$$\zeta = \eta + p \times \delta$$

with δusual least square estimator and $p$coefficient giving the relative weight to $\delta$with respect to the smoothing criterion.

The BSpline nodes are located on a regular spaced grid in the detector coordinate framset. At the edge of the reconstructed beam map area, 4 coincident nodes are added to avoid vanishing basis functions.

Let $B_{i,k+1}$, $k$degree B-Spline build using nodes { λ_i, ..., λ_{i+k+1}} (*De Boor & Cox*, 1972) :

$$B_{i,l+1}(x) = \frac{x - \lambda_i}{\lambda_{i+l} - \lambda_i} B_{i,l}(x) + \frac{\lambda_{i+l+1} - x}{\lambda_{i+l+1} - \lambda_{i+1}} B_{i+1,l}(x)$$
$$l = 1, \ldots, k$$

Simulations and errors

We estimate the reconstruction bias and noise in the measurements using an ensemble of simulated planet observations for each channel. Kept fixed in each simulation are:

- the input beam assumed: we use a supersampled version of the reconstructed BSpline beam (or whatever comes out of the current ongoing tests!)
- Astrophyical background is the same as that subtracted from the real data.
- StarTracker pointing (using the ptcor6 pointing model).

The following are varied in each simulation:

- detector noise realizations obtained by filtering randomly generated white noise with the measured noise PSDs
- random pointing errors with 2 arcsecond rms, and a spectrum that replicates the real errors.
- simulated glitches and the deglitching procedure
- Mars brightness temperature variability

400 simulated timelines are generated for each bolometer and for each of the two seasons of Mars observations used in the beam reconstruction. The simulated timelines are made into beam maps, projecting onto the BSpline basis in the same way as the real data.

The beam maps are propagated to effective beam window functions using the quickbeam approach (see effective beams below) and used to evaluate the reconstruction bias and to construct error eigenmodes in the effective beam window function.

Figure: random pointing error PSD Figures: error envelope plots (or should those go under effective beams?)

Residuals

There are two known beam effects that are not included in the main beam model and are estimated as a separate bias in flux and angular power spectrum measurement: 1. long tails due to errors in low frequency time response deconvolution, and 2. near sidelobes.

We stack all five observations of Jupiter to estimate the long time scale residuals due to incomplete deconvolution of the long time scale response.

Add some kind of mean tail plot

Near sidelobes are also evaluated using stacked Jupiter (hopefully they will just be part of the v53bis BSpline beams). The main features in the near sidelobes include a wide beam skirt, and dimpling lobes Add sidelobe plots and tables

Effective Beams

Several methods of effective beams determination have been developped and cross-validated. Need satisfactory comparison plot

FEBeCoP

To be coordinated with GracaSee Mitra et al (2011

FICSBell

Since the HFI beams are not azimuthally symmetric, the scanning strategy has to be taken into account in the effective beam response modelling. This is done using the FICSBell method (Hivon et al, in preparation), which generalizes to polarization and to include other sources of systematics the approach used for TT $C(l)$estimation in WMAP-3yr Hinshaw et al (2007) and by Smith et al (2007) in the detection of CMB lensing in WMAP maps. The different steps of the method used for this study can be summarized as follows:

1. The scanning related information (i.e., statistics of the orientation of each detector within each pixel) is computed first, and only once for a given observation campaign. Those orientation hit moments are only computed up to degree 4, for reasons described in point 2 below. At the same time, the first two moments of the distribution of samples within each pixel (ie, their center of mass and moments of inertia) are computed and stored on disc.
2. The scanning beam map or beam model of each detector $d$is analyzed into its Spherical Harmonics coefficients

where is the beam map centered on the North pole, and is the Spherical Harmonics basis function. Higher $s$indexes describes higher degrees of departure from azimuthal symmetry and, for HFI beams, the coefficients $b^d_{ls}$are decreasing functions of $s$at most $l$considered. It also appears that, for $l < 3000$, the coefficients with $|s| > 4$ account for 1%or less of the beam throughput. For this reason, only modes with $|s| \leq 4$are considered in the present analysis. Armitage-Caplan and Wandelt (2009) reached a similar conclusion in their deconvolution of Planck-LFI beams.

3. The b^d_{ls}coefficients computed above are used to generate s-spin weighted maps, as well as the first and second order derivatives, for a given CMB sky realization.

4. The spin weighted maps and orientation hit moments of the same order s are combined for all detectors involved, to provide an "observed" map. Similarly the local spatial derivatives are combined with the location hit moments to describe the effect of the non-ideal sampling of each pixel (see [sec:pixelization]). In this combination, the respective number of hits of each detector in each pixel is considered, as well as the weighting (generally proportional to the inverse noise variance) applied to each detector in order to minimize the final noise.
5. The power spectrum of this map can then be computed, and compared to the input CMB power spectrum to estimate the effective beam window function over the whole sky, or over a given region of the sky.

Monte-Carlo (MC) simulations in which the sky realisations are changed can be performed by repeating steps 3, 4 and 5. The impact of beam model uncertainties can be studied by including step 2 into the MC simulations.

QuickBeam

Planck observes the sky after convolution with a "scanning beam", which captures its effective response to the sky as a function of displacement from the nominal pointing direction. Decomposing the scanning beam into harmonic coefficients B_{lm}, each time-ordered data (TOD) sample can be modelled as (neglecting the contribution from instrumental noise, which is independent of beam asymmetry) where the TOD samples are indexed by i, and $\tilde{T}_{lm}$ is the underlying sky signal. The spin spherical harmonic ${}_sY_{lm}$ rotates the scanning beam to the pointing location (θ, ϕ), while the $e^{-is\alpha_i}$ factor gives it the correct orientation. Eq. may be evaluated with the "TotalConvolver" algorithm of Wandelt and Gorski (2001), accelerated using the "conviqt" recursion relations Prezeau and Reinecke (2010) This approach is implemented in LevelS. </ref>, although because it involves working with a TOD-sized objected it is necessarily slow.

On the small angular scales comparable to the size of the beam, it is a good approximation to assume that the procedure of mapmaking from TOD samples is essentially a process of binning: where $H(p)$ is the total number of hits in pixel $\hat{n}$.

Start with a normalized, rescaled harmonic transform of the beam B_{lm}, sky multipoles $\tilde{T}_{lm}$ and a scan history object $w(\hat{n}, s)$ given by $w(\hat{n}, s) = \sum_{j \in p} e^{is\alpha_j}/H(\hat{n})$ where the sum is over all hits j of pixel p at location $\hat{n}_p$, and α_j is the scan angle for observation j. The harmonic transform of this scan-strategy object is given by ${}_sw_{LM} = \int d^2\hat{n}\, {}_sY^*_{LM}(\hat{n}) w(\hat{n}, s)$. The beam-convolved observation is then given by $\tilde{T}(\hat{n}) = \sum_{slm} w(\hat{n}, -s) B_{ls} T_{lm}\, {}_sY_{lm}(\hat{n})$. Taking the ensemble average of the pseudo-Cl power spectrum of these T_{lm} we find

where is a cross-power spectrum of scan history objects. Note that the w(n,s) which we have used here can also incorporate a position dependent weighting to optimize the pseudo-Cl estimate, such as inverse-noise or a mask– the equations are unchanged. Writing the pseudo-Cl in position space (a la Dvorkin and Smith (2009)) with Wigner-d matrices we have

This integral can be implemented exactly using Gauss-Legendre quadrature, with a cost of . For simplicity, we've written all the equations here for the auto-spectrum of a single detector, but the generalization to a map made by adding several detectors with different weighting is straightforward. The cost to compute all of the necessary terms exactly in that case becomes .

Are beams really so difficult? On the flat-sky beam convolution is easy: just multiplication in Fourier space by a beam rotated onto the scan direction. Multiple hits with different scan directions are incorporated by averaging (as the "scan history" objects above encapsulate). Does the sphere really require everything to be so complicated? For a scan strategy which is fairly smooth across the sky, we can pretend that we are observing many independent flat-sky patches at high-L with fairly good accuracy. There is in fact a fairly good approximation to the beam convolved pseudo-Cl power spectrum which is essentially a flat-sky approximation. In the limit that $L \gg l_1$, with C_{l_2} and B_{l_2} being slowly-varying function in l_2 the pseudo-Cl sum above can be approximated as where the average $<>_p$ is

taken over the full sky. It's illustrative to consider three limits of this equation: for a "raster" scan strategy in which each pixel is observed with the same direction, we have and the predicted pseudo-Cl is just the power spectrum of the beam. For a "best-case" scan strategy, in which each pixel is observed many times with many different orientation angles, we have $< | w(, M) |^2 >_p = _{M0}$, and the transfer function is just the azimuthally symmetric part of the beam. Note that this is for a full-sky observation– in the presence of a mask, the average above produces an fsky factor, as expected. It just neglects the coupling between L multipoles (which can be calculated with the more complete equations above).

Pixelization Artifacts

- Several codes available to simulate effects of pixelization.
- Mixes the CMB gradient into a pixelization ``noise *with a level comparable to that of $2\mu Karcmin$ instrumental noise.*
- Quantitative estimate of effect should be included with each released map, but expect not to matter significantly for CMB analysis, as small compared to instrumental noise.

[sec:pixelization]

Planck maps are produced at resolution 11 $(N_{\rm side} = 2048)$, corresponding to pixels with a typical dimension of $1.7'$, comparable to the spacing between scanning rings . This results in an uneven distribution of hits within pixels, which introduces some complications in the analysis and interpretation of the maps. A sample of the hit distribution is illustrated in Fig. [fig:pixcoverage]. Below we discuss the simulation and modeling of this pixelization effect in more detail.

[!ht]

[fig:pixcoverage]

The collaboration has produced 3 codes which may be used to simulate the effect of pixelization on the observed sky, LevelS/TotalConvoler/Conviqt, FeBeCoP, and FICSBell references and further discussion of the three methods and how they each simulate the pixelization e$\diamond$ffect..

For the measurement of CMB fluctuations, it is also possible to gain intuition for the effects of pixelization analytically. On the small scales relevant to pixelization, the observed CMB is smooth, both due to physical damping as well as the convolution of the instrumental beam. Taylor expanding the CMB temperature about a pixel center to second order, the typical gradient amplitude is given by $\langle |\nabla T|^2 \rangle = \frac{1}{4\pi} \sum_l l(l+1)(2l+1) C_l^T W_l \approx 1 \times 10^9 \mu K^2/{\rm rad}^2$ where the approximate value is calculated for a ΛCDM cosmology with a $7'$ fwhm Gaussian beam. The typical curvature of the observed temperature, on the other hand is given by $\langle |\nabla^2 T|^2 \rangle = \frac{1}{4\pi} \sum_l [l(l+1)]^2 (2l+1) C_l^T W_l \approx 7 \times 10^{14} \mu K^2/{\rm rad}^4$. On the scales relevant to the maximum displacement from the center of a $1.7'$ pixel, the maximum displacement is , and so the gradient term tends to dominate, although the curvature term is still non-negligible. For each observation of a pixel, we can denote the displacement from the pixel center as $d = d_\theta + i d_\phi$. The average over all hits within a pixel gives an overall deflection vector which we will denote for a pixel center located at $\hat{n}$ as $d(\hat{n})$. This represents the center of mass of the hit distribution; in Fig. [fig:pixcoverage] we have plotted these average deflections using black arrows. The deflection field $d(\hat{n})$ may be decomposed into spin-1 spherical harmonics as $d_{lm} = \int_{4\pi} {}_1Y^*_{lm} d(\hat{n})$.

With a second order Taylor expansion of the CMB temperature about each pixel center, it is then possible to calculate the average pseudo-Cl power spectrum of the pixelized sky. This is given by

where $R^d = \langle |d|^2 \rangle /2$ is half the mean-squared deflection magnitude (averaged over hits within a pixel, as well as over pixels). C_l^{d+} is the sum of the gradient and curl power spectra of d_{lm}, and C_l^{d-} is the gradient spectrum minus the curl spectrum. The R^d term describes a smearing of the observed sky due to pixelization. For uniform pixel

coverage of $N_{\rm side} = 2048$pixels $\sqrt{\langle |d|^2 \rangle} = 0.725'$. For the hit distribution of Planck frequency maps, $R^d$is typically within maps, looks like will be better than 10%percent of this value, and so this term is accurately described by the pixel window function, which is derived under the assumption of uniform pixel coverage.
The effect of pixelization is essentially degenerate with that of gravitational lensing of the CMB, with the difference that it (1) acts on the beam-convolved sky, rather than the actual sky and (2) produces a curl-mode deflection field as well as a gradient mode. This is discussed further in cite lensing paper, where the subpixel deflection field constitutes a potential source of bias for the measured lensing potential. Indeed, Eq. [eqn:clt_pixelized] is just a slightly modified version of the usual first order CMB lensing power spectrum (Hu (2000), Lewis and Challinor (2006)) to accommodate curl modes.

A useful approximation to Eq. which is derived in the unrealistic limit that the deflection vectors are uncorrelated between pixels, but in practice gives a good description of the power induced by the pixelization, is that the $d(\hat{n})$ couples the CMB gradient into a source of noise with an effective level given by

where the average is taken over all pixels and $R^T$is half the mean-squared power in the CMB gradient: $R^T = \frac{1}{8\pi}\sum_l l(l+1)(2l+1)\tilde{C}_l^T$.For frequency-combined maps, $\sqrt{\langle |d(\hat{n})|^2 \rangle}$is typically on the order of $0.1'$, and so the induced noise is at the level of $\sigma^N \sim 2\mu K arcmin$. This is small compared to the instrumental contribution, although it does not disappear when taking cross-spectra, depending on how coherent the hit distributions of the two maps in the cross-spectrum are.

Map-making

Map-Making and photometric calibration

Introduction

This page will give an overview of the map-making and photometric calibration procedures used by the HFI DPC to build detector and frequency maps. This processing and its performances are described in the the HFI DPC Paper and the the HFI DPC Calibration co-Paper [which will be completed prior to this page].

To build HFI maps, we use the destriping approximation, in which noise is assumed to decompose into two components : white noise plus low frequency drifts. Using the sky redundancy, the low frequency drifts are modelled as one constant, or offset, per pointing period. To speed up the ulterior processing we first build intermediate products, by taking advantage of redundancies : we average signal and detector orientation on healpix pixels visited during each fixed pointing period, which we call hereafter 'ring'. Detector's pointing are corrected for slow drifts and aberration (displacement on the sky indouced by the satellite's motion). This intermediate product is called HPR for healpix pixel ring. They have been constructed using the same map resolution as the final HFI products (correspondontg to nside=2048). This new dataset is used as input in the following steps.

Photometric calibration

dipole calibration (100 to 353 GHz)

For the 2013 data release, the calibrator for the CMB frequency was the Solar dipole, as measured by the WMAP team (G. Hinshaw et al., Astrophys.J.Suppl.180:225-245,2009). We use a two components template fitting procedure, performed for each detector independently, to determine ring by ring an estimation of the dipole gain. The two fitted components are the Solar dipole and a sky template. We used the PSM for thermal dust emission at the detector's frequency as a first approximation of the sky template in pur early release. Using the HFI channel map

as a template brings negligible change in the averaged gain, but reduces the systematic ring-to-ring dispersion of our estimation. We average these estimations over a subset of rings in the first survey (2000 to 6000) in which the dipole's amplitude is high enough with respect to that of the sky template, to get a single dipole gain per detector.

Several pieces of evidence led us to the conclusion that out bolometers presented apparent gain variation with time, after comparing the 3rd scan of the sky with the first one. This was later (mid-2012) explained by inequalities in the steps of the analog-to-digital converters (ADC) used in each bolometer's electronic chain. These devices had to be characterized using warm data after the end of the HFI observations. This process is still on-going (01/2012).

In the mean time we used an empiric correction, looking for a gain estimation and an offset per ring. This amounts to solve the non-linear equation :

where d is s the detector measurement, both S the sky signal, g the detector gain, O the offset (for ring no i) are the unknowns to be determined, and n the noise. We linearized this equation starting from the constant gain approximation, to get a measurement of the apparent time-varying gains for each bolometer independently. The limitations of this process are intrinsic signal variability from one observation to the other, like polarization or intra-pixel gradient. This procedure was thus only used for the 100 to 217 GHz detectors, for which the dipole signal is brighter and galactic signal (and polarization). A mask was used to removed the inner part of the Galactic plane.

Higher frequency calibration (545 and 857 GHz)

We therefore finally derived the sub-mm channels' calibration for the 2013 Planck data release from the comparison of measurements of the Neptune and Uranus fluxes (with aperture photometry) with their expectations from the Moreno et al model of their atmospheres' emission. This procedure is justified, since for both planets, at the lower frequencies (100-353 Ghz), the fluxes we recover are in agreement within ~ +/-5\% with what is expected from the planet spectral model, and the HFI detector's band-passes.

We determined zero-level for the released maps is selected regions of the sky where dust emissions are low and well correlated with HI. We may thus estimate and subtract dust emissions using the Hi template, and CMB from a Planck component separated template. The remaining astrophysical zero level is that of CIB. By imposing that the vele we find is equal to that of the CIB model of Bethermin et al, we may aset the sezo level of our maps.

Building of Maps

Using the photometric calibration parameters, we build maps in two steps :

- we determine the destriping offsets using the full mission data
- we build the maps, using these offsets, by inverting the photometric equation :

where d is the destriped and calibrated signal at the HPR level. Detector's data are combined with an inverse noise weights derived from each detector's NEP. Q and U maps are build whenever possible. We propagate the white noise by building the 3x3 (or 1x1 if only I is reconstructed) covariance matrices in each pixel. At each frequency we build maps combining all detectors and independent detector sets. We use the offsets build for the full mission for building maps for each scan survey and for the nominal mission duration. We also build maps from the two independent halves of each rings. Altogether, more than 6000 maps are built at each release.

HPR and Maps are built in Galactic coordinates.

Noise properties

Map noise properties can be evaluated using several methods, thanks to the high level of observation redundancies. We can use the maps built from the difference between the first and second half of each rings, or compare individual sky scans, of detector sets with each other.

Low resolution (nside = 8, 16, 32 ?) pixel-to-pixel noise covariance matrices are build using an analytic approach from the measured noise power spectra.

Zodi correction

At the highest Planck frequencies, Zodiacal emission is visible in a survey difference map:

This map is a difference between the 857 GHz Survey 2 map and the 857 GHz Survey 1 map. This difference effectively removes Galactic and other emissions which originate far from Planck. As the Solar elongation is different for measurements of the same point on the sky for the two surveys, we see Zodiacal emission, while all emission from further sources is removed. The zodiacal emission follows the Ecliptic plane, which starts at the lower left of the image, then crosses the center of the plot towards the upper right. Note that the "arcs" at the top and bottom of the image are images of the Galactic center in the Far Sidelobes, which are discussed in the section below. Similar plots for other HFI frequencies, for maps both before and after removal, are shown here.

Zodiacal Emission is removed from the 353, 545 and 857 GHz channels. It is described in the HFI DPC Paper, but a synopsis of the procedure is as follows:

- During each survey, a large fraction of the sky has observations which all fall within a week of each other. That is, during a single survey, most pixels are observed during a short, well-defined period. The contribution from Zodiacal Emission to the total brightness seen, then, is well defined.
- We use the the COBE model of the Zodiacal Light to make predictions for this Zodiacal emission for those pixels observed over a span of one week or less, and use GRASP models of the beams to predict the emission from the Galaxy given our sidelobes. The templates from the COBE model are shown here.
- We fit the survey difference maps with these model templates to estimate the emissivity of each Zodi component and sidelobe at the Planck wavelengths. The results of these fits at each frequency are shown here.
- We reconstruct each ring of the the full mission using the combination of the COBE geometric model with the emissivities determined above and the sidelobe models.
- We remove the reconstruction above from each ring of data.
- We then make maps as described previously in this section. Maps with and without, as well as the differences between the two, are shown here. The survey differences before and after this removal are shown with and without Zodical emission removal here. The power spectra of what is removed from each map is shown here.

Far Sidelobes

The far sidelobe correction for the highest frequency HFI channels is described in the section above. Note that this correction is done only for the 857 and 545 GHz channels, as it is not seen at longer wavelengths. As for the Zodical emission correction, it is not important for the CMB.

We have made estimates of the contamination of the far sidelobes at 143 GHz by taking the 143 GHz map, adding the dipole, and passing it through our simulator, using a GRASP calculation of the far sidelobes for the 143-1a detector as the beam. The resulting maps is shown here:

While there is one small region that might reach 20 micro-K (this happens when the secondary spillover overlaps with the Galactic center), most of the map is quite quiet. This is evidenced by the power spectrum of the above map, which is quite small.

CO Correction

The extraction of CO maps from HFI maps is described in detail in the the CO Paper. The CO maps are produced by a combination of bolometer maps or frequency maps. The method is summarized [|here [1]]

References

[1] http://www.sciops.esa.int/wikiSI/planckpla/index.php?title=Science&instance=Planck_PLA_ES#CO_maps

Spectral response

HFI Spectral Response

This section outlines the unit conversion and colour correction protocol for Planck/HFI. Tables of unit conversion and colour correction coefficients will be included (there is not room for these in the P03d Co-Paper). Some of the checks on the unit conversion and colour correction coefficients will be described here also. Planet colour correction coefficients will be provided here (or perhaps in the joint HFI/LFI section). There will be links to the UcCC subsection of the PLA section, but the numbers and details belong here. The PLA UcCC subsection is primarily to introduce the software tools.

The band-average HFI spectral response data are shown in the figure below, and provided in the RIMO file [FIXME].

FIXME: insert figure.

The integration ranges used in determining the unit conversion and colour correction coefficients are verified through an iterative approach starting at one extreme and reducing to the band-centre for both the low and high frequency edges. The figure below demonstrates the stability in the integral once a sufficient data range has been employed. The range used in the official coefficients is thus sufficient to ensure that it falls within the flat region of the demonstration figure below.

FIXME: insert figure showing integral flattening once the range hs extended sufficiently out of band.

The band-average spectrum for a given frequency band is derived using a hit-map normalized inverse-square noise weighted detector spectrum average. Thus, the effective band-average spectrum changes depending on the region of sky in question, really the Planck coverage of any sky region. The histograms below demonstrate the variation across the sky of the detector weight coefficients, and thus the validity of using a single band-average spectrum for the entire sky map. Future analysis with the full Planck dataset may require incorporating the variation of the relative detector weights across the sky into understanding the differential spectral transmission between complementary maps (e.g. detset -1 cf. detset-2 maps).

FIXME: include detector weight histogram plots.

The following table presents basic characteristics of the HFI detector spectral repsonse, inclusing optical efficiency, effective frequency, etc.

FIXME: Add table from HFI_SPEC_TRANS_REPORT

Unit Conversion Tables

This section presents unit conversion coefficients for the HFI detectors (and LFI in some instances), including uncertainty estimates based on the uncertainty of the HFI detector spectral response. The derivation of the unit conversion coefficients is provided in planck2013-p02d.

Table 1: MJy/sr/K_{CMB} and ySZ/K_{CMB} unit conversion coefficients.

Band/Det. [GHz]	U_C [MJy/sr/K_{CMB}]	U_C [ySZ/K_{CMB}]
100-1a	238.2871 ± 0.7140	-0.24612 ± 0.00017
100-1b	241.8530 ± 0.6979	-0.24703 ± 0.00017
100-2a	244.2375 ± 0.7505	-0.24829 ± 0.00018
100-2b	243.3572 ± 0.7935	-0.24798 ± 0.00019
100-3a	246.0715 ± 0.7465	-0.24873 ± 0.00018
100-3b	240.1739 ± 0.7341	-0.24690 ± 0.00018
100-4a	246.7316 ± 0.7949	-0.24906 ± 0.00020
100-4b	247.6289 ± 0.7693	-0.24924 ± 0.00019
100-avg	244.0960 ± 0.3050	-0.24814 ± 0.0000741350
100-detset1	244.8649 ± 0.4196	-0.24833 ± 0.00010
100-detset2	243.7737 ± 0.3926	-0.24807 ± 0.0000950688
143-1a	366.4108 ± 0.2459	-0.35501 ± 0.00019
143-1b	369.5905 ± 0.2540	-0.35735 ± 0.00019
143-2a	366.7249 ± 0.2540	-0.35551 ± 0.00019
143-2b	370.7001 ± 0.2386	-0.35818 ± 0.00018
143-3a	360.0418 ± 0.2676	-0.35015 ± 0.00020
143-3b	365.9529 ± 0.2608	-0.35477 ± 0.00020
143-4a	371.3469 ± 0.2532	-0.35965 ± 0.00019
143-4b	369.0953 ± 0.2502	-0.35685 ± 0.00019
143-5	380.1162 ± 0.2340	-0.36557 ± 0.00018
143-6	373.3413 ± 0.2492	-0.36038 ± 0.00019
143-7	381.2511 ± 0.2467	-0.36660 ± 0.00019
143-8	376.1461 ± 0.2535	-0.36293 ± 0.00019
143-avg	371.7327 ± 0.0784	-0.35922 ± 0.0000594035
143-detset1	365.0304 ± 0.1332	-0.35398 ± 0.00010
143-detset2	369.3005 ± 0.1289	-0.35743 ± 0.0000969068
143-SWBs	378.5797 ± 0.1434	-0.36446 ± 0.00011
217-1	486.0322 ± 0.0359	4.34709 ± 0.01285
217-2	486.4008 ± 0.0373	4.02758 ± 0.01148
217-3	486.8924 ± 0.0363	4.11836 ± 0.01159
217-4	486.0164 ± 0.0350	4.43344 ± 0.01332
217-5a	479.8049 ± 0.0404	7.48401 ± 0.04083
217-5b	480.4364 ± 0.0396	6.97673 ± 0.03451

217-6a	480.3416 ± 0.0392	7.05081 ± 0.03492
217-6b	480.3544 ± 0.0397	7.01686 ± 0.03471
217-7a	481.0486 ± 0.0375	6.79755 ± 0.03214
217-7b	480.0012 ± 0.0397	7.69946 ± 0.04288
217-8a	479.8096 ± 0.0408	7.25645 ± 0.03840
217-8b	480.7686 ± 0.0386	6.86218 ± 0.03259
217-avg	483.6874 ± 0.0118	5.15309 ± 0.00592
217-detset1	480.3600 ± 0.0198	7.21293 ± 0.01879
217-detset2	480.3136 ± 0.0202	7.04561 ± 0.01783
217-SWBs	486.3306 ± 0.0181	4.23605 ± 0.00619
353-1	288.4183 ± 0.0212	0.16229 ± 0.0000249067
353-2	287.8701 ± 0.0223	0.16198 ± 0.0000253799
353-3a	289.2493 ± 0.0248	0.16231 ± 0.0000313162
353-3b	289.1951 ± 0.0226	0.16283 ± 0.0000259493
353-4a	286.6167 ± 0.0223	0.15887 ± 0.0000239865
353-4b	286.5976 ± 0.0229	0.15939 ± 0.0000249209
353-5a	289.9808 ± 0.0222	0.16446 ± 0.0000267670
353-5b	289.9004 ± 0.0229	0.16489 ± 0.0000272856
353-6a	288.8151 ± 0.0276	0.16299 ± 0.0000323775
353-6b	292.8348 ± 0.0251	0.16654 ± 0.0000304403
353-7	285.3414 ± 0.0273	0.15816 ± 0.0000340767
353-8	283.5120 ± 0.0248	0.15709 ± 0.0000261476
353-avg	287.4517 ± 0.0085	0.16110 ± 0.00000987580
353-detset1	289.6204 ± 0.0116	0.16376 ± 0.0000139126
353-detset2	287.9671 ± 0.0123	0.16090 ± 0.0000137521
353-SWBs	286.7861 ± 0.0120	0.16046 ± 0.0000138705
545-1	57.0831 ± 0.0489	0.06881 ± 0.0000563911
545-2	58.8825 ± 0.0457	0.06963 ± 0.0000516856
545-3	57.8794 ± 0.0858	0.06900 ± 0.00010
545-4	58.0595 ± 0.0515	0.06905 ± 0.0000591782
545-avg	58.0356 ± 0.0278	0.06918 ± 0.0000317698
545-detset1	58.0243 ± 0.0337	0.06924 ± 0.0000385529
545-detset2	58.0595 ± 0.0513	0.06905 ± 0.0000587272
857-1	2.1891 ± 0.0565	0.03784 ± 0.00083
857-2	2.3457 ± 0.0453	0.03816 ± 0.00062
857-3	2.2133 ± 0.0516	0.03785 ± 0.00075
857-4	2.4022 ± 0.0568	0.03818 ± 0.00076
857-avg	2.2681 ± 0.0270	0.03798 ± 0.00038
857-detset1	2.2643 ± 0.0356	0.03800 ± 0.00050

857-detset2	2.2730 ± 0.0401	0.03796 ± 0.00057

The unit conversion from MJy/sr to K_RJ (i.e. Tb) does not depend on the spectrum, so is the same across each frequency band.

Table 2: MJy/sr to Tb unit conversion.

Band (GHz)	U_C [K_{RJ}/(MJy/sr)]
100	0.0032548074
143	0.0015916707
217	0.00069120334
353	0.00026120163
545	0.00010958025
857	4.4316316e-05

Colour Correction, Powerlaw spectra

The following table presents colour correction coefficients for HFI (and LFI...TBD) detectors and bands. A subsequent table presents the colour corrections in terms of effective frequencies. Plots are also included demonstrating the variation in colour correction coefficients within a frequency band, over a range of spectral indices.

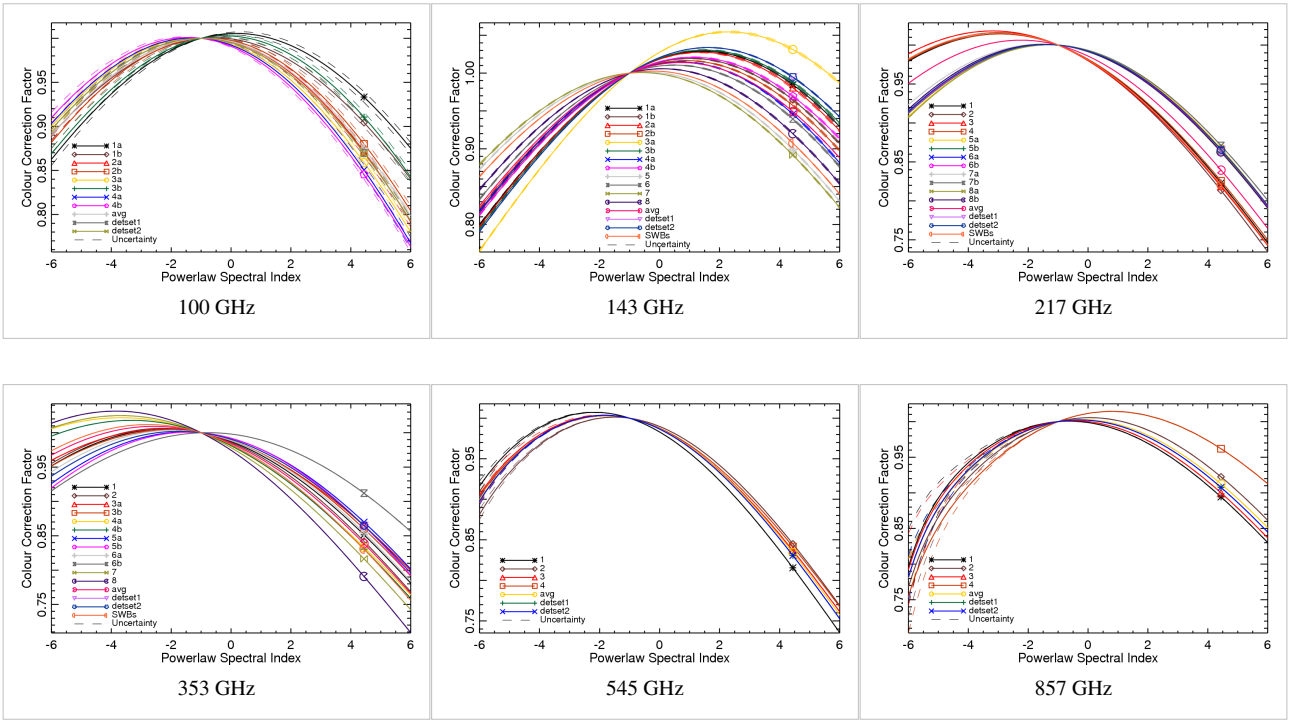

Band/Det. [GHz]	F_{CC}, S.I.: -4	-3	-2	-1	0	1	2	3	4
100-1a	0.93682 ± 0.00288	0.96513 ± 0.00194	0.98641 ± 0.00099	1	1.00548 ± 0.00099	1.00273 ± 0.00196	0.99180 ± 0.00289	0.97303 ± 0.00370	0.94693 ± 0.00439
100-1b	0.95469 ± 0.00359	0.97726 ± 0.00242	0.99252 ± 0.00121	1	0.99943 ± 0.00123	0.99080 ± 0.00236	0.97434 ± 0.00341	0.95048 ± 0.00433	0.91979 ± 0.00509
100-2a	0.95668 ± 0.00383	0.97967 ± 0.00259	0.99434 ± 0.00134	1	0.99626 ± 0.00131	0.98305 ± 0.00253	0.96064 ± 0.00361	0.92957 ± 0.00461	0.89055 ± 0.00535
100-2b	0.95213 ± 0.00378	0.97672 ± 0.00257	0.99289 ± 0.00128	1	0.99770 ± 0.00128	0.98597 ± 0.00250	0.96514 ± 0.00364	0.93578 ± 0.00466	0.89865 ± 0.00546
100-3a	0.96441 ± 0.00408	0.98520 ± 0.00275	0.99724 ± 0.00136	1	0.99327 ± 0.00129	0.97721 ± 0.00246	0.95227 ± 0.00347	0.91919 ± 0.00442	0.87887 ± 0.00508
100-3b	0.94194 ± 0.00321	0.96907 ± 0.00221	0.98866 ± 0.00111	1	1.00264 ± 0.00108	0.99640 ± 0.00210	0.98139 ± 0.00304	0.95797 ± 0.00390	0.92666 ± 0.00466
100-4a	0.96623 ± 0.00420	0.98652 ± 0.00283	0.99797 ± 0.00140	1	0.99234 ± 0.00135	0.97507 ± 0.00256	0.94864 ± 0.00364	0.91377 ± 0.00452	0.87135 ± 0.00521
100-4b	0.97085 ± 0.00368	0.98965 ± 0.00250	0.99955 ± 0.00125	1	0.99084 ± 0.00122	0.97224 ± 0.00234	0.94472 ± 0.00335	0.90909 ± 0.00422	0.86633 ± 0.00491
100-avg	0.95684 ± 0.00145	0.97975 ± 0.00099	0.99434 ± 0.00050	1	0.99640 ± 0.00049	0.98354 ± 0.00095	0.96174 ± 0.00136	0.93158 ± 0.00172	0.89381 ± 0.00204
100-detset1	0.96096 ± 0.00206	0.98250 ± 0.00142	0.99571 ± 0.00071	1	0.99510 ± 0.00068	0.98104 ± 0.00132	0.95818 ± 0.00188	0.92713 ± 0.00237	0.88868 ± 0.00275
100-detset2	0.95512 ± 0.00162	0.97860 ± 0.00109	0.99377 ± 0.00055	1	0.99694 ± 0.00054	0.98459 ± 0.00104	0.96324 ± 0.00148	0.93345 ± 0.00189	0.89598 ± 0.00220
143-1a	0.89624 ± 0.00086	0.93764 ± 0.00060	0.97263 ± 0.00031	1	1.01872 ± 0.00032	1.02801 ± 0.00063	1.02743 ± 0.00093	1.01688 ± 0.00121	0.99662 ± 0.00145
143-1b	0.90754 ± 0.00096	0.94559 ± 0.00067	0.97677 ± 0.00034	1	1.01443 ± 0.00036	1.01949 ± 0.00071	1.01492 ± 0.00104	1.00082 ± 0.00131	0.97759 ± 0.00158
143-2a	0.89562 ± 0.00093	0.93752 ± 0.00064	0.97272 ± 0.00033	1	1.01834 ± 0.00034	1.02703 ± 0.00067	1.02566 ± 0.00099	1.01422 ± 0.00129	0.99300 ± 0.00154
143-2b	0.91137 ± 0.00092	0.94831 ± 0.00063	0.97820 ± 0.00032	1	1.01294 ± 0.00032	1.01653 ± 0.00064	1.01056 ± 0.00094	0.99516 ± 0.00119	0.97074 ± 0.00143
143-3a	0.87293 ± 0.00080	0.92137 ± 0.00059	0.96420 ± 0.00031	1	1.02753 ± 0.00033	1.04577 ± 0.00069	1.05402 ± 0.00104	1.05201 ± 0.00138	1.03976 ± 0.00168
143-3b	0.89320 ± 0.00098	0.93577 ± 0.00068	0.97178 ± 0.00035	1	1.01941 ± 0.00037	1.02926 ± 0.00073	1.02918 ± 0.00106	1.01915 ± 0.00137	0.99948 ± 0.00167
143-4a	0.91028 ± 0.00088	0.94808 ± 0.00061	0.97836 ± 0.00031	1	1.01212 ± 0.00031	1.01421 ± 0.00061	1.00611 ± 0.00089	0.98805 ± 0.00113	0.96062 ± 0.00131
143-4b	0.90552 ± 0.00080	0.94424 ± 0.00056	0.97609 ± 0.00029	1	1.01513 ± 0.00029	1.02093 ± 0.00058	1.01721 ± 0.00085	1.00405 ± 0.00108	0.98188 ± 0.00129
143-5	0.94591 ± 0.00084	0.97224 ± 0.00057	0.99048 ± 0.00028	1	1.00048 ± 0.00028	0.99189 ± 0.00054	0.97451 ± 0.00078	0.94888 ± 0.00099	0.91575 ± 0.00116
143-6	0.92007 ± 0.00087	0.95452 ± 0.00060	0.98148 ± 0.00031	1	1.00943 ± 0.00031	1.00943 ± 0.00061	0.99996 ± 0.00089	0.98129 ± 0.00112	0.95395 ± 0.00133
143-7	0.95005 ± 0.00101	0.97507 ± 0.00068	0.99192 ± 0.00034	1	0.99900 ± 0.00033	0.98892 ± 0.00064	0.97009 ± 0.00092	0.94312 ± 0.00115	0.90883 ± 0.00134

143-8	0.92905 ± 0.00106	0.96094 ± 0.00070	0.98488 ± 0.00036	1	1.00574 ± 0.00035	1.00188 ± 0.00068	0.98858 ± 0.00098	0.96627 ± 0.00124	0.93573 ± 0.00138
143-avg	0.91412 ± 0.00031	0.95038 ± 0.00022	0.97935 ± 0.00011	1	1.01158 ± 0.00011	1.01364 ± 0.00022	1.00607 ± 0.00033	0.98907 ± 0.00042	0.96318 ± 0.00050
143-detset1	0.89061 ± 0.00043	0.93382 ± 0.00029	0.97071 ± 0.00015	1	1.02064 ± 0.00016	1.03182 ± 0.00031	1.03309 ± 0.00046	1.02433 ± 0.00060	1.00580 ± 0.00072
143-detset2	0.90504 ± 0.00052	0.94409 ± 0.00036	0.97612 ± 0.00018	1	1.01485 ± 0.00019	1.02009 ± 0.00038	1.01547 ± 0.00056	1.00108 ± 0.00071	0.97735 ± 0.00085
143-SWBs	0.93980 ± 0.00051	0.96809 ± 0.00034	0.98839 ± 0.00017	1	1.00250 ± 0.00017	0.99578 ± 0.00033	0.98006 ± 0.00048	0.95582 ± 0.00060	0.92382 ± 0.00070
217-1	1.01001 ± 0.00025	1.01437 ± 0.00017	1.01104 ± 0.0000834464	1	0.98146 ± 0.0000802765	0.95584 ± 0.00015	0.92373 ± 0.00022	0.88587 ± 0.00029	0.84309 ± 0.00035
217-2	1.01196 ± 0.00025	1.01614 ± 0.00017	1.01214 ± 0.0000851931	1	0.97999 ± 0.0000817160	0.95264 ± 0.00016	0.91866 ± 0.00023	0.87891 ± 0.00029	0.83436 ± 0.00034
217-3	1.01558 ± 0.00024	1.01798 ± 0.00016	1.01277 ± 0.0000788117	1	0.97995 ± 0.0000739414	0.95309 ± 0.00014	0.92006 ± 0.00019	0.88163 ± 0.00024	0.83866 ± 0.00028
217-4	1.01024 ± 0.00024	1.01432 ± 0.00016	1.01091 ± 0.0000810166	1	0.98175 ± 0.0000769260	0.95655 ± 0.00015	0.92496 ± 0.00021	0.88767 ± 0.00028	0.84549 ± 0.00033
217-5a	0.96844 ± 0.00026	0.98738 ± 0.00017	0.99803 ± 0.0000873238	1	0.99318 ± 0.0000845567	0.97777 ± 0.00016	0.95421 ± 0.00025	0.92318 ± 0.00032	0.88554 ± 0.00038
217-5b	0.97226 ± 0.00025	0.98994 ± 0.00017	0.99929 ± 0.0000838219	1	0.99202 ± 0.0000817184	0.97559 ± 0.00015	0.95120 ± 0.00022	0.91956 ± 0.00029	0.88156 ± 0.00034
217-6a	0.97150 ± 0.00026	0.98947 ± 0.00017	0.99908 ± 0.0000848909	1	0.99220 ± 0.0000806513	0.97593 ± 0.00016	0.95167 ± 0.00022	0.92012 ± 0.00028	0.88214 ± 0.00034
217-6b	0.97137 ± 0.00025	0.98943 ± 0.00017	0.99907 ± 0.0000817547	1	0.99219 ± 0.0000785606	0.97592 ± 0.00015	0.95169 ± 0.00022	0.92028 ± 0.00028	0.88257 ± 0.00033
217-7a	0.97678 ± 0.00025	0.99261 ± 0.00017	1.00045 ± 0.0000844965	1	0.99121 ± 0.0000835118	0.97430 ± 0.00016	0.94973 ± 0.00024	0.91817 ± 0.00031	0.88046 ± 0.00036
217-7b	0.96993 ± 0.00028	0.98809 ± 0.00019	0.99824 ± 0.0000955820	1	0.99328 ± 0.0000937668	0.97826 ± 0.00018	0.95537 ± 0.00026	0.92529 ± 0.00034	0.88885 ± 0.00040
217-8a	0.96801 ± 0.00027	0.98732 ± 0.00018	0.99810 ± 0.0000897456	1	0.99293 ± 0.0000858414	0.97713 ± 0.00017	0.95308 ± 0.00024	0.92152 ± 0.00030	0.88334 ± 0.00035
217-8b	0.97414 ± 0.00025	0.99113 ± 0.00016	0.99984 ± 0.0000788191	1	0.99161 ± 0.0000743292	0.97493 ± 0.00014	0.95048 ± 0.00020	0.91897 ± 0.00026	0.88126 ± 0.00031
217-avg	0.99378 ± 0.0000785663	1.00396 ± 0.0000523738	1.00607 ± 0.0000260772	1	0.98586 ± 0.0000247535	0.96403 ± 0.0000479011	0.93508 ± 0.0000688582	0.89977 ± 0.0000880719	0.85897 ± 0.00011
217-detset1	0.97210 ± 0.00011	0.98965 ± 0.0000713085	0.99907 ± 0.0000353487	1	0.99238 ± 0.0000335890	0.97642 ± 0.0000652875	0.95257 ± 0.0000978708	0.92152 ± 0.00013	0.88411 ± 0.00015
217-detset2	0.97122 ± 0.00013	0.98931 ± 0.0000871706	0.99901 ± 0.0000428016	1	0.99224 ± 0.0000412200	0.97599 ± 0.0000788817	0.95175 ± 0.00011	0.92024 ± 0.00014	0.88235 ± 0.00017
217-SWBs	1.01193 ± 0.00012	1.01566 ± 0.0000800628	1.01169 ± 0.0000388802	1	0.98083 ± 0.0000361511	0.95463 ± 0.0000686221	0.92201 ± 0.0000982270	0.88375 ± 0.00012	0.84069 ± 0.00015
353-1	0.99265 ± 0.00018	1.00266 ± 0.00012	1.00515 ± 0.0000594589	1	0.98729 ± 0.0000604515	0.96731 ± 0.00012	0.94058 ± 0.00017	0.90776 ± 0.00022	0.86965 ± 0.00027
353-2	0.99512 ± 0.00017	1.00448 ± 0.00012	1.00617 ± 0.0000594070	1	0.98602 ± 0.0000597532	0.96453 ± 0.00012	0.93604 ± 0.00018	0.90128 ± 0.00023	0.86111 ± 0.00028

353-3a	0.99494 ± 0.00021	1.00325 ± 0.00014	1.00498 ± 0.0000678294	1	0.98835 ± 0.0000641818	0.97024 ± 0.00012	0.94602 ± 0.00018	0.91620 ± 0.00023	0.88141 ± 0.00027
353-3b	0.99080 ± 0.00019	1.00090 ± 0.00013	1.00404 ± 0.0000629728	1	0.98875 ± 0.0000628625	0.97046 ± 0.00012	0.94549 ± 0.00018	0.91438 ± 0.00024	0.87780 ± 0.00028
353-4a	1.02156 ± 0.00017	1.02051 ± 0.00011	1.01332 ± 0.0000564405	1	0.98071 ± 0.0000532408	0.95573 ± 0.00010	0.92551 ± 0.00015	0.89056 ± 0.00019	0.85151 ± 0.00023
353-4b	1.01654 ± 0.00017	1.01770 ± 0.00011	1.01220 ± 0.0000572407	1	0.98127 ± 0.0000555070	0.95631 ± 0.00011	0.92561 ± 0.00016	0.88977 ± 0.00021	0.84951 ± 0.00025
353-5a	0.97711 ± 0.00018	0.99243 ± 0.00012	1.00016 ± 0.0000622265	1	0.99191 ± 0.0000608773	0.97608 ± 0.00012	0.95292 ± 0.00017	0.92307 ± 0.00022	0.88730 ± 0.00027
353-5b	0.97399 ± 0.00017	0.99066 ± 0.00011	0.99946 ± 0.0000586789	1	0.99213 ± 0.0000593907	0.97600 ± 0.00012	0.95198 ± 0.00017	0.92072 ± 0.00023	0.88306 ± 0.00028
353-6a	0.98767 ± 0.00023	0.99946 ± 0.00015	1.00364 ± 0.0000772503	1	0.98856 ± 0.0000760724	0.96957 ± 0.00015	0.94351 ± 0.00021	0.91103 ± 0.00027	0.87296 ± 0.00032
353-6b	0.96654 ± 0.00018	0.98394 ± 0.00013	0.99521 ± 0.0000644428	1	0.99812 ± 0.0000660710	0.98954 ± 0.00013	0.97439 ± 0.00019	0.95298 ± 0.00025	0.92575 ± 0.00030
353-7	1.02464 ± 0.00025	1.02337 ± 0.00016	1.01512 ± 0.0000779731	1	0.97828 ± 0.0000705538	0.95040 ± 0.00013	0.91695 ± 0.00019	0.87863 ± 0.00024	0.83621 ± 0.00028
353-8	1.03140 ± 0.00019	1.02872 ± 0.00013	1.01821 ± 0.0000632902	1	0.97446 ± 0.0000592252	0.94216 ± 0.00011	0.90384 ± 0.00017	0.86040 ± 0.00022	0.81279 ± 0.00026
353-avg	1.00188 ± 0.0000658139	1.00871 ± 0.0000438094	1.00811 ± 0.0000218270	1	0.98449 ± 0.0000211618	0.96190 ± 0.0000415137	0.93276 ± 0.0000608539	0.89776 ± 0.0000792146	0.85770 ± 0.0000959851
353-detset1	0.98298 ± 0.0000936819	0.99609 ± 0.0000621384	1.00185 ± 0.0000308546	1	0.99050 ± 0.0000300180	0.97352 ± 0.0000583752	0.94945 ± 0.0000846421	0.91889 ± 0.00011	0.88255 ± 0.00013
353-detset2	1.00524 ± 0.0000866191	1.01017 ± 0.0000579534	1.00845 ± 0.0000287729	1	0.98491 ± 0.0000278577	0.96343 ± 0.0000549193	0.93598 ± 0.0000788256	0.90310 ± 0.00010	0.86548 ± 0.00012
353-SWBs	1.00622 ± 0.0000959204	1.01174 ± 0.0000636195	1.00968 ± 0.0000312227	1	0.98285 ± 0.0000296202	0.95863 ± 0.0000571017	0.92789 ± 0.0000840579	0.89139 ± 0.00011	0.84997 ± 0.00013
545-1	0.98835 ± 0.00159	1.00344 ± 0.00071	1.00706 ± 0.00025	1	0.98297 ± 0.00014	0.95694 ± 0.00022	0.92302 ± 0.00026	0.88254 ± 0.00028	0.83687 ± 0.00028
545-2	0.96725 ± 0.00144	0.98922 ± 0.00066	0.99997 ± 0.00024	1	0.98982 ± 0.00013	0.97015 ± 0.00021	0.94196 ± 0.00027	0.90642 ± 0.00030	0.86485 ± 0.00032
545-3	0.97954 ± 0.00251	0.99694 ± 0.00116	1.00355 ± 0.00042	1	0.98686 ± 0.00023	0.96491 ± 0.00037	0.93512 ± 0.00044	0.89862 ± 0.00048	0.85665 ± 0.00050
545-4	0.97758 ± 0.00160	0.99548 ± 0.00074	1.00276 ± 0.00026	1	0.98774 ± 0.00015	0.96673 ± 0.00023	0.93790 ± 0.00027	0.90233 ± 0.00030	0.86123 ± 0.00031
545-avg	0.97732 ± 0.00079	0.99580 ± 0.00036	1.00316 ± 0.00013	1	0.98693 ± 0.0000723637	0.96474 ± 0.00011	0.93445 ± 0.00014	0.89725 ± 0.00016	0.85444 ± 0.00017
545-detset1	0.97720 ± 0.00106	0.99595 ± 0.00048	1.00335 ± 0.00017	1	0.98654 ± 0.0000918247	0.96380 ± 0.00014	0.93283 ± 0.00018	0.89487 ± 0.00019	0.85128 ± 0.00019
545-detset2	0.97758 ± 0.00156	0.99548 ± 0.00072	1.00276 ± 0.00026	1	0.98774 ± 0.00015	0.96673 ± 0.00024	0.93790 ± 0.00029	0.90233 ± 0.00032	0.86123 ± 0.00034
857-1	0.94232 ± 0.00807	0.97298 ± 0.00275	0.99165 ± 0.00075	1	0.99868 ± 0.00029	0.98825 ± 0.00039	0.96944 ± 0.00043	0.94315 ± 0.00044	0.91042 ± 0.00044
857-2	0.92120 ± 0.00664	0.95863 ± 0.00231	0.98447 ± 0.00064	1	1.00554 ± 0.00026	1.00139 ± 0.00036	0.98809 ± 0.00041	0.96642 ± 0.00043	0.93735 ± 0.00043

857-3	0.93838 ± 0.00745	0.97023 ± 0.00251	0.99024 ± 0.00069	1	1.00004 ± 0.00026	0.99089 ± 0.00036	0.97321 ± 0.00040	0.94789 ± 0.00041	0.91594 ± 0.00041
857-4	0.90936 ± 0.00683	0.94964 ± 0.00235	0.97945 ± 0.00065	1	1.01152 ± 0.00026	1.01417 ± 0.00035	1.00831 ± 0.00040	0.99445 ± 0.00042	0.97334 ± 0.00043
857-avg	0.93070 ± 0.00379	0.96497 ± 0.00128	0.98758 ± 0.00035	1	1.00270 ± 0.00013	0.99610 ± 0.00019	0.98082 ± 0.00021	0.95766 ± 0.00022	0.92761 ± 0.00022
857-detset1	0.93205 ± 0.00540	0.96604 ± 0.00182	0.98819 ± 0.00050	1	1.00196 ± 0.00019	0.99451 ± 0.00027	0.97830 ± 0.00029	0.95417 ± 0.00030	0.92315 ± 0.00030
857-detset2	0.92902 ± 0.00556	0.96363 ± 0.00192	0.98681 ± 0.00054	1	1.00364 ± 0.00021	0.99812 ± 0.00029	0.98402 ± 0.00032	0.96210 ± 0.00034	0.93330 ± 0.00034

Band/Det. [GHz]	$\nu_{\text{eff.}}$, S.I.: -4	-3	-2	-1	0	1	2	3	4
100-1a	97.066 ± 0.101	97.843 ± 0.099	98.641 ± 0.099	100	100.276 ± 0.096	101.102 ± 0.094	101.929 ± 0.092	102.756 ± 0.088	103.591 ± 0.084
100-1b	97.691 ± 0.126	98.462 ± 0.124	99.252 ± 0.121	100	100.871 ± 0.118	101.689 ± 0.112	102.510 ± 0.107	103.336 ± 0.101	104.178 ± 0.095
100-2a	97.653 ± 0.133	98.525 ± 0.132	99.434 ± 0.134	100	101.343 ± 0.128	102.333 ± 0.123	103.343 ± 0.117	104.381 ± 0.112	105.471 ± 0.105
100-2b	97.483 ± 0.131	98.371 ± 0.130	99.289 ± 0.128	100	101.189 ± 0.126	102.159 ± 0.122	103.138 ± 0.118	104.131 ± 0.114	105.160 ± 0.108
100-3a	97.889 ± 0.143	98.793 ± 0.141	99.724 ± 0.136	100	101.644 ± 0.125	102.619 ± 0.118	103.599 ± 0.110	104.588 ± 0.105	105.603 ± 0.097
100-3b	97.200 ± 0.114	98.019 ± 0.113	98.866 ± 0.111	100	100.626 ± 0.104	101.529 ± 0.100	102.445 ± 0.096	103.379 ± 0.092	104.348 ± 0.090
100-4a	97.944 ± 0.144	98.852 ± 0.143	99.797 ± 0.140	100	101.771 ± 0.132	102.786 ± 0.125	103.816 ± 0.118	104.868 ± 0.110	105.963 ± 0.103
100-4b	98.099 ± 0.125	99.010 ± 0.126	99.955 ± 0.125	100	101.913 ± 0.122	102.913 ± 0.117	103.919 ± 0.113	104.936 ± 0.109	105.979 ± 0.105
100-avg	97.662 ± 0.050	98.532 ± 0.050	99.434 ± 0.050	100	101.307 ± 0.048	102.267 ± 0.047	103.238 ± 0.045	104.225 ± 0.044	105.248 ± 0.042
100-detset1	97.808 ± 0.070	98.674 ± 0.072	99.571 ± 0.071	100	101.433 ± 0.068	102.386 ± 0.065	103.349 ± 0.062	104.327 ± 0.059	105.338 ± 0.056
100-detset2	97.601 ± 0.056	98.473 ± 0.055	99.377 ± 0.055	100	101.255 ± 0.053	102.217 ± 0.051	103.191 ± 0.049	104.182 ± 0.047	105.210 ± 0.044
143-1a	136.687 ± 0.044	137.855 ± 0.044	139.086 ± 0.045	143	141.708 ± 0.043	143.081 ± 0.042	144.484 ± 0.041	145.907 ± 0.040	147.346 ± 0.038
143-1b	137.246 ± 0.049	138.435 ± 0.049	139.678 ± 0.049	143	142.291 ± 0.049	143.643 ± 0.048	145.015 ± 0.046	146.398 ± 0.043	147.789 ± 0.042
143-2a	136.609 ± 0.048	137.825 ± 0.048	139.099 ± 0.048	143	141.791 ± 0.046	143.190 ± 0.045	144.613 ± 0.043	146.055 ± 0.042	147.516 ± 0.040
143-2b	137.429 ± 0.047	138.632 ± 0.047	139.882 ± 0.046	143	142.496 ± 0.044	143.845 ± 0.042	145.213 ± 0.041	146.598 ± 0.039	148.003 ± 0.038
143-3a	135.482 ± 0.041	136.648 ± 0.043	137.880 ± 0.044	143	140.506 ± 0.045	141.879 ± 0.046	143.275 ± 0.046	144.684 ± 0.045	146.095 ± 0.043
143-3b	136.494 ± 0.050	137.701 ± 0.050	138.965 ± 0.050	143	141.630 ± 0.050	143.011 ± 0.049	144.409 ± 0.046	145.814 ± 0.044	147.220 ± 0.043

143-4a	137.299 ± 0.046	138.574 ± 0.045	139.906 ± 0.044	143	142.706 ± 0.042	144.151 ± 0.040	145.613 ± 0.039	147.084 ± 0.037	148.561 ± 0.034
143-4b	137.135 ± 0.041	138.334 ± 0.042	139.581 ± 0.041	143	142.186 ± 0.040	143.524 ± 0.039	144.874 ± 0.037	146.230 ± 0.036	147.588 ± 0.034
143-5	139.128 ± 0.043	140.367 ± 0.042	141.638 ± 0.041	143	144.238 ± 0.038	145.551 ± 0.037	146.863 ± 0.036	148.174 ± 0.034	149.485 ± 0.033
143-6	137.838 ± 0.045	139.073 ± 0.044	140.351 ± 0.044	143	143.000 ± 0.042	144.355 ± 0.041	145.721 ± 0.039	147.098 ± 0.037	148.488 ± 0.035
143-7	139.332 ± 0.051	140.570 ± 0.050	141.844 ± 0.049	143	144.457 ± 0.045	145.776 ± 0.043	147.090 ± 0.041	148.394 ± 0.039	149.687 ± 0.036
143-8	138.254 ± 0.054	139.524 ± 0.052	140.838 ± 0.051	143	143.550 ± 0.048	144.926 ± 0.046	146.301 ± 0.043	147.668 ± 0.040	149.023 ± 0.036
143-avg	137.545 ± 0.016	138.771 ± 0.016	140.046 ± 0.016	143	142.709 ± 0.015	144.077 ± 0.015	145.457 ± 0.015	146.844 ± 0.014	148.235 ± 0.013
143-detset1	136.383 ± 0.022	137.566 ± 0.022	138.811 ± 0.022	143	141.450 ± 0.022	142.825 ± 0.021	144.223 ± 0.020	145.634 ± 0.019	147.052 ± 0.019
143-detset2	137.085 ± 0.026	138.308 ± 0.026	139.585 ± 0.026	143	142.265 ± 0.026	143.651 ± 0.025	145.055 ± 0.025	146.473 ± 0.023	147.904 ± 0.022
143-SWBs	138.822 ± 0.026	140.063 ± 0.025	141.340 ± 0.025	143	143.965 ± 0.024	145.294 ± 0.023	146.625 ± 0.022	147.955 ± 0.020	149.283 ± 0.019
217-1	216.066 ± 0.018	217.715 ± 0.018	219.396 ± 0.018	217	222.817 ± 0.018	224.543 ± 0.018	226.274 ± 0.019	228.011 ± 0.021	229.761 ± 0.025
217-2	216.108 ± 0.018	217.857 ± 0.018	219.635 ± 0.018	217	223.231 ± 0.018	225.028 ± 0.018	226.814 ± 0.019	228.587 ± 0.019	230.350 ± 0.021
217-3	216.487 ± 0.018	218.117 ± 0.017	219.771 ± 0.017	217	223.116 ± 0.016	224.790 ± 0.016	226.458 ± 0.016	228.118 ± 0.016	229.775 ± 0.017
217-4	216.127 ± 0.018	217.730 ± 0.018	219.368 ± 0.018	217	222.717 ± 0.017	224.413 ± 0.017	226.116 ± 0.018	227.825 ± 0.019	229.546 ± 0.022
217-5a	212.836 ± 0.019	214.684 ± 0.019	216.573 ± 0.019	217	220.421 ± 0.018	222.358 ± 0.018	224.293 ± 0.019	226.223 ± 0.021	228.153 ± 0.024
217-5b	213.124 ± 0.019	214.968 ± 0.018	216.846 ± 0.018	217	220.655 ± 0.018	222.564 ± 0.017	224.465 ± 0.017	226.355 ± 0.018	228.234 ± 0.019
217-6a	213.058 ± 0.019	214.914 ± 0.019	216.800 ± 0.018	217	220.619 ± 0.018	222.532 ± 0.018	224.441 ± 0.018	226.343 ± 0.018	228.245 ± 0.020
217-6b	213.041 ± 0.019	214.905 ± 0.019	216.798 ± 0.018	217	220.619 ± 0.017	222.523 ± 0.017	224.408 ± 0.017	226.271 ± 0.017	228.110 ± 0.018
217-7a	213.538 ± 0.018	215.299 ± 0.018	217.098 ± 0.018	217	220.766 ± 0.018	222.614 ± 0.018	224.458 ± 0.019	226.295 ± 0.019	228.123 ± 0.020
217-7b	213.010 ± 0.021	214.795 ± 0.021	216.618 ± 0.021	217	220.332 ± 0.020	222.198 ± 0.020	224.055 ± 0.020	225.896 ± 0.020	227.718 ± 0.020
217-8a	212.757 ± 0.020	214.655 ± 0.020	216.589 ± 0.019	217	220.510 ± 0.018	222.475 ± 0.018	224.432 ± 0.018	226.380 ± 0.019	228.324 ± 0.022
217-8b	213.279 ± 0.019	215.110 ± 0.018	216.966 ± 0.017	217	220.712 ± 0.016	222.581 ± 0.016	224.441 ± 0.016	226.287 ± 0.017	228.127 ± 0.021
217-avg	214.800 ± 0.006	216.544 ± 0.006	218.318 ± 0.006	217	221.914 ± 0.005	223.718 ± 0.005	225.517 ± 0.006	227.308 ± 0.006	229.096 ± 0.007

217-detset1	213.150 ± 0.008	214.955 ± 0.008	216.798 ± 0.008	217	220.548 ± 0.007	222.433 ± 0.007	224.312 ± 0.008	226.180 ± 0.009	228.039 ± 0.010
217-detset2	213.030 ± 0.010	214.893 ± 0.010	216.786 ± 0.009	217	220.614 ± 0.009	222.527 ± 0.009	224.429 ± 0.009	226.319 ± 0.009	228.200 ± 0.010
217-SWBs	216.201 ± 0.009	217.854 ± 0.009	219.537 ± 0.008	217	222.957 ± 0.008	224.676 ± 0.008	226.395 ± 0.008	228.113 ± 0.008	229.834 ± 0.010
353-1	349.478 ± 0.021	352.124 ± 0.021	354.818 ± 0.021	217	360.289 ± 0.022	363.032 ± 0.023	365.762 ± 0.023	368.469 ± 0.025	371.149 ± 0.027
353-2	349.711 ± 0.020	352.407 ± 0.020	355.178 ± 0.021	353	360.866 ± 0.023	363.742 ± 0.023	366.615 ± 0.024	369.467 ± 0.026	372.288 ± 0.027
353-3a	350.077 ± 0.027	352.393 ± 0.025	354.757 ± 0.024	353	359.591 ± 0.022	362.037 ± 0.022	364.488 ± 0.022	366.934 ± 0.022	369.368 ± 0.023
353-3b	349.440 ± 0.022	351.896 ± 0.022	354.426 ± 0.022	353	359.653 ± 0.023	362.323 ± 0.024	365.012 ± 0.025	367.709 ± 0.026	370.405 ± 0.028
353-4a	353.362 ± 0.020	355.505 ± 0.020	357.702 ± 0.020	353	362.224 ± 0.020	364.530 ± 0.020	366.853 ± 0.020	369.186 ± 0.020	371.521 ± 0.022
353-4b	352.599 ± 0.019	354.921 ± 0.020	357.305 ± 0.020	353	362.212 ± 0.021	364.709 ± 0.021	367.219 ± 0.022	369.730 ± 0.023	372.233 ± 0.024
353-5a	347.552 ± 0.022	350.274 ± 0.022	353.055 ± 0.022	353	358.726 ± 0.022	361.578 ± 0.022	364.418 ± 0.022	367.231 ± 0.022	370.005 ± 0.023
353-5b	347.060 ± 0.020	349.892 ± 0.020	352.811 ± 0.021	353	358.837 ± 0.022	361.905 ± 0.023	364.984 ± 0.024	368.057 ± 0.026	371.112 ± 0.029
353-6a	348.834 ± 0.027	351.530 ± 0.027	354.286 ± 0.027	353	359.913 ± 0.028	362.751 ± 0.029	365.583 ± 0.029	368.395 ± 0.030	371.177 ± 0.031
353-6b	346.756 ± 0.022	349.003 ± 0.022	351.310 ± 0.023	353	356.062 ± 0.024	358.487 ± 0.024	360.931 ± 0.025	363.384 ± 0.025	365.834 ± 0.026
353-7	353.439 ± 0.031	355.868 ± 0.029	358.338 ± 0.028	353	363.354 ± 0.025	365.877 ± 0.024	368.396 ± 0.024	370.906 ± 0.025	373.407 ± 0.028
353-8	353.919 ± 0.023	356.645 ± 0.023	359.428 ± 0.022	353	365.103 ± 0.022	367.964 ± 0.022	370.824 ± 0.025	373.678 ± 0.028	376.528 ± 0.034
353-avg	350.610 ± 0.008	353.208 ± 0.008	355.864 ± 0.008	353	361.289 ± 0.008	364.027 ± 0.008	366.763 ± 0.008	369.486 ± 0.009	372.192 ± 0.010
353-detset1	348.356 ± 0.011	350.970 ± 0.011	353.652 ± 0.011	353	359.156 ± 0.011	361.947 ± 0.011	364.744 ± 0.011	367.532 ± 0.011	370.302 ± 0.012
353-detset2	351.278 ± 0.010	353.602 ± 0.010	355.982 ± 0.010	353	360.870 ± 0.010	363.354 ± 0.011	365.850 ± 0.011	368.347 ± 0.011	370.837 ± 0.012
353-SWBs	351.075 ± 0.012	353.719 ± 0.011	356.419 ± 0.011	353	361.921 ± 0.011	364.692 ± 0.011	367.455 ± 0.011	370.203 ± 0.012	372.930 ± 0.013
545-1	536.802 ± 0.488	543.034 ± 0.252	548.855 ± 0.136	545	559.830 ± 0.048	565.023 ± 0.034	570.001 ± 0.027	574.744 ± 0.025	579.238 ± 0.023
545-2	532.896 ± 0.438	539.141 ± 0.234	544.983 ± 0.130	545	556.051 ± 0.047	561.311 ± 0.034	566.366 ± 0.029	571.194 ± 0.027	575.780 ± 0.025
545-3	535.490 ± 0.752	541.404 ± 0.409	546.939 ± 0.227	545	557.397 ± 0.080	562.362 ± 0.053	567.137 ± 0.040	571.706 ± 0.033	576.054 ± 0.030
545-4	535.198 ± 0.483	541.039 ± 0.260	546.508 ± 0.143	545	556.845 ± 0.049	561.756 ± 0.033	566.482 ± 0.026	571.006 ± 0.024	575.316 ± 0.022

545-avg	534.885 ± 0.243	541.002 ± 0.128	546.722 ± 0.070	545	557.535 ± 0.026	562.667 ± 0.019	567.596 ± 0.016	572.305 ± 0.015	576.778 ± 0.014
545-detset1	534.737 ± 0.326	540.984 ± 0.170	546.823 ± 0.092	545	557.860 ± 0.031	563.094 ± 0.021	568.118 ± 0.017	572.911 ± 0.015	577.458 ± 0.015
545-detset2	535.198 ± 0.471	541.039 ± 0.253	546.508 ± 0.141	545	556.845 ± 0.052	561.756 ± 0.038	566.482 ± 0.031	571.006 ± 0.028	575.316 ± 0.026
857-1	829.988 ± 4.775	840.870 ± 1.743	849.842 ± 0.646	857	866.045 ± 0.099	873.628 ± 0.048	880.885 ± 0.034	887.805 ± 0.030	894.378 ± 0.029
857-2	823.541 ± 3.974	834.506 ± 1.467	843.689 ± 0.550	857	860.548 ± 0.093	868.533 ± 0.049	876.219 ± 0.035	883.577 ± 0.030	890.587 ± 0.029
857-3	828.870 ± 4.453	839.678 ± 1.598	848.637 ± 0.594	857	864.918 ± 0.092	872.568 ± 0.046	879.900 ± 0.032	886.894 ± 0.028	893.535 ± 0.028
857-4	820.649 ± 4.152	830.916 ± 1.508	839.387 ± 0.557	857	854.755 ± 0.091	861.988 ± 0.043	868.940 ± 0.030	875.594 ± 0.026	881.939 ± 0.026
857-avg	826.562 ± 2.275	837.384 ± 0.820	846.356 ± 0.300	857	862.675 ± 0.048	870.355 ± 0.025	877.724 ± 0.018	884.765 ± 0.016	891.462 ± 0.016
857-detset1	826.845 ± 3.229	837.792 ± 1.158	846.878 ± 0.426	857	863.418 ± 0.067	871.201 ± 0.036	878.669 ± 0.027	885.803 ± 0.024	892.587 ± 0.024
857-detset2	826.214 ± 3.329	836.872 ± 1.225	845.697 ± 0.459	857	861.737 ± 0.073	869.284 ± 0.037	876.526 ± 0.026	883.446 ± 0.023	890.027 ± 0.023

Colour Correction, Modified Blackbody

This section presents colour correction coefficients for a variety of modified blackbody spectral profiles. A sample CIB spectrum, with $T = 13.6K, \beta = 1.4$, is chosen as one example. Three other examples are selected based on the variety of dust spectra used in typical HFI analysis. The first dust profile is $T = 18K, \beta = 1.6$, the second is $T = 17K, \beta = 1.5$, and the third (taken from the LMC region FIXME) is $T = 21K, \beta = 1.48$. Also shown are plots for a modified blackbody spectrum spanning a selection of the temperature/beta parameter space.

Table 5: Modified Blackbody Colour correction coefficients.

Band/Det. [GHz]	CC_{CIB}	CC_{dust1}	CC_{dust2}	CC_{dust3}
100-1a	0.96891 ± 0.00465	0.96531 ± 0.00477	0.96251 ± 0.00486	0.96494 ± 0.00478
100-1b	0.94535 ± 0.00440	0.94110 ± 0.00451	0.93779 ± 0.00459	0.94069 ± 0.00452
100-2a	0.92300 ± 0.00458	0.91757 ± 0.00469	0.91336 ± 0.00477	0.91704 ± 0.00469
100-2b	0.92954 ± 0.00480	0.92438 ± 0.00491	0.92037 ± 0.00499	0.92388 ± 0.00491
100-3a	0.91223 ± 0.00443	0.90661 ± 0.00452	0.90225 ± 0.00460	0.90607 ± 0.00453
100-3b	0.95291 ± 0.00463	0.94858 ± 0.00474	0.94522 ± 0.00483	0.94815 ± 0.00475
100-4a	0.90646 ± 0.00470	0.90054 ± 0.00481	0.89595 ± 0.00489	0.89997 ± 0.00481
100-4b	0.90164 ± 0.00451	0.89566 ± 0.00461	0.89103 ± 0.00469	0.89510 ± 0.00462
100-avg	0.92519 ± 0.00187	0.91993 ± 0.00191	0.91586 ± 0.00194	0.91942 ± 0.00191
100-detset1	0.92057 ± 0.00250	0.91521 ± 0.00255	0.91106 ± 0.00260	0.91470 ± 0.00256
100-detset2	0.92714 ± 0.00240	0.92192 ± 0.00245	0.91788 ± 0.00249	0.92142 ± 0.00246
143-1a	1.01638 ± 0.00133	1.01328 ± 0.00137	1.01109 ± 0.00140	1.01261 ± 0.00138
143-1b	0.99986 ± 0.00131	0.99627 ± 0.00135	0.99374 ± 0.00138	0.99553 ± 0.00136

143-2a	1.01363 ± 0.00135	1.01037 ± 0.00139	1.00808 ± 0.00142	1.00967 ± 0.00140
143-2b	0.99405 ± 0.00123	0.99027 ± 0.00127	0.98761 ± 0.00130	0.98950 ± 0.00128
143-3a	1.05255 ± 0.00151	1.05075 ± 0.00156	1.04946 ± 0.00160	1.05025 ± 0.00157
143-3b	1.01869 ± 0.00140	1.01568 ± 0.00144	1.01356 ± 0.00148	1.01503 ± 0.00145
143-4a	0.98667 ± 0.00130	0.98240 ± 0.00134	0.97940 ± 0.00137	0.98155 ± 0.00135
143-4b	1.00319 ± 0.00129	0.99977 ± 0.00133	0.99736 ± 0.00136	0.99906 ± 0.00134
143-5	0.94651 ± 0.00111	0.94129 ± 0.00114	0.93761 ± 0.00116	0.94032 ± 0.00115
143-6	0.97977 ± 0.00124	0.97552 ± 0.00128	0.97252 ± 0.00130	0.97468 ± 0.00128
143-7	0.94058 ± 0.00115	0.93517 ± 0.00118	0.93136 ± 0.00121	0.93418 ± 0.00119
143-8	0.96432 ± 0.00123	0.95953 ± 0.00127	0.95615 ± 0.00129	0.95862 ± 0.00127
143-avg	0.98776 ± 0.00040	0.98374 ± 0.00041	0.98091 ± 0.00042	0.98294 ± 0.00041
143-detset1	1.02404 ± 0.00073	1.02122 ± 0.00075	1.01923 ± 0.00077	1.02058 ± 0.00075
143-detset2	1.00011 ± 0.00066	0.99645 ± 0.00069	0.99386 ± 0.00070	0.99569 ± 0.00069
143-SWBs	0.95362 ± 0.00067	0.94859 ± 0.00069	0.94505 ± 0.00070	0.94765 ± 0.00069
217-1	0.88929 ± 0.00026	0.88089 ± 0.00027	0.87579 ± 0.00028	0.87851 ± 0.00028
217-2	0.88245 ± 0.00027	0.87368 ± 0.00028	0.86835 ± 0.00029	0.87119 ± 0.00028
217-3	0.88499 ± 0.00026	0.87654 ± 0.00027	0.87140 ± 0.00027	0.87415 ± 0.00027
217-4	0.89103 ± 0.00026	0.88276 ± 0.00027	0.87773 ± 0.00027	0.88041 ± 0.00027
217-5a	0.92654 ± 0.00029	0.91925 ± 0.00030	0.91481 ± 0.00031	0.91712 ± 0.00031
217-5b	0.92290 ± 0.00028	0.91552 ± 0.00029	0.91104 ± 0.00030	0.91338 ± 0.00029
217-6a	0.92346 ± 0.00028	0.91610 ± 0.00029	0.91162 ± 0.00030	0.91395 ± 0.00030
217-6b	0.92357 ± 0.00028	0.91625 ± 0.00029	0.91180 ± 0.00030	0.91412 ± 0.00029
217-7a	0.92144 ± 0.00028	0.91412 ± 0.00029	0.90967 ± 0.00030	0.91200 ± 0.00029
217-7b	0.92850 ± 0.00029	0.92145 ± 0.00030	0.91715 ± 0.00031	0.91939 ± 0.00030
217-8a	0.92492 ± 0.00029	0.91752 ± 0.00030	0.91302 ± 0.00031	0.91536 ± 0.00031
217-8b	0.92225 ± 0.00027	0.91493 ± 0.00028	0.91048 ± 0.00029	0.91281 ± 0.00029
217-avg	0.90314 ± 0.0000861543	0.89517 ± 0.0000896004	0.89032 ± 0.0000917018	0.89288 ± 0.0000905139
217-detset1	0.92480 ± 0.00014	0.91755 ± 0.00015	0.91314 ± 0.00015	0.91544 ± 0.00015
217-detset2	0.92357 ± 0.00014	0.91622 ± 0.00015	0.91175 ± 0.00015	0.91408 ± 0.00015
217-SWBs	0.88716 ± 0.00013	0.87870 ± 0.00013	0.87356 ± 0.00014	0.87630 ± 0.00014
353-1	0.92349 ± 0.00019	0.91335 ± 0.00020	0.90832 ± 0.00021	0.90908 ± 0.00021
353-2	0.91792 ± 0.00020	0.90719 ± 0.00021	0.90188 ± 0.00022	0.90268 ± 0.00021
353-3a	0.93046 ± 0.00023	0.92125 ± 0.00024	0.91668 ± 0.00025	0.91738 ± 0.00025
353-3b	0.92947 ± 0.00020	0.91980 ± 0.00022	0.91500 ± 0.00023	0.91571 ± 0.00022
353-4a	0.90649 ± 0.00019	0.89597 ± 0.00020	0.89076 ± 0.00021	0.89162 ± 0.00021
353-4b	0.90628 ± 0.00020	0.89544 ± 0.00021	0.89007 ± 0.00021	0.89094 ± 0.00021
353-5a	0.93790 ± 0.00020	0.92849 ± 0.00022	0.92382 ± 0.00022	0.92449 ± 0.00022
353-5b	0.93645 ± 0.00021	0.92655 ± 0.00023	0.92164 ± 0.00023	0.92232 ± 0.00023
353-6a	0.92679 ± 0.00025	0.91669 ± 0.00026	0.91168 ± 0.00027	0.91243 ± 0.00027

353-6b	0.96428 ± 0.00025	0.95730 ± 0.00026	0.95383 ± 0.00027	0.95427 ± 0.00027
353-7	0.89605 ± 0.00024	0.88454 ± 0.00025	0.87885 ± 0.00025	0.87979 ± 0.00025
353-8	0.88018 ± 0.00021	0.86715 ± 0.00022	0.86072 ± 0.00023	0.86176 ± 0.00023
353-avg	0.91429 ± 0.0000754475	0.90357 ± 0.0000803062	0.89825 ± 0.0000826753	0.89908 ± 0.0000821623
353-detset1	0.93393 ± 0.00011	0.92435 ± 0.00011	0.91960 ± 0.00012	0.92029 ± 0.00012
353-detset2	0.91853 ± 0.00011	0.90849 ± 0.00011	0.90350 ± 0.00012	0.90429 ± 0.00012
353-SWBs	0.90850 ± 0.00010	0.89736 ± 0.00011	0.89185 ± 0.00011	0.89271 ± 0.00011
545-1	0.92490 ± 0.00028	0.90745 ± 0.00029	0.90034 ± 0.00029	0.89825 ± 0.00029
545-2	0.94451 ± 0.00027	0.92908 ± 0.00028	0.92276 ± 0.00029	0.92083 ± 0.00029
545-3	0.93717 ± 0.00047	0.92141 ± 0.00048	0.91497 ± 0.00048	0.91305 ± 0.00048
545-4	0.93998 ± 0.00030	0.92462 ± 0.00031	0.91833 ± 0.00031	0.91645 ± 0.00031
545-avg	0.93662 ± 0.00017	0.92054 ± 0.00017	0.91397 ± 0.00017	0.91200 ± 0.00017
545-detset1	0.93505 ± 0.00020	0.91863 ± 0.00020	0.91193 ± 0.00021	0.90992 ± 0.00021
545-detset2	0.93998 ± 0.00030	0.92462 ± 0.00031	0.91833 ± 0.00031	0.91645 ± 0.00031
857-1	0.99656 ± 0.00043	0.98166 ± 0.00044	0.97627 ± 0.00044	0.97140 ± 0.00044
857-2	1.01159 ± 0.00036	0.99995 ± 0.00037	0.99562 ± 0.00037	0.99138 ± 0.00037
857-3	0.99957 ± 0.00041	0.98534 ± 0.00041	0.98017 ± 0.00042	0.97543 ± 0.00042
857-4	1.02479 ± 0.00046	1.01805 ± 0.00047	1.01540 ± 0.00047	1.01242 ± 0.00047
857-avg	1.00534 ± 0.00021	0.99259 ± 0.00021	0.98791 ± 0.00021	0.98349 ± 0.00021
857-detset1	1.00372 ± 0.00029	0.99035 ± 0.00029	0.98546 ± 0.00029	0.98088 ± 0.00029
857-detset2	1.00739 ± 0.00032	0.99543 ± 0.00032	0.99102 ± 0.00033	0.98680 ± 0.00033

Table 6: Modified Blackbody colour correction effective frequencies.

Band/Det. [GHz]	ν_{CIB}	ν_{dust1}	ν_{dust2}	ν_{dust3}
100-1a	102.926 ± 0.102	103.043 ± 0.102	103.133 ± 0.101	103.052 ± 0.102
100-1b	103.505 ± 0.100	103.623 ± 0.100	103.714 ± 0.099	103.632 ± 0.100
100-2a	104.590 ± 0.108	104.742 ± 0.107	104.859 ± 0.106	104.755 ± 0.107
100-2b	104.332 ± 0.108	104.475 ± 0.107	104.586 ± 0.107	104.487 ± 0.107
100-3a	104.787 ± 0.103	104.929 ± 0.102	105.038 ± 0.102	104.940 ± 0.102
100-3b	103.569 ± 0.104	103.704 ± 0.103	103.809 ± 0.103	103.715 ± 0.103
100-4a	105.078 ± 0.112	105.231 ± 0.111	105.349 ± 0.110	105.244 ± 0.111
100-4b	105.140 ± 0.107	105.286 ± 0.106	105.399 ± 0.106	105.298 ± 0.106
100-avg	104.425 ± 0.043	104.567 ± 0.043	104.678 ± 0.043	104.579 ± 0.043
100-detset1	104.525 ± 0.059	104.666 ± 0.058	104.775 ± 0.058	104.678 ± 0.058
100-detset2	104.382 ± 0.055	104.526 ± 0.055	104.637 ± 0.054	104.538 ± 0.055
143-1a	146.077 ± 0.043	146.306 ± 0.043	146.468 ± 0.043	146.341 ± 0.043
143-1b	146.563 ± 0.042	146.784 ± 0.042	146.941 ± 0.042	146.818 ± 0.042
143-2a	146.226 ± 0.042	146.458 ± 0.042	146.623 ± 0.042	146.494 ± 0.042
143-2b	146.760 ± 0.040	146.983 ± 0.040	147.141 ± 0.039	147.018 ± 0.039

143-3a	144.858 ± 0.047	145.081 ± 0.046	145.241 ± 0.046	145.115 ± 0.046
143-3b	145.984 ± 0.044	146.207 ± 0.044	146.366 ± 0.043	146.241 ± 0.043
143-4a	147.257 ± 0.042	147.492 ± 0.042	147.659 ± 0.042	147.529 ± 0.042
143-4b	146.392 ± 0.041	146.608 ± 0.041	146.761 ± 0.041	146.641 ± 0.041
143-5	148.324 ± 0.037	148.534 ± 0.036	148.682 ± 0.036	148.567 ± 0.036
143-6	147.257 ± 0.040	147.479 ± 0.039	147.635 ± 0.039	147.513 ± 0.039
143-7	148.545 ± 0.038	148.753 ± 0.038	148.899 ± 0.038	148.785 ± 0.038
143-8	147.828 ± 0.040	148.045 ± 0.040	148.198 ± 0.039	148.078 ± 0.040
143-avg	147.007 ± 0.013	147.229 ± 0.013	147.386 ± 0.013	147.263 ± 0.013
143-detset1	145.805 ± 0.023	146.030 ± 0.023	146.190 ± 0.023	146.064 ± 0.023
143-detset2	146.640 ± 0.021	146.868 ± 0.021	147.029 ± 0.021	146.903 ± 0.021
143-SWBs	148.108 ± 0.022	148.321 ± 0.022	148.471 ± 0.022	148.354 ± 0.022
217-1	227.910 ± 0.018	228.257 ± 0.019	228.468 ± 0.019	228.350 ± 0.019
217-2	228.488 ± 0.018	228.839 ± 0.019	229.053 ± 0.019	228.933 ± 0.019
217-3	228.026 ± 0.017	228.355 ± 0.017	228.556 ± 0.017	228.443 ± 0.017
217-4	227.727 ± 0.018	228.068 ± 0.018	228.276 ± 0.019	228.160 ± 0.019
217-5a	226.123 ± 0.019	226.504 ± 0.019	226.737 ± 0.020	226.606 ± 0.020
217-5b	226.259 ± 0.017	226.631 ± 0.018	226.858 ± 0.018	226.729 ± 0.018
217-6a	226.243 ± 0.019	226.619 ± 0.019	226.849 ± 0.019	226.719 ± 0.019
217-6b	226.180 ± 0.017	226.545 ± 0.017	226.768 ± 0.017	226.641 ± 0.017
217-7a	226.201 ± 0.018	226.563 ± 0.018	226.785 ± 0.018	226.659 ± 0.018
217-7b	225.807 ± 0.017	226.168 ± 0.017	226.389 ± 0.018	226.263 ± 0.018
217-8a	226.279 ± 0.019	226.663 ± 0.020	226.898 ± 0.020	226.765 ± 0.020
217-8b	226.193 ± 0.018	226.557 ± 0.018	226.779 ± 0.018	226.653 ± 0.018
217-avg	227.211 ± 0.006	227.566 ± 0.006	227.782 ± 0.006	227.660 ± 0.006
217-detset1	226.086 ± 0.009	226.454 ± 0.009	226.679 ± 0.009	226.551 ± 0.009
217-detset2	226.223 ± 0.009	226.595 ± 0.009	226.822 ± 0.009	226.693 ± 0.009
217-SWBs	228.015 ± 0.009	228.357 ± 0.009	228.565 ± 0.009	228.449 ± 0.009
353-1	367.442 ± 0.022	368.186 ± 0.022	368.556 ± 0.023	368.477 ± 0.023
353-2	368.379 ± 0.022	369.165 ± 0.023	369.555 ± 0.023	369.472 ± 0.023
353-3a	366.008 ± 0.024	366.681 ± 0.024	367.017 ± 0.024	366.944 ± 0.024
353-3b	366.675 ± 0.023	367.420 ± 0.024	367.791 ± 0.024	367.713 ± 0.024
353-4a	368.280 ± 0.022	368.928 ± 0.022	369.250 ± 0.022	369.183 ± 0.022
353-4b	368.758 ± 0.022	369.455 ± 0.023	369.801 ± 0.023	369.729 ± 0.023
353-5a	366.178 ± 0.022	366.948 ± 0.022	367.332 ± 0.022	367.248 ± 0.022
353-5b	366.887 ± 0.024	367.734 ± 0.025	368.155 ± 0.025	368.065 ± 0.025
353-6a	367.329 ± 0.028	368.102 ± 0.028	368.487 ± 0.028	368.404 ± 0.028
353-6b	362.470 ± 0.027	363.142 ± 0.027	363.479 ± 0.027	363.404 ± 0.027
353-7	369.930 ± 0.025	370.626 ± 0.026	370.972 ± 0.026	370.901 ± 0.026

353-8	372.546 ± 0.028	373.342 ± 0.030	373.736 ± 0.030	373.658 ± 0.030
353-avg	368.441 ± 0.009	369.193 ± 0.009	369.567 ± 0.009	369.488 ± 0.009
353-detset1	366.474 ± 0.012	367.241 ± 0.012	367.624 ± 0.012	367.542 ± 0.012
353-detset2	367.389 ± 0.012	368.079 ± 0.012	368.423 ± 0.012	368.350 ± 0.012
353-SWBs	369.145 ± 0.012	369.904 ± 0.012	370.281 ± 0.012	370.202 ± 0.012
545-1	570.556 ± 0.028	572.467 ± 0.027	573.239 ± 0.027	573.391 ± 0.027
545-2	566.970 ± 0.028	568.903 ± 0.027	569.687 ± 0.026	569.837 ± 0.026
545-3	567.692 ± 0.034	569.526 ± 0.031	570.268 ± 0.031	570.412 ± 0.031
545-4	567.037 ± 0.028	568.851 ± 0.027	569.586 ± 0.027	569.728 ± 0.027
545-avg	568.169 ± 0.016	570.059 ± 0.015	570.825 ± 0.015	570.973 ± 0.015
545-detset1	568.699 ± 0.020	570.624 ± 0.019	571.403 ± 0.019	571.554 ± 0.019
545-detset2	567.037 ± 0.027	568.851 ± 0.026	569.586 ± 0.026	569.728 ± 0.026
857-1	875.270 ± 0.035	879.728 ± 0.033	881.221 ± 0.033	882.236 ± 0.032
857-2	870.340 ± 0.034	875.044 ± 0.032	876.624 ± 0.032	877.693 ± 0.032
857-3	874.243 ± 0.036	878.746 ± 0.034	880.254 ± 0.033	881.277 ± 0.033
857-4	863.772 ± 0.036	867.990 ± 0.034	869.411 ± 0.033	870.359 ± 0.033
857-avg	872.073 ± 0.018	876.588 ± 0.017	878.102 ± 0.017	879.128 ± 0.017
857-detset1	872.923 ± 0.025	877.503 ± 0.023	879.038 ± 0.023	880.080 ± 0.023
857-detset2	870.996 ± 0.027	875.428 ± 0.026	876.915 ± 0.025	877.920 ± 0.025

CO unit conversion

This section presents the CO unit conversion coefficcients.

Table 7: CO unit conversion coefficients for the various HFI detectors and channel-averages

Band (GHz)	BC	Det.	CO line	F_{12CO} [$uK_{CMB}/K_{RJ}km/s$]	F_{13CO} [$uK_{CMB}/K_{RJ}km/s$]
100	00	1a	J1-0	10.87 ± 0.29	16.96 ± 0.75
100	01	1b	J1-0	12.61 ± 0.27	16.40 ± 0.71
100	20	2a	J1-0	14.69 ± 0.50	14.08 ± 0.61
100	21	2b	J1-0	12.01 ± 0.39	17.50 ± 0.63
100	40	3a	J1-0	16.36 ± 0.57	14.52 ± 0.64
100	41	3b	J1-0	11.78 ± 0.48	13.78 ± 0.51
100	80	4a	J1-0	19.09 ± 0.63	18.64 ± 0.79
100	81	4b	J1-0	16.11 ± 0.57	17.57 ± 0.80
100	100	avg	J1-0	14.78 ± 0.21	15.55 ± 0.26
143	02	1a	J1-0	0.0613 ± 0.0031	0.0022 ± 5.0163e-05
143	03	1b	J1-0	0.0437 ± 0.0022	0.0017 ± 5.5805e-05
143	30	2a	J1-0	0.0523 ± 0.0027	0.0020 ± 0.0001
143	31	2b	J1-0	0.0557 ± 0.0028	0.0022 ± 0.0001

143	50	3a	J1-0	0.0881 ± 0.0045	0.0030 ± 2.3871e-05
143	51	3b	J1-0	0.0737 ± 0.0036	0.0023 ± 0.0001
143	82	4a	J1-0	0.0489 ± 0.0024	0.0018 ± 8.9210e-05
143	83	4b	J1-0	0.0493 ± 0.0024	0.0019 ± 9.4426e-05
143	10	5	J1-0	0.0210 ± 0.0012	0.0012 ± 0.0001
143	42	6	J1-0	0.0579 ± 0.0029	0.0020 ± 0.0003
143	60	7	J1-0	0.0099 ± 0.0005	0.0005 ± 2.4544e-05
143	70	8	J1-0	0.0404 ± 0.0023	0.0018 ± 8.5655e-05
143	143	avg	J1-0	0.0470 ± 0.0008	0.0018 ± 4.4951e-05
143	02	1a	J2-1	0.0 ± 0.0	0.0 ± 0.0
143	03	1b	J2-1	0.0 ± 0.0	0.0 ± 0.0
143	30	2a	J2-1	0.0 ± 0.0	0.0 ± 0.0
143	31	2b	J2-1	0.0 ± 0.0	0.0 ± 0.0
143	50	3a	J2-1	0.0 ± 0.0	0.0 ± 0.0
143	51	3b	J2-1	0.0 ± 0.0	0.0 ± 0.0
143	82	4a	J2-1	0.0 ± 0.0	0.0 ± 0.0
143	83	4b	J2-1	0.0 ± 0.0	0.0 ± 0.0
143	10	5	J2-1	0.0 ± 0.0	0.0 ± 0.0
143	42	6	J2-1	0.0 ± 0.0	0.0 ± 0.0
143	60	7	J2-1	0.0 ± 0.0	0.0 ± 0.0
143	70	8	J2-1	0.0 ± 0.0	0.0 ± 0.0
143	143	avg	J2-1	0.0 ± 0.0	0.0 ± 0.0
217	04	1	J2-1	50.22 ± 0.36	34.42 ± 0.21
217	22	2	J2-1	42.47 ± 0.30	32.73 ± 0.21
217	52	3	J2-1	51.23 ± 0.35	37.37 ± 0.23
217	84	4	J2-1	47.75 ± 0.35	30.87 ± 0.19
217	11	5a	J2-1	43.97 ± 0.29	35.85 ± 0.22
217	12	5b	J2-1	43.68 ± 0.34	38.54 ± 0.22
217	43	6a	J2-1	38.92 ± 0.30	41.21 ± 0.25
217	44	6b	J2-1	40.75 ± 0.36	33.33 ± 0.21
217	61	7a	J2-1	45.50 ± 0.31	41.57 ± 0.26
217	62	7b	J2-1	43.58 ± 0.29	33.19 ± 0.20
217	71	8a	J2-1	45.30 ± 0.31	41.48 ± 0.25
217	72	8b	J2-1	41.78 ± 0.31	34.16 ± 0.21
217	217	avg	J2-1	45.85 ± 0.11	35.37 ± 0.07
353	05	1	J3-2	170.3 ± 1.3	82.5 ± 0.4
353	13	2	J3-2	174.0 ± 1.3	130.8 ± 0.7
353	23	3a	J3-2	185.4 ± 1.6	133.3 ± 0.8
353	24	3b	J3-2	200.7 ± 1.5	166.6 ± 0.9

353	32	4a	J3-2	172.9 ± 1.4	121.0 ± 0.7
353	33	4b	J3-2	140.9 ± 1.3	125.2 ± 0.7
353	53	5a	J3-2	150.3 ± 1.2	138.1 ± 0.7
353	54	5b	J3-2	159.8 ± 1.1	143.9 ± 0.8
353	63	6a	J3-2	148.9 ± 1.2	143.0 ± 0.9
353	64	6b	J3-2	166.4 ± 1.5	167.1 ± 1.0
353	45	7	J3-2	196.9 ± 1.4	110.9 ± 0.6
353	85	8	J3-2	185.3 ± 1.4	99.9 ± 0.6
353	353	avg	J3-2	175.1 ± 0.5	117.1 ± 0.2
545	14	1	J4-3	256.5 ± 2.5	47.8 ± 0.9
545	34	2	J4-3	268.3 ± 2.4	83.9 ± 1.0
545	55	3	J4-3	258.3 ± 3.2	59.7 ± 1.7
545	73	4	J4-3	230.7 ± 2.4	35.5 ± 1.1
545	545	avg	J4-3	252.5 ± 1.4	56.9 ± 0.6
545	14	1	J5-4	2216.1 ± 11.8	1144.5 ± 6.3
545	34	2	J5-4	2281.8 ± 12.3	1422.4 ± 7.6
545	55	3	J5-4	2349.2 ± 13.4	1845.6 ± 10.4
545	73	4	J5-4	2473.6 ± 13.7	1492.2 ± 8.1
545	545	avg	J5-4	2322.2 ± 7.3	1356.1 ± 4.3
857	25	1	J6-5	7794.4 ± 160.0	3264.7 ± 81.0
857	35	2	J6-5	6702.0 ± 111.9	1700.5 ± 43.7
857	65	3	J6-5	6978.7 ± 144.5	1417.9 ± 60.8
857	74	4	J6-5	7565.4 ± 145.4	1439.8 ± 57.3
857	857	avg	J6-5	7217.3 ± 71.4	2016.6 ± 30.4
857	25	1	J7-6	72291.9 ± 1440.7	61488.8 ± 1186.4
857	35	2	J7-6	62775.8 ± 995.9	64156.9 ± 969.1
857	65	3	J7-6	82316.7 ± 1523.9	57721.9 ± 1029.5
857	74	4	J7-6	87556.9 ± 1619.8	63467.8 ± 1119.9
857	857	avg	J7-6	74876.2 ± 694.6	61406.7 ± 545.5
857	25	1	J8-7	168443.0 ± 3337.6	136686.1 ± 2671.9
857	35	2	J8-7	145623.5 ± 2313.6	117751.3 ± 1825.7
857	65	3	J8-7	154861.1 ± 2861.8	126685.2 ± 2320.6
857	74	4	J8-7	125207.4 ± 2288.6	123683.8 ± 2230.9
857	857	avg	J8-7	151726.7 ± 1398.9	126570.5 ± 1151.8
857	25	1	J9-8	4941.8 ± 242.8	102261.9 ± 2036.6
857	35	2	J9-8	5619.9 ± 238.2	80172.8 ± 1263.2
857	65	3	J9-8	6897.2 ± 301.2	100933.8 ± 1853.0
857	74	4	J9-8	144.7 ± 232.1	51734.0 ± 988.8
857	857	avg	J9-8	4998.3 ± 131.9	88290.3 ± 821.8

Planet Colour Correction

As the planets within our solar system are used as calibration verification, and their spectra may deviate from the nominal Rayleigh-Jeans spectral profile, colour correction coefficients have been determined for each of the planets observed by Planck. This involves a model spectrum for each planet over the Planck Bands (cite rel. models here), and an understanding of the model uncertainties, and spectral uncertainties in order to determine the planet colour correction coefficient uncertainties. The table below summarizes the results for the planet colour correction coefficients.

FIXME: get into proper table format...

```
Band, BC, det., CC_SI=-2, CCE_SI=-2, CC_Mars1, CCE_Mars1, CC_Mars2,
CE_Mars2, CC_Mars3, CCE_Mars3, CC_Jup, CCE_Jup, CC_Sat, CCE_Sat, CC_Ur,
 CCE_Ur, CC_Nep, CCE_Nep
100 00 1a       0.99179524     0.0024569372       0.99136628
0.0028896212       0.99177756     0.0027920234       0.99136832
0.0028653367       0.99192571     0.0058583181       0.99226270
0.0051635052       0.99629477      0.0023507110        1.0000696
0.0023383064
100 01 1b       0.97434212     0.0023504173       0.97375068
0.0027664805       0.97430734     0.0026726654       0.97375361
0.0027429981       0.97441599     0.0056352787       0.97488177
0.0049649349       0.98002947     0.0022491406       0.98428882
0.0022335515
100 20 2a       0.96064335     0.0024812887       0.95985742
0.0028602119       0.96059429     0.0027710572       0.95986171
0.0028382682       0.96071444     0.0056396086       0.96134048
0.0049820244       0.96809857     0.0023651134       0.97276578
0.0023474124
100 21 2b       0.96513920     0.0026154215       0.96440156
0.0029987856       0.96509400     0.0029095399       0.96440543
0.0029770927       0.96521685     0.0057557103       0.96580167
0.0050993873       0.97217979     0.0024991748       0.97658077
0.0024855546
100 40 3a       0.95227079     0.0024217183       0.95141328
0.0028267431       0.95221319     0.0027357225       0.95141775
0.0028039782       0.95231097     0.0056369281       0.95298905
0.0049778541       0.96021386     0.0023229208       0.96555618
0.0023034938
100 41 3b       0.98139440     0.0024512185       0.98083549
0.0028571474       0.98136600     0.0027636093       0.98083842
0.0028339286       0.98151075     0.0057414268       0.98195360
0.0050633475       0.98700251     0.0023420047       0.99141841
0.0023273952
100 80 4a       0.94863992     0.0025572022       0.94773453
0.0029459918       0.94857907     0.0028574219       0.94773941
0.0029242937       0.94868107     0.0056758085       0.94939951
0.0050287996       0.95702542     0.0024475671       0.96255867
0.0024264874
```

```
100 81 4b       0.94472176     0.0024347784       0.94378680
0.0028136068       0.94465704     0.0027263078       0.94379172
0.0027919631       0.94474695     0.0055351329       0.94548546
0.0048926320       0.95329271     0.0023286029       0.95886516
0.0023080312
100 100 avg       0.96201584     0.0010140989       0.96125413
0.0017473936       0.96196792     0.0016180539       0.96125815
0.0017102511       0.96208289     0.0052173339       0.96268641
0.0044916060       0.96922184     0.0010542270       0.97410782
0.0010439924
143 02 1a        1.0274279    0.00069310170        1.0273780
0.0010929967        1.0274933    0.00097577618        1.0273952
0.0010617994        1.0277801     0.0040870736        1.0280921
0.0032092061        1.0303270    0.00062520368        1.0310322
0.00063324809
143 03 1b        1.0149215    0.00070866545        1.0147696
0.0010951536        1.0149853    0.00098107888        1.0147886
0.0010647845        1.0153107     0.0040423422        1.0157214
0.0031761456        1.0191177    0.00064083408        1.0196698
0.00064901275
143 30 2a        1.0256655    0.00071856612        1.0255947
0.0011051012        1.0257319    0.00098966074        1.0256126
0.0010743671        1.0260326     0.0040969243        1.0263760
0.0032170282        1.0288763    0.00064839386        1.0296126
0.00065702576
143 31 2b        1.0105600    0.00066156375        1.0103726
0.0010564197        1.0106237    0.00094037912        1.0103925
0.0010254397        1.0109642     0.0040132254        1.0114212
0.0031483366        1.0152188    0.00059867200        1.0157617
0.00060634902
143 50 3a        1.0540337    0.00079658097        1.0542126
0.0011819005        1.0540996     0.0010655460        1.0542247
0.0011511021        1.0542895     0.0042420340        1.0543570
0.0033359408        1.0539499    0.00071486962        1.0550431
0.00072497723
143 51 3b        1.0291866    0.00073197786        1.0291488
0.0011223489        1.0292516     0.0010059919        1.0291656
0.0010913951        1.0295330     0.0041396701        1.0298255
0.0032517812        1.0319238    0.00066040360        1.0326979
0.00066937901
143 82 4a        1.0061120    0.00070379842        1.0058677
0.0010944281        1.0061800    0.00097869910        1.0058899
0.0010635565        1.0065635     0.0040824417        1.0070911
0.0032056372        1.0116784    0.00063675289        1.0122041
0.00064498270
143 83 4b        1.0172157    0.00070622867        1.0170853
0.0010920808        1.0172783    0.00097799480        1.0171036
```

```
0.0010617064        1.0175901     0.0040386342        1.0179738
0.0031726240        1.0210933    0.00063851040        1.0217136
0.00064697273
143 10 5       0.97451281    0.00060130694       0.97403771
0.0010077414       0.97457462    0.00089211065       0.97406349
0.00097678507       0.97503467     0.0038957642       0.97578047
0.0030560406       0.98294909    0.00054954842       0.98306051
0.00055596656
143 42 6       0.99996107    0.00066668980       0.99968416
0.0010573354        1.0000246    0.00094266271       0.99970596
0.0010267065        1.0004048     0.0039909943        1.0009555
0.0031324957        1.0058087    0.00060469278        1.0062450
0.00061218052
143 60 7       0.97009182    0.00063299289       0.96958024
0.0010194157       0.97015385    0.00090626054       0.96960689
0.00098909047       0.97063066     0.0039043560       0.97140874
0.0030625003       0.97902883    0.00057634869       0.97905402
0.00058285699
143 70 8       0.98857904    0.00067452972       0.98820410
0.0010585037       0.98864304    0.00094536517       0.98822818
0.0010282681       0.98906878     0.0039713907       0.98971077
0.0031178738       0.99575904    0.00061283887       0.99604248
0.00062011604
143 143 avg        1.0070824    0.00021374022        1.0068614
0.00086409244        1.0071466    0.00071705691        1.0068821
0.00082483224        1.0075044     0.0040076546        1.0079914
0.0031228747        1.0122118    0.00021344720        1.0127057
0.00021557979
217 04 1       0.92372890    0.00014543105       0.92335527
0.00024240533       0.92408488    0.00019744716       0.92346228
0.00023023603       0.92564528     0.0015701413       0.94180278
0.0010131918       0.93820450    0.00012696036       0.95279110
0.00012462523
217 22 2       0.91865604    0.00014914031       0.91825965
0.00024397324       0.91902960    0.00019988489       0.91837207
0.00023202445       0.92064935     0.0015605936       0.93711772
0.0010080980       0.93393990    0.00013062592       0.94633963
0.00012956498
217 52 3       0.92005792    0.00014369930       0.91966886
0.00024222673       0.92041646    0.00019655457       0.91977696
0.00022986870       0.92194761     0.0015838572       0.93736052
0.0010206916       0.93487937    0.00012579592       0.94856537
0.00012450449
217 84 4       0.92495519    0.00014512127       0.92458715
0.00024358886       0.92530546    0.00019787179       0.92469247
0.00023121651       0.92680837     0.0015890382       0.94232617
0.0010241088       0.93919854    0.00012648258       0.95255081
```

```
0.00012451968
217 11 5a       0.95420528    0.00016517233       0.95395616
0.00026105946       0.95451165    0.00021582053       0.95404671
0.00024877594       0.95583734     0.0016393437       0.97066825
0.0010566672       0.96523516    0.00014388767       0.97794116
0.00014047459
217 12 5b       0.95119915    0.00015741187       0.95093690
0.00025282959       0.95150918    0.00020776743       0.95102877
0.00024059837       0.95285521     0.0016138199       0.96830417
0.0010403248       0.96255440    0.00013733322       0.97546140
0.00013434738
217 43 6a       0.95166719    0.00016000513       0.95140712
0.00025615709       0.95197683    0.00021074547       0.95149881
0.00024382949       0.95328677     0.0016297876       0.96784827
0.0010497778       0.96297893    0.00013941718       0.97494109
0.00013675603
217 44 6b       0.95169507    0.00015570745       0.95143404
0.00025362596       0.95200265    0.00020740357       0.95152524
0.00024108688       0.95330789     0.0016386924       0.96815314
0.0010553470       0.96297302    0.00013603545       0.97583895
0.00013324272
217 61 7a       0.94972963    0.00015239450       0.94946246
0.00025207770       0.95003715    0.00020563156       0.94955374
0.00023950395       0.95132855     0.0016287555       0.96583873
0.0010486024       0.96112182    0.00013270037       0.97286646
0.00013022047
217 62 7b       0.95537121    0.00016113948       0.95512752
0.00026061348       0.95566714    0.00021411649       0.95521510
0.00024801275       0.95688048     0.0016560033       0.97050533
0.0010660058       0.96606477    0.00014036063       0.97712304
0.00013754722
217 71 8a       0.95308368    0.00016110231       0.95282877
0.00025768691       0.95339507    0.00021184558       0.95292085
0.00024523592       0.95473572     0.0016464027       0.96936560
0.0010603617       0.96433301    0.00014032034       0.97700981
0.00013781597
217 72 8b       0.95048294    0.00015373978       0.95021787
0.00025301486       0.95079048    0.00020692295       0.95030911
0.00024053889       0.95210122     0.0016220164       0.96627247
0.0010445368       0.96184275    0.00013405319       0.97499412
0.00013086004
217 217 avg       0.93586113    4.7378428e-05       0.93553554
0.00020323701       0.93619662    0.00014455406       0.93563585
0.00018794390       0.93763539     0.0016001360       0.95291335
0.0010263908       0.94897105    4.1318756e-05       0.96194977
4.0574860e-05
353 05 1       0.94058043    0.00011332546       0.94098217
```

```
0.00011441096       0.94141295    0.00011288488       0.94116837
0.00011387941       0.94555005    0.00037131159       0.94844667
0.00017398739       0.95501386    9.6672425e-05       0.94252929
0.00010244836
353 13 2       0.93604223    0.00011766864       0.93646791
0.00011892386       0.93692586    0.00011730590       0.93666550
0.00011836793       0.94132594    0.00037197986       0.94433250
0.00017722200       0.95137461    0.00010038591       0.93875196
0.00010586665
353 23 3a       0.94601822    0.00013419995       0.94638004
0.00013494525       0.94677116    0.00013354759       0.94654860
0.00013446058       0.95047817    0.00037504681       0.95303302
0.00018638046       0.95908115    0.00011497526       0.94912779
0.00012047238
353 24 3b       0.94549039    0.00012107755       0.94587698
0.00012181912       0.94628057    0.00012041895       0.94605316
0.00012132239       0.95024077    0.00037357867       0.95295610
0.00017785405       0.95904147    0.00010291203       0.94782372
0.00010895011
353 32 4a       0.92550628    0.00011168432       0.92590043
0.00011280360       0.92638226    0.00011127256       0.92609866
0.00011226930       0.93061868    0.00036489332       0.93335202
0.00017140080       0.94131248    9.5161783e-05       0.93060586
0.00010232233
353 33 4b       0.92560740    0.00011535949       0.92601983
0.00011647515       0.92650963    0.00011494353       0.92622343
0.00011594320       0.93090737    0.00036576470       0.93376284
0.00017381066       0.94174044    9.8456132e-05       0.92965716
0.00010437055
353 53 5a       0.95292376    0.00012188150       0.95331003
0.00012272894       0.95368671    0.00012128687       0.95347921
0.00012222428       0.95752576    0.00037744312       0.96032758
0.00018013350       0.96572763    0.00010391665       0.95318252
0.00010850519
353 54 5b       0.95198172    0.00012562110       0.95239373
0.00012634361       0.95278451    0.00012493622       0.95257109
0.00012584674       0.95690100    0.00037545442       0.95986476
0.00018092809       0.96530501    0.00010679503       0.95260819
0.00011099594
353 63 6a       0.94350543    0.00014632473       0.94391092
0.00014710047       0.94433192    0.00014560840       0.94409518
0.00014658422       0.94846347    0.00038237367       0.95136826
0.00019551997       0.95766012    0.00012481655       0.94499853
0.00012943610
353 64 6b       0.97439004    0.00014454517       0.97469099
0.00014551843       0.97494197    0.00014385611       0.97481163
0.00014494673       0.97777798    0.00039581401       0.97992890
```

```
0.00019859126       0.98317463    0.00012209450       0.97339239
0.00012809685
353 45 7       0.91695423    0.00012676198       0.91738734
0.00012748245       0.91791853    0.00012616718       0.91760559
0.00012702172       0.92260648    0.00036124111       0.92566524
0.00017782391       0.93439356    0.00010927645       0.92339661
0.00011439164
353 85 8       0.90384202    0.00012261582       0.90433854
0.00012348863       0.90494364    0.00012202853       0.90458747
0.00012296857       0.91038829    0.00036092882       0.91389086
0.00017417894       0.92373414    0.00010434520       0.91163173
0.00011010402
353 353 avg       0.93323585    4.4062606e-05       0.93365358
4.7070290e-05       0.93411831    4.4557970e-05       0.93385153
4.6199076e-05       0.93848877    0.00035164656       0.94145185
0.00014110258       0.94870194    3.7658049e-05       0.93676117
3.9614753e-05
545 14 1       0.92302463    0.00016861905       0.92461756
0.00016804803       0.92501464    0.00016771153       0.92493336
0.00016787094       0.91708546    0.00015851497       0.80636759
0.00014498146       0.94179218    0.00015444168       0.95363288
0.00015667609
545 34 2       0.94195694    0.00016871427       0.94336773
0.00016811001       0.94370224    0.00016774858       0.94364108
0.00016791952       0.93574149    0.00015708569       0.82275030
0.00014416656       0.95787017    0.00015381168       0.97068422
0.00015578950
545 55 3       0.93512338    0.00027655893       0.93656096
0.00027600560       0.93691226    0.00027552445       0.93684341
0.00027578629       0.93104992    0.00025985046       0.81875193
0.00023124526       0.95176550    0.00025712338       0.96419783
0.00025990306
545 73 4       0.93789657    0.00018106184       0.93929799
0.00018048351       0.93963862    0.00018012702       0.93957268
0.00018030030       0.93488316    0.00016869839       0.82191908
0.00015426500       0.95404589    0.00016606602       0.96719779
0.00016790120
545 545 avg       0.93456594    9.9769955e-05       0.93603315
9.9429455e-05       0.93639001    9.9225109e-05       0.93632077
9.9322420e-05       0.92946031    9.3581163e-05       0.81720996
8.5125376e-05       0.95148319    9.1245529e-05       0.96409014
9.2283397e-05
857 25 1       0.96944437    0.00027856680       0.97151258
0.00027804692       0.97174365    0.00027784061       0.97174163
0.00027791474       0.98864826    0.00027967852       0.98899431
0.00027826822       0.98269193    0.00026752947       0.98870019
0.00026951231
```

```
857 35 2       0.98810255    0.00024194320       0.98982374
0.00024124537       0.99000266    0.00024103289       0.99000374
0.00024109823        1.0063799    0.00024222636        1.0057014
0.00024149148       0.99824571    0.00023048839        1.0042322
0.00023213953
857 65 3       0.97322233    0.00026529861       0.97521786
0.00026471472       0.97543817    0.00026450752       0.97543677
0.00026457792       0.99181933    0.00026601798       0.99151029
0.00026515330       0.98582708    0.00025417843       0.99174350
0.00025613279
857 74 4        1.0083172    0.00030474985        1.0094396
0.00030389953        1.0095398    0.00030362975        1.0095443
0.00030371607        1.0238004    0.00030485468        1.0254106
0.00030369029        1.0138754    0.00029033788        1.0204622
0.00029266176
857 857 avg       0.98090289    0.00013617145       0.98273089
0.00013584940       0.98292739    0.00013573943       0.98292724
0.00013577595       0.99918265    0.00013645470       0.99923102
0.00013587987       0.99210006    0.00013026850       0.99815419
0.00013122817
```

Conclusions

Summary remarks here...

HFI-Validation

The HFI validation is mostly modular. That is, each part of the pipeline, be it timeline processing, map-making, or any other, validates the results of its work at each step of the processing, looking specifically for known issues. In addition, we do additional validation with an eye towards overall system integrity by looking at generic differences between sets of maps, in which most problems will become apparent, whether known or not. Both these are described below.

Expected systematics and tests (bottom-up approach)

Like all experiments, Planck/HFI had a number of "issues" which it needed to track and verify were not compromising the data. While these are discussed in appropriate sections, here we gather them together to give brief summaries of the issues and refer the reader to the appropriate section for more details.

- Cosmic Rays - Unprotected by the atmosphere and more sensitive than previous bolometric experiment, HFI was subjected to many more cosmic ray hits than previous experiments. These were detected, the worst parts of the data flagged as unusable, and "tails" were modeled and removed. This is described in the section on glitch statistics and in the section on cosmic rays.
- Elephants - Cosmic rays also hit the 100 mK stage and cause the temperature to vary, inducing small temperature and thus noise variations in the detectors. These are effectively removed with the rest of the thermal fluctuations, described directly below.
- Thermal Fluctuations - HFI is an extremely stable instrument, but there are small thermal fluctuations. These are discussed in the timeline processing section on thermal decorrelation and in the section on 1.6 K and 4 K thermal

fluctuations.

- Popcorn Noise - Some channels were occasionally affected by what seems to be a "split-level" noise, which has been variously called popcorn noise or random telegraphic signal. These data are usually flagged. This is described in the section on noise stationarity and the section on Random Telegraphic Signal Noise
- Jumps - Similar to but distinct from popcorn noise, small jumps were occasionally found in the data streams. These data are usually corrected. This is described in the section on jump corrections.
- 4 K Cooler-Induced EM Noise - The 4 K cooler induced noise in the detectors with very specific frequency signatures, which is filtered. This is described in the section below on 4K line residuals, and their stability is discussed in the section on 4K cooler line stability.
- 4 K Cooler-Induced Microphonics - The mechanical cooler was shown in XXXXX to cause very little microphonic parasites in the detector data.
- Pointing-Change Microphonics - The changes in pointing after each pointing period were shown in XXXXX to cause very little microphonic parasitic signal in the detector data.
- Compression - Onboard compression is used to overcome our telemetry bandwidth limitations. This is explained in XXXXX.
- Noise Correlations - Correlations in noise between detectors seems to be negligble but for two polarization sensitive detectors in the same horn. This is discussed in XXXXX.
- Electrical Cross-Talk - Cross-talk is discussed in XXXXX.
- Pointing - The final pointing reconstruction for Planck is near the arcsecond level. This is discussed in XXXXX.
- Focal Plane Geometry - The relative positions of different horns in the focal plane is reconstructed using planets. This is discussed in XXXXX.
- Main Beam - The main beams for HFI are discussed in XXXXX.
- Ruze Envelope - Random imperfections or dust on the mirrors can increase the size of the beam a bit. This is discussed in XXXXX.
- Dimpling - The mirror support structure causes a pattern of small imperfections in the beams, which cause small sidelobe responses outside the main beam. This is discussed in XXXXX.
- Far Sidelobes - Small amounts of light can sometimes hit the detectors from just above the primary or secondary mirrors, or even from reflecting off the baffles. While small, when the Galactic center is in the right position, this can be detected in the highest frequency channels, so this is removed from the data. This is discussed in XXXXX.
- Planet Fluxes - Comparing the known fluxes of planets with the calibration on the CMB dipole is a useful check of calibration. This is done in XXXXX.
- Point Source Fluxes - As with planet fluxes, we also compare fluxes of known, bright point sources with the CMB dipole calibration. This is done in XXXXX.
- Time Constants - The HFI bolometers do not react instantaneously to light; there are small time constants, discussed XXXXX.
- ADC Correction - The HFI Analog-to-Digital Converters are not perfect, and are not used perfectly. Their effects on the calibration are discussed in XXXXX.
- Gain changes with Temperature Changes
- Optical Cross-Talk - This is discussed in XXXXX.
- Bandpass - The transmission curves, or "bandpass" has shown up in a number of places. This is discussed in XXXXX and YYYYY.
- Saturation - While this is mostly an issue only for Jupiter observations, it should be remembered that the HFI detectors cannot observe arbitrarily bright objects. This is discussed in XXXXX.

Generic approach to systematics

While we track and try to limit the individual effects listed above, and we do not believe there are other large effects which might compromise the data, we test this using a suite of general difference tests. As an example, the first and second years of Planck observations used almost exactly the same scanning pattern (they differed by one arc-minute at the Ecliptic plane). By differencing them, the fixed sky signal is almost completely removed, and we are left with only time variable signals, such as any gain variations and, of course, the statistical noise.

In addition, while Planck scans the sky twice a year, during the first six months (or survey) and the second six months (the second survey), the orientations of the scans and optics are actually different. Thus, by forming a difference between these two surveys, in addition to similar sensitivity to the time-variable signals seen in the yearly test, the survey difference also tests our understanding and sensitivity to scan-dependent noise such as time constant and beam asymmetries.

These tests use the `Yardstick` simulations below and culminate in the "Probabilities to Exceed" tests just after.

HFI simulations

The '`Yardstick`' simulations allows gauging various effects to see whether they need be included in monte-carlo to describe data. It also allows gauging the significance of validation tests on data (e.g. can null test can be described by the model?). They are completed by dedicated '`Desire`' simulations (`Desire` stands for DEtector SImulated REsponse), as well as Monte-Carlo simulations of the Beams determination to determine their uncertainty.

`Yardstick` simulations

The `Yardstick` V3.0 characterizes the DX9 data which is the basis of the data release. It goes through the following steps:

1. The input maps are computed using the Planck Sky Model, taking the RIMO bandpasses as input.
2. The `LevelS` is used to project input maps on timeline using the RIMO(B-Spline) scanning beam and the DX9 pointing (called ptcor6). The real pointing is affected by the aberration that is corrected by map-making. The `Yardstick` does not simulate aberration. Finally, the difference between the projected pointing from simulation and from DX9 is equal to the aberration.
3. The simulated noise timelines, that are added to the projected signal, have the same spectrum (low and high frequency) than the DX9 noise. For the`yardstick` V3.0 Althoough detectable, no correlation in time or between detectors have been simulated.
4. The simulation map making step use the DX9 sample flags.
5. For the low frequencies (100, 143, 217, 353), the `yardstick` output are calibrated using the same mechanism (e.g. dipole fitting) than DX9. This calibration step is not perfromed for higher frequency (545, 857) which use a differnt principle
6. The Official map making is run on those timelines using the same parameters than for real data.

A `yardstick` production is composed of

- all survey map (1,2 and nominal),
- all detector Detsets (from individual detectors to full channel maps).

The `Yardstick` V3.0 is based on 5 noise iterations for each map realization.

NB1: the `Yardstick` product is also the validating set for other implementations which are not using the HFI DPC production codes, an exemple of which are the so-called `FFP` simulations, where FFP stands for Full Focal Plane and are done in common by HFI & LFI. This is further described in HL-sims

NB2: A dedicated version has been used for Monte-Carlo simulations of the beams determination, or `MCB`. See Pointing&Beams#Simulations_and_errors

Desire simulations

Complementary to the Yardstick simulations, the Desire simulations are used in conjunction with the actual TOI processing, in order to investigate the impact of some systematics. The Desire pipeline allows to simulate the response of the HFI-instrument, including the non-linearity of the bolometers, the time transfer-function of the readout electronic chain, the conversion from power of the sky to ADU signal and the compression of the science data. It also includes various components of the noise like the glitches, the white and colored noise, the one-over-f noise and the RTS noise. Associated to the Planck Sky Model and LevelS tools, the Desire pipeline allows to perform extremely realistic simulations, compatible with the format of the output Planck HFI-data, including Science and House Keeping data. It goes through the following steps (see Fig. Desire End-to-End Simulations) :

1. The input maps are computed using the Planck Sky Model, taking the RIMO bandpasses as input;
2. The LevelS is used to project input maps into Time ordered Inputs TOIs, as described for the Yardstick simulations;
3. The TOIs of the simulated sky are injected into the Desire pipeline to produce TOIs in ADU, after adding instrument systematics and noise components;
4. The official TOI processing is applied on simulated data as done on real Planck-HFI TOIs;
5. The official map-making is run on those processed timelines using the same parameters as for real data;

This Desire simulation pipeline allows to explore systematics such as 4K lines or Glitches residual after correction by the official TOI processing, as described below.

Simulations versus data

The significance of various difference tests perfromed on data can be assessed in particular by comparing them with Yardstick realisations.

Yardstick production contains sky (generated with LevelS starting from PSM V1.77) and noise timeline realisations proceeded with the official map making. DX9 production was regenerated with the same code in order to get rid of possible differences that might appear for not running the official pipeline in the same conditions.

We compare statistical properties of the cross spectra of null test maps for the 100, 143, 217, 353 GHz channels. Null test maps can either be survey null test or half focal plane null test, each of which having a specific goal :

- survey1-survey2 (S1-S2) aim at isolating transfer function or pointing issues, while
- half focal plane null tests enable to focus on beam issues.

Comparing cross spectra we isolate systematic effects from the noise, and we can check whether they are properly simulated or need to. Spectra are computed with spice masking either DX9 point sources or simulated point sources, and masking the galactic plane with several mask width, the sky fraction from which spectra are computed are around 30%, 60% and 80%.

DX9 and the Y3.0 realisations are binned. For each bin we compute the statistical parameters (mean and variance) of the Yardstick distribution. The following figure is a typical example of a consistency test, it shows the differences between Y3.0 mean and DX9 considering the standard deviation of the yardstick. We also indicate chi square values, which are computed within larger bin : [0,20], [20,400], [400,1000][1000,2000], [2000, 3000], using the ratio between (DX9-Y3.0 mean)^2 and Y3.0 variance within each bin. This binned chi-square is only indicative: it may not be always significant, since DX9 variations sometimes disappear as we average them in a bin, the mean is then at the same scale as the yardstick one.

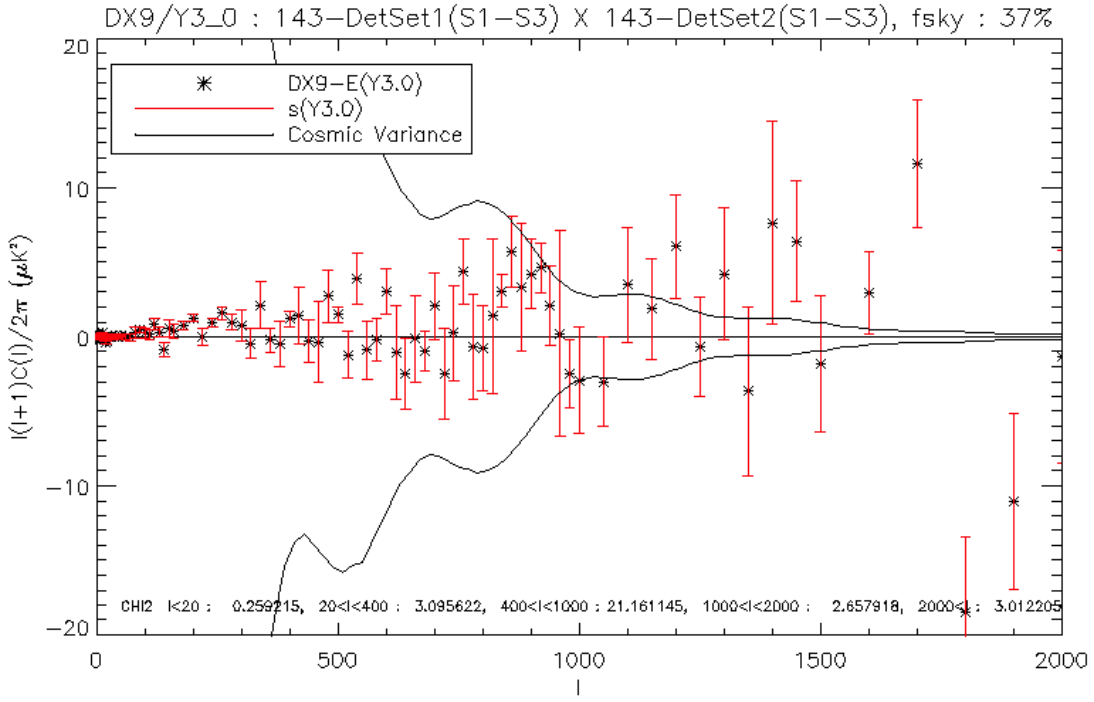

Example of consistency test for 143 survey null test maps.

Here will be a linlk to a (big) pdf file with all those plots, and/or a visualisation page.

Systematics Impact Estimates

Cosmic Rays

We have used `Desire` simulations to investigate the impact of glitch residuals at 143GHz. We remind that TOIs are highly affected by the impact of cosmic rays inducing glitches on the timelines. While the peak of the glitch signal is flagged and removed from the data, the glitch tail is removed from the signal during the TOI processing. We have quantified the efficiency and the impact of the official TOI processing when removing glitch tails on the scientific signal.

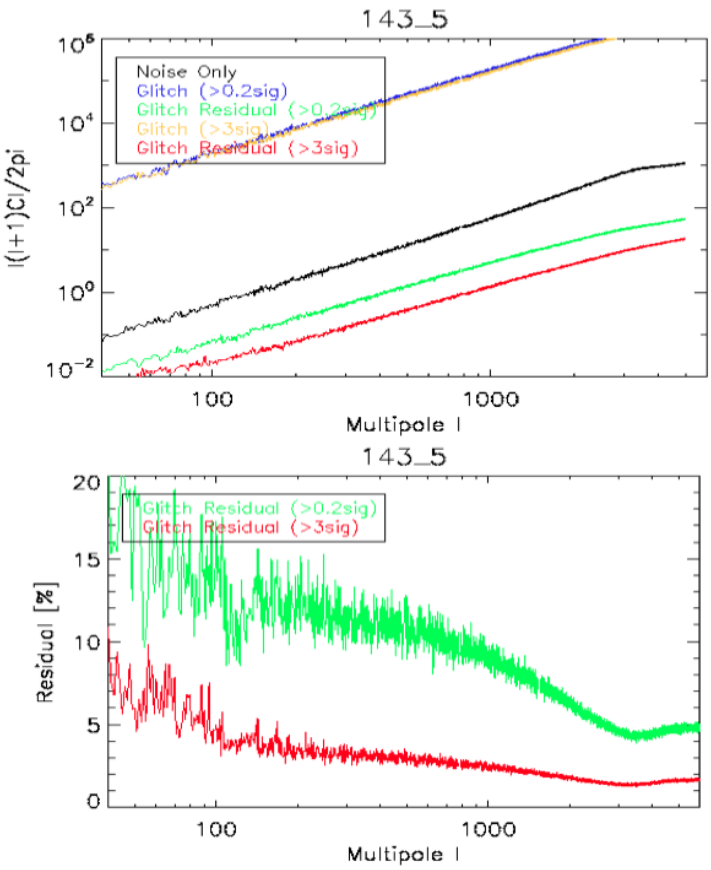

Comparison of Power SPectra with and without Glitch and Glitch corection

The Glitch model used in this set of simulations has been built using the real data extraction, in order to reproduce the 3 families observed (i.e. long, short and snail) and their relative distribution. This modelling has been validated on 143GHz channels, by comparing the glitch statistics of simulated timelines with real ones. Two types of models have been introduced for these simulations: the first only includes detectable glitches, with a glitch amplitude at the level of at least 3 times the noise level ; the second model also includes undetectable glitches until a level of 0.3 times the noise level.

The input sky used for these end-to-end simulations includes the CMB signal, our Galaxy, the compact sources and the planets. Not any other kind of systematics has been introduced, except the glitches associated with a white and colored noise to reproduce realistic data. For each bolometer three sets of simulated TOIs have been produced: (i) white plus colored noise only, (ii) noise plus "detectable glitches model" and (iii) noise plus "undetectable glitches model". On the simulated TOIs with glitches, two options of the TOI-processing have been used: with or without correction of the glitches (Despike Module), leading to a set of 5 processed TOIs. Maps and power spectra can be built on these sets of data.

It appears that in the case of the "detectable glitch model", the glitch tail residual represents less than 10% of the noise for ell<100 and less than 5% for ell>100. In the case of the "undetectable glitch model", these numbers goes to 20% for ell<100 and 15% for ell>100. Nevertheless the number of undetectable glitches remains largely unknown, and can only be extrapolated from power laws. Hence the results obtained for model 2 including undetectable glitches have to be taken as upper limits of the impact of glitch residuals on the power spectrum. These simulations also show that the glitch tail residuals do not produce any kind of 1/f supplementary noise.

1.6K and 4K stages Fluctuations

The 4K and 1.6K stages are thermally regulated. The level of (controlled) fluctuations is less than 20uK/sqrt(Hz) above the spin frequency (and below 0.2 Hz) for the 4K stage and 10uK/sqrt(Hz) for the the 1.6K stage. Using a typical coupling coefficient of 150 fW/K_4K, this translates into a noise of 3 aW/sqrt(Hz). This is 4% of the bolometer noise variance (with a NEP of typically 15aW/sqrt(Hz)), and is thus negligible.

RTS Noise

The Random Telegraphic Signal (RTS) noise, also called Popcorn Noise, appears as 2-levels jumps added on the baseline signal. Three bolometers are known to be affected by a high-RTS noise: 143-8, 545-3 and 857-4. While the 143-8 and 545-3 detectors are currently excluded from use in any products, other bolometers may show small amounts of small RTS.

We have investigated the probable impact of RTS noise present below the detection limit, i.e. 0.2 times the standard deviation noise of the signal. The `Desire` simulations with and without RTS noise have been produce on 143GHz bolometers. The analysis performed on the TOIS has shown that the impact measured is in perfect agreement with the expectation derived from the pre-launch RTS report. Residual RTS appears to be strongly limited, with a negligible impact on TOI noise – does not dominate over the 1/f noise at low frequencies (0.01Hz or below), and it would disappear rapidly above 1 Hz, very probably irrelevant at map level.

Baseline Jumps

Similar to but distinct from popcorn noise, small baseline jumps were occasionally found in the data streams. They differ from the RTS noise by a much longer duration of the plateau. These data are usually corrected by subtracting a constant baseline before and after the jumps. About 320 jumps are found per bolometers, this represents 16 jumps per day for hFI, i.e. 12800 over the mission lifetime. While the detection efficiency of the biggest jumps is extremely high, the question of the impact of the jumps with amplitudes lower than 0.5% of the standard deviation of signal is still open. `Desire` simulations are about to be produced to answer this.

Split-Level Noise

The Split-Level noise is the major component of the non-stationnary noise. It appears as a strong increase of the noise level during one or a few rings, and is characterized by the addition of anoher 1/f noise component. The impact of such a systematics effect is under investigation using dedicated `Desire` simulations at 143GHz.

Pointing-Change Microphonics

The "Thruster signal" is not present for all bolometer for 100, 143, 217 GHz. After the peak "Thruster signal", the relaxing time "normal noise" is about the same for all bolometers over channels, i.e. 12 seconds, but amplitude is different. Thus the effect of the manouver has decayed away long before the end of the "unstable" period, which would be minutes after the first thrust.

This effect can be neglected, and does not need to be included in the simulation runs.

Electrical Cross-Talk

The Electrical Cross-Talk consists in the electrical contamination received by a given channel and coming from the other channels of the focal plane. This is mainly driven by the locations of the channels inside the electronic devices of the readout chain, and not by their locations in the focal plane.

This effect has been first measured during the ground calibration phase, and then during the inflight 'Calibration, Performance and Validation' phase (CPV Phase) after launch. These two sets of measurements agree to show that the level of electrical cross-talk is smaller than 0.01% for SWBs and 0.1% for PSBs. These estimates have been confirmed by the analysis of the glitches. While the thousands of detected glitches have been flagged for a given channel, the signal of the neighbor channels have been stacked at the same dates of the glitch flags to reveal the amount of electrical contamination coming from the glitched signal. Strong glitches have also been used in the same scope in a second study. These two analysis based on glitches give the same estimates of electrical cross-talk as measured during calibration phases.

Hence the electrical cross-talk has a negligible impact on science data, except probably for PSBs on which further `Desire` simulations will be carried out.

Optical Cross-Talk

It has been shown using planets crossing that the optical cross-talk is negligible, with an upper limit of 0.01%. This effect can be neglected in the total budget error, without any end-to-end simulation.

Time Constant

The impact of the uncertainty of the time response has been studied using a set of 50 `Yardstick` simulations with CMB only on 8 143GHz bolometers. The set of 50 Time Transfer Function (TF)realizations have been chosen with a Low Frequency Excess Response (LFER) varying within 1.5% around its nominal value. While the same CMB sky map has been convolved through the optical beam, projected into TOIs and convolved with each of the 50 TF realizations, it has then been deconvolved by the nominal TF, leading to the deconvolved TOIs. Maps and power spectra have then been produced using these TOIs and compared to each others.

These simulations have shown that an uncertainty of 1.5% of the LFER yields 1% of error on the power spectrum at all scales, and even less at large scales.

4K lines Residuals

The 4K lines are the 4 K cooler induced noise in the detectors with very specific frequency signatures. They are filtered and corrected during the TOI-processing. The efficiency of this correction has been studied using two types of simulations at 143GHz: `Yardstick` and `Desire` simulations.

The `Yardstick` simulations have explored the impact of 4K lines residuals on CMB signal only, by adding a 4K lines pattern on the CMB TOIs, and by applying the same module of correction as used in the TOI-processing. The impact on the CMB power spectrum has been estimated by comparing the spectra obtained on data without 4K lines and data with corrected 4K lines.

The end-to-end `Desire` simulations include a complete sky (i.e. CMB, Galaxy and point sources) and the complete TOI-processing on the simulated data. The analysis and comparison is then performed on the maps directly and on the power spectra. It has been checked that the 4K lines modeling inputs used in the two sets of simulation are in agreement between them and with in-flight data. Those simulations have been performed on the full 143GHz channel, i.e. 12 detectors, and the full nominal mission range.

Both analysis converge to show that the 4K lines residual represent 2% to 2.5% maximum of the noise level at particular ell values affected by the 4K lines (such as ell=1800). These residuals are well below the one-sigma discrepancy of the noise itself at the same particular ell values.

Hence the 4K lines residuals are negligible. Nevertheless, the correlation between the 4K lines and the ADC correction discussed in XXXX may have an impact on the gain variation estimates at the end o the processing. This has still to be quantified.

Saturation

The Planck-HFI signal is converted into digital signal (Raw-Signal) by a 16 bit ADC. This signal is expressed in ADU, from 1 to 65535, and centered around 32768. A full saturation of the ADC corresponds to the value of 1310680 ADU, corresponding to the number of samples per half period times, N_sample, times 2^15. Nevertheless, the saturation of the ADC starts to appear when a fraction of the raw signal hits the 32767 (2^15) value.

We have used the SEB tool (standing for Simulation of Electronics and Bolometer) to simulate the response of the Readout Electronics Chain at a very high sampling, to mimic the high frequency behavior of the chain and investigate sub-period effects. It has been shown by this kind of simulations that the saturation of the ADC starts to appear if the signal is more then 7*10^5 - 8*10^5 ADU. Hence the variation of the gain, due to the saturation of the ADC, has an impact only when crossing Jupiter for SWB353GHz and SWB857GHz bolometers. This effect can be neglected.

PowerSpectra

This is the page regarding the HFI-based power spectra

We call intra-frequency checks those performed between detectors (or sets of) in the same frequency bands, which thus respond similarly to the sky emission. Interfrequency-checks on the other hand correspond to checks between detector in different frequency bands, imposing further reliance on a sky model to perform the test.

Intra-frequency checks

These compare the power spectra between various detector sets operating within the same frequency channel. They see the same sky, and should therefore give consistent results, up to the noise level, and up to color corrections due to their somewhat different spectral band passes. These corrections are rather small if one restricts the comparison to specific portions of the sky, for instance dominated by extra-Galactic components, like it is done for extracting the CMB power spectrum in the likelihood analysis where $f_{sky} \sim 0.4$.

Consistency checks

Figures taken from HFI DPC paper (P03). To be updated with new beam error when available.

The pictures shows in grey the prior deduced from the beam parameters uncertainty analysis. At 217 GHz, the distance between PSB and SWB suggests an accounted for effect (fortunately small enough for the likelihood analysis). The relative calibration appear to be at the 0.1% level.

This shows that whatever systematic effect might remain, it has to be common to all detectors within a frequency band to a very high level of accuracy.

Summary of HFI data characteristics

This page will contains mostly the same information as what will be in the summary section of the HFI DPC paper. It will center on a table similar to that in the Early DPC paper (shown below) which describes the most important characteristics and figures of the HFI instrument and data.

Table 4. Summary of the main characteristics of HFI early maps. The first column refers to following notes pertaining to the content of the line, while the units are between brackets [] at the right of column 2.

	HFI Early Maps - Main Characteristics							
a1	ν	[GHz]	100	143	217	353	545	857
a2	N_{Bolo}		8	11	12	12	3	3
a3	c_{WN}	[μK degree]	1.6	0.9	1.4	5.0	70	1180
b1	θ_S	[arcmin]	9.53	7.08	4.71	4.50	4.72	4.42
b2	$\Delta\theta_S$	[arcmin]	0.10	0.12	0.17	0.14	0.21	0.28
b3	e_S		1.20	1.03	1.13	1.10	1.17	1.35
b4	$\Delta\alpha_S$	[degree]	0.80	2.08	0.28	0.28	0.13	0.07
c1	$\overline{\theta_M}$	[arcmin]	9.88	7.18	4.87	4.65	4.72	4.39
c2	σ_{θ_M}	[arcmin]	0.04	0.02	0.03	0.04	0.06	0.05
c3	$\overline{e_M}$		1.15	1.01	1.06	1.05	1.14	1.19
c4	σ_{e_M}		0.02	0.01	0.02	0.02	0.03	0.05
d1	CMB relative calibration accuracy		$\lesssim$ 1%	$\lesssim$ 1%	$\lesssim$ 1%	$\lesssim$ 2%		
d2	CMB absolute calibration accuracy		$\lesssim$ 2%	$\lesssim$ 2%	$\lesssim$ 2%	$\lesssim$ 2%		
d3	FIRAS gain calibration accuracy						$\sim$ 7%	$\sim$ 7%
d4	FIRAS zero point uncertainty [MJy sr^{-1}]		0.8			1.4	2.2	1.7
e1	F_U	[MJy sr^{-1}/mK$_{CMB}$]	2.42 10^{-1}	3.69 10^{-1}	4.81 10^{-1}	2.88 10^{-1}	5.83 10^{-2}	2.24 10^{-3}
e2	ΔF_U		$\lesssim$ 1%	$\lesssim$ 1%	$\lesssim$ 1%	$\lesssim$ 1%	$\lesssim$ 1%	$\sim$ 3%
e3	$C(\alpha), \alpha = -2$		1.011	1.025	0.999	0.997	0.998	1.011
	$C(\alpha), \alpha = 0$		0.999	0.985	1.009	1.011	1.012	0.999
	$C(\alpha), \alpha = 1$		1.008	0.980	1.027	1.031	1.035	1.007
	$C(\alpha), \alpha = 2$		1.027	0.985	1.053	1.060	1.068	1.024
e4	F_{CO}	[μK$_{CMB}$/K$_{RJ}$ km s^{-1}]	14.2 ± 1.0		44.2 ± 1.0	171.0 ± 6.0		

This table is from the Early DPC paper, and will be updated when all figures are ready

Note that some of these parameters are available in the RIMO, which is described in detail in The RIMO section.

The LFI DPC

Overview

The LFI DPC processing is organized into different "Levels": 1,2,3,4 and S. In brief the Level-1 has the scope to analyze the data in a daily base, transform the telemetry packets in to timelines containing engineering values and feed it in the DPC database. Level-2 use the output of the Level-1 transforming raw TOI in to calibrated timelines with all the know systematic sources removed, those timelines are then used in the mapmaking process to create all the possible maps combinations. Level-3 use the Level-2 output of both DPC to derive astrophysical results like Catalogue, CMB map, foreground etc…. Level-S is the common simulation pipeline used to validate the results and any algorithm before its introduction into the official pipeline. Finally the Level-4 just act as a collector pointing used to reformat, document and deliver the products to the final archive.

Level 1: From packets to TOI

Level 1 takes input from the MOC's Data Distribution System (DDS), decompresses the raw data, and outputs Time Ordered Information for Level 2. This will be done by using software. The input to Level 1 are the telemetry (TM) and auxiliary data as they are released by the MOC (Mission Operation Centre). Level 1 will use TM data for performing a routine analysis (RTA) of the S/C and P/L with the aim of monitoring the overall health of the payload and detecting possible anomalies, and performing a quick-look data analysis of the science TM to monitor the operation of the observation plan and to verify the behavior of the instrument. Additional tasks of Level 1 relate to its role of instrument control and as the DPC interface with the MOC. Level-1 processing is described in detail in the Pre-processing section

Level 2: From TOI to Maps

The DPC Level 2 has many tasks. The first one is the creation of differenced data. Level 1 stores data from both Sky and Load. These two have to be properly combined to produce differenced data therefore reducing the impact of 1/f noise. This is done via the computation of the so-called gain modulation factor “R” which is derived taking the ratio of the mean signals from both Sky and Load. After differenced data are produced, the next step are the removal of know systematic effects and then the photometric calibration where calibrated means essentially that TOD are in physical units instead of engineering units; the following major task is the production of frequency maps calibrated and free from systematic effects (which is a complex task and involves several sub-pipelines). Level-2 processing is described in detail in the TOI processing section

Level 3: From Maps to Component

The aim of Level 3 is to transform the frequency maps produced by both instruments into preliminary maps of the underlying astrophysical components by means of pipeline processing and to provide other data sets including description of astrophysical sources (final catalogue of point sources, extended source maps and catalogues, description of global or statistical properties etc …). Data from both HFI and LFI are analyzed jointly to reach the final expected result. Level-3 processing is described in detail in the L3_LFI and HFI/LFI joint data processing section

Level S : A common HFI/LFI simulation software

Level S is the so-called "Simulation Level" software suite common to both consortia, which, given a sky model (generated by the Planck sky model, `PSM`), detectors pointing and beams, generates the infalling power on each detector. It can also provide a simplified description of eg. the noise. It is further described in the HFI/LFI common section.

LFI DPC Infrastructures

The LFI DPC provide a centralized hardware and software infrastructure to a large number of geographically distributed institution participating to the Planck mission. In few word the data are interfaced to a database where only meta-information are stored. This allow very high flexibility to eventually modify the product to be delivered.

Published Paper

The description of the pipeline applied to the *"Early Planck results"* can be found at the following link Planck early results. V. The Low Frequency Instrument data processing [1] and instrument performances are reported Planck early results. III. First assessment of the Low Frequency Instrument in-flight performance [2]

References

[1] http://www.aanda.org/index.php?option=com_article&access=standard&Itemid=129&url=/articles/aa/abs/2011/12/aa16484-11/aa16484-11.html

[2] http://www.aanda.org/index.php?option=com_article&access=standard&Itemid=129&url=/articles/aa/abs/2011/12/aa16480-11/aa16480-11.html

Pre-processing LFI

Overview

The first processing level of the LFI DPC is the so called Level 1. The source data of the Level 1 software includes:

- raw housekeeping telemetry packets retrieved from different satellite subsystems: the LFI instrument, the Sorption cooler, the HFI instrument and the Central Data Management Unit (CDMU).
- the LFI raw scientific telemetry
- Additional auxiliary data provided by the MOC and the Flight dynamics:
  - The Attitude History File (AHF)
  - Time correlation data (time correlation coefficients and time couples)
  - Command History data
  - The Sorption cooler out of limit data

Only a subset of the raw housekeeping telemetry packets is daily processed and converted into TOIs, i.e. those relevant to the LFI Daily Quality Report production and the estimation of the LFI instrument systematic effects.

The LFI scientific telemetry

Each LFI radiometer provides two analog outputs, one for each amplifier chain. In a nominal configuration, each output yields a sequence of alternating V_{sky}, V_{load}signals at the frequency of the phase switch. By changing the phase switches configuration, the output can be a sequence of either V_{sky}or V_{load}signals.

The conversion from analog to digital form of each radiometer output is performed by a 14 bits Analog-to-Digital Converter (ADC) in the Data Acquisition Electronics unit (DAE). The DAE transforms the signal in the range [-2.5 V, +2.5 V]: first it applies a tunable *offset*, O_{DAE}, then it amplifies the signal with a tunable *gain*, G_{DAE}, in order to make full use of the resolution of the ADC, and finally the signal is integrated. To eliminate phase switch raise transients, the integration takes into account a *blanking time*, i.e. a blind time in the integrator where data are not considered. The default value of the blanking time is 7.5 μs. Both the O_{DAE}, the $G_{DAE}$and the blanking time are parameters set through the LFI on-board software. The equation applied to transform a given input signal V_{in}into an output $V_{out}$is:

$$V_{out} = G_{DAE}(V_{in} + O_{DAE}) + Z_{DAE}$$

with $G_{DAE} = 1, 2, 3, 4, 6, 8, 12, 16, 24, 48$, $O_{DAE}$is one of 255 possible offset steps from +0 up to +2.5 V and where $Z_{DAE}$is a small offset introduced by the DAE when applying a selected gain. The values of $G_{DAE}$and $O_{DAE}$are set by sending, through specific telecommands, the DAE Gain Index (DGI) and the DAE Offset Index (DOI) associated to the desired values.

The ADC quantizes the V_{out}uniformly in the range $-2.5V \leq V_{adc} \leq +2.5V$, so that the quantization step is $q_{ADC} = 5.0/2^{14} = 0.30518$mV. The quantization formula is

$$S = \text{round}\left(\frac{V_{out} + 2.5}{q_{ADC}}\right),$$

and the output is stored as an unsigned integer of 16 bits.

The digitized scientific data is then processed by the Radiometer Electronics Box Assembly (REBA) which runs the LFI on-board software. For each LFI detector, the REBA processes the data in the form of time series which are split into telemetry packets. To satisfy the LFI assigned telemetry budget limit of 53.5 Kbps, the REBA implements 7 acquisition modes (processing types) which reduce the scientific data rate by applying a number of processing steps. The following figure illustrates the main steps of the on-board processing and the corresponding processing types (PTypes).

PType 0

in this mode the REBA just packs the raw data of the selected channel without any processing.

PType 1

consecutive S_{sky}or S_{load}samples are coadded and stored as unsigned integers of 32 bits. The number of consecutive samples to be coadded is specified by the N_{aver}parameter.

PType 2

in this mode, two main processing steps are applied. First, pairs of averaged $S_{sky}$and S_{load}samples, respectively $\overline{S}_{sky}$and $\overline{S}_{load}$, are mixed by applying two different gain modulation factors, GMF1 and GMF2: The operations are performed as floating point operations. Then the two values obtained are requantized, converting them into two 16-bit signed integers:

PType 3

with respect to PType 2, in this mode only a single gain modulation factor is used, GMF1, obtaining:

$$P = \overline{S}_{sky} - \text{GMF1} \cdot \overline{S}_{load}$$

and analogously to PType 2, the value is requantized obtaining a 16-bit signed integer.

PTypes 4, 5, 6

with the processing types PType 4, PType 5 and PType 6, the REBA performs a loss-less adaptive arithmetic compression of the data obtained respectively with the processing types PType 0, PType 2 and PType 3. The compressor takes couples of 16 bit numbers and stores them in the output stream up to the complete filling of the data segment for the packet in process.

A set of REBA processing parameters — N_{aver}, GMF1, GMF2, q and Offset — is selected for each of the 44 LFI channels.They are also included in a teartiary header of each scientific telemetry packet sent to ground. The REBA can acquire data from a channel in two modes at the same time. This capability is used to verify the effect of a certain processing type on the data quality. So, in nominal conditions, the LFI instrument uses PType 5 for all its 44 detectors and every 15 minutes a single detector, in turn, is also processed with PType 1, in order to periodically check the gain modulation factors and the second quantization parameters. The other processing types are mainly used for diagnostic, testing or contingency purposes.

Packets generated by the REBA follow the ESA Packet Telemetry Standard and Packet Telecommand Standard, the CCSDS Packet Telemetry recommendations and the ESA Packet Utilization Standard (PUS). The packet structure for an LFI scientific telemetry packet is shown in the following figure.

From packets to raw TOIs

On a daily basis, the LFI Level 1 software pipeline retrieves the housekeeping and scientific telemetry packets dumped from the satellite on-board memory through the MOC Data Disposition System (DDS). The Level 1 software has to recover most accurately the values of the original (averaged) sky and load samples acquired on-board. Data acquired with PTypes 4, 5 and 6 is first uncompressed. The loss-less compression applied on-board is simply inverted and the number of samples obtained is checked with the value stored in the tertiary header.

The digitized data, processed by the REBA, are not in physical units but in ADU (Analog to Digital Unit). Conversion of $S_{sky}$and S_{load}in Volt requires the Data Source Address (DSA), i.e. the radiometer and detector from which the data are generated, the blanking time (indicized by the Blancking Time Index, BTI), the DGI and the DOI. The DSA and BTI values are recovered from the packet tertiary header, while the DGI and DOI values are recovered from the LFI HK telemetry. Hence, the value in Volt is obtained as:

$$V_i = \frac{S_i \cdot q_{ADC} - Z_{DAE} - 2.5}{G_{DAE}} - O_{DAE} \approx \frac{S_i - \tilde{Z}_{DAE}(\mathrm{DSA}, \mathrm{BTI}, \mathrm{DGI})}{\tilde{G}_{DAE}(\mathrm{DSA}, \mathrm{BTI}, \mathrm{DGI})} - \tilde{O}_{DAE}(\mathrm{DSA}, \mathrm{BTI}, \mathrm{DOI})$$

where $\tilde{G}_{DAE}(\mathrm{DSA}, \mathrm{BTI}, \mathrm{DGI})$, $\tilde{O}_{DAE}(\mathrm{DSA}, \mathrm{BTI}, \mathrm{DOI})$and $\tilde{Z}_{DAE}(\mathrm{DSA}, \mathrm{BTI}, \mathrm{DGI})$are look-up tables estimated during the LFI ground calibration campaign with:

- $\tilde{G}_{DAE}(\mathrm{DSA}, \mathrm{BTI}, \mathrm{DGI}) \approx \frac{G_{DAE}}{q_{ADC}}$,
- $\tilde{O}_{DAE}(\mathrm{DSA}, \mathrm{BTI}, \mathrm{DOI}) \approx O_{DAE}$,
- $\tilde{Z}_{DAE}(\mathrm{DSA}, \mathrm{BTI}, \mathrm{DGI}) \approx \frac{Z_{DAE} + 2.5}{q_{ADC}}$.

This conversion is the only processing required by PTypes 0 and 3 and it is the last step in the processing of all the other processing types. Since PType 1 data is just coadded on-board, the division by $N_{aver}$is performed by the Level 1 software. PType 2 and 5 data have to be dequantized by:

$$P_i = \frac{Q_i}{q} - \mathrm{Offset}$$

and then demixed to obtain $\overline{S}_{sky}$and $\overline{S}_{load}$:

On-board time reconstruction

The On-Board Time (OBT) reconstruction for scientific data has to take into account the phase switch status and the processing type applied on-board. If the phase switch is off, it means that the packet contains consecutive values of either sky or load samples, and the sampling frequency, $f_{sampling}$, is 8192 Hz. Denoting with $i \geq 0$ the sample index within the packet, for PType 0 and 4 we have that:

$$t_i^{obt} = t_0^{obt} + i\frac{1}{f_{sampling}},$$

where t_0^{obt} is the on-board time of the packet (t_{pkt}^{obt}) and $i = 0$ denotes the first sample in the packet. If the switching status is on, either consecutive pairs of (sky, load) samples or (load, sky) samples are stored in the packets. Hence, consecutive couples of samples have the same time stamp and $f_{sampling}$= 4096 Hz.

For averaged data (PTypes 1, 2, 3, 5, 6), the first sample of a scientific packet is the sum (mean) of N_{aver} samples, and the packet time, t_{pkt}^{obt}, is the time of the first of the N_{aver} samples. In this case, t_0^{obt} is computed as:

$$t_0^{obt} = t_{pkt}^{obt} + \frac{N_{aver} - 1}{2}\frac{1}{f_{sampling}}$$

and

$$t_i^{obt} = t_0^{obt} + i\frac{N_{aver}}{f_{sampling}}, \text{for } \; i \geq 1$$

Housekeeping telemetry handling

Some information should be added for the handling of the housekeeping telemetry, using the Mission Information Base (MIB)

Auxiliary data handling

Some information concerning the handling of the Attitude History Files, Time Correlation data and Time Couples, OBT/UTC conversion, Out Of Limit data

TOI processing LFI

Overview

The LFI Level2 Pipeline analyzes each horn of the instrument separately, one pointing period at time, and store results in object the length of an OD. Each diode of the horn is corrected from systematic, differentiated and then combined with its complementary diode in the same radiometer. The horn is then calibrated and the photometric calibration is applied.

Pre-processing

Before the run of the Level2 pipeline and to improve the analysis the Mission information and data sampling divisions are stored in the database.

The Mission information is a set of objects, one for each Operational Day (OD, as defined in REFERENCE??), in which are stored Pointing Period data: DPC pointing ID (where 1 is the first pointing of the nominal mission), PSO pointing ID, start OBT of the pointing maneuver, start OBT of the stable pointing, end OBT of the pointing, spin axis ecliptic longitude and latitude.

The sampling information is a set of objects, one for each LFI frequency, in which are stored for each pointing ID: start OBT of the pointing maneuver, start OBT of the stable pointing, end OBT of the pointing, number of samples of the pointing, number of stable samples of the pointing, start sample of the stable pointing and sample number from the start of the nominal mission. Valid samples and OBTs are defined where any of the radiometers from that frequency cohort contain valid data.

ADC Correction

During analysis it appeared that white noise and calibration seemed affected by something in common. It turn out to be a non linearity in the Analogic/Digital Converter on board. More on P02 and P02a.

Evaluation

The mathematical model represents the digital ADC output as:

$$X = (V - \Delta)\gamma + x_0$$

where V is the voltage input, γ is the DAE gain, Δ is the DAE offset and x_0 is the DAE T_{zero}.

We can model the non-linearity as a function of the input voltage $R(V)$. So we have the apparent inferred voltage V' and we can link it to the actual input voltage with:

$$((V - \Delta)\gamma + x_0)R(V) = X = ((V' - \Delta)\gamma + x_0$$

so that:

$$R(V) = \frac{(V' - \Delta)\gamma + x_0}{(V - \Delta)\gamma + x_0}$$

Since $V >> \Delta$ and $V\gamma >> x_0$ we can use the much simpler relation:

$$R(V) = \frac{V'}{V}$$

and we expect it to be very near to unity for all V.

To find the response curve we have only the apparent voltage to work with, so we had to use the inverse response function $R'(V')$ and replace the real input voltage with T_{sys} times the time varying gain factor $G(t)$.

$$V = V'R'(V') = G(t)T_{sys}$$

If we introduce a small signal on top of T_{sys}which leads to increased detected voltage and corresponding apparent voltage increment:

$$V + \delta V = (V^{'} + \delta V^{'}) = (V^{'} + \delta V^{'})R^{'}(V^{'} + \delta V^{'}) = G(t)(T_{sys} + \delta T)$$

so carrying out the differentiation respect to $V^{'}$to the relation between true and apparent signal voltage leads to:

$$\delta V = \left(V^{'} \frac{dR^{'}(V^{'})}{dV^{'} + R^{'}(V^{'})} \right) \delta V^{'} = G(t)\delta T$$

We now assume $T_{sys}$and $\delta T$are fixed and that the variations are due to slow drifts in the gain. So we can isolate the terms:

$$V^{'} = \frac{G(t)T_{sys}}{R^{'}(V^{'})}$$

$$\delta V^{'} = \frac{G(t)\delta T}{V^{'} \frac{dR^{'}(V^{'})}{dV} + R^{'}(V^{'})}$$

Combining the equations through the gain factor to remove it:

$$\frac{V^{'} R^{'}(V^{'})}{T_{sys}} = \frac{\delta V^{'} \frac{dR^{'}(V^{'})}{dV^{'}} + R^{'}(V^{'})}{\delta T}$$

Rearranging and putting $a = \frac{\delta T}{T_{sys}}$

$$\frac{dR^{'}(V^{'})}{dV^{'}} = \left(\frac{a}{dV^{'}} - \frac{1}{V^{'}} \right) R^{'}(V^{'})$$

So there is the expected direct proportionality of $\delta V^{'}$to $V^{'}$due to the assumption that the variations in voltage are due to overall gain drift, so the amplitude of voltage and signal will vary together. Then there is the additional differential term which will pull signal amplitude away from the linear relationship. So if we plot measured white noise or dipole gain factor against recovered voltage we should see this linear curve with variations due to local slope changes at particular voltages. The linear part can be taken out and the differential part fitted. This was numerically integrated up to get the inverse response curve, what we need to convert the measured voltages to corrected voltages.

Application

For each of the 44 LFI diodes there is the corresponding object in the Database. Each object contains 4 columns: the input voltages coming from the sky channel and the corresponding linearized output, the input voltages coming from the reference channel and the corresponding linearized output.

Data loaded by the module are used to initialize two different interpolators using CSPLINE and the functions from gsl (GNU Scientific Libraries [1]) libraries. The interpolators are then used to correct each sample.

Spikes Removal

Some of the LFI receivers exhibit a small artifact with exactly 1 second repetition, which visible in the power spectra. The effect is a set of spikes at 1 Hz and harmonics. The spurious signal is very well modeled and is removed from the timelines. More information can be found in P02 and P02a.

Modeling

The cause of the spikes at 1 Hz and harmonics is a tiny 1 second square wave embedded in affected channels. The method to estimate the 1 Hz signal is to build a template in time domain synchronized with the spurious signal. The first step is dividing each second of data into time bins using OBT. The number of bins is computed using:

$$nbins = fsamp * template\_resolution$$

where fsamp is the sampling frequency and is 136 at 70 GHz, 80 at 44 GHz and 56 at 30 GHz. Then the bins vector is initialized with time intervals. To avoid aliasing effects template resolution is $\sqrt{3}$. We can write the process adding an index to the time sample: lower index denotes the particular time sample, while the upper index labels the bin into which the sample falls. The linear filter can be written as:

$$s(t_i^j) = a_j \left(1 - \Delta x(t_i^j)\right) + a_{j+1}\Delta x(t_i^j)$$

Here $\Delta x(t_i^j)$is the filter weight which is determined by where within the bin sample lies. If we use $t^j$with only an upper index to denote the start of each bin, then we can write the filter weight as follows:

$$\Delta x(t_i^j) = \frac{t_i^j - t^j}{t^{j+1} - t^j}$$

In other words, the filter weight is the time sample value minus the start of the bin divided by the width of the bin.

We must estimate the parameters $a_j$from the data. With the assumption that the instrument has stable noise properties, we can use a least square algorithm to estimate the bin values:

This can be represented in matrix equation:

$$M_{jk}a_k = b_j$$

with the following definitions:

$$M_{k,k-1} = \sum_i (1 - \Delta x(t_i^{k-1}))\Delta x(t_i^{k-1})$$
$$M_{k,k} = \sum_i (1 - \Delta x(t_i^k))^2 \Delta x(t_i^{k-1})^2$$
$$M_{k,k+1} = \sum_i (1 - \Delta x(t_i^k))\Delta x(t_i^k)$$
$$M_{k,k+n}(|n| > 1) = 0$$
$$b_j = \sum_i d_i^k (1 - \Delta x(t_k^i)) + d_i^{k-1}\Delta x(t_i^{k-1})$$

With these definitions we have to make use of periodic boundary conditions to obtain the correct results, such that if $k = 0, k - 1 = n - 1$and $k = n - 1, k + 1 = 0$. Once this is done, we have a symmetric tridiagonal matrix with additional values at the upper right and lower left corners of the matrix. The matrix is solved with LU decomposition. In order to be certain of the numerical accuracy of the result, we can perform a simple iteration. The solving of the linear system and the iterative improvement of the solution are implemented as suggested in Numerical Recipes.

Application

For each of the 44 LFI diodes there is the corresponding object in the Database. Because of the amplitude of the spikes we choose to apply the correction only on the 44 GHz radiometers. Each object contains 3 columns: the bins start time vector, the sky amplitudes and the reference amplitudes.

For each sample the value to be subtracted is computed using:

$$V = skyAmp_k(1 - \Delta x(t_k)) + skyAmp_{k+1}\Delta x(t_k)$$

where k is the index of the bins at a given time.

Gaps Filling

During the mission some of the data packets were lost (see P02). Moreover in two different and very peculiar situations LFI was shutdown and restarted, giving inconsistencies in data sampling. All of those data aren't used for scientific purpose but to avoid discrepancies in data analysis all of the radiometers at the same frequency must have the same samples.

To accomplish this the length of the data stream to be reduced in a specific pointing period is compared with the data stored in the sample information object. If the length is not the same the OBT vector is filled with missing sample times, the data vector is filled with zeros and in the flag column the bit for gap is raised.

Gain Modulation Factor

The pseudo-correlation design of the LFI radiometers allows a dramatic reduction of $1/f$ noise when the V_{sky} and V_{load} outputs are differenced. The two streams are slightly unbalanced, as one looks at the 2.7 K sky and the other looks at the ~4.5 K reference load. To force the mean of the difference to zero, the load signal is multiplied by the Gain Modulation Factor (R). For each pointing period this factor is computed using:

$$R = \frac{< V_{sky} >}{< V_{load} >}$$

Then the data are differenced using:

This value for R minimizes the 1/f and the white noise in the difference timestream. The i index represents the diode and can be 0 or 1.

At this point the maneuver flag bit is set to identify which samples have missing data, using the information stored in the sampling information object. This identifies which data to ignore in the next step of the Pipeline.

The R values are stored in the database. At the same time the mean values of V_{sky} and V_{load} are stored in order to be used in other steps of the analysis.

Diode Combination

The two complementary diodes of each radiometer are combined. The relative weights of the diodes in the combination are chosen for optimal noise. We assign relative weights to the uncalibrated diode streams based on their first order calibrated noise.

Evaluation

From first order calibration we compute an absolute gain G_0 and G_1, subtract an estimated sky signal and calculate the calibrated white noise σ_0 and σ_1, for the pair of diodes. The weights for the two diodes (i = 0 or 1) are:

$$W_i = \frac{\sigma_i^2}{G_{01}} \frac{1}{\sigma_0^2 + \sigma_1^2}$$

where the weighted calibration constant is given by:

$$G_{01} = \frac{1}{\sigma_0^2 + \sigma_1^2} [G_0 \sigma_1^2 + G_1 \sigma_0^2]$$

The weights are fixed to a single value per diode for the entire dataset. Small variations in the relative noise of the diodes would in principle suggest recalculating the weights on shorter timescales, however, we decided a time varying weight could possibly induce more significant subtle systematics, so chose a single best estimate for the weights for each diode pair.

Horn	Weight M-00	Weight M-01	Weight S-10	Weight S-11
18	0.567304963	0.432695037	0.387168785	0.612831215
19	0.502457723	0.497542277	0.55143474	0.44856526
20	0.523020094	0.476979906	0.476730576	0.523269424
21	0.500324722	0.499675278	0.563712153	0.436287847
22	0.536283158	0.463716842	0.553913461	0.446086539
23	0.508036034	0.491963966	0.36160661	0.63839339
24	0.602269189	0.397730811	0.456037835	0.543962165
25	0.482050606	0.517949394	0.369618239	0.630381761
26	0.593126369	0.406873631	0.424268188	0.575731812
27	0.519877701	0.480122299	0.484831449	0.515168551
28	0.553227696	0.446772304	0.467677355	0.532322645

Application

The weights in the table above are used in the formula:

$$TOI_{diff} = w_0 TOI_{diff0} + w_1 TOI_{diff1}$$

Planet Flagging

Why we flag planets.

Extraction Method

The planets Temperature have been estimated from chunk of samples affected, plus a surrounding region, projected onto a grid (microstripes), by assuming an elliptical Gaussian beam using parameters from instrument database.

Microstripes are a way to extract and store relevant samples for planets detection. Relevant samples are samples affected by the planet plus samples in the neighbor. The search radius to select samples as relevant is 5 deg around the planet position, computed at the pointing period mid time. For each sample we store SCET (Spacecraft Event Time), pointing directions and calibrated temperature. Destriping is applied during application.

Random errors are estimated by taking the variance of samples entering each micromap pixel. This is fast and the major problems (near a bright source the noise gives a larger value and it is difficult to extract the correlation matrix) causes the noise to be overestimated by a factor of two that in this situation is not a major drawback.

The apparent position of Planets as seen from Planck at a given time is derived from JPL Horizon [2]. Position are sampled in tables at steps of 15 minutes and then linearly interpolated at the sampling frequency of each detector. JPL Horizons tables allow also to derive other quantities such as the Planet-Planck distance and the Planet-Sun distance nad the planet angular diameter affecting the apparent brightness of the planet.

The antenna temperature is a function of the dilution factor, according to:

$$T_{ant,obs} = 4log2 T_{ant,1} \left(\frac{\theta}{b_{fwhm}} \right)^2$$

where $T_{ant,obs}$ and $T_{ant,1}$ are the observed and reduced T_{ant}, θ the instantaneous planets angular diameter and b_{fwhm} the beam full width half maximum.

With the above definition $T_{ant,1}$ could be considered as the T_{ant} for a planet with $b_{fwhm} = \theta$, but a more convenient view is to take a Reference Dilution factor D_0, as the dilution factor for a standardized planet angular

diameter and beam fwhm b_{fwhm}, θ_0, to have:

$$D_0 = \left(\frac{\theta_0}{b_0}\right)^2$$

leading to the following definition of a standardized T_{ant}:

$$T_{ant,obs} = 4log2T_{ant,0}\left(\frac{b_{fwhm,0}}{b_{fwhm}}\frac{\theta}{\theta_0}\right)^2$$

with the advantage of removing variations among different detectors and transits while keeping the value of T_{ant} similar to that seen by the instrument and then allowing a prompt comparison of signals and sensitivities.

Application

The OBT vector found by the search are saved in a set of object, one for each horn. In Level2 Pipeline those OBTs are compared with the OBT vector of the data to raise planet bit flag where needed.

Photometric Calibration

Photometric calibration is the procedure used to convert data from volts to kelvin. The source of the calibration is the well known CMB dipole, caused by the motion of the Solar System with respect to the CMB reference frame. To this signal we add the modulation induced by the orbital motion of Planck around the Sun. The resulting signal is then convoluted with the horn beam to get the observed Dipole.

Beam Convolved Dipole

In computing the beam convolved dipole we used an elegant algorithm to save time and computing power. In computing the cosmological dipole signal it is common to assume a pencil-like beam acting as a Dirac delta function. In this case a dipole timeline is defined as:

$$\Delta T_{D,\delta}(t) = \mathbf{P}_E(t) \cdot \mathbf{D}_E$$

where $\mathbf{P}_E(t)$is the pointing direction, in the observer reference frame and $\mathbf{D}_E$is the dipole axis scaled by the dipole amplitude again in the same reference frame.

In general the true signal would have to be convolved with the beam pattern of the given radiometer, usually described as a fixed map in the beam reference frame or as a time dependent map in the observer reference frame. In this case it is easiest to describe the convolution in the beam reference frame, since the function to be convolved is described by a single vector.

Denoting with $\mathcal{U}(t)$the matrix converting from the observer to the beam reference frame, so that:

$$\mathcal{U}(t)\mathbf{P}_E(t) = \mathbf{e}_z$$

the instantaneous dipole direction in the beam reference frame is:

$$\mathbf{D}(t) = \mathcal{U}(t)\mathbf{D}_E$$

By denoting with $\mathbf{P}$a pointing direction in the beam reference frame then:

$$\Delta T_D(t) = N\int_{4\pi} B(\mathbf{P})\mathbf{P}\cdot\mathbf{D}(t)d^3\mathbf{P}$$

where $\mathbf{N}$is a normalization costant.

$$N^{-1} = \int_{4\pi} B(\mathbf{P})d^3\mathbf{P}$$

Denoting with $\mathbf{P}_x$, $\mathbf{P}_y$, $\mathbf{P}_z$the three cartesian components of the $\mathbf{P}$the integral of the dot product can be decomposed into three independent integrals:

$$S_x = N \int_{4\pi} B(\mathbf{P}) P_x d^3\mathbf{P}$$
$$S_y = N \int_{4\pi} B(\mathbf{P}) P_y d^3\mathbf{P}$$
$$S_z = N \int_{4\pi} B(\mathbf{P}) P_z d^3\mathbf{P}$$

those integrals define a time independent vector characteristic of each radiometer and constant over the mission.

Detector ID	S_x	S_y	S_z
LFI18S	1.4105692317321994e-03	-3.7689062388084022e-04	9.9999893412338192e-01
LFI18M	1.1200251268914613e-03	-3.2838598619563524e-04	9.9999931885294768e-01
LFI19S	1.7861136968831050e-03	-4.4036975450455066e-04	9.9999830793473898e-01
LFI19M	1.4292780457919835e-03	-4.7454175238335579e-04	9.9999886598655352e-01
LFI20S	1.7008692096818349e-03	-6.1036624911600191e-04	9.9999836724715374e-01
LFI20M	1.5548897911626446e-03	-5.9289001736737262e-04	9.9999861539862389e-01
LFI21S	1.6975720932854463e-03	6.0961185087824777e-04	9.9999837330986663e-01
LFI21M	1.5486274949897787e-03	5.9228926426513112e-04	9.9999862547220986e-01
LFI22S	1.7861136968831245e-03	4.4036975450366470e-04	9.9999830793473898e-01
LFI22M	1.4292780457920242e-03	4.7454175238250377e-04	9.9999886598655352e-01
LFI23S	1.4105692317321714e-03	3.7689062387997129e-04	9.9999893412338203e-01
LFI23M	1.1200251268914476e-03	3.2838598619481239e-04	9.9999931885294757e-01
LFI24S	3.4636411743209074e-04	-2.8530917087092225e-07	9.9999994001590664e-01
LFI24M	4.3939553230170735e-04	-2.9414231975370517e-07	9.9999990346573508e-01
LFI25S	-1.0428719495964051e-04	1.9328051933678115e-04	9.9999997588341061e-01
LFI25M	-1.1004766833423990e-04	2.7656488668259429e-04	9.9999995570068612e-01
LFI26S	-1.0428719495970346e-04	-1.9328051933760877e-04	9.9999997588341061e-01
LFI26M	-1.1004766833430009e-04	-2.7656488668343130e-04	9.9999995570068612e-01
LFI27S	1.6613273546973915e-03	6.6518363019636186e-04	9.9999839875979735e-01
LFI27M	1.5583345016298123e-03	6.4183510236962536e-04	9.9999857981963269e-01
LFI28S	1.6633788116048607e-03	-6.6629002345089925e-04	9.9999839461297824e-01
LFI28M	1.5571200481047094e-03	-6.4144198187461837e-04	9.9999858196366442e-01

By using this characteristic vector the calculation of the convolved dipole is simply defined by a dot product of the vector $\mathbf{S}$by the dipole axis rotated in the beam reference frame.

$$\Delta T(t) = \mathbf{S}^T \mathcal{U}(t) \mathbf{D}_E$$

Binning

In order to simplify the computation and to reduce the amount of data used in the calibration procedure the data are phase binned in map with Nside 256. During phase binning all the data with flagged for maneuvers, planets, gaps and the ones flagged in Level1 analysis as not recoverable are discharged.

Fit

The first order calibration values are given by a Least Square Fit between the signal and the dipole. For each pointing a gain (g_k) and an offset (b_k) values are computed minimizing:

$$\chi^2 = \sum_{i \in k} \frac{[\Delta V(t_i) - \Delta V_m(t_i|g_k, b_k)]^2}{rms_i^2}$$

The sum includes samples outside a Galactic mask.

Mademoiselle

The largest source of error in the fit arises from unmodeled sky signal $\Delta T_a$from CMB anisotropy. To correct this we iteratively project the calibrated data (without the dipole) onto a map, scan this map to produce a new TOD with astrophysical signal removed, and finally run a simple destriping algorithm to find the corrections to the gain and offset factors.

To reduce the impact of the noise during the iterative procedure the sky estimation is built using data from both radiometers of the same horn.

Smoothing

To improve accuracy given by the iterative algorithm and remove noise from the solution a smoothing algorithm must be performed. We used two different algorithms: OSG for the 44 and 70 GHz radiometers, and DV/V Fix for the 30 GHz. The reasons behind this choice can be found in P02b.

OSG

OSG is a python code that performs smoothing with a 3 step algorithm.

The first step is a Moving Average Window: the gain and offset factors are streams containing one value for each pointing period, that we call dipole fit raw streams. The optimized window has a length of 600 pointing periods.

The second step is a wavelet algorithm, using pywt (Discrete Wavelet Transform in Python [3]) libraries. Both dipole fit raw streams and averaged streams are denoised using wavelets of the Daubechies family extending the signals using symmetric-padding.

The third step is the combination of dipole fit raw and averaged denoised signal using knowledge about the instrument performance during the mission.

4 K total-power and Fix

For the 30 GHz channels we used 4K total-power to track gain changes. The theory and explanation of the choice can be found in P02b.

The algorithm uses V_{load}mean values computed during differentiation and raw gains as they are after iterative calibration, performing a linear weighted fit between the two streams using as weight the dipole variance in single pointing periods. The fit is a single parameter fit, so the offsets are put to zero in this smoothing method. It uses the gsl libraries.

In addition to the smoothing, to better follow sudden gain changes due to instrument configuration changes, a fix algorithm is implemented. The first step is the application of the 4k total-power smoothed gains to the data and the

production of single radiometer maps in the periods between events. The resulting maps are then fit with dipole maps covering the same period of time producing two factor for each radiometer: $corrM$ is the result of the fit using the main radiometer and $corrS$ the one coming from the side radiometer. The correction to be applied to the gain values is then computed as:

$$corr = \frac{1}{1 + \frac{corrM + corrS}{2}}$$

Gain Application

The last step in TOI processing is the creation of the calibrated stream. For each sample we have:

where t is the time and k is the pointing period. $convDip$ is the CMB Dipole convolved with the beam.

References

[1] http://www.gnu.org/software/gsl/
[2] http://ssd.jpl.nasa.gov/?horizons
[3] http://www.pybytes.com/pywavelets/

TOI-Noise LFI

Overview

This pipeline step aims at the reconstruction of the noise parameters from calibrated flight TOI. The goal is two-folds: one the one side we need to know the actual noise properties of our instrument in order to properly take them into account especially during the following processing and analysis steps like map-making and power spectrum estimation. On the other side evaluation of noise properties along the instrument life-time is a way to track down possible variations, anomalies and general deviations from the expected behaviour.

Operations

Noise estimation is performed on calibrated data and since we would like to track possible noise variations along mission life-time, we select data in chunks of 5 ODs (Operational Days). These data are processed by the ROMA Iterative Generalized Least Square (IGLS) map-making algorithm which includes a noise estimation tool. In general an IGLS map-making is a quite consuming in terms of time and resources required. However the length of the data is such that running on the DPC cluster in very short time (~1-2 minutes).

The method implemented can be summerized as follows. We model the calibrated TOI as

$$\mathbf{\Delta T} = \mathbf{P} \mathbf{m} + \mathbf{n}$$

where $\mathbf{n}$ is the noise vector and $\mathbf{P}$ is the pointing matrix that links a pixel in the map $\mathbf{m}$ with a sample in the TOI $\mathbf{d}$. The zero-th order estimation of the signal is obtained simply rebinning TOI into a map. Then an iterative approach follows in which both signal and noise are estimated according to

$$\mathbf{\hat{n}_i} = \mathbf{\Delta T} - \mathbf{P\hat{m}_i}$$

$$\mathbf{\hat{m}_{i+1}} = \mathbf{(P^T\hat{N}_i^{-1}P)^{-1}P^T\hat{N}_i^{-1}\Delta T}$$

where $\mathbf{\hat{N}_i}$ is the noise covariance matrix in time domain out from iteration i. After three iterations convergence is achieved.

We then perform an FFT (Fast Fourier Transform) on the noise time stream out from the iterative approach and then fit the resulting spectrum.

Fitting Pipeline

In the very first release of Planck data, once noise spectra were extracted a simply log-periodogram fitting approach was applied to derive the most important noise parameters (white noise level, knee-frequency and slope of the low-frequency noise component). However during mission life-time there were some specific events (e.g. the switch over of the sorption coolers) that we expect were able to cause variation in instrument behaviour and hence in its noise properties. In this respect we have improved our fitting pipeline adding a Monte Carlo Markov Chain approach to estimate noise parameters.

MCMC approach

This new approach allows us to improve our noise model. Indeed this can be parametrized by the usual combination of white plus $1/f$ noise

$$P(f) = \sigma^2 \left[1 + \left(\frac{f}{f_k}\right)^{\beta}\right]$$

with three basic noise parameters. However it is also possible to work with a functional form with two more parameters as

$$P(f) = \sigma^2 \left[1 + \left(\frac{f}{f_{k1}}\right)^{\beta_1} + \left(\frac{f}{f_{k2}}\right)^{\beta_2}\right]$$

This latter could be useful when there are clearly two different behaviour in the low-frequency part of the spectrum where, beside usual radiometric $1/f$ noise, appears signature of thermal fluctuations induced noise.

As for the white noise part, this is, as before, computed making a simple average of noise spectrum on the last 10% of frequency bins. This percentage works well for almost all radiometers at 44 and 70 GHz but it is indeed quite delicate for the 30 GHz radiometers which show typical values of knee-frequency around 100 mHz and, therefore, require a smaller number to get an un-biased white noise estimation. Once white noise is computed, the code creates Markov Chains for the other parameters. Discarding the burn-in period of the chains we can directly get from the chain samples distribution, the expected value and variance of each noise parameters sampled.

The left panel of the following Figure shows a typical spectrum at 70 GHz with superimposed the simple log-periodogram fit (purple line) and the new MCMC derived spectrum (blue line). The right panel instead shows distribution for knee-frequency and slope derived from the example spectrum.

The final noise parameters

As already reported we know that during the nominal operations there was a quite dramatic change in LFI induced by the switch over of the two sorption coolers and particularly we expect to see the effect of degradation of the performance of the first sorption cooler and the onset of the redundant one.

In the following figure we report a set of noise frequency spectra for three LFI radiometers (LFI28M, LFI24S and LFI18M) from the beginning of the operation till the time of the current data release. Some comments are in order. First of all the white noise level is extremely stable in all the three cases (but this is also true for all the LFI radiometer). Also knee-frequency and low-frequency slope are quite stable till OD 326. After that period spectra show a noise increase and two slopes for the low-frequency part which become more evident for spectra around OD 366 and OD 466 where the first cooler starts to be less effective and produces low-frequency thermal noise. After the switch-over to the redundant cooler data still present (the very last spectrum) thermal noise at very low-frequency. This behaviour is almost present in all radiometers with different trends ranging from the small effect shown by LFI24S to more prominent effect as shown by LFI28M and LFI18M.

Pointing LFI

Detector Pointing

Detector pointing reconstruction requires knowledge of the spacecraft attitude and the location of the horns in the focal plane. The AHF (Attitude History File REFERENCE??) gives the orientation of the spacecraft spin axis in quaternions sampled at 8 Hz, as well as the beginning and the end times for each pointing period.

The computation needs to initialize the horn and beam information: it reads the θ, $\phi$and ψposition and rotation angles from the instrument database and builds the rotation matrix from the spin axis to the focal plane ($ax2det$). At the same time the major corrections are initialized.

Wobble Angle

Wobble angles are the angles which defines the relationship between the Principal Axis Reference Frame of Planck and the Body Reference Frame of Planck, both of which have their origin in the Planck Baricenter (ACMS, AHF-ICD).

Pointings are determined by a set of rotations converting coordinates in the STR reference frame to ecliptical reference frame, i.e. defining the rotation matrix $R_{ecl,str}$. The matrix can be decomposend in a sequence of matrix mutiplications:

$$R_{ecl,str} = R_{ecl,A} R_{A,B} R_{B,str}$$

here we used $R_{rfb,rfa}$to denote transformation from Rerference Frame RFA to Reference Frame RFB, and $R_{rfa,rfb} = R^{-1}_{rfb,rfa}$.

The $R_{B,str}$converts from STR coordinates to Body Reference Frame coordinates, it is a constant matrix.

$$\begin{bmatrix} \cos\beta & 0 & -\sin\beta \\ 0 & 1 & 0 \\ \sin\beta & 0 & \cos\beta \end{bmatrix}$$

where $\beta = 85deg$is the STR boresight angle assumed to be constant and aligned with the telescope LOS, but this is not the case. The STR is located on the SVM, at about 1.5 m from the origin of the Body reference frame, a change in its position of 0.15 mm will result in a change of its orientation of about 10^{-4}radiants about 20 arcsec.

There is no way to measure directly those changes. So the effect is that to have an apparent change in the ψ_1, ψ_2 (tilt angles as defined in the AHF) and ψ_3(azimuth angle as defined in the AHF) angles: the reason is apparent immediately when looking at the way a perturbation in STR reference frame orientation propagates.

AHF provides wobble angle measures at 1 minute (ψ_1, ψ_2) and one OD (ψ_3) rate. Indeed $\psi_3$is provided at each pointing period but measures within each given OD are constant.

Assuming to have quaternions represented by rotation matrix $R_{ecl,B}(t)$at a time t, and assuming to have representative values of true wobble angles $\psi_{1,0}$, $\psi_{2,0}$, $\psi_{3,0}$and a way to estimate the apparent $\delta\psi_1(t)$, $\delta\psi_2(t)$, $\delta\psi_3(t)$it is possible to remove the apparent effect.

With the available information it can be done for $\psi_1$and ψ_2.

The correction algorithm initializes two rotation matrices as references using $\psi_1$and $\psi_2$from the first pointing period of the nominal mission:

$$R_{psi1} = \begin{bmatrix} \cos\psi_{1,ref} & \sin\psi_{1,ref} & 0 \\ -\sin\psi_{1,ref} & \cos\psi_{1,ref} & 0 \\ 0 & 0 & 1 \end{bmatrix}$$

$$R_{psi2} = \begin{bmatrix} \cos\psi_{2,ref} & 0 & -\sin\psi_{2,ref} \\ 0 & 1 & 0 \\ \sin\psi_{2,ref} & 0 & \cos\psi_{2,ref} \end{bmatrix}$$

Then, for each pointing period, builds two correction matrices using $\psi_1$and $\psi_2$as provided by the AHF in the Observation section:

$$R^T_{psi1} = \begin{bmatrix} \cos\psi_1 & -\sin\psi_1 & 0 \\ \sin\psi_1 & \cos\psi_1 & 0 \\ 0 & 0 & 1 \end{bmatrix}$$

$$R^T_{psi2} = \begin{bmatrix} \cos\psi_2 & 0 & \sin\psi_2 \\ 0 & 1 & 0 \\ -\sin\psi_2 & 0 & \cos\psi_2 \end{bmatrix}$$

From these matrices the correction matrix is build:

$$R = R^T_{psi1} R^T_{psi2} R_{psi2} R_{psi1}$$

Each quaternion of the AHF is finally corrected using R.

Stellar Aberration

The corrected quaternions are interpolated using Spherical Linear Interpolation algorithm and transformed in cartesian vector, which we call DPT. For each sample the stellar aberration correction is applied:

$$DPT = DPT - \frac{v_{sat}}{c}$$

where $v_{sat}$is the satellite velocity and $c$is the speed of light. After this operation the vector is normalized.

Finally the cartesian vetor is converted in Ecliptic Coordinates, the detector pointing.

Beam Rotation

The rotation of the beam with respect the north direction is the ψangle and is computed rotating the corrected quaternions Qusing:

$$R = R_\theta R_\phi Qax2det$$

The resulting rotation matrix represents the rotation of the beam, the \psi angle is then:

$$\psi = -\arctan(R[0][1], R[0][0])$$

Beams LFI

Wish List

list of information to be inserted in the explanatory supplements

- Description of LFI FOV.

- Description of various telescope models as reported in the beam paper.

- Format of beam data

- Definition of various coordinate frames for beams

Overview

LFI is observing the sky with 11 pairs of beams associated with the 22 pseudo-correlation radiometers. Each beam of the radiometer pair (Radiometer Chain Assembly - RCA) is named as LFIXXM or LFIXXS. XX is the RCA number ranging from 18 to 28; M and S are the two polarization namely main-arm and side-arm of the Orthomode transduccers #darcangelo2009b.

Main Beams and Focal Plane calibration

As the focal plane calibration we refer to the determination of the beam pointing parameters in the nominal Line of Sight (LOS) frame through main beam measurments using Jupiter transits. the parametes that characterise the beam pointing are the following:

- THETA_UV (θ_{uv})
- PHI_UV (ϕ_{uv})

They are calculated starting from u,v coordinates derived form the beam reconstruction algorithm as

$\theta_{uv} = \arcsin(u^2+v^2)$

$\phi_{uv} = \arctan(v/u)$

Three additional angles are used to characterize the beams in the RIMO:

- TILT
- PSI_UV (ψ_{uv})
- PSI_POL (ψ_{pol})

the Tilt angle is the angle between the major axis of the gaussian fitting and the U-axis **CHECK THIS**

ψ_{uv} and ψ_{pol} are **not** derived from measurements but they are extimated form **optical simulations**. They are the quantities that represent the polarization direction of each beam, in the following approximation: **the M- and S- beams of the same RCA point at the same direction on the sky**

Effective beams

TBW

Window Functions

TBW

Sidelobes

There is no direct measurements of sidelobes for LFI. The sidelobe pattern is estimated by simulations taking into account the geometry of the telescope and the satellite structure. In figure

References

<biblio force=false>

1. References

</biblio>

Map-making LFI

Map-making

The input of the map-making step consists of the calibrated timelines, along with the corresponding pointing information. The main output consists of temperature and polarization maps. An important part of the map-making step is the removal of correlated 1/f noise.

LFI maps were constructed with the Madam map-making code, version 3.7.4. The code is based on generalized destriping technique, where the correlated noise component is modeled as a sequence of constant offset, "baselines". The baseline solution is constrained by a noise filter. As auxiliary information the code produces a hit count map and a white noise covariance matrix. No beam information is used, but the signal is assigned to the pixel where the center of the beam falls.

In the first release the chosen baseline length was one second. This gives a good noise removal, without being computationally heavy. The noise filter was built according to the noise parameters listed in Table XX.

Flagged samples were excluded from the analysis. The galaxy region was masked out in the destriping phase, to redúce error arising from strong signal gradients. Radiometers were combined according to the horn-uniform weighting scheme to minimize systematics. The polarization component was included in the analysis, although only the temperature maps are released. A detailed description of the map-making procedure is given in … (LFI processing paper, map-making section).

The maps are in Healpix format, at resolution nside=1024, in nested pixeling scheme. Unobserved pixels are marked by a special value.

The released maps are in galactic coordinates. The conversion from ecliptic to galactic coordinate system is described by rotation matrix

```
( -0.054882486,  0.494116468, -0.867661702,
  -0.993821033, -0.110993846, -0.000346354,
  -0.096476249,  0.86228144,   0.497154957 )
```

The conversion was applied to the input pointing data, prior to the construction of the map.

Table XX:

For each LFI radiometer, list

-white noise sigma

-knee frequency

-slope

-min frequency

-horn-uniform weight

Caption: noise parameters used in the construction of the noise filter, and the radiometer weights.

Low-resolution maps and Noise Covariance Matrices

To fully exploit the information contained in the large scale structure of the microwave sky, a pixel-pixel covariances are needed in the maximum likelihood estimation of the CMB power spectrum. However, full covariance matrices are impossible to employ at the native map resolution due to resource limitations. A low-resolution dataset is therefore required at the low-l analysis. This dataset consists of low-resolution maps, and descriptions of residual noise present in those maps given by pixel-pixel noise covariance matrices (NCVMs).

The low-resolution dataset can currently be utilized efficiently only at resolution $N_{\textrm side} = 16$, or lower. All the low-resolution data products are produced at this target resolution.

Low Resolution Maps

Number of different schemes to obtain the low resolution maps are discussed in #keskitalo2009. We chose to downgrade the maps using the inverse noise weighting. See #for discussion.

Inputs

We took the high resolution maps described in LFI-Map-making and the corresponding 3×3 matrices as an input for this analysis step.

Production

The high resolution maps were downgraded to $N_\mathrm{side} = 16$ using inverse noise weights (given by the 3×3 matrices), and subsequently the temperature part was smoothed with a symmetric Gaussian beam with $\mbox{FWHM} = 440\,\mbox{arcmin}$.

Noise Covariance Matrices

The statistical description of the residual noise in the maps is given in the form of a pixel-to-pixel noise covariance matrix (NCVM), as described in #keskitalo2009.

Inputs

The noise model was given in the form of the three noise parameters: white noise level σ, slope, and knee frequency f_{knee}. We actually used three sets of noise parameters one for the entire mission (nominal mission), and one per each sky survey (SS1 and SS2).

We used the same pointing as in the noise Monte Carlo simulations. See the description in Noise Monte Carlo simulations.

We used the gap files produced during the making of the flight maps to leave out samples that were flagged bad for various reasons.

Production

The output of the NCVM module of Madam map-maker are inverse NCVMs. Since the inverse matrices are additive, we divided the computations into a number of small chucks to save computational resources. Therefore we firstly calculated one inverse NCVM per radiometer per survey at resolution $N_\mathrm{side}=32$, and secondly combined the individual inverse matrices to form the actual inverse matrices. The map-making parameters were almost identical to the standard map-making runs. The differing parameter values are listed below:

```
- Baseline lengths were 0.25 s/ 8 samples, 0.50 s/ 24 samples, and 0.50 s/39 samples for 30 GHz, 44 GHz, and 70GHz, respectively.
```

- The calculations were performed at resolution $N_\mathrm{side} = 32$.

- No destriping mask was applied.

- The horns were weighted optimally.

To get the noise covariance from its inverse, the matrices are inverted using the eigen decomposition of a matrix. The monopole of the temperature map cannot be resolved by the map-maker, and thus the matrix becomes singular. The ill-determined mode is left out of the analysis.

Having calculated the eigen decomposition in the previous step, we can apply the same linear operators to modify the eigenvectors as was applied to the high resolution maps while downgrading them. The eigenvectors are downgraded to $N_\mathrm{side} = 16$ using inverse noise weights, and subsequently the temperature part is smoothed with a symmetric Gaussian beam with $\mbox{FWHM} = 440\,\mbox{arcmin}$.

The final matrices are then recomposed from the original eigenvalues and modified eigenvectors.

The low resolution noise covariance matrices

- are in C binary format files.

- are organized in block form,

```
$$
\left (\begin{matrix}
 II & IQ & IU \\
 QI & QQ & QU \\
 UI & UQ & UU
 \end{matrix} \right).
$$
```

- are in HEALPix nested pixelisation scheme. Resolution is $N_\mathrm{side} = 16$, and thus there are $N_\mathrm{pix} = 3072$ pixels.

- are in Galactic coordinates.

- have units $\mathrm{K}_{\mathrm{CMB}}$.

- uncovered pixels are marked with

- T-only?

- number of files

Half-ring jackknife Noise Maps

Overview

In order to estimate the noise directly at the map level and in the angular power spectra, we divided the time-ordered data into two halves and produced half-ring jackknife maps as described in Planck First Results: II. The Low Frequency Instrument performance and data processing.

Briefly: Instead of using the full time ordered data as described above, we produced two sets of maps using either only the first half of each pointing period (map named $\mathbf{j_1}$ below) or only the second half of each pointing period (map named $\mathbf{j_2}$). At each pixel p, these half-ring jackknife maps $\mathbf{j_1}$ and $\mathbf{j_2}$ contain the same sky signal, since they result from the same scanning pattern on the sky. However, because of instrumental noise, the maps $\mathbf{j_1}$ and $\mathbf{j_2}$ are not identical.

We estimated the noise level in each map $\mathbf{m}$ made using the full(ring) data, by constructing a half-ring difference map

$\mathbf{n_{m}}(p) = [\mathbf{j_1}(p) - \mathbf{j_2}(p)] \ / \ \mathbf{w_{\rm hit}}(p)\,,$

with weights

$\mathbf{w_{hit}}(p) = \sqrt{ \mathbf{hit_{full}}(p) \left[\frac{1}{\mathbf{hit_1}(p)} +

```
      \frac{1}{\mathbf{hit_2}(p)} \right]}\,$.
```

Here $\mathbf{hit_{full}}(p) = \mathbf{hit_1}(p) + \mathbf{hit_2}(p)$ is the hit count at pixel p in the full map $\mathbf{m}$, while $\mathbf{hit_1}$ and $\mathbf{hit_2}$ are the hit counts of $\mathbf{j_1}$ and $\mathbf{j_2}$, respectively. The weight factor $\mathbf{w_{hit}}(p)$ is equal to 2 only in those pixels where $\mathbf{hit_1}(p) = \mathbf{hit_2}(p)$. In a typical pixel, $\mathbf{hit_1}(p)$ will differ slightly from $\mathbf{hit_2}(p)$ and hence the weight factor is $\mathbf{w_{hit}}(p) > 2$.

The half-ring difference maps $\mathbf{n_{m}}$ are the most direct measure of the noise in the actual maps. The other noise estimates (NCVM and noise Monte Carlo) rely on specific modelling of the noise and this modelling can be validated by comparing to the half-ring difference maps. However, the half-ring difference maps can only capture the noise that varies faster than half of the duration of the pointing period, i.e., the noise whose frequency is $f \gtrsim 2/20\,\mbox{min} = 1.7\,$mHz.

We calculated the noise maps $\mathbf{n_{m}}$, from half-ring jackknife maps for temperature (I) and polarization (Q and U) and as a first quality check of the maps (and as one of the tests of the whole data processing pipeline up to the maps) tested both numerically and visually that these noise maps divided pixel-by-pixel by square root of the white noise covariance maps were approximately Gaussian with variance near to unity. Temperature noise maps for the nominal survey and for the first and second sky surveys are shown in the next subsection. Further we calculated from the noise maps the temperature and polarization (E and B mode) auto-correlation and cross-correlation noise angular power spectra by anafast and compared to these the results from the white noise covariance matrices and from the noise Monte Carlo simulations. A similar comparison was made between downgraded half-ring noise maps, downgraded noise Monte Carlo maps and the low resolution noise covariance maps. Detailed results are presented in the Systematic Effects paper.

Examples of Half-ring Difference Maps and Noise Angular Power Spectra

Hit Count Weighted Half-ring Difference Maps

Here we show some hitcount weighted half-ring difference maps, i.e., noise maps for temperature. The columns are for different LFI frequencies: 30, 44, and 70 GHz. The rows are the nominal survey (a bit more than 1 year of observations), survey 1 (the first sky survey, approx first half a year of observations) and survey 2 (the second sky survey, approx the second half a year of observations). Some features are visible in particular in the galactic plane. These are due to "gradient leakage". (In regions where the gradient in the sky signal is very large even a tiny difference in the pointing of the first and second half of each pointing period causes the signal to "leak" to the half-ring difference map. In practice this is not a problem for noise estimation, since these regions - the galaxy, orion, crab nebula, etc - will be masked in the cosmology analysis.

Half-ring difference maps calculated at the native nside 1024 resolution. Columns: frequency (30, 44, 70 GHz), rows: sky survey (nominal, survey_1, survey_2).

Half-ring difference maps (the same as above, but) **smoothed** with 60 arcmin fwhm Gaussian. Columns: frequency (30, 44, 70 GHz), rows: sky survey (nominal, survey_1, survey_2).

Hit Count Weighted Half-ring Difference Maps Normalized by sqrt of white noise variance at each pixel

Now we show the same as above, but divided by the square root of the estimate of white noise variance in each pixel. These normalized noise maps should be approximately Gaussian with a unit variance (at the native resolution), apart from some stripes that are due to correlated (non-Gaussian) 1/f noise. The large-scale 1/f noise is more apparent in the smoothed version of the figure that follows after the native resolution version.

Normalized Half-ring difference maps calculated at the native nside 1024 resolution. Columns: frequency (30, 44, 70 GHz), rows: sky survey (nominal, survey_1, survey_2).

Normalized Half-ring difference maps (the same as above, but) **smoothed** with 60 arcmin fwhm Gaussian. Columns: frequency (30, 44, 70 GHz), rows: sky survey (nominal, survey_1, survey_2).

Noise Anglular Power Spectra from Half-ring Difference Maps

The noise angular power spectra calculated by anafast from half-ring difference temperature maps and normalized by the sky coverage to estimate the noise level if there was a full sky coverage in order to make a comparison of different surveys easier. Columns: frequency (30, 44, 70 GHz). Colors: black = nominal, red = survey_1, blue = survey_2.

Comparison of Noise Calculated from Half-ring Difference and from Other Noise Estimates

Here we compare noise angular power spectra estimated from half-ring difference maps (RED) to the estimate from white noise covariance maps (BLUE) and the full noise Monte Carlo simulations (BLACK, top curve 16% quantile, middle curve 50% quantile, i.e., median, and bottom curve 84% quantile) - see the next section for the details of noise Monte Carlo.

Nominal survey:

Survey_1:

Survey_2:

High-ell average (l=1150..1800) noise relative to the white noise estimate

The same as previous figures, but the noise comparison made from the high ell tails off the angular power spectra where the white noise dominates. We have taken the average of C_l from the multipoles between 1150 and 1800, and subtracted the white noise estimate. Half-ring difference noise estimate is RED, the full noise Monte Carlo estimate is BLACK, and the white noise estimate from noise Monte Carlo is GREEN. The white noise estimate from the white noise covariance map (WNC), BLUE, has been subtracted from all the results.

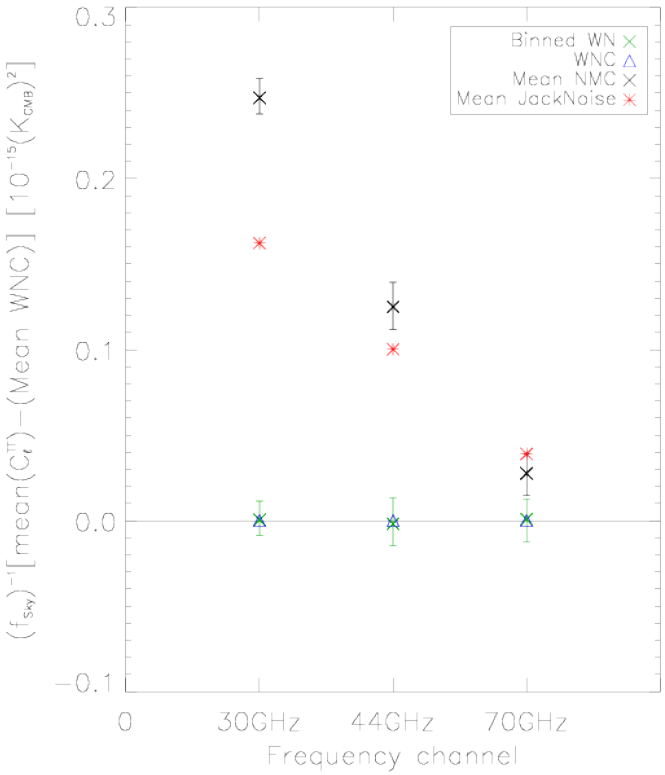

Nominal survey:

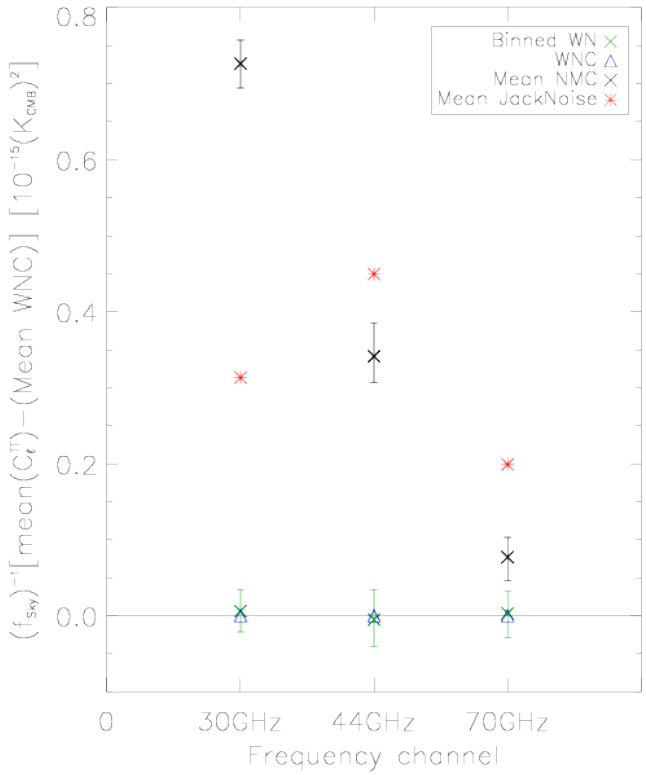

Survey_1:

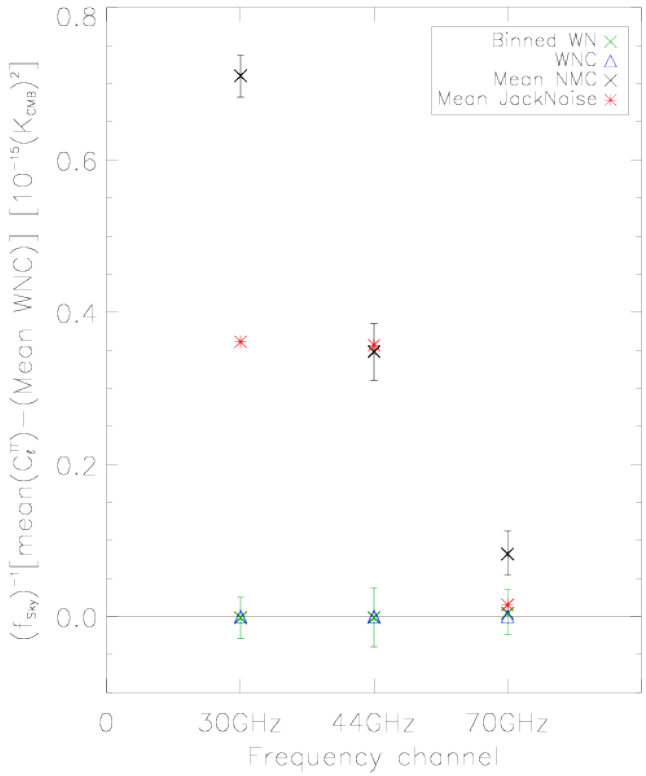

Survey_2:

Noise Monte Carlo Simulation

Overview

Calculating and handling full pixel-to-pixel noise covariance matrices for Planck maps if feasible only at low resolution. To support the analysis of high-resolution maps, a Monte Carlo set of noise maps were produced. These maps were produced from noise timelines using the same map-making procedure as for the flight data. In the noise Monte Carlo it was possible to follow exactly the map-making procedure used for the flight maps, whereas for the calculation of noise covariance matrices some approximations had to be made. Such noise Monte Carlos were produced at two levels of the analysis: 1) LFI Monte Carlo (MC) as part of the LFI data processing, and 2) Full Focal Plane (FFP) Monte Carlo as part of the joint HFI/LFI data processing. This page describes the LFI noise MC. For the FFP MC, see HL-sims.

Inputs

The noise MC uses a three-parameter (white noise level (σ), slope, and knee frequency (f_knee)) noise model, where the noise consists of white noise and correlated ($1/f$) noise and the latter has a power spectrum

$$ P(f) = \frac{2\sigma^2}{f_\mathrm{sample}}\left(\frac{f}{f_\mathrm{knee}}\right)^\mathrm{slope} $$.

Here f_sample is the sampling frequency of the instrument. The noise parameters were determined separately for each radiometer as described in TOI-Noise LFI, assuming they stayed constant over the mission.

The detector pointing was reconstructed from satellite pointing, focal-plane geometry, pointing correction (tilt angle), and sample timing, using Level-S simulation software. The same pointing solution (two focal planes) was used as for the LFI flight maps. Due to numerical accuracy, the detector pointing in the noise MC was not exactly the same as for the flight maps, but some data samples (of the order of one in a thousand) whose pointing was near the pixel boundary ended up assigned to the neighboring pixel. During the map-making from the flight data, a gap file was produced to represent the samples that were omitted from map-making due to various flags. This gap file was used in the noise MC instead of the full set of flags. The flight map-making used a destriping mask to exclude regions of strong signal gradients from contributing to the noise baseline solution. These same destriping masks (one for each frequency channel) were used for the noise MC.

Production

The noise was generated internally in the Madam map-making code using a Stochastic Differential Equation (SDE) method, to avoid time-consuming writing and reading noise timelines to/from disk. Noise for each pointing period was generated separately, using a double-precision random number seed constructed from the realization number, radiometer number, and the pointing period number; to allow regeneration of the same noise realization when needed. White noise and $1/f$ noise were generated separately.

The same map-making code (Madam) with the same parameter settings was used for the noise MC as for the flight maps. In addition to the destriped maps from the full noise (output maps), also binned maps from just the white noise (binned white noise maps) were produced; they represent the white noise part of the output maps. The difference between these two maps represent the residual correlated noise in the output map. The maps were made at Healpix resolution $N_\mathrm{side} = 1024$. For low-resolution analysis, these maps were downgraded (and the temperature part was smoothed) to $N_\mathrm{side} = 32$ and $N_\mathrm{side} = 16$.

When the noise MC for the first Planck data release was performed, calibrated data for five sky surveys were available. In addition to frequency maps for the nominal survey and the full survey (all five sky surveys), single-survey and 70 GHz horn-pair maps were produced in the noise MC, resulting in 27 different cases of LFI maps, a subset of the map cases produced from the flight data. For each case 102--1026 realizations were produced.

Usage

These noise Monte Carlo maps were used for a number of things in LFI data analysis. They were compared to the low-resolution noise covariance matrices, generated for the same noise model to see the impact of the approximations in the noise covariance matrix calculation. They were compared to the half-ring noise maps to see how well the noise model matches the noise in the flight maps (noting, however, that the half-ring noise maps misrepresent the lowest noise frequencies in the flight maps, and contain some effects from the sky signal). They were also used in power spectrum estimation and non-Gaussianity estimation.

Examples

As an example, we show below images of the first realization of the 70 GHz frequency map noise for the nominal survey. The images are in order: destriped full noise, binned white noise, residual correlated noise. Note that it is difficult to see any difference between the first too images, since the residual correlated noise is more than an order of magnitude below the white noise level. The units are CMB K.

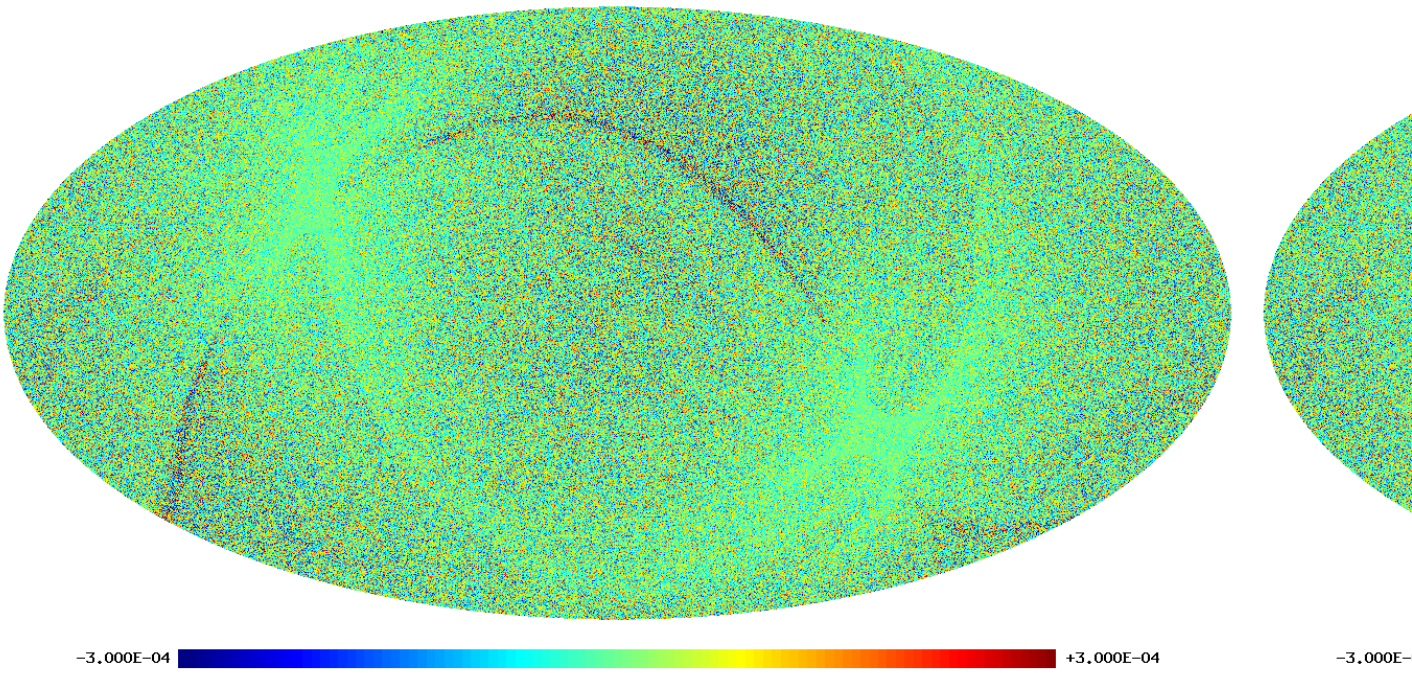

The following two images show the statistics of the angular power spectra of 101 realizations of the 70 GHz frequency map noise for the nominal survey. The thick black line shows the median C_ℓ, and the green line the mean C_ℓ. Thin black lines show the minimum, 16% quantile, 84% quantile, and the maximum C_ℓ. The red line is the 102nd realization. The first plot is for the full noise in the output map, the second plot is for the residual correlated noise.

The Bibliography

<biblio force=false>

1. References

</biblio>

LFI systematic effect uncertainties

Overview

TBW

LFI-Validation

Overview

Data validation is a step of paramount importance in the complex process of data analysis and the extraction of the final scientific goals of an experiment. The LFI approach to data validation is based upon null-tests approach and here we present the rationale behind envisaged/performed null-tests and the actual results for the present data release. Also we will provide results of the same kind of tests performed on previous release to show the overall improvements in the data quality.

Null-tests approach

In general null-tests are performed in order to highlight possible issues in the data related to instrumental systematic effect not properly accounted for within the processing pipeline and related to known events of the operational conditions (e.g. switch-over of the sorption coolers) or to intrinsic instrument properties coupled with sky signal like stray-light contamination.

Such null-tests are expected to be performed considering data on different time scales ranging from 1-minute to one year of observations, at different unit level (radiometer, horn, horn-pair, within frequency and cross-frequency both in total intensity and, when applicable, to polarisation.

This is quite demanding in terms of all possible combinations. In addition some tools are already available and can be properly used for this kind of analysis. However it may be possible that on some specific time-scale, detailed tools have to be developed in order to produce the desired null-test results. In this respect the actual half-ring jack-knives are suitable to track any effects on pointing period times scales. On time-scales between half-ring and survey there are lot of possibilities. It has to be verified if the actual code producing half-ring jack-knives (madam) can handle data producing jack-knives of larger (e.g. 1 hour) times scales.

It is fundamental that such test have to be performed on DPC data product with clear and identified properties (e.g. single R, DV/V single fit, etc.) in order to avoid any possible mis-understanding due to usage of non homogeneous data sets.

Many of the null-tests proposed are done at map level with sometime compression of their statistical information into an angular power spectrum. However together with full-sky maps it is interesting to have a closer look on some specific sources. I would be important to compare fluxes from both polarized and un-polarized point sources with different radiometers in order to asses possible calibration mis-match and/or polarization leakage issues. Such comparison will also possibly indicate problems related to channel central frequencies. The proposed set of sources would be: M42, Tau A, Cas A and Cyg A. However other H{\sc II} regions like Perseus are valuable. One can compare directly their fluxes from different sky surveys and/or the flux of the difference map and how this is consistent with instrumental noise.

Which kind of effect is probed with a null-test on a specific time scale? Here it is a simple list. At survey time scale it is possible to underlying any side-lobes effects, while on time scales of full-mission, it is possible to have an indication of calibration problems when observing the sky with the same S/C orientation. Differences at this time

scale between horns at the same frequency may also reveal central frequency and beam issues.

Total Intensity Null Tests

In order to highlight different issues, several time scales and data combinations are considered. The following table is a sort of null-test matrix to be filled with test results. It should be important to try to set a sort of pass/fail criteria for each of the tests and to be prepared to detailed actions in order to avoid and correct any failure of the tests. To assess the results an idea could be to proceed as in the nominal pipeline $i.e.$ to compare the angular power spectra of null test maps with a fiducial angular power spectrum of a white noise map. This could be made automatic and, in case the test does not pass then a more thorough investigation could be performed. This will provide an overall indication of the residuals. However structures in the residual are important as well as the overall average level and visual inspection of the data is therefore fundamental.

Concerning null-tests on various time scales a comment is in order. At large time scales (i.e. of the order of a survey or more) it is clear that the basic data set will be made of the single survey maps at radiometer/horn/frequency level that will be properly combined to obtain the null-test under consideration. For example at 6 months time scale we will analysis maps of the difference between different surveys for the radiometer/horn/frequency under test. On the other hand at 12 months time scale we will combine surveys 1 and 2 together to be compared with the same combination for surveys 3 and 4. At full-mission time scale, the analysis it is not always possible e.g. at radiometer level we have only one full-mission data set. However it would be interesting to combine odd surveys together and compare them with even surveys again combined together. On shorter time scales (i.e. less than a survey) the data products to be considered are different and will be the output of the jack-knives code when different time scales are considered: the usual half-ring JK on pointing period time scale and the new, if possible, jack-knives on 1 minute time scale. Therefore null-tests will use both surveys/full-mission maps as well as tailored jack-knives maps.

The following table reports our total intensity null-tests matrix with a $\checkmark$ where tests are possible.

Data Set	1minute	1 hour	Survey	Full Mission
Radiometer (M/S)	$\checkmark$	$\checkmark$	$\checkmark$	$\checkmark$
Horn (M+S)	$\checkmark$	$\checkmark$	$\checkmark$	$\checkmark$
Horn Pair^1			$\checkmark$	$\checkmark$
Frequency	$\checkmark$	$\checkmark$	$\checkmark$	$\checkmark$
Cross-Frequency			$\checkmark$	$\checkmark$

^{1} this is (M+S)/2 and differences are between couple of horns (e.g. (28M+28S)/2- (27M+27S)/2)

Polarisation Null Tests

The same arguments applies also for polarization analysis with only some differences regarding the possible combination producing polarized data. Radiometer will not be available, instead of sum between M and S radiometer we will consider their difference.

Data Set	1minute	1 hour	Survey	Full Mission
Horn (M-S)	$\checkmark$	$\checkmark$	$\checkmark$	$\checkmark$
Horn Pair^1			$\checkmark$	$\checkmark$
Frequency	$\checkmark$	$\checkmark$	$\checkmark$	$\checkmark$
Cross-Frequency			$\checkmark$	$\checkmark$

^{1} this is difference between couple of horns (e.g. (28M-28S)/2- (27M-27S)/2)

Practical Considerations

For practical purposed and visual inspection of the null-tests results it would be useful to produce results smoothed at 3° (and at 10° for highlight larger angular scales) for all the total intensity maps. For polarization, as we already did several times when comparing to $WMAP$ data, a downgrade of the product at $N_{\rm side}=128$ would be useful to highlight large scale residuals. These considerations are free to evolve according to our needs.

Due to large possibilities and number of data sets to be considered, it would be desirable to have sort of automatic tools that ingest two, or more, inputs maps and produce difference map(s) and corresponding angular power spectrum(spectra). This has been implemented using Python language and interacting directly with FITS files of a specific data release. The code is parallel and can run both at NERSC and at DPC producing consistent results. In addition for each null-tests performed a JSON DB file is produced in which main test informations are stored together with interesting computed quantities like mean, standard deviation of the residual maps. Beside JSON files also GIF images of the null-test are produced. Such JSON and GIF files are used to create (both with Python again and with Scheme) a report in form of an HTML page from the LFI Wiki.

Together with images, power spectra of the residual are also produced and compared with the expected level of white noise derived from the half-ring jack-knifes. With these quantities are combined to produce a sort of χ^2. This gives an indication of the deviation of the residuals with respect to the white noise level. Of course underlying signal does not posses a Gaussian statistic and therefore with non-Gaussian data, the χ^2 tests is less meaningful. However this gives an hint on the presence of residuals which in some cases are indeed expected: in fact making difference between odd and even survey at horn and frequency level, is a way to show the signature of the external stray-light which, although properly accounted for during the calibration procedure, has not been removed from the data.

Data Release Results

L3 LFI

LFI specific L3 activities: masks, MCQA, etc

MCQA

TBW

Summary LFI

HFI/LFI joint data processing

HFI/LFI common processing uses as basic input the maps at the 9 frequencies covered by the two instruments.

The goal is to obtain various catalogues, identify the different astrophysical components whose superposition leads to the observed sky, and provides a statistical characterisation of the CMB, in particular through a likelihood code (of a particular theoretical C(l) given Planck data).

Catalogues

Are described here

Component maps

Are described here

Power spectra and likelihood code

Are described here

Simulations

Are described here

Scientific analysis products

Are described here

Compact Source catalogues

Planck Catalogue of Compact Sources

The Planck Catalogue of Compact Sources (PCCS) is a sample of reliable sources, both Galactic and extragalactic, extracted directly from the Planck nominal maps. The first public version of the PCCS is derived from the data acquired by Planck between August 13 2009 and November 26 2010. The PCCS consists of nine lists of sources, extracted independently from each of Planck's nine frequency channels. It is fully described in #planck2013-p05.

The whole PCCS can be downloaded here [1].

Detection procedure

The Mexican Hat Wavelet 2 (MHW2; Gonzalez-Nuevo et al., 2006) is the base algorithm used to produce the single channel catalogues of the PCCS. Although each DPC has is own implementation of this algorithm (IFCAMEX and HFI-MHW), the results are compatible at least at the statistical uncertainty level. Additional algorithms are also implemented, like the multi-frequency Matrix Multi-filters (MTXF; Herranz et al., 2009) and the Bayesian PowellSnake (Carvalho et al. 2009), but for the current version of the PCCS they are used just for the validation of the results obtained by the MHW2.

The full-sky maps are divided into a sufficient number of overlapping flat patches in such a way that 100% of the sky is covered. Each patch is then filtered by the MHW2 with a scale that is optimised to provide the maximum signal-to-noise ratio in the filtered maps. A sub-catalogue of objects is produced for each patch and then, at the end of the process, all the sub-catalogues are merged together, removing repetitions. For each channel, a parent sample is created containing all the sources detected with a signal-to-noise greater than 4. These 9 lists, that contain the positions, native flux densities and errors, are used as inputs in the validation step. The results of the validation process are finally used to decided the final thresholding or removal of spurious sources, defining the final PCCS.

Bandfilling is the process by which flux density estimates at specific bands are generated based on source positions defined in another band. For the current PCCS release we compute the flux density at 217, 353, and 545 GHz at the positions of each source detected at 857 GHz, using aperture photometry. Bandfilling is not attempted at other frequencies due to the variation in spatial resolution across the bands, which makes multifrequency associations challenging, especially in crowded regions such as the Galactic Plane.

Photometry

In addition of the native flux density estimation provided by the detection algorithm, three additional measurements are obtained for each of the source in the parent samples. These additional flux density estimations are based on aperture photometry, PSF fitting and Gaussian fitting (see #planck2013-p05 for a detailed description of these additional photometries). The native flux density estimation is the only one that is obtained directly from the filtered maps while for the others the flux density estimates has a local background subtracted. The flux density estimations have not been colour corrected. Colour corrections are available in [reference to the Color Correction description].

Validation process

The parent sample lists constitute only the starting point for the validation process. The results of the validation (both internal and external depending on the kind of information used) determine the final selection of sources to be included in the PCCS.

Internal validation

The PCCS is validated through an internal Monte-Carlo quality assessment (MCQA) process that uses large numbers of source injection and detection loops on realistic simulated maps to constrain detection characteristics.

Source injection consists on the introduction of fake sources in the real maps. The positions of the injected sources are chosen in order to avoid existing detections in the real maps and previously injected sources. By analysing the recovered injected sources we can determine several statistical properties of the detection process: completeness, photometry accuracy, variation of sensitivity along the sky, etc.

On the other hand, in order to study the number of false detections, also known as Purity, we need to perform realistic all-sky simulations. [Description or reference of the simulation used].

External validation

At the lowest frequencies of Planck, it is possible to validate PCCS source identifications using external data sets, particularly large-area radio surveys. This kind of validation allow us also to characterize the detection process, i.e. to determine the Completeness, Purity and positional accuracy. Moreover, the external validation offers the opportunity for an absolute validation of the different photometries, directly related with the calibration and the knowledge of the beams.

At higher frequencies, surveys as the South-Pole Telescope (SPT), the Atacama Cosmology Telescope (ACT) and H-ATLAS or HERMES form Herschel will also be very important, although only for limited regions of the sky. In particular, the Herschel synergy is crucial to study the possible contamination of the catalogues caused by the Galactic cirrus at high frequencies.

This statistical characterization of the detection process is used to choose the best signal-to-noise threshold for each channel in order to maximize the Completeness without penalizing the Purity.

Cautionary notes

- Statistical Character : warnings about the statistical analysis of this catalogue... Completeness levels for statistical analysis as number counts, usage of sensitivity maps at fixed completeness level, etc
- Variability: At radio frequencies, many of the extragalactic sources are highly variable. A small fraction of them vary even on time scales of a few hours based on the brightness of the same source as it passes through the different Planck horns (refs?). Follow-up observations of these sources might show significant differences in flux density compared to the values in the data products. Although the maps used for the PCCS are based on ~2.5 sky coverages, the current version of the PCCS provides only a single average flux density estimate over all Planck data samples that were included in the all sky maps and does not contain any measure of the variability of the sources.
- Contamination from CO: At infrared/submillimetre frequencies (100GHz and above), the Planck bandpasses straddle energetically significant CO lines (refs?). The effect is the most significant at 100GHz, where the line might contribute more than 50% of the measured flux density. Follow-up observations of these sources, especially those associated with Galactic star-forming regions, at a similar frequency but different bandpass, should correct for the potential contribution of line emission to the continuum flux density of the source. See Planck HFI Core Team (2011b) for details.

- Photometry: Each source has multiple measures of photometry APERFLUX, GAUFLUX, PSFFLUX and DETFLUX (or native) as defined above. The appropriate photometry to be used depends on the nature of the source. For sources which are unresolved at the spatial resolution of Planck, APERFLUX and DETFLUX are most appropriate. Even in this regime, PSF fits of faint sources fail and consequently these have a PSFFLUX value of NaN (Not a Number). For bright resolved sources, GAUSFLUX might be most appropriate although GAUSFLUX appears to overestimate the flux of sources close to the Galactic plane due to an inability to fit for the contribution of the Galactic background at the spatial resolution of the data.
- Cirrus/ISM: A significant fraction of the sources detected in the upper HFI bands could be associated with Galactic interstellar medium features or cirrus. The IRAS 100μm surface brightness in MJy sr1 for each of the sources, which is commonly used as a proxy for cirrus, is available through a search of the ERCSC with IRSA. Candidate ISM features can also be selected by choosing objects with EXTENDED=1 although nearby Galactic and extragalactic sources which are extended at Planck spatial resolution will meet this criterion. Alternately, the value of CIRRUS in the catalogue can be utilised to flag sources which might be clustered together and thereby associated with ISM structure.

Planck SZ Cluster Catalogue

The Planck SZ Cluster Catalogue is a nearly full-sky list of reliable SZ clusters detected in the Planck data. It is fully described in [reference to the Planck Cosmology and Product Paper 05a]. The catalogue is derived from the HFI frequency channel maps after masking and filling the bright point sources (SNR >= 10) from the PCCS single-frequency catalogues in those channels. Three detection methods were used to construct the catalogue: two implementations of the Matched Multi-Filter (MMF) algorithm and PowellSnakes (PwS), a Bayesian algorithm. A Galactic dust mask (leaving 85% of the sky) and a point source mask are applied a posteriori to remove detections in the portion of the sky where foregrounds are likely to cause spurious detections.

The master catalogue contains the merger of the catalogues from the three detection methods. The individual catalogues are also provided for the expert user in order to assess the consistency of the methods. The completeness and reliability of the catalogues have been assessed through internal and external validation. The catalogue has a reliability of 85% (TBC).

Early Release Compact Source Catalogue

The ERCSC is a list of high reliability (>90%) sources, both Galactic and extragalactic, derived from the data acquired by Planck between August 13 2009 and June 6 2010. The ERCSC consists of:

- nine lists of sources, extracted independently from each of Planck's nine frequency channels
- two lists extracted using multi-channel criteria: the Early Cold Cores catalogue (ECC), consisting of Galactic dense and cold cores, selected mainly on the basis of their temperature ; and the Early Sunyaev-Zeldovich catalogue (ESZ), consisting of galaxy clusters selected by the spectral signature of the Sunyaev-Zeldovich effect.

The whole ERCSC can be downloaded here [2].

The ERCSC is also accessible via the NASA/IPAC Infrared Science Archive [3].

The Bibliography

<biblio force=false>

1. References

</biblio>

References

[1] http://www.sciops.esa.int/index.php?project=planck&page=Planck_Legacy_Archive
[2] http://www.sciops.esa.int/index.php?project=PLANCK&page=Planck_Data_Products
[3] http://irsa.ipac.caltech.edu/Missions/planck.html

CMB map cleaning from foreground emissions

CMB Cleaning

C2

The main product to express cosmological constraints posed by Planck data is a Likelihood code. One of its by-product is the derived Maximum-likelihood CMB spectrum.

NB: This is very much a scientific product, whose development status will be described in a dedicated talk at the review.

Principles used to build the Planck Likelihood

We have used an hybrid approach for the likelihood which is:

- Pixel-based at low-ell
- based on fine-grained pseudo-CL at high-ell. I.e. it uses all independent groupings of detectors at 100, 143 and 217GHz.

This allows easy “Planck-Ext” (stitching of high(er)-ell likelihoods, in particular ACT & SPT).

The Planck code, CLIK, provides a unique interface (and it allows internally to keep cross-checking with various approaches), at V4.1 now (V1 was mid-2011).

We derived from CLIK our “best” CTT, together with a basic (diagonal) error estimate, which will allow making plots & quick model checks, comparison with various sources of uncertainties comparison with the CTT derived from the CMB map(s) issued from Component Separation activities…

`CLIK` - The Planck C(l) LIKelihood code

This section is a copy/extract of the private wiki pages of the collaboration, from which the updates will be made for major Exp.Sup. releases

[-*Last modified 2012-10-10* -]

`clik` is a package with both a code and data files to distribute the current planck likelihood. It is available from ESA through the [PLA [1]] under *operational files*, then clicking the *supplementary data* icon on the toolbar

---

Overview

```
Here follows a description of the last release of clik
```

!! **Version 4.0**

Main improvements for this release are the addition of

- CAMspec_v5.2dust hi-ell likelihood,
- plik_dx9_v2 hi-ell likelihood and
- an early october version of the actspt likelihood.

Partial compatibility between those likelihood has been implemented : all three share the same cib modeling and either CAMspec or plik can be this way used with actspt. CAMspec further use the same sz and szXcib modeling. plik neglect the sz and szXcib foregrounds for now (as they approximatively cancel in planck range of ells).

No update has been made on the low-ell likelihood. To recover the files (still compatible with the last version of the code) one has to retrieve clik v3.5 and use the file contained therein.

Beware that the previous CAMspec files will not work with the current release.

Code

`clik` code is at version *4.0b2*

Known issues

- none for now.

Changes:

- from *3.5*

```
** inclusion of actspt
** removal of dependency on gel
** removal/cleanup of lot's of legacy code
** better discovery of the hdf5 version (in particular version 1.8.X compiled in pure 1.6.X compatibility mode)
** better detection of some weird python install
** plik likelihood code has been improved and is now 20times faster
** correction for the C++ boilerplate
** correction of the clik_config scripts with the addition of laking libs
```

Data

- hi-ell

```
** plik_dx9_v2.clik
** CAMspec_5.2dust.clik
```

- hi-ell non planck

```
** actspt_2012_10_08.clik
```

Changes:

- CAMspec has changed a lot and now include beam parameters
- actspt is new
- new easily modifiable foreground modeling module for plik.

An important note for actspt

As for the low-ell likelihood, actspt code relies on data being installed in a specific place. The file is usable as is, but will dump some data in /tmp at each initialization. If this is not a desirable behaviour, data can be dumped once and for all by following the procedure described here.

Exemple of output

We'll give here an actual exemple of use and result of an exploration

Also Link to where we shall make available all the explorations of the (model/data) combinations we shall release in the scientific product section

Current Best-fit CMB spectrum

This is still evolving

References

[1] http://www.sciops.esa.int/index.php?project=planck&page=Planck_Legacy_Archive

HL-sims

The PSM or *"Planck Sky Model"* is an updated version (using knowledge derived from Planck observations) of the software tool described in Ref to the PSM paper of 2012. This can take in actual band-passes (in a RIMO) and create sky maps and catalogues at the specified frequencies. It can be supplemented by ad-hoc simulation software for particular (theoretical) CMB maps

The Level S (LS in short) is a generic simulation tool common to HFI and LFI. One version was described in ref to the old LS paper. It can take in input the output of the PSM, a pointing and beam description in order to generate the infalling power on detectors as a function of time. It can additionnaly create some noise realisation as a very simplified version of the actual instruments. Alternatively, the output can be used as input to a detailed simulation of the instrumental behaviour.

The PSM together with the LS therefore provide two basic bricks of a more extensive instrument specific simulation environment. For HFI, see HFI-Validation#sims.

Joint simulations provides an environment for checking algorithms in a realistic context. The latest series is the "FFP6", which provides a Full Focal Plane simulation of the DPC maps in the 2013 data release. They were initially provided (partially) "blind", ie without knowledge of the actual sky components used, but with an exact description of the Bandpasses, beams, and calibration.

CMB maps simulations

The basic maps are simple Gaussian realisation determined by their power spectrum generated by, eg., CAMB external Ref to CAMB site and papers Here.

Several non-Gaussian signatures can also be generated by dedicated software, like the lensing-induced deformations, a version of which is included in the standard PSM package. But other cases have been developped within Planck as part of its scientific preaparation, in particular the f_{NL} and g_{NL} maps of Ref to Elzner and Wandelt paper and the string maps of ref to Ringeval and Bouchet paper }}. Maybe also, the Bianchi model or other non sts=atistically anisotropic cases. For convenience, they are available through the PLA Link here to PLA once ESA has finsihed developing the interface.

Planck Sky Model PSM

this is the abstract of the pre-launch PSM paper, arXiv:1207.3675

The Planck Sky Model (PSM) is a parametric model for the generation of all-sky, few arcminute resolution maps of sky emission at submillimetre to centimetre wavelengths, in both intensity and polarisation. Several options are implemented to model the cosmic microwave background, Galactic diffuse emission (synchrotron, free-free, thermal and spinning dust, CO lines), Galactic H-II regions, extragalactic radio sources, dusty galaxies, and thermal and kinetic Sunyaev-Zeldovich signals from clusters of galaxies. Each component is simulated by means of educated interpolations/extrapolations of data sets available at the time of the launch of the Planck mission, complemented by state-of-the-art models of the emission.

Distinctive features of the simulations are: spatially varying spectral properties of synchrotron and dust; different spectral parameters for each point source; modeling of the clustering properties of extragalactic sources and of the power spectrum of fluctuations in the cosmic infrared background.

The PSM enables the production of random realizations of the sky emission, constrained to match observational data within their uncertainties, and is implemented in a software package that is regularly updated with incoming information from observations. The model is expected to serve as a useful tool for optimizing planned microwave and sub-millimetre surveys and to test data processing and analysis pipelines. It is, in particular, used for the

development and validation of data analysis pipelines within the planck collaboration. A version of the software that can be used for simulating the observations for a variety of experiments is made available on a dedicated website.

Level S `LS`

The `LS` software package simulates the incoming sky radiation on detectors as a function of time. ref to LS docs , paps

FFP6 data set

The sixth round of simulations of the "Full Focal Plane" of Planck encompasses the basic characteristics of Planck (Temperature) maps in support of scientific analyses, from component separation and power spectrum estimation to measures of non-gaussianity. They are simplified/idealsized in the sense that TOI processing is considered perfect. (For HFI for instance, there are no transfer function nor pointing error, no 4K nor glitch residuals, no noise correlation, etc). But the actual pointing, spectral banpasses, beams, noise determinations were used.

The basis sky maps are available here - link to PLA, including for convenience the individual components (which were initially hidden to the Planck collaboration, but for the generators :-)).

Science

In addition to formal deliverables, The Planck scientific collaboration will make available useful additional information. In particular, some scientific publications will obtain informations best given in numerical form, and this section will cover all those, i.e. provide an overview of the product, a reference to the publication for in-depth description, and links to the numerical information in the PLA.

NB: The following content is only indicative (20/10/2012), and will evolve according to what the Planck Sceince Team deeems fit to publication at the time when the supplement will be frozen for the 2013 data release.

Science Maps

Here will be the specific product which are not obtained by the general component separation approach. These scientific products may be available only in some fraction of the sky and/or using dedicated ancillary data, etc.

CO maps

CO rotational transition line emission is present in all HFI bands but for the 143 GHz channel. It is especially significant in the 100, 217 and 353 GHz channels (due to the 115 (1-0), 230 (2-1) and 345 GHz (3-2) CO transitions). This emission comes essentially from the Galactic interstellar medium and is mainly located at low and intermediate Galactic latitudes. Three approaches have been used to extract CO velocity-integrated emission maps from HFI maps and produce three types of CO products. A full description of these products is given in #planck2013-p03a. The 3 Type 1 maps at 115, 230, and 345 GHz are of low contamination, in particular in the Galactic Plane, but with a low signal-to-noise ratio. Two Type 2 maps (115 and 230 GHz) have a larger signal-to-noise ratio and are tailored for medium and high galactic latitude studies. Finally, one Type 3 map contains the best signal-to-noise ratio for one generic CO line and can be used to locate the faintest molecular regions. The products are described in [| this Section [1]].

Diffuse SZ map

Planck large frequency coverage between 30 and 857 GHZ allows us to measure the thermal Sunyaev-Zeldovich (tSZ) effect -- inverse Compton scattering of CMB photons in hot electrons -- on clusters of galaxies and inter-clusters cosmic web filaments. Using the Planck frequency channels from 100 to 857 GHz and especially tailored component separation methods we have produced a first full-sky map of the tSZ effect in Compton parameter units. This map has been internally validated by inter-comparison of the maps obtained from different component separation methods and by cross-correlation with foreground templates. From this we have proved that the Planck all-sky Compton parameter map is dominated by the tSZ emission in the multipole range from 100 to 800.

REF P05b

Thermal dust model

One of the major Galactic foreground for CMB studies is interstellar thermal dust emission. It is observed everywhere on the sky, from the Galactic plane to the faintest areas at high Galactic latitudes. The CMB fades toward higher frequencies, whereas the thermal dust emission spectrum increases, and so dust becomes the dominant signal in the submillimetre. The frequency coverage and sensitivity of HFI are such that a more precise model of thermal dust emission is possible compare to previous experiments. The model of thermal dust emission is based on a modified black body fit using HFI data at 857, 545 and 353 GHz together with IRAS (IRIS) data at 100 micron. Three all-sky maps are obtained from the fit : dust temperature (T), dust spectral index (Beta) and dust optical depth at 353 GHz (Tau353). From this dust model a fourth map giving an estimate of the dust reddening E(B-V) is also provided. These products are described in [| this Section [2]].

Cosmological parameters

While papers concerned with parameters will describe the salient results obtained by the collaboration, we plan to make available constraints posed by PLanck on a rather large number of (model/data set) combinations.

In addition, here are specific parametrisation/models considered for the inflation paper:

1. Harrison-Zeldovich (HZ), HZ + free number of relativistic degrees of freedom, HZ + free Helium abundance
2. \Lambda CDM (LCDM)
3. LCDM + tensors (r)
4. LCDM + running, LCDM + running + r
5. LCDM by PCA on reionization, LCDM + r by PCA on reionization
6. LCDM + r + curvature
7. Inflaton potential reconstruction in the observable range (standard cosmological parameters plus inflationary potential parameters)
8. LCDM + super-imposed oscillations (currently LCDM model plus 3 parameters, others to be considered)
9. LCDM + r for generalized scalar field (without tensor-to-scalar consistency condition)
10. LCDM + isocurvature (including uncorrelated or anti-correlated mixture, broken law power spectrum).

MCMC Chains for the Planck likelihood

In addition to the paramter constraints, we will probably (TBC) make available MCMC chains.

PICO training sets

PICO interpolates the CMB powerspectrum as a function of cosmological parameters for very fast and very accurate parameter estimation. (See http://arxiv.org/abs/astro-ph/0606709 and http://arxiv.org/abs/0712.0194)

Because PICO is trained using CAMB calls on the highest accuracy settings, PICO can in some cases be more accurate than CAMB on default accuracy.

PICO comes with easy interfaces into CAMB and CosmoMC

The latest PICO version will be available here as well as the PICO website http://cosmos.astro.illinois.edu/pico/.

Therefore delivery through PLA is TBC (but we shall at least refer to the specific version used)

References

<biblio force=false>

1. References

</biblio>

References

[1] http://www.sciops.esa.int/wikiSI/planckpla/index.php?title=Astrophysical_component_maps&instance=Planck_PLA_ES#CO_emission_maps

[2] http://www.sciops.esa.int/wikiSI/planckpla/index.php?title=Astrophysical_component_maps&instance=Planck_PLA_ES#Dust_optical_depth_map_and_model

Planck Legacy Archive

Planck Legacy Archive

Introduction

The Planck Legacy Archive (PLA) contains all public products originating from the Planck mission. A graphical user interface accessible from this page allows to list, display, inspect, select, and download these products.

The first public product present in the Planck Legacy Archive was the Early-Release Compact Source Catalogue (ERCSC) released in January 2011.

As of January 2013, the PLA contains all temperature maps per Planck frequency, as well as ancillary maps like Survey maps, detector maps, etc. It also contains the first public version of the Planck Catalogue of Compact Sources and information about the spacecraft, instrument and survey history, notably through all the operational files and the Planck Operations State History (POSH).

Purpose

The PLA will mainly serve the needs of professional astrophysicists wishing to carry out astronomical research, related to various astronomy fields as the Cosmic Microwave Background, extragalactic astronomy, Galactic interstellar medium, and Solar System studies, among others. In addition to these professional users, a number of others will be browsing the PLA, including members of the general public and members of the press. In both cases, they will be looking for general information on the Planck satellite and its scientific results, news about Planck, pictures and other public-relations material, among other things.

Contents

The Planck Legacy Archive contains the following classes of products as of January 2013:

- frequency maps at all nine frequencies of Planck (in temperature only)
- sky component maps per frequency per component
- various ancillary maps like survey maps, detector maps, detector set maps, etc
- the first version of the Planck Legacy Catalogue of Compact Sources
- the Early-Release Compact Source Catalogue (since January 11th, 2011)
- operational files for the first six surveys (approximately first three years of Planck routine operations): pointing lists (programmed and achieved), orbit information, data-quality reports, instrument health reports, etc)
- the Planck Operational State History (POSH) - the "state vector" of the Planck mission
- documents associated to the above products

In addition to these public products, the same archive has an internal part (Planck Internal Archive or PIA) containing products restricted to the Planck collaboration.

Software

The data browsing and retrieval from the PLA interface involves the following actions:

- there are several search panels or tabs (Maps, Catalogues, Time-Ordered Information, Documents...) which offer a set of filters to set the search criteria for the data queries
- after executing a query, a new result panel is automatically created with the result contents
- each result tab contains a list of the data which match the specified query. From this page several operations can be performed, depending on the type of data to be retrieved (e.g. display a set of sources, save result tables as XML or CSV, send them to another application, download the products, etc).

Some products require authentication (only those pertaining to the Planck Internal Archive, restricted to some people in the Planck Collaboration). The user must enter their username and password (Planck LDAP credentials) in the login window. If authorisation is granted, the status bar in the left bottom corner of the application window will be updated to the current user's ID and login time.

A general set of help pages is present on the Java interface. Please refer to these pages for further explanations on the software.

Access

The PLA main page can be accessed here [1].

The Java interface can also be directly launched from here [2].

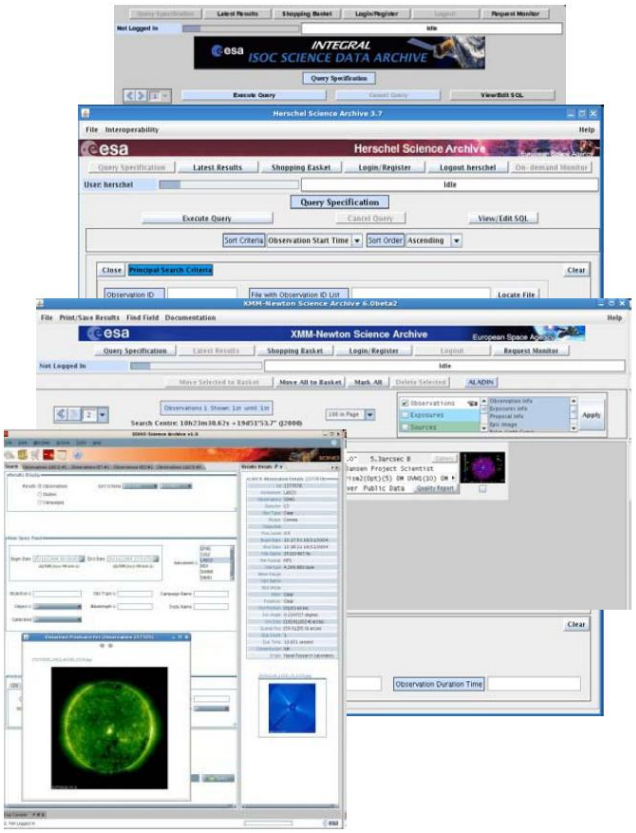

The Planck Legacy Archive Java interface is part of the general archiving effort developed by the Science Archives Team at ESAC

Trouble shooting for the PLA Java client

To run the PLA your web browser must be Java compliant (Java version 1.5.x or higher is required for running the PLA), if not please install the latest Java following the instructions provided here [3].

In case of problem, and to make sure that you are using the latest version of our software, please clean your Java Web Start cache (see below) and run the application again. If the problem persists, please open a web browser (Internet Explorer, Mozilla Firefox, Safari, ...) and send us the output from this page [4] (which lists your configuration) along with the description of your problem. If the problem is related to data searching, it will be very helpful if you include the contents of your Log Console, which you'll find at the bottom of the ERCSC window, when you contact us (see Helpdesk section).

How to clean your Java Web Start cache on Windows systems:

- Click on the "Start" icon in the lower left hand corner of your screen, followed by clicking on the "Run" menu choice.
- In the run box, type "javaws -viewer" (w/o the quotes) and hit "Enter".
- Select all the entries and then click on the "Remove Selected Applications/Items/Entries" button/icon.

On Linux systems:

- Find out what version of Java you are running by and typing in "java -version" at the command line (w/o the quotes).
- Type in the command "$JAVA_HOME/jre/javaws/javaws" or "$JAVA_HOME/jre/javaws/javaws -viewer" on the command line if your Java version is 1.5 or 1.6 respectively.
- Select all the entries and then click on the "Remove Selected Applications/Items/Entries" button/icon.

On Mac OS X systems:

- Find out what version of Java you are using by running "Applications/Utilities/Terminal" and typing in "java -version" at the command line (w/o the quotes).
- Type in the command "javaws" or "javaws -viewer" on the command line if your Java version is 1.5 or 1.6 respectively.
- Select all the entries and then click on the "Remove Selected Applications/Items/Entries" button/icon.

On Windows systems, in case of trouble with Java WebStart and Comodo Firewall:

- When trying to launch the archive interface, Java WebStart may return the error “splash recv failed”.
- Possible solution: Add Java WebStart to the list of authorized applications in the Comodo Firewall.

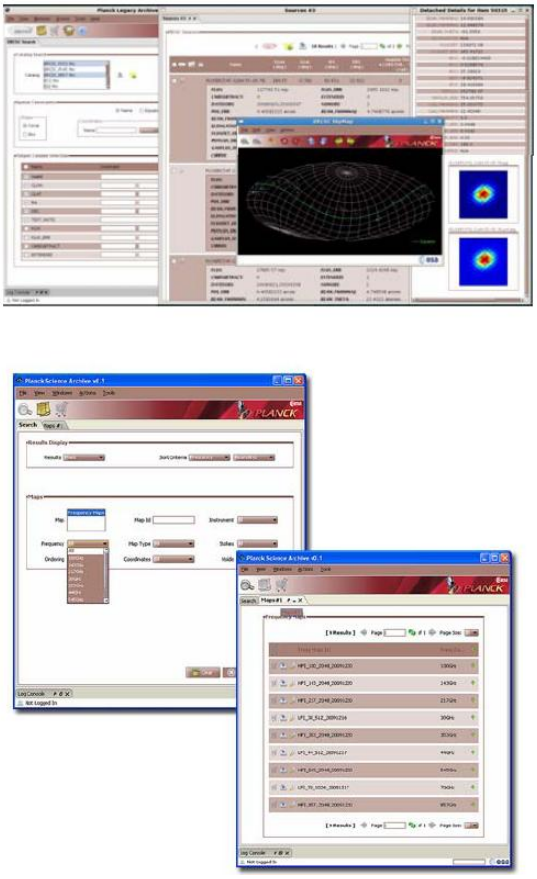

Illustration of the specific case of the Planck Legacy Archive interface

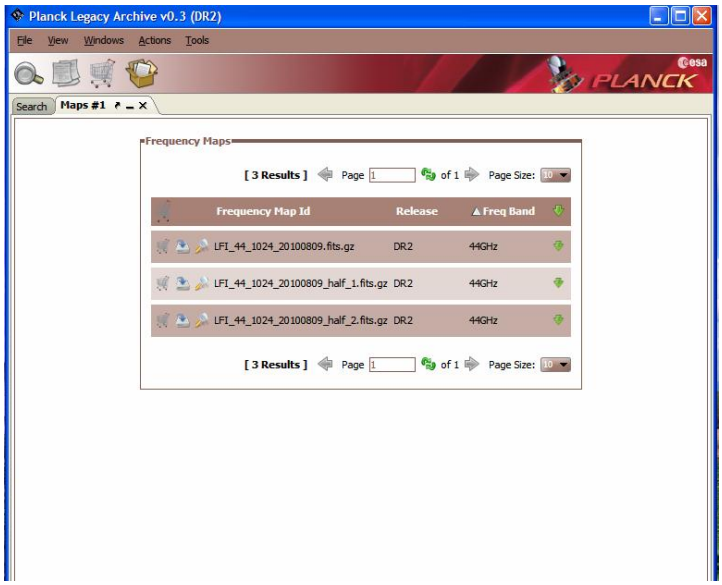

Illustration of the specific case of the Planck Legacy Archive interface

Planck Legacy Archive Helpdesk

The PLA Helpdesk consists of the three scientists of Planck Science Office. For some questions related to data products and instruments, the questions may be re-directed to data-processing or instrument specialists in science institutes of the Planck Ground Segment.

In order to send a request to the Helpdesk, please fill in the form at: [[5]]

("Submit a ticket")

References

[1] http://www.sciops.esa.int/index.php?page=Planck_Legacy_Archive&project=planck
[2] http://pla.esac.esa.int/pla/pla.jnlp
[3] http://www.java.com/en/download/manual.jsp
[4] http://www.java.com/en/download/testjava.jsp
[5] http://www.sciops.esa.int/helpdesk_pia

Mission science products

NB. This page being use for experimenting with structure

Contents of this chapter

Timelines - [Not for 1st Rel]

Semi-raw signal timelines • Calibrated signal timelines • Pointing timelines • FITS file structure

Single detector maps - [Not for 1st Rel] or incorporate later into Frequency Maps

Frequency Maps -

Introduction • Types of maps • List of products • FITS file structure

Component maps -

CMB maps • Synchrotron & free-free • Anomalous dust emission • Dust opacity • CO emission

Catalogues -

ERCSC • Compact Sources • SZ Clusters)

Angular power spectra -

Spectra#Sky power spectra • Spectra#CMB power spectrum

The RIMOs -

Detector-level data • Map-level data • Band transmissions • Detector noise spectra • Beam Window Functions

Effective beams -

page not yet started … TBW by ??

Likelihood Code -

page refers to C2 section …TBW by Benabed

Colour correction code -

page not yet started … should be in software utilities section??

*Note: headings that are **Not for 1st Rel** will not be exported to the external (and public) version of the XS, but are maintained here for completeness*

AMo: this page is under construction and still very preliminary - pending a better definition of what this section will contain, and a more detailed listing of its contents. Also, while I have done nearly all of the writing so far, LFI and PSO should be sharing the task ….

The *Mission Science Products* *AMo: I don't know of any good definition from a user point of view (i.e. what's in the PLAlist v0.95 or what's in the Science Implementation Plan have limited value). In practice I would tend to regroup the items in 5.1 and 5.2 into a single section (which I would bring to top level of the TOC), and I am not sure about how to handle the other sections of 5. So the rest of this section should be revised.* are those data and associated characterization products that are produced by the DPCs using exclusively (or almost) data from the Planck mission. Thy are defined in the Science Implementation Plan (ref), though additional products have been added later. They do not include specific products that come out of the special processing performed in the context of the scientific papers, normally products that require extensive use of external dataset. These, when delivered, are described in the Additional Science Products section below.

The Mission Data Products described in this chapter are:

- different flavors of **sky maps**, i.e., maps of the full signal received from the sky, processed via the DPC pipelines; these represent the best view of the sky at the Planck frequencies that the DPCs could produce at this time;
- **catalogues** of point sources, one per frequency band, and of the SZ clusters (of which there are several compiled with different extraction methods);
- astrophysical **component maps** (with more that one map for some components), which attempt to separate the different astrophysical components, namely the CMB (various examples obtained with different extraction methods), and several foregrounds;
- a **Dust opacity map and model** derived from the dust component but using also external information;
- **sky power spectra** for selected combination of detectors useful for Likelihood studies, and obtained with the DPC's best estimate of the beam window function;
- a **CMB power spectrum**;
- A set of instrument-level data compiled into the **RIMO** (Reduced Instrument Model), such as beam properties, noise levels, bandpass profiles, and more. There is one RIMO for each instrument.
- the **effective beams** … Should this be here or in ancillary data?

Also included as Mission Products are two software packages:

- the Likelihood code package, which is itself split into a software package and a data package,
- the Unit Conversion and Color Correction (UcCC) package Should this be here or in the software utilities section?, which is used together with the bandpass profiles in the RIMO.

There are no low-level science products in this first release of Planck data, in particular no timeline data (raw or processed signal, pointing), and in general no data at the single detector level. Other products of scientific analyses that were built with extensive use of external data are given in Additional products, and mission and payload information are in later chapters.

The data products are packaged into FITS files that contain a main product (e.g., a signal map) and one or more other products to characterize it (e.g., an error map and a hit-count map). Depending on the details of the products, the data are writting into a single *BINTABLE* or a few extensions. The RIMO is also packaged into a FITS file, but given the nature of its different elements it was necessary to use several hundred *BINTABLE* extensions.

The software is delivered as a tarball of code, and if necessary a second tarball of associated data is also delivered. The details depend on the code and are described elsewhere in this document.

This chapter is divided by type of product. Each section contain is a brief description of how each type of product is obtained, while the details of the processing are given in the HFI Data Processing chapter, and any known problems with the product. The list of product files is then given, and sample FITS headers are given and explained.

Timelines

There will be no timelines in the 1st data release.

Semi-raw signal timelines

HFI timelines

Originally defined to be the raw (ADU) data demodulated and converted to engineering units (V) via the HFI transfer functions (includes 3-pt filtering?). But (1) this is not the same demodulation method as used in the TOI prod pipeline, and (2) the ADC correction (or at least one method thereof) implies a modification of the raw data before demodulation. Thus what the HFI will deliver is not yet decided

LFI timelines

TBW

Cleaned and calibrated signal timelines

HFI processing

The calibrated timelines are produced by the *TOIprod* pipeline (link to wiki; link to paper) which in brief performs the following operations:

demodulation

> this is performed around a variable level which is determined from the valid input data (a validity flat from a previous version of the processing is determined for this purpose), and the data are converted to engineering units (V) using known conversion coefficients.

despiking

> using the demodulated data converted to V (by the transfer function) the glitches are identified and fitted with templates. A glitch flag is produced that identifies the strongest part of the glitches, and a timeline of glitch tails is produced from the template fits, and subtracted from the demodulated timeline from step 1. Finally, the flagged ranges are replaced with data from TBC *(is this done here, if not where?)*

dark template removal

> *TBW*

conversion to absorbed power

> the timeline is converted to watts of absorbed power using the bolometer function. This includes a non-linearity correction

removal of the 4K cooler lines

> *TBW*

at this point a timeline in W and a glitch flag are written to disk

deconvolution by the time transfer function

TBW

jump correction

removes some (relatively rare) jumps in the signal baseline

at this point a *tau-deconvolved* and *jump-corrected* timeline and its associated glitch flag are written to disk. These timelines are later used in the flux calibration and mapmaking stages

Note that these timelines contain the full sky signal, i.e. including the solar and orbital dipoles and the Zodiacal light. The dipoles are necessary for the flux calibration and are removed by the pipeline at the mapmaking stage.

Need to discuss dipoles removal and conversion to astrophysical units at the export stage

LFI processing

TBW

Pointing timelines

The pointing is determined starting from the AHF produced by MOC, which gives the direction and orientation of the LOS of a fiducial position in the focal plane at frequencies of 8Hz during stable pointing and 4 Hz during maneuvers (TBC for details, reference). This is interpolated to the times of data observation (ref to method), corrected for the wobble and other time-dependent offsets determined from the observed positions of a large number of sources around the sky, and finally converted to the LOS of each detector using the quaternions in the IMO (which are determined from observations of bright planets - see the Focal plane reconstruction pipeline).

Details of delivery are TBD

FITS file structure

The FITS files will begin with a minimal primary header that will be followed by several BINTABLE extensions: the first one for the OBT and its (global) flag, the following ones for each detector signal data and its (local) flag.

Filenames will be of the form *{H\|L}FI_HscN-DDDD-R-yyymmdd.fits*, where *DDDD* is the OD number, *sc* indicates science data, and N=1-5 for the 5 HFI files, and *R* indicates it is reduced (i.e., cleaned and calibrated) data.

NB. this is the current name used in DPC exchanges, perhaps it should be changed … eg. replace the date with the release number. Will also indicate that they are calibrated in astrophysical units and will have the dipoles removed, thus they are for delivery to the external community.

Header keywords

An example is given below.

EXTENSION 0:

```
SIMPLE  =                    T / file does conform to FITS standard
BITPIX  =                   32 / number of bits per data pixel
NAXIS   =                    0 / number of data axes
EXTEND  =                    T / FITS dataset may contain extensions
COMMENT   FITS (Flexible Image Transport System) format is defined in 'Astronomy
COMMENT   and Astrophysics', volume 376, page 359; bibcode: 2001A&A...376..359H
EFDD_VER= '99.9    '
ICD_VER = '99.9    '
IMO     = 'IMO_2_62'
DATE    = '2012-09-04T13:45:59' / file creation date (YYYY-MM-DDThh:mm:ss UT)
```

```
END
```

where EFDD_VER and ICD_VER are the versions of the respective documents in which the structure is defined (dummy values in the example).

EXTENSION 1: OBT

```
XTENSION= 'BINTABLE'           / binary table extension
BITPIX  =                    8 / 8-bit bytes
NAXIS   =                    2 / 2-dimensional binary table
NAXIS1  =                    9 / width of table in bytes
NAXIS2  =             15573106 / number of rows in table
PCOUNT  =                    0 / size of special data area
GCOUNT  =                    1 / one data group (required keyword)
TFIELDS =                    2 / number of fields in each row
TTYPE1  = 'OBT     '           / label for field   1
TFORM1  = '1K      '           / data format of field: 8-byte INTEGER
TUNIT1  = '2**(-16)sec'        / physical unit of field
TTYPE2  = 'Flag    '           / label for field   2
TFORM2  = '1B      '           / data format of field: BYTE
TUNIT2  = 'N/A     '           / physical unit of field
EXTNAME = 'OBT     '           / name of this binary table extension
TIMEZERO= '1660237181'
END
```

where TIMEZERO is the value of the first timesample in the units of TUNIT1

EXTENSION 2: 14_545_1_LFER4_JC_v51

This is the first of the extensions containing the detector data, and is followed by more like it for the other detectors.

```
XTENSION= 'BINTABLE'           / binary table extension
BITPIX  =                    8 / 8-bit bytes
NAXIS   =                    2 / 2-dimensional binary table
NAXIS1  =                    5 / width of table in bytes
NAXIS2  =             15573106 / number of rows in table
PCOUNT  =                    0 / size of special data area
GCOUNT  =                    1 / one data group (required keyword)
TFIELDS =                    2 / number of fields in each row
TTYPE1  = 'Signal  '           / label for field   1
TFORM1  = '1E      '           / data format of field: 4-byte REAL
TUNIT1  = 'KCMB    '           / physical unit of field
TTYPE2  = 'Flag    '           / label for field   2
TFORM2  = '1B      '           / data format of field: BYTE
TUNIT2  = 'N/A     '           / physical unit of field
EXTNAME = '14_545_1_LFER4_JC_v51' / name of this binary table extension
TIMEZERO= '1660237181'
CHANNEL = '545-1   '
END
```

Note that NAXIS must be the same for all extensions.

NB. may want to change EXTNAME to be just the detector name; the rest was for internal purposes only

Frequency Maps

General description

Sky maps give the best estimate of the unpolarised signal from the sky after removal, as far as possible, of known systematic effects and of the dipole signals induced by the motion of the solar system in the CMB and of the Planck satellite in the solar system. Sky maps are provided for the nominal Planck mission and also, separately,for the first two single surveys, the third one being covered only for a small part during the nominal mission. The details of the start and end times of each are given in this table.

For characterization purposes, are also provided maps covering the nominal survey but using only half of the available data. These are the *ringhalf_{1\|2}* maps, which are built using the first and second half of the stable pointing part of the data in each pointing period. These maps are used extensively to investigate the (high frequency) noise properties the maps themselves and of other products described elsewhere (see e.g., the data validation section).

To help in further processing, there are also masks of the Galactic Plane and of point sources, each provided for several different depths

All sky maps are in Healpix format, with Nside of 2048 for HFI and of 1024 for LFI, in Galactic coordinates, and Nested ordering. The signal is given in units of K_{cmb} for 33-353 GHz, and of MJy/sr (for a constant νF_ν energy distribution) for 545 and 857 GHz. Each sky map is packaged into a *BINTABLE* extension of a FITS file together with a hit-count map (or hit map, for short) and a variance map, and additional information is given in the FITS file header. The structure of the FITS file is given in the FITS file structure section below.

Types of maps

Full channel maps

> Full channel maps are built using all the valid detectors of a frequency channel and cover the nominal mission. For HFI, the 143-8 and 545-3 bolometers are rejected entirely as they are seriously affected by RTS noise. Images in the HFI-DPC paper (#planck2013-p03; can be copied here once produced with the final color scheme).

Single survey maps

> Single survey maps are built using all valid detectors of a frequency channel, but cover separately the different sky surveys.

Half-ring maps

> Half-ring maps are built using only the first or the second half of the stable pointing period data. There are thus two half-ring maps per frequency channel named *ringhalf_1* and *ringhalf_2* respectively. These maps are built for characterization purposes in order to perform null tests. In particular, the difference between the two half-ring maps at a given frequency give a good estimate of the high frequency noise in the data.

Caveats and known issues

Map zero-level

For the 100 to 857 GHz maps, due to recent evolutions in the calibration scheme, the zero levels could not be set to their optimal levels especially for Galactic studies in time for the data release. A recipe for adjusting these zero levels to astrophysical values is given in the HFI Calibration paper #planck2013-p03f .

For the 30, 44 and 70 GHz, maps are corrected for zero level monopole by applying an offset correction, see LFI Calibration paper #planck2013-p02b (summary to be included here, add a note about the offset applied that is indicated in the header comment keywords AG).

The Zodiacal light and the Far-Side Lobes

Insert here how these are seen in the differences of the single survey maps

Artifacts near caustics of the scanning strategy

TBW if still an issue??

Production process

Sky maps are produced by combining appropriately the data of all working detectors in a frequency channel over some period of the mission. They give the best estimate of the signal from the sky (unpolarised) after removal, as far as possible, of known systematic effects and of the dipole signals induced by the motion of the solar system in the CMB and of the Planck satellite in the solar system. In particular, they include the Zodiacal light emission (Zodi for short) and also the scattering from the far-side lobes of the beams (FSL). More on this below.

HFI processing

The inputs to the mapmaking are TOIs of signal that have been cleaned (as far as possible) of instrumental effects and calibrated in absorbed watts. While the processing involved is described in detail in the TOI processing section, we give a very brief summary here for convenience. That pipeline performs the following operations:

demodulation

this is performed around a variable level which is determined from the valid input data (a validity flag from a previous version of the processing is used for this purpose), and the data are converted to engineering units (V) using known conversion coefficients.

despiking

using the demodulated data converted to V (by the transfer function) the glitches are identified and fitted with templates. A glitch flag is produced that identifies the strongest part of the glitches, and a timeline of glitch tails is produced from the template fits, and subtracted from the demodulated timeline from step 1. Finally, the flagged ranges are replaced with data from an average over the pointing period (TBC)

dark template removal

the two dark bolometers are demodulated and despiked as above; the resulting timelines are then smoothed and used as an indicator of the overall temperature variations of the bolometer plate. Where the variations are consistent with each other, they are combined and removed from the bolometer signal timelines using appropriate coupling coefficients. The few percent of the data where they are not consistent are flagged on the timelines.

conversion to absorbed power

the timeline is converted to watts of absorbed power using the bolometer function. This includes a non-linearity correction; removal of the 4K cooler lines: the electromagnetic interference of the 4K cooler with the bolometer readout wires induces some sharp lines in the signal power spectra at frequencies of the 4K

cooler's fundamental and its multiples, folded by the signal modulations. Fourier coefficients of the relevant lines are determined on a per-ring basis, and then removed from the data. The quality of the removal depends on the bolometer.

deconvolution by the time transfer function

this is done to correct for the non-instantaneous time response of the bolometers. The function itself is modeled using 4 parameters which are adjusted primarily on the planet data and also from comparisons of the northward and southward scans of the Galactic Plane. It is then removed using Fourier techniques, which has the side-effect of increasing the noise at high frequencies.

jump correction

removes some (relatively rare: 0.3 jumps per bolometer per pointing period, on average) jumps in the signal baseline. The jumps are detected characterized on smoothed TOIs, and corrected by adding a constant to part of the signal timeline. The origin of the jumps is not known.

The results of this processing are a timeline of signal (in absorbed watts) and a *valid data* flag timeline for each of the 50 valid bolometers processed; these timelines contain the full sky signal, i.e., including the solar and orbital dipoles, the Zodiacal light, and contributions from the Far-Side lobes. The dipoles are necessary for the flux calibration and are removed at the mapmaking stage. The remaining two bolometers (143-8 and 535-3) show semi-random jumps in the signal level, typically jumping over 2-5 different *pseudo-baseline* levels, a behavior known as *Random Telegraphic Signal*, so that these are commonly called the RTS bolometers. Finally, ring-level statistics of different types (mean, median, rms, kurtosis, etc.) are determined on a per-ring basis for all timelines, and a selection based on these statistics is used to discard anomalous rings, which are recorded in a ring-level flag for each valid bolometer timeline.

Throughout this processing, bright planets (Mars, Jupiter, Saturn, Uranus) and bright asteroids are masked in the timeline in order to avoid ringing effects in the processing. Since they move on the sky, the portion of the sky masked during one survey is observed during one, and no hole is left in the final map. In parallel, the planet data are processed in a similar way, but with different parameters for the despiking step, and without the final jump correction step. These results are processed separately to determine the beam shapes and the focal plane geometry.

The pointing is determined starting from the AHF produced by MOC, which gives the direction and orientation of the LOS of a fiducial position in the focal plane at frequencies of 8Hz during stable pointing and 4 Hz during maneuvers (TBC for details, reference). This is interpolated to the times of data observation (ref to method), corrected for the wobble and other time-dependent offsets determined from the observed positions of a large number of sources around the sky, and finally converted to the LOS of each detector using the quaternions in the IMO (which are determined from observations of bright planets - see the Focal plane reconstruction pipeline).

The mapmaking pipeline is described in detail in the Map-making section, and a brief summary is given here for convenience.

The cleaned TOIs of signal of each detector, together with their flags, produced by the TOI processing pipeline, and the TOIs of pointing (quaternions), described in Detectors pointing and beams, are the inputs to the mapmaking step.

The input signal TOIs are expressed in Watts from the sky absorbed by the bolometer, and their associated flags are used to samples or full rings to discard. Are discarded periods of unstable pointing and pointing maneuvers in general, glitched data, transits over bright planets (since they move, the *hole* flagged during one survey is covered during another sky survey), and some full rings are discarded if their noise properties differ significantly from the nominal value and the few rings of duration longer than 90 min, since the pointing is not sufficiently stable over such long periods (details in Discarded rings section). The preparation of input pointing TOIs is described in Detectors pointing and beams. In brief, the STR (StarTracker) pointing produced by Flight Dynamics is interpolated to the detector sampling frequency in order to obtain a tuple of pointing quaternions for each sample and corrected for certain known effects. The angular offset between the STR line of sight and that of each bolometer is reflected in the

Focal Plane Geometry, which is determined from the observation of bright planets. Also, the STR pointing timeline is corrected for slowly varying offsets between the STR and the HFI focal plane using observations of all planets and of other (fixed) bright sources.

Using the pointing TOIs, the signal TOIs are first used to build Healpix rings using the nearest grid point method; each ring containing the combined data of one pointing period. These are then calibrated in brightness, cleaned of the dipole signals, and projected onto Healpix maps as explained in the following sections.

The cleaned TOIs must be calibrated in astrophysical units. At 100-353 GHz, the flux calibration gains are determined for each pointing period (or ring) from the solar-motion dipole after removal of the small dipole induced by the motion of the Planck satellite in the solar system. The solar-motion dipole from WMAP (REF) is used for this purpose. This gain by ring is then smoothed with a window of width 50 rings, which reveals an apparent variation of ~1-2% on a scale of 100s to 1000s of rings for the 100-217 GHz channels, and is applied to the Watt data. At 353GHz, where the solar motion dipole is weaker compared to the signal, no gain variation is detected, and a single fixed gain is applied to all rings. At 545 and 857 GHz the gain is determined from the observation of Uranus and Neptune (Jupiter is not used because its brightness produced some non-linearity in the bolometer response) and comparison to recent models (REF) made explicitly for this mission. A single gain is applied to all rings at these frequencies. Prior to projecting the Healpix rings (HPRs) onto a map, a destriping approach is used to remove low-frequency noise. The noise is modelled as the sum of a white noise component and a constant, or *offset*, per pointing period which represents the low frequency 1/f noise. The offsets are determined by minimizing the differences between HPRs at their crossings. After subtracting these offsets, calibrated data are projected onto Healpix maps, with the data of each bolometer weighted by a factor of 1/NET of that bolometer, and accounting for the slight different band transmission profiles of the bolometers in each band.

These maps provide the main mission products. A second, reduced, set of maps, cleaned of the Zodiacal emission of the FSL leakage is also produced for the nominal mission and the two single surveys, but not for the half-rings (since the contribution would be the same for the two halves of each ring). For this purpose, the the Zodiacal emission and the FSL contamination, which are not fixed on the sky, are modeled separately at HPR-level, and subtracted from the signal HPR before projecting them onto the maps.

Together with signal maps, hit count and variance maps are also produced. The hit maps give the (integer) number of valid TOI-level samples that contribute to the signal of each pixel. All valid samples are counted in the same way, i.e., there is no weighting factor applied. The variance maps project the white noise estimate, provided by the NETs, in the sky domain.

LFI processing

LFI maps were constructed with the Madam map-making code, version 3.7.4. The code is based on generalized destriping technique, where the correlated noise component is modeled as a sequence of constant offset, called baselines. A noise filter was used to constrain the baseline solution allowing the use of 1 second baselines.

Radiometers were combined according to the horn-uniform weighting scheme to minimize systematics. The used weights are listed in Map-making. The flagged samples were excluded from the analysis by setting their weights to C_{w}^{-1} = 0. The galaxy region was masked out in the destriping phase, to reduce error arising from strong signal gradients. The polarization component was included in the analysis, although only the temperature maps are released.

A detailed description of the map-making procedure is given in #planck2013-p02. See also section Map-making.

Inputs

HFI inputs

- The cleaned TOIs of signal of each detector, together with their flags, produced by the TOI processing pipeline
- The TOIs of pointing (quaternions), described in Detectors pointing and beams
- Bolometer-level characterization data, from the DPC's internal IMO (not distributed)
- Planck orbit data used to compute and remove the earth dipole
- WMAP solar dipole information used to calibrate the CMB channels
- Planet models used to calibrate the Galactic channels.

LFI inputs

The Madam map-maker takes as an input:

- The calibrated timelines (for details see TOI Processing)
- The detector pointings (for details see Detector pointing)
- The noise information in the form of three-parameter (white noise level (σ), slope, and knee frequency (f_knee)) noise model (for details see RIMO)

Related products

A description of other products that are related and share some commonalities with the product being described here. E.g. if the description is of a generic product (e.g. frequency maps), all the products falling into that type should be listed and referenced.

File names

The FITS filenames are of the form *{H\|L}FI_SkyMap_fff_nnnn_R1.nn_{type}_{coverage}_{type}.fits*, where *fff* are three digits to indicate the Planck frequency band, and *nnnn* is the Healpix Nside of the map, *coverage* indicates which part of the mission is covered, and the optional *type* indicates the subset of input data used. A full list of products, by their names, is given in the List of products below. **to be reviewed**

The list of products containing sky maps are given below, grouped by type

Outstanding: link to archive objects / LFI to fill in their products

Full channel maps

Frequency	FITS file name
30GHz	LFI_SkyMap_030_1024_R1.mm_nominal.fits [1]
44GHz	LFI_SkyMap_044_1024_R1.mm_nominal.fits [2]
70GHz	LFI_SkyMap_070_1024_R1.mm_nominal.fits [3]
100GHz	HFI_SkyMap_100_2048_R1.10_nominal.fits [4]
143GHz	HFI_SkyMap_143_2048_R1.10_nominal.fits [5]
217GHz	HFI_SkyMap_217_2048_R1.10_nominal.fits [6]
353GHz	HFI_SkyMap_353_2048_R1.10_nominal.fits [7]
545GHz	HFI_SkyMap_545_2048_R1.10_nominal.fits [8]

857GHz	HFI_SkyMap_857_2048_R1.10_nominal.fits [9]

Single survey maps

Frequency	Survey 1 FITS file name	Survey 2 FITS file name
30GHz	LFI_SkyMap_030_1024_R1.mm_survey_1.fits [1]	LFI_SkyMap_030_1024_R1.mm_survey_2.fits [1]
44GHz	LFI_SkyMap_044_1024_R1.mm_survey_1.fits [2]	LFI_SkyMap_044_1024_R1.mm_survey_2.fits [2]
70GHz	LFI_SkyMap_070_1024_R1.mm_survey_1.fits [3]	LFI_SkyMap_070_1024_R1.mm_survey_2.fits [3]
100GHz	HFI_SkyMap_100_2048_R1.10_survey_1.fits [4]	HFI_SkyMap_100_2048_R1.10_survey_2.fits [4]
143GHz	HFI_SkyMap_143_2048_R1.10_survey_1.fits [5]	HFI_SkyMap_143_2048_R1.10_survey_2.fits [5]
217GHz	HFI_SkyMap_217_2048_R1.10_survey_1.fits [6]	HFI_SkyMap_217_2048_R1.10_survey_2.fits [6]
353GHz	HFI_SkyMap_353_2048_R1.10_survey_1.fits [7]	HFI_SkyMap_353_2048_R1.10_survey_2.fits [7]
545GHz	HFI_SkyMap_545_2048_R1.10_survey_1.fits [8]	HFI_SkyMap_545_2048_R1.10_survey_2.fits [8]
857GHz	HFI_SkyMap_857_2048_R1.10_survey_1.fits [9]	HFI_SkyMap_857_2048_R1.10_survey_2.fits [9]

Half-ring maps

Frequency	Half-ring 1 FITS file name	Half-ring 2 FITS file name
30GHz	LFI_SkyMap_030_1024_R1.mm_nominal_ringhalf_1.fits [1]	LFI_SkyMap_030_1024_R1.mm_nominal_ringhalf_2.fits [1]
44GHz	LFI_SkyMap_044_1024_R1.mm_nominal_ringhalf_1.fits [2]	LFI_SkyMap_044_1024_R1.mm_nominal_ringhalf_2.fits [2]
70GHz	LFI_SkyMap_070_1024_R1.mm_nominal_ringhalf_1.fits [3]	LFI_SkyMap_070_1024_R1.mm_nominal_ringhalf_2.fits [3]
100GHz	HFI_SkyMap_100_2048_R1.nn_nominal_ringhalf_1.fits [4]	HFI_SkyMap_100_2048_R1.nn_nominal_ringhalf_2.fits [4]
143GHz	HFI_SkyMap_143_2048_R1.nn_nominal_ringhalf_1.fits [5]	HFI_SkyMap_143_2048_R1.nn_nominal_ringhalf_2.fits [5]
217GHz	HFI_SkyMap_217_2048_R1.nn_nominal_ringhalf_1.fits [6]	HFI_SkyMap_217_2048_R1.nn_nominal_ringhalf_2.fits [6]
353GHz	HFI_SkyMap_353_2048_R1.nn_nominal_ringhalf_1.fits [7]	HFI_SkyMap_353_2048_R1.nn_nominal_ringhalf_2.fits [7]
545GHz	HFI_SkyMap_545_2048_R1.nn_nominal_ringhalf_1.fits [8]	HFI_SkyMap_545_2048_R1.nn_nominal_ringhalf_2.fits [8]
857GHz	HFI_SkyMap_857_2048_R1.nn_nominal_ringhalf_1.fits [9]	HFI_SkyMap_857_2048_R1.nn_nominal_ringhalf_2.fits [9]

Zodi and Far-side-lobes corrected maps

```
HFI_SkyMap_100_2048_R1.nn_nominal_ZodiCorrected.fits
HFI_SkyMap_143_2048_R1.nn_nominal_ZodiCorrected.fits
HFI_SkyMap_217_2048_R1.nn_nominal_ZodiCorrected.fits
HFI_SkyMap_353_2048_R1.nn_nominal_ZodiCorrected.fits
HFI_SkyMap_545_2048_R1.nn_nominal_ZodiCorrected.fits
HFI_SkyMap_857_2048_R1.nn_nominal_ZodiCorrected.fits
```

```
HFI_SkyMap_100_2048_R1.nn_survey_1_ZodiCorrected.fits
HFI_SkyMap_143_2048_R1.nn_survey_1_ZodiCorrected.fits
HFI_SkyMap_217_2048_R1.nn_survey_1_ZodiCorrected.fits
```

```
HFI_SkyMap_353_2048_R1.nn_survey_1_ZodiCorrected.fits
HFI_SkyMap_545_2048_R1.nn_survey_1_ZodiCorrected.fits
HFI_SkyMap_857_2048_R1.nn_survey_1_ZodiCorrected.fits
HFI_SkyMap_100_2048_R1.nn_survey_2_ZodiCorrected.fits
HFI_SkyMap_143_2048_R1.nn_survey_2_ZodiCorrected.fits
HFI_SkyMap_217_2048_R1.nn_survey_2_ZodiCorrected.fits
HFI_SkyMap_353_2048_R1.nn_survey_2_ZodiCorrected.fits
HFI_SkyMap_545_2048_R1.nn_survey_2_ZodiCorrected.fits
HFI_SkyMap_857_2048_R1.nn_survey_2_ZodiCorrected.fits
```

FITS file structure

The FITS files for the sky maps contain a minimal primary header with no data, and a *BINTABLE* extension (EXTENSION 1, EXTNAME = 'FREQ-MAP') containing the data. The structure is shows schematically in the figure at right.

The *FREQ-MAP* extension contains is a 3-column table of that contain the signal, variance, and hit-count maps, all in Healpix format, in columns 1, 2, and 3, respectively. The number of rows is 50331648 for HFI and 12582912 for LFI, corresponding to the number of pixels in a Healpix map of Nside= 2048 and 1024, respectively (N.B: Npix = 12 Nside^2). The three columns are *I_STOKES* for the intensity (or temperature) signal, *II_COV* for the variance, and *HIT* for the hit-count. The exact order of the columns in the figure is indicative only, and the details can be found in the keywords.

Keywords indicate the coordinate system (GALACTIC), the Healpix ordering scheme (NESTED), the units (K_cmb or MJy/sr) of each column, and of course the frequency channel (FREQ). The COMMENT fields give a one-line summary of the product, and some other information useful for traceability within the DPCs. The original filename is also given in the *FILENAME* keyword as are the datasum and the md5 checksum for the extension. The *BAD_DATA* keyword gives the value used by Healpix to indicate pixels for which no signal is present (these will also have a hit-count value of 0). The COMMENT fields give further information including some traceability data for the DPC's. The main parameters are summarised below:

Map file data structure

Column Name	Data Type	Units	Description
1. EXTNAME = 'FREQ-MAP' : Data columns			
I_STOKES	Real*4	K_cmb or MJy/sr	The signal map
II_COV	Real*4	K_cmb^2 or (MJy/sr)^2	The variance map
HIT	Int*4	none	The hit-count map
Keywords			
PIXTYPE	string	HEALPIX	
COORDSYS	string	GALACTIC	Coordinate system
ORDERING	string	NESTED	Healpix ordering
NSIDE	Int	1024 or 2048	Healpix Nside for LFI and HFI, repsectively
FIRSTPIX	Int*4	0	First pixel number
LASTPIX	Int*4	12582912 or 50331647	Last pixel number, for LFI and HFI, repsectively
FREQ	string	nnn	The frequency channel (3 chars)

The same structure applies to all *SkyMap* products, independent of whether they are full channel, survey of half-ring. The distinction between the types of maps is present in the FITS filename (and in the traceability comment fields).

References

<biblio force=false>

1. References

</biblio>

References

[1] http://pladev.esac.esa.int/pla/aio/metadata-action?RESOURCE_CLASS=FREQUENCY_MAP&SELECTED_FIELDS=MAP.MAP_ID,MAP.SIZE,MAP_PERIOD.NAME,INSTRUMENT.NAME&INSTRUMENT.NAME=LFI&FREQUENCY.VALUE=30&MAP_PERIOD.NAME=Nominal&FREQUENCY_MAP.JACKKNIFE=&RELEASE.NAME=PR1&RETURN_TYPE=HTML

[2] http://pladev.esac.esa.int/pla/aio/metadata-action?RESOURCE_CLASS=FREQUENCY_MAP&SELECTED_FIELDS=MAP.MAP_ID,MAP.SIZE,MAP_PERIOD.NAME,INSTRUMENT.NAME&INSTRUMENT.NAME=LFI&FREQUENCY.VALUE=44&MAP_PERIOD.NAME=Nominal&FREQUENCY_MAP.JACKKNIFE=&RELEASE.NAME=PR1&RETURN_TYPE=HTML

[3] http://pladev.esac.esa.int/pla/aio/metadata-action?RESOURCE_CLASS=FREQUENCY_MAP&SELECTED_FIELDS=MAP.MAP_ID,MAP.SIZE,MAP_PERIOD.NAME,INSTRUMENT.NAME&INSTRUMENT.NAME=LFI&FREQUENCY.VALUE=70&MAP_PERIOD.NAME=Nominal&FREQUENCY_MAP.JACKKNIFE=&RELEASE.NAME=PR1&RETURN_TYPE=HTML

[4] http://pladev.esac.esa.int/pla/aio/metadata-action?RESOURCE_CLASS=FREQUENCY_MAP&SELECTED_FIELDS=MAP.MAP_ID,MAP.SIZE,MAP_PERIOD.NAME,INSTRUMENT.NAME&INSTRUMENT.NAME=HFI&FREQUENCY.VALUE=100&MAP_PERIOD.NAME=Nominal&FREQUENCY_MAP.JACKKNIFE=&RELEASE.NAME=PR1&RETURN_TYPE=HTML

[5] http://pladev.esac.esa.int/pla/aio/metadata-action?RESOURCE_CLASS=FREQUENCY_MAP&SELECTED_FIELDS=MAP.MAP_ID,MAP.SIZE,MAP_PERIOD.NAME,INSTRUMENT.NAME&INSTRUMENT.NAME=HFI&FREQUENCY.VALUE=143&MAP_PERIOD.NAME=Nominal&FREQUENCY_MAP.JACKKNIFE=&RELEASE.NAME=PR1&RETURN_TYPE=HTML

[6] http://pladev.esac.esa.int/pla/aio/metadata-action?RESOURCE_CLASS=FREQUENCY_MAP&SELECTED_FIELDS=MAP.MAP_ID,MAP.SIZE,MAP_PERIOD.NAME,INSTRUMENT.NAME&INSTRUMENT.NAME=HFI&FREQUENCY.VALUE=217&MAP_PERIOD.NAME=Nominal&FREQUENCY_MAP.JACKKNIFE=&RELEASE.NAME=PR1&RETURN_TYPE=HTML

[7] http://pladev.esac.esa.int/pla/aio/metadata-action?RESOURCE_CLASS=FREQUENCY_MAP&SELECTED_FIELDS=MAP.MAP_ID,MAP.SIZE,MAP_PERIOD.NAME,INSTRUMENT.NAME&INSTRUMENT.NAME=HFI&FREQUENCY.VALUE=353&MAP_PERIOD.NAME=Nominal&FREQUENCY_MAP.JACKKNIFE=&RELEASE.NAME=PR1&RETURN_TYPE=HTML

[8] http://pladev.esac.esa.int/pla/aio/metadata-action?RESOURCE_CLASS=FREQUENCY_MAP&SELECTED_FIELDS=MAP.MAP_ID,MAP.SIZE,MAP_PERIOD.NAME,INSTRUMENT.NAME&INSTRUMENT.NAME=HFI&FREQUENCY.VALUE=545&MAP_PERIOD.NAME=Nominal&FREQUENCY_MAP.JACKKNIFE=&RELEASE.NAME=PR1&RETURN_TYPE=HTML

[9] http://pladev.esac.esa.int/pla/aio/metadata-action?RESOURCE_CLASS=FREQUENCY_MAP&SELECTED_FIELDS=MAP.MAP_ID,MAP.SIZE,MAP_PERIOD.NAME,INSTRUMENT.NAME&INSTRUMENT.NAME=HFI&FREQUENCY.VALUE=857&MAP_PERIOD.NAME=Nominal&FREQUENCY_MAP.JACKKNIFE=&RELEASE.NAME=PR1&RETURN_TYPE=HTML

The RIMO

Overview

The RIMO, or *Reduced Instrument Model* is a FITS file containing selected instrument characteristics that are needed by users who work with the released data products. It is described in detail in *The HFI and LFI RIMO ICD* (ref). There will be two RIMOs, one for each instrument, which will follow the same overall structure, but will differ in the details. The type of data in the RIMO can be:

Parameter

: namely scalars to give properties such as a noise level or a representative beam FWHM

Table

: to give, e.g., filter transmission profiles or noise power spectra

Image

: namely 2-D "flat" array, to give, e.g., the beam correlation matrices

The FITS file begins with primary header that contains some keywords that mainly for internal use and no data. The different types of data are written into different BINTABLE (for parameters and tables) or IMAGE (for 2-D arrays) extensions, as described below.

Map-level parameter data

The map-level data table contains the effective beam solid angle (total and out to different multiples of the beamFWHM) and noise information. It is written into a BINTABLE extension named *MAP_PARAMS* whose structure is as follows:

FREQUENCY

: a 3-digit string giving the reference frequency in GHz, i.e., of the form *044* or *217*

OMEGA_F, *OMEGA_F_ERR*

: the full beam solid angle and its uncertainty, in armin^2

OMEGA_1, *OMEGA_1_DISP*

: the beam solid angle out to 1FWHM, and its dispersion, in arcmin^2

OMEGA_2, *OMEGA_2_DISP*

: the beam solid angle out to 2FWHM, and its dispersion, in arcmin^2

FWHM

: FWHM of a Gaussian beam having the same (total) solid angle, in sr. This is the best value for source flux determination

FWHMGAUS

: FWHM derived from best Gaussian fit to beam maps, in sr. This is the best value for source identification

NOISE

: This is the typical noise/valid observation sample as derived from the high *ell* spectra of the half-ring maps, in the units of the corresponding map

For the Omega columns, the 'DISP' (for *dispersion*) column gives an estimate of the spatial variation as a function of position on the sky. This is the variation induced by combining the scanning beam determined from the planet observations with the scanning strategy, as described in Detectors pointing & beam.

Effective band transmission profiles

The effective filter bandpasses are given in different BINTABLE extensions. The extension is named *BANDPASS_{name}*, where *name* specified the frequency channel. In the case of the maps, the bandpasses are a weighted average of the bandpasses of the detectors that are used to build the map. For details see #planck2013-p03d. The bandpasses are given as 4-column tables containing:

WAVENUMBER

the wavenumber in cm-1, conversion to GHz is accomplished by multiplying by $10^{-7}c$[mks].

TRANSMISSION

the transmission (normalized to 1 at the max for HFI and to have an integral of 1 for LFI)

ERROR

the statistical $1-\sigma$uncertainty for the transmission profile (not provided for LFI).

FLAG

a flag indicating if the data point is an independent frequency data point (nominally the case), or an FTS instrument line shape (ILS)-interpolated data point. The frequency data has been over-sampled by a factor of ~10 to assist in CO component separation efforts #planck2013-p03a, #planck2013-p03d.

The number of rows will differ among the different extensions, but are the same, by construction, within each extension.

Beam Window Functions

Beam window functions and associated error descriptions are written into a BINTABLE for each *detection unit*, where *detection unit* consists of an auto or a cross product of one or two frequency maps or detset maps used in the likelihood. Here they are:

- the 6 HFI frequency channels, producing 21 extensions
  - 100, 143, 217, 353, 545, 857
- 26 detsets, producing 351 extensions; the detsets used are, by frequency channel:
  - 100-DS1, 100-DS2,
  - 143-DS1, 143-DS2, 143-5, 143-6, 143-7,
  - 217-DS1, 217-DS2, 217-1, 217-2, 217-3, 217-4,
  - 353-DS1, 353-DS2, 353-1, 353-2, 353-7, 353-8,
  - 545-1, 545-2, 545-4,
  - 857-1, 857-2, 857-3, 857-4

and the extension names are of the form *BEAM_WF_U1XU2* where U1 and U2 are one (possibly the same) detection unit from one of the main groups above (i.e. there are no cross products between detsets and frequency channels, or between HFI and LFI). Each extension contains the columns:

- *NOMINAL* (Real*4) with the window function proper,
- *EIGEN_n* (Real*4, n=1-5), with the error modes.

and the following keywords

- *NUMVECT* (Integer) specified the number of eigenmode vectors, and
- *LMIN* and *LMAX* (Integer) which give the length of nominal vector
- *LMIN_EM* and *LMAX_EM* (Integer) that give the range of the valid samples of the eigenmode vectors. Here *LMAX_EM* is always less than or equal to *LMAX*, and the values between *LMAX_EM*+1 and LMAX is set to NaN

Beam Correlation Matrix

Two of these matrices are given, in two *IMAGE* extensions

- CORREL_FREQ, for the frequency channels (21 units),
- CORREL_DETS for the detsets (351 units).

Each is a symmetric matrix with 1-valued diagonal, made of NBEAMS*NBEAMS blocks, each block being NMODES*NMODES in size. Each row- (and column-) block entry relates to the B(l) model whose name is indicated in ROW_U1XU2 keywords, and the corresponding eigenmodes are stored in a HDU of the same name.

Effective Beams

TBW

Product description

A general description of the product, including e.g. figures related to the contents (e.g. maps, tables), and some explanation of its scientific meaning. If there are scientific warnings about the use of the product (User's caveats), they should also be given here, or at least references to other explanatory documents (papers etc).

Production process

Description of the Pipeline used to generate the product. In particular any limitations and approximations used in the data processing should be listed. Avoiding detailed descriptions of methods and referring to other parts of the ES and/or the relevant Planck papers for the details. References however should be quite detailed (i.e. it is not enough to direct the user to a paper, but the relevant section in the paper should be provided).

Inputs

A list (and brief description to the extent possible) of the input data used to generate this product (down to file names), as well as any external ancillary data sets which were used.

Related products

A description of other products that are related and share some commonalities with the product being described here. E.g. if the description is of a generic product (e.g. frequency maps), all the products falling into that type should be listed and referenced.

Meta data

A detailed description of the data format of each file, including header keywords for fits files, extension names, column names, formats….

Catalogues

Product description

A general description of the product, including e.g. figures related to the contents (e.g. maps, tables), and some explanation of its scientific meaning. If there are scientific warnings about the use of the product (User's caveats), they should also be given here, or at least references to other explanatory documents (papers etc).

The Planck Catalogue of Compact Sources (PCCS) comprises a set of nine single-frequency source catalogues. The catalogues contain high-reliability sources, both Galactic and extragalactic, detected over the entire sky, making use of the nominal mission data. No polarization information is provided for the sources at this time. The PCCS differs in philosophy from the ERCSC in that it puts more emphasis on the completeness of the catalogue, with-out reducing notably the reliability of the detected sources. The greater amount of data, different selection process and the improvements in the calibration and map-making processing (#planck2013-p02,#planck2013-p03 and references therein) help the PCCS to improve upon the performance of the ERCSC.

Table 1: PCCS characteristics

Channel	30	44	70	100	143	217	353	545	857
Frequency [GHz]	28.4	44.1	70.4	100.0	143.0	217.0	353.0	545.0	857.0
Beam FWHM [arcmin]	32.38	27.10	13.30	9.88	7.18	4.87	4.65	4.72	4.39
SNR threshold	4.0	4.0	4.0	4.6	4.7	4.8	4.9/6.0	4.7/7.0	4.9/7.0
#	1256	731	939	2813	4616	14215	18507	14572	20076
# (|b| > 30°)	572	258	332	599	795	1523	2074	1694	3804

Before using the PCCS, please read the Cautionary Notes in the PCCS general description section.

For full details, see paper #planck2013-p05.

Production process

For a description of the production and validation processes of the PCCS see the corresponding section.

Inputs

The data obtained from the Planck nominal mission between 2009 August 13 and 2010 November 27, corresponding to operational days 91--636, have been processed into full-sky maps by the HFI and LFI Data Processing Centres (DPCs). A description of the processing can be found in #planck2013-p02,#planck2013-p03. The data consist of two complete sky surveys and 60% of the third survey. This implies that the flux densities of sources obtained from the nominal mission maps are the average of at least two observations. The nine Planck frequency channel maps are used as input to the source detection pipelines. For the high-frequency channels, 353, 545 and 857 GHz, the model of the Zodiacal Light Emission (ZLE) (?) has been subtracted from the maps before detecting the sources. The relevant properties of the frequency maps and main parameters used to generate the catalogues are summarized in Table 1.

A list (and brief description to the extent possible) of the input data used to generate this product (down to file names), as well as any external ancillary data sets which were used.

- frequency maps
- RIMO
- effective beams

To be reviewed and compiled by Joaquin/Mark.

Related products

A description of other products that are related and share some commonalities with the product being described here. E.g. if the description is of a generic product (e.g. frequency maps), all the products falling into that type should be listed and referenced.

link to pages with other catalogues

1. ERCSC
2. SZ catalogue

File names

COM_PCCS_030_R1.mm.fits

COM_PCCS_044_R1.mm.fits

COM_PCCS_070_R1.mm.fits

COM_PCCS_100_R1.mm.fits

COM_PCCS_143_R1.mm.fits

COM_PCCS_217_R1.mm.fits

COM_PCCS_353_R1.mm.fits

COM_PCCS_545_R1.mm.fits

COM_PCCS_857_R1.mm.fits

Meta Data

The PCCS source list in each frequency is structured as a FITS binary table having one row for each detected source.

The FITS primary header will have the following structure:

FITS primary header

FITS Keyword	Data Type	Units	Description
INSTRUME	String		LFI or HFI
VERSION	String		Version of PCCS
DATE	String		Date file created:yyyy-mm-dd
ORIGIN	String		Name of organization responsible for the data (LFI-DPC – HFI-DPC)
TELESCOP	String		PLANCK
CREATOR	String		Pipeline Version
DATE-OBS	String	days	Start-up time of the survey: yyyy-mm-dd
DATE-END	String	days	Ending time of the survey: yyyy-mm-dd

The Fits extension is composed by several columns described below:

FITS header

Column Name	Data Type	Units	Description
Identification			
NAME	String		Source name – see Note 1
Source Position			
GLON	Real*8	degrees	Galactic longitude based on extraction algorithm
GLAT	Real*8	degrees	Galactic latitude based on extraction algorithm
RA	Real*8	degrees	Right ascension (J2000) transformed from (GLON,GLAT)
DEC	Real*8	degrees	Declination (J2000) transformed from (GLON,GLAT)
Photometry			
DETFLUX	Real*4	mJy	Flux density of source as determined by detection method
DETFLUX_ERR	Real*4	mJy	Uncertainty (1 sigma) in derived flux density from detection method
APERFLUX	Real*4	mJy	Flux density of source as determined from the aperture photometry
APERFLUX_ERR	Real*4	mJy	Uncertainty (1 sigma) in derived flux density from the aperture photometry
PSFFLUX	Real*4	mJy	Flux density of source as determined from PSF fitting
PSFFLUX_ERR	Real*4	mJy	Uncertainty (1 sigma) in derived flux density from PSF fitting
GAUFLUX	Real*4	mJy	Flux density of source as determined from 2-D Gaussian fitting
GAUFLUX_ERR	Real*4	mJy	Uncertainty (1 sigma) in derived flux density from 2-D Gaussian fitting
GAU_SEMI1	Real*4	arcmin	Gaussian fit along axis 1 (see Note 4 for axis definition)
GAU_SEMI1_ERR	Real*4	arcmin	Uncertainty (1 sigma) in derived Gaussian fit along axis 1
GAU_SEMI2	Real*4	arcmin	Gaussian fit along axis 2
GAU_SEMI2_ERR	Real*4	arcmin	Uncertainty (1 sigma) in derived Gaussian fit along axis 2
GAU_THETA	Real*4	deg	Gaussian fit orientation angle counting anti-clockwise from the x -axis
GAU_THETA_ERR	Real*4	deg	Uncertainty (1 sigma) in derived gaussian fit orientation angle
GAU_FWHM_EFF	Real*4	arcmin	Gaussian fit effective FWHM
Flags and validation			
EXTENDED	Integer*2		Flag indicated that source is extended
CIRRUS_N	Integer*4		Number of sources detected at 857 GHz within HFI TBC degrees
EXT_VAL	Integer*2		Flag indicated external validation - see Note 2
ERCSC	String		Name of the ERCSC counterpart if any
ONLY 857 GHz Catalogue			
APERFLUX_217	Real*4	mJy	Source flux density at 217 GHz (best estimation) of the object detected at 857
APERFLUX_ERR_217	Real*4	mJy	Uncertainty in source flux density
APERFLUX_353	Real*4	mJy	Source flux density at 353 GHz (best estimation) of the object detected at 857
APERFLUX_ERR_353	Real*4	mJy	Uncertainty in source flux density
APERFLUX_545	Real*4	mJy	Source flux density at 545 GHz (best estimation) of the object detected at 857
APERFLUX_ERR_545	Real*4	mJy	Uncertainty in source flux density

Note 1.- Source name designations consist of a prefix and a positional qualifier, the latter is in Galactic coordinates and specified as "Glll.ll±bb.bb" where the (l,b) values are truncated. The prefix used in the single band portion of the

PCCS is PLCK1 ddd PCCS catalogue at ddd GHz.

For example, a source detected at (l,b) = (120.237, 4.231) in the 545 GHz Planck map would be labelled PLCK545 G120.23±04.23.

Note 2.- The EXTENDED flag has the value of 0 if the source is compact and the value of 1 is it extended. The source size is determined by the geometric mean of the Gaussian fit FWHMs, with the criteria for extension being sqrt(GAU_FWHMMAJ * GAU_FWHMIN) > 1.5 times the beam FWHM.

Note 3.- The EXT_VAL flag has the value of 0, 1, or 2, based on the following conditions:

- 2 – The source has a clear counterpart in one of the catalogues considered as ancillary data.
- 1 – The source has NOT a clear counterpart in one of the catalogues considered as ancillary data but it has been detected by the internal multi-frequency method.
- 0 – The source has NOT a clear counterpart in one of the catalogues considered as ancillary data and it has NOT been detected by the internal multi-frequency method.

Note 4.- The x axis is defined for each source as parallel to the constant colatitude line, with the same direction as the longitude. Therefore the position angles are measured anticlockwise from the x axis.

```
XTENSION= 'BINTABLE'           /Written by IDL:  Tue Feb 26 17:50:21 2013
BITPIX  =                    8 /
NAXIS   =                    2 /Binary table
NAXIS1  =                  145 /Number of bytes per row
NAXIS2  =                 1256 /Number of rows
PCOUNT  =                    0 /Random parameter count
GCOUNT  =                    1 /Group count
TFIELDS =                   24 /Number of columns
DATE    = '2013-02-26'         /Creation date
INSTRUME= 'LFI     '           /Low Frequency Instrument
VERSION = '1.0     '           /Version of PCCS
ORIGIN  = 'LFI-DPC '           /Organisation responsible for data
TELESCOP= 'PLANCK  '           /Planck
CREATOR = 'Nov12-v03'          /Pipeline version
DATE-OBS= '2009-08-13'         /Start time of the survey
DATE-END= '2010-11-26'         /End time of the survey
EXTNAME = 'PCCS1_f030'         /Extension name
TFORM1  = '23A     '           /Character string
TTYPE1  = 'NAME    '           /Label for column 1
TUNIT1  = 'None    '           /Units of column 1
TFORM2  = '1D      '           /Real*8 (double precision)
TTYPE2  = 'GLON    '           /Label for column 2
TUNIT2  = 'degrees '           /Units of column 2
TFORM3  = '1D      '           /Real*8 (double precision)
TTYPE3  = 'GLAT    '           /Label for column 3
TUNIT3  = 'degrees '           /Units of column 3
TFORM4  = '1D      '           /Real*8 (double precision)
TTYPE4  = 'RA      '           /Label for column 4
TUNIT4  = 'degrees '           /Units of column 4
TFORM5  = '1D      '           /Real*8 (double precision)
TTYPE5  = 'DEC     '           /Label for column 5
TUNIT5  = 'degrees '           /Units of column 5
```

```
TFORM6  = '1E      '           /Real*4 (floating point)
TTYPE6  = 'DETFLUX '           /Label for column 6
TUNIT6  = 'mJy     '           /Units of column 6
TFORM7  = '1E      '           /Real*4 (floating point)
TTYPE7  = 'DETFLUX_ERR'        /Label for column 7
TUNIT7  = 'mJy     '           /Units of column 7
TFORM8  = '1E      '           /Real*4 (floating point)
TTYPE8  = 'APERFLUX'           /Label for column 8
TUNIT8  = 'mJy     '           /Units of column 8
TFORM9  = '1E      '           /Real*4 (floating point)
TTYPE9  = 'APERFLUX_ERR'       /Label for column 9
TUNIT9  = 'mJy     '           /Units of column 9
TFORM10 = '1E      '           /Real*4 (floating point)
TTYPE10 = 'PSFFLUX '           /Label for column 10
TUNIT10 = 'mJy     '           /Units of column 10
TFORM11 = '1E      '           /Real*4 (floating point)
TTYPE11 = 'PSFFLUX_ERR'        /Label for column 11
TUNIT11 = 'mJy     '           /Units of column 11
TFORM12 = '1E      '           /Real*4 (floating point)
TTYPE12 = 'GAUFLUX '           /Label for column 12
TUNIT12 = 'mJy     '           /Units of column 12
TFORM13 = '1E      '           /Real*4 (floating point)
TTYPE13 = 'GAUFLUX_ERR'        /Label for column 13
TUNIT13 = 'mJy     '           /Units of column 13
TFORM14 = '1E      '           /Real*4 (floating point)
TTYPE14 = 'GAU_SEMI1'          /Label for column 14
TUNIT14 = 'arcmin  '           /Units of column 14
TFORM15 = '1E      '           /Real*4 (floating point)
TTYPE15 = 'GAU_SEMI1_ERR'      /Label for column 15
TUNIT15 = 'arcmin  '           /Units of column 15
TFORM16 = '1E      '           /Real*4 (floating point)
TTYPE16 = 'GAU_SEMI2'          /Label for column 16
TUNIT16 = 'arcmin  '           /Units of column 16
TFORM17 = '1E      '           /Real*4 (floating point)
TTYPE17 = 'GAU_SEMI2_ERR'      /Label for column 17
TUNIT17 = 'arcmin  '           /Units of column 17
TFORM18 = '1E      '           /Real*4 (floating point)
TTYPE18 = 'GAU_THETA'          /Label for column 18
TUNIT18 = 'degrees '           /Units of column 18
TFORM19 = '1E      '           /Real*4 (floating point)
TTYPE19 = 'GAU_THETA_ERR'      /Label for column 19
TUNIT19 = 'degrees '           /Units of column 19
TFORM20 = '1E      '           /Real*4 (floating point)
TTYPE20 = 'GAU_FWHM_EFF'       /Label for column 20
TUNIT20 = 'arcmin  '           /Units of column 20
TFORM21 = '1I      '           /Integer*2 (short integer)
TTYPE21 = 'EXTENDED'           /Label for column 21
```

```
TUNIT21 = '0/1     '           /Units of column 21
TNULL21 =                   -1 /Null value for column 21
TFORM22 = '1I      '           /Integer*2 (short integer)
TTYPE22 = 'CIRRUS_N'           /Label for column 22
TUNIT22 = 'None    '           /Units of column 22
TNULL22 =                   -1 /Null value for column 22
TFORM23 = '1I      '           /Integer*2 (short integer)
TTYPE23 = 'EXT_VAL '           /Label for column 23
TUNIT23 = '0/1/2   '           /Units of column 23
TNULL23 =                   -1 /Null value for column 23
TFORM24 = '24A     '           /Character string
TTYPE24 = 'ERCSC   '           /Label for column 24
TUNIT24 = 'None    '           /Units of column 24
```

Early Release Compact Source Catalogue

see ERCSC

Note to LM: move this to a separate page

The Bibliography

<biblio force=false>

1. References

</biblio>

Catalogues ERCSC

The Plank Early Release Compact Source Catalogue was the first Planck product to be publicly released in Jan 2011. It was produced with a very rapid turnaround to facilitate follow-up observations with existing cryogenic observatories such as Herschel. It contained a list of all high reliability sources, both Galactic and extragalactic, that were derived from the first all sky coverage by Planck. The data that went into the ERCSC comprised all observations undertaken between 13 August 2009 and 6 June 2010, corresponding to Planck operational days 91–389. Since the Planck scan strategy results in the entire sky being observed every 6 months, the data considered in the ERCSC release corresponded to the first sky coverage and 60% of the second sky coverage. The goals on photometric accuracy were 30% while the positional accuracy goal translated to a positional root mean square (RMS) uncertainty that is less than 1/5 of the beam full width at half maximum (FWHM).

The ERCSC consisted of single frequency source lists, one at each of the nine Planck frequencies. The number of sources in the lists range from 705 at 30 GHz to 8988 at 857 GHz. No attempt was made to cross-match the sources from the different frequencies due to the wide range of spatial resolutions (33 arcmin at 30 GHz to 4.3 arcmin at 857 GHz) spanned by Planck. Two additional catalogues which consisted of a list of Cold Cores of interstellar molecular clouds within the Galaxy and a list of galaxy clusters detected through the Sunyaev- Zel’dovich effect, were provided. These consisted of candidate sources that were detected using multifrequency algorithms that use the distinct spectral signature of such sources through the Planck frequency channels. The early Cold Cores (ECC) list comprised of 915 sources while the early Sunyaev-Zel'dovich (ESZ) effect detected cluster list consisted of 189 sources. In all, there are more than 15000 unique sources in these early catalogues.

In order to generate the ERCSC, four source detection algorithms were run as part of the ERCSC pipeline. A Monte-Carlo algorithm based on the injection and extraction of artificial sources into the Planck maps was implemented to select reliable sources among all extracted candidates such that the cumulative reliability of the catalogue is >90%. Reliability is defined as the fraction of sources in the catalog which have measured flux densities which are within 30% of their true flux density. There is no requirement on completeness for the ERCSC. As a result of the Monte-Carlo assessment of reliability of sources from the different techniques, an implementation of the PowellSnakes source extraction technique was used at the five frequencies between 30 and 143GHz while the SExtractor technique was used between 217 and 857GHz. The 10σ photometric flux density limit of the catalogue at $|b| > 30$ deg is 0.49, 1.0, 0.67, 0.5, 0.33, 0.28, 0.25, 0.47 and 0.82 Jy at each of the nine frequencies between 30 and 857GHz. Sources which are up to a factor of ~2 fainter than this limit, and which are present in "clean" regions of the Galaxy where the sky background due to emission from the interstellar medium is low, are included in the ERCSC if they meet the high reliability criterion. The sensitivity of the ERCSC is shown in the figure below. The Planck ERCSC sources have known associations to stars with dust shells, stellar cores, radio galaxies, blazars, infrared luminous galaxies and Galactic interstellar medium features. A significant fraction of unclassified sources are also present in the catalogs.

The multifrequency information from Planck allows some basic classification of the sources to be undertaken. In the Galactic plane, at frequencies below 100 GHz, the majority of the sources are dominated by synchrotron or free-free emission. At the higher frequencies, the sources are almost exclusively dominated by thermal dust emission. At high Galactic latitudes however, the synchrotron sources dominate the source counts to 217 GHz with dusty sources being the primary source population at 353 GHz and higher. Recent attempts to classify a subset of the Planck 857 GHz sources at high latitudes based on cross-correlations with sources in other catalogs such as WISE and SDSS, found that almost half of them are associated with stars and low-redshift galaxies while a significant fraction (44%) might be interstellar medium features (Johnson et al 2013, AAS, 22135218J).

Full details on the construction, contents and usage of the ERCSC, ECC and ESZ catalogues can be found in Planck Early Results VII, VIII and XXIII (Planck Collaboration 2011, A&A, A7, A8 and A23 respectively).

Figure: The Planck ERCSC flux density limit, quanitfied as the faintest ERCSC source at |b|<10 deg (dashed black line) and at |b|>30 deg (solid black line), is shown relative to other wide area surveys (From Planck Collaboration 2011, A&A, 536, A7). Also shown are spectra of known sources of foreground emission as red lines. The ERCSC sensitivity is worse in the Galactic plane due to the strong contribution of ISM emission, especially at submillimeter wavelengths. At face value, the WMAP and Planck flux density limits appear to be comparable at the lowest frequencies, but the Planck ERCSC is much more complete as discussed in Planck Collaboration (2011).

Frequency maps angular power spectra

Here will be a number of power spectra.

- For HFI, these are the auto and cross-spectra of the 13 detector (set) maps at 100, 143 and 217GHz, all masked with mask2 for ease of comparison. These are the maps used in the High-ell likelihood, although in the likelihood the cross-spectra used are obtained with different masks according to specific cross-spectra.
- For LFI, these will be at 30, 40, and 70 GHz. To Be filled by Polenta

HFI frequency maps power spectra

Outstanding:EFH to add the purpose of these spectra and of the associated covariance matrices, and a description of how they are obtained, including the inputs used to build them (maps, beams, mask), AMo to add description of FITS file with sample header. NB. contrary to the R1.00 (pre-)delivery, in the R1.10 final delivery each spectrum and associated covar matrix will be packaged together in a single file.

Product description

A general description of the product, including e.g. figures related to the contents (e.g. maps, tables), and some explanation of its scientific meaning. If there are scientific warnings about the use of the product (User's caveats), they should also be given here, or at least references to other explanatory documents (papers etc).

Production process

Description of the Pipeline used to generate the product. In particular any limitations and approximations used in the data processing should be listed. Avoiding detailed descriptions of methods and referring to other parts of the ES and/or the relevant Planck papers for the details. References however should be quite detailed (i.e. it is not enough to direct the user to a paper, but the relevant section in the paper should be provided).

Inputs

A list (and brief description to the extent possible) of the input data used to generate this product (down to file names), as well as any external ancillary data sets which were used.

Related products

A description of other products that are related and share some commonalities with the product being described here. E.g. if the description is of a generic product (e.g. frequency maps), all the products falling into that type should be listed and referenced.

Meta data

A detailed description of the data format of each file, including header keywords for fits files, extension names, column names, formats….

LFI frequency maps power spectra

Product description

The angular power spectrum provides information about the distribution of power on the sky map at the various angular scales. It is especially important for CMB, because it is characterized by a number of features, most notably the acoustic peaks, that encode the dependence from cosmological parameters. Therefore, angular power spectra are the basic inputs for the Planck Likelihood Code, and for estimation of cosmological parameters in general.

For this release we have computed only temperature power spectra. Polarization is not included.

Please note that these spectra come from frequency maps. No component separation has been applied, and we have only masked Galactic Plane and detected point sources. Units are μK^2_{CMB}.

Production process

Spectra are computed using cROMAster, a implementation of the pseudo-Cl method described in Hivon et al, 2002 [1]. In addition to the original approach, our implementation allows for estimation of cross-power spectra from two or more maps (see Polenta et al, 2005, [2] for details). The software package uses HEALPix [3] modules for spherical harmonic transform and Cl calculation. The schematic of the estimation process is as follows:

- computing the a_lm coefficients from the input temperature map after masking Galactic Plane and point sources.
- computing the pseudo power spectrum from the alms.
- estimating the bias due to the noise power spectrum of the map from noise-only Monte Carlo simulations based on detector noise properties
- correcting for the effect of the adopted mask by computing the mode-mode coupling kernel corresponding to that mask
- deconvolving the effect due to the finite angular resolution of the telescope by using the beam window function
- deconvolving the effect due to the finite size of the pixel in the map by using a pixel window function
- binning the power spectrum from individual multipoles into bandpowers
- estimating error bars on bandpowers from signal plus noise Monte Carlo simulations, where signal simulations include only CMB anisotropies.

Inputs

- LFI Frequency Maps
- Galactic Plane and point source masks
- Beam window functions
- Monte Carlo simulations
- binning scheme

Related products

A description of other products that are related and share some commonalities with the product being described here. E.g. if the description is of a generic product (e.g. frequency maps), all the products falling into that type should be listed and referenced.

Meta data

A detailed description of the data format of each file, including header keywords for fits files, extension names, column names, formats….

References

[1] http://adsabs.harvard.edu/abs/2002ApJ...567....2H
[2] http://adsabs.harvard.edu/abs/2005JCAP...11..001P
[3] http://healpix.sourceforge.net/

Astrophysical component maps

Overview

This section is very preliminary. Its purpose is to give examples of what these products could look like.

This section describes the astrophysical component maps are similar products that are provided in a joint effort by the two DPC. These products are derived from some or all of the nine channel maps described above using different techniques and, in some cases, using other constraints from external data sets. Here we give a brief description of the product and how it is obtained, followed by a description of the FITS file containing the data and associated information.

Two different types of structure are used for these products depending on whether the astrophysical component varies with frequency:

independent of frequency

: in this case a single map to give the structure suffices. It will (optionally) be accompanied by an uncertainty map a mask and possibly a beam window function, and a method will be given to convert the structure map to the map at a given frequency. This applies to the CMB and to the dust opacity.

variable with frequency

: in this case the file will contain up to 10 signal maps, for the 10 Planck frequencies, accompanied (optionally) by uncertainties a mask.

CMB maps

NOTE: Text in red to be removed when filling the contents

Product description

A general description of the product, including e.g. figures related to the contents (e.g. maps, tables), and some explanation of its scientific meaning. If there are scientific warnings about the use of the product (User's caveats), they should also be given here, or at least references to other explanatory documents (papers etc).

Three different estimates of the CMB are produced. The subsections below give a brief description of each method, and what are its advantages. Details of the motivations can be found in the corresponding paper #planck2013-06[06].

The CMB data are in thermodynamic temperature units (uK_cmb), and the residuals are in the units of the original sky map (K_cmb for the CMB channels, and MJy/sr for the Galactic channels). As usual, all maps are in Galactic coordinate and use Nested ordering scheme.

SMICA

Cardoso to write brief intro with purpose, production method, inputs used, constraints

NILC

Cardoso to write brief intro with purpose, production method, inputs used, constraints

Sevem

The aim of Sevem is to produce clean CMB maps at one or several frequencies by using a procedure based on template fitting. The templates are internal, i.e., they are constructed from Planck data, avoiding the need for external data sets, which usually complicates the analyses and may introduce inconsistencies. The method has been successfully applied to Planck simulations Leach et al., 2008 and to WMAP polarisation data Fernandez-cobos et al., 2012. In the cleaning process, no assumptions about the foregrounds or noise levels are needed, rendering the technique very robust.

Production process

Description of the Pipeline used to generate the product. In particular any limitations and approximations used in the data processing should be listed. Avoiding detailed descriptions of methods and referring to other parts of the ES and/or the relevant Planck papers for the details. References however should be quite detailed (i.e. it is not enough to direct the user to a paper, but the relevant section in the paper should be provided).

SMICA

Cardoso to write brief intro with purpose, production method, inputs used, constraints

NILC

Cardoso to write brief intro with purpose, production method, inputs used, constraints

Sevem

The templates are constructed by subtracting two neighbouring Planck frequency channel maps, after first smoothing them to a common resolution to ensure that the CMB signal is properly removed. A linear combination of the templates is then subtracted from the Planck sky map at the frequency to be cleaned, in order to produce the clean CMB. The coefficients of the linear combination are obtained by minimising the variance of the clean map outside a given mask. Although we exclude very contaminated regions during the minimization, the subtraction is performed for all pixels and, therefore, the cleaned maps cover the full-sky (although we expect that foreground residuals are

present in the excluded areas).

An additional level of flexibility can also be considered: the linear coefficients can be the same for all the sky, or several regions with different sets of coefficients can be considered. The regions are then combined in a smooth way, by weighting the pixels at the boundaries, to avoid discontinuities in the clean maps. In order to take into account the different spectral behaviour of the foregrounds at low and high galactic latitudes, we have chosen to use two regions: the region with the 3 per cent brightest Galactic emission, and the region with the remaining 97 per cent of the sky.

Our final CMB map has then been constructed by combining the 143 and 217 GHz cleaned maps by weighting the maps in harmonic space taking into account the noise level, the resolution and a rough estimation of the foreground residuals of each map (obtained from realistic simulations). This final map has a resolution corresponding to a Gaussian beam of fwhm=5 arcminutes.

Inputs

A list (and brief description to the extent possible) of the input data used to generate this product (down to file names), as well as any external ancillary data sets which were used.

SMICA

Cardoso to write brief intro with purpose, production method, inputs used, constraints

NILC

Cardoso to write brief intro with purpose, production method, inputs used, constraints

Sevem

The inputs maps used are all the Planck frequency channels. In particular, we have cleaned the 100, 143 GHz and 217 GHz maps using four templates constructed as the difference of the following Planck channels (smoothed to a common resolution): (30-44)GHz, (44-70)GHz, (545-353)GHz and (857-545)GHz. [from Laura Bonavera & Belen Barreiro, 18.feb.2013]

Related products

A description of other products that are related and share some commonalities with the product being described here. E.g. if the description is of a generic product (e.g. frequency maps), all the products falling into that type should be listed and referenced.

File names

The FITS files corresponding to the three CMB products are the following:

- COM_CompMap_CMB-nilc_2048_R1.10.fits
- COM_CompMap_CMB-sevem_2048_R1.10.fits
- COM_CompMap_CMB-smica_2048_R1.10.fits

Meta Data

A detailed description of the data format of each file, including header keywords for fits files, extension names, column names, formats….

Each CMB products is delivered as a FITS file that contains four data extensions (nos. 1-4) in addition to a primary extension (no. 0) with no data. They contain:

Ext 1, 'COMP-MAP' : a CMB signal map accompanied by an uncertainty map, and two mask, all at Nside 2048. The CMB has been inpainted with likely values in regions where it could not be determined (namely over the Galactic Plane and some bright sources); the inpainted area covers ~3% of the sky. The uncertainty map is derived from the half-ring maps, which thus misses the low frequency components of the noise, but provides a reasonable estimate of the uncertainties at hi l, but not at low l, where residuals from the foregrounds become important. The masks are a validity mask to indicate where the resulting CMB is considered valid, and an inpainting mask to indicate where the CMB was inpainted.

Ext 2, 'FGDS-LFI' : foregrounds at the three LFI frequencies, at Nside 1024, built by smoothing the CMB map to the resolution of the given frequency

Ext 3, 'FGDS-HFI' : foregrounds at the six HFI frequencies, at Nside 2048, built by smoothing the CMB map to the resolution of the given frequency

Ext 4, 'BEAM-WF' : the beam transfer function, out to a value of ell that depends on the method and that is given in the header

Maps of astrophysical foregrounds

We describe diffuse foreground products for the Planck 2013 release. See Planck paper P06-Component Separation #planck2013-p06 for a detailed description and astrophysical discussion of those.

Product description

Low frequency foreground component

The products below contain the result of the fitting for one foreground component at low frequencies in Planck bands, along with its spectral behavior parametrized by a power law spectral index. Amplitude and spectral indeces are evaluated at Nside 256 (see below in the production process), along with standard deviation from sampling and instrumental noise on both. An amplitude solution at Nside=2048 is also given, along with standard deviation from sampling and instrumental noise as well as solutions on halfrings. The beam profile associated to this component is also provided as a secondary Extension in the Nside 2048 product.

Thermal dust

The products below contain the result of the fitting for one foreground component at high frequencies in Planck bands, along with its spectral behavior parametrized by temperature and emissivity. Amplitude, temperature and emissivity are evaluated at Nside 256 (see below in the production process), along with standard deviation from sampling and instrumental noise on all of them. An amplitude solution at Nside=2048 is also given, along with standard deviation from sampling and instrumental noise as well as solutions on halfrings. The beam profile associated to this component is provided.

Sky mask

The delivered mask is defined as the sky region where the fitting procedure was conducted and the solutions presented here were obtained. It is made by masking a region where the Galactic emission is too intense to perform the fitting, plus the masking of brightest point sources.

Production process

CODE: COMMANDER-RULER. The code exploits a parametrization of CMB and main diffuse foreground observables. The naive resolution of input frequency channels is reduced to Nside=256 first. Parameters related to the foreground scaling with frequency are estimated at that resolution by using Markov Chain Monte Carlo analysis using Gibbs sampling. The foreground parameters make the foreground mixing matrix which is applied to the data at full resolution in order to obtain the provided products at Nside=2048. In the Planck paper P06-Component Separation #planck2013-p06 additional material is discussed, specifically concerning the sky region where the solutions are reliable, in terms of chi2 maps.

Inputs

Nominal frequency maps at 30, 44, 70, 100, 143, 217, 353 GHz (LFI 30 GHz frequency maps [1], LFI 44 GHz frequency maps [2] and LFI 70 GHz frequency maps [3], HFI 100 GHz frequency maps [4], HFI 143 GHz frequency maps [5],HFI 217 GHz frequency maps [6] and HFI 353 GHz frequency maps [7]) and their II column corresponding to the noise covariance matrix. Halfrings at the same frequencies. Beam window functions as reported in the LFI and HFI RIMO.

Related products

None.

File names

- Low frequency component at Nside 256: COM_CompMap_Lfreqfor-commrul_0256_R1.00.fits
- Low frequency component at Nside 2048: COM_CompMap_Lfreqfor-commrul_2048_R1.00.fits
- Thermal dust at Nside 256: COM_CompMap_dust-commrul_0256_R1.00.fits
- Thermal dust at Nside 2048: COM_CompMap_dust-commrul_2048_R1.00.fits
- Mask: COM_CompMap_Mask-rulerminimal_2048.fits

Meta Data

Low frequency foreground component

Low frequency component at Nside 256

File name: COM_CompMap_Lfreqfor-commrul_0256_R1.00.fits

Name HDU -- COMP-MAP

Column 1: I -- uK_CMB

Column 2: I_stdev -- uK_CMB

Column 3: Beta -- No Unit

Column 4: B_stdev -- No Unit

Comment: The Intensity is normalized at 30 GHz

Comment: The intensity was estimated during mixing matrix estimation

Low frequency component at Nside 2048

File name: COM_CompMap_Lfreqfor-commrul_2048_R1.00.fits

Name HDU -- COMP-MAP

Column 1: I -- uK_CMB

Column 2: I_stdev -- uK_CMB

Column 3: I_hr1 -- uK_CMB

Column 4: I_hr2 -- uK_CMB

Comment: The intensity was computed after mixing matrix application

Nome HDU -- BeamWF

Column 1: Temperature (meaning the beam profile) -- None

Comment: Beam window function used in the Component separation process

Thermal dust

Thermal dust component at Nside=256

File name: COM_CompMap_dust-commrul_0256_R1.00.fits

Name HDU -- COMP-MAP

Column 1: I -- MJy/sr

Column 2: I_stdev -- MJy/sr

Column 3: Em -- none

Column 4: Em_stdev -- none

Column 5: T -- uK_CMB

Column 6: T_stdev -- uK_CMB

COMMENT: The intensity is normalized at 353 GHz

Thermal dust component at Nside=2048

File name: COM_CompMap_dust-commrul_2048_R1.00.fits

Name HDU -- COMP-MAP

Column 1: I -- MJy/sr

Column 2: I_stdev -- MJy/sr

Column 2: I_hr1 -- MJy/sr

Column 3: I_hr2 -- MJy/sr

Name HDU -- BeamWF

Column 1: Temperature (meaning the beam profile) -- None

Comment: Beam window function used in the Component separation process

Sky mask

File name: COM_CompMap_Mask-rulerminimal_2048.fits

Nome HDU -- COMP-MASK

Column 1: Mask

Dust optical depth map and model

Thermal emission from interstellar dust is captured by Planck-HFI over the whole sky, at all frequencies from 100 to 857 GHz. This emission is well modelled by a modified black body in the far-infrared to millimeter range. It is produced by the biggest interstellar dust grain that are in thermal equilibrium with the radiation field from stars. The grains emission properties in the sub-millimeter are therefore directly linked to their absorption properties in the UV-visible range. By modelling the thermal dust emission in the sub-millimeter, a map of dust reddening in the visible can then be constructed.

Model of thermal dust emission

The model of the thermal dust emission is based on a modify black body fit to the data I_nu:
I_nu = A B_nu(T) nu^beta.
where B_nu(T) is the Planck function for dust equilibirum temperature T, A is the amplitude of the MBB and beta the dust spectral index. The dust optical depth at frequency nu is :
Tau_nu = I_nu / B_nu(T) = A nu^beta

The dust parameters provided are T, beta and Tau_353. They were obtained by fitting the Planck data at 353, 545 and 857 GHz together with the IRAS (IRIS) 100 micron data. All maps (in Healpix nside=2048) were smoothed to a common resolution of 5 arcmin. The CMB anisotropies, clearly visible at 353 GHz, were removed from all the HFI maps using the SMICA map. An offset was removed from each map to obtained a meaningful Galactic zero level, using a correlation with the LAB 21 cm data in diffuse areas of the sky (N_HI < 2x10^20 cm^-2). Because the dust emission is so well correlated between frequencies in the Rayleigh-Jeans part of the dust spectrum, the zero level of the 545 and 353 GHz were improved by correlating with the 857 GHz over a larger mask (N_HI < 3x10^20 cm^-2). Faint residual dipole structures, identified in the 353 and 545 GHz maps, were removed prior to the fit.

The MBB fit was performed using a chi-square minimization, assuming errors for each data point that include instrumental noise, calibration uncertainties (on both the dust emission and the CMB anisotropies) and uncertainties on the zero level. Because of the known degeneracy between T and Beta in the presence of noise, we produced a model of dust emission using data smoothed to 35 arcmin; at such resolution no systematic bias of the parameters is observed. The map of the spectral index Beta at 35 arcmin was than used to fit the data for T and Tau_353 at 5 arcmin.

E(B-V) map :

For the production of the E(B-V) map, we used Planck and IRAS data from which point sources in diffuse areas were removed to avoid contamination by galaxies. In the hypothesis of constant dust emission cross-section, the optical depth map Tau_353 is proportional to dust column density. It can then be used to estimate E(B-V), also proportional to dust column density in the hypothesis of a constant differential absorption cross-section between the B and V bands. Given those assumptions :
E(B-V) = q Tau_353.
To estimate the calibration factor q, we followed a method similar to Mortsell (2013) based on SDSS reddening measurements (E(g-r) which corresponds closely to E(B-V)) of 77 429 Quasars (Schneider et al. 2007). The interstellar HI column densities covered on the lines of sight of this sample ranges from 0.5 to 10x10^20 cm^-2. Therefore this sample allows to estimate q in the diffuse ISM where dust properties are expected to vary less than in denser clouds where coagulation and grain growth might modify dust emission and absorption cross sections.

Dust optical depth products

The characteristics of the dust model maps are the following.

- Dust temperature : nside 2048, fwhm=5 arcmin, units=Kelvin
- Dust spectral index : nside=2048, fwhm=35 arcmin, no units
- Dust optical depth at 353 GHz : nside=2048, fwhm=5 arcmin, no units
- Dust reddening E(B-V) : nside=2048, fwhm=5 arcmin, units=magnitude, obtained with data from which point sources were removed.

These maps and their associated uncertainty maps are written into a single extension whose structure is shows below.

```
;-------------------------------------------------------------------------------
; EXTENSION 1: COMP-MAP
; - Header
;-------------------------------------------------------------------------------
MRDFITS: Binary table.  8 columns by  1 rows.
XTENSION= 'BINTABLE'           /Written by IDL:  Mon Feb  4 11:33:34 2013
BITPIX  =                    8 /
NAXIS   =                    2 /Binary table
NAXIS1  =           1610612736 /Number of bytes per row
NAXIS2  =                    1 /Number of rows
PCOUNT  =                    0 /Random parameter count
GCOUNT  =                    1 /Group count
TFIELDS =                    8 /Number of columns
COMMENT
COMMENT  *** End of mandatory fields ***
COMMENT
EXTVER  =                    1 /Extension version
DATE    = '2013-02-04'         /Creation date
COMMENT
COMMENT  *** Column names ***
COMMENT
TTYPE1  = 'TAU353  '           / opacity 353GHz
TTYPE2  = 'TAU353ERR'          / opacity 353GHz
TTYPE3  = 'A_V     '           / Extinction
TTYPE4  = 'A_V_ERR '           / Error on A_V
TTYPE5  = 'T_HF    '           / T for hi freq correction
TTYPE6  = 'T_HF_ERR'           / T for hi freq correction
TTYPE7  = 'BETAHF  '           / Beta for hi freq correction
TTYPE8  = 'BETAHFERR'          / Mask
COMMENT
COMMENT  *** Column formats ***
COMMENT
TFORM1  = '50331648E'          /
TFORM2  = '50331648E'          /
TFORM3  = '50331648E'          /
TFORM4  = '50331648E'          /
TFORM5  = '50331648E'          /
TFORM6  = '50331648E'          /
```

```
TFORM7  = '50331648E'          /
TFORM8  = '50331648E'          /
COMMENT
COMMENT  *** Column units ***
COMMENT
TUNIT1  = 'none    '           /
TUNIT2  = 'none    '           /
TUNIT3  = 'mag     '           /
TUNIT4  = 'mag     '           /
TUNIT5  = 'K       '           /
TUNIT6  = 'K       '           /
TUNIT7  = 'none    '           /
TUNIT8  = 'none    '           /
COMMENT
COMMENT  *** Planck params ***
COMMENT
EXTNAME = 'COMP-MAP'           / Extension name
AST-COMP= 'DUST_OPA'           / Component
COORSYS = 'GALACTIC'           / Coordinate system
ORDERING= 'NESTED  '           / Healpix ordering
NSIDE   =                 2048 / Healpix Nside
FIRSTPIX=                    0 /
LASTPIX =             50331647 /
BAD_DATA=         -1.63750E+30 / bad pixel value
FILENAME= 'HFI_CompMap_DustOpacity_2048_R1.00.fits' / FITS filename
CHECKSUM= '7DPW8CMU7CMU7CMU'   / HDU checksum created 2013-02-04T10:33:35
PROCVER = 'DX9     '           / Product version
COMMENT
COMMENT  see Planck Eplanatory Supplement Ch. 999 for
COMMENT  for description of the model and how to use it.
COMMENT
END
```

CO emission maps

CO rotational transition line emission is present in all HFI bands but for the 143 GHz channel. It is especially significant in the 100, 217 and 353 GHz channels (due to the 115 (1-0), 230 (2-1) and 345 GHz (3-2) CO transitions). This emission comes essentially from the Galactic interstellar medium and is mainly located at low and intermediate Galactic latitudes. Three approaches (summarised below) have been used to extract CO velocity-integrated emission maps from HFI maps and to make three types of CO products. An introduction is given in Section and a full description of these products is given in #planck2013-p03a.

- Type 1 product: it is based on a single channel approach using the fact that each CO line has a slightly different transmission in each bolometer at a given frequency channel. These transmissions can be evaluated from bandpass measurements that were performed on the ground or empirically determined from the sky using existing ground-based CO surveys. From these, the J=1-0, J=2-1 and J=3-2 CO lines can be extracted independently. As this approach is based on individual bolometer maps of a single channel, the resulting Signal-to-Noise ratio (SNR) is relatively low. The benefit, however, is that these maps do not suffer from contamination from other HFI channels (as is the case for the other approaches) and are more reliable, especially in the Galactic Plane.

- Type 2 product: this product is obtained using a multi frequency approach. Three frequency channel maps are combined to extract the J=1-0 (using the 100, 143 and 353 GHz channels) and J=2-1 (using the 143, 217 and 353 GHz channels) CO maps. Because frequency channels are combined, the spectral behaviour of other foregrounds influences the result. The two type 2 CO maps produced in this way have a higher SNR than the type 1 maps at the cost of a larger possible residual contamination from other diffuse foregrounds.
- Type 3 product: using prior information on CO line ratios and a multi-frequency component separation method, we construct a combined CO emission map with the largest possible SNR. This type 3 product can be used as a sensitive finder chart for low-intensity diffuse CO emission over the whole sky.

The released Type 1 CO maps have been produced using the MILCA-b algorithm, Type 2 maps using a specific implementation of the Commander algorithm, and the Type 3 map using the full Commander-Ruler component separation pipeline (see above).

Characteristics of the released maps are the following. We provide Healpix maps with Nside=2048. For one transition, the CO velocity-integrated line signal map is given in K_RJ.km/s units. A conversion factor from this unit to the native unit of HFI maps (K_CMB) is provided in the header of the data files and in the RIMO. Four maps are given per transition and per type:

- The signal map
- The standard deviation map (same unit as the signal),
- A null test noise map (same unit as the signal) with similar statistical properties. It is made out of half the difference of half-ring maps.
- A mask map (0B or 1B) giving the regions (1B) where the CO measurement is not reliable because of some severe identified foreground contamination.

All products of a given type belong to a single file. Type 1 products have the native HFI resolution i.e. approximately 10, 5 and 5 arcminutes for the CO 1-0, 2-1, 3-2 transitions respectively. Type 2 products have a 15 arcminute resolution The Type 3 product has a 5.5 arcminute resolution.

A typical header for these data is given below. It contains a keyword giving the conversion between the CO velocity-integrated units (K.km/s) and the HFI map native units (K_CMB). However, users are to use CO subtraction with care, as it will necessarily add noise to the result.

```
XTENSION= 'BINTABLE'           /Written by IDL:  Fri Dec 14 14:29:27 2012
BITPIX  =                    8 /
NAXIS   =                    2 /Binary table
NAXIS1  =           1308622848 /Number of bytes per row
NAXIS2  =                    1 /Number of rows
PCOUNT  =                    0 /Random parameter count
GCOUNT  =                    1 /Group count
TFIELDS =                    8 /Number of columns
COMMENT
COMMENT  *** End of mandatory fields ***
COMMENT
EXTVER  =                    1 /Extension version
DATE    = '2012-12-14'         /Creation date
COMMENT
COMMENT  *** Column names ***
COMMENT
TTYPE1  = 'I10     '           / Intensity
TTYPE2  = 'E10     '           / Error
TTYPE3  = 'N10     '           / Nulltest
```

```
TTYPE4  = 'M10     '           / Mask
TTYPE5  = 'I21     '           / Intensity
TTYPE6  = 'E21     '           / Error
TTYPE7  = 'N21     '           / Nulltest
TTYPE8  = 'M21     '           / Mask
COMMENT
COMMENT  *** Column formats ***
COMMENT
TFORM1  = '50331648E'          /
TFORM2  = '50331648E'          /
TFORM3  = '50331648E'          /
TFORM4  = '50331648B'          /
TFORM5  = '50331648E'          /
TFORM6  = '50331648E'          /
TFORM7  = '50331648E'          /
TFORM8  = '50331648B'          /
COMMENT
COMMENT  *** Column units ***
COMMENT
TUNIT1  = 'Krj km/s'           /
TUNIT2  = 'Krj km/s'           /
TUNIT3  = 'Krj km/s'           /
TUNIT4  = 'none    '           /
TUNIT5  = 'Krj km/s'           /
TUNIT6  = 'Krj km/s'           /
TUNIT7  = 'Krj km/s'           /
TUNIT8  = 'none    '           /
COMMENT
COMMENT  *** Planck params ***
COMMENT
EXTNAME = 'COMP-MAP'           / Extension name
AST-COMP= 'CO-LINE '           / Component
COORSYS = 'GALACTIC'           / Coordinate system
ORDERING= 'NESTED  '           / Healpix ordering
NSIDE   =                 2048 / Healpix Nside
FIRSTPIX=                    0 /
LASTPIX =             50331647 /
BAD_DATA=         -1.63750E+30 / bad pixel value
FILENAME= 'HFI_CompMap_CO-line_2048_R1.01.fits' / FITS filename
PROCVER = 'DX9     '           / Product version
COMMENT
COMMENT  Multiply by these factors to convert Kcmb
COMMENT
CNV(1-0)=    1.42144524614E-05 / Conv factor in Kcmb/(Krj*km/s)
CNV(2-1)=    4.43577255985E-05 / Conv factor in Kcmb/(Krj*km/s)
COMMENT
COMMENT ---------------------------------------------------------------------
```

```
COMMENT HFI-DMC objects:
COMMENT group: /data/dmc/MISS03/DATA/CO_PRODUCT_TYPE2/
COMMENT Creation date  - object name
COMMENT 12-11-30 14:21 - 115GHz_CO_J1-0_type2
COMMENT 12-11-30 14:23 - 230GHz_CO_J2-1_type2
COMMENT 12-11-30 14:22 - 115GHz_CO_J1-0_STDDEV_type2
COMMENT 12-11-30 14:24 - 230GHz_CO_J2-1_STDDEV_type2
COMMENT 12-11-30 14:22 - 115GHz_CO_J1-0_NULL_type2
COMMENT 12-11-30 14:23 - 230GHz_CO_J2-1_NULL_type2
COMMENT 12-11-30 16:29 - 115GHz_CO_J1-0_MASK_type2
COMMENT 12-11-30 16:31 - 230GHz_CO_J2-1_MASK_type2
COMMENT ------------------------------------------------------------------------
END
```

Other maps

This section will be for the various CIB maps, and others. The overall structure of the FITS files will be similar to the cases above, though the details will be tailored to the individual products.

References

<biblio force=false>

1. References

</biblio>

CMB spectrum & Likelihood Code

Cosmological Parameters

Cosmological parameter tables

TBW by A.Lewis

Description

A general description of the product, including e.g. figures related to the contents (e.g. maps, tables), and some explanation of its scientific meaning. If there are scientific warnings about the use of the product (User's caveats), they should also be given here, or at least references to other explanatory documents (papers etc).

Production process

How it is produced, giving inputs used, both internal (Planck) and external.

Caveats and known issues

The title says it all.

Related products

A description of other products that are related and share some commonalities with the product being described here. E.g. if the description is of a generic product (e.g. frequency maps), all the products falling into that type should be listed and referenced.

File names

- A pdf of the results in , which is suitable for human reading.
- A text file is in … which is suitable for electronic reading.

The structure of the text file is … see e.g., Frequency Maps for sample tables

Specially processed maps

Overview

A general description of the product, including e.g. figures related to the contents (e.g. maps, tables), and some explanation of its scientific meaning. If there are scientific warnings about the use of the product (User's caveats), they should also be given here, or at least references to other explanatory documents (papers etc).

Lensing map

Description

The fiducial Planck lensing potential map is made from a minimum variance combination of the 143 and 217 GHz Planck maps on approximately 70% of the sky, using 857GHz as a dust template. This is the same lens reconstruction on which the Planck lensing likelihood is based.

We distribute:

PHIBAR

: A (transfer-function convolved) map of the lensing potential, in NSIDE 2048 HEALPix RING format. It is obtained by convolving the lensing potential estimate \hat{\phi} with the lensing response function $R_L^{\phi\phi}$.

MASK

: This is a NSIDE 2048 HEALPix map, containing the analysis mask used in the lens reconstruction.

RLPP

: This column contains the response function $R_L^{\phi\phi}$.

NLPP

: This column contains a sky-averaged estimate of the noise power spectrum of PHIBAR. The noise is highly coloured. Note that there is some dependence of the noise power spectrum with the local noise level of the map. Note that the noise power spectrum estimate here is not sufficiently accurate for a power spectrum analysis.

[From Duncan Hanson, Feb.2013]

Production process

The construction of these quantities are described in detail in Sec. 2.1 of P12_Lensing. This map has been band-limited between multipoles $10 \le L \le 2048$. The response function $R_L^{\phi\phi}$ here is analogous to the the beam transfer function in a CMB temperature or polarization map. We have chosen to distribute this transfer-function convolved map rather than the normalized lens reconstruction as it is a significantly more localized function of the CMB temperature map from which it is derived. This is discussed further in Appendix A of P12_Lensing.

Inputs

This product is built from the 143 and 217 GHz Planck sky maps.

File names and format

A single file named *COM_CompMap_Lensing_2048_R1.10.fits* with two BINTABLE extensions containing the items described above.

Column Name	Data Type	Units	Description
1. EXTNAME = 'LENS-MAP' : Data columns			
PHIBAR	Real*4	none	Map of the lensing potential
MASK	Int	none	Region over which the lensing potential is reconstructed
Keywords			
PIXTYPE	HEALPIX		
COORDSYS	GALACTIC	Coordinate system	
ORDERING	NESTED	Healpix ordering	
NSIDE	2048	Healpix Nside	
FIRSTPIX	0		
LASTPIX	50331647		
2. EXTNAME = 'TransFun' : Data columns			
RLPP	Real*4	none	Response function (see above)
NLPP	Real*4	none	sky-averaged noise spectrum
Keywords			
L_MIN	0		
L_MAX	2048		

Additional angular power spectra

These are the spectra which are neither the frequency map ones not the cmb one , which are already described in previous sections (on frequency maps and cmb spectrum and likelihood). OIf that exists this is the place for SZ power spectrum , CIB power spectrum, etc...

Additional Angular Power spectrum number 1

NOTE: Text in red to be removed when filling the contents

Product description

A general description of the product, including e.g. figures related to the contents (e.g. maps, tables), and some explanation of its scientific meaning. If there are scientific warnings about the use of the product (User's caveats), they should also be given here, or at least references to other explanatory documents (papers etc).

Production process

Description of the Pipeline used to generate the product. In particular any limitations and approximations used in the data processing should be listed. Avoiding detailed descriptions of methods and referring to other parts of the ES and/or the relevant Planck papers for the details. References however should be quite detailed (i.e. it is not enough to direct the user to a paper, but the relevant section in the paper should be provided).

Inputs

A list (and brief description to the extent possible) of the input data used to generate this product (down to file names), as well as any external ancillary data sets which were used.

Related products

A description of other products that are related and share some commonalities with the product being described here. E.g. if the description is of a generic product (e.g. frequency maps), all the products falling into that type should be listed and referenced.

Meta Data

A detailed description of the data format of each file, including header keywords for fits files, extension names, column names, formats….

Additional Science products

Scientific data used to generate Planck products

Simulation data

NOTE: not in the 1st release, probably between the 1st and 2nd....

Survey history

NOTE: Text in red to be removed when filling the contents

Product description

A general description of the product, including e.g. figures related to the contents (e.g. maps, tables), and some explanation of its scientific meaning. If there are scientific warnings about the use of the product (User's caveats), they should also be given here, or at least references to other explanatory documents (papers etc).

Production process

Description of the Pipeline used to generate the product. In particular any limitations and approximations used in the data processing should be listed. Avoiding detailed descriptions of methods and referring to other parts of the ES and/or the relevant Planck papers for the details. References however should be quite detailed (i.e. it is not enough to direct the user to a paper, but the relevant section in the paper should be provided).

Inputs

A list (and brief description to the extent possible) of the input data used to generate this product (down to file names), as well as any external ancillary data sets which were used.

Related products

A description of other products that are related and share some commonalities with the product being described here. E.g. if the description is of a generic product (e.g. frequency maps), all the products falling into that type should be listed and referenced.

Format

A detailed description of the data format of each file, including header keywords for fits files, extension names, column names, formats….

Pre-Programmed Pointing Lists

The Pre-Programmed Pointing Lists (PPL) are made by Planck Science Office from the Baseline Scanning Strategy with the help of the Software Planning and Performance Tool. They are sent to MOC/FD for use in making the Augmented Pre-Programmed Pointing Lists (APPL) used for commanding the spacecraft attitude.

The PPL file name is the following: YYYYMMDD_yyyymmdd_NNNN_X.PPL

with YYYYMMDD = start date of the valid span of the PPL file

yyyymmdd = end date of the valid span of the PPL file

NNNN = unique sequence number, in the range 0000 ≤ NNNN ≤ 9999, incrementing sequentially throughout the mission and uniquely identifying each new PPL file that is generated (i.e. no repeated numbers and no gaps in the sequence of PPLs) o 0000-8999 reserved for PSO o 9000-9999 reserved for attitude manoeuvres generated by MOC

X = type of PPL, as follows: o R = Routine (standard 4-week PPL) o C = Contingency (3-day replanning) o L = Long-Term PPL (LTPPL) o S = Special

PPLs contain the following information in ASCII columns:

- pointing reference number
- Ecliptic longitude
- Ecliptic latitude
- nominal start time for pointing
- earliest allowed start time
- latest allowed start time
- nominal dwell time
- observation type
- comments

PPLs can be found in the Planck Legacy Archive in the "Time-Ordered Information: Operational Files" section, ordered normally by periods of a month.

Detailed information about the PPL's can be found here: PPL ICD [1]

Augmented Pre-Programmed Pointing Lists

APPLs are made by MOC / Flight Dynamics using pointing information (PPLs) from the Planck Science Office.

The APPLs incorporate information about the Operational Days boundaries in order to fit pointings into each OD.

APPLs are grouped ans summarized by MOC to form files called the APPL Summary Files or APS. These are delivered in the Planck Legacy Archive in the "Time-Ordered Information: Operational Files" section, by Operational Day.

Detailed information about the APPL's can be found here: APPL Interface Control Document [2]

Attitude History Files

The pointing history of Planck is described in the Attitude History Files (AHF) sequence. All the AHF can be found in the Planck Legacy Archive, for three different methods of computation (AHF, DHF, GHF).

The GHF are made using refined pointing information from the Fiber Optics Gyroscope.

Available information concerning the AHF can be found here: AHF Interface Control Document [3]

Focal plane geometry

The Spacecraft-Instrument Alignment Matrix (SIAM) contains all the geometry information for each detector of both instruments with respect to the main optical frame.

The last updated SIAM is provided in the Planck Legacy Archive in the "Time-Ordered Information: Operational Files" section.

Information about the structure of the SIAM can be found here: SIAM ICD [4]

Orbit file

The orbit file is produced by the Flight Dynamics team at ESOC and contains the information of the Planck orbital history throughout the whole mission (since launch).

Planck operational state history

The Planck Operational State History (POSH) provides an easily accessible summary of the status of the Planck spacecraft, throughout the course of its mission. It should be useful to scientists as a complement to the data they are analyzing.

Due to the type and quantity of data that describes the state of a satellite and its instruments, it is common for it to be spread over a large number of files and formats which may have to be retrieved from a large number of systems. In addition there are a significant number of potentially interesting occurrences during the mission which are not found in any one single repository; examples are mission milestones, definitions of operational days and anomalous events. The initial motivation for the creation of the POSH was to provide the state of the spacecraft and its instruments in an easily accessible way at any given time. States to be included were the operational phases and the operational status/mode of each of the major payload components. The intention being that this information could be used to assist not only in the operational work in monitoring the status of the survey but also as a data source that could be consulted whilst analyzing science data.

Two main record types are stored in the POSH:

EVENTS, consisting of occurrences during the mission that can be described by a start and end time (e.g. survey boundaries, anomalies, ODs, manoeuvres). The definition of an event is provided for operational purposes; it may or may not agree with the definition of an event for data analysis purposes (e.g. the boundaries of a survey may be defined in a different way in the pipeline).

HOUSE KEEPING (HK) SUMMARY which consists of some HK timelines with one data point per pointing period (e.g. temperatures, position in the sky, drift rates, sun angles). This data set contains a very compact operational summary of the mission (not an exhaustive list of HK).

References

[1] http://www.rssd.esa.int/llink/livelink/fetch/-60063/65211/65216/200039/2785625/PGS-ICD-017_Pre-programmed_Pointing_List_%5BPPL%5D.pdf?nodeid=2785628&vernum=-2
[2] http://www.rssd.esa.int/llink/livelink/fetch/-60063/65211/65216/200039/2785625/PGS-ICD-050_Augmented_Pre-programmed_Pointing_List_%5BAPPL%5D.pdf?nodeid=2865927&vernum=-2
[3] http://www.rssd.esa.int/llink/livelink/fetch/-60063/65211/65216/200039/2785625/PGS-ICD-006_Attitude_History_File_%5BAHF%5D.pdf?nodeid=2808899&vernum=-2
[4] http://www.rssd.esa.int/llink/livelink/fetch/-60063/65211/65216/200039/2785625/PGS-ICD-039_Spacecraft_Instrument_Alignment_Matrix_%5BSIAM%5D.pdf?nodeid=2831007&vernum=-2

Satellite history

MOC information about satellite history will come at the end of the Planck mission. There is no information for PLA1.

Design and performance documentation

The design and performance documentation (if any) can be downloaded from the "documents" tab of the Planck Legacy Archive interface.

Payload design

Instrument performance

Documentation

Spectral response per detector

Polarisation responses

Photometric responses

Main beam

4π beams

Systematics effects

Telescope

Thermal

Design, performance and calibration documentation

There is no such documentation available for PLA1.

FOG

Fiber-Optic Giroscope data are not provided in the PLA1 release.

Software utilities

Unpack and Display

There is no "unpack and display" software for PLA1.

Unit Conversion and Colour Correction

The unit conversion and colour correction software (UC_CC) consists of a set of IDL procedures and functions that read the band transmission from the DPC RIMOs and perform the requested conversions. The package is delivered as a tarfile and contains a detailed instruction manual. The data and software file requirements are provided below along with basic use instructions and some simple examples. The full list of its contents is:

```
UC_CC_v102/get_hfibolo_list.pro
UC_CC_v102/hfi_co_correction.pro
UC_CC_v102/hfi_colour_correction.pro
UC_CC_v102/hfi_lfi_test_script.pro
UC_CC_v102/hfi_lfi_test_script_PLA_RIMO.pro
UC_CC_v102/hfi_read_avg_bandpass.pro
UC_CC_v102/hfi_read_bandpass.pro
UC_CC_v102/hfi_unit_conversion.pro
UC_CC_v102/lfi_read_avg_bandpass.pro
UC_CC_v102/lfi_read_bandpass.pro
UC_CC_v102/LFI_fastcc.pro
UC_CC_v102/LFI_fastcc_test.pro
UC_CC_v102/README.txt
UC_CC_v102/Instructions.pdf
```

The package is currently available on [[1]]

Relevant Documentation

Please refer to the Spectral Response sections of the Explanatory Supplement (i.e. 2.2.1.2, 4.4.5, and 4.6), as well as the Spectral Response Paper #planck2013-p03d for details of the derivation of the detector spectra and band-average spectra included in the RIMO files, as well as additional details on the unit conversion and colour correction methodology, philosophy, and implementation. This section concentrates on the use of the provided UC_CC software itself, leaving the other sections to provide the basis for it.

Tarfile Distribution Package

This section provides a brief explanation of each file included in the UC_CC distribution.

1. `get_hfibolo_list.pro`: used to provide basic detector information (i.e. names) within subsequent routines.
2. `hfi_read_bandpass.pro`: a routine to get the desired detector level spectral transmission data (HFI) and output in a structure format used by the other routines.
3. `hfi_read_avg_bandpass.pro`: a routine to get the desired HFI band-average spectral transmission data and output in a structure format used by the other routines.
4. `hfi_unit_conversion.pro`: a routine that accepts spectral response information and outputs unit conversion coefficients.
5. `hfi_colour_correction.pro`: a routine that accepts spectral response information and outputs colour correction coefficients.
6. `hfi_co_correction.pro`: a routine that accepts spectral response information and outputs CO conversion coefficients.
7. `lfi_read_bandpass.pro`: a routine to get the desired detector level spectral transmission data (LFI) and output in a structure format used by the other routines.
8. `lfi_read_avg_bandpass.pro`: a routine to get the desired LFI band-average spectral transmission data and output in a structure format used by the other routines.
9. `hfi_lfi_test_script.pro`: a sample script providing examples of calling the various routines.
10. `hfi_lfi_test_script_PLA_RIMO.pro`: a sample script providing examples of calling the various routines using the PLA RIMO file (without detector-level spectra).
11. `LFI_fastcc.pro`: a routine to calculate LFI colour corrections using quadratic approximations (faster than integrating each time).
12. `LFI_fastcc_test.pro`: a sample script providing examples of calling the LFI_fastcc routine.
13. `README.txt`: a text file providing basic instructions and expected output for the hfi_lfi_test_script.pro file (basic introduction and precursor to this document).

Required Input Data

The UC_CC routines require access to the Planck spectral response data. This is nominally provided in the RIMO files included in the same location as this package. The ingestion routines are written in such a way as to accept updated RIMO files (provided the `.fits` header structure uses the same naming conventions as currently / previously implemented). For users with access to the HFI databases on magique3 (i.e. members of the HFI Core-team), the software is also able to access the spectral response data directly from the HFI IMO (see examples below for details). The software is written to allow use of the PLA RIMO file which includes only band-average spectra, as well as the full RIMO (with detector level spectra) which will be made available through the PLA in a future release.

A user may provide a unique model spectrum about which to generate colour correction coefficients specific to the model input (see §2.6.5), however this is not required for standard colour correction coefficients based on power-law spectral indices and/or modified blackbody spectra.

Required Software Packages

This software has been tested on IDL versions 6.4, 7.1, 8.0, 8.1, and 8.2. It requires use of the `mrdfits.pro` file, and related sub-routines, from *the IDL Astronomy User's Library* to read the RIMO `.fits` files. This library should be included with most IDL Healpix distributions, and is otherwise freely available online (http://idlastro.gsfc.nasa.gov/). The UC_CC routines will not work with the RIMO `.fits` files without routines from this library! The routines provided will work with either the full (internal) RIMO files containing detector level spectra, or the PLA (external) RIMO files with only frequency-band level spectra. To date the software has not been tested on the PLA RIMO files (this should change soon, and needs to prior to the data release).

Software Initialization

No installation is required. It is recommended to add the UC_CC scripts to a directory within your IDL path, or add the UC_CC directory to your IDL path. As some of the UC_CC files contain multiple functions/procedures, it is also recommended to compile each of the UC_CC `.pro` files prior to running scripts using the respective routines; `get_hfibolo_list.pro` should be compiled before any of the other routines.

Software Use

The following section outlines basic use of the UC_CC IDL scripts and provides examples.

Spectral Input

The UC_CC routines accept individual detector and band-average spectra structures as input. The `hfi_read_bandpass.pro` and `hfi_read_avg_bandpass.pro` routines are used to obtain this data for HFI, and the `lfi_read_bandpass.pro` and `lfi_read_avg_bandpass.pro` routines are used to obtain this data for LFI. The spectra can be restored from either a RIMO file, or an IMO database (if access to such is available). The routines return the transmission spectra by default, but are also configured to return the spectral uncertainty and interpolation flag as additional output parameters. Here are some example IDL commands using these routines:

```
hfi_bp = hfi_read_bandpass(/RIMO, PATH_RIMO='/path/to/RIMO/file/', $

         NAME_RIMO='Name_of_RIMO_file.fits', FLG_INFO=flg, ER_INFO=er, /FLAG)
hfi_bp_withCO = hfi_read_bandpass(/RIMO, PATH_RIMO='/path/to/file', $

         NAME_RIMO='Name_of_RIMO_file.fits', FLG_INFO=flg_withCO, $

         ER_INFO=er_withCO, FLAG = 0)
hfi_avg = hfi_read_avg_bandpass(/RIMO, PATH_RIMO='/path/to/RIMO/file/', $

         NAME_RIMO='Name_of_RIMO_file.fits', FLG_INFO=flg_avg, ER_INFO=er_avg, /FLAG)
hfi_avg_withCO = hfi_read_avg_bandpass(/RIMO, PATH_RIMO='/path/to/file', $

         NAME_RIMO='Name_of_RIMO_file.fits', FLG_INFO=flg_avg_withCO, $

         ER_INFO=er_avg_withCO, FLAG = 0)
lfi_bp = lfi_read_bandpass(/RIMO, PATH_RIMO='/path/to/RIMO/file/', $

         NAME_RIMO='Name_of_LFI_RIMO_file.fits', ER_INFO=er)
lfi_avg = lfi_read_avg_bandpass(/RIMO, PATH_RIMO='/path/to/RIMO/file/', $
```

```
        NAME_RIMO='Name_of_LFI_RIMO_file.fits', ER_INFO=er_avg)
```

In the above examples, `hfi_bp`, `hfi_bp_withCO`, and `lfi_bp` represent IDL structures containing individual detector spectra. The variables `er` and `er_avg` containt the spectral uncertainty within a structure similar to that of the spectra. The `flg` and `flg_avg` structures contain the CO interpolation flag indiciating if a spectral data point is uniquely measured from the calibration data (i.e. `flg[i] = 0`), or interpolated (i.e. `flg[i] = 1`, see Ex. Supp. for more details). No such flag exists for LFI. If the `FLAG` keyword is set, flagged data points are removed from the spectral structures prior to being output; i.e. `FLAG=0` outputs all data and `FLAG=1` outputs only un-flagged data points, the default setting if FLAG is not input is the `FLAG=1` setting. With the `RIMO` keyword set, there must be a `RIMO.fits` file in the `PATH_RIMO` directory of the `NAME_RIMO` keyword value. The routines may also get the spectra from an IMO database (this requires the user to have access to an IMO data base with details available within the Planck collaboration).

The output of the ...read_bandpass.pro routines is an array of IDL structures. The other UC_CC routines are written in such a way as to accept these structures as input. The software has been modularized such that the subroutines within the scripts can accept input spectra in other formats. This level of use of the UC_CC routines is beyond this introduction, however. Those interested are directed to look through the original source code of the subroutines, paying particular attention to the subroutines without the hfi_ prefix within each script; these routines may be called externally. Further queries may be directed towards the authors (esp. Spencer).

The LFI RIMO files follow a different convention than that of HFI, so the ingestion routine also accounts for this. The LFI RIMO file frequency bins represent the bin start frequency rather than the bin centre frequency, and the convention is such that the transmission data need to be scaled by λ^2 to be consistent with the HFI spectra. Both of these modifications are performed within the `lfi_read_bandpass` and `lfi_read_avg bandpass` routines, so their output structures are in the format expected by the remaining UC_CC routines.

The UC_CC routines follow HFI unit conversion and colour correction conventions, and have been developed primarily for use with HFI data processing. Functionality has also been included for the LFI spectra. The UC_CC routines LFI output has been verified against internal LFI coefficients for the combined case of K $_{CMB}$ to T $_b$ unit conversion and colour correction for spectral indices ranging from -2 to $+4$. This validation confirmed that the UC_CC code treats the LFI spectra in the same way as in other LFI data processing, and thus all of the UC_CC LFI output is expected to conform with official LFI data processing.

UC_CC Output

The UC_CC routines output conversion coefficients as arrays of IDL structures. This ensures that the detector name and coefficient are paired, and any additional information may also be provided, e.g. the CO rotational transition line in the case of a CO coefficient. It is important to note that the output for the 143-8 and 545-3 detector coefficients is intentionally set to -10^9 in all cases. These two detectors have been excluded from HFI data processing due to their noise characteristics, and thus do not contribute to the band-average spectra or band-average coefficients. Ground measurements for these detectors do exist, and it is possible to determine these coefficients if needed, but they have been intentionally hidden from standard use.

Coefficient Uncertainty Estimate

An optional function of this software is to output an uncertainty for every unit conversion and colour correction coefficient determined. This requires spectral uncertainty as input (HFI only at present), and has uncertainty of other parameters as optional depending on the colour correction (e.g. CO radial velocity, dust temperature or emissivity, spectral index uncertainty, user-supplied spectral profile uncertainty (see §6.5), etc.). The GETERR keyword instructs the routines to calculate the coefficient uncertainty via NITER (another keyword) iterations of a Monte-Carlo uncertainty simulation. This requires the BP_ERR keyword to be set to the detector uncertainty (output

from the hfi_read_bandpass routine), and/or the band-average spectral uncertainty to be set via the EABP (Error in Average Band-Pass) keyword (output from the hfi_read_avg_bandpass routine). Please refer to the test scripts for details on how these routine calls are performed. In principle it is possible to determine uncertainties for the LFI colour corrections, based on errors in the spectral index, dust temperature, etc. without spectral uncertainty; this is beyond the scope of this introduction and is left as an exercise (contact the authors for assistance if needed). The colour correction routine accepts various error keywords for use in the GETERR uncertainty estimate. These include ER_ALPHA, ER_TBD, ER_BETABD, ER_INU, associated with the ALPHA, TBD, BETABD, and INU input keywords. The default setting is zero to allow the uncertainty estimate to be strictly based on the spectral uncertainty. If any of the additional error keywords are set, then this additional uncertainty is combined with the spectral uncertainty in the simulation run. The defualt number of itereations is 2. Obviously this will not provide an accurate estimate, but not task processing time if accidentally set. The example routines use 100 iterations. Published uncertainty results typically use 10000 iterations (but this obviously takes longer to compute).

Unit Conversion

The hfi_unit_conversion.pro routine will yield a structure of unit conversion coefficients for the provided spectral input, on a frequency channel and individual detector level for both LFI and HFI. It accepts an IDL structure containing individual detector spectra as input. It also accepts a band-average structure array as an additional keyword input, and outputs coefficients derived from the provided detector average spectrum. If this ABP optional keyword input is not provided, then the optional AVG_UC keyword output is not returned, and the main output returned by the function is set to zero (the individual bolometer coefficients are still returned via the keyword outputs).

```
hfi_100_uc = hfi_unit_conversion(BP_INFO=hfi_bp, '100',hfibolo_100_uc, $

         ABP=hfi_avg, AVG_UC=AVG_100_UC, CH_UC=ch_100_uc)
```

```
help, hfibolo_100_uc, /STRUCT ; Displays details of the structure contents.
uc_KCMB2MJy_100_1a = hfibolo_100_uc[0].KCMB2MJYSR
uc_KCMB2YSZ_100_2b = hfibolo_100_uc[3].KCMB2YSZ
uc_MJY2TB_100_avg = avg_100_uc.MJY2TB
lfi_44_uc = hfi_unit_conversion(BP_INFO=lfi_bp, '44', lfibolo_44_uc, $
         /lfi, ABP=lfi_avg, AVG_UC=AVG_44_UC)
```

In the above expressions, both the `hfi_100_uc` and `avg_100_uc` variables contain the coefficients determined using the band-average spectrum, and the `ch_100_uc` variable contains the average of the individual detector coefficients; these two variable sets may be similar but are not expected to be identical. The hfibolo_100_uc variable contains the individual detector values. The UC_CC unit conversion script accepts both LFI and HFI spectra in the format output by the corresponding read_..._bandpass routine. Details of the unit conversion equations are available in planck2013-p03d.

Colour Correction

The colour correction routine works in much the same way as the unit conversion. It requires individual detector spectra as input, and band-average spectral input is optional, with the same caveats as above (§2.8). The colour correction routine has three distinct modes of operation. The first mode is a powerlaw spectral index where the output is a multiplicative coefficient for conversion *from* a spectral index of -1 *to* a user-supplied spectral index, α. The second is a modified blackbody where the conversion is *from* a -1spectral index *to* a Planck function of temperature, T, and emissivity $\propto \nu^{\beta}$(normalized by a $\nu_c^{\beta} B_{\nu}(\nu_c, T)$factor). The third is *from* a -1spectral index *to* a user supplied spectral profile. One example of this use is in the provision of colour correction coefficients for

Mars, Jupiter, Saturn, Uranus, and Neptune where planet model spectra is provided as the user-specified spectral profile. Details of the colour correction equations are available in the Ex. Supp. An additional set of keywords have been added to the colour correction routines to provide the relevant effective frequency for a given spectral index, modified blackbody profile, or user-specified spectral profile. Examples of this use are included in the hfi_lfi_test_script.pro file. It is stressed that the use of effective frequencies is not within the official data processing philosophy of Planck; these outputs are provided strictly to allow comparison with other experiments that have adopted the effective frequency approach.

```
;    Determine a powerlaw colour correction for 100 GHz detectors.

hfi_100_cc = hfi_color_correction(BP_INFO=hfi_bp, '100', hfibolo_100_cc, $

    /POWERLAW, ALPHA=2.0, ABP=hfi_avg, AVG_CC=AVG_100_cc)

help, hfibolo_100_cc, /struct    ;    Print info about the detector output.

    ;    Determine a modified blackbody colour correction for Beta = 1.8 and T = 18 K.

hfi_545_cc = hfi_color_correction(BP_INFO=hfi_bp, '545', hfibolo_545_cc, /MODBLACKBODY, $

    TBD = 18d, BETABD = 1.8d, ABP=hfi_avg, CH_CC=CH_545_CC, AVG_CC=AVG_545_CC)

    print, hfibolo_545_cc.BOLONAME

    print, hfibolo_545_cc.CC
```

- Note that 545-3 is set to -10^9as this detector is not included in flight data products due to excessive noise.

```
    ;    Try to use a user-input spectrum

nu = (hfi_avg[5].freq)    ;    in Hz

Inu = COS((hfi_avg[5].trans)) ;    some arb. profile

hfi_857_cc = hfi_color_correction(BP_INFO=hfi_bp, '857', nu, Inu, hfibolo_857_cc, $

    ABP=hfi_avg, CH_CC=CH_857_CC, AVG_CC=AVG_857_CC)

print, hfibolo_857_cc.BOLONAME

    print, hfibolo_857_cc.CC
```

```
    ;    Try to use another user-input spectrum

nu = (hfi_avg[5].freq)    ;    in Hz

Inu = LOG((hfi_avg[5].trans)) ;    some arb. profile

hfi_857_cc = hfi_color_correction(BP_INFO=hfi_bp, '857', nu, Inu, hfibolo_857_cc, $
```

```
    ABP=hfi_avg, CH_CC=CH_857_CC, AVG_CC=AVG_857_CC)

print, hfibolo_857_cc.BOLONAME

    print, hfibolo_857_cc.CC
```

The variable CH_CC represents the average of the individual detector coefficients. The AVG_CC keyword and the function return value are both the output variable for the colour correction based on the band-average spectrum (i.e. the spectra are averaged and single coefficients are determined, not the averaging of multiple coefficients). The hfibolo_... variable is the output for the individual detector coefficients. For the user specified spectral profile, i.e. nu and Inu provided by the user, the frequency sampling of nu and Inu must match that of the corresponding transmission spectra. This was demonstrated above by setting nu = (hfi_avg[5].freq) from the transmission structure array.

CO Correction

The CO correction routine provides conversion for CO emission from units of K $_{CMB}$ to units of K km/s. The input and output formats are similar to the other UC_CC routines as described above. It is advised to use the `FLAG=0` setting in obtaining the detector and band-average spectra for the CO coefficients whereas it is recommended to use the `FLAG=1` or `/FLAG` setting for generation of any of the other coefficients (§2.6.1).

```
  ; Determine CO coefficients for 100 GHz detectors, COJ1-0 transition.
vrad = 0d ; radial velocity of 0 km/s.
    hfi_100_co = hfi_co_correction( BP_INFO=hfi_bp_withCO, '100', hfibolo_100_co, $
    hfibolo_100_13co, vrad=vrad, ABP=hfi_avg_withCO, AVG_CO=AVG_100_CO, $
    AVG_13CO=AVG_100_13CO, CH_CO=CH_100_CO, CH_13CO=CH_100_13CO, $
    BP_FLG=flg_withCO, FABP=flg_avg_withCO)

print, hfibolo_100_co.BOLONAME ; print the detector names
print, hfibolo_100_co.COLINE ; print the lower J value of the CO transition
print, hfibolo_100_co.CC ; print the CO coefficients
print, hfibolo_100_13co.CC ; print the 13CO coefficients

; Repeat the above while also getting an uncertainty estimate.
hfi_100_co_wEr = hfi_co_correction( BP_INFO=hfi_bp_withCO, '100', hfibolo_100_co_wEr, $
    hfibolo_100_13co_wEr, vrad=vrad, ABP=hfi_avg_withCO, AVG_CO=AVG_100_CO_wEr, $
    AVG_13CO=AVG_100_13CO_wEr, CH_CO=CH_100_CO_wEr, CH_13CO=CH_100_13CO_wEr, $
    BP_FLG=flg_withCO, FABP=flg_avg_withCO, BP_ERR=hfi_er_withCO, EABP=hfi_er_avg_withCO, $
    /GETERR, NITER=100)

print, hfibolo_100_co.BOLONAME ; print the detector names
print, hfibolo_100_co.COLINE ; print the lower J value of the CO transition
print, hfibolo_100_co.CC ; print the CO coefficients
print, hfibolo_100_co.ER ; print the CO coefficient uncertainties
print, hfibolo_100_13co.CC ; print the 13CO coefficients
print, hfibolo_100_13co.ER ; print the 13CO coefficient uncertainties

; Use a different vrad and get the coefficients for the 143 GHz detectors.
```

```
; You do not have to set the BP_FLG and FABP keywords, but the result is more accurate if you do.

vrad = -30d ; radial velocity of -30 km/s (towards viewer).
hfi_143_co = hfi_co_correction( BP_INFO=hfi_bp_withCO, '143', hfibolo_143_co, $
    hfibolo_143_13co, vrad=vrad, ABP=hfi_avg_withCO, AVG_CO=AVG_143_CO, $
    AVG_13CO=AVG_143_13CO, CH_CO=CH_143_CO, CH_13CO=CH_143_13CO)

print, hfibolo_143_co.BOLONAME ; print the detector names
print, hfibolo_143_co.COLINE ; There are two 143 GHz lines inc. (both coeffs. very small)
print, hfibolo_143_co.CC ; print the CO coefficients

; Use another vrad and get the coefficients for the 857 GHz detectors.
vrad = 60d ; radial velocity of 60 km/s (away from viewer).
hfi_857_co = hfi_co_correction( BP_INFO=hfi_bp_withCO, '857', hfibolo_857_co, $
    hfibolo_857_13co, vrad=vrad, ABP=hfi_avg_withCO, AVG_CO=AVG_857_CO, $
    AVG_13CO=AVG_857_13CO, CH_CO=CH_857_CO, CH_13CO=CH_857_13CO)

print, hfibolo_857_co.BOLONAME ; print the detector names
print, hfibolo_857_co.COLINE ; There are four 857 GHz lines
print, hfibolo_857_co.CC ; print the CO coefficients
```

Although it is possible to determine CO coefficients for all 9 of the lowest rotational transitions for each HFI channel, the UC_CC routine only outputs those within, or nearly within the relevant spectral band. The two out-of-band 143 GHz coefficients are included as a confirmation of the CO rejection within this band.

Nested Correction

Combinations of the above coefficients may be used to obtain additional correction factors. A few illustrative examples are included below.

Colour correction from $\alpha = -2$ to $\alpha = 4$

The colour correction from a spectral index of -2 to 4 is done by first computing the conversion from both indices to -1, and then producing the correct ratio of the two.

```
    ;    Determine the -2 to -1 correction, and the 4 to -1 correction

alpha1 = -2d ;   the first  CC spectral index

alpha2 =  4d ;   the second CC spectral index

hfi_100_a1_cc = hfi_colour_correction(BP_INFO=hfi_bp, '100', hfibolo_100_a1_cc, $

    /POWERLAW, ALPHA=alpha1, ABP=hfi_avg, AVG_CC=AVG_100_a1_cc)

    ;    The above converts from -1 to alpha1

hfi_100_a2_cc = hfi_colour_correction(BP_INFO=hfi_bp, '100', hfibolo_100_a2_cc, $

    /POWERLAW, ALPHA=alpha2, ABP=hfi_avg, AVG_CC=AVG_100_a2_cc)
```

```
    ;    The above converts from -1 to alpha2

hfibolo_100_m2_to_4_cc = hfibolo_100_a1_cc    ;   Use this as a placeholder.

cc_m1_to_m2 = hfibolo_100_a1_cc.CC    ;  Coeffs. for -1 to -2

cc_m1_to_4  = hfibolo_100_a2_cc.CC    ;  Coeffs. for -1 to  4

cc_m2_to_4  = cc_m1_to_4/cc_m1_to_m2  ;  ratio the coeffs.

hfibolo_100_m2_to_4_cc.CC = cc_m2_to_4    ;  Set the structure values to the coeff. ratios.

print, cc_m1_to_m2    ;  the -1 -> -2 coeffs.

print, cc_m1_to_4     ;  the -1 ->  4 coeffs.

print, cc_m2_to_4     ;  the -2 ->  4 coeffs.
```

It is important to get the correct numerator and denominator when determining nested/combined unit conversion and colour correction ratios. Colour correction coefficients are from spectral index -1 *to* spectral index α by definition. The units of the unit conversion coefficients should be clear. The IRAS convention implies a spectral index of -1, so the unit conversion coefficients yielding results in units of MJy/sr are expected to have an associated spectral index of -1.

Unit conversion / colour correction from K $_{\mathrm{CMB}}$ to $\alpha = 2$

In order to convert between units of K $_{\mathrm{CMB}}$ to MJy/sr with an effective spectral index of $\alpha = 2$ requires both a unit conversion and a colour correction.

```
    ;    Determine the K_CMB to MJy/sr conversion (alpha=-1)

hfi_100_uc = hfi_unit_conversion(BP_INFO=hfi_bp, '100',hfibolo_100_uc, $

    ABP=hfi_avg, AVG_UC=AVG_100_UC)

uc_100_KCMB2MJy = hfibolo_100_uc.KCMB2MJYSR    ;    The UC Coeffs.

    ;    Determine the -1 to 2 colour correction.

hfi_100_cc = hfi_color_correction(BP_INFO=hfi_bp, '100', hfibolo_100_cc, $

    /POWERLAW, ALPHA=2.0, ABP=hfi_avg, AVG_CC=AVG_100_cc)

cc_100_m1_to_2 = hfibolo_100_cc.CC    ;    The CC coeffs.

uccc_100_Kcmb_to_2 = uc_100_KCMB2MJy*cc_100_m1_to_2    ;    Units are still MJy/sr/Kcmb

print, uccc_100_Kcmb_to_2    ;    Print the UC/CC Coeffs.
```

The above examples should demonstrate the basic idea. Users are welcome to experiment with various combinations of data conversion.

LFI quadratic (fast) Colour Correction

The IDL routine 'LFI_fastcc' provides a quick and easy method of calculating the colour corrections that should be applied to Planck LFI data depending on the source spectra. It uses quadratic fits of the form $cc=A + B\times\alpha + C\times\alpha^2$ to the tabulated values in section 2 of P02b Planck/LFI Calibration#planck2013-p02b. It does not have any external dependencies.

The routine can be called for the band averaged maps as

```
LFI_fastcc(freq,spectra)
```

where *freq* is one of 28.4, 44.1 or 70.4; or for individual RCA as

```
LFI_fastcc(70.4,spectra,detector=18)
```

(for the 70GHz RCA number 18).

Also included is the LFI_fastcc_test.pro script. This reproduces the tabulated values using the quadratic fits, and demonstrates that the values from the quadratic fit agree with those in the table to an accuracy of ~0.1%.

The conventions for the spectra and corrections are the same as in the paper, i.e. the measured values should be *multiplied* by the colour corrections to obtain the colour-corrected value.

Conclusions

The basic function and structure of the UC_CC routines has been described with command-line examples provided. Further details on the derivation of the equations used within the routines is found in the references cited above, i.e. #planck2013-p03d.

References

<biblio force=false>

1. References

</biblio>

Print and Plot

There is no "print and plot" software for PLA1.

Analysis

There is no "analysis" software for PLA1.

Format Conversion

There is no "format conversion" software for PLA1.

References

[1] http://externaltools.planck.fr

Appendix

Appendix

Band-Average Spectral Transmission

The derivation of the band-average spectral transmission data products is described here. This section will include figures of each band and histograms of the full-sky weight maps (verification of the detector relative weight coefficients used).

Additional Spectral Characterization Data

This section provides additional HFI spectral characterization data to that presented in the main body of the Explanatory Supplement. Where an example for a single detector may have been included above, this section will contain the same information for all detectors.

FIXME: insert table of spetral band parameters (cut-on, cut-off, effective frequency, opt. efficiency, etc.)

FIXME: insert plots of individual detector interferograms.

FIXME: insert plots of waveguide/IAS/filter spectral stitching for each detector, grouped into frequency-bands.

FIXME: insert plots of each spectral transmission, full range, with log inset for OOB regions.

Glossary

- **calibration** [HFI meaning]: For a single detector, the absolute calibration is gain factor between the measured signal (watts absorbed by the detector) and the sky signal (in astrophysical units); can vary with time. For a set of detectors, the relative calibration is the difference in the calibration between detector pairs. The latter can be measured very accurately from the observations of the same source by different detectors, and is only slightly affected by the differences in the detector spectral responses, which are similar; the former requires observations of sources with well modeled spectral energy distributions or well known spectra, and requires that the detector's spectral bandpass also be well known.
- **calibration** [LFI meaning]:absolute calibration refers to the 0th order calibration for each channel, 1 single number, while the relative calibration refers to the component of the calibration that varies pointing period by pointing period.
- **detector set** [HFI meaning]: a detector set (aka detset aka quad) is a combinaison of two pairs of Polarization Sensitive Bolometers pairs at the proper orientations. The lists of detsets is given in here.
- **DMC** : Data Management Component, the databases used at the HFI and LFI DPCs
- **effective beam** [HFI meaning]: the effective beam at the map level is the overall angular response to the sky in a map pixel, which results from the combined effect of the instrumental response, the scanning strategy and the data processing.
- **far sidelobe** [HFI meaning]: the response to the sky of a detector more than 5 degrees from the beam centroid.
- **half ring difference** : difference between the map built using the first half of each pointing period (typically 20 minutes of contiguous data) and the one built with the second half. This difference effectively removes the sky signal and most of the correlated noise, leaving only the noise components that have time scales of < ~ 20 min.

- **HPR** [HFI meaning]: HEALPix Rings are introduced to avoid any additional binning of the data. We choose a sky pixelization as a basis for this ring making (HEALPix, Górski et al. 2005). HPR are therefore partial sky maps produced via a projection onto the sky of each single pointing period separately.
- **IMO** [HFI meaning]: the HFI Instrument MOdel is a central repository containing the models (or a link to them) and sets of fixed parameters used in these models describing for example how photons are gathered and transformed into data. IMO is oriented toward the data reduction and data processing. IMO is also used to monitor the instrument health. IMO represents at any time the official knowledge of the instrument response. It is intended to represent its best current knowledge agreed on by the project and applicable to the data processing. IMO does not represent the knowledge of the instrument. It is a knowledge of its response, (e.g. how photons are gathered and transformed into data). It is a simplified fraction of this knowledge directly useful to reduce the data. The IMO is restricted to the sole parameters used in the DPC. IMO does not contain timelines, nor maps, although it can provide links to calibration timelines (e.g. gain evolution) and calibration maps (e.g. beam maps). Models do not need to be unique (not a single model for a single process). Depending on the purpose for which they are used, they can be more or less sophisticated. (e.g. bolometer models, beam representations, very simplified for first assessment of pointing parameters, ...). IMO does not choose between them : it contains the parameters for each of them at the same time. See HFI RIMO.
- **main beam** [HFI meaning] Response to the sky within 23 arcminutes of the centroid of response.
- **near sidelobe** [HFI meaning] Response to the sky between 23 arcminutes and 5 degrees from the main beam centroid.
- **OD** : Operation Day definition is geometric visibility driven as it runs from the start of a DTCP (satellite Acquisition Of Signal) to the start of the next DTCP. Given the different ground stations and spacecraft will takes which station for how long, the OD duration varies but it is basically once a day.
- **optical beam** [HFI meaning] The response to the sky due to optics alone.
- **PBR** [HFI meaning]: Phase Bin Rings provide a compressed and higher signal-to-noise ratio rendition of the original Time Order Data
- **polarization leakage** [HFI meaning]: in general, systematic effects mix the I,Q,U signals. Given the amplitudes of the sky signals, leakage from temperature to polarisation can be dramatic for polarisation analysis.
- **ring** [HFI meaning]: at the HFI DPC level the ring is the time intervalle between two First Thurster Firings as defined in AHF description document [2]. It thus starts with a satellite slew and thus an unstable pointing period and continue with a satellite dwell and thus stable pointing period.
- **RIMO** [HFI meaning]: The RIMO, or Reduced Instrument Model is a FITS file containing selected instrument characteristics that are needed by users who work with the released data products.
- **sample** [HFI meaning]
- **scanning beam** [HFI meaning]: the scanning is defined as the beam measured from the response to a point source of the full optical and electronic system, after the filtering.
- **scanning beam** [LFI meaning]: the actual beam which couples the optics of the instrument with the scanning movement of the satellite (beam smearing). It can be measured from planet observations.
- **SOVT** : System Operation and Validation Test
- **spectral response** (or bandpass): steady state response of a detector system (i.e., detector and its electronics + horn + filter) as a function of frequency. It does not consider the temporal response and associated transfer function.
- **survey** [HFI meaning]: sky surveys (aka Scan #)are defined in terms of the direction of the satellite's spin axis. Survey periods are given here.
- **TOD** [HFI meaning]: Time-Ordered Data
- **TOD** [LFI meaning]: Time-Ordered Data, refers to calibrated data
- **TOI** [HFI meaning]: Time Ordered Information
- **TOI** [LFI meaning]: Time Ordered Information, refers to uncalibrated data

- **warm units** : JFET, Bellow, PAU et REU

Acronym list

- **calibration** [HFI meaning]: For a single detector, the absolute calibration is gain factor between the measured signal (watts absorbed by the detector) and the sky signal (in astrophysical units); can vary with time. For a set of detectors, the relative calibration is the difference in the calibration between detector pairs. The latter can be measured very accurately from the observations of the same source by different detectors, and is only slightly affected by the differences in the detector spectral responses, which are similar; the former requires observations of sources with well modeled spectral energy distributions or well known spectra, and requires that the detector's spectral bandpass also be well known.
- **calibration** [LFI meaning]:absolute calibration refers to the 0th order calibration for each channel, 1 single number, while the relative calibration refers to the component of the calibration that varies pointing period by pointing period.
- **detector set** [HFI meaning]: a detector set (aka detset aka quad) is a combinaison of two pairs of Polarization Sensitive Bolometers pairs at the proper orientations. The lists of detsets is given in here.
- **DMC** : Data Management Component, the databases used at the HFI and LFI DPCs
- **effective beam** [HFI meaning]: the effective beam at the map level is the overall angular response to the sky in a map pixel, which results from the combined effect of the instrumental response, the scanning strategy and the data processing.
- **far sidelobe** [HFI meaning]: the response to the sky of a detector more than 5 degrees from the beam centroid.
- **half ring difference** : difference between the map built using the first half of each pointing period (typically 20 minutes of contiguous data) and the one built with the second half. This difference effectively removes the sky signal and most of the correlated noise, leaving only the noise components that have time scales of < ~ 20 min.
- **HPR** [HFI meaning]: HEALPix Rings are introduced to avoid any additional binning of the data. We choose a sky pixelization as a basis for this ring making (HEALPix, Górski et al. 2005). HPR are therefore partial sky maps produced via a projection onto the sky of each single pointing period separately.
- **IMO** [HFI meaning]: the HFI Instrument MOdel is a central repository containing the models (or a link to them) and sets of fixed parameters used in these models describing for example how photons are gathered and transformed into data. IMO is oriented toward the data reduction and data processing. IMO is also used to monitor the instrument health. IMO represents at any time the official knowledge of the instrument response. It is intended to represent its best current knowledge agreed on by the project and applicable to the data processing. IMO does not represent the knowledge of the instrument. It is a knowledge of its response, (e.g. how photons are gathered and transformed into data). It is a simplified fraction of this knowledge directly useful to reduce the data. The IMO is restricted to the sole parameters used in the DPC. IMO does not contain timelines, nor maps, although it can provide links to calibration timelines (e.g. gain evolution) and calibration maps (e.g. beam maps). Models do not need to be unique (not a single model for a single process). Depending on the purpose for which they are used, they can be more or less sophisticated. (e.g. bolometer models, beam representations, very simplified for first assessment of pointing parameters, ...). IMO does not choose between them : it contains the parameters for each of them at the same time. See HFI RIMO.
- **main beam** [HFI meaning] Response to the sky within 23 arcminutes of the centroid of response.
- **near sidelobe** [HFI meaning] Response to the sky between 23 arcminutes and 5 degrees from the main beam centroid.
- **OD** : Operation Day definition is geometric visibility driven as it runs from the start of a DTCP (satellite Acquisition Of Signal) to the start of the next DTCP. Given the different ground stations and spacecraft will takes which station for how long, the OD duration varies but it is basically once a day.

- **optical beam** [HFI meaning] The response to the sky due to optics alone.
- **PBR** [HFI meaning]: Phase Bin Rings provide a compressed and higher signal-to-noise ratio rendition of the original Time Order Data
- **polarization leakage** [HFI meaning]: in general, systematic effects mix the I,Q,U signals. Given the amplitudes of the sky signals, leakage from temperature to polarisation can be dramatic for polarisation analysis.
- **ring** [HFI meaning]: at the HFI DPC level the ring is the time intervalle between two First Thurster Firings as defined in AHF description document [2]. It thus starts with a satellite slew and thus an unstable pointing period and continue with a satellite dwell and thus stable pointing period.
- **RIMO** [HFI meaning]: The RIMO, or Reduced Instrument Model is a FITS file containing selected instrument characteristics that are needed by users who work with the released data products.
- **sample** [HFI meaning]
- **scanning beam** [HFI meaning]: the scanning is defined as the beam measured from the response to a point source of the full optical and electronic system, after the filtering.
- **scanning beam** [LFI meaning]: the actual beam which couples the optics of the instrument with the scanning movement of the satellite (beam smearing). It can be measured from planet observations.
- **SOVT** : System Operation and Validation Test
- **spectral response** (or bandpass): steady state response of a detector system (i.e., detector and its electronics + horn + filter) as a function of frequency. It does not consider the temporal response and associated transfer function.
- **survey** [HFI meaning]: sky surveys (aka Scan #)are defined in terms of the direction of the satellite's spin axis. Survey periods are given here.
- **TOD** [HFI meaning]: Time-Ordered Data
- **TOD** [LFI meaning]: Time-Ordered Data, refers to calibrated data
- **TOI** [HFI meaning]: Time Ordered Information
- **TOI** [LFI meaning]: Time Ordered Information, refers to uncalibrated data
- **warm units** : JFET, Bellow, PAU et REU

References

References

<biblio>

1. planck2013-p01 bibtex=@BOOK{planck2013-p01,

author = {Planck Collaboration 01,}, title = {P01 Mission}, journal = {Submitted to A&A}, keywords = {Astrophysics}, year = {2013} }

1. planck2013-p01a bibtex=@BOOK{planck2013-p01a,

author = {Planck Collaboration 01a,}, title = {P01a Consistency Tests}, journal = {Submitted to A&A}, keywords = {Astrophysics}, year = {2013} }

1. planck2013-p02 bibtex=@BOOK{planck2013-p02,

author = {Planck Collaboration 02,}, title = {P02 LFI Processing}, journal = {Submitted to A&A}, keywords = {Astrophysics}, year = {2013} }

1. planck2013-p02a bibtex=@BOOK{planck2013-p02a,

author = {Planck Collaboration 02a,}, title = {P02a LFI Systematics}, journal = {Submitted to A&A}, keywords = {Astrophysics}, year = {2013} }

1. planck2013-p02b bibtex=@BOOK{planck2013-p02b,

author = {Planck Collaboration 02b,}, title = {P02b LFI Calibration}, journal = {Submitted to A&A}, keywords = {Astrophysics}, year = {2013} }

1. planck2013-p02c bibtex=@BOOK{planck2013-p02c,

author = {Planck Collaboration 02c,}, title = {P02c LFI Polarization}, journal = {Submitted to A&A}, keywords = {Astrophysics}, year = {2013} }

1. planck2013-p02d bibtex=@BOOK{planck2013-p02d,

author = {Planck Collaboration 02d,}, title = {P02d LFI Beams}, journal = {Submitted to A&A}, keywords = {Astrophysics}, year = {2013} }

1. planck2013-p03 bibtex=@BOOK{planck2013-p03,

author = {Planck Collaboration 03,}, title = {P03 HFI Processing}, journal = {Submitted to A&A}, keywords = {Astrophysics}, year = {2013} }

1. planck2013-p03a bibtex=@BOOK{planck2013-p03a,

author = {Planck Collaboration 03a,}, title = {P03a CO}, journal = {Submitted to A&A}, keywords = {Astrophysics}, year = {2013} }

1. planck2013-p03b bibtex=@BOOK{planck2013-p03b,

author = {Planck Collaboration 03b,}, title = {P03b HFI Spire Cross Calibration}, journal = {Submitted to A&A}, keywords = {Astrophysics}, year = {2013} }

1. planck2013-p03c bibtex=@BOOK{planck2013-p03c,

author = {Planck Collaboration 03c,}, title = {P03c HFI Transfer Function and Beams}, journal = {Submitted to A&A}, keywords = {Astrophysics}, year = {2013} }

1. planck2013-p03d bibtex=@BOOK{planck2013-p03d,

author = {Planck Collaboration 03d,}, title = {P03d HFI Spectral Bands}, journal = {Submitted to A&A}, keywords = {Astrophysics}, year = {2013} }

1. planck2013-p03e bibtex=@BOOK{planck2013-p03e,

author = {Planck Collaboration 03e,}, title = {P03e HFI Glitch}, journal = {Submitted to A&A}, keywords = {Astrophysics}, year = {2013} }

1. planck2013-p03f bibtex=@BOOK{planck2013-p03f,

author = {Planck Collaboration 03f,}, title = {P03f HFI Calibration}, journal = {Submitted to A&A}, keywords = {Astrophysics}, year = {2013} }

1. planck2013-p03g bibtex=@BOOK{planck2013-p03g,

author = {Planck Collaboration 03g,}, title = {P03g HFI Polarization}, journal = {Submitted to A&A}, keywords = {Astrophysics}, year = {2013} }

1. planck2013-p04 bibtex=@BOOK{planck2013-p04,

author = {Planck Collaboration 04,}, title = {P04 Telescope}, journal = {Submitted to A&A}, keywords = {Astrophysics}, year = {2013} }

1. planck2013-p05 bibtex=@BOOK{planck2013-p05,

author = {Planck Collaboration 05,}, title = {P05 PCCS}, journal = {Submitted to A&A}, keywords = {Astrophysics}, year = {2013} }

1. planck2013-p05a bibtex=@BOOK{planck2013-p05a,

author = {Planck Collaboration 05a,}, title = {P05a Planck Cluster Sample}, journal = {Submitted to A&A}, keywords = {Astrophysics}, year = {2013} }

1. planck2013-p05b bibtex=@BOOK{planck2013-p05b,

author = {Planck Collaboration 05b,}, title = {P05b SZ PowerSpectrum Bispectrum Py}, journal = {Submitted to A&A}, keywords = {Astrophysics}, year = {2013} }

1. planck2013-p06 bibtex=@BOOK{planck2013-p06,

author = {Planck Collaboration 06,}, title = {P06 Component Separation}, journal = {Submitted to A&A}, keywords = {Astrophysics}, year = {2013} }

1. planck2013-p06a bibtex=@BOOK{planck2013-p06a,

author = {Planck Collaboration 06a,}, title = {P06a Synchrotron Model}, journal = {Submitted to A&A}, keywords = {Astrophysics}, year = {2013} }

1. planck2013-p06b bibtex=@BOOK{planck2013-p06b,

author = {Planck Collaboration 06b,}, title = {P06b Submillimeter Dust Model}, journal = {Submitted to A&A}, keywords = {Astrophysics}, year = {2013} }

1. planck2013-p07 bibtex=@BOOK{planck2013-p07,

author = {Planck Collaboration 07,}, title = {P07 Power Spectra}, journal = {Submitted to A&A}, keywords = {Astrophysics}, year = {2013} }

1. planck2013-p08 bibtex=@BOOK{planck2013-p08,

author = {Planck Collaboration 08,}, title = {P08 Likelihood}, journal = {Submitted to A&A}, keywords = {Astrophysics}, year = {2013} }

1. planck2013-p09 bibtex=@BOOK{planck2013-p09,

author = {Planck Collaboration 09,}, title = {P09 Isotropy and Statistics}, journal = {Submitted to A&A}, keywords = {Astrophysics}, year = {2013} }

1. planck2013-p09a bibtex=@BOOK{planck2013-p09a,

author = {Planck Collaboration 09a,}, title = {P09a Fnl Bispectrum Trispectrum}, journal = {Submitted to A&A}, keywords = {Astrophysics}, year = {2013} }

1. planck2013-p10 bibtex=@BOOK{planck2013-p10,

author = {Planck Collaboration 10,}, title = {P10 Parameters Extras}, journal = {Submitted to A&A}, keywords = {Astrophysics}, year = {2013} }

1. planck2013-p11 bibtex=@BOOK{planck2013-p11,

author = {Planck Collaboration 11,}, title = {P11 Parameters Planck Alone and Planck plus External Data}, journal = {Submitted to A&A}, keywords = {Astrophysics}, year = {2013} }

1. planck2013-p12 bibtex=@BOOK{planck2013-p12,

author = {Planck Collaboration 12,}, title = {P12 Lensing}, journal = {Submitted to A&A}, keywords = {Astrophysics}, year = {2013} }

1. planck2013-p13 bibtex=@BOOK{planck2013-p13,

author = {Planck Collaboration 13,}, title = {P13 CIB Lensing}, journal = {Submitted to A&A}, keywords = {Astrophysics}, year = {2013} }

1. planck2013-p14 bibtex=@BOOK{planck2013-p14,

author = {Planck Collaboration 14,}, title = {P14 ISW}, journal = {Submitted to A&A}, keywords = {Astrophysics}, year = {2013} }

1. planck2013-p15 bibtex=@BOOK{planck2013-p15,

author = {Planck Collaboration 15,}, title = {P15 Cosmological Constraints from Clusters}, journal = {Submitted to A&A}, keywords = {Astrophysics}, year = {2013} }

1. planck2013-p16 bibtex=@BOOK{planck2013-p16,

author = {Planck Collaboration 16,}, title = {P16 Reionization}, journal = {Submitted to A&A}, keywords = {Astrophysics}, year = {2013} }

1. planck2013-p17 bibtex=@BOOK{planck2013-p17,

author = {Planck Collaboration 17,}, title = {P17 Inflation}, journal = {Submitted to A&A}, keywords = {Astrophysics}, year = {2013} }

1. planck2013-p18 bibtex=@BOOK{planck2013-p18,

author = {Planck Collaboration 18,}, title = {P18 Non Standard Inflation}, journal = {Submitted to A&A}, keywords = {Astrophysics}, year = {2013} }

1. planck2013-p19 bibtex=@BOOK{planck2013-p19,

author = {Planck Collaboration 19,}, title = {P19 Geometry and Topology}, journal = {Submitted to A&A}, keywords = {Astrophysics}, year = {2013} }

1. planck2013-p20 bibtex=@BOOK{planck2013-p20,

author = {Planck Collaboration 20,}, title = {P20 Strings and Other Defects}, journal = {Submitted to A&A}, keywords = {Astrophysics}, year = {2013} }

1. planck2013-p21 bibtex=@BOOK{planck2013-p21,

author = {Planck Collaboration 21,}, title = {P21 Magnetic Fields}, journal = {Submitted to A&A}, keywords = {Astrophysics}, year = {2013} }

1. planck2013-p22 bibtex=@BOOK{planck2013-p22,

author = {Planck Collaboration 22,}, title = {P22 Dark Matter Annihilation}, journal = {Submitted to A&A}, keywords = {Astrophysics}, year = {2013} }

1. planck2013-p23 bibtex=@BOOK{planck2013-p23,

author = {Planck Collaboration 23,}, title = {P23 Birefringence}, journal = {Submitted to A&A}, keywords = {Astrophysics}, year = {2013} }

1. planck2013-p24 bibtex=@BOOK{planck2013-p24,

author = {Planck Collaboration 24,}, title = {P24 Parity Violation}, journal = {Submitted to A&A}, keywords = {Astrophysics}, year = {2013} }

1. planck2013-p25 bibtex=@BOOK{planck2013-p25,

author = {Planck Collaboration 25,}, title = {P25 Variation of Fundamental Constants}, journal = {Submitted to A&A}, keywords = {Astrophysics}, year = {2013} }

1. planck2013-p26 bibtex=@BOOK{planck2013-p26,

author = {Planck Collaboration 26,}, title = {P26 Planck Sky Model}, journal = {Submitted to A&A}, keywords = {Astrophysics}, year = {2013} }

1. planck2013-p27 bibtex=@BOOK{planck2013-p27,

author = {Planck Collaboration 27,}, title = {P27 Simulations}, journal = {Submitted to A&A}, keywords = {Astrophysics}, year = {2013} }

1. planck2013-p28 bibtex=@BOOK{planck2013-p28,

author = {Planck Collaboration 28,}, title = {P28 Explanatory Supplement}, journal = {Submitted to A&A}, keywords = {Astrophysics}, year = {2013} }

1. planck2012-I bibtex=@ARTICLE{planck2012-I,

author = {Planck Collaboration I,}, title = {Planck intermediate results. I. Further validation of new Planck clusters with XMM-Newton}, journal = {A&A}, year = {2012}, volume = {543}, pages = {A102} }

1. planck2012-II bibtex=@BOOK{planck2012-II,

author = {Planck and AMI Collaborations,}, title = {Planck intermediate results. II. Comparison of Sunyaev-Zeldovich measurements from Planck and from the Arcminute Microkelvin Imager for 11 galaxy clusters}, journal = {Submitted to A&A}, keywords = {Astrophysics}, year = {2012}, publisher = {Submitted to A&A, [arXiv:astro-ph/1204.1318]} }

1. planck2012-III bibtex=@BOOK{planck2012-III,

author = {Planck Collaboration III,}, title = {Planck intermediate results. III. The relation between galaxy cluster mass and Sunyaev-Zeldovich signal}, journal = {Submitted to A&A}, keywords = {Astrophysics}, year = {2012}, publisher = {Submitted to A&A, [arXiv:astro-ph/1204.2743]} }

1. planck2012-IV bibtex=@BOOK{planck2012-IV,

author = {Planck Collaboration IV,}, title = {Planck intermediate results. IV. The XMM-Newton validation programme for new Planck clusters}, journal = {Submitted to A&A}, keywords = {Astrophysics}, year = {2012}, publisher = {Submitted to A&A, [arXiv:astro-ph/1205.3376]} }

1. planck2012-V bibtex=@BOOK{planck2012-V,

author = {Planck Collaboration V,}, title = {Planck intermediate results. V. Pressure profiles of galaxy clusters from the Sunyaev-Zeldovich effect}, journal = {Submitted to A&A}, keywords = {Astrophysics}, year = {2012}, publisher = {Submitted to A&A, [arXiv:astro-ph/1207.4061]} }

1. planck2012-VI bibtex=@BOOK{planck2012-VI,

author = {Planck Collaboration VI,}, title = {Planck intermediate results. VI. The dynamical structure of PLCKG214.6+37.0, a Planck discovered triple system of galaxy clusters}, journal = {Submitted to A&A}, keywords = {Astrophysics}, year = {2012}, publisher = {Submitted to A&A, [arXiv:astro-ph/1207.4009]} }

1. planck2012-VII bibtex=@BOOK{planck2012-VII,

author = {Planck Collaboration VII,}, title = {Planck intermediate results. VII. Statistical properties of infrared and radio extragalactic sources from the Planck Early Release Compact Source Catalogue at frequencies between 100 and 857 GHz}, journal = {Submitted to A&A}, keywords = {Astrophysics}, year = {2012}, publisher = {Submitted to A&A, [arXiv:astro-ph/1207.4706]} }

1. planck2012-VIII bibtex=@BOOK{planck2012-VIII,

author = {Planck Collaboration VIII,}, title = {Planck intermediate results. VIII. Filaments between interacting clusters}, journal = {Submitted to A&A}, keywords = {Astrophysics}, year = {2012}, publisher = {Submitted to A&A, [arXiv:astro-ph/1208.5911]} }

1. planck2012-IX bibtex=@BOOK{planck2012-IX,

author = {Planck Collaboration IX,}, title = {Planck intermediate results. IX. Detection of the Galactic haze with Planck}, journal = {Submitted to A&A}, keywords = {Astrophysics}, year = {2012}, publisher = {Submitted to A&A, [arXiv:astro-ph/1208.5483]} }

1. planck2012-X bibtex=@BOOK{planck2012-X,

author = {Planck Collaboration X,}, title = {Planck intermediate results. X. Physics of the hot gas in the Coma cluster}, journal = {Submitted to A&A}, keywords = {Astrophysics}, year = {2012}, publisher = {Submitted to A&A, [arXiv:astro-ph/1208.3611]} }

1. planck2012-XI bibtex=@BOOK{planck2012-XI,

author = {Planck Collaboration XI,}, title = {Planck intermediate results. XI. The gas content of dark matter halos: the Sunyaev-Zeldovich-stellar mass relation for locally brightest galaxies}, journal = {Submitted to A&A}, keywords = {Astrophysics}, year = {2012}, publisher = {Submitted to A&A, [arXiv:astro-ph/1212.4131]} }

1. planck2013-XII bibtex=@BOOK{planck2013-XII,

author = {Planck Collaboration XII,}, title = {Planck intermediate results. XII. Diffuse Galactic components in the Gould Belt System}, journal = {Submitted to A&A}, keywords = {Astrophysics}, year = {2013}, publisher = {Submitted to A&A, [arXiv:astro-ph/1301.5839]} }

1. planck2011-1-1 bibtex=@ARTICLE{planck2011-1.1,

author = {Planck Collaboration I,}, title = {Planck early results. I. The Planck mission}, journal = {A&A}, year = {2011}, volume = {536}, pages = {A1}, url={http://dx.doi.org/10.1051/0004-6361/201116464} }

1. planck2011-1-3 bibtex=@ARTICLE{planck2011-1.3,

author = {Planck Collaboration II,}, title = {Planck early results. II. The thermal performance of Planck}, journal = {A&A}, year = {2011}, volume = {536}, pages = {A2} }

1. planck2011-1-4 bibtex=@ARTICLE{planck2011-1.4,

author = {Mennella, A. and Butler, R. C. and Curto, A. and Cuttaia, F. and Davis, R. J. and Dick, J. and Frailis, M. and Galeotta, S. and Gregorio, A. and Kurki-Suonio, H. and Lawrence, C. R. and Leach, S. and Leahy, J. P. and Lowe, S. and Maino, D. and Mandolesi, N. and Maris, M. and Martínez-González, E. and Meinhold, P. R. and Morgante, G. and Pearson, D. and Perrotta, F. and Polenta, G. and Poutanen, T. and Sandri, M. and Seiffert, M. D. and Suur-Uski, A.-S. and Tavagnacco, D. and Terenzi, L. and Tomasi, M. and Valiviita, J. and Villa, F. and Watson, R. and Wilkinson, A. and Zacchei, A. and Zonca, A. and Aja, B. and Artal, E. and Baccigalupi, C. and Banday, A. J. and Barreiro, R. B. and Bartlett, J. G. and Bartolo, N. and Battaglia, P. and Bennett, K. and Bonaldi, A. and Bonavera, L. and Borrill, J. and Bouchet, F. R. and Burigana, C. and Cabella, P. and Cappellini, B. and Chen, X. and Colombo, L. and Cruz, M. and Danese, L. and D'Arcangelo, O. and Davies, R. D. and de Gasperis, G. and de Rosa, A. and de Zotti, G. and Dickinson, C. and Diego, J. M. and Donzelli, S. and Efstathiou, G. and Enßlin, T. A. and Eriksen, H. K. and Falvella, M. C. and Finelli, F. and Foley, S. and Franceschet, C. and Franceschi, E. and Gaier, T. C. and Génova-Santos, R. T. and George, D. and Gómez, F. and González-Nuevo, J. and Górski, K. M. and Gruppuso, A. and Hansen, F. K. and Herranz, D. and Herreros, J. M. and Hoyland, R. J. and Hughes, N. and Jewell,

J. and Jukkala, P. and Juvela, M. and Kangaslahti, P. and Keihänen, E. and Keskitalo, R. and Kilpia, V.-H. and Kisner, T. S. and Knoche, J. and Knox, L. and Laaninen, M. and Lähteenmäki, A. and Lamarre, J.-M. and Leonardi, R. and León-Tavares, J. and Leutenegger, P. and Lilje, P. B. and López-Caniego, M. and Lubin, P. M. and Malaspina, M. and Marinucci, D. and Massardi, M. and Matarrese, S. and Matthai, F. and Melchiorri, A. and Mendes, L. and Miccolis, M. and Migliaccio, M. and Mitra, S. and Moss, A. and Natoli, P. and Nesti, R. and N{\o}rgaard-Nielsen, H. U. and Pagano, L. and Paladini, R. and Paoletti, D. and Partridge, B. and Pasian, F. and Pettorino, V. and Pietrobon, D. and Pospieszalski, M. and Prézeau, G. and Prina, M. and Procopio, P. and Puget, J.-L. and Quercellini, C. and Rachen, J. P. and Rebolo, R. and Reinecke, M. and Ricciardi, S. and Robbers, G. and Rocha, G. and Roddis, N. and Rubino-Martín, J. A. and Savelainen, M. and Scott, D. and Silvestri, R. and Simonetto, A. and Sjoman, P. and Smoot, G. F. and Sozzi, C. and Stringhetti, L. and Tauber, J. A. and Tofani, G. and Toffolatti, L. and Tuovinen, J. and Türler, M. and Umana, G. and Valenziano, L. and Varis, J. and Vielva, P. and Vittorio, N. and Wade, L. A. and Watson, C. and White, S. D. M. and Winder, F.}, title = {Planck early results. III. First assessment of the Low Frequency Instrument in-flight performance}, journal = {A&A}, year = {2011}, volume = {536}, pages = {A3}, }

1. planck2011-1-5 bibtex=@ARTICLE{planck2011-1.5,

author = {Planck HFI Core Team,}, title = {Planck early results, IV. First assessment of the High Frequency Instrument in-flight performance}, journal = {A&A}, year = {2011}, volume = {536}, pages = {A4} }

1. planck2011-1-6 bibtex=@ARTICLE{planck2011-1.6,

author = {Zacchei, A. and Maino, D. and Baccigalupi, C. and Bersanelli, M. and Bonaldi, A. and Bonavera, L. and Burigana, C. and Butler, R. C. and Cuttaia, F. and de Zotti, G. and Dick, J. and Frailis, M. and Galeotta, S. and González-Nuevo, J. and Górski, K. M. and Gregorio, A. and Keihänen, E. and Keskitalo, R. and Knoche, J. and Kurki-Suonio, H. and Lawrence, C. R. and Leach, S. and Leahy, J. P. and López-Caniego, M. and Mandolesi, N. and Maris, M. and Matthai, F. and Meinhold, P. R. and Mennella, A. and Morgante, G. and Morisset, N. and Natoli, P. and Pasian, F. and Perrotta, F. and Polenta, G. and Poutanen, T. and Reinecke, M. and Ricciardi, S. and Rohlfs, R. and Sandri, M. and Suur-Uski, A.-S. and Tauber, J. A. and Tavagnacco, D. and Terenzi, L. and Tomasi, M. and Valiviita, J. and Villa, F. and Zonca, A. and Banday, A. J. and Barreiro, R. B. and Bartlett, J. G. and Bartolo, N. and Bedini, L. and Bennett, K. and Binko, P. and Borrill, J. and Bouchet, F. R. and Bremer, M. and Cabella, P. and Cappellini, B. and Chen, X. and Colombo, L. and Cruz, M. and Curto, A. and Danese, L. and Davies, R. D. and Davis, R. J. and de Gasperis, G. and de Rosa, A. and de Troia, G. and Dickinson, C. and Diego, J. M. and Donzelli, S. and Dörl, U. and Efstathiou, G. and Enßlin, T. A. and Eriksen, H. K. and Falvella, M. C. and Finelli, F. and Franceschi, E. and Gaier, T. C. and Gasparo, F. and Génova-Santos, R. T. and Giardino, G. and Gómez, F. and Gruppuso, A. and Hansen, F. K. and Hell, R. and Herranz, D. and Hovest, W. and Huynh, M. and Jewell, J. and Juvela, M. and Kisner, T. S. and Knox, L. and Lähteenmäki, A. and Lamarre, J.-M. and Leonardi, R. and León-Tavares, J. and Lilje, P. B. and Lubin, P. M. and Maggio, G. and Marinucci, D. and Martínez-González, E. and Massardi, M. and Matarrese, S. and Meharga, M. T. and Melchiorri, A. and Migliaccio, M. and Mitra, S. and Moss, A. and N{\o}rgaard-Nielsen, H. U. and Pagano, L. and Paladini, R. and Paoletti, D. and Partridge, B. and Pearson, D. and Pettorino, V. and Pietrobon, D. and Prézeau, G. and Procopio, P. and Puget, J.-L. and Quercellini, C. and Rachen, J. P. and Rebolo, R. and Robbers, G. and Rocha, G. and Rubi{\ no-Martín}, J. A. and Salerno, E. and Savelainen, M. and Scott, D. and Seiffert, M. D. and Silk, J. I. and Smoot, G. F. and Sternberg, J. and Stivoli, F. and Stompor, R. and Tofani, G. and Toffolatti, L. and Tuovinen, J. and Türler, M. and Umana, G. and Vielva, P. and Vittorio, N. and Vuerli, C. and Wade, L. A. and Watson, R. and White, S. D. M. and Wilkinson, A. }, title = {Planck early results. V. The Low Frequency Instrument data processing}, journal = {A&A}, year = {2011}, volume = {536}, pages = {A5}, }

1. planck2011-1-7 bibtex=@ARTICLE{planck2011-1.7,

author = {Planck HFI Core Team,}, title = {Planck early results. VI. The High Frequency Instrument data processing}, journal = {A&A}, year = {2011}, volume = {536}, pages = {A6} }

1. planck2011-1-10 bibtex=@ARTICLE{planck2011-1.10,

author = {Planck Collaboration VII,}, title = {Planck early results. VII. The Early Release Compact Source Catalogue}, journal = {A&A}, year = {2011}, volume = {536}, pages = {A7} }

1. planck2011-1-10sup bibtex=@BOOK{planck2011-1.10sup,

author = {Planck Collaboration,}, title = {The Explanatory Supplement to the Planck Early Release Compact Source Catalogue}, keywords = {Astrophysics}, year = {2011}, publisher = {ESA} }

1. planck2011-5-1a bibtex=@ARTICLE{planck2011-5.1a,

author = {Planck Collaboration VIII,}, title = {Planck early results. VIII. The all-sky early Sunyaev-Zeldovich cluster sample}, journal = {A&A}, year = {2011}, volume = {536}, pages = {A8} }

1. planck2011-5-1b bibtex=@ARTICLE{planck2011-5.1b,

author = {Planck Collaboration IX,}, title = {Planck early results. IX. XMM-Newton follow-up for validation of Planck cluster candidates}, journal = {A&A}, year = {2011}, volume = {536}, pages = {A9} }

1. planck2011-5-2a bibtex=@ARTICLE{planck2011-5.2a,

author = {Planck Collaboration X,}, title = {Planck early results. X. Statistical analysis of Sunyaev-Zeldovich scaling relations for X-ray galaxy clusters}, journal = {A&A}, year = {2011}, volume = {536}, pages = {A10} }

1. planck2011-5-2b bibtex=@ARTICLE{planck2011-5.2b,

author = {Planck Collaboration XI,}, title = {Planck early results. XI. Calibration of the local galaxy cluster Sunyaev-Zeldovich scaling relations}, journal = {A&A}, year = {2011}, volume = {536}, pages = {A11} }

1. planck2011-5-2c bibtex=@ARTICLE{planck2011-5.2c,

author = {Planck Collaboration XII,}, title = {Planck early results. XII. Cluster Sunyaev-Zeldovich optical Scaling relations}, journal = {A&A}, year = {2011}, volume = {536}, pages = {A12} }

1. planck2011-6-1 bibtex=@ARTICLE{planck2011-6.1,

author = {Planck Collaboration XIII,}, title = {Planck early results. XIII. Statistical properties of extragalactic radio sources in the Planck Early Release Compact Source Catalogue}, journal = {A&A}, year = {2011}, volume = {536}, pages = {A13} }

1. planck2011-6-2 bibtex=@ARTICLE{planck2011-6.2,

author = {Planck Collaboration XIV,}, title = {Planck early results. XIV. Early Release Compact Source Catalogue validation and extreme radio sources}, journal = {A&A}, year = {2011}, volume = {536}, pages = {A14} }

1. planck2011-6-3a bibtex=@ARTICLE{planck2011-6.3a,

author = {Planck Collaboration XV,}, title = {Planck early results. XV. Spectral energy distributions and radio continuum spectra of northern extragalactic radio sources}, journal = {A&A}, year = {2011}, volume = {536}, pages = {A15} }

1. planck2011-6-4a bibtex=@ARTICLE{planck2011-6.4a,

author = {Planck Collaboration XVI,}, title = {Planck early results. XVI. The Planck view of nearby galaxies}, journal = {A&A}, year = {2011}, volume = {536}, pages = {A16} }

1. planck2011-6-4b bibtex=@ARTICLE{planck2011-6.4b,

author = {Planck Collaboration XVII,}, title = {Planck early results. XVII. Origin of the submillimetre excess dust emission in the Magellanic Clouds}, journal = {A&A}, year = {2011}, volume = {536}, pages = {A17} }

1. planck2011-6-6 bibtex=@ARTICLE{planck2011-6.6,

author = {Planck Collaboration XVIII,}, title = {Planck early results. XVIII. The power spectrum of cosmic infrared background anisotropies}, journal = {A&A}, year = {2011}, volume = {536}, pages = {A18} }

1. planck2011-7-0 bibtex=@ARTICLE{planck2011-7.0,

author = {Planck Collaboration XIX,}, title = {Planck early results. XIX. All-sky temperature and dust optical depth from Planck and IRAS --- constraints on the dark gas in our Galaxy}, journal = {A&A}, year = {2011}, volume = {536}, pages = {A19} }

1. planck2011-7-2 bibtex=@ARTICLE{planck2011-7.2,

author = {Planck Collaboration XX,}, title = {Planck early results. XX. New light on anomalous microwave emission from spinning dust grains}, journal = {A&A}, year = {2011}, volume = {536}, pages = {A20} }

1. planck2011-7-3 bibtex=@ARTICLE{planck2011-7.3,

author = {Planck Collaboration XXI,}, title = {Planck early results. XXI. Properties of the interstellar medium in the Galactic plane}, journal = {A&A}, year = {2011}, volume = {536}, pages = {A21} }

1. planck2011-7-7a bibtex=@ARTICLE{planck2011-7.7a,

author = {Planck Collaboration XXII,}, title = {Planck early results. XXII. The submillimetre properties of a sample of Galactic cold clumps}, journal = {A&A}, year = {2011}, volume = {536}, pages = {A22} }

1. planck2011-7-7b bibtex=@ARTICLE{planck2011-7.7b,

author = {Planck Collaboration XXIII,}, title = {Planck early results. XXIII. The Galactic cold core population revealed by the first all-sky survey}, journal = {A&A}, year = {2011}, volume = {536}, pages = {A23} }

1. planck2011-7-12 bibtex=@ARTICLE{planck2011-7.12,

author = {Planck Collaboration XXIV,}, title = {Planck early results. XXIV. Dust in the diffuse interstellar medium and the Galactic halo}, journal = {A&A}, year = {2011}, volume = {536}, pages = {A24} }

1. planck2011-7-13 bibtex=@ARTICLE{planck2011-7.13,

author = {Planck Collaboration XXV,}, title = {Planck early results. XXV. Thermal dust in nearby molecular clouds}, journal = {A&A}, year = {2011}, volume = {536}, pages = {A25} }

1. planck2011-5-1c bibtex=@ARTICLE{planck2011-5.1c,

author = {Planck Collaboration XXVI,}, title = {Planck early results. XXVI. Detection with Planck and confirmation by XMM-Newton of PLCK G266.6-27.3, an exceptionally X-ray luminous and massive galaxy cluster at z 1}, journal = {A&A}, year = {2011}, volume = {536}, pages = {A26} }

1. planck2011-6-3b bibtex=@ARTICLE{planck2011-6.3b,

author = {Giommi, P. and Polenta, G. and Lähteenmäki, A. and Thompson, D. J. and Capalbi, M. and Cutini, S. and Gasparrini, D. and González-Nuevo, J. and León-Tavares, J. and López-Caniego, M. and Mazziotta, M. N. and Monte, C. and Perri, M. and Rain{\`o}, S. and Tosti, G. and Tramacere, A. and Verrecchia, F. and Aller, H. D. and Aller, M. F. and Angelakis, E. and Bastieri, D. and Berdyugin, A. and Bonaldi, A. and Bonavera, L. and Burigana, C. and Burrows, D. N. and Buson, S. and Cavazzuti, E. and Chincarini, G. and Colafrancesco, S. and Costamante, L. and Cuttaia, F. and D'Ammando, F. and de Zotti, G. and Frailis, M. and Fuhrmann, L. and Galeotta, S. and Gargano, F. and Gehrels, N. and Giglietto, N. and Giordano, F. and Giroletti, M. and Keihänen, E. and King, O. and Krichbaum, T. P. and Lasenby, A. and Lavonen, N. and Lawrence, C. R. and Leto, C. and Lindfors, E. and Mandolesi, N. and Massardi, M. and Max-Moerbeck, W. and Michelson, P. F. and Mingaliev, M. and Natoli, P. and Nestoras, I. and Nieppola, E. and Nilsson, K. and Partridge, B. and Pavlidou, V. and Pearson, T. J. and Procopio, P. and Rachen, J. P. and Readhead, A. and Reeves, R. and Reimer, A. and Reinthal, R. and Ricciardi, S. and Richards, J. and Riquelme, D. and Saarinen, J. and Sajina, A. and Sandri, M. and Savolainen, P. and Sievers, A. and Sillanpää, A. and Sotnikova, Y. and Stevenson, M. and Tagliaferri, G. and Takalo, L. and Tammi, J. and Tavagnacco, D. and Terenzi, L. and Toffolatti, L. and Tornikoski, M. and Trigilio, C. and Turunen, M. and Umana, G. and Ungerechts, H. and Villa, F. and Wu, J. and Zacchei, A. and Zensus, J. A. and Zhou, X.}, title = {Simultaneous Planck, Swift, and Fermi observations of X-ray and {γ}-ray selected blazars}, journal = {A&A}, year = {2012}, volume = {541}, pages = {A160} }

1. ade2010 bibtex=@ARTICLE{ade2010,

author = {Ade, P. A. R. and Savini, G. and Sudiwala, R. and Tucker, C. and Catalano, A. and Church, S. and Colgan, R. and Desert, F. X. and Gleeson, E. and Jones, W. C. and Lamarre, J.-M. and Lange, A. and Longval, Y. and Maffei, B. and Murphy, J. A. and Noviello, F. and Pajot, F. and Puget, J.-L. and Ristorcelli, I. and Woodcraft, A. and Yurchenko, V.}, title = {Planck pre-launch status: The optical architecture of the HFI}, journal = {A&A}, keywords = {cosmic microwave background, space vehicles: instruments, instrumentation: detectors, instrumentation: polarimeters, submillimeter: general, techniques: photometric}, year = {2010}, month = {sep}, volume = {520}, pages = {A11+}, doi = {10.1051/0004-6361/200913039}, adsurl = {http://adsabs.harvard.edu/abs/2010A%26A..
.520A..11A}, adsnote = {Provided by the SAO/NASA Astrophysics Data System} }

1. bersanelli2010 bibtex=@ARTICLE{bersanelli2010,

author = {Bersanelli, M. and Mandolesi, N. and Butler, R. C. and Mennella, A. and Villa, F. and Aja, B. and Artal, E. and Artina, E. and Baccigalupi, C. and Balasini, M. and Baldan, G. and Banday, A. and Bastia, P. and Battaglia, P. and Bernardino, T. and Blackhurst, E. and Boschini, L. and Burigana, C. and Cafagna, G. and Cappellini, B. and Cavaliere, F. and Colombo, F. and Crone, G. and Cuttaia, F. and D'Arcangelo, O. and Danese, L. and Davies, R. D. and Davis, R. J. and de Angelis, L. and de Gasperis, G. C. and de La Fuente, L. and de Rosa, A. and de Zotti, G. and Falvella, M. C. and Ferrari, F. and Ferretti, R. and Figini, L. and Fogliani, S. and Franceschet, C. and Franceschi, E. and Gaier, T. and Garavaglia, S. and Gomez, F. and Gorski, K. and Gregorio, A. and Guzzi, P. and Herreros, J. M. and Hildebrandt, S. R. and Hoyland, R. and Hughes, N. and Janssen, M. and Jukkala, P. and Kettle, D. and Kilpiä, V. H. and Laaninen, M. and Lapolla, P. M. and Lawrence, C. R. and Lawson, D. and Leahy, J. P. and Leonardi, R. and Leutenegger, P. and Levin, S. and Lilje, P. B. and Lowe, S. R. and Lubin, P. M. and Maino, D. and Malaspina, M. and Maris, M. and Marti-Canales, J. and Martinez-Gonzalez, E. and Mediavilla, A. and Meinhold, P. and Miccolis, M. and Morgante, G. and Natoli, P. and Nesti, R. and Pagan, L. and Paine, C. and Partridge, B. and Pascual, J. P. and Pasian, F. and Pearson, D. and Pecora, M. and Perrotta, F. and Platania, P. and Pospieszalski, M. and Poutanen, T. and Prina, M. and Rebolo, R. and Roddis, N. and Rubiño-Martin, J. A. and Salmon, M. J. and Sandri, M. and Seiffert, M. and Silvestri, R. and Simonetto, A. and Sjoman, P. and Smoot, G. F. and Sozzi, C. and Stringhetti, L. and Taddei, E. and Tauber, J. and Terenzi, L. and Tomasi, M. and Tuovinen, J. and Valenziano, L. and Varis, J. and Vittorio, N. and Wade, L. A. and Wilkinson, A. and Winder, F. and Zacchei, A. and Zonca, A.}, title = {Planck pre-launch status: Design and description of the Low Frequency Instrument}, journal = {A&A}, archivePrefix = {arXiv}, eprint = {1001.3321}, primaryClass = {astro-ph.IM}, keywords = {cosmic microwave background, cosmology: observations, space vehicles: instruments}, year = {2010}, month = {sep}, volume = {520}, pages = {A4+}, doi = {10.1051/0004-6361/200912853}, adsurl = {http://adsabs.harvard.edu/abs/2010A%26A...520A..
.4B}, adsnote = {Provided by the SAO/NASA Astrophysics Data System} }

1. lamarre2010 bibtex=@ARTICLE{lamarre2010,

author = {Lamarre, J.-M. and Puget, J.-L. and Ade, P. A. R. and Bouchet, F. and Guyot, G. and Lange, A. E. and Pajot, F. and Arondel, A. and Benabed, K. and Beney, J.-L. and Benoît, A. and Bernard, J.-P. and Bhatia, R. and Blanc, Y. and Bock, J. J. and Bréelle, E. and Bradshaw, T. W. and Camus, P. and Catalano, A. and Charra, J. and Charra, M. and Church, S. E. and Couchot, F. and Coulais, A. and Crill, B. P. and Crook, M. R. and Dassas, K. and de Bernardis, P. and Delabrouille, J. and de Marcillac, P. and Delouis, J.-M. and Désert, F.-X. and Dumesnil, C. and Dupac, X. and Efstathiou, G. and Eng, P. and Evesque, C. and Fourmond, J.-J. and Ganga, K. and Giard, M. and Gispert, R. and Guglielmi, L. and Haissinski, J. and Henrot-Versillé, S. and Hivon, E. and Holmes, W. A. and Jones, W. C. and Koch, T. C. and Lagardère, H. and Lami, P. and Landé, J. and Leriche, B. and Leroy, C. and Longval, Y. and Macías-Pérez, J. F. and Maciaszek, T. and Maffei, B. and Mansoux, B. and Marty, C. and Masi, S. and Mercier, C. and Miville-Deschênes, M.-A. and Moneti, A. and Montier, L. and Murphy, J. A. and Narbonne, J. and Nexon, M. and Paine, C. G. and Pahn, J. and Perdereau, O. and Piacentini, F. and Piat, M. and Plaszczynski, S. and Pointecouteau, E. and Pons, R. and Ponthieu, N. and Prunet, S. and Rambaud, D. and Recouvreur, G. and Renault, C. and Ristorcelli, I. and Rosset, C. and Santos, D. and Savini, G. and Serra, G. and Stassi, P. and Sudiwala, R. V. and Sygnet, J.-F. and Tauber, J. A. and Torre, J.-P. and Tristram, M. and Vibert, L. and Woodcraft, A. and Yurchenko,

V. and Yvon, D. }, title = {Planck pre-launch status: The HFI instrument, from specification to actual performance}, journal = {A&A}, keywords = {cosmic microwave background, space vehicles: instruments, submillimeter: general, techniques: photometric, techniques: polarimetric}, year = {2010}, month = {sep}, volume = {520}, pages = {A9+}, doi = {10.1051/0004-6361/200912975}, adsurl = {http://adsabs.harvard.edu/abs/2010A%26A…520A…9L}, adsnote = {Provided by the SAO/NASA Astrophysics Data System} }

1. leahy2010 bibtex=@ARTICLE{leahy2010,

author = {Leahy, J. P. and Bersanelli, M. and D'Arcangelo, O. and Ganga, K. and Leach, S. M. and Moss, A. and Keihänen, E. and Keskitalo, R. and Kurki-Suonio, H. and Poutanen, T. and Sandri, M. and Scott, D. and Tauber, J. and Valenziano, L. and Villa, F. and Wilkinson, A. and Zonca, A. and Baccigalupi, C. and Borrill, J. and Butler, R. C. and Cuttaia, F. and Davis, R. J. and Frailis, M. and Francheschi, E. and Galeotta, S. and Gregorio, A. and Leonardi, R. and Mandolesi, N. and Maris, M. and Meinhold, P. and Mendes, L. and Mennella, A. and Morgante, G. and Prezeau, G. and Rocha, G. and Stringhetti, L. and Terenzi, L. and Tomasi, M. }, title = {Planck pre-launch status: Expected LFI polarisation capability}, journal = {A&A}, keywords = {polarization, instrumentation: polarimeters, space vehicles: instruments, techniques: polarimetric, cosmic microwave background}, year = {2010}, month = {sep}, volume = {520}, pages = {A8+}, doi = {10.1051/0004-6361/200912855}, adsurl = {http://adsabs.harvard. edu/ abs/ 2010A%26A. . . 520A. . . 8L}, adsnote = {Provided by the SAO/NASA Astrophysics Data System} }

1. maffei2010 bibtex=@ARTICLE{maffei2010,

author = {Maffei, B. and Noviello, F. and Murphy, J. A. and Ade, P. A. R. and Lamarre, J.-M. and Bouchet, F. R. and Brossard, J. and Catalano, A. and Colgan, R. and Gispert, R. and Gleeson, E. and Haynes, C. V. and Jones, W. C. and Lange, A. E. and Longval, Y. and McAuley, I. and Pajot, F. and Peacocke, T. and Pisano, G. and Puget, J.-L. and Ristorcelli, I. and Savini, G. and Sudiwala, R. and Wylde, R. J. and Yurchenko, V.}, title = {Planck pre-launch status: HFI beam expectations from the optical optimisation of the focal plane}, journal = {A&A}, keywords = {space vehicles: instruments, submillimeter: general, telescopes, cosmic microwave background, instrumentation: polarimeters, instrumentation: detectors}, year = {2010}, month = {sep}, volume = {520}, pages = {A12+}, doi = {10.1051/0004-6361/200912999}, adsurl = {http:/ / adsabs. harvard. edu/ abs/ 2010A%26A. . . 520A. . 12M}, adsnote = {Provided by the SAO/NASA Astrophysics Data System} }

1. mandolesi2010 bibtex=@ARTICLE{mandolesi2010,

author = {Mandolesi, N. and Bersanelli, M. and Butler, R. C. and Artal, E. and Baccigalupi, C. and Balbi, A. and Banday, A. J. and Barreiro, R. B. and Bartelmann, M. and Bennett, K. and Bhandari, P. and Bonaldi, A. and Borrill, J. and Bremer, M. and Burigana, C. and Bowman, R. C. and Cabella, P. and Cantalupo, C. and Cappellini, B. and Courvoisier, T. and Crone, G. and Cuttaia, F. and Danese, L. and D'Arcangelo, O. and Davies, R. D. and Davis, R. J. and de Angelis, L. and de Gasperis, G. and de Rosa, A. and de Troia, G. and de Zotti, G. and Dick, J. and Dickinson, C. and Diego, J. M. and Donzelli, S. and Dörl, U. and Dupac, X. and Enßlin, T. A. and Eriksen, H. K. and Falvella, M. C. and Finelli, F. and Frailis, M. and Franceschi, E. and Gaier, T. and Galeotta, S. and Gasparo, F. and Giardino, G. and Gomez, F. and Gonzalez-Nuevo, J. and Górski, K. M. and Gregorio, A. and Gruppuso, A. and Hansen, F. and Hell, R. and Herranz, D. and Herreros, J. M. and Hildebrandt, S. and Hovest, W. and Hoyland, R. and Huffenberger, K. and Janssen, M. and Jaffe, T. and Keihänen, E. and Keskitalo, R. and Kisner, T. and Kurki-Suonio, H. and Lähteenmäki, A. and Lawrence, C. R. and Leach, S. M. and Leahy, J. P. and Leonardi, R. and Levin, S. and Lilje, P. B. and López-Caniego, M. and Lowe, S. R. and Lubin, P. M. and Maino, D. and Malaspina, M. and Maris, M. and Marti-Canales, J. and Martinez-Gonzalez, E. and Massardi, M. and Matarrese, S. and Matthai, F. and Meinhold, P. and Melchiorri, A. and Mendes, L. and Mennella, A. and Morgante, G. and Morigi, G. and Morisset, N. and Moss, A. and Nash, A. and Natoli, P. and Nesti, R. and Paine, C. and Partridge, B. and Pasian, F. and Passvogel, T. and Pearson, D. and Pérez-Cuevas, L. and Perrotta, F. and Polenta, G. and Popa, L. A. and Poutanen, T. and Prezeau, G. and Prina, M. and Rachen, J. P. and Rebolo, R. and Reinecke, M. and Ricciardi, S. and Riller, T. and Rocha, G. and Roddis, N. and Rohlfs, R. and Rubiño-Martin, J. A. and Salerno, E. and Sandri, M. and Scott, D. and Seiffert, M. and

Silk, J. and Simonetto, A. and Smoot, G. F. and Sozzi, C. and Sternberg, J. and Stivoli, F. and Stringhetti, L. and Tauber, J. and Terenzi, L. and Tomasi, M. and Tuovinen, J. and Türler, M. and Valenziano, L. and Varis, J. and Vielva, P. and Villa, F. and Vittorio, N. and Wade, L. and White, M. and White, S. and Wilkinson, A. and Zacchei, A. and Zonca, A. }, title = {Planck pre-launch status: The Planck-LFI programme}, journal = {A&A}, archivePrefix = {arXiv}, eprint = {1001.2657}, primaryClass = {astro-ph.CO}, keywords = {cosmic microwave background, space vehicles: instruments, instrumentation: detectors, instrumentation: polarimeters, submillimeter: general, telescopes}, year = {2010}, month = {sep}, volume = {520}, pages = {A3+}, doi = {10.1051/0004-6361/200912837}, adsurl = {http:// / adsabs. harvard. edu/ abs/ 2010A%26A. . . 520A. . . 3M}, adsnote = {Provided by the SAO/NASA Astrophysics Data System} }

1. mennella2010 bibtex=@ARTICLE{mennella2010,

author = {Mennella, A. and Bersanelli, M. and Butler, R. C. and Cuttaia, F. and D'Arcangelo, O. and Davis, R. J. and Frailis, M. and Galeotta, S. and Gregorio, A. and Lawrence, C. R. and Leonardi, R. and Lowe, S. R. and Mandolesi, N. and Maris, M. and Meinhold, P. and Mendes, L. and Morgante, G. and Sandri, M. and Stringhetti, L. and Terenzi, L. and Tomasi, M. and Valenziano, L. and Villa, F. and Zacchei, A. and Zonca, A. and Balasini, M. and Franceschet, C. and Battaglia, P. and Lapolla, P. M. and Leutenegger, P. and Miccolis, M. and Pagan, L. and Silvestri, R. and Aja, B. and Artal, E. and Baldan, G. and Bastia, P. and Bernardino, T. and Boschini, L. and Cafagna, G. and Cappellini, B. and Cavaliere, F. and Colombo, F. and de La Fuente, L. and Edgeley, J. and Falvella, M. C. and Ferrari, F. and Fogliani, S. and Franceschi, E. and Gaier, T. and Gomez, F. and Herreros, J. M. and Hildebrandt, S. and Hoyland, R. and Hughes, N. and Jukkala, P. and Kettle, D. and Laaninen, M. and Lawson, D. and Leahy, P. and Levin, S. and Lilje, P. B. and Maino, D. and Malaspina, M. and Manzato, P. and Marti-Canales, J. and Martinez-Gonzalez, E. and Mediavilla, A. and Pasian, F. and Pascual, J. P. and Pecora, M. and Peres-Cuevas, L. and Platania, P. and Pospieszalsky, M. and Poutanen, T. and Rebolo, R. and Roddis, N. and Salmon, M. and Seiffert, M. and Simonetto, A. and Sozzi, C. and Tauber, J. and Tuovinen, J. and Varis, J. and Wilkinson, A. and Winder, F. }, title = {Planck pre-launch status: Low Frequency Instrument calibration and expected scientific performance}, journal = {A&A}, archivePrefix = {arXiv}, eprint = {1001.4562}, primaryClass = {astro-ph.IM}, keywords = {cosmic microwave background, telescopes, space vehicles: instruments, instrumentation: detectors, instrumentation: polarimeters, submillimeter: general}, year = {2010}, month = {sep}, volume = {520}, pages = {A5+}, doi = {10.1051/0004-6361/200912849}, adsurl = {http:// / adsabs. harvard. edu/ abs/ 2010A%26A. . . 520A. . . 5M}, adsnote = {Provided by the SAO/NASA Astrophysics Data System} }

1. pajot2010 bibtex=@ARTICLE{pajot2010,

author = {Pajot, F. and Ade, P. A. R. and Beney, J.-L. and Bréelle, E. and Broszkiewicz, D. and Camus, P. and Carabétian, C. and Catalano, A. and Chardin, A. and Charra, M. and Charra, J. and Cizeron, R. and Couchot, F. and Coulais, A. and Crill, B. P. and Dassas, K. and Daubin, J. and de Bernardis, P. and de Marcillac, P. and Delouis, J.-M. and Désert, F.-X. and Duret, P. and Eng, P. and Evesque, C. and Fourmond, J.-J. and Fran&ccedel;ois, S. and Giard, M. and Giraud-Héraud, Y. and Guglielmi, L. and Guyot, G. and Haissinski, J. and Henrot-Versillé, S. and Hervier, V. and Holmes, W. and Jones, W. C. and Lamarre, J.-M. and Lami, P. and Lange, A. E. and Lefebvre, M. and Leriche, B. and Leroy, C. and Macias-Perez, J. and Maciaszek, T. and Maffei, B. and Mahendran, A. and Mansoux, B. and Marty, C. and Masi, S. and Mercier, C. and Miville-Deschenes, M.-A. and Montier, L. and Nicolas, C. and Noviello, F. and Perdereau, O. and Piacentini, F. and Piat, M. and Plaszczynski, S. and Pointecouteau, E. and Pons, R. and Ponthieu, N. and Puget, J.-L. and Rambaud, D. and Renault, C. and Renault, J.-C. and Rioux, C. and Ristorcelli, I. and Rosset, C. and Savini, G. and Sudiwala, R. and Torre, J.-P. and Tristram, M. and Vallée, D. and Veneziani, M. and Yvon, D.}, title = {Planck pre-launch status: HFI ground calibration}, journal = {A&A}, keywords = {cosmic microwave background, space vehicles: instruments, submillimeter: general}, year = {2010}, month = {sep}, volume = {520}, pages = {A10+}, doi = {10.1051/0004-6361/200913203}, adsurl = {http://adsabs. harvard. edu/ abs/ 2010A%26A. . . 520A. . 10P}, adsnote = {Provided by the SAO/NASA Astrophysics Data System} }

1. rosset2010 bibtex=@ARTICLE{rosset2010,

author = {Rosset, C. and Tristram, M. and Ponthieu, N. and Ade, P. and Aumont, J. and Catalano, A. and Conversi, L. and Couchot, F. and Crill, B. P. and Désert, F.-X. and Ganga, K. and Giard, M. and Giraud-Héraud, Y. and Haïssinski, J. and Henrot-Versillé, S. and Holmes, W. and Jones, W. C. and Lamarre, J.-M. and Lange, A. and Leroy, C. and Macías-Pérez, J. and Maffei, B. and de Marcillac, P. and Miville-Deschênes, M.-A. and Montier, L. and Noviello, F. and Pajot, F. and Perdereau, O. and Piacentini, F. and Piat, M. and Plaszczynski, S. and Pointecouteau, E. and Puget, J.-L. and Ristorcelli, I. and Savini, G. and Sudiwala, R. and Veneziani, M. and Yvon, D.}, title = {Planck pre-launch status: High Frequency Instrument polarization calibration}, journal = {A&A}, archivePrefix = {arXiv}, eprint = {1004.2595}, primaryClass = {astro-ph.CO}, keywords = {space vehicles: instruments, techniques: polarimetric, instrumentation: polarimeters, instrumentation: detectors, cosmic microwave background, submillimeter: general}, year = {2010}, month = {sep}, volume = {520}, pages = {A13+}, doi = {10.1051/0004-6361/200913054}, adsurl = {http:/ / adsabs. harvard. edu/ abs/ 2010A%26A. . . 520A. . 13R}, adsnote = {Provided by the SAO/NASA Astrophysics Data System} }

1. sandri2010 bibtex=@ARTICLE{sandri2010,

author = {Sandri, M. and Villa, F. and Bersanelli, M. and Burigana, C. and Butler, R. C. and D'Arcangelo, O. and Figini, L. and Gregorio, A. and Lawrence, C. R. and Maino, D. and Mandolesi, N. and Maris, M. and Nesti, R. and Perrotta, F. and Platania, P. and Simonetto, A. and Sozzi, C. and Tauber, J. and Valenziano, L.}, title = {Planck pre-launch status: Low Frequency Instrument optics}, journal = {A&A}, keywords = {cosmic microwave background, space vehicles: instruments, instrumentation: detectors, submillimeter: general, telescopes}, year = {2010}, month = {sep}, volume = {520}, pages = {A7+}, doi = {10.1051/0004-6361/200912891}, adsurl = {http://adsabs.harvard.edu/abs/2010A%26A...520A...7S}, adsnote = {Provided by the SAO/NASA Astrophysics Data System} }

1. tauber2010a bibtex=@ARTICLE{tauber2010a,

author = {Tauber, J. A. and Mandolesi, N. and Puget, J.-L. and Banos, T. and Bersanelli, M. and Bouchet, F. R. and Butler, R. C. and Charra, J. and Crone, G. and Dodsworth, J. and et al.}, title = {Planck pre-launch status: The Planck mission}, journal = {A&A}, keywords = {cosmic microwave background, space vehicles: instruments, instrumentation: detectors, instrumentation: polarimeters, submillimeter: general, radio continuum: general}, year = {2010}, month = {sep}, volume = {520}, pages = {A1+}, doi = {10.1051/0004-6361/200912983}, adsurl = {http://adsabs.harvard.edu/abs/2010A%26A...520A...1T}, adsnote = {Provided by the SAO/NASA Astrophysics Data System} }

1. tauber2010b bibtex=@ARTICLE{tauber2010b,

author = {Tauber, J. A. and Norgaard-Nielsen, H. U. and Ade, P. A. R. and Amiri Parian, J. and Banos, T. and Bersanelli, M. and Burigana, C. and Chamballu, A. and de Chambure, D. and Christensen, P. R. and Corre, O. and Cozzani, A. and Crill, B. and Crone, G. and D'Arcangelo, O. and Daddato, R. and Doyle, D. and Dubruel, D. and Forma, G. and Hills, R. and Huffenberger, K. and Jaffe, A. H. and Jessen, N. and Kletzkine, P. and Lamarre, J. M. and Leahy, J. P. and Longval, Y. and de Maagt, P. and Maffei, B. and Mandolesi, N. and Martí-Canales, J. and Martín-Polegre, A. and Martin, P. and Mendes, L. and Murphy, J. A. and Nielsen, P. and Noviello, F. and Paquay, M. and Peacocke, T. and Ponthieu, N. and Pontoppidan, K. and Ristorcelli, I. and Riti, J.-B. and Rolo, L. and Rosset, C. and Sandri, M. and Savini, G. and Sudiwala, R. and Tristram, M. and Valenziano, L. and van der Vorst, M. and van't Klooster, K. and Villa, F. and Yurchenko, V.}, title = {Planck pre-launch status: The optical system}, journal = {A&A}, keywords = {cosmic microwave background, space vehicles: instruments, instrumentation: detectors, instrumentation: polarimeters, submillimeter: general, telescopes}, year = {2010}, month = {sep}, volume = {520}, pages = {A2+}, doi = {10.1051/0004-6361/200912911}, adsurl = {http://adsabs.harvard.edu/abs/2010A%26A...520A...2T}, adsnote = {Provided by the SAO/NASA Astrophysics Data System} }

1. villa2010 bibtex=@ARTICLE{villa2010,

author = {Villa, F. and Terenzi, L. and Sandri, M. and Meinhold, P. and Poutanen, T. and Battaglia, P. and Franceschet, C. and Hughes, N. and Laaninen, M. and Lapolla, P. and Bersanelli, M. and Butler, R. C. and Cuttaia, F. and D'Arcangelo, O. and Frailis, M. and Franceschi, E. and Galeotta, S. and Gregorio, A. and Leonardi, R. and Lowe, S. R. and Mandolesi, N. and Maris, M. and Mendes, L. and Mennella, A. and Morgante, G. and Stringhetti, L. and Tomasi, M. and Valenziano, L. and Zacchei, A. and Zonca, A. and Aja, B. and Artal, E. and Balasini, M. and Bernardino, T. and Blackhurst, E. and Boschini, L. and Cappellini, B. and Cavaliere, F. and Colin, A. and Colombo, F. and Davis, R. J. and de La Fuente, L. and Edgeley, J. and Gaier, T. and Galtress, A. and Hoyland, R. and Jukkala, P. and Kettle, D. and Kilpia, V.-H. and Lawrence, C. R. and Lawson, D. and Leahy, J. P. and Leutenegger, P. and Levin, S. and Maino, D. and Malaspina, M. and Mediavilla, A. and Miccolis, M. and Pagan, L. and Pascual, J. P. and Pasian, F. and Pecora, M. and Pospieszalski, M. and Roddis, N. and Salmon, M. J. and Seiffert, M. and Silvestri, R. and Simonetto, A. and Sjoman, P. and Sozzi, C. and Tuovinen, J. and Varis, J. and Wilkinson, A. and Winder, F.}, title = {Planck pre-launch status: Calibration of the Low Frequency Instrument flight model radiometers}, journal = {A&A}, archivePrefix = {arXiv}, eprint = {1005.2541}, primaryClass = {astro-ph.IM}, keywords = {cosmic microwave background, space vehicles: instruments, instrumentation: detectors, techniques: miscellaneous}, year = {2010}, month = {sep}, volume = {520}, pages = {A6+}, doi = {10.1051/0004-6361/200912860}, adsurl = {http://adsabs.harvard.edu/abs/2010A%26A...520A...6V}, adsnote = {Provided by the SAO/NASA Astrophysics Data System} }

1. artal2009 bibtex=@ARTICLE{artal2009,

author = {Artal, E. and Aja, B. and de la Fuente, M. L. and Pascual, J. P. and Mediavilla, A. and Martinez-Gonzalez, E. and Pradell, L. and de Paco, P. and Bara, M. and Blanco, E. and García, E. and Davis, R. and Kettle, D. and Roddis, N. and Wilkinson, A. and Bersanelli, M. and Mennella, A. and Tomasi, M. and Butler, R. C. and Cuttaia, F. and Mandolesi, N. and Stringhetti, L.}, title = {LFI 30 and 44 GHz receivers Back-End Modules}, journal = {Journal of Instrumentation}, archivePrefix = {arXiv}, eprint = {1001.4771}, primaryClass = {astro-ph.IM}, year = {2009}, month = {dec}, volume = {4}, pages = {2003-+}, doi = {10.1088/1748-0221/4/12/T12003}, adsurl = {http://adsabs.harvard.edu/abs/2009JInst...4T2003A}, adsnote = {Provided by the SAO/NASA Astrophysics Data System} }

1. battaglia2009 bibtex=@ARTICLE{battaglia2009,

author = {Battaglia, P. and Franceschet, C. and Zonca, A. and Bersanelli, M. and Butler, R. C. and D'Arcangelo, O. and Davis, R. J. and Galeotta, S. and Guzzi, P. and Hoyland, R. and Hughes, N. and Jukkala, P. and Kettle, D. and Laaninen, M. and Leonardi, R. and Maino, D. and Mandolesi, N. and Meinhold, P. and Mennella, A. and Platania, P. and Terenzi, L. and Tuovinen, J. and Varis, J. and Villa, F. and Wilkinson, A.}, title = {Advanced modelling of the Planck-LFI radiometers}, journal = {Journal of Instrumentation}, archivePrefix = {arXiv}, eprint = {1001.4659}, primaryClass = {astro-ph.IM}, year = {2009}, month = {dec}, volume = {4}, pages = {2014-+}, doi = {10.1088/1748-0221/4/12/T12014}, adsurl = {http://adsabs.harvard.edu/abs/2009JInst...4T2014B}, adsnote = {Provided by the SAO/NASA Astrophysics Data System} }

1. cuttaia2009 bibtex=@ARTICLE{cuttaia2009,

author = {Cuttaia, F. and Mennella, A. and Stringhetti, L. and Maris, M. and Terenzi, L. and Tomasi, M. and Villa, F. and Bersanelli, M. and Butler, R. C. and Cappellini, B. and Cuevas, L. P. and D'Arcangelo, O. and Davis, R. and Frailis, M. and Franceschet, C. and Franceschi, E. and Gregorio, A. and Hoyland, R. and Leonardi, R. and Lowe, S. and Mandolesi, N. and Meinhold, P. and Mendes, L. and Roddis, N. and Sandri, M. and Valenziano, L. and Wilkinson, A. and Zacchei, A. and Zonca, A. and Battaglia, P. and De Nardo, S. and Grassi, S. and Lapolla, M. and Leutenegger, P. and Miccolis, M. and Silvestri, R.}, title = {Planck-LFI radiometers tuning}, journal = {Journal of Instrumentation}, archivePrefix = {arXiv}, eprint = {1001.4648}, primaryClass = {astro-ph.IM}, year = {2009}, month = {dec}, volume = {4}, pages = {2013-+}, doi = {10.1088/1748-0221/4/12/T12013}, adsurl = {http://adsabs.harvard.edu/abs/2009JInst...4T2013C}, adsnote = {Provided by the SAO/NASA Astrophysics Data System} }

1. darcangelo2009a bibtex=@ARTICLE{darcangelo2009a,

author = {D'Arcangelo, O. and Figini, L. and Simonetto, A. and Villa, F. and Pecora, M. and Battaglia, P. and Bersanelli, M. and Butler, R. C. and Cuttaia, F. and Garavaglia, S. and Guzzi, P. and Mandolesi, N. and Mennella, A. and Morgante, G. and Pagan, L. and Valenziano, L. }, title = {The Planck-LFI flight model composite waveguides}, journal = {Journal of Instrumentation}, archivePrefix = {arXiv}, eprint = {1001.4711}, primaryClass = {astro-ph.IM}, year = {2009}, month = {dec}, volume = {4}, pages = {2007-+}, doi = {10.1088/1748-0221/4/12/T12007}, adsurl = {http://adsabs.harvard.edu/abs/2009JInst...4T2007D}, adsnote = {Provided by the SAO/NASA Astrophysics Data System} }

1. darcangelo2009b bibtex=@ARTICLE{darcangelo2009b,

author = {D'Arcangelo, O. and Simonetto, A. and Figini, L. and Pagana, E. and Villa, F. and Pecora, M. and Battaglia, P. and Bersanelli, M. and Butler, R. C. and Garavaglia, S. and Guzzi, P. and Mandolesi, N. and Sozzi, C.}, title = {The Planck-LFI flight model ortho-mode transducers}, journal = {Journal of Instrumentation}, archivePrefix = {arXiv}, eprint = {1001.4686}, primaryClass = {astro-ph.IM}, year = {2009}, month = {dec}, volume = {4}, pages = {2005-+}, doi = {10.1088/1748-0221/4/12/T12005}, url = {http://adsabs.harvard.edu/abs/2009JInst...4T2005D}, adsurl = {http://adsabs.harvard.edu/abs/2009JInst...4T2005D}, adsnote = {Provided by the SAO/NASA Astrophysics Data System} }

1. davis2009 bibtex=@ARTICLE{davis2009,

author = {Davis, R. J. and Wilkinson, A. and Davies, R. D. and Winder, W. F. and Roddis, N. and Blackhurst, E. J. and Lawson, D. and Lowe, S. R. and Baines, C. and Butlin, M. and Galtress, A. and Shepherd, D. and Aja, B. and Artal, E. and Bersanelli, M. and Butler, R. C. and Castelli, C. and Cuttaia, F. and D'Arcangelo, O. and Gaier, T. and Hoyland, R. and Kettle, D. and Leonardi, R. and Mandolesi, N. and Mennella, A. and Meinhold, P. and Pospieszalski, M. and Stringhetti, L. and Tomasi, M. and Valenziano, L. and Zonca, A.}, title = {Design, development and verification of the 30 and 44 GHz front-end modules for the Planck Low Frequency Instrument}, journal = {Journal of Instrumentation}, archivePrefix = {arXiv}, eprint = {1001.4743}, primaryClass = {astro-ph.IM}, year = {2009}, month = {dec}, volume = {4}, pages = {2002-+}, doi = {10.1088/1748-0221/4/12/T12002}, adsurl = {http://adsabs.harvard.edu/abs/2009JInst...4T2002D}, adsnote = {Provided by the SAO/NASA Astrophysics Data System} }

1. frailis2009 bibtex=@ARTICLE{frailis2009,

author = {Frailis, M. and Maris, M. and Zacchei, A. and Morisset, N. and Rohlfs, R. and Meharga, M. and Binko, P. and Türler, M. and Galeotta, S. and Gasparo, F. and Franceschi, E. and Butler, R. C. and D'Arcangelo, O. and Fogliani, S. and Gregorio, A. and Lowe, S. R. and Maggio, G. and Malaspina, M. and Mandolesi, N. and Manzato, P. and Pasian, F. and Perrotta, F. and Sandri, M. and Terenzi, L. and Tomasi, M. and Zonca, A.}, title = {A systematic approach to the Planck LFI end-to-end test and its application to the DPC Level 1 pipeline}, journal = {Journal of Instrumentation}, archivePrefix = {arXiv}, eprint = {1001.4838}, primaryClass = {astro-ph.IM}, year = {2009}, month = {dec}, volume = {4}, pages = {2021-+}, doi = {10.1088/1748-0221/4/12/T12021}, adsurl = {http://adsabs.harvard.edu/abs/2009JInst...4T2021F}, adsnote = {Provided by the SAO/NASA Astrophysics Data System} }

1. herreros2009 bibtex=@ARTICLE{herreros2009,

author = {Herreros, J. M. and Gómez, M. F. and Rebolo, R. and Chulani, H. and Rubiño-Martin, J. A. and Hildebrandt, S. R. and Bersanelli, M. and Butler, R. C. and Miccolis, M. and Peña, A. and Pereira, M. and Torrero, F. and Franceschet, C. and López, M. and Alcalá, C.}, title = {The Planck-LFI Radiometer Electronics Box Assembly}, journal = {Journal of Instrumentation}, archivePrefix = {arXiv}, eprint = {1001.4696}, primaryClass = {astro-ph.IM}, year = {2009}, month = {dec}, volume = {4}, pages = {2008-+}, doi = {10.1088/1748-0221/4/12/T12008}, adsurl = {http://adsabs.harvard.edu/abs/2009JInst...4T2008H}, adsnote = {Provided by the SAO/NASA Astrophysics Data System} }

1. malaspina2009 bibtex=@ARTICLE{malaspina2009,

author = {Malaspina, M. and Franceschi, E. and Battaglia, P. and Binko, P. and Butler, R. C. and D'Arcangelo, O. and Fogliani, S. and Frailis, M. and Franceschet, C. and Galeotta, S. and Gasparo, F. and Gregorio, A. and Lapolla, M. and Leonardi, R. and Maggio, G. and Mandolesi, N. and Manzato, P. and Maris, M. and Meharga, M. and Meinhold, P. and Morisset, N. and Pasian, F. and Perrotta, F. and Rohlfs, R. and Sandri, M. and Tomasi, M. and Türler, M. and Zacchei, A. and Zonca, A.}, title = {LFI Radiometric Chain Assembly (RCA) data handling ``Rachel*},* journal = {Journal of Instrumentation}, archivePrefix = {arXiv}, eprint = {1001.4787}, primaryClass = {astro-ph.IM}, year = {2009}, month = {dec}, volume = {4}, pages = {2017-+}, doi = {10.1088/1748-0221/4/12/T12017}, adsurl = {http://adsabs.harvard.edu/abs/2009JInst…4T2017M}, adsnote = {Provided by the SAO/NASA Astrophysics Data System} }

1. maris2009 bibtex=@ARTICLE{maris2009,

author = {Maris, M. and Tomasi, M. and Galeotta, S. and Miccolis, M. and Hildebrandt, S. and Frailis, M. and Rohlfs, R. and Morisset, N. and Zacchei, A. and Bersanelli, M. and Binko, P. and Burigana, C. and Butler, R. C. and Cuttaia, F. and Chulani, H. and D'Arcangelo, O. and Fogliani, S. and Franceschi, E. and Gasparo, F. and Gomez, F. and Gregorio, A. and Herreros, J. M. and Leonardi, R. and Leutenegger, P. and Maggio, G. and Maino, D. and Malaspina, M. and Mandolesi, N. and Manzato, P. and Meharga, M. and Meinhold, P. and Mennella, A. and Pasian, F. and Perrotta, F. and Rebolo, R. and Türler, M. and Zonca, A.}, title = {Optimization of Planck-LFI on-board data handling}, journal = {Journal of Instrumentation}, archivePrefix = {arXiv}, eprint = {1001.4737}, primaryClass = {astro-ph.IM}, year = {2009}, month = {dec}, volume = {4}, pages = {2018-+}, doi = {10.1088/1748-0221/4/12/T12018}, adsurl = {http://adsabs.harvard.edu/abs/2009JInst…4T2018M}, adsnote = {Provided by the SAO/NASA Astrophysics Data System} }

1. meinhold2009 bibtex=@ARTICLE{meinhold2009,

author = {Meinhold, P. and Leonardi, R. and Aja, B. and Artal, E. and Battaglia, P. and Bersanelli, M. and Blackhurst, E. and Butler, C. R. and Cuevas, L. P. and Cuttaia, F. and D'Arcangelo, O. and Davis, R. and de la Fuente, M. L. and Frailis, M. and Franceschet, C. and Franceschi, E. and Gaier, T. and Galeotta, S. and Gregorio, A. and Hoyland, R. and Hughes, N. and Jukkala, P. and Kettle, D. and Laaninen, M. and Leutenegger, P. and Lowe, S. R. and Malaspina, M. and Mandolesi, R. and Maris, M. and Martínez-González, E. and Mendes, L. and Mennella, A. and Miccolis, M. and Morgante, G. and Roddis, N. and Sandri, M. and Seiffert, M. and Salmón, M. and Stringhetti, L. and Poutanen, T. and Terenzi, L. and Tomasi, M. and Tuovinen, J. and Varis, J. and Valenziano, L. and Villa, F. and Wilkinson, A. and Winder, F. and Zacchei, A. and Zonca, A. }, title = {Noise properties of the Planck-LFI receivers}, journal = {Journal of Instrumentation}, archivePrefix = {arXiv}, eprint = {1001.4608}, primaryClass = {astro-ph.IM}, year = {2009}, month = {dec}, volume = {4}, pages = {2009-+}, doi = {10.1088/1748-0221/4/12/T12009}, adsurl = {http://adsabs.harvard.edu/abs/2009JInst…4T2009M}, adsnote = {Provided by the SAO/NASA Astrophysics Data System} }

1. mennella2009 bibtex=@ARTICLE{mennella2009,

author = {Mennella, A. and Villa, F. and Terenzi, L. and Cuttaia, F. and Battaglia, P. and Bersanelli, M. and Butler, R. C. and D'Arcangelo, O. and Artal, E. and Davis, R. and Frailis, M. and Franceschet, C. and Galeotta, S. and Gregorio, A. and Hughes, N. and Jukkala, P. and Kettle, D. and Kilpiä, V.-H. and Laaninen, M. and Lapolla, P. M. and Leonardi, R. and Leutenegger, P. and Lowe, S. and Mandolesi, N. and Maris, M. and Meinhold, P. and Mendes, L. and Miccolis, M. and Morgante, G. and Roddis, N. and Sandri, M. and Silvestri, R. and Stringhetti, L. and Tomasi, M. and Tuovinen, J. and Valenziano, L. and Zacchei, A. and Varis, J. and Wilkinson, A. and Zonca, A.}, title = {The linearity response of the Planck-LFI flight model receivers}, journal = {Journal of Instrumentation}, archivePrefix = {arXiv}, eprint = {1001.4610}, primaryClass = {astro-ph.IM}, year = {2009}, month = {dec}, volume = {4}, pages = {2011-+}, doi = {10.1088/1748-0221/4/12/T12011}, adsurl = {http://adsabs.harvard.edu/abs/2009JInst...4T2011M}, adsnote = {Provided by the SAO/NASA Astrophysics Data System} }

1. morgante2009 bibtex=@ARTICLE{morgante2009,

author = {Morgante, G. and Pearson, D. and Melot, F. and Stassi, P. and Terenzi, L. and Wilson, P. and Hernandez, B. and Wade, L. and Gregorio, A. and Bersanelli, M. and Butler, C. and Mandolesi, N. }, title = {Cryogenic characterization of the Planck sorption cooler system flight model}, journal = {Journal of Instrumentation}, archivePrefix = {arXiv}, eprint = {1001.4628}, primaryClass = {astro-ph.IM}, year = {2009}, month = {dec}, volume = {4}, pages = {2016-+}, doi = {10.1088/1748-0221/4/12/T12016}, adsurl = {http://adsabs.harvard.edu/abs/2009JInst...4T2016M}, adsnote = {Provided by the SAO/NASA Astrophysics Data System} }

1. terenzi2009a bibtex=@ARTICLE{terenzi2009a,

author = {Terenzi, L. and Lapolla, M. and Laaninen, M. and Battaglia, P. and Cavaliere, F. and De Rosa, A. and Hughes, N. and Jukkala, P. and Kilpiä, V.-H. and Morgante, G. and Tomasi, M. and Varis, J. and Bersanelli, M. and Butler, R. C. and Ferrari, F. and Franceschet, C. and Leutenegger, P. and Mandolesi, N. and Mennella, A. and Silvestri, R. and Stringhetti, L. and Tuovinen, J. and Valenziano, L. and Villa, F.}, title = {Cryogenic environment and performance for testing the Planck radiometers}, journal = {Journal of Instrumentation}, archivePrefix = {arXiv}, eprint = {1001.4644}, primaryClass = {astro-ph.IM}, year = {2009}, month = {dec}, volume = {4}, pages = {2015-+}, doi = {10.1088/1748-0221/4/12/T12015}, adsurl = {http://adsabs.harvard.edu/abs/2009JInst...4T2015T}, adsnote = {Provided by the SAO/NASA Astrophysics Data System} }

1. terenzi2009b bibtex=@ARTICLE{terenzi2009b,

author = {Terenzi, L. and Salmon, M. J. and Colin, A. and Mennella, A. and Morgante, G. and Tomasi, M. and Battaglia, P. and Lapolla, M. and Bersanelli, M. and Butler, R. C. and Cuttaia, F. and D'Arcangelo, O. and Davis, R. and Franceschet, C. and Galeotta, S. and Gregorio, A. and Hughes, N. and Jukkala, P. and Kettle, D. and Laaninen, M. and Leutenegger, P. and Leonardi, R. and Mandolesi, N. and Maris, M. and Meinhold, P. and Miccolis, M. and Roddis, N. and Sambo, L. and Sandri, M. and Silvestri, R. and Tuovinen, J. and Valenziano, L. and Varis, J. and Villa, F. and Wilkinson, A. and Zonca, A.}, title = {Thermal susceptibility of the Planck-LFI receivers}, journal = {Journal of Instrumentation}, archivePrefix = {arXiv}, eprint = {1001.4653}, primaryClass = {astro-ph.IM}, year = {2009}, month = {dec}, volume = {4}, pages = {2012-+}, doi = {10.1088/1748-0221/4/12/T12012}, adsurl = {http://adsabs.harvard.edu/abs/2009JInst...4T2012T}, adsnote = {Provided by the SAO/NASA Astrophysics Data System} }

1. tomasi2009 bibtex=@ARTICLE{tomasi2009,

author = {Tomasi, M. and Mennella, A. and Galeotta, S. and Lowe, S. R. and Mendes, L. and Leonardi, R. and Villa, F. and Cappellini, B. and Gregorio, A. and Meinhold, P. and Sandri, M. and Cuttaia, F. and Terenzi, L. and Maris, M. and Valenziano, L. and Salmon, M. J. and Bersanelli, M. and Binko, P. and Butler, R. C. and D'Arcangelo, O. and Fogliani, S. and Frailis, M. and Franceschi, E. and Gasparo, F. and Maggio, G. and Maino, D. and Malaspina, M. and Mandolesi, N. and Manzato, P. and Meharga, M. and Morgante, G. and Morisset, N. and Pasian, F. and Perrotta, F. and Rohlfs, R. and Türler, M. and Zacchei, A. and Zonca, A.}, title = {Off-line radiometric analysis of Planck-LFI data}, journal = {Journal of Instrumentation}, archivePrefix = {arXiv}, eprint = {1001.4642}, primaryClass = {astro-ph.IM}, year = {2009}, month = {dec}, volume = {4}, pages = {2020-+}, doi = {10.1088/1748-0221/4/12/T12020}, adsurl = {http://adsabs.harvard.edu/abs/2009JInst...4T2020T}, adsnote = {Provided by the SAO/NASA Astrophysics Data System} }

1. tomasi2010 bibtex=@ARTICLE{tomasi2010,

author = {Tomasi, M. and Cappellini, B. and Gregorio, A. and Colombo, F. and Lapolla, M. and Terenzi, L. and Morgante, G. and Bersanelli, M. and Butler, R. C. and Galeotta, S. and Mandolesi, N. and Maris, M. and Mennella, A. and Valenziano, L. and Zacchei, A.}, title = {Dynamic validation of the Planck-LFI thermal model}, journal = {Journal of Instrumentation}, archivePrefix = {arXiv}, eprint = {1001.4646}, primaryClass = {astro-ph.IM}, year = {2010}, month = {jan}, volume = {5}, pages = {1002-+}, doi = {10.1088/1748-0221/5/01/T01002}, adsurl = {http://adsabs.harvard.edu/abs/2010JInst...5.1002T}, adsnote = {Provided by the SAO/NASA Astrophysics Data System} }

1. valenziano2009 bibtex=@ARTICLE{valenziano2009,

author = {Valenziano, L. and Cuttaia, F. and De Rosa, A. and Terenzi, L. and Brighenti, A. and Cazzola, G. P. and Garbesi, A. and Mariotti, S. and Orsi, G. and Pagan, L. and Cavaliere, F. and Biggi, M. and Lapini, R. and Panagin, E. and Battaglia, P. and Butler, R. C. and Bersanelli, M. and D'Arcangelo, O. and Levin, S. and Mandolesi, N. and Mennella, A. and Morgante, G. and Morigi, G. and Sandri, M. and Simonetto, A. and Tomasi, M. and Villa, F. and Frailis, M. and Galeotta, S. and Gregorio, A. and Leonardi, R. and Lowe, S. R. and Maris, M. and Meinhold, P. and Mendes, L. and Stringhetti, L. and Zonca, A. and Zacchei, A.}, title = {Planck-LFI: design and performance of the 4 Kelvin Reference Load Unit}, journal = {Journal of Instrumentation}, archivePrefix = {arXiv}, eprint = {1001.4778}, primaryClass = {astro-ph.IM}, year = {2009}, month = {dec}, volume = {4}, pages = {2006-+}, doi = {10.1088/1748-0221/4/12/T12006}, adsurl = {http://adsabs.harvard.edu/abs/2009JInst...4T2006V}, adsnote = {Provided by the SAO/NASA Astrophysics Data System} }

1. varis2009 bibtex=@ARTICLE{varis2009,

author = {Varis, J. and Hughes, N. J. and Laaninen, M. and Kilpiä, V.-H. and Jukkala, P. and Tuovinen, J. and Ovaska, S. and Sjöman, P. and Kangaslahti, P. and Gaier, T. and Hoyland, R. and Meinhold, P. and Mennella, A. and Bersanelli, M. and Butler, R. C. and Cuttaia, F. and Franceschi, E. and Leonardi, R. and Leutenegger, P. and Malaspina, M. and Mandolesi, N. and Miccolis, M. and Poutanen, T. and Kurki-Suonio, H. and Sandri, M. and Stringhetti, L. and Terenzi, L. and Tomasi, M. and Valenziano, L.}, title = {Design, development, and verification of the Planck Low Frequency Instrument 70 GHz Front-End and Back-End Modules}, journal = {Journal of Instrumentation}, archivePrefix = {arXiv}, eprint = {1001.4661}, primaryClass = {astro-ph.IM}, year = {2009}, month = {dec}, volume = {4}, pages = {2001-+}, doi = {10.1088/1748-0221/4/12/T12001}, adsurl = {http://adsabs.harvard.edu/abs/2009JInst...4T2001V}, adsnote = {Provided by the SAO/NASA Astrophysics Data System} }

1. villa2009 bibtex=@ARTICLE{villa2009,

author = {Villa, F. and D'Arcangelo, O. and Pecora, M. and Figini, L. and Nesti, R. and Simonetto, A. and Sozzi, C. and Sandri, M. and Battaglia, P. and Guzzi, P. and Bersanelli, M. and Butler, R. C. and Mandolesi, N.}, title = {Planck-LFI flight model feed horns}, journal = {Journal of Instrumentation}, archivePrefix = {arXiv}, eprint = {1001.4633}, primaryClass = {astro-ph.IM}, year = {2009}, month = {dec}, volume = {4}, pages = {2004-+}, doi = {10.1088/1748-0221/4/12/T12004}, adsurl = {http://adsabs.harvard.edu/abs/2009JInst...4T2004V}, adsnote = {Provided by the SAO/NASA Astrophysics Data System} }

1. zacchei2009 bibtex=@ARTICLE{zacchei2009,

author = {Zacchei, A. and Frailis, M. and Maris, M. and Morisset, N. and Rohlfs, R. and Meharga, M. and Binko, P. and Türler, M. and Galeotta, S. and Gasparo, F. and Franceschi, E. and Butler, R. C. and Cuttaia, F. and D'Arcangelo, O. and Fogliani, S. and Gregorio, A. and Leonardi, R. and Lowe, S. R. and Maino, D. and Maggio, G. and Malaspina, M. and Mandolesi, N. and Manzato, P. and Meinhold, P. and Mendes, L. and Mennella, A. and Morgante, G. and Pasian, F. and Perrotta, F. and Sandri, M. and Stringhetti, L. and Terenzi, L. and Tomasi, M. and Zonca, A.}, title = {Level 1 on-ground telemetry handling in Planck-LFI}, journal = {Journal of Instrumentation}, archivePrefix = {arXiv}, eprint = {1001.4730}, primaryClass = {astro-ph.IM}, year = {2009}, month = {dec}, volume = {4}, pages = {2019-+}, doi = {10.1088/1748-0221/4/12/T12019}, adsurl = {http://adsabs.harvard.edu/abs/2009JInst...4T2019Z}, adsnote = {Provided by the SAO/NASA Astrophysics Data System} }

1. zonca2009 bibtex=@ARTICLE{zonca2009,

author = {Zonca, A. and Franceschet, C. and Battaglia, P. and Villa, F. and Mennella, A. and D'Arcangelo, O. and Silvestri, R. and Bersanelli, M. and Artal, E. and Butler, R. C. and Cuttaia, F. and Davis, R. J. and Galeotta, S. and Hughes, N. and Jukkala, P. and Kilpiä, V.-H. and Laaninen, M. and Mandolesi, N. and Maris, M. and Mendes, L. and Sandri, M. and Terenzi, L. and Tuovinen, J. and Varis, J. and Wilkinson, A.}, title = {Planck-LFI radiometers' spectral response}, journal = {Journal of Instrumentation}, archivePrefix = {arXiv}, eprint = {1001.4589},

primaryClass = {astro-ph.IM}, year = {2009}, month = {dec}, volume = {4}, pages = {2010-+}, doi = {10.1088/1748-0221/4/12/T12010}, adsurl = {http://adsabs.harvard.edu/abs/2009JInst...4T2010Z}, adsnote = {Provided by the SAO/NASA Astrophysics Data System} }

1. holmes2008 bibtex=@ARTICLE{holmes2008,

author = {Holmes, W. A. and Bock, J. J. and Crill, B. P. and Koch, T. C. and Jones, W. C. and Lange, A. E. and Paine, C. G.}, title = {Initial test results on bolometers for the Planck high frequency instrument}, journal = { Appl. Opt}, year = {2008}, month = {nov}, volume = {47}, pages = {5996-+}, doi = {10.1364/AO.47.005996}, adsurl = {http://adsabs.harvard.edu/abs/2008ApOpt..47.5996H}, adsnote = {Provided by the SAO/NASA Astrophysics Data System} }

1. bhandari2004 bibtex=@ARTICLE{bhandari2004,

author = {Bhandari, P. and Prina, M. and Bowman, R. C. and Paine, C. and Pearson, D. and Nash, A.}, title = {Sorption coolers using a continuous cycle to produce 20 K for the Planck flight mission}, journal = {Cryogenics}, year = {2004}, month = {jun}, volume = {44}, pages = {395-401}, adsurl = {http://adsabs.harvard.edu/abs/2004Cryo...44..395B}, adsnote = {Provided by the SAO/NASA Astrophysics Data System} }

1. planck2005-bluebook bibtex=@ARTICLE{planck2005-bluebook,

author = {Planck Collaboration,}, title = {The Scientific Programme of Planck}, journal = {ESA publication ESA-SCI(2005)/01}, eprint = {arXiv:astro-ph/0604069}, keywords = {Astrophysics}, year = {2005}, adsurl = {http://adsabs.harvard.edu/abs/2006astro.ph..4069T}, adsnote = {Provided by the SAO/NASA Astrophysics Data System} }

1. bennett2010 bibtex=@ARTICLE{bennett2010,

author = {Bennett, C. L. and Hill, R. S. and Hinshaw, G. and Larson, D. and Smith, K. M. and Dunkley, J. and Gold, B. and Halpern, M. and Jarosik, N. and Kogut, A. and Komatsu, E. and Limon, M. and Meyer, S. S. and Nolta, M. R. and Odegard, N. and Page, L. and Spergel, D. N. and Tucker, G. S. and Weiland, J. L. and Wollack, E. and Wright, E. L.}, title = {Seven-year Wilkinson Microwave Anisotropy Probe (WMAP) Observations: Are There Cosmic Microwave Background Anomalies?}, journal = {Aps}, archivePrefix = {arXiv}, eprint = {1001.4758}, primaryClass = {astro-ph.CO}, keywords = {cosmic background radiation, cosmological parameters, cosmology: observations, dark matter, early universe, instrumentation: detectors, large-scale structure of universe, space vehicles, space vehicles: instruments, telescopes}, year = {2011}, month = {feb}, volume = {192}, pages = {17-+}, doi = {10.1088/0067-0049/192/2/17}, adsurl = {http://adsabs.harvard.edu/abs/2011ApJS..192...17B}, adsnote = {Provided by the SAO/NASA Astrophysics Data System} }

1. gold2010 bibtex=@ARTICLE{gold2010,

author = {Gold, B. and Odegard, N. and Weiland, J. L. and Hill, R. S. and Kogut, A. and Bennett, C. L. and Hinshaw, G. and Chen, X. and Dunkley, J. and Halpern, M. and Jarosik, N. and Komatsu, E. and Larson, D. and Limon, M. and Meyer, S. S. and Nolta, M. R. and Page, L. and Smith, K. M. and Spergel, D. N. and Tucker, G. S. and Wollack, E. and Wright, E. L.}, title = {Seven-year Wilkinson Microwave Anisotropy Probe (WMAP) Observations: Galactic Foreground Emission}, journal = {Aps}, archivePrefix = {arXiv}, eprint = {1001.4555}, primaryClass = {astro-ph.GA}, keywords = {cosmic background radiation, cosmology: observations, diffuse radiation, Galaxy: halo, Galaxy: structure, ISM: structure}, year = {2011}, month = {feb}, volume = {192}, pages = {15-+}, doi = {10.1088/0067-0049/192/2/15}, adsurl = {http://adsabs.harvard.edu/abs/2011ApJS..192...15G}, adsnote = {Provided by the SAO/NASA Astrophysics Data System} }

1. jarosik2010 bibtex=@ARTICLE{jarosik2010,

author = {Jarosik, N. and Bennett, C. L. and Dunkley, J. and Gold, B. and Greason, M. R. and Halpern, M. and Hill, R. S. and Hinshaw, G. and Kogut, A. and Komatsu, E. and Larson, D. and Limon, M. and Meyer, S. S. and Nolta, M. R. and Odegard, N. and Page, L. and Smith, K. M. and Spergel, D. N. and Tucker, G. S. and Weiland, J. L. and Wollack, E. and Wright, E. L.}, title = {Seven-year Wilkinson Microwave Anisotropy Probe (WMAP) Observations:

Sky Maps, Systematic Errors, and Basic Results}, journal = {Aps}, archivePrefix = {arXiv}, eprint = {1001.4744}, primaryClass = {astro-ph.CO}, keywords = {cosmic background radiation, space vehicles: instruments}, year = {2011}, month = {feb}, volume = {192}, pages = {14-+}, doi = {10.1088/0067-0049/192/2/14}, adsurl = {http://adsabs.harvard.edu/abs/2011ApJS..192...14J}, adsnote = {Provided by the SAO/NASA Astrophysics Data System} }

1. komatsu2010 bibtex=@ARTICLE{komatsu2010,

author = {Komatsu, E. and Smith, K. M. and Dunkley, J. and Bennett, C. L. and Gold, B. and Hinshaw, G. and Jarosik, N. and Larson, D. and Nolta, M. R. and Page, L. and Spergel, D. N. and Halpern, M. and Hill, R. S. and Kogut, A. and Limon, M. and Meyer, S. S. and Odegard, N. and Tucker, G. S. and Weiland, J. L. and Wollack, E. and Wright, E. L.}, title = {Seven-year Wilkinson Microwave Anisotropy Probe (WMAP) Observations: Cosmological Interpretation}, journal = {Aps}, archivePrefix = {arXiv}, eprint = {1001.4538}, primaryClass = {astro-ph.CO}, keywords = {cosmic background radiation, cosmology: observations, dark matter, early universe, space vehicles}, year = {2011}, month = {feb}, volume = {192}, pages = {18-+}, doi = {10.1088/0067-0049/192/2/18}, adsurl = {http://adsabs.harvard.edu/abs/2011ApJS..192...18K}, adsnote = {Provided by the SAO/NASA Astrophysics Data System} }

1. larson2010 bibtex=@ARTICLE{larson2010,

author = {Larson, D. and Dunkley, J. and Hinshaw, G. and Komatsu, E. and Nolta, M. R. and Bennett, C. L. and Gold, B. and Halpern, M. and Hill, R. S. and Jarosik, N. and Kogut, A. and Limon, M. and Meyer, S. S. and Odegard, N. and Page, L. and Smith, K. M. and Spergel, D. N. and Tucker, G. S. and Weiland, J. L. and Wollack, E. and Wright, E. L.}, title = {Seven-year Wilkinson Microwave Anisotropy Probe (WMAP) Observations: Power Spectra and WMAP-derived Parameters}, journal = {Aps}, archivePrefix = {arXiv}, eprint = {1001.4635}, primaryClass = {astro-ph.CO}, keywords = {cosmic background radiation, cosmological parameters, cosmology: observations, dark matter, early universe, space vehicles: instruments}, year = {2011}, month = {feb}, volume = {192}, pages = {16-+}, doi = {10.1088/0067-0049/192/2/16}, adsurl = {http://adsabs.harvard.edu/abs/2011ApJS..192...16L}, adsnote = {Provided by the SAO/NASA Astrophysics Data System} }

1. weiland2010 bibtex=@ARTICLE{weiland2010,

author = {Weiland, J. L. and Odegard, N. and Hill, R. S. and Wollack, E. and Hinshaw, G. and Greason, M. R. and Jarosik, N. and Page, L. and Bennett, C. L. and Dunkley, J. and Gold, B. and Halpern, M. and Kogut, A. and Komatsu, E. and Larson, D. and Limon, M. and Meyer, S. S. and Nolta, M. R. and Smith, K. M. and Spergel, D. N. and Tucker, G. S. and Wright, E. L.}, title = {Seven-year Wilkinson Microwave Anisotropy Probe (WMAP) Observations: Planets and Celestial Calibration Sources}, journal = {Aps}, archivePrefix = {arXiv}, eprint = {1001.4731}, primaryClass = {astro-ph.CO}, keywords = {galaxies: individual: Cygnus A 3C274, ISM: supernova remnants, planets and satellites: general, radio continuum: general, space vehicles: instruments}, year = {2011}, month = {feb}, volume = {192}, pages = {19-+}, doi = {10.1088/0067-0049/192/2/19}, adsurl = {http://adsabs.harvard.edu/abs/2011ApJS..192...19W}, adsnote = {Provided by the SAO/NASA Astrophysics Data System} }

1. hinshaw2009 bibtex=@ARTICLE{hinshaw2009,

author = {Hinshaw, G. and Weiland, J. L. and Hill, R. S. and Odegard, N. and Larson, D. and Bennett, C. L. and Dunkley, J. and Gold, B. and Greason, M. R. and Jarosik, N. and Komatsu, E. and Nolta, M. R. and Page, L. and Spergel, D. N. and Wollack, E. and Halpern, M. and Kogut, A. and Limon, M. and Meyer, S. S. and Tucker, G. S. and Wright, E. L.}, title = {Five-Year Wilkinson Microwave Anisotropy Probe (WMAP) Observations: Data Processing, Sky Maps, and Basic Results}, journal = {Aps}, eprint = {0803.0732}, keywords = {Astrophysics}, year = {2009}, month = {Feb}, volume = {180}, pages = {225-245}, adsurl = {http://adsabs.harvard.edu/abs/2008arXiv0803.0732H}, adsnote = {Provided by the SAO/NASA Astrophysics Data System} }

1. hill2009 bibtex=@ARTICLE{hill2009,

author = {Hill, R. S. and Weiland, J. L. and Odegard, N. and Wollack, E. and Hinshaw, G. and Larson, D. and Bennett, C. L. and Halpern, M. and Page, L. and Dunkley, J. and Gold, B. and Jarosik, N. and Kogut, A. and Limon, M. and Nolta, M.R. and Spergel, D. N. and Tucker, G. S. and Wright, E. L.}, title = {Five-Year Wilkinson Microwave Anisotropy Probe (WMAP) Observations: Beam Maps and Window Functions}, journal = {Aps}, eprint = {0803.0570}, keywords = {Astrophysics}, year = {2009}, month = {Feb}, volume = {180}, pages = {246-264}, adsurl = {http:// adsabs. harvard. edu/ abs/ 2008arXiv0803. 0570H}, adsnote = {Provided by the SAO/NASA Astrophysics Data System} }

1. gold2009 bibtex=@ARTICLE{gold2009,

author = {Gold, B. and Bennett, C. L. and Hill, R. S. and Hinshaw, G. and Odegard, N. and Spergel, D. N. and Weiland, J. and Dunkley, J. and Halpern, M. and Jarosik, N. and Kogut, A. and Komatsu, E. and Larson, D. and Meyer, S. S. and Nolta, M.R. and Wollack, E. and Wright, E. L.}, title = {Five-Year Wilkinson Microwave Anisotropy Probe (WMAP) Observations: Galactic Foreground Emission}, journal = {Aps}, eprint = {0803.0715}, keywords = {Astrophysics}, year = {2009}, month = {Feb}, volume = {180}, pages = {265-282}, adsurl = {http:// adsabs. harvard. edu/ abs/ 2008arXiv0803. 0715G}, adsnote = {Provided by the SAO/NASA Astrophysics Data System} }

1. wright2009 bibtex=@ARTICLE{wright2009,

author = {Wright, E. L. and Chen, X. and Odegard, N. and Bennett, C. L. and Hill, R. S. and Hinshaw, G. and Jarosik, N. and Komatsu, E. and Nolta, M. R. and Page, L. and Spergel, D. N. and Weiland, J. L. and Wollack, E. and Dunkley, J. and Gold, B. and Halpern, M. and Kogut, A. and Larson, D. and Limon, M. and Meyer, S. S. and Tucker, G. S.}, title = {Five-Year Wilkinson Microwave Anisotropy Probe (WMAP) Observations: Source Catalog}, journal = {Aps}, eprint = {0803.0577}, keywords = {Astrophysics}, year = {2009}, month = {Feb}, volume = {180}, pages = {283-295}, adsurl = {http://adsabs.harvard.edu/abs/2008arXiv0803.0577W}, adsnote = {Provided by the SAO/NASA Astrophysics Data System} }

1. nolta2009 bibtex=@ARTICLE{nolta2009,

author = {Nolta, M. R. and Dunkley, J. and Hill, R. S. and Hinshaw, G. and Komatsu, E. and Larson, D. and Page, L. and Spergel, D. N. and Bennett, C. L. and Gold, B. and Jarosik, N. and Odegard, N. and Weiland, J. L. and Wollack, E. and Halpern, M. and Kogut, A. and Limon, M. and Meyer, S. S. and Tucker, G. S. and Wright, E.L.}, title = {Five-Year Wilkinson Microwave Anisotropy Probe (WMAP) Observations: Angular Power Spectra}, journal = {Aps}, eprint = {0803.0593}, keywords = {Astrophysics}, year = {2009}, month = {Feb}, volume = {180}, pages = {296-305}, adsurl = {http:// adsabs. harvard. edu/ abs/ 2008arXiv0803. 0593N}, adsnote = {Provided by the SAO/NASA Astrophysics Data System} }

1. dunkley2009 bibtex=@ARTICLE{dunkley2009,

author = {Dunkley, J. and Komatsu, E. and Nolta, M. R. and Spergel, D. N. and Larson, D. and Hinshaw, G. and Page, L. and Bennett, C. L. and Gold, B. and Jarosik, N. and Weiland, J. L. and Halpern, M. and Hill, R. S. and Kogut, A. and Limon, M. and Meyer, S. S. and Tucker, G. S. and Wollack, E. and Wright, E. L.}, title = {Five-Year Wilkinson Microwave Anisotropy Probe (WMAP) Observations: Likelihoods and Parameters from the WMAP data}, journal = {Aps}, eprint = {0803.0586}, keywords = {Astrophysics}, year = {2009}, month = {Feb}, volume = {180}, pages = {306-376}, adsurl = {http:// adsabs. harvard. edu/ abs/ 2008arXiv0803. 0586D}, adsnote = {Provided by the SAO/NASA Astrophysics Data System} }

1. komatsu2009 bibtex=@ARTICLE{komatsu2009,

author = {Komatsu, E. and Dunkley, J. and Nolta, M. R. and Bennett, C. L. and Gold, B. and Hinshaw, G. and Jarosik, N. and Larson, D. and Limon, M. and Page, L. and Spergel, D. N. and Halpern, M. and Hill, R. S. and Kogut, A. and Meyer, S. S. and Tucker, G. S. and Weiland, J. L. and Wollack, E. and Wright, E. L.}, title = {Five-Year Wilkinson Microwave Anisotropy Probe (WMAP) Observations: Cosmological Interpretation}, journal = {Aps}, eprint = {0803.0547}, keywords = {Astrophysics}, year = {2009}, month = {Feb}, volume = {180}, pages

= {330-376}, adsurl = {http://adsabs.harvard.edu/abs/2008arXiv0803.0547K}, adsnote = {Provided by the SAO/NASA Astrophysics Data System} }

1. kogut2007 bibtex=@ARTICLE{kogut2007,

author = {Kogut, A. and Dunkley, J. and Bennett, C. L. and Doré, O. and Gold, B. and Halpern, M. and Hinshaw, G. and Jarosik, N. and Komatsu, E. and Nolta, M. R. and Odegard, N. and Page, L. and Spergel, D. N. and Tucker, G. S. and Weiland, J. L. and Wollack, E. and Wright, E. L.}, title = {Three-Year Wilkinson Microwave Anisotropy Probe (WMAP) Observations: Foreground Polarization}, journal = {Ap}, eprint = {arXiv:0704.3991}, year = {2007}, month = {aug}, volume = {665}, pages = {355-362}, doi = {10.1086/519754}, adsurl = {http://adsabs.harvard.edu/abs/2007ApJ...665..355K}, adsnote = {Provided by the SAO/NASA Astrophysics Data System} }

1. jarosik2007 bibtex=@ARTICLE{jarosik2007,

author = {Jarosik, N. and Barnes, C. and Greason, M. R. and Hill, R. S. and Nolta, M. R. and Odegard, N. and Weiland, J. L. and Bean, R. and Bennett, C. L. and Doré, O. and Halpern, M. and Hinshaw, G. and Kogut, A. and Komatsu, E. and Limon, M. and Meyer, S. S. and Page, L. and Spergel, D. N. and Tucker, G. S. and Wollack, E. and Wright, E. L.}, title = {Three-Year Wilkinson Microwave Anisotropy Probe (WMAP) Observations: Beam Profiles, Data Processing, Radiometer Characterization, and Systematic Error Limits}, journal = {Aps}, eprint = {arXiv:astro-ph/0603452}, year = {2007}, month = {jun}, volume = {170}, pages = {263-287}, doi = {10.1086/513697}, adsurl = {http://adsabs.harvard.edu/abs/2007ApJS..170..263J}, adsnote = {Provided by the Smithsonian/NASA Astrophysics Data System} }

1. hinshaw2007 bibtex=@ARTICLE{hinshaw2007,

author = {Hinshaw, G. and Nolta, M. R. and Bennett, C. L. and Bean, R. and Doré, O. and Greason, M. R. and Halpern, M. and Hill, R. S. and Jarosik, N. and Kogut, A. and Komatsu, E. and Limon, M. and Odegard, N. and Meyer, S. S. and Page, L. and Peiris, H. V. and Spergel, D. N. and Tucker, G. S. and Verde, L. and Weiland, J. L. and Wollack, E. and Wright, E. L.}, title = {Three-Year Wilkinson Microwave Anisotropy Probe (WMAP) Observations: Temperature Analysis}, journal = {Aps}, eprint = {arXiv:astro-ph/0603451}, year = {2007}, month = {jun}, volume = {170}, pages = {288-334}, doi = {10.1086/513698}, adsurl = {http://adsabs.harvard.edu/abs/2007ApJS..170..288H}, adsnote = {Provided by the Smithsonian/NASA Astrophysics Data System} }

1. page2007 bibtex=@ARTICLE{page2007,

author = {Page, L. and Hinshaw, G. and Komatsu, E. and Nolta, M. R. and Spergel, D. N. and Bennett, C. L. and Barnes, C. and Bean, R. and Doré, O. and Dunkley, J. and Halpern, M. and Hill, R. S. and Jarosik, N. and Kogut, A. and Limon, M. and Meyer, S. S. and Odegard, N. and Peiris, H. V. and Tucker, G. S. and Verde, L. and Weiland, J. L. and Wollack, E. and Wright, E. L.}, title = {Three-Year Wilkinson Microwave Anisotropy Probe (WMAP) Observations: Polarization Analysis}, journal = {Aps}, eprint = {arXiv:astro-ph/0603450}, year = {2007}, month = {jun}, volume = {170}, pages = {335-376}, doi = {10.1086/513699}, adsurl = {http://adsabs.harvard.edu/abs/2007ApJS..170..335P}, adsnote = {Provided by the Smithsonian/NASA Astrophysics Data System} }

1. spergel2007 bibtex=@ARTICLE{spergel2007,

author = {Spergel, D. N. and Bean, R. and Doré, O. and Nolta, M. R. and Bennett, C. L. and Dunkley, J. and Hinshaw, G. and Jarosik, N. and Komatsu, E. and Page, L. and Peiris, H. V. and Verde, L. and Halpern, M. and Hill, R. S. and Kogut, A. and Limon, M. and Meyer, S. S. and Odegard, N. and Tucker, G. S. and Weiland, J. L. and Wollack, E. and Wright, E. L.}, title = {Three-Year Wilkinson Microwave Anisotropy Probe (WMAP) Observations: Implications for Cosmology}, journal = {Aps}, eprint = {arXiv:astro-ph/0603449}, year = {2007}, month = {jun}, volume = {170}, pages = {377-408}, doi = {10.1086/513700}, adsurl = {http://adsabs.harvard.edu/abs/2007ApJS..170..377S}, adsnote = {Provided by the Smithsonian/NASA Astrophysics Data System} }

1. nolta2004 bibtex=@Article{nolta2004,

author = {Nolta, M. R. and Wright, E. L. and Page, L. and Bennett, C. L. and Halpern, M. and Hinshaw, G. and Jarosik, N. and Kogut, A. and Limon, M. and Meyer, S. S. and Spergel, D. N. and Tucker, G. S. and Wollack, E.},

title = {First Year Wilkinson Microwave Anisotropy Probe (WMAP) Observations: Dark Energy Induced Correlation with Radio Sources}, journal = {Astrophys. J.}, volume = {608}, year = {2004}, pages = {10-15}, eprint = {astro-ph/0305097}, }

1. bennett2003a bibtex=@article{bennett2003a,

author = {Bennett, C. L. and Halpern, M. and Hinshaw, G. and Jarosik, N. and Kogut, A. and Limon, M. and Meyer, S. S. and Page, L. and Spergel, D. N. and Tucker, G. S. and Wollack, E. and Wright, E. L. and Barnes, C. and Greason, M. R. and Hill, R. S. and Komatsu, E. and Nolta, M. R. and Odegard, N. and Peiris, H. V. and Verde, L. and Weiland, J. L.}, title = {First-Year Wilkinson Microwave Anisotropy Probe (WMAP) Observations: Preliminary Maps and Basic Results}, journal = {Aps}, year = {2003}, month = {sep}, volume = {148}, pages = {1-27}, adsurl = {http://adsabs.harvard.edu/cgi-bin/nph-bib_query?bibcode=2003ApJS..148....1B&db_key=AST}, adsnote = {Provided by the NASA Astrophysics Data System} }

1. page2003a bibtex=@article{page2003a,

author = {Page, L. and Barnes, C. and Hinshaw, G. and Spergel, D. N. and Weiland, J. L. and Wollack, E. and Bennett, C. L. and Halpern, M. and Jarosik, N. and Kogut, A. and Limon, M. and Meyer, S. S. and Tucker, G. S. and Wright, E. L.}, title = {First-Year Wilkinson Microwave Anisotropy Probe (WMAP) Observations: Beam Profiles and Window Functions}, journal = {Aps}, year = {2003}, month = {sep}, volume = {148}, pages = {39-50}, adsurl = {http://adsabs.harvard.edu/cgi-bin/nph-bib_query?bibcode=2003ApJS..148...39P&db_key=AST}, adsnote = {Provided by the NASA Astrophysics Data System} }

1. hinshaw2003a bibtex=@article{hinshaw2003a,

author = {Hinshaw, G. and Barnes, C. and Bennett, C. L. and Greason, M. R. and Halpern, M. and Hill, R. S. and Jarosik, N. and Kogut, A. and Limon, M. and Meyer, S. S. and Odegard, N. and Page, L. and Spergel, D. N. and Tucker, G. S. and Weiland, J. L. and Wollack, E. and Wright, E. L.}, title = {First-Year Wilkinson Microwave Anisotropy Probe (WMAP) Observations: Data Processing Methods and Systematic Error Limits}, journal = {Aps}, year = {2003}, volume = {148}, pages = {63-95}, adsurl = {http:/ / adsabs. harvard. edu/ cgi-bin/ nph-bib_query?bibcode=2003ApJS..148...63H&db_key=AST}, adsnote = {Provided by the NASA Astrophysics Data System} }

1. spergel2003 bibtex=@article{spergel2003,

author = {Spergel, D. N. and Verde, L. and Peiris, H. V. and Komatsu, E. and Nolta, M. R. and Bennett, C. L. and Halpern, M. and Hinshaw, G. and Jarosik, N. and Kogut, A. and Limon, M. and Meyer, S. S. and Page, L. and Tucker, G. S. and Weiland, J. L. and Wollack, E. and Wright, E. L.}, title = {First-Year Wilkinson Microwave Anisotropy Probe (WMAP) Observations: Determination of Cosmological Parameters}, journal = {Aps}, year = {2003}, month = {sep}, volume = {148}, pages = {175-194}, adsurl = {http:/ / adsabs. harvard. edu/ cgi-bin/ nph-bib_query?bibcode=2003ApJS..148..175S&db_key=AST}, adsnote = {Provided by the NASA Astrophysics Data System} }

1. bennett2003b bibtex=@article{bennett2003b,

author = {Bennett, C. L. and Hill, R. S. and Hinshaw, G. and Nolta, M. R. and Odegard, N. and Page, L. and Spergel, D. N. and Weiland, J. L. and Wright, E. L. and Halpern, M. and Jarosik, N. and Kogut, A. and Limon, M. and Meyer, S. S. and Tucker, G. S. and Wollack, E. }, title = {First-Year Wilkinson Microwave Anisotropy Probe (WMAP) Observations: Foreground Emission}, journal = {Aps}, year = {2003}, volume = {148}, pages = {97-117}, adsurl = {http:/ / adsabs. harvard. edu/ cgi-bin/ nph-bib_query?bibcode=2003ApJS. . 148. . . 97B& db_key=AST}, adsnote = {Provided by the NASA Astrophysics Data System} }

1. barnes2003 bibtex=@article{barnes2003,

author = {Barnes, C. and Hill, R. S. and Hinshaw, G. and Page, L. and Bennett, C. L. and Halpern, M. and Jarosik, N. and Kogut, A. and Limon, M. and Meyer, S. S. and Tucker, G. S. and Wollack, E. and Wright, E. L.}, title = {First-Year Wilkinson Microwave Anisotropy Probe (WMAP) Observations: Galactic Signal Contamination from

Sidelobe Pickup}, journal = {Aps}, year = {2003}, month = {sep}, volume = {148}, pages = {51-62}, adsurl = {http://adsabs.harvard.edu/cgi-bin/nph-bib_query?bibcode=2003ApJS..148...51B&db_key=AST}, adsnote = {Provided by the NASA Astrophysics Data System} }

1. peiris2003 bibtex=@article{peiris2003,

author = {Peiris, H. V. and Komatsu, E. and Verde, L. and Spergel, D. N. and Bennett, C. L. and Halpern, M. and Hinshaw, G. and Jarosik, N. and Kogut, A. and Limon, M. and Meyer, S. S. and Page, L. and Tucker, G. S. and Wollack, E. and Wright, E. L.}, title = {First-Year Wilkinson Microwave Anisotropy Probe (WMAP) Observations: Implications For Inflation}, journal = {Aps}, year = {2003}, month = {sep}, volume = {148}, pages = {213-231}, adsurl = {http://adsabs.harvard.edu/cgi-bin/nph-bib_query?bibcode=2003ApJS..148..213P&db_key=AST}, adsnote = {Provided by the NASA Astrophysics Data System} }

1. page2003b bibtex=@article{page2003b,

author = {Page, L. and Nolta, M. R. and Barnes, C. and Bennett, C. L. and Halpern, M. and Hinshaw, G. and Jarosik, N. and Kogut, A. and Limon, M. and Meyer, S. S. and Peiris, H. V. and Spergel, D. N. and Tucker, G. S. and Wollack, E. and Wright, E. L.}, title = {First-Year Wilkinson Microwave Anisotropy Probe (WMAP) Observations: Interpretation of the TT and TE Angular Power Spectrum Peaks}, journal = {Aps}, year = {2003}, month = {sep}, volume = {148}, pages = {233-241}, adsurl = {http:/ / adsabs. harvard. edu/ cgi-bin/ nph-bib_query?bibcode=2003ApJS..148..233P&db_key=AST}, adsnote = {Provided by the NASA Astrophysics Data System} }

1. jarosik2003 bibtex=@article{jarosik2003,

author = {Jarosik, N. and Barnes, C. and Bennett, C. L. and Halpern, M. and Hinshaw, G. and Kogut, A. and Limon, M. and Meyer, S. S. and Page, L. and Spergel, D. N. and Tucker, G. S. and Weiland, J. L. and Wollack, E. and Wright, E. L.}, title = {First-Year Wilkinson Microwave Anisotropy Probe (WMAP) Observations: On-Orbit Radiometer Characterization}, journal = {Aps}, year = {2003}, month = {sep}, volume = {148}, pages = {29-37}, adsurl = {http://adsabs.harvard.edu/cgi-bin/nph-bib_query?bibcode=2003ApJS..148...29J&db_key=AST}, adsnote = {Provided by the NASA Astrophysics Data System} }

1. verde2003 bibtex=@article{verde2003,

author = {Verde, L. and Peiris, H. V. and Spergel, D. N. and Nolta, M. R. and Bennett, C. L. and Halpern, M. and Hinshaw, G. and Jarosik, N. and Kogut, A. and Limon, M. and Meyer, S. S. and Page, L. and Tucker, G. S. and Wollack, E. and Wright, E. L.}, title = {First-Year Wilkinson Microwave Anisotropy Probe (WMAP) Observations: Parameter Estimation Methodology}, journal = {Aps}, year = {2003}, volume = {148}, pages = {195-211}, adsurl = {http://adsabs.harvard.edu/cgi-bin/nph-bib_query?bibcode=2003ApJS..148..195V&db_key=AST}, adsnote = {Provided by the NASA Astrophysics Data System} }

1. kogut2003 bibtex=@article{kogut2003,

author = {Kogut, A. and Spergel, D. N. and Barnes, C. and Bennett, C. L. and Halpern, M. and Hinshaw, G. and Jarosik, N. and Limon, M. and Meyer, S. S. and Page, L. and Tucker, G. S. and Wollack, E. and Wright, E. L.}, title = {First-Year Wilkinson Microwave Anisotropy Probe (WMAP) Observations: Temperature-Polarization Correlation}, journal = {Aps}, year = {2003}, month = {sep}, volume = {148}, pages = {161-173}, adsurl = {http:// adsabs. harvard. edu/ cgi-bin/ nph-bib_query?bibcode=2003ApJS. . 148. . 161K& db_key=AST}, adsnote = {Provided by the NASA Astrophysics Data System} }

1. komatsu2003 bibtex=@article{komatsu2003,

author = {Komatsu, E. and Kogut, A. and Nolta, M. R. and Bennett, C. L. and Halpern, M. and Hinshaw, G. and Jarosik, N. and Limon, M. and Meyer, S. S. and Page, L. and Spergel, D. N. and Tucker, G. S. and Verde, L. and Wollack, E. and Wright, E. L.}, title = {First-Year Wilkinson Microwave Anisotropy Probe (WMAP) Observations: Tests of Gaussianity}, journal = {Aps}, year = {2003}, month = {sep}, volume = {148}, pages = {119-134}, adsurl = {http://adsabs.harvard.edu/cgi-bin/nph-bib_query?bibcode=2003ApJS..148..119K&db_key=AST}, adsnote

= {Provided by the NASA Astrophysics Data System} }

1. hinshaw2003b bibtex=@article{hinshaw2003b,

author = {Hinshaw, G. and Spergel, D. N. and Verde, L. and Hill, R. S. and Meyer, S. S. and Barnes, C. and Bennett, C. L. and Halpern, M. and Jarosik, N. and Kogut, A. and Komatsu, E. and Limon, M. and Page, L. and Tucker, G. S. and Weiland, J. L. and Wollack, E. and Wright, E. L.}, title = {First-Year Wilkinson Microwave Anisotropy Probe (WMAP) Observations: The Angular Power Spectrum}, journal = {Aps}, year = {2003}, volume = {148}, pages = {135-159}, adsurl = {http://adsabs.harvard.edu/cgi-bin/nph-bib_query?bibcode=2003ApJS..148..135H&db_key=AST}, adsnote = {Provided by the NASA Astrophysics Data System} }

1. delabrouille2012 bibtex=@ARTICLE{delabrouille2012,

author = {Delabrouille, J. and Betoule, M. and Melin, J.-B. and Miville-Deschênes, M.-A. and Gonzalez-Nuevo, J. and Le Jeune, M. and Castex, G. and de Zotti, G. and Basak, S. and Ashdown, M. and Aumont, J. and Baccigalupi, C. and Banday, A. and Bernard, J.-P. and Bouchet, F. R. and Clements, D. L. and da Silva, A. and Dickinson, C. and Dodu, F. and Dolag, K. and Elsner, F. and Fauvet, L. and Fa&yuml, G. and Giardino, G. and Leach, S. and Lesgourgues, J. and Liguori, M. and Macias-Perez, J. F. and Massardi, M. and Matarrese, S. and Mazzotta, P. and Montier, L. and Mottet, S. and Paladini, R. and Partridge, B. and Piffaretti, R. and Prezeau, G. and Prunet, S. and Ricciardi, S. and Roman, M. and Schaefer, B. and Toffolatti, L.}, title = {The pre-launch Planck Sky Model: a model of sky emission at submillimetre to centimetre wavelengths}, journal = {ArXiv e-prints}, archivePrefix = {arXiv}, eprint = {1207.3675}, primaryClass = {astro-ph.CO}, keywords = {Astrophysics - Cosmology and Extragalactic Astrophysics}, year = {2012}, month = {jul}, adsurl = {http://adsabs.harvard.edu/abs/2012arXiv1207.3675D}, adsnote = {Provided by the SAO/NASA Astrophysics Data System} }

1. armitage-caplan2009 bibtex=@ARTICLE{armitage-caplan2009,

author = {Armitage-Caplan, C. and Wandelt, B. D.}, title = {PReBeaM for Planck: A Polarized Regularized Beam Deconvolution Map-Making Method}, journal = {Aps}, archivePrefix = {arXiv}, eprint = {0807.4179}, keywords = {cosmic microwave background, cosmology: observations, methods: data analysis}, year = {2009}, month = {apr}, volume = {181}, pages = {533-542}, doi = {10.1088/0067-0049/181/2/533}, adsurl = {http://adsabs.harvard.edu/abs/2009ApJS..181..533A}, adsnote = {Provided by the SAO/NASA Astrophysics Data System} }

1. ashdown2007a bibtex=@ARTICLE{ashdown2007a,

author = {Ashdown, M. A. J. and Baccigalupi, C. and Balbi, A. and Bartlett, J. G. and Borrill, J. and Cantalupo, C. and de Gasperis, G. and Górski, K. M. and Heikkilä, V. and Hivon, E. and Keihänen, E. and Kurki-Suonio, H. and Lawrence, C. R. and Natoli, P. and Poutanen, T. and Prunet, S. and Reinecke, M. and Stompor, R. and Wandelt, B.}, title = {Making maps from Planck LFI 30 GHz data}, journal = {A&A}, eprint = {arXiv:astro-ph/0702483}, keywords = {cosmology: cosmic microwave background, methods: data, analysis, techniques: image processing, cosmology: observations}, year = {2007}, month = {aug}, volume = {471}, pages = {361-380}, doi = {10.1051/0004-6361:20077312}, adsurl = {http://adsabs.harvard.edu/abs/2007A%26A...471..361A}, adsnote = {Provided by the SAO/NASA Astrophysics Data System} }

1. ashdown2007b bibtex=@ARTICLE{ashdown2007b,

author = {Ashdown, M. A. J. and Baccigalupi, C. and Balbi, A. and Bartlett, J. G. and Borrill, J. and Cantalupo, C. and de Gasperis, G. and Górski, K. M. and Hivon, E. and Keihänen, E. and Kurki-Suonio, H. and Lawrence, C. R. and Natoli, P. and Poutanen, T. and Prunet, S. and Reinecke, M. and Stompor, R. and Wandelt, B. and {The Planck CTP Working Group} }, title = {Making sky maps from Planck data}, journal = {A&A}, eprint = {arXiv:astro-ph/0606348}, keywords = {cosmology: cosmic microwave background, methods: data analysis}, year = {2007}, month = {may}, volume = {467}, pages = {761-775}, doi = {10.1051/0004-6361:20065829}, adsurl = {http://adsabs.harvard.edu/abs/2007A%26A...467..761A}, adsnote = {Provided by the SAO/NASA Astrophysics Data System} }

1. ashdown2009 bibtex=@ARTICLE{ashdown2009,

author = {Ashdown, M. A. J. and Baccigalupi, C. and Bartlett, J. G. and Borrill, J. and Cantalupo, C. and de Gasperis, G. and de Troia, G. and Górski, K. M. and Hivon, E. and Huffenberger, K. and Keihänen, E. and Keskitalo, R. and Kisner, T. and Kurki-Suonio, H. and Lawrence, C. R. and Natoli, P. and Poutanen, T. and Prézeau, G. and Reinecke, M. and Rocha, G. and Sandri, M. and Stompor, R. and Villa, F. and Wandelt, B. and {The Planck Ctp Working Group}}, title = {Making maps from Planck LFI 30 GHz data with asymmetric beams and cooler noise}, journal = {A&A}, archivePrefix = {arXiv}, eprint = {0806.3167}, keywords = {cosmology: cosmic microwave background, methods: data analysis, cosmology: observations}, year = {2009}, month = {jan}, volume = {493}, pages = {753-783}, doi = {10.1051/0004-6361:200810381}, adsurl = {http://adsabs.harvard.edu/abs/2009A%26A...493..753A}, adsnote = {Provided by the SAO/NASA Astrophysics Data System} }

1. aumont2010 bibtex=@ARTICLE{aumont2010,

author = {Aumont, J. and Conversi, L. and Thum, C. and Wiesemeyer, H. and Falgarone, E. and Macías-Pérez, J. F. and Piacentini, F. and Pointecouteau, E. and Ponthieu, N. and Puget, J. L. and Rosset, C. and Tauber, J. A. and Tristram, M.}, title = {Measurement of the Crab nebula polarization at 90 GHz as a calibrator for CMB experiments}, journal = {A&A}, keywords = {ISM: supernova remnants, polarization, cosmology: cosmic background radiation}, year = {2010}, month = {may}, volume = {514}, pages = {A70+}, doi = {10.1051/0004-6361/200913834}, adsurl = {http://adsabs.harvard.edu/abs/2010A%26A...514A..70A}, adsnote = {Provided by the SAO/NASA Astrophysics Data System} }

1. cappellini2003 bibtex=@ARTICLE{cappellini2003,

author = {Cappellini, B. and Maino, D. and Albetti, G. and Platania, P. and Paladini, R. and Mennella, A. and Bersanelli, M.}, title = {Optimized in-flight absolute calibration for extended CMB surveys}, journal = {A&A}, eprint = {arXiv:astro-ph/0309317}, keywords = {cosmology: cosmic microwave background, methods: data analysis}, year = {2003}, month = {oct}, volume = {409}, pages = {375-385}, doi = {10.1051/0004-6361:20030927}, adsurl = {http://adsabs.harvard.edu/abs/2003A%26A...409..375C}, adsnote = {Provided by the SAO/NASA Astrophysics Data System} }

1. colombo2009 bibtex=@ARTICLE{colombo2009,

author = {Colombo, L. P. L. and Pierpaoli, E. and Pritchard, J. R. }, title = {Cosmological parameters after WMAP5: forecasts for Planck and future galaxy surveys}, journal = {MNRAS}, archivePrefix = {arXiv}, eprint = {0811.2622}, keywords = {galaxies: statistics , cosmic microwave background , cosmological parameters , large-scale structure of Universe}, year = {2009}, month = {oct}, volume = {398}, pages = {1621-1637}, doi = {10.1111/j.1365-2966.2009.14802.x}, adsurl = {http://adsabs.harvard.edu/abs/2009MNRAS.398.1621C}, adsnote = {Provided by the SAO/NASA Astrophysics Data System} }

1. dupac2005 bibtex=@ARTICLE{dupac2005,

author = {Dupac, X. and Tauber, J.}, title = {Scanning strategy for mapping the Cosmic Microwave Background anisotropies with Planck}, journal = {A&A}, eprint = {arXiv:astro-ph/0409405}, keywords = {cosmic microwave background, methods: observational}, year = {2005}, month = {jan}, volume = {430}, pages = {363-371}, doi = {10.1051/0004-6361:20041526}, adsurl = {http://adsabs.harvard.edu/abs/2005A%26A...430..363D}, adsnote = {Provided by the SAO/NASA Astrophysics Data System} }

1. hanson2009 bibtex=@ARTICLE{hanson2009,

author = {Hanson, D. and Rocha, G. and Górski, K.}, title = {Lensing reconstruction from Planck sky maps: inhomogeneous noise}, journal = {MNRAS}, archivePrefix = {arXiv}, eprint = {0907.1927}, keywords = {gravitational lensing , methods: numerical , cosmic microwave background , cosmology: observations}, year = {2009}, month = {dec}, volume = {400}, pages = {2169-2173}, doi = {10.1111/j.1365-2966.2009.15614.x}, adsurl = {http://adsabs.harvard.edu/abs/2009MNRAS.400.2169H}, adsnote = {Provided by the SAO/NASA Astrophysics Data System} }

1. huffenberger2010 bibtex=@ARTICLE{huffenberger2010,

author = {Huffenberger, K. M. and Crill, B. P. and Lange, A. E. and Górski, K. M. and Lawrence, C. R.}, title = {Measuring Planck beams with planets}, journal = {A&A}, archivePrefix = {arXiv}, eprint = {1007.3468}, primaryClass = {astro-ph.CO}, keywords = {cosmic microwave background, cosmological parameters, cosmology: observations}, year = {2010}, month = {feb}, volume = {510}, pages = {A58+}, doi = {10.1051/0004-6361/200913117}, adsurl = {http://cdsads.u-strasbg.fr/abs/2010A%26A...510A..58H}, adsnote = {Provided by the SAO/NASA Astrophysics Data System} }

1. leach2008 bibtex=@ARTICLE{leach2008,

author = {Leach, S. M. and Cardoso, J.-F. and Baccigalupi, C. and Barreiro, R. B. and Betoule, M. and Bobin, J. and Bonaldi, A. and Delabrouille, J. and de Zotti, G. and Dickinson, C. and Eriksen, H. K. and González-Nuevo, J. and Hansen, F. K. and Herranz, D. and Le Jeune, M. and López-Caniego, M. and Martínez-González, E. and Massardi, M. and Melin, J.-B. and Miville-Deschênes, M.-A. and Patanchon, G. and Prunet, S. and Ricciardi, S. and Salerno, E. and Sanz, J. L. and Starck, J.-L. and Stivoli, F. and Stolyarov, V. and Stompor, R. and Vielva, P. }, title = {Component separation methods for the PLANCK mission}, journal = {A&A}, archivePrefix = {arXiv}, eprint = {0805.0269}, keywords = {cosmology: cosmic microwave background, methods: data analysis}, year = {2008}, month = {nov}, volume = {491}, pages = {597-615}, doi = {10.1051/0004-6361:200810116}, adsurl = {http://adsabs.harvard.edu/abs/2008A%26A...491..597L}, adsnote = {Provided by the SAO/NASA Astrophysics Data System} }

1. massardi2006 bibtex=@INPROCEEDINGS{massardi2006,

author = {Massardi, M.}, title = {Realistic point source maps at Planck frequencies}, booktitle = {CMB and Physics of the Early Universe}, year = {2006}, adsurl = {http://adsabs.harvard.edu/abs/2006cmb..confE..45M}, adsnote = {Provided by the SAO/NASA Astrophysics Data System} }

1. mennella2002 bibtex=@ARTICLE{mennella2002,

author = {Mennella, A. and Bersanelli, M. and Burigana, C. and Maino, D. and Mandolesi, N. and Morgante, G. and Stanghellini, G.}, title = {PLANCK: Systematic effects induced by periodic fluctuations of arbitrary shape}, journal = {A&A}, eprint = {arXiv:astro-ph/0111078}, keywords = {COSMOLOGY: COSMIC MICROWAVE BACKGROUND, OBSERVATIONS, INSTRUMENTATION: DETECTORS, MISCELLANEOUS, METHODS: ANALYTICAL}, year = {2002}, month = {mar}, volume = {384}, pages = {736-742}, doi = {10.1051/0004-6361:20020024}, adsurl = {http://adsabs.harvard.edu/abs/2002A%26A...384..736M}, adsnote = {Provided by the SAO/NASA Astrophysics Data System} }

1. mennella2003 bibtex=@ARTICLE{mennella2003,

author = {Mennella, A. and Bersanelli, M. and Seiffert, M. and Kettle, D. and Roddis, N. and Wilkinson, A. and Meinhold, P.}, title = {Offset balancing in pseudo-correlation radiometers for CMB measurements}, journal = {A&A}, eprint = {arXiv:astro-ph/0307558}, keywords = {cosmology: cosmic microwave background, observations, instrumentation: detectors, methods: analytical}, year = {2003}, month = {nov}, volume = {410}, pages = {1089-1100}, doi = {10.1051/0004-6361:20031266}, adsurl = {http://adsabs.harvard.edu/abs/2003A%26A...410.1089M}, adsnote = {Provided by the SAO/NASA Astrophysics Data System} }

1. natoli2001 bibtex=@ARTICLE{natoli2001,

author = {Natoli, P. and de Gasperis, G. and Gheller, C. and Vittorio, N. }, title = {A Map-Making algorithm for the Planck Surveyor.}, journal = {A&A}, eprint = {arXiv:astro-ph/0101252}, keywords = {COSMIC MICROWAVE BACKGROUND ANISOTROPIES, METHODS: DATA ANALYSIS}, year = {2001}, month = {jun}, volume = {372}, pages = {346-356}, doi = {10.1051/0004-6361:20010393}, adsurl = {http://adsabs.harvard.edu/abs/2001A%26A...372..346N}, adsnote = {Provided by the SAO/NASA Astrophysics Data System} }

1. reinecke2006 bibtex=@ARTICLE{reinecke2006,

author = {Reinecke, M. and Dolag, K. and Hell, R. and Bartelmann, M. and Enßlin, T. A.}, title = {A simulation pipeline for the Planck mission}, journal = {A&A}, eprint = {arXiv:astro-ph/0508522}, keywords = {cosmology:

cosmic microwave background, cosmology: large-scale structure of Universe, methods: numerical}, year = {2006}, month = {jan}, volume = {445}, pages = {373-373}, doi = {10.1051/0004-6361:20053413}, adsurl = {http://adsabs.harvard.edu/abs/2006A%26A...445..373R}, adsnote = {Provided by the SAO/NASA Astrophysics Data System} }

1. ricciardi2007 bibtex=@ARTICLE{ricciardi2007,

author = {Ricciardi, S.}, title = {Planck Reference Sky versus WMAP}, journal = {New Astronomy Review}, year = {2007}, month = {mar}, volume = {51}, pages = {310-315}, doi = {10.1016/j.newar.2006.11.054}, adsurl = {http://adsabs.harvard.edu/abs/2007NewAR..51..310R}, adsnote = {Provided by the SAO/NASA Astrophysics Data System} }

1. rocha2009 bibtex=@ARTICLE{rocha2009,

author = {Rocha, G. and Contaldi, C. R. and Bond, J. R. and Gorski, K. M. }, title = {Application of XFaster power spectrum and likelihood estimator to Planck}, journal = {ArXiv e-prints}, archivePrefix = {arXiv}, eprint = {0912.4059}, keywords = {Astrophysics - Cosmology and Extragalactic Astrophysics, Astrophysics - Instrumentation and Methods for Astrophysics}, year = {2009}, month = {dec}, adsurl = {http://adsabs.harvard.edu/abs/2009arXiv0912.4059R}, adsnote = {Provided by the SAO/NASA Astrophysics Data System} }

1. seiffert2002 bibtex=@ARTICLE{seiffert2002,

author = {Seiffert, M. and Mennella, A. and Burigana, C. and Mandolesi, N. and Bersanelli, M. and Meinhold, P. and Lubin, P.}, title = {1/f noise and other systematic effects in the Planck-LFI radiometers}, journal = {A&A}, eprint = {arXiv:astro-ph/0206093}, keywords = {cosmology: cosmic microwave background, observations, instrumentation: detectors, methods: analytical}, year = {2002}, month = {sep}, volume = {391}, pages = {1185-1197}, doi = {10.1051/0004-6361:20020880}, adsurl = {http://adsabs.harvard.edu/abs/2002A%26A...391.1185S}, adsnote = {Provided by the SAO/NASA Astrophysics Data System} }

1. white2006 bibtex=@ARTICLE{white2006,

author = {White, M.}, title = {Cosmological science enabled by Planck}, journal = {New Astronomy Reviews}, eprint = {arXiv:astro-ph/0606643}, year = {2006}, month = {dec}, volume = {50}, pages = {938-944}, doi = {10.1016/j.newar.2006.09.008}, adsurl = {http://adsabs.harvard.edu/abs/2006NewAR..50..938W}, adsnote = {Provided by the SAO/NASA Astrophysics Data System} }

1. buehler1996 bibtex=@INPROCEEDINGS{buehler1996,

author = {Buehler, P. and Desorgher, L. and Zehnder, A.}, title = {Simple Instruments for Continuous Measurement of Trapped Particles}, booktitle = {Environment Modeling for Space-Based Applications}, year = {1996}, series = {ESA Special Publication}, volume = {392}, editor = {T.-D. Guyenne \& A. Hilgers}, month = {dec}, pages = {87-+}, adsurl = {http://adsabs.harvard.edu/abs/1996ESASP.392...87B}, adsnote = {Provided by the SAO/NASA Astrophysics Data System} }

1. cantalupo2010 bibtex=@ARTICLE{cantalupo2010,

author = {Cantalupo, C. M. and Borrill, J. D. and Jaffe, A. H. and Kisner, T. S. and Stompor, R.}, title = {MADmap: A Massively Parallel Maximum Likelihood Cosmic Microwave Background Map-maker}, journal = {Aps}, archivePrefix = {arXiv}, eprint = {0906.1775}, primaryClass = {astro-ph.CO}, keywords = {cosmic background radiation, cosmology: observations, methods: data analysis, methods: numerical}, year = {2010}, month = {mar}, volume = {187}, pages = {212-227}, doi = {10.1088/0067-0049/187/1/212}, adsurl = {http://adsabs.harvard.edu/abs/2010ApJS..187..212C}, adsnote = {Provided by the SAO/NASA Astrophysics Data System} }

1. degasperis2005 bibtex=@ARTICLE{degasperis2005,

author = {de Gasperis, G. and Balbi, A. and Cabella, P. and Natoli, P. and Vittorio, N.}, title = {ROMA: A map-making algorithm for polarised CMB data sets}, journal = {A&A}, eprint = {arXiv:astro-ph/0502142}, keywords = {cosmology: cosmic microwave background, methods: statistical, methods: data analysis}, year =

{2005}, month = {jun}, volume = {436}, pages = {1159-1165}, doi = {10.1051/0004-6361:20042512}, adsurl = {http:/ / adsabs. harvard. edu/ abs/ 2005A%26A. . . 436. 1159D}, adsnote = {Provided by the SAO/NASA Astrophysics Data System} }

1. finkbeiner1999 bibtex=@ARTICLE{finkbeiner1999,

author = {Finkbeiner, D. P. and Davis, M. and Schlegel, D. J.}, title = {Extrapolation of Galactic Dust Emission at 100 Microns to Cosmic Microwave Background Radiation Frequencies Using FIRAS}, journal = {Ap}, eprint = {arXiv:astro-ph/9905128}, keywords = {ISM: DUST, EXTINCTION, INFRARED: ISM: CONTINUUM, SUBMILLIMETER}, year = {1999}, month = {oct}, volume = {524}, pages = {867-886}, doi = {10.1086/307852}, adsurl = {http:/ / cdsads. u-strasbg. fr/ abs/ 1999ApJ. . . 524. . 867F}, adsnote = {Provided by the SAO/NASA Astrophysics Data System} }

1. fixsen1997 bibtex=@ARTICLE{fixsen1997,

author = {Fixsen, D. J. and Weiland, J. L. and Brodd, S. and Hauser, M. G. and Kelsall, T. and Leisawitz, D. T. and Mather, J. C. and Jensen, K. A. and Schafer, R. A. and Silverberg, R. F. }, title = {Comparison of the COBE FIRAS and DIRBE Calibrations}, journal = {Ap}, eprint = {arXiv:astro-ph/9707192}, keywords = {COSMOLOGY: COSMIC MICROWAVE BACKGROUND, INFRARED: GENERAL, INSTRUMENTATION: PHOTOMETERS}, year = {1997}, month = {dec}, volume = {490}, pages = {482-+}, doi = {10.1086/304906}, adsurl = {http:/ / cdsads. u-strasbg. fr/ abs/ 1997ApJ. . . 490. . 482F}, adsnote = {Provided by the SAO/NASA Astrophysics Data System} }

1. gorski2005 bibtex=@ARTICLE{gorski2005,

author = {Górski, K. M. and Hivon, E. and Banday, A. J. and Wandelt, B. D. and Hansen, F. K. and Reinecke, M. and Bartelmann, M.}, title = {HEALPix: A Framework for High-Resolution Discretization and Fast Analysis of Data Distributed on the Sphere}, journal = {Ap}, eprint = {arXiv:astro-ph/0409513}, keywords = {Cosmology: Cosmic Microwave Background, Cosmology: Observations, Methods: Statistical}, year = {2005}, month = {apr}, volume = {622}, pages = {759-771}, doi = {10.1086/427976}, adsurl = {http://adsabs.harvard.edu/abs/2005ApJ…622..759G}, adsnote = {Provided by the SAO/NASA Astrophysics Data System} }

1. keihanen2004 bibtex=@ARTICLE{keihanen2004,

author = {Keihänen, E. and Kurki-Suonio, H. and Poutanen, T. and Maino, D. and Burigana, C.}, title = {A maximum likelihood approach to the destriping technique}, journal = {A&A}, eprint = {arXiv:astro-ph/0304411}, keywords = {methods: data analysis, cosmology: cosmic microwave background}, year = {2004}, month = {dec}, volume = {428}, pages = {287-298}, doi = {10.1051/0004-6361:200400060}, adsurl = {http://cdsads.u-strasbg.fr/abs/2004A%26A...428..287K}, adsnote = {Provided by the SAO/NASA Astrophysics Data System} }

1. keihanen2005 bibtex=@ARTICLE{keihanen2005,

author = {Keihänen, E. and Kurki-Suonio, H. and Poutanen, T. }, title = {MADAM- a map-making method for CMB experiments}, journal = {MNRAS}, eprint = {arXiv:astro-ph/0412517}, keywords = {methods: data analysis, cosmic microwave background}, year = {2005}, month = {jun}, volume = {360}, pages = {390-400}, doi = {10.1111/j.1365-2966.2005.09055.x}, adsurl = {http:/ / cdsads. u-strasbg. fr/ abs/ 2005MNRAS. 360. . 390K}, adsnote = {Provided by the SAO/NASA Astrophysics Data System} }

1. keihanen2010 bibtex=@ARTICLE{keihanen2010,

author = {Keihänen, E. and Keskitalo, R. and Kurki-Suonio, H. and Poutanen, T. and Sirviö, A.-S.}, title = {Making cosmic microwave background temperature and polarization maps with MADAM}, journal = {A&A}, archivePrefix = {arXiv}, eprint = {0907.0367}, primaryClass = {astro-ph.CO}, keywords = {cosmology: cosmic microwave background, methods: data analysis}, year = {2010}, month = {feb}, volume = {510}, pages = {A57+}, doi = {10.1051/0004-6361/200912813}, adsurl = {http:/ / adsabs. harvard. edu/ abs/ 2010A%26A. . . 510A. . 57K}, adsnote = {Provided by the SAO/NASA Astrophysics Data System} }

1. kurki-suonio2009 bibtex=@ARTICLE{kurki-suonio2009,

author = {Kurki-Suonio, H. and Keihänen, E. and Keskitalo, R. and Poutanen, T. and Sirviö, A.-S. and Maino, D. and Burigana, C.}, title = {Destriping CMB temperature and polarization maps}, journal = {A&A}, archivePrefix = {arXiv}, eprint = {0904.3623}, primaryClass = {astro-ph.IM}, keywords = {methods: data analysis, cosmology: cosmic microwave background}, year = {2009}, month = {nov}, volume = {506}, pages = {1511-1539}, doi = {10.1051/0004-6361/200912361}, adsurl = {http:/ / adsabs. harvard. edu/ abs/ 2009A%26A. . . 506. 1511K}, adsnote = {Provided by the SAO/NASA Astrophysics Data System} }

1. macias2007 bibtex=@ARTICLE{macias2007,

author = {Macías-Pérez, J. F. and Lagache, G. and Maffei, B. and Ganga, K. and Bourrachot, A. and Ade, P. and Amblard, A. and Ansari, R. and Aubourg, E. and Aumont, J. and Bargot, S. and Bartlett, J. and Benoît, A. and Bernard, J.-P. and Bhatia, R. and Blanchard, A. and Bock, J. J. and Boscaleri, A. and Bouchet, F. R. and Camus, P. and Cardoso, J.-F. and Couchot, F. and de Bernardis, P. and Delabrouille, J. and Désert, F.-X. and Doré, O. and Douspis, M. and Dumoulin, L. and Dupac, X. and Filliatre, P. and Fosalba, P. and Gannaway, F. and Gautier, B. and Giard, M. and Giraud-Héraud, Y. and Gispert, R. and Guglielmi, L. and Hamilton, J.-C. and Hanany, S. and Henrot-Versillé, S. and Hristov, V. and Kaplan, J. and Lamarre, J.-M. and Lange, A. E. and Madet, K. and Magneville, C. and Marrone, D. P. and Masi, S. and Mayet, F. and Murphy, J. A. and Naraghi, F. and Nati, F. and Patanchon, G. and Perdereau, O. and Perrin, G. and Plaszczynski, S. and Piat, M. and Ponthieu, N. and Prunet, S. and Puget, J.-L. and Renault, C. and Rosset, C. and Santos, D. and Starobinsky, A. and Strukov, I. and Sudiwala, R. V. and Teyssier, R. and Tristram, M. and Tucker, C. and Vanel, J.-C. and Vibert, D. and Wakui, E. and Yvon, D.}, title = {Archeops in-flight performance, data processing, and map making}, journal = {A&A}, eprint = {arXiv:astro-ph/0603665}, keywords = {methods: data analysis, cosmic microwave background}, year = {2007}, month = {jun}, volume = {467}, pages = {1313-1344}, doi = {10.1051/0004-6361:20065258}, adsurl = {http://cdsads.u-strasbg.fr/abs/2007A%26A...467.1313M}, adsnote = {Provided by the SAO/NASA Astrophysics Data System} }

1. maino2002 bibtex=@ARTICLE{maino2002,

author = {Maino, D. and Burigana, C. and Górski, K. M. and Mandolesi, N. and Bersanelli, M.}, title = {Removing 1/f noise stripes in cosmic microwave background anisotropy observations}, journal = {A&A}, eprint = {arXiv:astro-ph/0202271}, keywords = {methods: data analysis, cosmology: cosmic microwave background}, year = {2002}, month = {may}, volume = {387}, pages = {356-365}, doi = {10.1051/0004-6361:20020242}, adsurl = {http:/ / cdsads. u-strasbg. fr/ abs/ 2002A%26A. . . 387. . 356M}, adsnote = {Provided by the SAO/NASA Astrophysics Data System} }

1. melin2006 bibtex=@ARTICLE{melin2006,

author = {Melin, J.-B. and Bartlett, J. G. and Delabrouille, J. }, title = {Catalog extraction in SZ cluster surveys: a matched filter approach}, journal = {A&A}, eprint = {arXiv:astro-ph/0602424}, keywords = {large-scale structure of Universe, galaxies: clusters: general, methods: data analysis}, year = {2006}, month = {nov}, volume = {459}, pages = {341-352}, doi = {10.1051/0004-6361:20065034}, adsurl = {http:/ / adsabs. harvard. edu/ abs/ 2006A%26A...459..341M}, adsnote = {Provided by the SAO/NASA Astrophysics Data System} }

1. poutanen2006 bibtex=@ARTICLE{poutanen2006,

author = {Poutanen, T. and de Gasperis, G. and Hivon, E. and Kurki-Suonio, H. and Balbi, A. and Borrill, J. and Cantalupo, C. and Doré, O. and Keihänen, E. and Lawrence, C. R. and Maino, D. and Natoli, P. and Prunet, S. and Stompor, R. and Teyssier, R. }, title = {Comparison of map-making algorithms for CMB experiments}, journal = {A&A}, eprint = {arXiv:astro-ph/0501504}, keywords = {methods: data analysis, cosmology: cosmic microwave background}, year = {2006}, month = {apr}, volume = {449}, pages = {1311-1322}, doi = {10.1051/0004-6361:20052845}, adsurl = {http://adsabs.harvard.edu/abs/2006A%26A…449.1311P}, adsnote = {Provided by the SAO/NASA Astrophysics Data System} }

1. pratt1978 bibtex=@BOOK{pratt1978,

author = {Pratt, W. K.}, title = {Digital image processing}, booktitle = {A Wiley-Interscience Publication, New York: Wiley, 1978}, year = {1978}, editor = {Pratt, W. K.}, adsurl = {http://adsabs.harvard.edu/abs/1978dip..book.....P}, adsnote = {Provided by the SAO/NASA Astrophysics Data System} }

1. prunet2001 bibtex=@ARTICLE{prunet2001,

author = {Prunet, S. and Ade, P. A. R. and Bock, J. J. and Bond, J. R. and Borrill, J. and Boscaleri, A. and Coble, K. and Crill, B. P. and de Bernardis, P. and De Gasperis, G. and De Troia, G. and Farese, P. C. and Ferreira, P. G. and Ganga, K. and Giacometti, M. and Hivon, E. and Hristov, V. V. and Iacoangeli, A. and Jaffe, A. H. and Lange, A. E. and Martinis, L. and Masi, S. and Mason, P. and Mauskopf, P. D. and Melchiorri, A. and Miglio, L. and Montroy, T. and Netterfield, C. B. and Pascale, E. and Piacentini, F. and Pogosyan, D. and Pongetti, F. and Prunet, S. and Rao, S. and Romeo, G. and Ruhl, J. E. and Scaramuzzi, F. and Sforna, D. and Vittorio, N.}, title = {Noise estimation in CMB time-streams and fast map-making. Application to the BOOMERanG98 data}, journal = {ArXiv Astrophysics e-prints}, eprint = {arXiv:astro-ph/0101073}, keywords = {Astrophysics}, year = {2001}, month = {jan}, adsurl = {http://adsabs.harvard.edu/abs/2001astro.ph..1073P}, adsnote = {Provided by the SAO/NASA Astrophysics Data System} }

1. shoemake1985 bibtex=@inproceedings{shoemake1985,

author = Shoemake, Ken, title = {Animating rotation with quaternion curves}, booktitle = {SIGGRAPH '85: Proceedings of the 12th annual conference on Computer graphics and interactive techniques}, year = {1985}, isbn = {0-89791-166-0}, pages = {245--254}, doi = {http://doi.acm.org/10.1145/325334.325242}, publisher = {ACM}, address = {New York, NY, USA}, }

1. shuster1993 bibtex=@ARTICLE{shuster1993,

author = {Shuster, M. D.}, title = {Survey of attitude representations}, journal = {Journal of the Astronautical Sciences}, keywords = {ATTITUDE CONTROL, FLIGHT MECHANICS, KINEMATIC EQUATIONS, SATELLITE ORIENTATION, SATELLITE ROTATION, COVARIANCE, ERRORS, KINEMATICS, TRANSFORMATIONS (MATHEMATICS)}, year = {1993}, month = {oct}, volume = {41}, pages = {439-517}, adsurl = {http://adsabs.harvard.edu/abs/1993JAnSc..41..439S}, adsnote = {Provided by the SAO/NASA Astrophysics Data System} }

1. swinyard2010 bibtex=@ARTICLE{swinyard2010,

author = {Swinyard, B. M. and Hartogh, P. and Sidher, S. and Fulton, T. and Lellouch, E. and Jarchow, C. and Griffin, M. J. and Moreno, R. and Sagawa, H. and Portyankina, G. and Blecka, M. and Banaszkiewicz, M. and Bockelee-Morvan, D. and Crovisier, J. and Encrenaz, T. and Kueppers, M. and Lara, L. and Lis, D. and Medvedev, A. and Rengel, M. and Szutowicz, S. and Vandenbussche, B. and Bensch, F. and Bergin, E. and Billebaud, F. and Biver, N. and Blake, G. and Blommaert, J. and de Val-Borro, M. and Cernicharo, J. and Cavalie, T. and Courtin, R. and Davis, G. and Decin, L. and Encrenaz, P. and de Graauw, T. and Jehin, E. and Kidger, M. and Leeks, S. and Orton, G. and Naylor, D. and Schieder, R. and Stam, D. and Thomas, N. and Verdugo, E. and Waelkens, C. and Walker, H.}, title = {The Herschel-SPIRE submillimetre spectrum of Mars}, journal = {A&A}, archivePrefix = {arXiv}, eprint = {1005.4579}, primaryClass = {astro-ph.EP}, keywords = {instrumentation: spectrographs, space vehicles: instruments, planets and satellites: atmospheres, planets and satellites: individual: Mars, planets and satellites: composition}, year = {2010}, month = {jul}, volume = {518}, pages = {L151+}, doi = {10.1051/0004-6361/201014717}, adsurl = {http://adsabs.harvard.edu/abs/2010A%26A...518L.151S}, adsnote = {Provided by the SAO/NASA Astrophysics Data System} }

1. carvalho2009 bibtex=@ARTICLE{carvalho2009,

author = {Carvalho, P. and Rocha, G. and Hobson, M. P.}, title = {A fast Bayesian approach to discrete object detection in astronomical data sets - PowellSnakes I}, journal = {MNRAS}, archivePrefix = {arXiv}, eprint = {0802.3916}, keywords = {methods: data analysis , cosmic microwave background , cosmology: observations}, year = {2009}, month = {mar}, volume = {393}, pages = {681-702}, doi = {10.1111/j.1365-2966.2008.14016.x}, adsurl

= {http:/ / adsabs. harvard. edu/ abs/ 2009MNRAS. 393. . 681C}, adsnote = {Provided by the SAO/NASA Astrophysics Data System} }

1. colombi2009 bibtex=@ARTICLE{colombi2009,

author = {Colombi, S. and Jaffe, A. and Novikov, D. and Pichon, C. }, title = {Accurate estimators of power spectra in N-body simulations}, journal = {MNRAS}, archivePrefix = {arXiv}, eprint = {0811.0313}, keywords = {methods: analytical , methods: data analysis , methods: N-body simulations , methods: numerical , methods: statistical , large-scale structure of Universe}, year = {2009}, month = {feb}, volume = {393}, pages = {511-526}, doi = {10.1111/j.1365-2966.2008.14176.x}, adsurl = {http://cdsads.u-strasbg.fr/abs/2009MNRAS.393..511C}, adsnote = {Provided by the SAO/NASA Astrophysics Data System} }

1. dame2001 bibtex=@ARTICLE{dame2001,

author = {Dame, T. M. and Hartmann, D. and Thaddeus, P.}, title = {The Milky Way in Molecular Clouds: A New Complete CO Survey}, journal = {Ap}, eprint = {arXiv:astro-ph/0009217}, keywords = {Galaxy: Structure, ISM: Clouds, ISM: Molecules, Radio Lines: ISM, Galaxy: Solar Neighborhood, Stars: Formation}, year = {2001}, month = {feb}, volume = {547}, pages = {792-813}, doi = {10.1086/318388}, adsurl = {http://cdsads.u-strasbg.fr/abs/2001ApJ...547..792D}, adsnote = {Provided by the SAO/NASA Astrophysics Data System} }

1. ferreira2000 bibtex=@ARTICLE{ferreira2000,

author = {Ferreira, P. G. and Jaffe, A. H.}, title = {Simultaneous estimation of noise and signal in cosmic microwave background experiments}, journal = {MNRAS}, eprint = {arXiv:astro-ph/9909250}, keywords = {COSMIC MICROWAVE BACKGROUND}, year = {2000}, month = {feb}, volume = {312}, pages = {89-102}, doi = {10.1046/j.1365-8711.2000.03108.x}, url={http:/ / onlinelibrary. wiley. com/ doi/ 10. 1046/ j. 1365-8711. 2000. 03108. x/abstract} adsurl = {http://cdsads.u-strasbg.fr/abs/2000MNRAS.312…89F}, adsnote = {Provided by the SAO/NASA Astrophysics Data System} }

1. giorgini1996 bibtex=@INPROCEEDINGS{giorgini1996,

author = {Giorgini, J. D. and Yeomans, D. K. and Chamberlin, A. B. and Chodas, P. W. and Jacobson, R. A. and Keesey, M. S. and Lieske, J. H. and Ostro, S. J. and Standish, E. M. and Wimberly, R. N.}, title = {JPL's On-Line Solar System Data Service}, booktitle = {Bulletin of the American Astronomical Society}, year = {1996}, series = {Bulletin of the American Astronomical Society}, volume = {28}, month = {sep}, pages = {1158-+}, adsurl = {http:/ / ukads. nottingham. ac. uk/ abs/ 1996DPS. . . . 28. 2504G}, adsnote = {Provided by the SAO/NASA Astrophysics Data System} }

1. mitra2010 bibtex=@ARTICLE{mitra2010,

author = {Mitra, S. and Rocha, G. and Górski, K. M. and Huffenberger, K. M. and Eriksen, H. K. and Ashdown, M. A. J. and Lawrence, C. R. }, title = {Fast Pixel Space Convolution for Cosmic Microwave Background Surveys with Asymmetric Beams and Complex Scan Strategies: FEBeCoP}, journal = {Aps}, archivePrefix = {arXiv}, eprint = {1005.1929}, primaryClass = {astro-ph.CO}, keywords = {cosmic background radiation, methods: data analysis}, year = {2011}, month = {mar}, volume = {193}, pages = {5-+}, doi = {10.1088/0067-0049/193/1/5}, adsurl = {http://adsabs.harvard.edu/abs/2011ApJS..193....5M}, adsnote = {Provided by the SAO/NASA Astrophysics Data System} }

1. onishi2002 bibtex=@ARTICLE{onishi2002,

author = {Onishi, T. and Mizuno, A. and Kawamura, A. and Tachihara, K. and Fukui, Y.}, title = {A Complete Search for Dense Cloud Cores in Taurus}, journal = {Ap}, keywords = {ISM: Clouds, ISM: Individual: Name: Taurus Cloud Complex, ISM: Molecules, Radio Lines: ISM, Stars: Formation}, year = {2002}, month = {aug}, volume = {575}, pages = {950-973}, doi = {10.1086/341347}, adsurl = {http://cdsads.u-strasbg.fr/abs/2002ApJ...575..950O}, adsnote = {Provided by the SAO/NASA Astrophysics Data System} }

1. rocha2010a bibtex=@ARTICLE{rocha2010a,

author = {Rocha, G. and Pagano, L. and Górski, K. M. and Huffenberger, K. M. and Lawrence, C. R. and Lange, A. E.}, title = {Markov chain beam randomization: a study of the impact of PLANCK beam measurement errors on cosmological parameter estimation}, journal = {A&A}, archivePrefix = {arXiv}, eprint = {0907.5254}, primaryClass = {astro-ph.CO}, keywords = {cosmic microwave background, cosmology: observations, methods: data analysis}, year = {2010}, month = {apr}, volume = {513}, pages = {A23+}, doi = {10.1051/0004-6361/200913032}, adsurl = {http:/ / adsabs. harvard. edu/ abs/ 2010A%26A. . . 513A. . 23R}, adsnote = {Provided by the SAO/NASA Astrophysics Data System} }

1. rocha2010b bibtex=@ARTICLE{rocha2010b,

author = {Rocha, G. and Contaldi, C. R. and Colombo, L. P. L. and Bond, J. R. and Gorski, K. M. and Lawrence, C. R.}, title = {Performance of XFaster likelihood in real CMB experiments}, journal = {ArXiv e-prints}, archivePrefix = {arXiv}, eprint = {1008.4948}, primaryClass = {astro-ph.CO}, keywords = {Astrophysics - Cosmology and Extragalactic Astrophysics}, year = {2010}, month = {aug}, adsurl = {http:/ / adsabs. harvard. edu/ abs/ 2010arXiv1008.4948R}, adsnote = {Provided by the SAO/NASA Astrophysics Data System} }

1. spencer2010 bibtex=@ARTICLE{spencer2010,

author = {Spencer, L. D. and Naylor, D. A. and Swinyard, B. M.}, title = {Performance evaluation of the Herschel/SPIRE imaging Fourier transform spectrometer through ground-based measurements}, journal = {Measurement Science and Technology}, year = {2010}, month = {jun}, volume = {21}, number = {6}, pages = {065601-+}, doi = {10.1088/0957-0233/21/6/065601}, adsurl = {http://cdsads. u-strasbg. fr/ abs/ 2010MeScT. . 21f5601S}, adsnote = {Provided by the SAO/NASA Astrophysics Data System} }

1. widrow bibtex=@ARTICLE{widrow56,

author = {Widrow, B}, title = {A Study of Rough Amplitude Quantization by Means of Nyquist Sampling Theory}, journal = {IRE Transactions on Circuit Theory}, year = {1956}, month = {dec}, volume = {CT-3(4)}, number = {}, pages = {266-276, }

1. banta bibtex=@ARTICLE{1053732,

author={Banta, E.}, journal={Information Theory, IEEE Transactions on}, title={On the autocorrelation function of quantized signal plus noise}, year={1965}, month={jan}, volume={11}, number={1}, pages={ 114 - 117}, keywords={Autocorrelation;Entropy;Fourier series;Gaussian noise;Mutual information;Noise level;Quantum dots;Voltage; Correlation functions; Quantization (signal); Signal quantization;}, doi={10.1109/TIT.1965.1053732}, ISSN={0018-9448},}

</biblio>

Planck Collaboration

A pictorial overview of the major participating funding agencies and scientific institutes.

The Planck Scientific Collaboration consists of all the scientists which have contributed to the development of the Planck mission, and who participate in the scientific exploitation of the Planck data during the proprietary period, which nominally ends with the release of the scientific products to the community 3.5 yrs after launch, i.e. in January 2013. A complete database of all members of the Planck Collaboration can be searched online [1]. Each individual is a member of one or more among four Consortia of scientists:

- The LFI Consortium, Principal Investigator N. Mandolesi of the Istituto di Astrofisica Spaziale e Fisica Cosmica (Bologna, Italy);
- The HFI Consortium, Principal Investigator J.L. Puget of the Institut d'Astrophysique Spatiale (Orsay, France), and co-PI F.R. Bouchet of the Institut d'Astrophysique de Paris (Paris, France);
- The DK-Planck Consortium, led by H.U. Norgaard-Nielsen of the Danish National Space Institute (Copenhagen, Denmark);
- ESA's Planck Science Office, Project Scientist J. Tauber.

The Planck instruments, LFI and HFI were designed, built, tested and delivered to ESA by dedicated teams under the direction of the LFI and HFI Principal Investigators and Project Managers.

The ground operations of the Planck satellite are based on 4 geographically distributed centres:

- The Mission Operations Centre (MOC), located at ESA's Operations Centre in Darmstadt (Germany), is responsible for all aspects of flight control and of the health and safety of the Planck satellite, including both instruments. It plans and executes all necessary satellite activities, including instrument commanding requests by the instrument operations centres. MOC communicates with the satellite using ESA's 35-m antenna located in

New Norcia (Australia) over a daily 3-hour period, during which it uplinks a scheduled activity timeline which is autonomously executed by the satellite, and downlinks the science and housekeeping (HK) data acquired by the satellite during the past 24 hours. The downlinked data are transferred from New Norcia to the MOC over a period of typically 8 hours; at MOC they are put onto a data server from where they are retrieved by the two Data Processing Centres.

- The Planck Science Office (PSO), located at ESA's European Space Astronomy Centre in Madrid (Spain) is responsible for coordinating scientific operations of the Planck instruments, and for planning the sky surveying strategy. It provides to MOC a detailed pointing plan with a periodicity of about 1 month. PSO also develops and operates the archive which stores and distribute the final scientific products to the community.
- The LFI Operations and Data Processing Centre, located at the Osservatorio Astronomico di Trieste (Italy), is responsible for the optimal operation of the LFI instrument, and for the processing of the data acquired by LFI into the final scientific products of the mission.
- The HFI Operations and Data Processing Centres, located respectively at the Institut d'Astrophysique Spatiale in Orsay (France) and at the Institut d'Astrophysique de Paris (France), are similarly responsible for the optimal operation of the HFI instrument, and (with several other institutes in France and the UK) for the processing of the data acquired by HFI into the final scientific products of the mission.

The Planck Science Team (see membership [2]) is a formal body set up by ESA at the inception of the project to represent the scientific interests of the mission, which has had a key advisory role to the development of the satellite, payload and ground segment. It is a recognised principle of the mission that the scientific exploitation of Planck during the proprietary period is a joint venture between the involved Consortia, and the Science Team is the body which has taken the role to organise, plan, coordinate, and oversee all the common activities in this respect. All members of the Planck Scientific Collaboration have agreed to abide by the policies set by the Science Team with regard to data access and publication of scientific results.

The scientific activities of the Planck Collaboration within the proprietary period are organised in "Projects", which consist of teams of people who are responsible to write papers on specific scientific topics on behalf of the whole Collaboration. "Working groups" gather Projects in similar areas. Coordinators of Working Groups and Leaders of Projects are nominated by the Planck Science Team. Papers by the Planck Collaboration are based on the scientific programme described in the Planck Bluebook; their authorship is extensive and ordered alphabetically. Individual members who have made important contributions to Planck over many years are referred to as "Planck Scientists" and have the right to co-author all these papers. Other members of the Planck Collaboration are referred to as "Planck Associates" and have the right to co-author papers to which they have contributed. Papers describing technical aspects or very specialized science topics, are prepared by ad-hoc teams and have non-alphabetic author order.

An internal reviewing process ensures that scientific papers submitted for publication by the Planck Collaboration are consistent with each other and of high scientific quality. This process is led by an internal Editorial Board which is led by Planck's Survey Scientists and consists of senior members of the Planck Collaboration. The Editorial Board makes recommendations to the Planck Science Team on the readiness for submission of all Planck papers. The Science Team makes the final decisions.

Funding

Planck is a project of the European Space Agency - ESA - with instruments provided by two scientific Consortia funded by ESA member states (in particular the lead countries: France and Italy) with contributions from NASA (USA), and telescope reflectors provided in a collaboration between ESA and a scientific Consortium led and funded by Denmark.

ESA has managed the project since its inception in 1993 and funded the development of the satellite, its launch, and its operations.

The Planck LFI project (including instrument development and operation, data processing and scientific analysis) is developed by an international consortium led by Italy and involving Canada, Finland, Germany, Norway, Spain, Switzerland, UK, and USA. The Italian contribution is funded by the Italian Space Agency (ASI) and INAF.

The Planck HFI instrument and associated Data Processing Centre were designed, built, and are operated by an international consortium of laboratories, universities and institutes, with important contributions from industry, under the leadership of the PI institute, the Institut d'Astrophysique Spatiale at Orsay, France. The instrument and associated Data Processing Centre are funded in particular by CNES, CNRS, NASA, STFC, and ASI.

The reflectors of Planck's telescope were developed by a collaboration between ESA and a scientific Consortium (DK-Planck) led and funded by Denmark.

The Planck Collaboration acknowledges the support of: ESA; CNES and CNRS/INSU-IN2P3-INP (France); ASI, CNR, and INAF (Italy); NASA and DoE (USA); STFC and UKSA (UK); CSIC, MICINN and JA (Spain); Tekes, AoF and CSC (Finland); DLR and MPG (Germany); CSA (Canada); DTU Space (Denmark); SER/SSO (Switzerland); RCN (Norway); SFI (Ireland); FCT/MCTES (Portugal); and DEISA (EU).

- European Space Agency [3]
- France
  - CNES [4]: Centre National des Etudes Spatiales
  - CNRS/INSU-IN2P3-INP: Centre National de la Recherche Scientifique/ Institut National des Sciences de l'Univers- Institut National de Physique Nucleaire et de Physique des Particules- Institut National Polytechnique
- Italy
  - ASI: Agenzia Spaziale Italiana
  - CNR: Consiglio Nazionale della Ricerca
  - INAF: Istituto Nazionale di Astrofisica
- United States of America
  - NASA: National Air and Space Administration
  - DoE: Department of Energy
- United Kingdom
  - STFC: Science and Technology Facilities Council
  - UKSA: UK Space Agency
- Spain
  - CSIC: Consejo Superior de Investigaciones Cientificas
  - MICINN: Ministerio de Ciencia e Innovacion
  - JA: Junta de Andalucia
- Finland
  - Tekes: Finnish Funding Agency for Technology and Innovation
  - AoF: Academy of Finland
  - CSC - IT Center for Science
- Germany

  - DLR: Deutsches Zentrum fuer Luft- und Raumfahrt
  - MPG: Max-Planck-Gesellschaft zur Foerderung der Wissenschaften
- Canada
  - CSA: Canadian Space Agency
- Denmark
  - DTU Space: Danmarks Tekniske Universitet/Institut for Rumforskning og-teknologi
- Switzerland
  - SER/SSO: State Secretariat for Education and Research/Swiss Space Office
- Norway
  - RCN: Research Council of Norway
  - NSC: Norwegian Space Centre
- Ireland
  - SFI: Science Foundation Ireland
- Portugal
  - FCT/MCTES: Fundacao para a Ciencia e a Tecnologia/ Ministerio da Ciencia, Tecnologia e Ensino Superior
- European Union
  - DEISA: Distributed European Infrastructure for Supercomputing Applications

References

[1] http://www.rssd.esa.int/index.php?project=IDIS&page=people

[2] http://www.rssd.esa.int/index.php?project=PLANCK&page=Science_Team

[3] http://www.esa.int

[4] http://www.cnes.fr

Article Sources and Contributors

Main Page *Source*: http://www.sciops.esa.int/wikiSI/planckpla/index.php?oldid=4928 *Contributors*: Acoulais, Agregori, Amennell, Amoneti, Azacchei, Dmaino, Ekeihane, Fbouchet, Jvalivii, Kganga, Lmendes, Lspencer, Lvibert, MediaWiki default, Mfrailis, Rbailey, Rleonard, Xdupac

The Planck mission *Source*: http://www.sciops.esa.int/wikiSI/planckpla/index.php?oldid=3558 *Contributors*: Lmendes

The satellite *Source*: http://www.sciops.esa.int/wikiSI/planckpla/index.php?oldid=3614 *Contributors*: Lmendes, Rleonard

The service module *Source*: http://www.sciops.esa.int/wikiSI/planckpla/index.php?oldid=3616 *Contributors*: Lmendes, Rleonard

Thermal design *Source*: http://www.sciops.esa.int/wikiSI/planckpla/index.php?oldid=3653 *Contributors*: Lmendes, Rleonard

HFI design, qualification, and performance *Source*: http://www.sciops.esa.int/wikiSI/planckpla/index.php?oldid=4737 *Contributors*: Acoulais, Bcrill, Fpajot, Fpiacent, Jlamarre, Kganga, Lmendes, Lspencer, Lvibert

HFI cryogenics *Source*: http://www.sciops.esa.int/wikiSI/planckpla/index.php?oldid=4738 *Contributors*: Fpajot, Lmendes, Lvibert

HFI cold optics *Source*: http://www.sciops.esa.int/wikiSI/planckpla/index.php?oldid=4739 *Contributors*: Jlamarre, Lmendes, Lspencer, Lvibert

HFI detection chain *Source*: http://www.sciops.esa.int/wikiSI/planckpla/index.php?oldid=4740 *Contributors*: Jhaissin, Jlamarre, Lmendes, Lvibert, Splaszcz

HFI time response model *Source*: http://www.sciops.esa.int/wikiSI/planckpla/index.php?oldid=4741 *Contributors*: Jlamarre, Lmendes, Lvibert

HFI operations *Source*: http://www.sciops.esa.int/wikiSI/planckpla/index.php?oldid=4743 *Contributors*: Lmendes, Lvibert

HFI perfsummary *Source*: http://www.sciops.esa.int/wikiSI/planckpla/index.php?oldid=4744 *Contributors*: Lmendes

HFI inst annexes *Source*: http://www.sciops.esa.int/wikiSI/planckpla/index.php?oldid=4745 *Contributors*: Lmendes, Lspencer, Lvibert

HFIspecEFF *Source*: http://www.sciops.esa.int/wikiSI/planckpla/index.php?oldid=4596 *Contributors*: Lspencer

HFIspecBREF *Source*: http://www.sciops.esa.int/wikiSI/planckpla/index.php?oldid=4611 *Contributors*: Lspencer

HFIspecFT *Source*: http://www.sciops.esa.int/wikiSI/planckpla/index.php?oldid=4608 *Contributors*: Lspencer

HFIspecWG *Source*: http://www.sciops.esa.int/wikiSI/planckpla/index.php?oldid=3919 *Contributors*: Lspencer

HFIspecCOtable *Source*: http://www.sciops.esa.int/wikiSI/planckpla/index.php?oldid=3925 *Contributors*: Lspencer

HFI data compression *Source*: http://www.sciops.esa.int/wikiSI/planckpla/index.php?oldid=4638 *Contributors*: Lvibert

HFI operations timeline *Source*: http://www.sciops.esa.int/wikiSI/planckpla/index.php?oldid=4986 *Contributors*: Lvibert

LFI design, qualification, and performance *Source*: http://www.sciops.esa.int/wikiSI/planckpla/index.php?oldid=5023 *Contributors*: Agregori, Lmendes

LFIAppendix *Source*: http://www.sciops.esa.int/wikiSI/planckpla/index.php?oldid=5028 *Contributors*: Agregori, Lmendes

The telescope *Source*: http://www.sciops.esa.int/wikiSI/planckpla/index.php?oldid=4747 *Contributors*: Lmendes, Rleonard

The standard radiation environment monitor *Source*: http://www.sciops.esa.int/wikiSI/planckpla/index.php?oldid=1888 *Contributors*: Lmendes, Xdupac

The fiber optic gyro unit *Source*: http://www.sciops.esa.int/wikiSI/planckpla/index.php?oldid=3111 *Contributors*: Lmendes, Rleonard

Ground segment overview *Source*: http://www.sciops.esa.int/wikiSI/planckpla/index.php?oldid=4233 *Contributors*: Lmendes, Xdupac

Contingencies *Source*: http://www.sciops.esa.int/wikiSI/planckpla/index.php?oldid=4235 *Contributors*: Lmendes, Rleonard

Operational history *Source*: http://www.sciops.esa.int/wikiSI/planckpla/index.php?oldid=4236 *Contributors*: Lmendes, Rleonard

Survey scanning and performance *Source*: http://www.sciops.esa.int/wikiSI/planckpla/index.php?oldid=4237 *Contributors*: Lmendes, Xdupac

Thermal environment *Source*: http://www.sciops.esa.int/wikiSI/planckpla/index.php?oldid=4238 *Contributors*: Lmendes, Rleonard

Radiation environment *Source*: http://www.sciops.esa.int/wikiSI/planckpla/index.php?oldid=4239 *Contributors*: Lmendes

Pointing performance *Source*: http://www.sciops.esa.int/wikiSI/planckpla/index.php?oldid=4240 *Contributors*: Lmendes, Xdupac

Data flow overview *Source*: http://www.sciops.esa.int/wikiSI/planckpla/index.php?oldid=4245 *Contributors*: Lmendes, Rleonard

On-board processing *Source*: http://www.sciops.esa.int/wikiSI/planckpla/index.php?oldid=4246 *Contributors*: Lmendes

MOC data transfer and storage *Source*: http://www.sciops.esa.int/wikiSI/planckpla/index.php?oldid=4247 *Contributors*: Lmendes, Rleonard

The HFI DPC *Source*: http://www.sciops.esa.int/wikiSI/planckpla/index.php?oldid=4308 *Contributors*: Amoneti, Fbouchet, Fdesert, Kganga, Lmendes, Lspencer, Lvibert

Pre-processing *Source*: http://www.sciops.esa.int/wikiSI/planckpla/index.php?oldid=4291 *Contributors*: Amoneti, Lmendes, Lvibert

TOI processing *Source*: http://www.sciops.esa.int/wikiSI/planckpla/index.php?oldid=4698 *Contributors*: Amoneti, Crenault, Fdesert, Lmendes, Lsanselm

Pointing&Beams *Source*: http://www.sciops.esa.int/wikiSI/planckpla/index.php?oldid=4802 *Contributors*: Ajaffe, Bcrill, Ehivon, Fbouchet, Fpajot, Lmendes

Map-making *Source*: http://www.sciops.esa.int/wikiSI/planckpla/index.php?oldid=4562 *Contributors*: Amoneti, Fdesert, Kganga, Lmendes, Operdere, Xdupac

Spectral response *Source*: http://www.sciops.esa.int/wikiSI/planckpla/index.php?oldid=4435 *Contributors*: Amoneti, Lmendes, Lspencer

HFI-Validation *Source*: http://www.sciops.esa.int/wikiSI/planckpla/index.php?oldid=4725 *Contributors*: Fbouchet, Kganga, Lmendes, Lmontier, Lvibert, Stechene

PowerSpectra *Source*: http://www.sciops.esa.int/wikiSI/planckpla/index.php?oldid=4305 *Contributors*: Ehivon, Fbouchet, Lmendes

Summary of HFI data characteristics *Source*: http://www.sciops.esa.int/wikiSI/planckpla/index.php?oldid=4307 *Contributors*: Lmendes, Lvibert

The LFI DPC *Source*: http://www.sciops.esa.int/wikiSI/planckpla/index.php?oldid=4258 *Contributors*: Azacchei, Lmendes

Pre-processing LFI *Source*: http://www.sciops.esa.int/wikiSI/planckpla/index.php?oldid=3051 *Contributors*: Mfrailis

TOI processing LFI *Source*: http://www.sciops.esa.int/wikiSI/planckpla/index.php?oldid=4310 *Contributors*: Lmendes, Pleahy, Pmeinhol, Sgaleott

TOI-Noise LFI *Source*: http://www.sciops.esa.int/wikiSI/planckpla/index.php?oldid=2547 *Contributors*: Dmaino

Pointing LFI *Source*: http://www.sciops.esa.int/wikiSI/planckpla/index.php?oldid=4729 *Contributors*: Lmendes, Sgaleott

Beams LFI *Source*: http://www.sciops.esa.int/wikiSI/planckpla/index.php?oldid=4949 *Contributors*: Agregori, Fvilla, Lmendes

Map-making LFI *Source*: http://www.sciops.esa.int/wikiSI/planckpla/index.php?oldid=4630 *Contributors*: Assirvio, Azacchei, Ekeihane, Hkurkis, Jvalivii, Lmendes

LFI systematic effect uncertainties *Source*: http://www.sciops.esa.int/wikiSI/planckpla/index.php?oldid=4317 *Contributors*: Agregori, Lmendes

LFI-Validation *Source*: http://www.sciops.esa.int/wikiSI/planckpla/index.php?oldid=4319 *Contributors*: Dmaino, Lmendes

L3 LFI *Source*: http://www.sciops.esa.int/wikiSI/planckpla/index.php?oldid=4748 *Contributors*: Agregori, Lmendes

Summary LFI *Source*: http://www.sciops.esa.int/wikiSI/planckpla/index.php?oldid=4749 *Contributors*: Lmendes

HFI/LFI joint data processing *Source*: http://www.sciops.esa.int/wikiSI/planckpla/index.php?oldid=4263 *Contributors*: Fbouchet, Joagonza, Lmendes

Compact Source catalogues *Source*: http://www.sciops.esa.int/wikiSI/planckpla/index.php?oldid=4930 *Contributors*: Joagonza, Lmendes

CMB map cleaning from foreground emissions *Source*: http://www.sciops.esa.int/wikiSI/planckpla/index.php?oldid=4323 *Contributors*: Fbouchet, Lmendes

C2 *Source*: http://www.sciops.esa.int/wikiSI/planckpla/index.php?oldid=4732 *Contributors*: Fbouchet, Lmendes

HL-sims *Source*: http://www.sciops.esa.int/wikiSI/planckpla/index.php?oldid=4750 *Contributors*: Fbouchet, Lmendes

Science *Source*: http://www.sciops.esa.int/wikiSI/planckpla/index.php?oldid=4947 *Contributors*: Fbouchet, Fdesert, Jmacias, Lmendes, Lvibert, Mmiville

Planck Legacy Archive *Source*: http://www.sciops.esa.int/wikiSI/planckpla/index.php?oldid=3421 *Contributors*: Lmendes, Xdupac

Mission science products *Source*: http://www.sciops.esa.int/wikiSI/planckpla/index.php?oldid=4757 *Contributors*: Amoneti, Lmendes

Timelines *Source*: http://www.sciops.esa.int/wikiSI/planckpla/index.php?oldid=4756 *Contributors*: Amoneti, Lmendes

Frequency Maps *Source*: http://www.sciops.esa.int/wikiSI/planckpla/index.php?oldid=5033 *Contributors*: Agregori, Amoneti, Assirvio, Azacchei, Crenault, Ekeihane, Fdesert, Lmendes, Operdere

The RIMO *Source*: http://www.sciops.esa.int/wikiSI/planckpla/index.php?oldid=5053 *Contributors*: Amoneti, Lmendes, Lspencer

Effective Beams *Source*: http://www.sciops.esa.int/wikiSI/planckpla/index.php?oldid=4784 *Contributors*: Agregori, Lmendes

Catalogues *Source*: http://www.sciops.esa.int/wikiSI/planckpla/index.php?oldid=5032 *Contributors*: Agregori, Amoneti, Joagonza, Lmendes, Lvibert, Mashdown, Xdupac

Catalogues ERCSC *Source*: http://www.sciops.esa.int/wikiSI/planckpla/index.php?oldid=3725 *Contributors*: Crangara

Frequency maps angular power spectra *Source*: http://www.sciops.esa.int/wikiSI/planckpla/index.php?oldid=5042 *Contributors*: Fbouchet, Gpolenta, Lmendes

Astrophysical component maps *Source*: http://www.sciops.esa.int/wikiSI/planckpla/index.php?oldid=4982 *Contributors*: Agregori, Amoneti, Cbacciga, Fdesert, Lmendes, Mmiville

CMB spectrum & Likelihood Code *Source*: http://www.sciops.esa.int/wikiSI/planckpla/index.php?oldid=4765 *Contributors*: Agregori, Fbouchet, Lmendes, Mfreschi

Cosmological Parameters *Source*: http://www.sciops.esa.int/wikiSI/planckpla/index.php?oldid=5039 *Contributors*: Agregori, Amoneti, Lmendes

Specially processed maps *Source*: http://www.sciops.esa.int/wikiSI/planckpla/index.php?oldid=4993 *Contributors*: Agregori, Amoneti, Lmendes

Additional angular power spectra *Source*: http://www.sciops.esa.int/wikiSI/planckpla/index.php?oldid=4775 *Contributors*: Agregori, Amoneti, Fbouchet, Lmendes

Additional Science products *Source*: http://www.sciops.esa.int/wikiSI/planckpla/index.php?oldid=2564 *Contributors*: Lmendes

Scientific data used to generate Planck products *Source*: http://www.sciops.esa.int/wikiSI/planckpla/index.php?oldid=4777 *Contributors*: Lmendes

Simulation data *Source*: http://www.sciops.esa.int/wikiSI/planckpla/index.php?oldid=4779 *Contributors*: Agregori, Lmendes

Survey history *Source*: http://www.sciops.esa.int/wikiSI/planckpla/index.php?oldid=4780 *Contributors*: Lmendes, Rleonard, Xdupac

Satellite history *Source*: http://www.sciops.esa.int/wikiSI/planckpla/index.php?oldid=3418 *Contributors*: Lmendes, Xdupac

Payload design *Source*: http://www.sciops.esa.int/wikiSI/planckpla/index.php?oldid=2581 *Contributors*: Lmendes

Instrument performance *Source*: http://www.sciops.esa.int/wikiSI/planckpla/index.php?oldid=2583 *Contributors*: Lmendes

Telescope *Source*: http://www.sciops.esa.int/wikiSI/planckpla/index.php?oldid=2584 *Contributors*: Lmendes

Thermal *Source*: http://www.sciops.esa.int/wikiSI/planckpla/index.php?oldid=3415 *Contributors*: Lmendes, Xdupac

FOG *Source*: http://www.sciops.esa.int/wikiSI/planckpla/index.php?oldid=3422 *Contributors*: Lmendes, Xdupac

Software utilities *Source*: http://www.sciops.esa.int/wikiSI/planckpla/index.php?oldid=3939 *Contributors*: Lmendes, Lspencer, Mpeel, Xdupac

Appendix *Source*: http://www.sciops.esa.int/wikiSI/planckpla/index.php?oldid=3300 *Contributors*: Lmendes, Lspencer

Glossary *Source*: http://www.sciops.esa.int/wikiSI/planckpla/index.php?oldid=4980 *Contributors*: Bcrill, Lmendes, Lvibert, Rleonard

Acronym list *Source*: http://www.sciops.esa.int/wikiSI/planckpla/index.php?oldid=3369 *Contributors*: Bcrill, Lmendes, Lvibert, Rleonard

References *Source*: http://www.sciops.esa.int/wikiSI/planckpla/index.php?oldid=4019 *Contributors*: Lmendes, Splaszcz

Planck Collaboration *Source*: http://www.sciops.esa.int/wikiSI/planckpla/index.php?oldid=1719 *Contributors*: Rleonard, Xdupac

Image Sources, Licenses and Contributors

file:Planck_Logos.jpg *Source*: http://www.sciops.esa.int/wikiSI/planckpla/index.php?title=File:Planck_Logos.jpg *License*: unknown *Contributors*: Rleonard

file:PlanckMissionTimeline.JPG *Source*: http://www.sciops.esa.int/wikiSI/planckpla/index.php?title=File:PlanckMissionTimeline.JPG *License*: unknown *Contributors*: Xdupac

file:HerschelPlanckLaunch.jpg *Source*: http://www.sciops.esa.int/wikiSI/planckpla/index.php?title=File:HerschelPlanckLaunch.jpg *License*: unknown *Contributors*: Xdupac

file:PLANCK_HERSCHEL_LAUNCH.jpg *Source*: http://www.sciops.esa.int/wikiSI/planckpla/index.php?title=File:PLANCK_HERSCHEL_LAUNCH.jpg *License*: unknown *Contributors*: Xdupac

file:Cooldown.jpg *Source*: http://www.sciops.esa.int/wikiSI/planckpla/index.php?title=File:Cooldown.jpg *License*: unknown *Contributors*: Xdupac

File:381-Herschel_reflection_in_Primary_Reflector_H.jpg *Source*: http://www.sciops.esa.int/wikiSI/planckpla/index.php?title=File:381-Herschel_reflection_in_Primary_Reflector_H.jpg *License*: unknown *Contributors*: Rleonard

Image:HFI_horns.jpg *Source*: http://www.sciops.esa.int/wikiSI/planckpla/index.php?title=File:HFI_horns.jpg *License*: unknown *Contributors*: Lvibert

Image:HFI_2_4_1_JML_SignalFormation.png *Source*: http://www.sciops.esa.int/wikiSI/planckpla/index.php?title=File:HFI_2_4_1_JML_SignalFormation.png *License*: unknown *Contributors*: Acoulais

Image:HFI_2_4_1_overal_cryo.jpg *Source*: http://www.sciops.esa.int/wikiSI/planckpla/index.php?title=File:HFI_2_4_1_overal_cryo.jpg *License*: unknown *Contributors*: Fpajot

Image:HFI_2_4_1_JML_FeedHorns.png *Source*: http://www.sciops.esa.int/wikiSI/planckpla/index.php?title=File:HFI_2_4_1_JML_FeedHorns.png *License*: unknown *Contributors*: Acoulais

Image:HFI_2_4_1_JML_beam.png *Source*: http://www.sciops.esa.int/wikiSI/planckpla/index.php?title=File:HFI_2_4_1_JML_beam.png *License*: unknown *Contributors*: Acoulais

Image:HFI_2_4_1_JML_PowerDiff.png *Source*: http://www.sciops.esa.int/wikiSI/planckpla/index.php?title=File:HFI_2_4_1_JML_PowerDiff.png *License*: unknown *Contributors*: Acoulais

Image:HFI_2_4_1_JML_FarField.png *Source*: http://www.sciops.esa.int/wikiSI/planckpla/index.php?title=File:HFI_2_4_1_JML_FarField.png *License*: unknown *Contributors*: Acoulais

Image:HFI_2_4_1_JML_FarField2.png *Source*: http://www.sciops.esa.int/wikiSI/planckpla/index.php?title=File:HFI_2_4_1_JML_FarField2.png *License*: unknown *Contributors*: Acoulais

File:HFI_FilterPlots_100GHz.png *Source*: http://www.sciops.esa.int/wikiSI/planckpla/index.php?title=File:HFI_FilterPlots_100GHz.png *License*: unknown *Contributors*: Lspencer

File:HFI_FilterPlots_143GHz.png *Source*: http://www.sciops.esa.int/wikiSI/planckpla/index.php?title=File:HFI_FilterPlots_143GHz.png *License*: unknown *Contributors*: Lspencer

File:HFI_FilterPlots_217GHz.png *Source*: http://www.sciops.esa.int/wikiSI/planckpla/index.php?title=File:HFI_FilterPlots_217GHz.png *License*: unknown *Contributors*: Lspencer

File:HFI_FilterPlots_353GHz.png *Source*: http://www.sciops.esa.int/wikiSI/planckpla/index.php?title=File:HFI_FilterPlots_353GHz.png *License*: unknown *Contributors*: Lspencer

File:HFI_FilterPlots_545GHz.png *Source*: http://www.sciops.esa.int/wikiSI/planckpla/index.php?title=File:HFI_FilterPlots_545GHz.png *License*: unknown *Contributors*: Lspencer

File:HFI_FilterPlots_857GHz.png *Source*: http://www.sciops.esa.int/wikiSI/planckpla/index.php?title=File:HFI_FilterPlots_857GHz.png *License*: unknown *Contributors*: Lspencer

Image:OOBstitch_bc00_Prad_Apod5_v302_sm.png *Source*: http://www.sciops.esa.int/wikiSI/planckpla/index.php?title=File:OOBstitch_bc00_Prad_Apod5_v302_sm.png *License*: unknown *Contributors*: Lspencer

Image:COflags_v300_sm.png *Source*: http://www.sciops.esa.int/wikiSI/planckpla/index.php?title=File:COflags_v300_sm.png *License*: unknown *Contributors*: Lspencer

Image:COJ10_HFI100_SpecTrans_v300_Apod5_sm.png *Source*: http://www.sciops.esa.int/wikiSI/planckpla/index.php?title=File:COJ10_HFI100_SpecTrans_v300_Apod5_sm.png *License*: unknown *Contributors*: Lspencer

Image:HFI_2_4_1_FPiacentini_bolo1.png *Source*: http://www.sciops.esa.int/wikiSI/planckpla/index.php?title=File:HFI_2_4_1_FPiacentini_bolo1.png *License*: unknown *Contributors*: -

Image:HFI_2_4_1_FPiacentini_bolo2.png *Source*: http://www.sciops.esa.int/wikiSI/planckpla/index.php?title=File:HFI_2_4_1_FPiacentini_bolo2.png *License*: unknown *Contributors*: Acoulais

Image:HFI_2_4_1_FPiacentini_table1.png *Source*: http://www.sciops.esa.int/wikiSI/planckpla/index.php?title=File:HFI_2_4_1_FPiacentini_table1.png *License*: unknown *Contributors*: Acoulais

Image:HFI_2_4_1_FPiacentini_FocalPlaneLayout.png *Source*: http://www.sciops.esa.int/wikiSI/planckpla/index.php?title=File:HFI_2_4_1_FPiacentini_FocalPlaneLayout.png *License*: unknown *Contributors*: Acoulais

Image:HFI_2_4_1_FPiacentini_FocalPlaneGeo.png *Source*: http://www.sciops.esa.int/wikiSI/planckpla/index.php?title=File:HFI_2_4_1_FPiacentini_FocalPlaneGeo.png *License*: unknown *Contributors*: Acoulais

Image:HFI_2_4_1_FPiacentini_table2.jpeg *Source*: http://www.sciops.esa.int/wikiSI/planckpla/index.php?title=File:HFI_2_4_1_FPiacentini_table2.jpeg *License*: unknown *Contributors*: Acoulais

File:BREF_LowF_Apod5_avgSpec_SN_sm.png *Source*: http://www.sciops.esa.int/wikiSI/planckpla/index.php?title=File:BREF_LowF_Apod5_avgSpec_SN_sm.png *License*: unknown *Contributors*: Lspencer

File:BREF_HighF_Apod5_avgSpec_SN_sm.png *Source*: http://www.sciops.esa.int/wikiSI/planckpla/index.php?title=File:BREF_HighF_Apod5_avgSpec_SN_sm.png *License*: unknown *Contributors*: Lspencer

File:Bref_LowF_HighF_SN_sm.png *Source*: http://www.sciops.esa.int/wikiSI/planckpla/index.php?title=File:Bref_LowF_HighF_SN_sm.png *License*: unknown *Contributors*: Lspencer

File:BREF_LowF_Apod5_avgSpec_SN_100_sm.png *Source*: http://www.sciops.esa.int/wikiSI/planckpla/index.php?title=File:BREF_LowF_Apod5_avgSpec_SN_100_sm.png *License*: unknown *Contributors*: Lspencer

File:BREF_LowF_Apod5_avgSpec_SN_143_sm.png *Source*: http://www.sciops.esa.int/wikiSI/planckpla/index.php?title=File:BREF_LowF_Apod5_avgSpec_SN_143_sm.png *License*: unknown *Contributors*: Lspencer

File:BREF_LowF_Apod5_avgSpec_SN_217_sm.png *Source*: http://www.sciops.esa.int/wikiSI/planckpla/index.php?title=File:BREF_LowF_Apod5_avgSpec_SN_217_sm.png *License*: unknown *Contributors*: Lspencer

File:BREF_HighF_Apod5_avgSpec_SN_353_sm.png *Source*: http://www.sciops.esa.int/wikiSI/planckpla/index.php?title=File:BREF_HighF_Apod5_avgSpec_SN_353_sm.png *License*: unknown *Contributors*: Lspencer

File:BREF_HighF_Apod5_avgSpec_SN_545_sm.png *Source*: http://www.sciops.esa.int/wikiSI/planckpla/index.php?title=File:BREF_HighF_Apod5_avgSpec_SN_545_sm.png *License*: unknown *Contributors*: Lspencer

File:BREF_HighF_Apod5_avgSpec_SN_857_sm.png *Source*: http://www.sciops.esa.int/wikiSI/planckpla/index.php?title=File:BREF_HighF_Apod5_avgSpec_SN_857_sm.png *License*: unknown *Contributors*: Lspencer

Image:SNall_sm.png *Source*: http://www.sciops.esa.int/wikiSI/planckpla/index.php?title=File:SNall_sm.png *License*: unknown *Contributors*: Lspencer

File:PreRatioIFGM_bc00_Prad_Apod5_v300_sm.png *Source*: http://www.sciops.esa.int/wikiSI/planckpla/index.php?title=File:PreRatioIFGM_bc00_Prad_Apod5_v300_sm.png *License*: unknown *Contributors*: Lspencer

File:IFGM_Ls_ds.png *Source*: http://www.sciops.esa.int/wikiSI/planckpla/index.php?title=File:IFGM_Ls_ds.png *License*: unknown *Contributors*: Lspencer

Image:PreRatioSpec_bc00_Prad_Apod5_v300_avgSpec_SN_sm.png *Source*: http://www.sciops.esa.int/wikiSI/planckpla/index.php?title=File:PreRatioSpec_bc00_Prad_Apod5_v300_avgSpec_SN_sm.png *License*: unknown *Contributors*: Lspencer

Image:setting.png *Source*: http://www.sciops.esa.int/wikiSI/planckpla/index.php?title=File:Setting.png *License*: unknown *Contributors*: Splaszcz

Image:cl_DPU_217unlensed.png *Source*: http://www.sciops.esa.int/wikiSI/planckpla/index.php?title=File:Cl_DPU_217unlensed.png *License*: unknown *Contributors*: Splaszcz

File:LFI_schema.jpg *Source*: http://www.sciops.esa.int/wikiSI/planckpla/index.php?title=File:LFI_schema.jpg *License*: unknown *Contributors*: Agregori

File:schema.jpg *Source*: http://www.sciops.esa.int/wikiSI/planckpla/index.php?title=File:Schema.jpg *License*: unknown *Contributors*: Agregori

File:rca_schematic.jpg *Source*: http://www.sciops.esa.int/wikiSI/planckpla/index.php?title=File:Rca_schematic.jpg *License*: unknown *Contributors*: Agregori

File:phase_switch_operation.jpg *Source*: http://www.sciops.esa.int/wikiSI/planckpla/index.php?title=File:Phase_switch_operation.jpg *License*: unknown *Contributors*: Agregori

File:FUNCT_tests_schedule_vs_K-eps-converted-to.jpg *Source*: http://www.sciops.esa.int/wikiSI/planckpla/index.php?title=File:FUNCT_tests_schedule_vs_K-eps-converted-to.jpg *License*: unknown *Contributors*: Agregori

File:fh1.jpg *Source*: http://www.sciops.esa.int/wikiSI/planckpla/index.php?title=File:Fh1.jpg *License*: unknown *Contributors*: Agregori

File:fh2.jpg *Source*: http://www.sciops.esa.int/wikiSI/planckpla/index.php?title=File:Fh2.jpg *License*: unknown *Contributors*: Agregori

File:omt.jpg *Source*: http://www.sciops.esa.int/wikiSI/planckpla/index.php?title=File:Omt.jpg *License*: unknown *Contributors*: Agregori
File:fem1.jpg *Source*: http://www.sciops.esa.int/wikiSI/planckpla/index.php?title=File:Fem1.jpg *License*: unknown *Contributors*: Agregori
File:fembem70.jpg *Source*: http://www.sciops.esa.int/wikiSI/planckpla/index.php?title=File:Fembem70.jpg *License*: unknown *Contributors*: Agregori
File:bem1.jpg *Source*: http://www.sciops.esa.int/wikiSI/planckpla/index.php?title=File:Bem1.jpg *License*: unknown *Contributors*: Agregori
File:bem2.jpg *Source*: http://www.sciops.esa.int/wikiSI/planckpla/index.php?title=File:Bem2.jpg *License*: unknown *Contributors*: Agregori
File:4krl.jpg *Source*: http://www.sciops.esa.int/wikiSI/planckpla/index.php?title=File:4krl.jpg *License*: unknown *Contributors*: Agregori
File:4kload.jpg *Source*: http://www.sciops.esa.int/wikiSI/planckpla/index.php?title=File:4kload.jpg *License*: unknown *Contributors*: Agregori
File:4krl_t.jpg *Source*: http://www.sciops.esa.int/wikiSI/planckpla/index.php?title=File:4krl_t.jpg *License*: unknown *Contributors*: Agregori
File:OBS.jpg *Source*: http://www.sciops.esa.int/wikiSI/planckpla/index.php?title=File:OBS.jpg *License*: unknown *Contributors*: Agregori
File:compression.jpg *Source*: http://www.sciops.esa.int/wikiSI/planckpla/index.php?title=File:Compression.jpg *License*: unknown *Contributors*: Agregori
File:compr1.jpg *Source*: http://www.sciops.esa.int/wikiSI/planckpla/index.php?title=File:Compr1.jpg *License*: unknown *Contributors*: Agregori
File:compr2.jpg *Source*: http://www.sciops.esa.int/wikiSI/planckpla/index.php?title=File:Compr2.jpg *License*: unknown *Contributors*: Agregori
File:LFI_OpsMode.jpg *Source*: http://www.sciops.esa.int/wikiSI/planckpla/index.php?title=File:LFI_OpsMode.jpg *License*: unknown *Contributors*: Agregori
File:LFIfreq.jpg *Source*: http://www.sciops.esa.int/wikiSI/planckpla/index.php?title=File:LFIfreq.jpg *License*: unknown *Contributors*: Agregori
File:Colorcorr.jpg *Source*: http://www.sciops.esa.int/wikiSI/planckpla/index.php?title=File:Colorcorr.jpg *License*: unknown *Contributors*: Agregori
File:band1.jpg *Source*: http://www.sciops.esa.int/wikiSI/planckpla/index.php?title=File:Band1.jpg *License*: unknown *Contributors*: Agregori
File:band2.jpg *Source*: http://www.sciops.esa.int/wikiSI/planckpla/index.php?title=File:Band2.jpg *License*: unknown *Contributors*: Agregori
File:stability.jpg *Source*: http://www.sciops.esa.int/wikiSI/planckpla/index.php?title=File:Stability.jpg *License*: unknown *Contributors*: Agregori
File:Sensor_position.jpg *Source*: http://www.sciops.esa.int/wikiSI/planckpla/index.php?title=File:Sensor_position.jpg *License*: unknown *Contributors*: Agregori
File:Din_t1.jpg *Source*: http://www.sciops.esa.int/wikiSI/planckpla/index.php?title=File:Din_t1.jpg *License*: unknown *Contributors*: Agregori
File:Susc_t.jpg *Source*: http://www.sciops.esa.int/wikiSI/planckpla/index.php?title=File:Susc_t.jpg *License*: unknown *Contributors*: Agregori
file:ESOC.jpg *Source*: http://www.sciops.esa.int/wikiSI/planckpla/index.php?title=File:ESOC.jpg *License*: unknown *Contributors*: Xdupac
file:ESAC_6.JPG *Source*: http://www.sciops.esa.int/wikiSI/planckpla/index.php?title=File:ESAC_6.JPG *License*: unknown *Contributors*: Xdupac
file:GS.jpg *Source*: http://www.sciops.esa.int/wikiSI/planckpla/index.php?title=File:GS.jpg *License*: unknown *Contributors*: Xdupac
file:GSPlanck.JPG *Source*: http://www.sciops.esa.int/wikiSI/planckpla/index.php?title=File:GSPlanck.JPG *License*: unknown *Contributors*: Xdupac
file:FocalPlane.png *Source*: http://www.sciops.esa.int/wikiSI/planckpla/index.php?title=File:FocalPlane.png *License*: unknown *Contributors*: Rleonard
File:ScannStrategy.png *Source*: http://www.sciops.esa.int/wikiSI/planckpla/index.php?title=File:ScannStrategy.png *License*: unknown *Contributors*: Xdupac
File:Cycloidal_scanning.JPG *Source*: http://www.sciops.esa.int/wikiSI/planckpla/index.php?title=File:Cycloidal_scanning.JPG *License*: unknown *Contributors*: Xdupac
File:Crab_Nebula.jpg *Source*: http://www.sciops.esa.int/wikiSI/planckpla/index.php?title=File:Crab_Nebula.jpg *License*: unknown *Contributors*: Xdupac
File:Mars.jpg *Source*: http://www.sciops.esa.int/wikiSI/planckpla/index.php?title=File:Mars.jpg *License*: unknown *Contributors*: Xdupac
File:PlanckMissionTimeline.JPG *Source*: http://www.sciops.esa.int/wikiSI/planckpla/index.php?title=File:PlanckMissionTimeline.JPG *License*: unknown *Contributors*: Xdupac
file:PointingPerformance2011.JPG *Source*: http://www.sciops.esa.int/wikiSI/planckpla/index.php?title=File:PointingPerformance2011.JPG *License*: unknown *Contributors*: Xdupac
file:PointingPerformance2011latitude.JPG *Source*: http://www.sciops.esa.int/wikiSI/planckpla/index.php?title=File:PointingPerformance2011latitude.JPG *License*: unknown *Contributors*: Xdupac
file:PointingPerformanceCorrelation.jpg *Source*: http://www.sciops.esa.int/wikiSI/planckpla/index.php?title=File:PointingPerformanceCorrelation.jpg *License*: unknown *Contributors*: Xdupac
File:GroundSegment.png *Source*: http://www.sciops.esa.int/wikiSI/planckpla/index.php?title=File:GroundSegment.png *License*: unknown *Contributors*: Rleonard
File:HFI_4_4_1_deltatos.png *Source*: http://www.sciops.esa.int/wikiSI/planckpla/index.php?title=File:HFI_4_4_1_deltatos.png *License*: unknown *Contributors*: Lvibert
File:HFI_4_4_1_deltatoszoom.png *Source*: http://www.sciops.esa.int/wikiSI/planckpla/index.php?title=File:HFI_4_4_1_deltatoszoom.png *License*: unknown *Contributors*: Lvibert
File:HFI_4_4_1_ringduration.png *Source*: http://www.sciops.esa.int/wikiSI/planckpla/index.php?title=File:HFI_4_4_1_ringduration.png *License*: unknown *Contributors*: Lvibert
File:HFI_4_4_1_OBTUTC.png *Source*: http://www.sciops.esa.int/wikiSI/planckpla/index.php?title=File:HFI_4_4_1_OBTUTC.png *License*: unknown *Contributors*: Lvibert
File:10_143_5_PBR_10800RING_LFER4_JC.jpg *Source*: http://www.sciops.esa.int/wikiSI/planckpla/index.php?title=File:10_143_5_PBR_10800RING_LFER4_JC.jpg *License*: unknown *Contributors*: Fdesert
File:10_143_5_rcircles_LFER4_JC.jpg *Source*: http://www.sciops.esa.int/wikiSI/planckpla/index.php?title=File:10_143_5_rcircles_LFER4_JC.jpg *License*: unknown *Contributors*: Fdesert
File:10_143_5_fft_LFER4_JC.jpg *Source*: http://www.sciops.esa.int/wikiSI/planckpla/index.php?title=File:10_143_5_fft_LFER4_JC.jpg *License*: unknown *Contributors*: Fdesert
File:14_545_1_PBR_10800RING_LFER4_JC.jpg *Source*: http://www.sciops.esa.int/wikiSI/planckpla/index.php?title=File:14_545_1_PBR_10800RING_LFER4_JC.jpg *License*: unknown *Contributors*: Fdesert
File:14_545_1_rcircles_LFER4_JC.jpg *Source*: http://www.sciops.esa.int/wikiSI/planckpla/index.php?title=File:14_545_1_rcircles_LFER4_JC.jpg *License*: unknown *Contributors*: Fdesert
File:14_545_1_fft_LFER4_JC.jpg *Source*: http://www.sciops.esa.int/wikiSI/planckpla/index.php?title=File:14_545_1_fft_LFER4_JC.jpg *License*: unknown *Contributors*: Fdesert
File:baseline.jpg *Source*: http://www.sciops.esa.int/wikiSI/planckpla/index.php?title=File:Baseline.jpg *License*: unknown *Contributors*: Fdesert
File:figIntermPaperGR.jpg *Source*: http://www.sciops.esa.int/wikiSI/planckpla/index.php?title=File:FigIntermPaperGR.jpg *License*: unknown *Contributors*: Fdesert
File:group10_143_5.jpg *Source*: http://www.sciops.esa.int/wikiSI/planckpla/index.php?title=File:Group10_143_5.jpg *License*: unknown *Contributors*: Fdesert
File:group14_545_1.jpg *Source*: http://www.sciops.esa.int/wikiSI/planckpla/index.php?title=File:Group14_545_1.jpg *License*: unknown *Contributors*: Fdesert
File:T90.jpg *Source*: http://www.sciops.esa.int/wikiSI/planckpla/index.php?title=File:T90.jpg *License*: unknown *Contributors*: Fdesert
File:10_143_5_4Klines.jpg *Source*: http://www.sciops.esa.int/wikiSI/planckpla/index.php?title=File:10_143_5_4Klines.jpg *License*: unknown *Contributors*: Fdesert
File:14_545_1_4Klines.jpg *Source*: http://www.sciops.esa.int/wikiSI/planckpla/index.php?title=File:14_545_1_4Klines.jpg *License*: unknown *Contributors*: Fdesert
File:spinfreq1.jpg *Source*: http://www.sciops.esa.int/wikiSI/planckpla/index.php?title=File:Spinfreq1.jpg *License*: unknown *Contributors*: Fdesert
File:jump_exe.png *Source*: http://www.sciops.esa.int/wikiSI/planckpla/index.php?title=File:Jump_exe.png *License*: unknown *Contributors*: Fdesert
File:10_143_5_smooth_Watt.jpg *Source*: http://www.sciops.esa.int/wikiSI/planckpla/index.php?title=File:10_143_5_smooth_Watt.jpg *License*: unknown *Contributors*: Fdesert
File:14_545_1_smooth_Watt.jpg *Source*: http://www.sciops.esa.int/wikiSI/planckpla/index.php?title=File:14_545_1_smooth_Watt.jpg *License*: unknown *Contributors*: Fdesert
File:stddev_group10_143_5.jpg *Source*: http://www.sciops.esa.int/wikiSI/planckpla/index.php?title=File:Stddev_group10_143_5.jpg *License*: unknown *Contributors*: Fdesert
File:stddev_group_14_545_1.jpg *Source*: http://www.sciops.esa.int/wikiSI/planckpla/index.php?title=File:Stddev_group_14_545_1.jpg *License*: unknown *Contributors*: Fdesert
File:23_353_TwoLevel.jpg *Source*: http://www.sciops.esa.int/wikiSI/planckpla/index.php?title=File:23_353_TwoLevel.jpg *License*: unknown *Contributors*: Fdesert
File:HFI_4_4_2_RTSexample13.jpg *Source*: http://www.sciops.esa.int/wikiSI/planckpla/index.php?title=File:HFI_4_4_2_RTSexample13.jpg *License*: unknown *Contributors*: Fdesert
File:HFInominal_IntegrationTime.jpg *Source*: http://www.sciops.esa.int/wikiSI/planckpla/index.php?title=File:HFInominal_IntegrationTime.jpg *License*: unknown *Contributors*: Fdesert
File:SSOflag_10_143_5J.png *Source*: http://www.sciops.esa.int/wikiSI/planckpla/index.php?title=File:SSOflag_10_143_5J.png *License*: unknown *Contributors*: Crenault
File:SSOflag_10_143_5S.png *Source*: http://www.sciops.esa.int/wikiSI/planckpla/index.php?title=File:SSOflag_10_143_5S.png *License*: unknown *Contributors*: Crenault
File:SSOflag_10_143_5M.png *Source*: http://www.sciops.esa.int/wikiSI/planckpla/index.php?title=File:SSOflag_10_143_5M.png *License*: unknown *Contributors*: Crenault
File:SSOflag_10_143_5a.png *Source*: http://www.sciops.esa.int/wikiSI/planckpla/index.php?title=File:SSOflag_10_143_5a.png *License*: unknown *Contributors*: Crenault
File:SSOflag_25_857_1J.png *Source*: http://www.sciops.esa.int/wikiSI/planckpla/index.php?title=File:SSOflag_25_857_1J.png *License*: unknown *Contributors*: Crenault
File:SSOflag_25_857_1S.png *Source*: http://www.sciops.esa.int/wikiSI/planckpla/index.php?title=File:SSOflag_25_857_1S.png *License*: unknown *Contributors*: Crenault
File:SSOflag_25_857_1M.png *Source*: http://www.sciops.esa.int/wikiSI/planckpla/index.php?title=File:SSOflag_25_857_1M.png *License*: unknown *Contributors*: Crenault

File:SSOflag_25_857_1a.png *Source*: http://www.sciops.esa.int/wikiSI/planckpla/index.php?title=File:SSOflag_25_857_1a.png *License*: unknown *Contributors*: Crenault

Image:FocalPlane.png *Source*: http://www.sciops.esa.int/wikiSI/planckpla/index.php?title=File:FocalPlane.png *License*: unknown *Contributors*: Rleonard

File:CCplot_100GHz_wEr_88mm.png *Source*: http://www.sciops.esa.int/wikiSI/planckpla/index.php?title=File:CCplot_100GHz_wEr_88mm.png *License*: unknown *Contributors*: Lspencer

File:CCplot_143GHz_wEr_88mm.png *Source*: http://www.sciops.esa.int/wikiSI/planckpla/index.php?title=File:CCplot_143GHz_wEr_88mm.png *License*: unknown *Contributors*: Lspencer

File:CCplot_217GHz_wEr_88mm.png *Source*: http://www.sciops.esa.int/wikiSI/planckpla/index.php?title=File:CCplot_217GHz_wEr_88mm.png *License*: unknown *Contributors*: Lspencer

File:CCplot_353GHz_wEr_88mm.png *Source*: http://www.sciops.esa.int/wikiSI/planckpla/index.php?title=File:CCplot_353GHz_wEr_88mm.png *License*: unknown *Contributors*: Lspencer

File:CCplot_545GHz_wEr_88mm.png *Source*: http://www.sciops.esa.int/wikiSI/planckpla/index.php?title=File:CCplot_545GHz_wEr_88mm.png *License*: unknown *Contributors*: Lspencer

File:CCplot_857GHz_wEr_88mm.png *Source*: http://www.sciops.esa.int/wikiSI/planckpla/index.php?title=File:CCplot_857GHz_wEr_88mm.png *License*: unknown *Contributors*: Lspencer

File:DX9_Y3_consistency.png *Source*: http://www.sciops.esa.int/wikiSI/planckpla/index.php?title=File:DX9_Y3_consistency.png *License*: unknown *Contributors*: Stechene

Image:Glitch_PowerSPectra_Expla.png *Source*: http://www.sciops.esa.int/wikiSI/planckpla/index.php?title=File:Glitch_PowerSPectra_Expla.png *License*: unknown *Contributors*: Lmontier

File:table.png *Source*: http://www.sciops.esa.int/wikiSI/planckpla/index.php?title=File:Table.png *License*: unknown *Contributors*: Kganga

File:Comparison_Cls_NMC_WNC_JN_WNCmean_removed_nominal_nomask.png *Source*: http://www.sciops.esa.int/wikiSI/planckpla/index.php?title=File:Comparison_Cls_NMC_WNC_JN_WNCmean_removed_nominal_nomask.png *License*: unknown *Contributors*: Jvalivii

File:Comparison_Cls_NMC_WNC_JN_WNCmean_removed_survey1_nomask.png *Source*: http://www.sciops.esa.int/wikiSI/planckpla/index.php?title=File:Comparison_Cls_NMC_WNC_JN_WNCmean_removed_survey1_nomask.png *License*: unknown *Contributors*: Jvalivii

File:Comparison_Cls_NMC_WNC_JN_WNCmean_removed_survey2_nomask.png *Source*: http://www.sciops.esa.int/wikiSI/planckpla/index.php?title=File:Comparison_Cls_NMC_WNC_JN_WNCmean_removed_survey2_nomask.png *License*: unknown *Contributors*: Jvalivii

File:LFI_4_5_5_4_madam_mask_1sec_DB10_1_noise_70GHz_all_DX9delta_nom_1024outmap.00000.gif *Source*: http://www.sciops.esa.int/wikiSI/planckpla/index.php?title=File:LFI_4_5_5_4_madam_mask_1sec_DB10_1_noise_70GHz_all_DX9delta_nom_1024outmap.00000.gif *License*: unknown *Contributors*: Hkurkis

File:LFI_4_5_5_4_madam_mask_1sec_DB10_1_white_70GHz_all_DX9delta_nom_1024binmap.00000.gif *Source*: http://www.sciops.esa.int/wikiSI/planckpla/index.php?title=File:LFI_4_5_5_4_madam_mask_1sec_DB10_1_white_70GHz_all_DX9delta_nom_1024binmap.00000.gif *License*: unknown *Contributors*: Hkurkis

File:LFI_4_5_5_4_madam_mask_1sec_DB10_1_rcnoise_70GHz_all_DX9delta_nom_1024map.00000.gif *Source*: http://www.sciops.esa.int/wikiSI/planckpla/index.php?title=File:LFI_4_5_5_4_madam_mask_1sec_DB10_1_rcnoise_70GHz_all_DX9delta_nom_1024map.00000.gif *License*: unknown *Contributors*: Hkurkis

file:Archives.JPG *Source*: http://www.sciops.esa.int/wikiSI/planckpla/index.php?title=File:Archives.JPG *License*: unknown *Contributors*: Xdupac

file:PLA.JPG *Source*: http://www.sciops.esa.int/wikiSI/planckpla/index.php?title=File:PLA.JPG *License*: unknown *Contributors*: Xdupac

file:PLAview.JPG *Source*: http://www.sciops.esa.int/wikiSI/planckpla/index.php?title=File:PLAview.JPG *License*: unknown *Contributors*: Xdupac

File:Planck_Logos.jpg *Source*: http://www.sciops.esa.int/wikiSI/planckpla/index.php?title=File:Planck_Logos.jpg *License*: unknown *Contributors*: Rleonard